

Reference

NBS
PUBLICATIONS



NIST
PUBLICATIONS

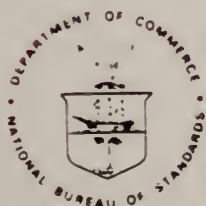
NBSIR 83-2742 (R)

Photonuclear Data - Abstract Sheets 1955 - 1982 Volume VII (Sulphur - Calcium)

E. G. Fuller, Henry Gerstenberg

U.S. DEPARTMENT OF COMMERCE
National Bureau of Standards
National Measurement Laboratory
Center for Radiation Research
Gaithersburg, MD 20899

October 1984



U.S. DEPARTMENT OF COMMERCE

NATIONAL BUREAU OF STANDARDS

QC
100
.U56
83-2742
1984

NBSIR 83-2742

**PHOTONUCLEAR DATA - ABSTRACT SHEETS
1955 - 1982
VOLUME VII (SULPHUR - CALCIUM)**

E. G. Fuller, Henry Gerstenberg

U.S. DEPARTMENT OF COMMERCE
National Bureau of Standards
National Measurement Laboratory
Center for Radiation Research
Gaithersburg, MD 20899

October 1984

**U.S. DEPARTMENT OF COMMERCE, Malcolm Baldrige, *Secretary*
NATIONAL BUREAU OF STANDARDS, Ernest Ambler, *Director***

TABLE OF CONTENTS

Table of Contents	i
Introduction.	1
Sulphur (Natural)	3
Sulphur (A=32).	45
Sulphur (A=33).	135
Sulphur (A=34).	139
Sulphur (A=36).	149
Chlorine (Natural).	153
Chlorine (A=34)	165
Chlorine (A=35)	171
Chlorine (A=36)	195
Chlorine (A=37)	199
Argon (A=36).	207
Argon (A=38).	217
Argon (A=40).	227
Potassium (Natural)	259
Potassium (A=37).	273
Potassium (A=39).	277
Potassium (A=41).	306
Calcium (Natural)	313
Calcium (A=40).	317
Calcium (A=41).	487
Calcium (A=42).	499
Calcium (A=44).	521
Calcium (A=48).	547
Definition of Abbreviations and Symbols	563

Photonuclear Data-Abstract Sheets 1955-1982

I. Introduction

As used in connection with this collection of data-abstract sheets, the term photonuclear data is taken to mean any data leading to information on the electromagnetic matrix element between the ground state and excited states of a given nuclide. The most common types of reactions included in this compilation are: (e,e') , (γ,γ) , (γ,γ') , (γ,n) , (γ,p) , etc. as well as ground-state particle capture reactions, e.g. (α,γ_0) . Two reactions which fit the matrix element criterion are not included in the compilation because of their rather special nature. These are heavy particle Coulomb excitation and the thermal neutron capture reaction (n,γ_0) . While the energy region of particular interest extends from 0 to 150 MeV, papers are indexed which report measurements in the region from 150 MeV to 4 GeV. Most of the experiments listed are concerned with the excitation energy range from 8 to 30 MeV, the region of the photonuclear giant resonance.

The hierarchical grouping of the photonuclear data-abstract sheets within the file is by: 1. Target Element, 2. Target Isotope, and 3. by the Bibliographic Reference Code assigned to the paper from which the data on the sheet were abstracted. In this file, colored pages are used to mark the beginning and end of the sheets for each chemical element. A brief historical sketch of the element is given on the divider sheet marking the start of each section; the information for this sketch was derived from references such as the Encyclopaedia Britannica. In those cases where the sheets for a given element make up a major part of a volume, colored pages are also used to delineate sections pertaining to the individual isotopes of the element. Each of the sections of the file, as delineated by two colored divider sheets, represents a 27 year history of the study of electromagnetic interactions in either a specific nuclide or a specific element.

The data-abstract sheets are filed under the element and/or isotope in which the ground-state electromagnetic transition takes place. For example, the abstract sheet for a total neutron yield measurement for a naturally occurring copper sample would appear in the elemental section of the copper file. On the other hand, a measurement of the ^{62}Cu 9.73 minute positron activity produced in the same sample by photons with energies below the three-neutron separation energy for ^{65}Cu (28.68 MeV) would be filed with the sheets for ^{63}Cu . Similarly a measurement of the ground-state neutron capture cross section in ^{12}C would be filed under ^{13}C while the corresponding ground-state alpha-particle capture cross section would be filed under ^{16}O .

At the end of this volume there is a master list of the abbreviations that have been used in the index section of the abstract sheets. The listings are those used in the final published index, Photonuclear Data Index, 1973-1981, NBSIR 82-2543, issued in August 1982 by the U. S. Department of Commerce, National Bureau of Standards, Washington, DC 20234. In some cases two notations are entered for the same quantity. The second entry is the abbreviation that was used in one or more of the earlier published editions of the index.

SULFUR

Z=16

The name sulfur was derived from the Latin word *suphurum* and was often called brimstone (burning stone). Sulfur is one of the few elements found in the earth's crust as an elemental form. It was easily recognized by the ancients because of its color and the resulting odor when burned. Early records indicate it was used in religious ceremonies, witchcraft, cosmetics, medicine, and warfare. It was also employed for the fumigation of buildings and the bleaching of cloth.

S

ELEM. SYM.	A	Z
S		16
REF. NO.		JOC
55 R1 1		

METHOD

Cloud chamber in magnetic field

REACTION	RESULT	EXCITATION ENERGY	SOURCE		DETECTOR		ANGLE
			TYPE	RANGE	TYPE	RANGE	
G ₂ D	RLY	THR - 65	C	65	CCH-I		4PI

RATIO TO PROTONS

$$\frac{Y_D}{Y_P} = .15 \pm .04$$

TABLE I. Reported photodeuteron/photoproton yields.

Element	Ratio	Maximum x-ray energy Mev	Reference
Beryllium	0.21 ^a	310	1
Copper	0.14 ^a	310	1
Copper	0.31 ^b	24	2
Copper	0.76 ^c	65	3
Cerium	0.05 ^b	24	4
Cobalt	0.02 ^b	24	5
Carbon	0.12 ^a	310	1
Lead	0.24 ^a	310	1
Sulfur	0.15 ^d	65	present work

^a Two-crystal telescope at 90°. Both particles have 40-Mev average energy.

^b Obtained with nuclear emulsion. Particles were identified by grain counting.

^c Magnetic cloud chamber. Particles in equal range and solid angle intervals. Measured protons were 1.1 to 1.8 Mev. Deuterons were in energy interval 1.2 to 2.3 Mev.

^d Conditions identical to (c). Ratio computed for thin target based on thick target observations.

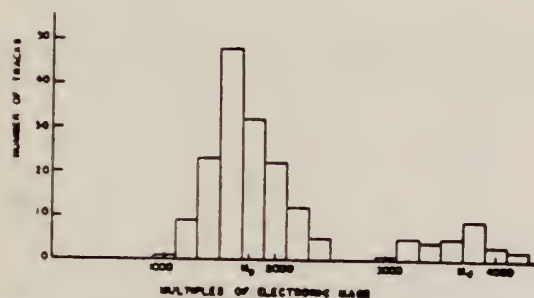


FIG. 1. Observed mass distribution of particles from sulfur.
Ratio of No. of deuterons to No. of protons = 0.19 ± 0.04 .

Method Betatron; photon scattering; NaI spectrometer

Ref. No.	EH
56 Fu 1	

Reaction	E or ΔE	E_0	Γ	$\int \sigma dE$	$J\pi$	Notes
$S(\gamma, \gamma)$	Bremss. 4-40					Detector at 120° . Cross sections given here are 13% too high due to erroneous $\cos \beta$ factor in denominator of Eq. 5. [See footnote 8 in Phys. Rev. <u>106</u> , 993 (1957)].

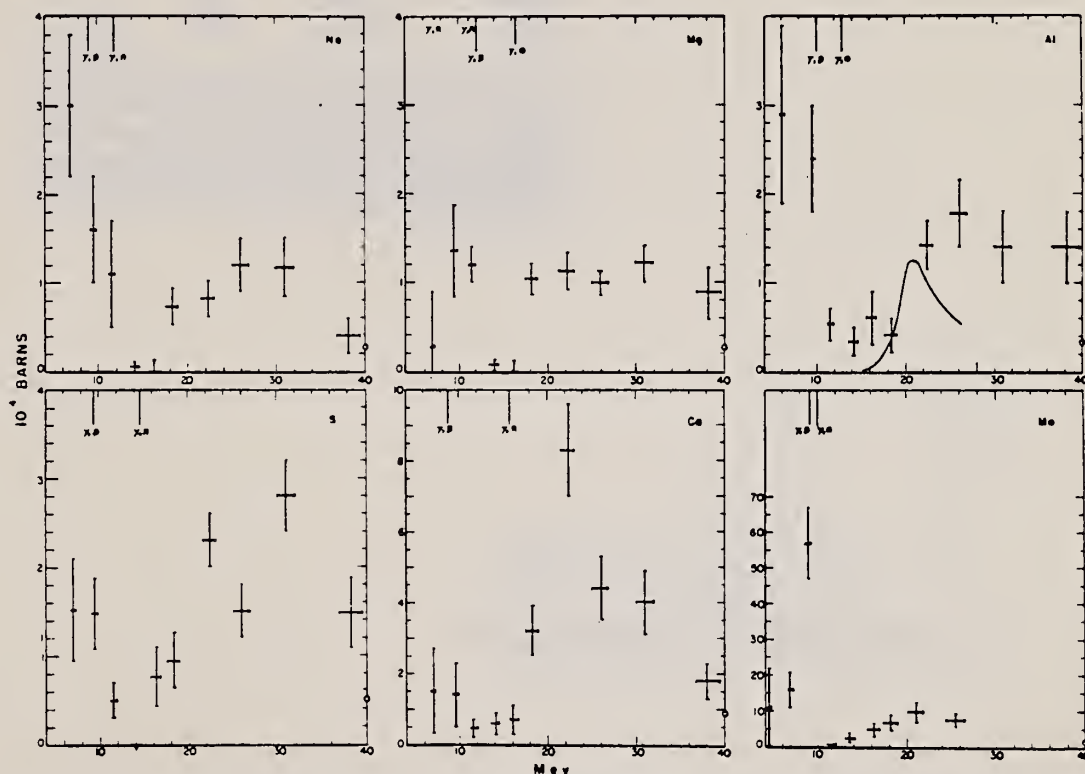


FIG. 4. The elastic scattering cross sections for Na, Mg, Al, S, Ca, and Mn. The indicated spread in energy is the width of the differential discriminator channel, and the standard deviations are based only on the number of counts. The vertical lines at the top represent the particle thresholds for the most important isotopes. The open circles at the extreme right indicate the magnitude of the Thomson cross section for Z free protons scattering coherently. The solid curve superimposed on the Al data is the scattering cross section calculated from the dispersion relation by substituting for $\sigma_0(E)$ in Eq. (6) the sum of the neutron and proton yield^{1,18} cross sections.

Ref. J. Dular, G. Kernel, M. Kregar, M.V. Mihailović, G. Pregl,
M. Rosina, C. Zupančič
Nuclear Phys. 14, 131 (1959)

Elem. Sym.

A

Z

S

16

Method

Compton Spectrometer; 30 MeV Betatron

Ref. No.

59 Du 1

EH

Reaction	E or ΔE	E_0	Γ	$\int \sigma dE$	$J\pi$	Notes
(μ_t)	Bremss. 28.9 30.3					817

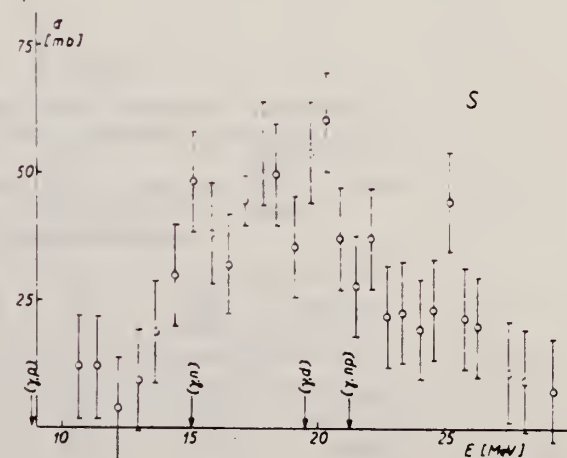


Fig. 7. Nuclear absorption cross section for S.

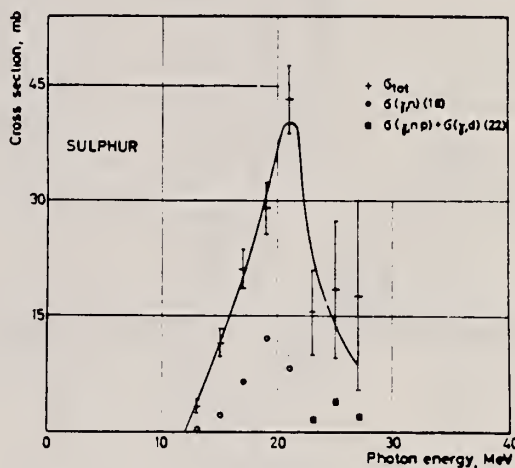
Elem. Sym.	A	Z
S		16

Method 30 MeV synchrotron; NaI(Tl) scintillator spectrometer; photon spectrum	Ref. No. 59 Ko 1	EH
---	---------------------	----

Reaction	E or ΔE	E ₀	Γ	∫σdE	Jπ	Notes
S (μ _t)	Bremss. 30.5	21	6.6	$\int_{10}^{27} = 0.30 \text{ MeV-mb}$		

TABLE 2
Experimentally determined giant resonance data: peak energy, E_{max}, width at half height, ΔE, and integrated cross section, $\int_{10 \text{ MeV}}^{27 \text{ MeV}} \sigma dE$, and values of $\int_0^\infty \sigma dE$ predicted by the dipole sum rule.

Absorber	E _{max} (MeV)	ΔE (MeV)	$\int_{10 \text{ MeV}}^{27 \text{ MeV}} \sigma dE$	$\int_0^\infty \sigma dE$
Carbon	23	4.6	0.12	0.18
Aluminium	21.5	7.8	0.24	0.40
Sulphur	21	6.6	0.30	0.48
Iron	19.5	9.4	0.76	0.84



¹⁷ B. Ziegler, Z. Physik 152 (1958) 566.
¹⁸ J. Halpern and A. K. Mann, Phys. Rev. 83 (1951) 370.
¹⁹ R. Montalbetti, L. Katz and J. Goldemberg, Phys. Rev. 91 (1953) 659.
²⁰ L. W. Jones and K. M. Terwilliger, Phys. Rev. 91 (1953) 699.
²¹ W. C. Barber, W. D. George and D. D. Reagan, Phys. Rev. 98 (1955) 73.
²² F. Ferraro, R. Malvano, S. Menardi and O. Terracini, Nuclear Physics 9 (1958) 32.
²³ L. Katz and A. S. Penfold, Phys. Rev. 81 (1951) 815.
²⁴ S. A. E. Johansson, Phys. Rev. 97 (1955) 1186.

Ref. V.P. Chizhov
Zhur. Eksp. i Teoret. Fiz. 38, 809 (1960)
Soviet Phys. JETP 11, 587 (1960)

Elem. Sym.	A	Z
S		16

Method 90 MeV Bremsstrahlung; scintillator counter telescope

Ref. No.	JHH
60 Ch 1	

Reaction	E or ΔE	E ₀	Γ	∫σdE	Jπ	Notes
S(γ,p)						Energy Range of particles detected: E_d - 15.5-30 MeV E_p - 15.5-30 MeV E_t - 17-30 MeV Ratios: $\sigma(\gamma,d)/\sigma(\gamma,p) \}$ at $\theta = 90^\circ$ $\sigma(\gamma,t)/\sigma(\gamma,d)$
S(γ,d)						
S(γ,t)						

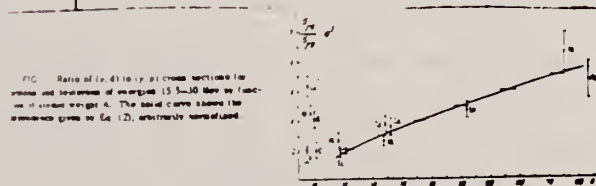


TABLE I

Element	$100N_p/N_d$	Element	$100N_p/N_d$	Element	$100N_p/N_d$	Element	$100N_p/N_d$
Li ⁶	30±3	S	39±8	Ni	10±4	In	5±2.5
Li ⁷	22.5±2.5	Si	10.7±4	Co	2.5±2	Ta	10±4
Be	13±6	S	4±4	Cu	2±2	Au	3±3

Ref. K. Reibel, A.K. Mann
Phys. Rev. 118, 701 (1960)

Elem. Sym. A Z

S

16

Method γ 's from $F^{19}(\gamma, \alpha\gamma)$ reaction; protons from Van de Graaff; NaI

Ref. No.
60 Re 1

JHH

Reaction	E or ΔE	E_0	Γ	$\int \sigma dE$	$J\pi$	Notes
$S(\gamma, \gamma)$	~ 7					$\langle \bar{\sigma} \rangle (E_p = 2.05 \text{ MeV}) = 0.074 \pm 0.011 \text{ mb}$ Detector at 90° .

Method 30 MeV electron synchrotron; emulsions; magnetic analysis.

Ref. No.	
61 Fo 1	JHH

Reaction	E or ΔE	E_0	Γ	$\int \sigma dE$	$J\pi$	Notes
(γ, p)	Bremss. 30			Angle Unknown		No significant (γ, d) yield detected.

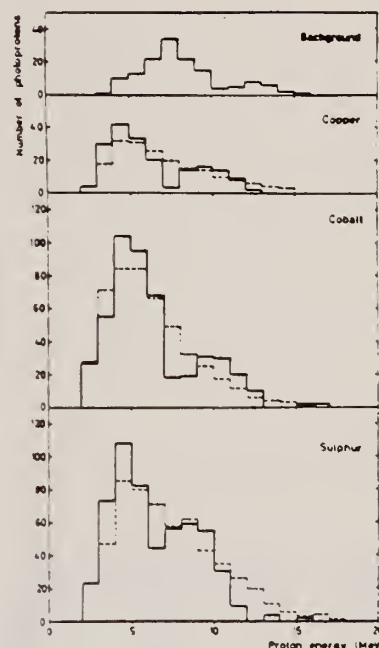


Figure 8: Energy distribution of the photoproton tracks giving intersection points in the area $-8.4 > x_t > -11.6$ and $-3.0 < x_t < 3.0$

The lowest section shows the photoprotons from the sulphur exposure. The dashed line is the expected distribution from ref. 19 [Cujec-Dobovisek, Congr. Intern. de Phys. Nucleaire (1958) 634]. The second section shows the photoprotons from the cobalt exposure. The dashed line is the expected distribution from ref. 20 [Toms and Stephens, Phys. Rev. 95, 1209 (1954)]. The third section shows the photoprotons from the copper exposure. The dashed line is the expected distribution from ref. 21 [Lin'kova et al, Soviet JETP 38, 780 (1960)]. The background is subtracted in these 3 sections, but shown in the uppermost section. It originates from the entrance window.

M. Masuda
J. Phys. Soc. 16, 1801 (1961)

ELEM. STM. A		
S		16
REF. NO.	61 Ma 2	NVB

METHOD
Betatron; proton angular distribution; ZnS scintillator

REACTION	RESULT	EXCITATION ENERGY	SOURCE		DETECTOR		ANGLE
			TYPE	RANGE	TYPE	RANGE	
G, XP	NOX	9 - 21	C	21	SCI - I	1 - 10	DST

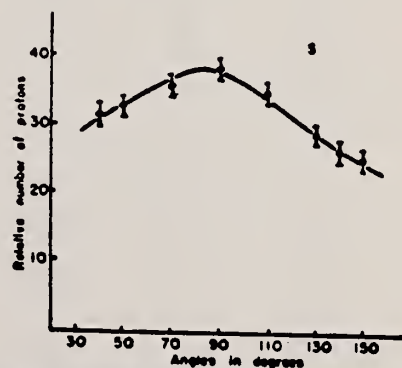


Fig. 6. Angular distribution of photo-protons from sulfur. The experimental dots fit the expression, $1 + 0.57 \sin^2 \theta (1 + 0.23 \cos \theta)^2$.

Method 25 MeV betatron; photon scattering; NaI(Tl) spectrometer;
ion chamber.

Ref. No.	
61 To 1	NVB

Reaction	E or ΔE	E ₀	Γ	∫σdE	Jπ	Notes
S(γ,γ)	Bremss. 5-12	8.5				Detector at 120° Table II from J. Phys. Soc. Japan <u>18</u> , 17-22 (1963)

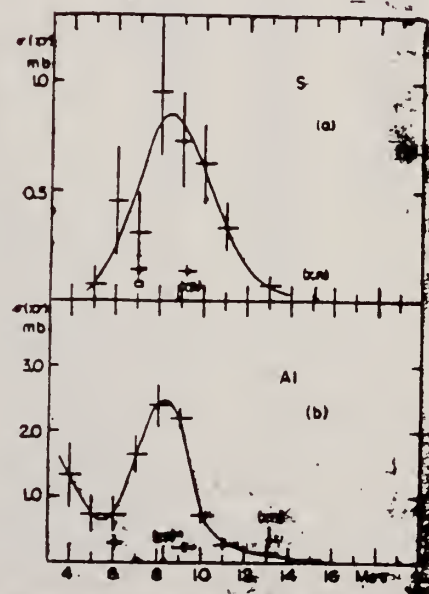
References

- 1) E. G. Fuller and E. Hayward: Phys. Rev. **101** (1956) 692.
- 2) see E. Segre: *Experimental Nuclear Physics*, vol. 1, p. 346.
- 3) J. S. Levin and D. J. Hughes: Phys. Rev. **101** (1956) 1328.
- 4) K. Reibel and A. K. Mahn: Phys. Rev. **118** (1960) 701.

Table II. The correction of the energy scale.

Energy in Ref. 1	should be read
4.0 Mev	3.3 Mev
6.0	5.5
8.0	7.7
10.0	9.9
12.0	12.1
14.0	14.3

Figure showing two plots of cross-section (mb) versus energy (Mev) for S and Al. Plot (a) for S shows a peak around 8 Mev. Plot (b) for Al shows a peak around 8 Mev. Both plots have energy in Mev on the x-axis and cross-section in mb on the y-axis.



Ref. K. Shoda, K. Abe, T. Ishizuka, N. Kawamura, M. Kimura
J. Phys. Soc. Japan 17, 735 (1962)

Elem. Sym.	A	Z
S		16

Method 25 MeV betatron; proton yield; scintillator; ion chamber

Ref. No.	
62 Sh 11	NVB

Reaction	E or ΔE	E_0	Γ	$\int \sigma dE$	$J \pi$	Notes <u>966</u>
$S(\gamma, p)$	Bremss. Th4 - 24	19.3	6 MeV	$\int_0^{23} = 0.26 \text{ MeV-b}$		$\sigma_{\text{max}} = 41.6 \text{ mb.}$ 6 detectors at angles: 20° 55° $90^\circ (2)$ 125° 160° Measured all protons above $E_0 = 1.5 \text{ MeV}$

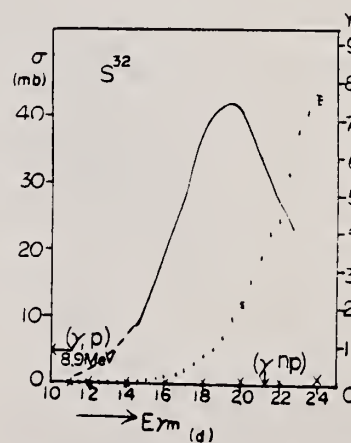


Fig. 3. Photoproton yield and cross section curves for a) Mg, b) Al, c) Si, d) S. Arrows in the figure show the threshold energies. The backgrounds observed without targets are shown by x.

Method Synchrotron; neutron yield; BF_3 counters; NBS chamber monitor

Ref. No. 63 Bo 1 JHH

Reaction	E or ΔE	E_0	Γ	$\int \sigma dE$	$J\pi$	Notes
$S(\gamma, n)$	Bremss. 10-30			$\int_{th}^{28} = 81 \text{ MeV-mb}$		For " E_0 " and " $\sigma(\text{mb})$ ", see Table III below.

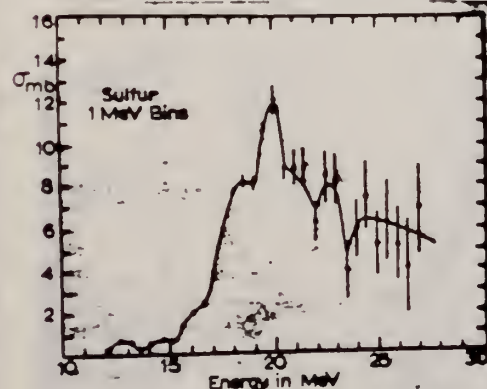
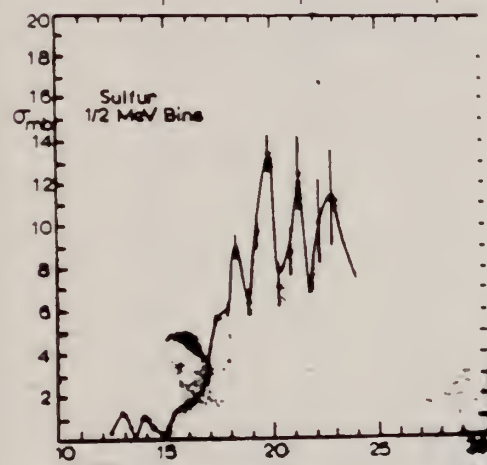


Fig. 4. $S(\gamma, n)$ cross section unfolded using $\frac{1}{2}$ -MeV bins (top curve) and 1-MeV bins (lower curve).

TABLE III. Summary of data from this experiment giving energy positions of levels found in our cross sections and corresponding data from other experiments.

Element	University of Virginia E (MeV)	University of Virginia σ (mb)	Govt. E (MeV)	Govt. σ (mb)	Kimura* E (MeV)	Kimura* σ (mb)
S	16.0	1.2				
	18.5	8.4	18			
	19.75	14.7	18.9		18.9	
	20.75	18.4	20		20.0	
	22.75	9.4	21.4		21.4	
	24.25	7.1				
P	University of Virginia		Mutsuro†			
	E (MeV)	σ (mb)	E (MeV)	σ (mb)		
	14.75	1.0	13.5	0		
	15.75	5.6	14.6	4		
	17.25	9.2	15.8	14		
	18.25	10.2	17.5	21		
	19.25	11.5	19.0	22		
	20.25	13.6	20.3	22		
S	University of Virginia		Mutsuro†			
	E (MeV)	σ (mb)	E (MeV)	σ (mb)		
	16	1.7	15.7	7		
	17.5	6.0	16.8	10		
	18.25	9.0	17.9	20		
	19.75	13.4	18.75	11		
	21.25	12.5	19.7	16		
	22.75	11.3				
	24.0	9.0				

* See Refs. 12, 13, and 14.
† See Ref. 15.

TABLE II. Integrated cross-section values obtained from the (γ, n) cross sections of elements measured in this laboratory.*

Element	Limits of integration threshold to	$\int \sigma dE$ MeV-mb	Dipole sum rule $X=0$ MeV-mb	% of DSR exhausted by (γ, n)
O	31 MeV	46	240	19
Mg	29	84	360	23
Al	28	97.5	405	24
Si	28	80	420	19
P	28	127	465	27
S	28	81	480	17
Ca	28	74	600	12
N	25	60	210	29
	50	116		55
Ar	25	392	600	65
	50	598		100
Li	25	39	105	37
	50	93		89

* See Refs. 1, 12, and 13.

† L. N. Bolen and W. D. Whitehead, Phys. Rev. Letters 9, 458 (1962).

‡ R. L. Bramblett, J. C. Coldwell, and S. C. Fultz, University of California Lawrence Radiation Laboratory Report UCRL 7156 (unpublished).

§ F. W. K. Firk and E. R. Rae, International Symposium on Direct Interactions and Nuclear Reaction Mechanisms, Padua, 1962 (to be published).

|| N. Mutsuro, K. Kageyama, M. Mishina, T. Nakagawa, E. Tanaka, and M. Kimura, J. Phys. Soc. Japan 17, 1672 (1962).

¶ N. Mutsuro, K. Kageyama, M. Mishina, E. Tanaka, and M. Kimura, J. Phys. Soc. Japan 17, 1673 (1962).

||| R. W. Fast, P. A. Flournoy, R. S. Tickle, and W. D. Whitehead, Phys. Rev. 118, 535 (1960).

|||| K. Min, L. N. Bolen, and W. D. Whitehead, Phys. Rev. 132, 740 (1963).

Ref.

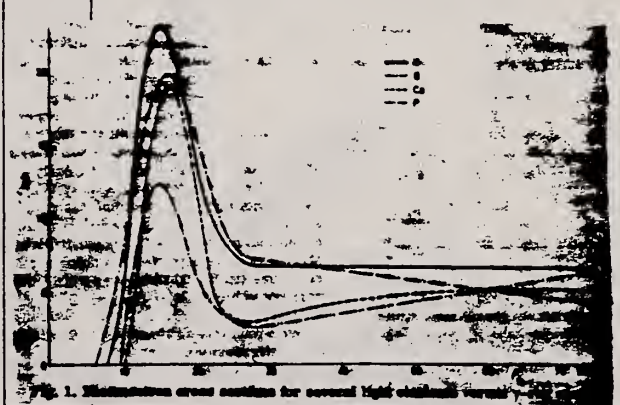
S. Costa, F. Ferrero, S. Ferromi, B. Minetti, C. Molino
R. Malvagi
Phys. Letters 6, 226 (1963)

Elem. Sym.	A	Z
S		16

Method

100 MeV Synchrotron; 4π neutron detector; calculated integrated cross sections - fitted with polynomial of degree η

Ref. No.	
63 Co 3	207

Reaction	E or ΔE	E_0	Γ	$\int \sigma dE$	$J\pi$	Notes
(γ, xn)						$\sigma_b = \int \frac{\sigma(E)}{E} dE$ gets $(\vec{v}_p \cdot \vec{v}_n - \vec{v}_n \cdot \vec{v}_{n1})$ $= (R_n^2 - R_p^2 - \frac{3}{\pi^2} \frac{E_n^2}{E^2} \sigma_b \frac{A-1}{A^2}) \times \frac{2}{A-2}$ See "Boron" for plots of this and $\int \sigma dE/60 \text{ MeV/A}$.
						

Ref. N. Mutsuro, K. Kageyama, M. Mishina, E. Tanaka, T. Aizawa, M. Kimura
J. Phys. Soc. Japan 18, 599 (1963)

Elem. Sym.	A	Z
S		16

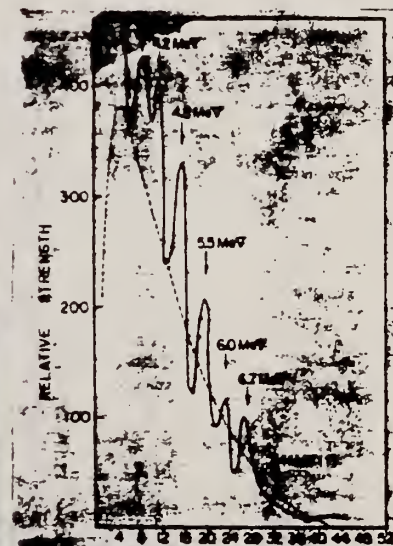
Method 25 MeV betatron; neutron yield and spectrum; BF_3 counter,
scintillator; NBS chamber

Ref. No.	
63 Mu 2	NVB

Reaction	E or ΔE	E ₀	Γ	∫σdE	Jπ	Notes																											
S(γ, xn)	Bremss.			22.5		Used (n,p) reaction in Stilbene to get n-spectrum for E _γ max. ~ 24 MeV, θ = 90°.																											
	E _γ max: 14-24	E _γ : 15.7 16.8 17.9 18.8 19.7 20.6		∫ ₀ ^{22.5} = 60±6 MeV-mb																													
	Δ E: 0.25 or 0.1	E _n : 6.7 6.0 5.5 4.8 4.2 3.6 3.0				<p>Table II. Characteristic constants of emitted neutron spectrum in S(γ, n) reaction.</p> <p>Values of E (MeV) are deduced on the assumption that all neutron groups are produced by the ground state transition.</p> <table><tr><th>E_n MeV</th><th>Relative Strength</th><th>E MeV</th></tr><tr><td>7.4</td><td>—</td><td>22.4</td></tr><tr><td>6.7</td><td>1</td><td>21.8</td></tr><tr><td>6.0</td><td>1</td><td>21.1</td></tr><tr><td>5.5</td><td>2</td><td>20.6</td></tr><tr><td>4.8</td><td>3</td><td>19.9</td></tr><tr><td>4.2</td><td>3</td><td>19.3</td></tr><tr><td>3.6</td><td>3</td><td>18.7</td></tr><tr><td>3.0</td><td>—</td><td>18.0</td></tr></table>	E _n MeV	Relative Strength	E MeV	7.4	—	22.4	6.7	1	21.8	6.0	1	21.1	5.5	2	20.6	4.8	3	19.9	4.2	3	19.3	3.6	3	18.7	3.0	—	18.0
E _n MeV	Relative Strength	E MeV																															
7.4	—	22.4																															
6.7	1	21.8																															
6.0	1	21.1																															
5.5	2	20.6																															
4.8	3	19.9																															
4.2	3	19.3																															
3.6	3	18.7																															
3.0	—	18.0																															

12) M. Kimura, et al. To be published in J. Phys. Soc. Japan

12) M. Kimura, et al. To be published in J. Phys. Soc. Japan



Method Betatron; proton spectrum; nuclear emulsion

Ref. No.	NVB
63 Sh 4	

Reaction	E or ΔE	E_0	Γ	$\int \sigma dE$	$J\pi$	Notes
----------	-----------------	-------	----------	------------------	--------	-------

$S(\gamma, xp)$	Bremss. 24.0					
-----------------	-----------------	--	--	--	--	--

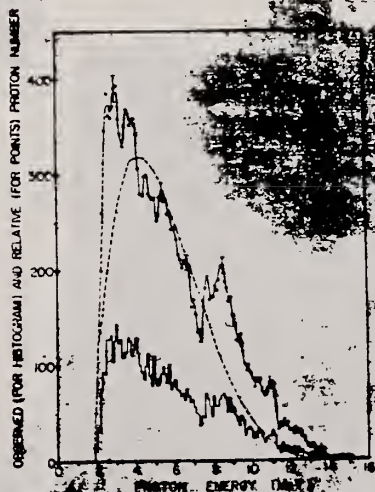


Fig. 1. The energy spectrum of photo-neutrons from S^{32} . The histogram is observed one. The solid line is a smoothed one. The dashed line is a calculated one using the statistical theory.

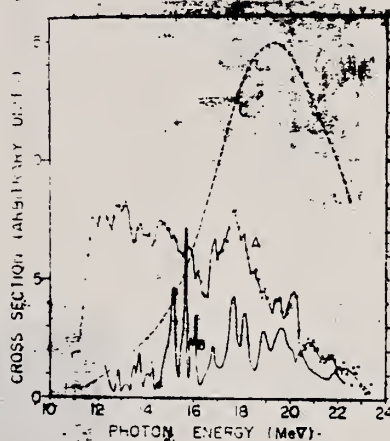


Fig. 2. Comparison of cross sections for $S^{32}(\gamma, p)P^{32}$. A. Present cross section assuming ground state transitions. B. Cross section of $S^{32}(\gamma, p)P^{32}$ obtained from $P^{32}(\gamma, \gamma)S^{32}(\gamma, n)$. C. Total cross section of $S^{32}(\gamma, p)P^{32}$.

K. Shoda, K. Abe, T. Ishizuka, N. Kawamura, and M. Kimura: J. Phys. Soc. Japan 17 (1963) 750.

- 4) N. W. Tanner: private communication. D. S. Gemmel: private communication.
- 5) M. Kimura, K. Shoda, N. Mutsuro, M. Sugawara, K. Abe, K. Kageyama, M. Mishina, A. Ono, T. Ishizuka, S. Mori, N. Kawamura, T. Nakagawa, and E. Tanaka: to be published

METHOD					REF. NO.	
Van de Graaff; resonance fluorescence					64 Bo 1	NVB
REACTION	RESULT	EXCITATION ENERGY	SOURCE		DETECTOR	
			TYPE	RANGE	TYPE	RANGE
G,G	LFT	1-3	C	1 - 3	NAI-D	100
		(0.5 - 3.0)		(0.5 - 3.0)		

ABI

TABLE I
Cases of observed resonance fluorescence

Nucleus multipol.	State (MeV)	Spin	I_0, I'	$T(g^2 I_0^2 I'^2)^{-1}$ (sec).	Mean lifetime T BCW (sec)	Mean lifetime T other (sec)	Ref.	Γ_0/Γ_w BCW
S^{32}	0.00 2.32	0 ⁺ 2 ⁺	1	$8.6 \pm 2.8 \times 10^{-14}$	$27 \pm 9 \times 10^{-14}$	16×10^{-14}	41	7

METHOD

Linac

REF. NO.

64 F1 1

JOC

REACTION	RESULT	EXCITATION ENERGY	SOURCE		DETECTOR		ANGLE
			TYPE	RANGE	TYPE	RANGE	
G,XN	SPC	THR-25	C	23,25	TØF-D		70

TABLE 2

Energy levels in S^{32} observed in the reactions $S^{32}(\gamma, n)S^{31}$ and $P^{31}(p, \gamma_e)S^{32}$

$S^{32}(\gamma, n)S^{31}$ (MeV)	$P^{31}(p, \gamma_e)S^{32}$ (MeV)	$S^{32}(\gamma, n)S^{31}$ (MeV)	$P^{31}(p, \gamma_e)S^{32}$ (MeV)
17.08	17.04	18.62	18.60
17.21	17.20		18.69
17.42 ± 0.03	17.43	18.81	18.80
17.48	17.50	18.88	18.88
17.61	17.62	19.03	
17.70	17.71	19.24	
17.88	17.90	19.34	
17.96	17.967	19.42	
18.12	18.08	19.65	
18.16 ± 0.04	18.15	19.74	
18.30	18.33	19.88	
18.37	18.44	20.15	
18.56	18.56	20.62 ± 0.06	

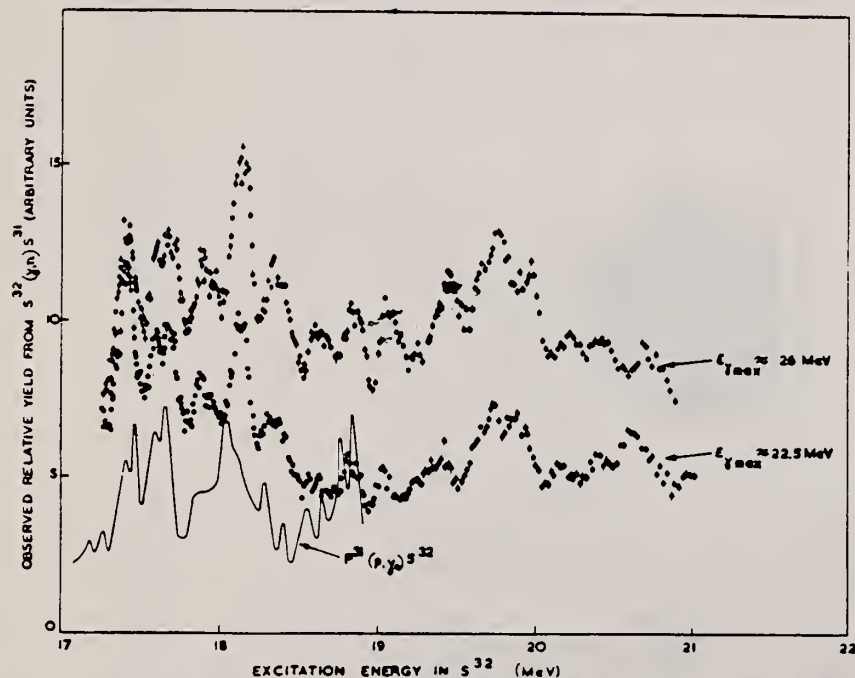


Fig. 2. The observed relative yields of photoneutrons from the reaction $S^{32}(\gamma, n)S^{31}$ (assuming ground state neutrons only) for bremsstrahlung energies of 22.5 and 25 MeV. The $P^{31}(p, \gamma_e)S^{32}$ data²⁴ are shown in the region below 20 MeV. Uncertainties in the background prevent a quantitative measurement of the non-ground state (or evaporation) spectrum of photoneutrons.

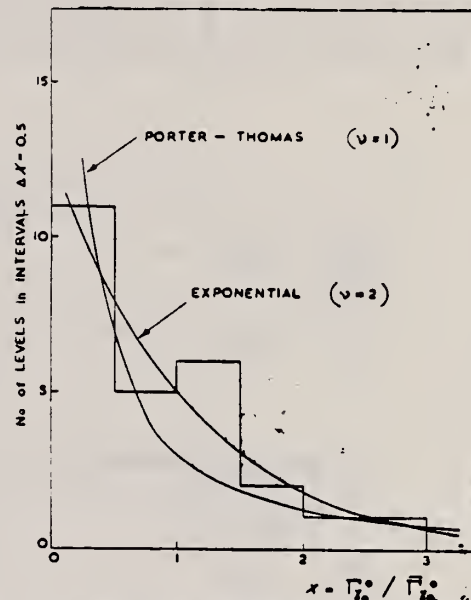


Fig. 3. The distribution of ground state γ -ray transitions for 26 levels in S^{32} assuming E1 transitions. Comparisons are made with a Porter-Thomas and an exponential distribution. (Here $\Gamma_0^2 \equiv \Gamma_0/E_\gamma^2$ and $P(x)dx = (1/2\sqrt{\pi})(\frac{1}{2}x)^{-1/2} \exp(-\frac{1}{2}x)dx$ is the Porter-Thomas distribution).

B. S. Ishkhanov, I. M. Kapitonov, V. G. Shevchenko and B. A. Yur'ev
Phys. Letters 2, 162 (1964)

S

16

METHOD

Betatron

REF. NO.

64 Is 1

JOC

REACTION	RESULT	EXCITATION ENERGY	SOURCE		DETECTOR		ANGLE
			TYPE	RANGE	TYPE	RANGE	
G, XP	ABX	THR - 32	C	15-32	SCI-D	0-3	UNK

818

Table 2
Measurements results

Element	Maximum cross section (b)	Peak position (MeV)	Peak half-width (MeV)	Integrated cross section $\int_0^{32} \sigma(E) dE$ (MeV, b)
P	0.043	21	10	0.36 ± 0.06
S	0.050	21	9	0.37 ± 0.05
Mg	0.018	22.5	11	0.18 ± 0.04
	0.018	26.0		

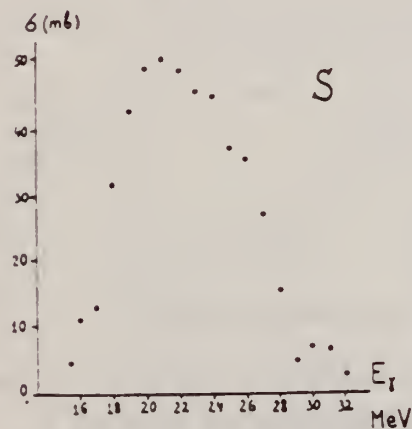


Fig. 4. The (γ, p) cross section for S.

REF.

J.M. Wyckoff, B. Ziegler, H.W. Koch, and R. Uhlig
Phys. Rev. 137, B576-94 (1965)

S

16

METHOD

REF. NO.

Synchrotron; ion chamber monitor

65 Wy 1

NVB

REACTION	RESULT	EXCITATION ENERGY	SOURCE		DETECTOR		ANGLE
			TYPE	RANGE	TYPE	RANGE	
G,MU-T	ABX	10 - 35	C	90	SCI-D		4PI

43+

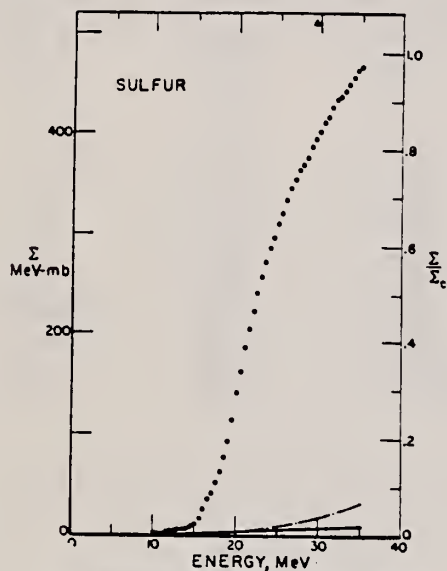
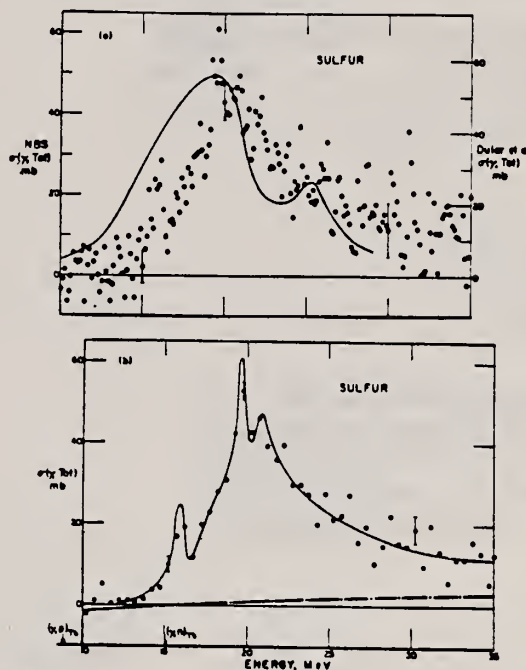


FIG. 20. Sulfur total photonuclear cross section integrated over energy.

FIG. 19. Sulfur total photonuclear cross section. The solid line on (a) represents the $\sigma(\gamma, \text{Tot})$ data of Dular *et al.* (Ref. 5) using the right-hand ordinate scale.

METHOD

Betatron

REF. NO.

66 Ho 3

JDM

REACTION	RESULT	EXCITATION ENERGY	SOURCE		DETECTOR		ANGLE
			TYPE	RANGE	TYPE	RANGE	
G, A	SPC	THR-31	C	31	SCD-D	3-13	130

TABLE I

Experimental data and results

Element	Mg	Al	S	Ni	Cu	Zn	Error (%)
target thickness (mg/cm ²)	0.81	1.54	0.80	2.50	2.68	3.00	5 ^{a)}
dose (r)	6190	25400	23200	3880	5840	4220	10
yield absolute (10 ⁴ /mole · r) for $E_m > 3.16$ MeV	0.61	0.93	1.46	1.65	0.92	2.42	11 ^{a)}
yield relative to Ni	0.36	0.56	0.88	1	0.55	1.43	5 ^{a)}
$Y_{\gamma, \sigma}/Y_{\gamma, tot}(\%)$	9.6	11.4	12.4	7.0	3.2	^{b)}	
nuclear temp. θ (MeV)	1.43	1.48	1.46	1.04		0.91	10
level density parameter a (MeV ⁻¹)	5.1	4.8	4.9	8.6		10.8	10

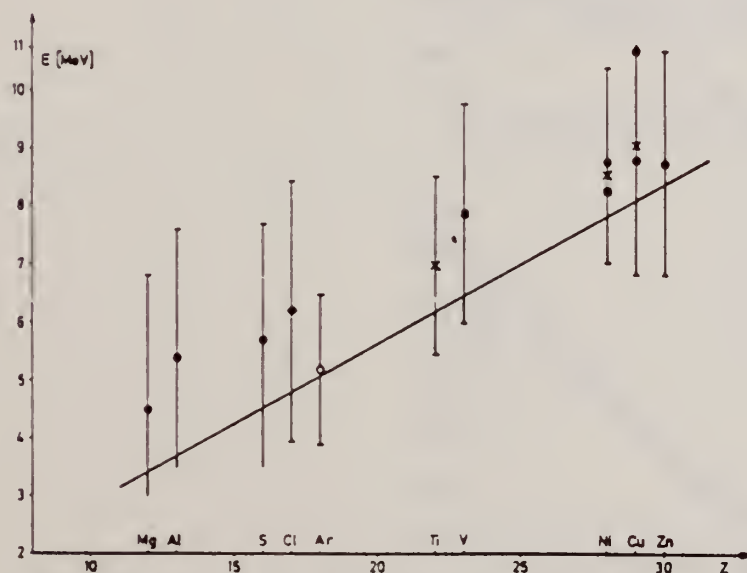
^{a)} For S, the error of the target thickness has been 10 %, of the absolute yield 14 % and of the relative yield 10 %.^{b)} For Zn $\sigma_{\gamma, tot}$ is not known.

Fig. 4. Position of the peaks in different photoalpha spectra plotted against Z of the target nuclei. \times : Scheer *et al.*⁽¹⁰⁾, \blacksquare : Kregar and Povh⁽⁹⁾, \blacktriangle : Meneghetti and Vitale⁽⁸⁾, \blacklozenge : Erdős *et al.*⁽¹⁾, \circ : Komar *et al.*⁽⁷⁾, \bullet : this work. The signs show the position of the maximum, the bars give the widths at half maximum. The curve shows the height of the Coulomb barrier.

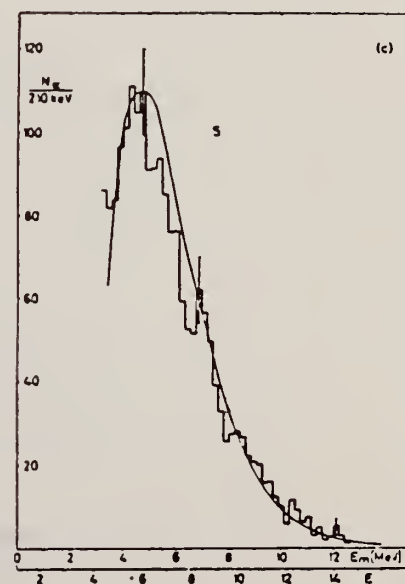


Fig. 3 (c)

REF.	H. Lichtblau and B.M. Spicer Aust. J. Phys. <u>19</u> , 297 (1966)				ELEM. SYM.	A	Z	
J					S		16	
PI								
METHOD					REF. NO.			
35 MeV Betatron; NBS ionization chamber					66 Li 1		JDM	
S								
REACTION		RESULT	EXCITATION ENERGY	SOURCE		DETECTOR		ANGLE
				TYPE	RANGE	TYPE	RANGE	
G,P		SPC	THR - 32	C	32	SCI-D	1 - 20	90

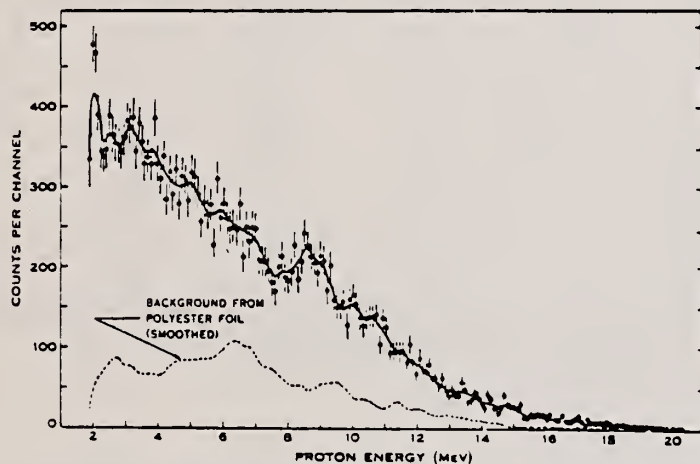


Fig. 6.—Energy spectrum of photoprotons from sulphur, with bremsstrahlung end-point energy 32 MeV.

REF.

B. S. Ishkhanov, I. M. Kapitonov, V. G. Shevchenko, and B. A. Yur'ev
 J. Nucl. Phys. (USSR) 4, 765 (1966)
 Soviet J. Nucl. Phys. 4, 544 (1967)

ELEM. SYM. A

S

16

REF. NO.

67 Is 1

joc

METHOD

[Page 1 of 2]

REACTION	RESULT	EXCITATION ENERGY	SOURCE		DETECTOR		ANGLE
			TYPE	RANGE	TYPE	RANGE	
G,P	ABX	THR-35	C	22-35	EMU-D	3	DST

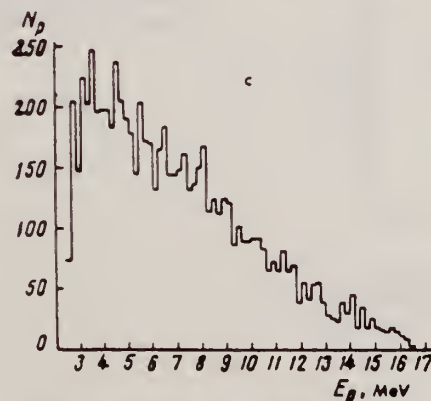
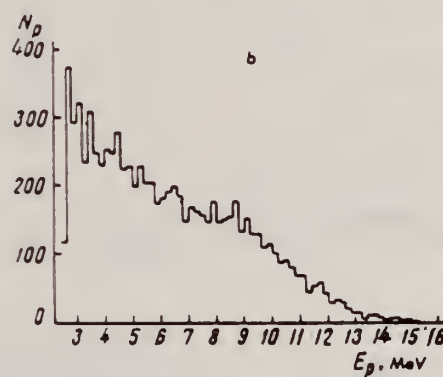
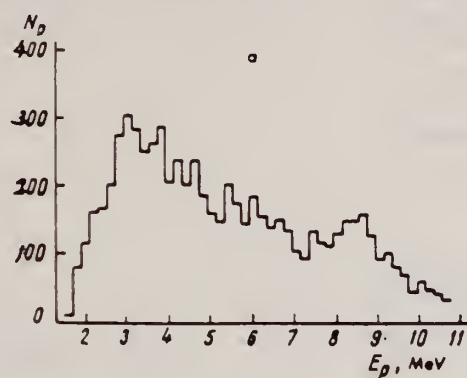


Fig. 1. Energy distribution of photoprotons from S^{32} , obtained by irradiation with bremsstrahlung of the following energies: a - $E_{\gamma max} = 22$ MeV, b - $E_{\gamma max} = 25$ MeV, c - $E_{\gamma max} = 34$ MeV.

REF. B. S. Ishkhanov, I. M. Kapitonov, V. G. Shevchenko, and B. A. Yur'ev
J. Nucl. Phys. (USSR) 4, 765 (1966)
Soviet J. Nucl. Phys. 4, 544 (1967)

ELEM. SYM.	A	Z
S		16
REF. NO.		joc
67 Is 1		

METHOD [Page 2 of 2]

REACTION	RESULT	EXCITATION ENERGY	SOURCE		DETECTOR		ANGLE
			TYPE	RANGE	TYPE	RANGE	

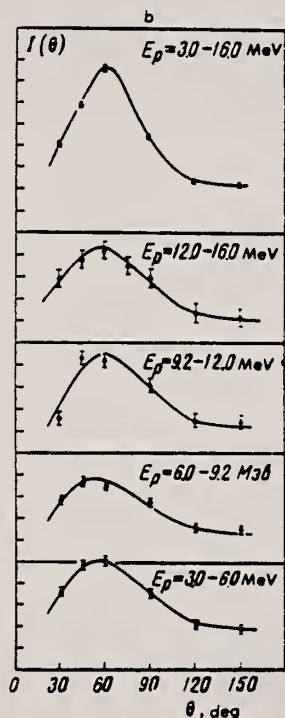
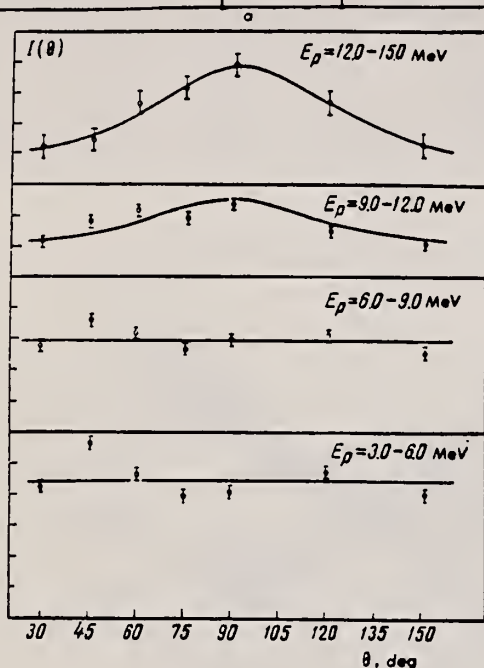


Fig. 2. Angular distributions of individual energy groups of photoprotons from S^{32} , obtained with bremsstrahlung of the following energies: a- $E_{\gamma\max} = 25$ MeV, b- $E_{\gamma\max} = 34$ MeV.

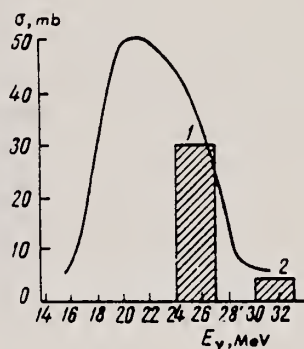


Fig. 3. Cross section for the reaction $S^{32}(\gamma, p)$. The smooth curve is the experimental cross section. The crosshatched columns are the results obtained by Neudachin and Shevchenko,^[1] as follows: 1 - cross section for the transition $1p_{1/2} \rightarrow 1d_{3/2}$; 2 - cross section for the transition $1p_{3/2} \rightarrow 1d_{5/2}$.

METHOD

REF. NO.	
68 Ab 5	egf

REACTION	RESULT	EXCITATION ENERGY	SOURCE		DETECTOR		ANGLE
			TYPE	RANGE	TYPE	RANGE	
G, XP	SPC	THR-24	C	21-24	SCD-D	2-14	90

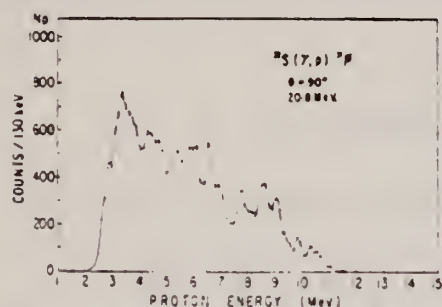


Fig. 1. Energy spectrum of photoprotons from sulphur at 90°, with bremsstrahlung end-point energy 20.8 MeV.

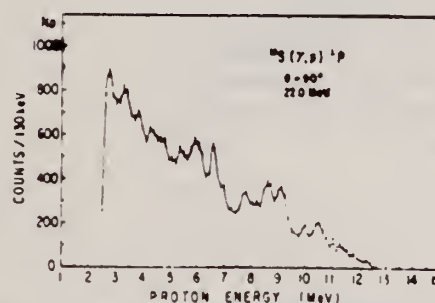


Fig. 2. Energy spectrum of photoprotons from sulphur at 90°, with bremsstrahlung end-point energy 22.0 MeV.

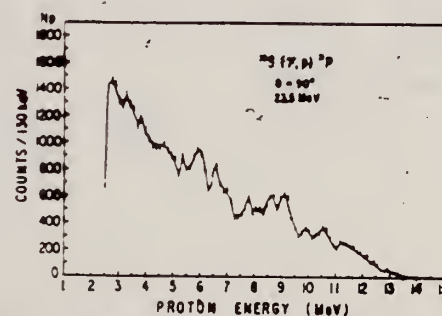


Fig. 3. Energy spectrum of photoprotons from sulphur at 90°, with bremsstrahlung end-point energy 23.5 MeV.

B. S. Dolbilkin, A. I. Isakov, V. I. Korin, L. E. Lazareva, and
 F. A. Nikolaev
 Yad. Fiz. 8, 1080 (1968)
 Sov. J. Nucl. Phys. 8, 626 (1969)

ELEM. SIM.

S

16

METHOD

REF. NO.

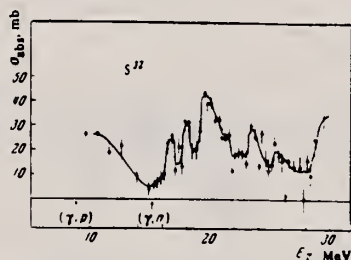
68 Do 1

egf

REACTION	RESULT	EXCITATION ENERGY	SOURCE		DETECTOR		ANGLE
			TYPE	RANGE	TYPE	RANGE	
G, MU-T	ABX	10-30	C	260	MGP-D	10-30	4PI

859

FIG. 1. γ -ray absorption cross-section curve for sulfur.



METHOD

REF. NO.

68 Go 6

HMG

REACTION	RESULT	EXCITATION ENERGY	SOURCE		DETECTOR		ANGLE
			TYPE	RANGE	TYPE	RANGE	
G,XN	ABX	14-30	C	14-30	BF3-I		4PI

432

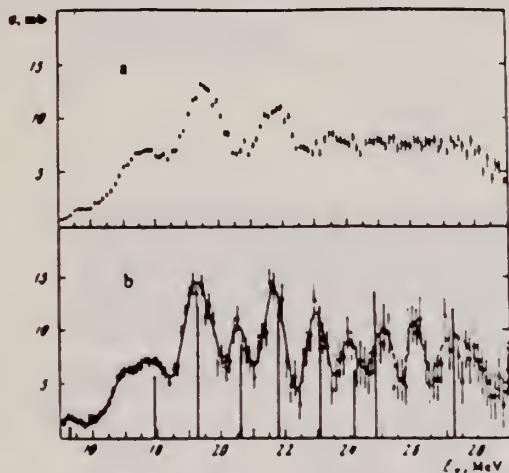


FIG. 3. Cross section for the reaction $S^{32}(\gamma, n)$. The computational step $\Delta E = 1$ MeV (a) and 0.5 MeV (b). The vertical bars are the results obtained by Goryachev et al. [8]

Table II. Parameters of resonances observed in the cross section for $S^{32}(\gamma, n)$

E^0 , MeV	σ_{int} , MeV-mb	E^0 , MeV	E^0 , MeV	σ_{int} , MeV-mb	E^0 , MeV
Our data		data of [7]	data of [11]	data of [12]	data of [13]
1.6 ± 0.1	1	16	15.7	$\left. \begin{matrix} 15.7 \\ 16.0 \end{matrix} \right\} \begin{matrix} 0.8 \\ 0.6 \end{matrix} \right\}$	1.4
16.8 ± 0.1	3.5		16.8	$\left. \begin{matrix} 16.8 \\ 17.1 \end{matrix} \right\} \begin{matrix} 2.0 \\ 0.8 \end{matrix} \right\}$	2.8
17.5 ± 0.1	4.6	17.5		$\left. \begin{matrix} 17.5 \\ 17.7 \end{matrix} \right\} \begin{matrix} 2.5 \\ 2.5 \end{matrix} \right\}$	5
(17.9)			17.9		$\left. \begin{matrix} 17.21; 17.42; \\ 17.48; 17.61; \\ 17.70; 17.88 \end{matrix} \right\}$
		18.25		$\left. \begin{matrix} 18.2 \\ 18.5 \end{matrix} \right\} \begin{matrix} 4.5 \\ 2.0 \end{matrix} \right\}$	$\left. \begin{matrix} 17.96; 18.12 \\ 18.16; 18.30 \end{matrix} \right\}$
19.0 ± 0.1	14.4		18.75	$\left. \begin{matrix} 18.9 \\ 19.2 \end{matrix} \right\} \begin{matrix} 5.5 \\ 6.5 \end{matrix} \right\}$	12
19.6 ± 0.1	7.1				$\left. \begin{matrix} 18.37; 18.56; \\ 18.62; 18.81; \\ 18.88; 19.03; \\ 19.24; 19.34 \end{matrix} \right\}$
20.5 ± 0.1	5.2	19.75	19.7	$\left. \begin{matrix} 19.55 \\ 19.9 \end{matrix} \right\} \begin{matrix} 7.0 \\ 7.5 \end{matrix} \right\}$	$\left. \begin{matrix} 19.42; 19.66; \\ 19.74; 19.88; \\ 20.15 \end{matrix} \right\}$
				$\left. \begin{matrix} 20.3 \\ 20.55 \end{matrix} \right\} \begin{matrix} 7.5 \\ 4.0 \end{matrix} \right\}$	11.5
21.5 ± 0.1	15.3	21.25			20.62
23.0 ± 0.1	8.4	22.75		21.6	6.5
~ 27	15.4				

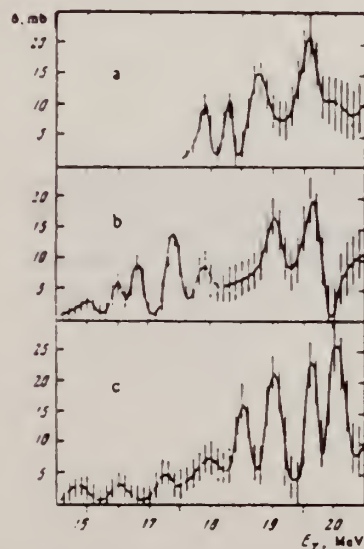


FIG. 5. Cross sections for the reactions: a - $Si^{28}(\gamma, n)$, b - $S^{32}(\gamma, n)$, c - $Ca^{40}(\gamma, n)$. Computational step $\Delta E = 0.2$ MeV.

METHOD

REF. NO.

68 Ka 1

HMG

REACTION	RESULT	EXCITATION ENERGY	SOURCE		DETECTOR		ANGLE
			TYPE	RANGE	TYPE	RANGE	
G,N	ABX	50-85	C	55,85	TOF-D	10-85	67
							(67.5)

NEUT ENGY SPEC

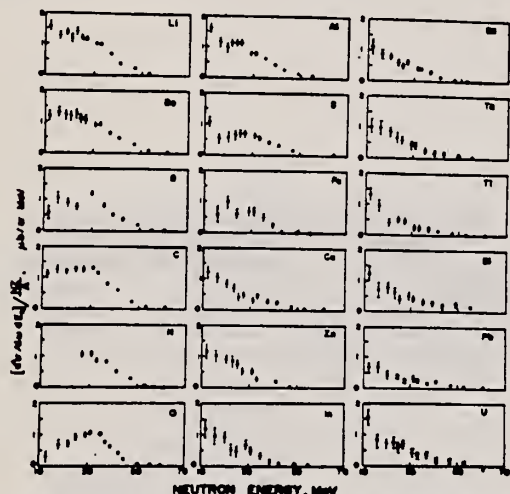


FIG. 6. Observed neutron spectra due to 55-85-MeV difference photon spectra. The effective cross sections have been divided by NZ/A .

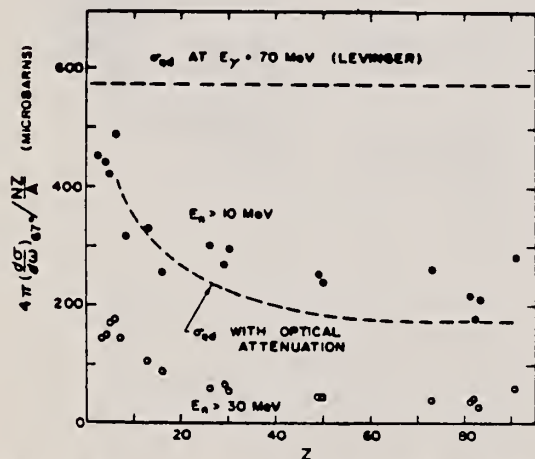


FIG. 7. Effective cross sections for production of fast neutrons with energies greater than 10 MeV (solid circles) and 30 MeV (open circles) by the 55-85-MeV photon difference spectrum. The dashed curves are modified quasideuteron model predictions as discussed in the text.

TABLE I. Comparison of present cross-section values in mb for production of high-energy photoneutrons by 55-85-MeV photons with measured cross sections $\sigma(\gamma, T_n)$, also in mb, for total photoneutron production. The present cross-section values are uncertain by 8 to 10% because of counting statistics and normalization errors; in addition all values depend on an absolute normalization in terms of the deuteron photodisintegration cross section, which is known to about 10% at these energies.

Target	$4\pi(d\sigma/d\Omega)/N\Delta$ ($E_n > 10$ MeV) [Present experiment]	$\sigma(\gamma, T_n)$ Jones and Terwilliger ^a	$\sigma(\gamma, T_n)$ Costa <i>et al.</i> ^b	Other results
Li	0.75		1.0	
Be	1.0	2.7	2.3	2.3 ^c
B	1.0		1.4	
C	1.5	1.3	1.4	2.4 ^d
O	1.3		1.6	
Al	2.8	5.5	4.6	8 ^d
S	2.1		4.4	6.5 ^d
Fe	4.2	16	12	
Cu	4.3	20	19	
Zn	4.4		15	
In	7.4			
Sn	7.0			
Ta	10.7	95		
Tl	10.7			
Pb	8.3	100		
Bi	13			
U	16	65		

^a Average cross sections between 55 and 85 MeV, as read from Figs. 4 and 5 of Ref. 4.

^b $\int_{55}^{85} \sigma_{\text{total}} dE - \int_{55}^{85} \sigma_{\text{dd}} dE/50$, as taken from Fig. 4 of Ref. 5 and Table I of Ref. 6.

^c S. Costa, L. Pasqualini, G. Piragino, and L. Roasio, Nuovo Cimento 42, 306 (1966).

^d G. Bishop, S. Costa, S. Ferromi, R. Malvase, and G. Riccio, Nuovo Cimento 42, 148 (1966).

REF.

K. Abe, N. Kawamura, M. Kanazawa and N. Mutsuro
J. Phys. Soc. Japan 26, 203 (1969)

ELEM. SYM.

A

Z

S

16

METHOD

REF. NO.

69 Ab 1

egf

REACTION	RESULT	EXCITATION ENERGY	SOURCE		DETECTOR		ANGLE
			TYPE	RANGE	TYPE	RANGE	
G,XP	SPC	THR-26	C	26	SCD-D	2-14	90

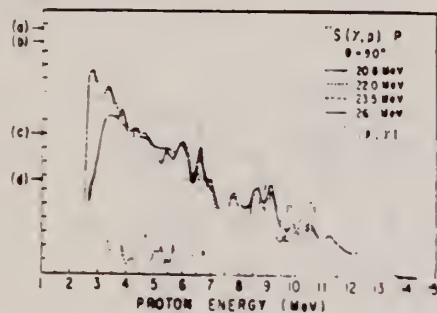


Fig. 2. Photoproton spectra from $S(\gamma, p)$. A result from ${}^A P(\rho, \gamma)$ data is superposed for reference.

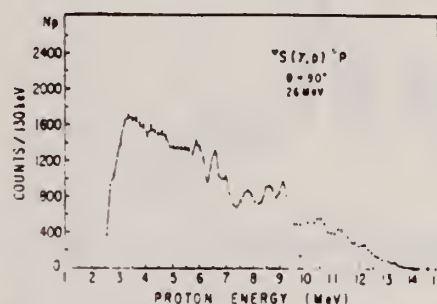


Fig. 1. Energy spectrum of photoprotons from sulphur at 90° , with bremsstrahlung end-point energy 26 MeV.

METHOD

REF. NO.

69 No 1

egf

REACTION	RESULT	EXCITATION ENERGY	SOURCE		DETECTOR		ANGLE
			TYPE	RANGE	TYPE	RANGE	
G, NA24	ABY	78-999	C	100-999	ACT-I		4PI

999 = 1.2 GEV

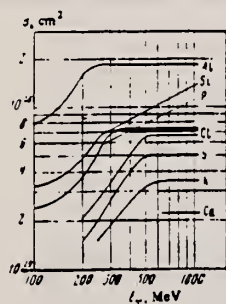


FIG. 2. Cross sections as a function of -ray energy.

Table I

Reaction	Nucleons emitted	Threshold, MeV	Target	Distribution of isotopes, %
Al ²⁷ → Na ²⁴	2p, n	31	Al	100
Si ²⁸ → Na ²⁶	3p, n	43	Si	92.27
P ³¹ → Na ²⁸	4p, 3n	69	P	100
S ³² → Na ²⁹	5p, 3n	78	S	95.02
Cl ³⁵ → Na ³⁰	6p, 5n	104	NH ₄ Cl	75.4
K ³⁹ → Na ³²	8p, 7n	140	K ₂ CO ₃	93.18
Ca ⁴⁰ → Na ³³	9p, 7n	148	CaO	96.97

*The threshold was calculated as the binding energy of the emitted nucleons.

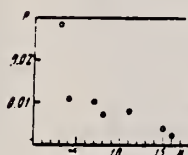
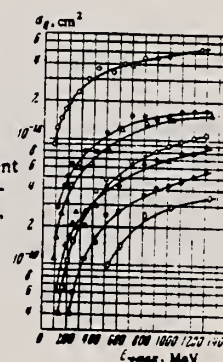


FIG. 3. Dependence of P on number of nucleons which have left the nucleus.

Table II. Cross sections for reactions in the saturation region

Reaction	σ_0 , 10^{-22} cm ²	Reaction	σ_0 , 10^{-22} cm ²
Al ²⁷ → Na ²⁴	195 ± 20	Cl ³⁵ → Na ³⁰	69 ± 7
Si ²⁸ → Na ²⁶	72 ± 8	K ³⁹ → Na ³²	35 ± 5
P ³¹ → Na ²⁸	74 ± 8	Ca ⁴⁰ → Na ³³	22 ± 3
S ³² → Na ²⁹	52 ± 6		

FIG. 1. Cross section σ_Q per equivalent photon as a function of maximum bremsstrahlung energy. Points: ○ - Al, ● - Si, △ - P, ▲ - S, □ - Cl, ■ - K, ◇ - Ca.



According to the photomesonic mechanism, the cross section for the reaction can be written in the form

$$\sigma = \sigma_0 A P. \quad (1)$$

Here σ_0 is the total cross section for interaction of the photon with a free nucleon with inclusion of the nucleon motion in the nucleus (σ_0 , as has been shown by Roos and Peterson,^[6] depends only weakly on photon energy for $E_\gamma > 300$ MeV); A is the number of nucleons in the nucleus, and P is the probability that the reaction will proceed by a given channel.

METHOD

REF. NO.

70 Wu 1

egf

REACTION	RESULT	EXCITATION ENERGY	SOURCE		DETECTOR		ANGLE
			TYPE	RANGE	TYPE	RANGE	
G,N	ABX	16-19	C	16-22	TOF-D		90

Cross section relative to $D(\gamma, n)p$

820 GROUND STATE

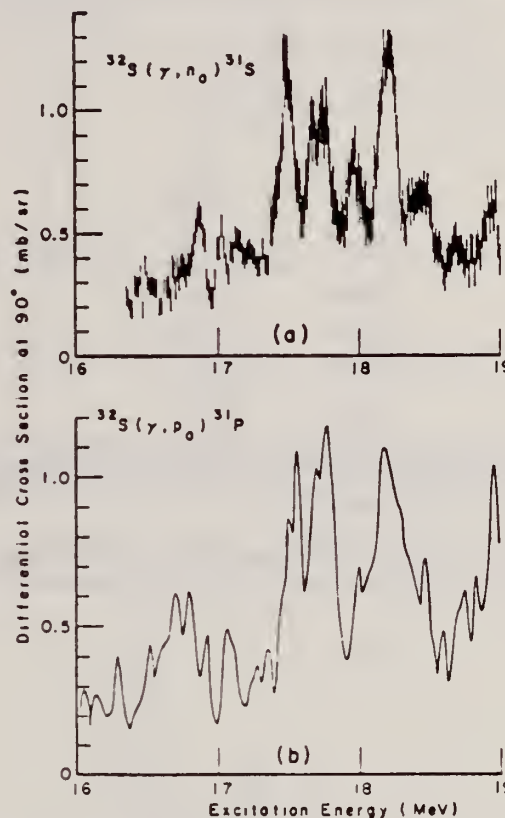


Fig. 5a. The observed $^{32}\text{S}(\gamma, n_0)^{31}\text{S}$ differential cross section at 90° . 5b. The $^{32}\text{S}(\gamma, p_0)^{31}\text{P}$ differential cross section at 90° deduced from the inverse reaction 2). The magnitude of the cross section is that of ref. 18), also measured relative to the cross section for the $D(\gamma, n)p$ reaction.

METHOD

REF. NO.

71 Co 2

egf

REACTION	RESULT	EXCITATION ENERGY	SOURCE		DETECTOR		ANGLE
			TYPE	RANGE	TYPE	RANGE	
G,XN	ABI	36-64	C	10-64	BF3-I		4PI

FAST N YIELD

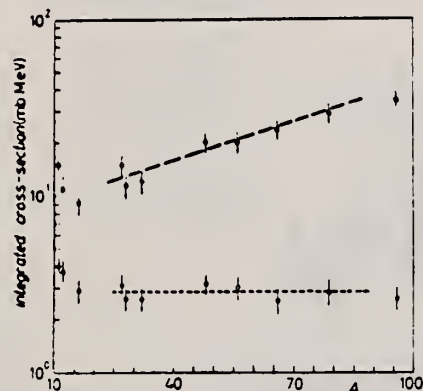


Fig. 2.

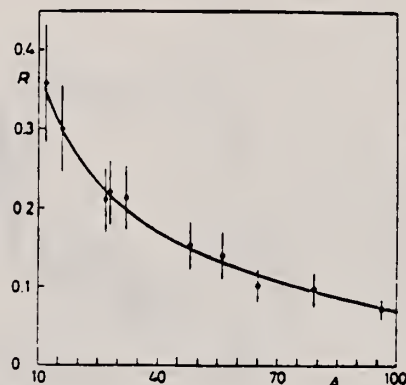


Fig. 3.

Fig. 2. - Experimental photoneutron cross-sections integrated over photon energy between 36 and 64 MeV and divided by NZ/A are plotted as a function of the mass number. Black dots are total cross-sections not corrected for neutron multiplicity; open circles represent fast neutron cross-sections (see text). The dashed lines are drawn only to guide the eye.

Fig. 3. - The ratio between fast and total photoneutron integrated cross-sections as a function of the mass number A . The solid line represents a fit of the ratios calculated for some nuclei by taking into account the theoretical neutron energy spectra given by GABRIEL and ALMILLER (*) and the efficiencies of our detector (see Fig. 1).

METHOD

REF. NO.

71 Fa 1

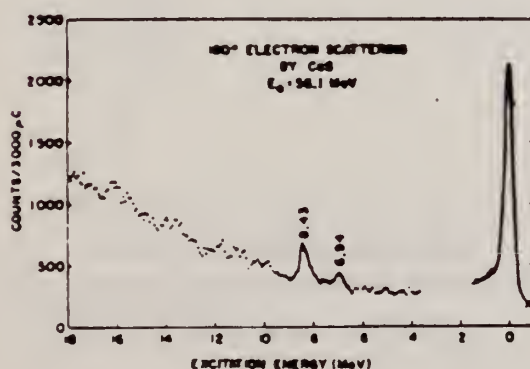
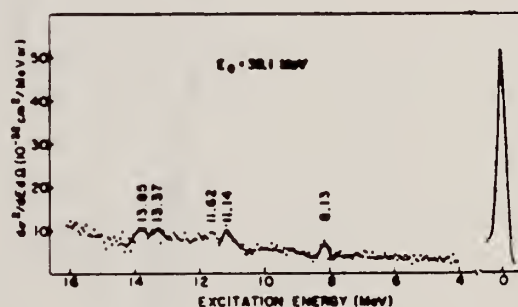
hmg

REACTION	RESULT	EXCITATION ENERGY	SOURCE		DETECTOR		ANGLE
			TYPE	RANGE	TYPE	RANGE	
E, E/	ABX	8-12	D	39, 56	MAG-D		180

5 LEVELS

TABLE I. Differential cross sections, spin and parity, transition radius, and radiation width for energy levels in ^{40}Ca and ^{22}S , including DWBA corrections.

Nucleus	Level energy (MeV)	$(d\sigma/d\Omega)_M$ ($10^{-34} \text{ cm}^2/\text{sr}$)	$(d\sigma/d\Omega)_{DW}$	J^π	R (fm)	Γ_γ (eV)
^{40}Ca	5.94 ± 0.07	34 ± 8	23 ± 12	$(1^-, 2^-)$		
	6.94 ± 0.07	38 ± 7	60 ± 19	(1^-)		
	8.43 ± 0.07	102 ± 12	119 ± 21	2^-	4.3 ± 0.5	$2.6^{+1.5}_{-1.0} \times 10^{-4}$
	10.34 ± 0.06	40 ± 13	129 ± 22	(1^+)	$3.5^{+1.5}_{-1.0}$	$7.0^{+1.5}_{-1.0}$
^{22}S	8.13 ± 0.07	38 ± 13	104 ± 31	1^+	$3.4^{+1.5}_{-1.0}$	$2.8^{+1.5}_{-1.0}$
	10.82 ± 0.07	48 ± 12	67 ± 37	1^+	$2.0^{+1.5}_{-1.0}$	$2.9^{+1.5}_{-1.0}$
				2^-	$5.0^{+1.5}_{-1.0}$	$7^{+1.5}_{-1.0} \times 10^{-4}$
	11.14 ± 0.07	54 ± 12	219 ± 46	1^+	3.9 ± 0.3	$18.9^{+1.5}_{-1.0}$
	11.62 ± 0.07	48 ± 12	123 ± 39	1^+	$3.4^{+1.5}_{-1.0}$	$9.7^{+1.5}_{-1.0}$

^a If the data and equations yield $R^2 < 0$, the lower limit of R is taken to be zero.FIG. 4. Spectrum obtained by 180° scattering of 39.1-MeV electrons from CaS. The gap in the spectrum is present because a preliminary survey showed no structure of interest in this region.FIG. 5. Differential cross section for 180° scattering of 39.1-MeV electrons from sulphur. This spectrum is the result of a subtraction of a Ca spectrum from a CaS spectrum. The gap in the spectrum exists because a preliminary survey showed no structure of interest in this region.



Tatsuya Saito
Bull. Chem. Soc. Japan 44, 1800 (1971)

S

16

METHOD

REF. NO.

71 Sa 2

egf

REACTION	RESULT	EXCITATION ENERGY	SOURCE		DETECTOR		ANGLE
			TYPE	RANGE	TYPE	RANGE	
G,NA24	ABX	THR-250	C	20-250	ACT-I		4PI
G,4P	ABX	THR-250	C	20-250	ACT-I		4PI

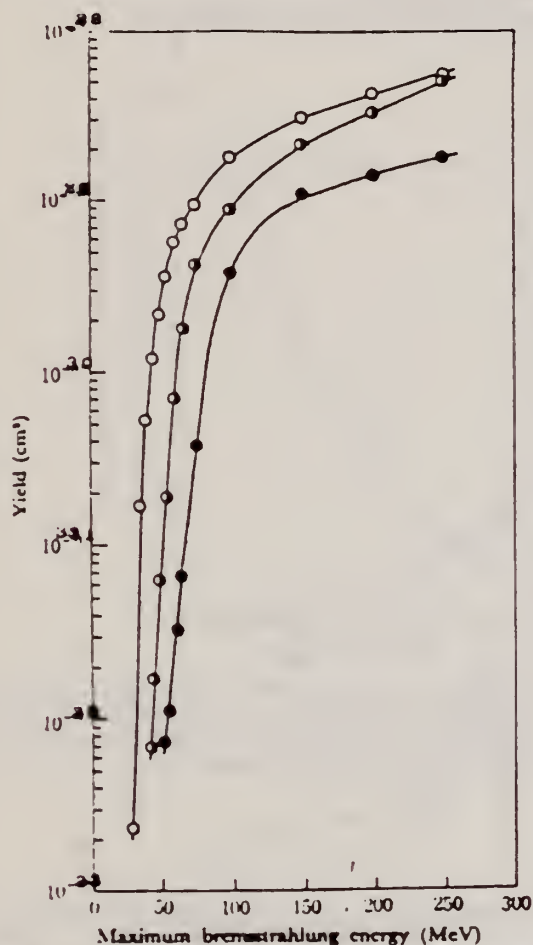


Fig. 4. The yield curves for the reactions $^{28}\text{Si} \rightarrow ^{28}\text{Na}$, $^{31}\text{P} \rightarrow ^{28}\text{Na}$, and $^{32}\text{S} \rightarrow ^{28}\text{Na}$.
○: $^{28}\text{Si} \rightarrow ^{28}\text{Na}$, ○: $^{31}\text{P} \rightarrow ^{28}\text{Na}$, ●: $^{32}\text{S} \rightarrow ^{28}\text{Na}$

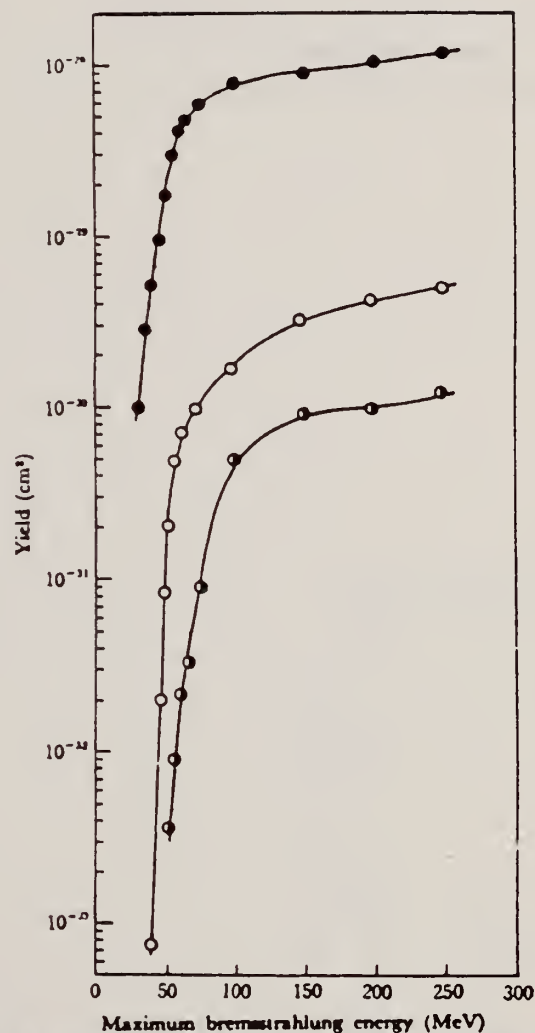


Fig. 5. The yield curves for the reactions $^{28}\text{Si}(\gamma,2p)^{26}\text{Mg}$, $^{31}\text{P}(\gamma,3p)^{26}\text{Mg}$, and $^{32}\text{S}(\gamma,4p)^{26}\text{Mg}$.
●: $^{28}\text{Si}(\gamma,2p)^{26}\text{Mg}$, ○: $^{31}\text{P}(\gamma,3p)^{26}\text{Mg}$, ○: $^{32}\text{S}(\gamma,4p)^{26}\text{Mg}$

(over)

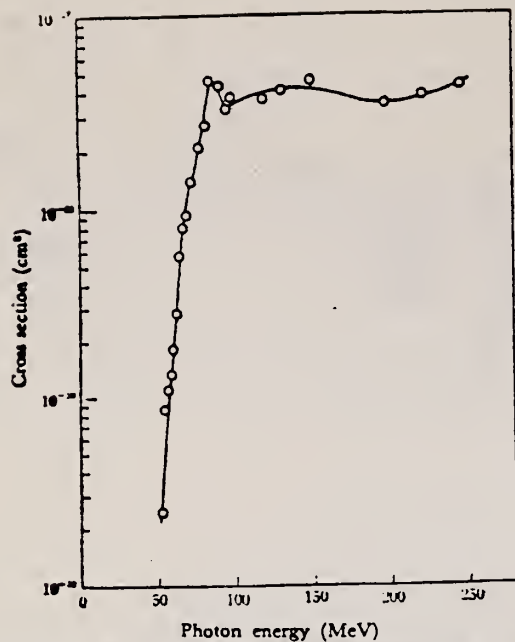


Fig. 9. The excitation function for the reaction $^{32}\text{S} \rightarrow ^{34}\text{Na}$.

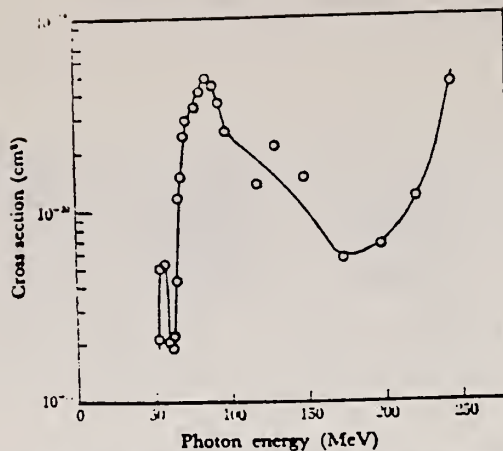


Fig. 12. The excitation function for the reaction $^{32}\text{S}(\gamma,4p)^{32}\text{Mg}$.

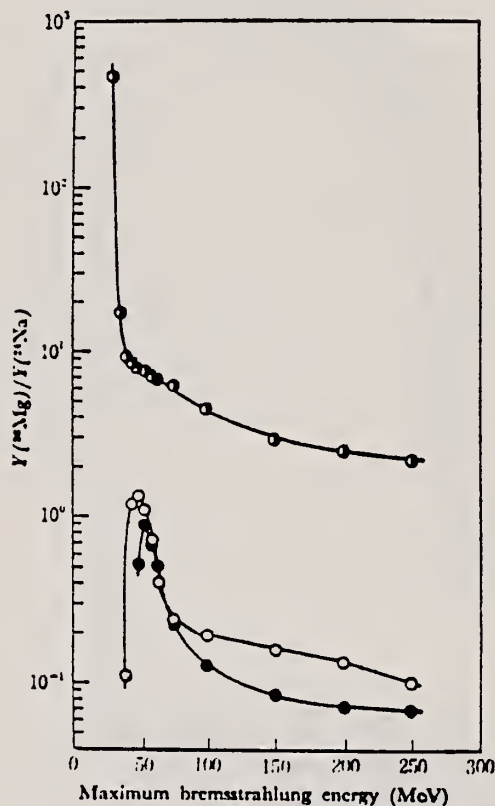


Fig. 13. Yield ratios versus maximum bremsstrahlung energy.
 ○: $Y(^{32}\text{Si}(\gamma,2p)^{32}\text{Mg})/Y(^{32}\text{Si} \rightarrow ^{31}\text{Na})$
 ○: $Y(^{31}\text{P}(\gamma,3p)^{32}\text{Mg})/Y(^{31}\text{P} \rightarrow ^{31}\text{Na})$
 ●: $Y(^{32}\text{S}(\gamma,4p)^{32}\text{Mg})/Y(^{32}\text{S} \rightarrow ^{31}\text{Na})$

ELEM. SYM.	A	Z
S		16
REF. NO.		
73 Ja 3		egf

METHOD					REF. NO.		
					73 J _a 3	egf	
REACTION	RESULT	EXCITATION ENERGY	SOURCE		DETECTOR		ANGLE
			TYPE	RANGE	TYPE	RANGE	
G, NA24	ABY	THR-999	C	100-999	ACT-I		4PT

999=1 GEV

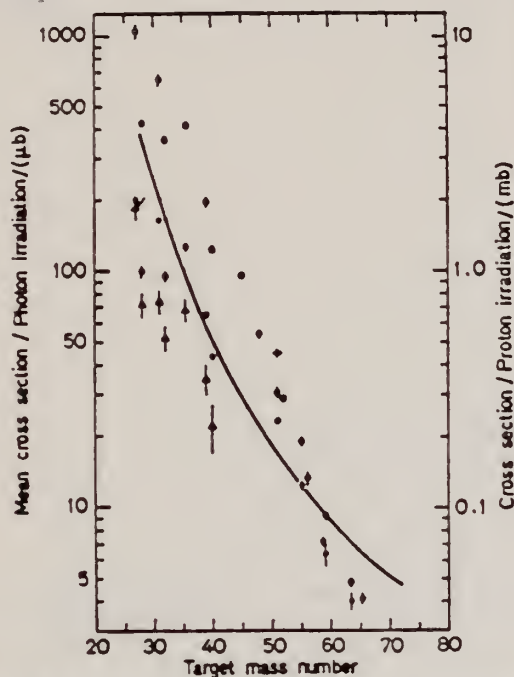


Fig. 7. Mean cross sections for ^{24}Na production as a function of target mass number. Present work filled circles. Noga *et al.* [3] open triangles. Kumbartzki *et al.* [13] cross and Korteling *et al.* [1] 400 MeV protons open circles. The solid line gives the mean cross sections calculated by Jonsson *et al.* [17]

- ¹Korteling, R.G. *et al.*, J. Inorg. Nucl. Chem. 29, 2863 (1967).
³Noga, V.I. *et al.*, Sov. J. Nucl. Phys. 9, 637 (1969).
¹³Kumbartzki, G. *et al.*, Nucl. Phys. A176, 23 (1971).
¹⁷Jonsson, G.G. *et al.*, LUNP7212, Oct. 1972, to be published in Physica Scripta.

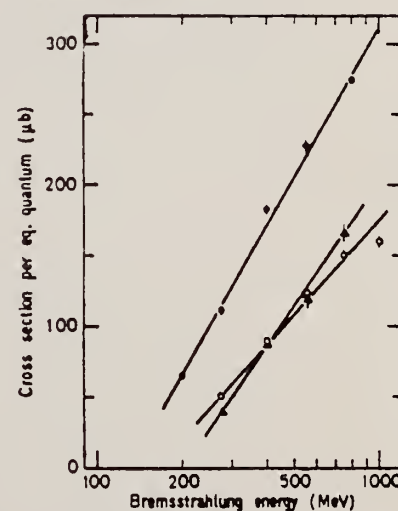


Fig. 3. The determined yields for the reactions $^{31}\text{P} \rightarrow ^{24}\text{Na}$ (filled circles), $^{32}\text{S} \rightarrow ^{24}\text{Na}$ (open circles) and $^{35,37}\text{Cl} \rightarrow ^{24}\text{Na}$ (filled triangles)



REF.

A. Veyssiere, H. Beil, R. Bergere, P. Carlos, A. Lepretre, and
A. De Miniac
Nucl. Phys. **A227**, 513 (1974)

ELEM. SYM. A Z

S

16

METHOD

REF. NO.

74 Va 1

egf

REACTION	RESULT	EXCITATION ENERGY	SOURCE		DETECTOR		ANGLE
			TYPE	RANGE	TYPE	RANGE	
* G, N	ABX	15- 32	D	15- 32	BF3-I		4PI
** $G, 2N$	ABX	29- 32	D	29- 32	BF3-I		4PI
*** G, NP	ABX	21- 30	D	21- 30	BF3-I		4PI

* 894
** 892
*** 893

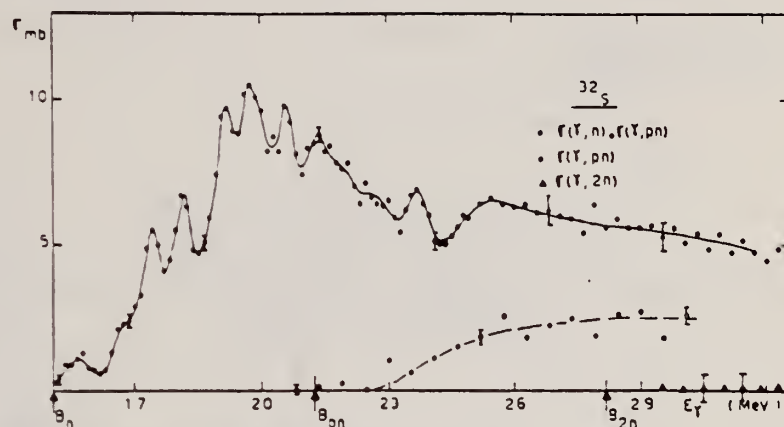


Fig. 8. Partial photoneutron cross sections $[\sigma(\gamma, n) + \sigma(\gamma, pn)]$, $\sigma(\gamma, pn)$ and $\sigma(\gamma, 2n)$ of ^{32}S .

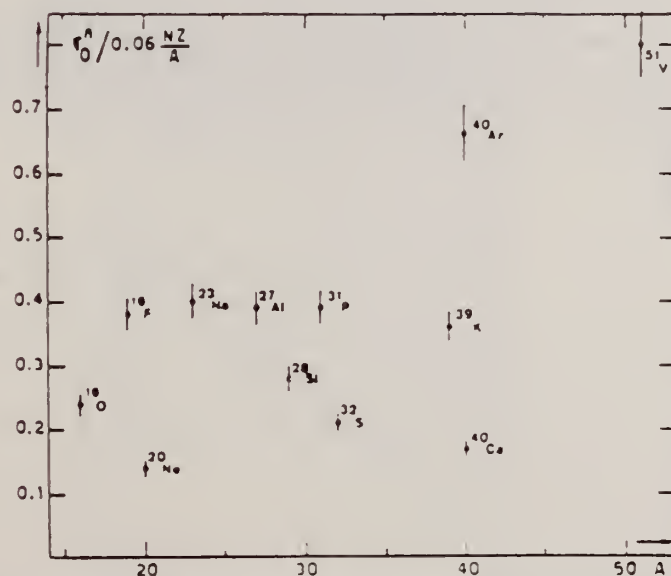


Fig. 22. Ratio of experimental integrated photoneutron cross section σ_0^n over the Thomas, Reiche and Kuhn sum rule $[0.06 NZ/A]$. Numerical values and upper integration limits E_M are taken from table 3. Also $\Delta\sigma_0^n = \pm 7\%$ for all nuclei.

(over)

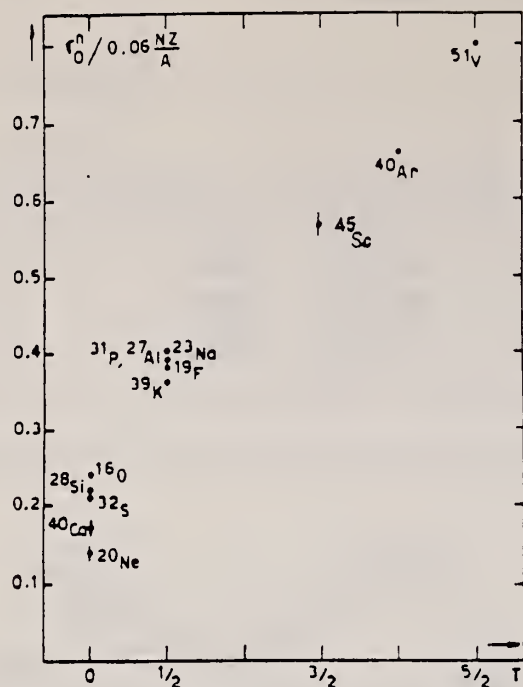


Fig. 24. The $[\sigma_0^n/(0.06 NZ/A)]$ ratio as a function of isospin T . Possible overall errors of $\pm 7\%$ are to be applied to all nuclei shown.

TABLE 3
Experimental integrated photoneutron cross sections $\sigma_0^n = \int_0^{E_M} \sigma_{Tn}(E) dE$ compared with the classical sum rule $[0.06 NZ/A]$ of Thomas, Reich and Kuhn

	$T = 0$					$T = \frac{1}{2}$					$T = \frac{3}{2}$	$T = 2$	$T = \frac{5}{2}$
Nucleus	^{16}O	^{20}Ne	^{28}Si	^{32}S	^{40}Ca	^{19}F	^{23}Na	^{27}Al	^{31}P	^{39}K	^{45}Sc	^{40}Ar	^{51}V
σ_0^n (MeV · mb)	58 ± 4	42 ± 3	94 ± 7	98 ± 7	100 ± 7	108 ± 7	137 ± 9	158 ± 10	182 ± 12	210 ± 14	383 ± 25	393 ± 28	602 ± 42
$\sigma_0^n/(0.06 NZ/A)$	0.24	0.14	0.22	0.21	0.17	0.38	0.40	0.39	0.39	0.36	0.57	0.66	0.8
E_M (MeV)	30	26.7	30	30	29.5	29	30	30	29	30	28.1	26.7	28

REF.

V. di Napoli, G. Rosa, F. Salvetti, M. L. Terranova,
H. G. de Carvalho, J. B. Martins, O. A. P. Tavares
J. Inorg. Nucl. Chem. **37**, 1101 (1975)

ELEM. SYM.

A

Z

S

16

METHOD

REF. NO.

75 Di 4

egf

REACTION	RESULT	EXCITATION ENERGY	SOURCE		DETECTOR		ANGLE
			TYPE	RANGE	TYPE	RANGE	
G,F18	ABY	THR-999	C	300-999	ACT-I		4PI
G,NA22	ABY	THR-999	C	300-999	ACT-I		4PI
G,NA24	ABY	THR-999	C	300-999	ACT-I		4PI

999 = 1 GEV

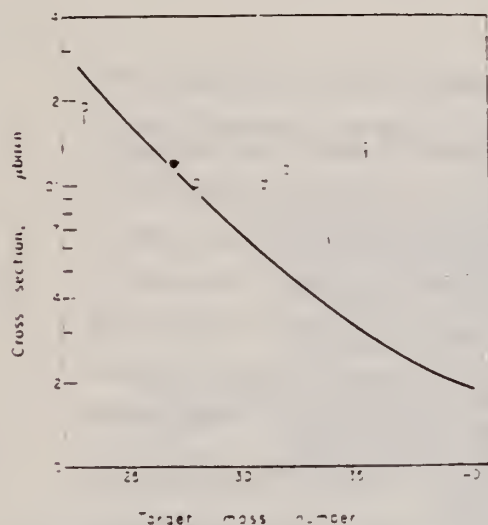


Fig. 2. Mean absolute cross section of ^{18}F photoproduction vs the target mass number. Open triangle: energy range 0.15-0.72 GeV. Ref. [18]. Filled circle: energy range 0.3-1 GeV. Ref. [3]. Open circles: present work. The curve has been calculated by means of Eqn (1).

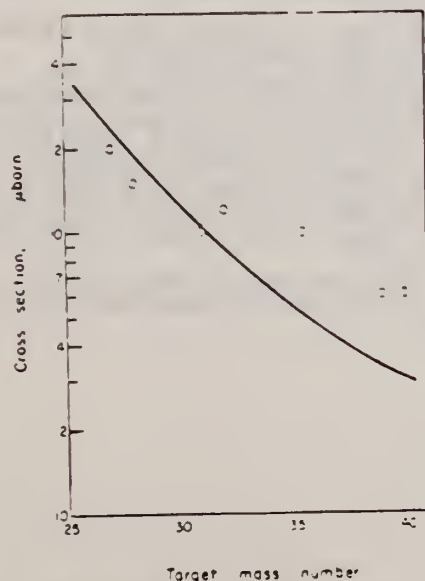


Fig. 3. Mean absolute cross section of ^{23}Na photoproduction vs the target mass number. The curve has been calculated by means of Eqn (1).

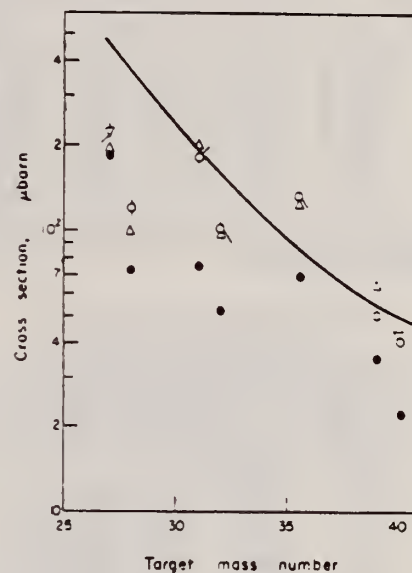


Fig. 4. Mean absolute cross section of ^{24}Na photoproduction vs the target mass number. Filled circles: energy range 0.1-1 GeV. Ref. [20]. Reversed open triangle: energy range 0.3-1 GeV. Ref. [8]. Open triangles: energy range 0.25-1 GeV. Ref. [19]. Open circles: present work. The curve has been calculated by means of Eqn (1).

Table 2. Cross-section per equivalent quantum $\sigma_0(\mu\text{b})$ of photoproduction of ^{18}F

Target nucleus	Bremsstrahlung maximum energy $E_0(\text{GeV})$				
	0.20	0.40	0.55	0.75	1.00
^{23}Na	590 ± 30	640 ± 30	720 ± 30	780 ± 30	830 ± 30
$^{27}\text{Al}^a$	116 ± 7	172 ± 6	202 ± 6	245 ± 5	270 ± 5
^{28}Si	80 ± 10	110 ± 10	145 ± 10	170 ± 10	200 ± 10
^{31}P	60 ± 10	90 ± 10	130 ± 10	150 ± 10	180 ± 10
^{32}S	55 ± 10	90 ± 10	125 ± 10	160 ± 10	190 ± 10
^{37}Cl	185 ± 20	230 ± 20	270 ± 20	310 ± 20	350 ± 20
^{39}K	35 ± 5	50 ± 5	65 ± 5	75 ± 5	90 ± 5
^{40}Ca	5 ± 2	20 ± 3	35 ± 5	45 ± 5	60 ± 5

^aThe results for ^{27}Al have already been published (see [3]) and are reported for comparison.

(over)

Table 3. Cross-section per equivalent quantum $\sigma_0(\mu\text{b})$ of photoproduction of ^{23}Na

Target nucleus	Bremsstrahlung maximum energy E_0 (GeV)				
	0.30	0.40	0.55	0.75	1.00
^{27}Al	490 ± 20	560 ± 20	667 ± 20	690 ± 20	745 ± 20
^{28}Si	290 ± 20	330 ± 20	380 ± 20	430 ± 20	470 ± 20
^{31}P	230 ± 20	250 ± 20	290 ± 20	330 ± 20	350 ± 20
^{32}S	206 ± 10	240 ± 10	280 ± 10	320 ± 10	350 ± 10
$^{35,37}\text{Cl}$	230 ± 10	260 ± 10	290 ± 10	320 ± 10	350 ± 10
^{39}K	30 ± 3	50 ± 5	65 ± 5	80 ± 5	100 ± 5
^{40}Ca	5 ± 2	20 ± 3	45 ± 5	60 ± 5	60 ± 5

Table 4. Cross-section per equivalent quantum $\sigma_0(\mu\text{b})$ of photoproduction of ^{24}Na

Target nucleus	Bremsstrahlung maximum energy E_0 (GeV)				
	0.30	0.40	0.55	0.75	1.00
$^{27}\text{Al}^*$	370 ± 10	440 ± 10	500 ± 20	550 ± 20	660 ± 20
^{28}Si	100 ± 10	140 ± 10	160 ± 10	210 ± 10	240 ± 10
^{31}P	100 ± 20	160 ± 20	200 ± 20	270 ± 20	310 ± 20
^{32}S	120 ± 10	160 ± 10	180 ± 10	210 ± 10	240 ± 10
$^{35,37}\text{Cl}$	65 ± 10	100 ± 10	140 ± 10	190 ± 10	220 ± 10
^{39}K	20 ± 5	35 ± 5	55 ± 5	65 ± 5	80 ± 5
^{40}Ca	12 ± 3	25 ± 5	35 ± 5	50 ± 5	60 ± 5

*The results for ^{27}Al have already been published (see [8]) and are reported for comparison.

Table 5. Mean absolute cross-section $\bar{\sigma}_0(\mu\text{b})$ in the energy range 0.3–1 GeV

Target nucleus	Produced radionuclide		
	^{18}F	^{24}Na	^{24}Na
^{23}Na	190 ± 30		
$^{27}\text{Al}^*$	120 ± 10	200 ± 20	220 ± 20
^{28}Si	100 ± 10	150 ± 20	120 ± 10
^{31}P	100 ± 10	100 ± 20	180 ± 20
^{32}S	110 ± 10	120 ± 10	100 ± 10
$^{35,37}\text{Cl}$	135 ± 20	100 ± 10	130 ± 10
^{39}K	45 ± 5	60 ± 5	50 ± 5
^{40}Ca	46 ± 5	60 ± 5	40 ± 5

*The results for the photoproduction of ^{18}F and ^{24}Na from ^{27}Al have already been published (Ref. [3] and [8], respectively).

- V. di Napoli and M. L. Terranova, *J. inorg. nucl. Chem.* **36**, 3633 (1974).
- V. di Napoli, A. M. Lacerenza, F. Salvetti, S. M. Terenzi, H. G. de Carvalho and J. B. Martins, *J. inorg. nucl. Chem.* **35**, 1419 (1973).
- C. M. Lederer, J. M. Hollander and I. Perlman, *Table of Isotopes*, 6th Edn Wiley, New York (1967).
- R. G. Korteling and A. A. Caretto, Jr., *J. inorg. nucl. Chem.* **29**, 2863 (1967).
- R. G. Korteling and A. A. Caretto, Jr., *Phys. Rev. C* **1**, 193 (1970).
- R. G. Korteling and A. A. Caretto, Jr., *Phys. Rev. C*, 1960 (1970).
- V. di Napoli, A. M. Lacerenza, F. Salvetti, H. G. de Carvalho and J. B. Martins, *Lett. Nuovo Cimento* **1**, 835 (1971).
- I. Halpern, R. J. Debs, J. T. Eisinger, A. W. Fairhall and H. G. Richter, *Phys. Rev.* **97**, 1327 (1955).
- C. B. Fulmer, K. S. Toth, I. R. Williams, T. H. Handley, C. F. Dell, E. L. Callis, T. M. Jenkins and J. M. Wyckoff, *Phys. Rev. C* **2**, 1371 (1970).
- G. J. Kumbartzki, U. Kim and C. K. Kwan, *Nucl. Phys. A* **160**, 237 (1970).
- G. J. Kumbartzki and U. Kim, *Nucl. Phys. A* **176**, 23 (1971).
- K. Lindgren and G. G. Jonsson, *Nucl. Phys. A* **197**, 71 (1972).
- C. E. Roos and V. Z. Peterson, *Phys. Rev.* **124**, 1610 (1961).
- T. A. Gabriel and R. G. Alsmiller, Jr., *Phys. Rev.* **182**, 1033 (1969).
- G. G. Jonsson and K. Lindgren, *Phys. Scr.* **7**, 49 (1973).
- G. Rudstam, *Z. Naturf.* **21a**, 1027 (1966).
- A. Masaike, *J. phys. Soc. Japan* **19**, 427 (1964).
- A. Järund, B. Friberg and B. Forkman, Private communication to G. G. Jonsson and K. Lindgren, quoted in Ref. [16]; see also A. Järund, B. Friberg and B. Forkman, University of Lund Report No. LUNP-7303, 1973 (unpublished).
- V. I. Noga, Yu. N. Ranyuk and P. V. Sorokin, *Yad. Fiz.* **9**, 1152 (1969) (transl.: *Sov. J. Nucl. Phys.* **9**, 673 (1969)).
- T. Methasiri and S. A. E. Johansson, *Nucl. Phys. A* **167**, 97 (1971).
- J. R. Nix and E. Sassi, *Nucl. Phys.* **81**, 61 (1966).
- W. D. Myers and W. J. Swiatecki, *Nucl. Phys.* **81**, 1 (1966).

REF. A. S. Danagulyan, N. A. Demekhina
Yad. Fiz. 24, 681 (1976)
Sov. J. Nucl. Phys. 24, 355 (1976)

ELEM. SYM.	A	Z
S		16
REF. NO.		76 Da 4
		hmg

REACTION	RESULT	EXCITATION ENERGY	SOURCE		DETECTOR		ANGLE
			TYPE	RANGE	TYPE	RANGE	
G,NA24	ABX	THR* 5	C	2* 5	ACT-I		4PI

*ENERGY, GEV

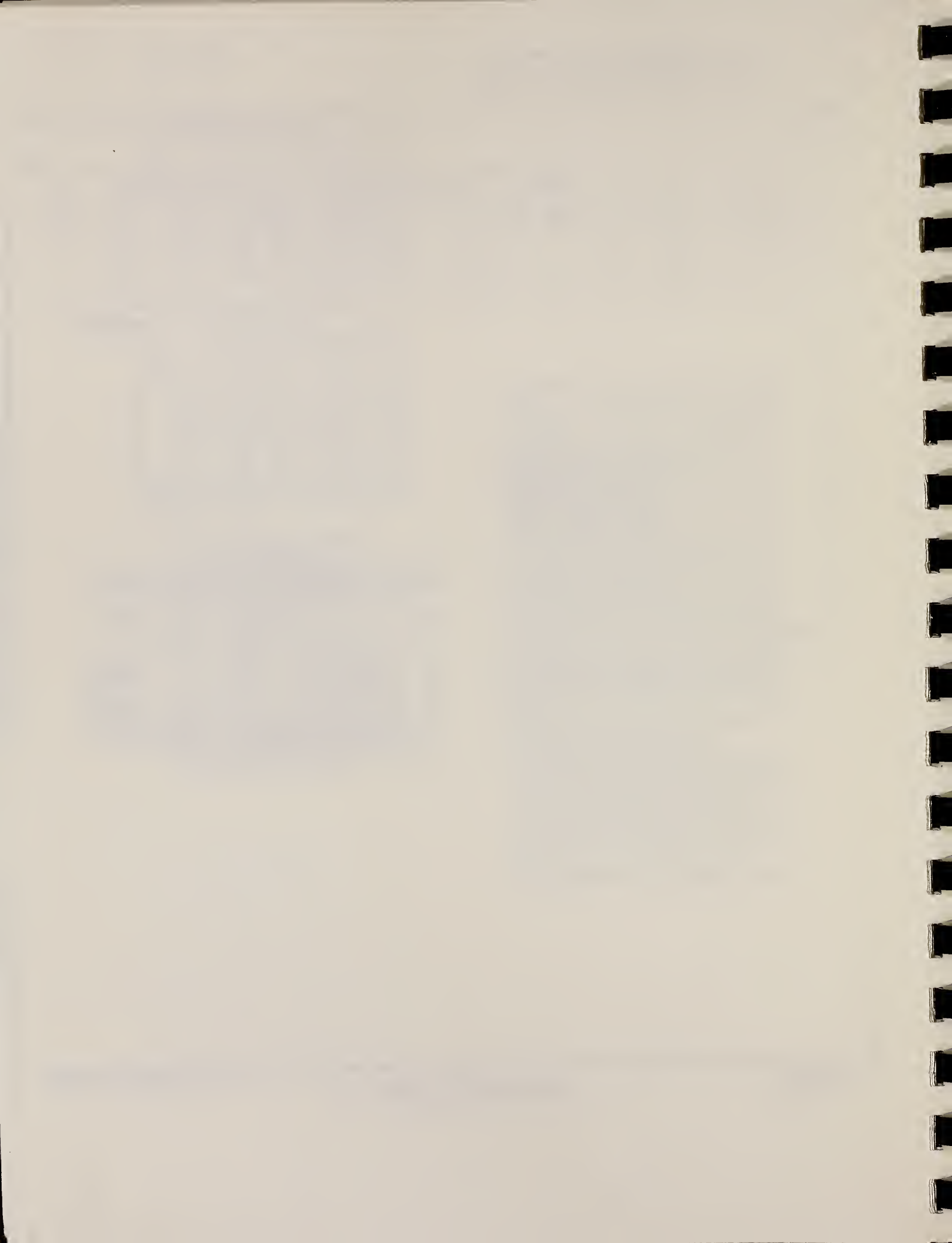


FIG. 2. Yield values and theoretical values according to the modified Rudstam formula as a function of the target charge number Z_1 . Points: ●—experiment, ○—theory.

TABLE I. Experimental yields and reaction cross sections obtained in the measurements at the Erevan electron accelerator.

Target nucleus	Reaction yield, mb					Reaction cross section, mb
	E_{max} , GeV					
	1	3	4	4.5	5	
^{27}Al	0.31 ± 0.06	0.87		0.87		0.07213 ± 0.0346
^{28}Si	0.27 ± 0.02	0.28		0.29		0.0267 ± 0.013
^{35}S	0.24 ± 0.02	0.22		0.27		0.0323 ± 0.0155
Cl	0.28 ± 0.03	0.30		0.28		—
^{39}K	0.1 ± 0.01	0.125		0.15		0.06 ± 0.0288
^{40}Ca	0.066 ± 0.01	0.09		0.115		0.035 ± 0.0168
^{51}V	0.085 ± 0.02	0.094 ± 0.02	0.098 ± 0.02		0.082 ± 0.025	0.019
^{55}Mn	0.079 ± 0.02	0.073 ± 0.02	0.087 ± 0.017		0.088 ± 0.015	0.01078 ± 0.0056
Ca	0.029 ± 0.006	0.037 ± 0.007	0.046 ± 0.007		0.034 ± 0.007	0.00547 ± 0.0028

Note. The reaction cross sections have been calculated in the $1/E$ approximation of the bremsstrahlung spectrum.



S
A=32

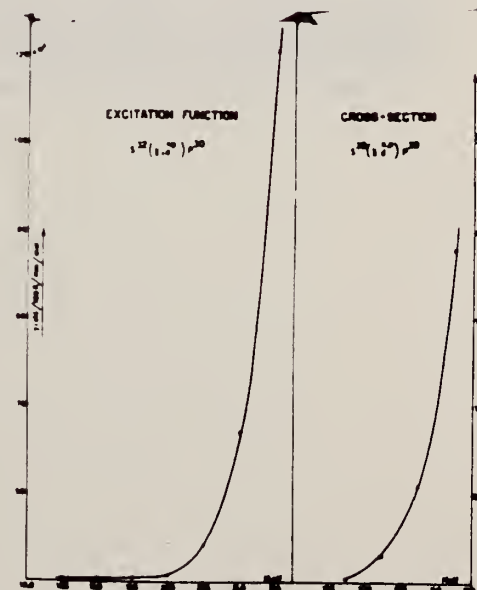
S
A=32

S
A=32

M.D. DeSouza Santos, J. Goldemberg, R.R. Pieroni, E. Silva,
O.A. Borello, S.S. Villaca, J.L. Lopes
Int. Conf. Peaceful Uses of Atomic Energy II (UN, NY) 169 (1955)

ELEM. SYM.	A	Z
S	32	16

METHOD					REF. NO.		EGF
Betatron; neutron, proton yield; radioactivity; r-chamber					55 De 1		
REACTION	RESULT	EXCITATION ENERGY	SOURCE		DETECTOR		ANGLE
			TYPE	RANGE	TYPE	RANGE	
G, NP	ABX	18-22	C	18-22	ACT-I		4PI



REF.

S.S. Villaca, J. Goldemberg
An. Acad. Brasil. Cienc. 27, 427 (1955)

ELEM. SYM. A Z

S

32

16

METHOD

Betatron; ion chamber monitor

REF. NO.

55 V1 1

NVB

REACTION	RESULT	EXCITATION ENERGY	SOURCE		DETECTOR		ANGLE
			TYPE	RANGE	TYPE	RANGE	
G,D	ABX	19-22	C	17-22	ACT-I		4PI

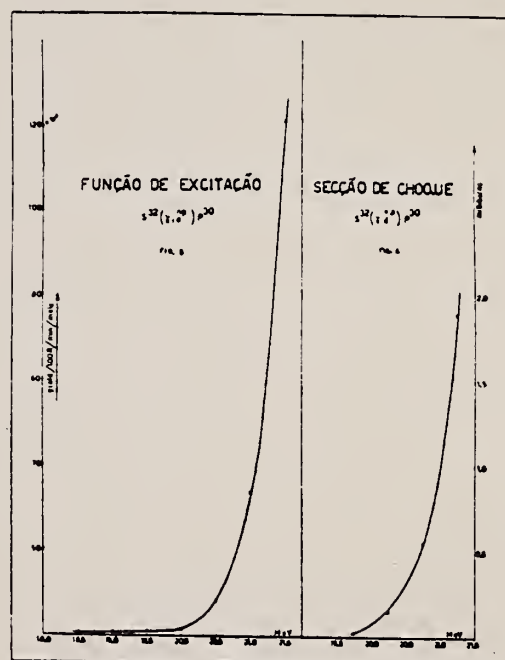
INCLUDES G, NP

Fig. 5 u 6

METHOD

REF. NO.

56 He 3

hmg

REACTION	RESULT	EXCITATION ENERGY	SOURCE		DETECTOR		ANGLE
			TYPE	RANGE	TYPE	RANGE	
E, E/	FMF	1-7	D	187	MAG-D		DST

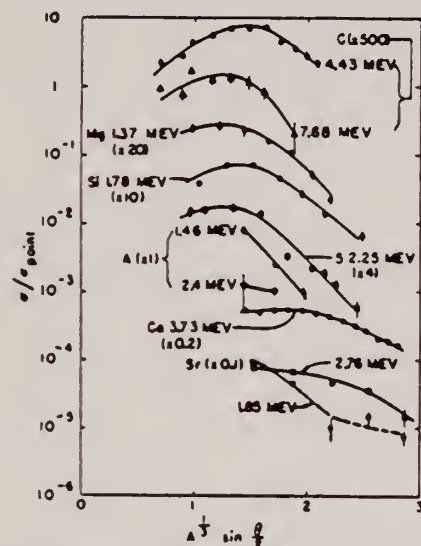


FIG. 3. Inelastic angular distributions (observed cross section divided by Peasback point-charge cross sections). The results of Hahn *et al.* (reference 8) for Ca and of Fregeau and Hofstadter (reference 11) are included for comparison.

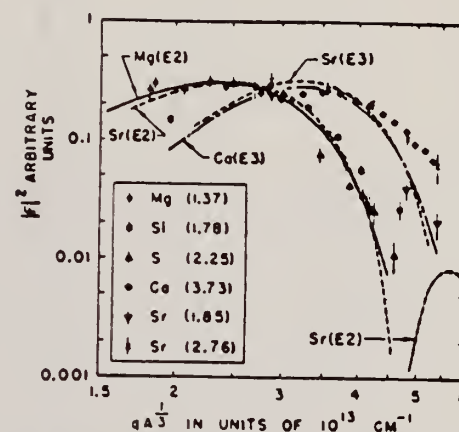


FIG. 7. Inelastic "universal curves." A composite plot of inelastic data from Mg, Si, S, Ca, and Sr against $q/1$. The various form factors are arbitrarily normalized to minimize the spread of points. The point from sulfur and the point from silicon which seem to deviate from the "universal curve" are assumed to contain undetected experimental errors. The curves labeled Mg(E2), Sr(E2), Ca(E3), and Sr(E3) are calculated for electric-quadrupole and-octupole transitions using the "smeared δ -function" transition charge densities of Sec. V, and are arbitrarily normalized.

Ref. No.	
58 Go 3	EH

Excitation Function
 $S^{32}(\gamma, d) p^{30}$

x Katz et al
 O Goldberg and Marquez

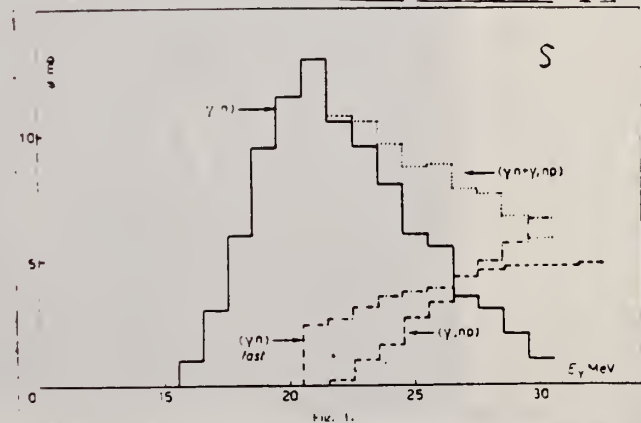
Relative Scale

MeV

Ref. U. Farinelli, F. Ferrero, S. Ferroni, R. Malvano, E. Silva Nuovo Cimento <u>12</u> , 89 (1959)	Elem. Sym.	A	Z
	S	32	16

Method	Ref. No.	
Activation; Si(n,p) detector	59 Fa 1	EH

Reaction	E or ΔE	E ₀	Γ	∫σdE	Jπ	Notes
S ³² (γ,n)	30	21±0.5	6	∫ ³⁰ = 0.093 MeV-mb		
S ³² (γ,pn)	30	> 30		∫ ³⁰ = 0.028 MeV-mb		
S ³² (γ,n!)	30	> 30		∫ ³⁰ = 0.040 MeV-mb		



Elem. Sym.	A	Z
S	32	16
Ref. No.		JHH
60 Fe 1		

Method 31 MeV betatron; activation; NaI; neutron counters

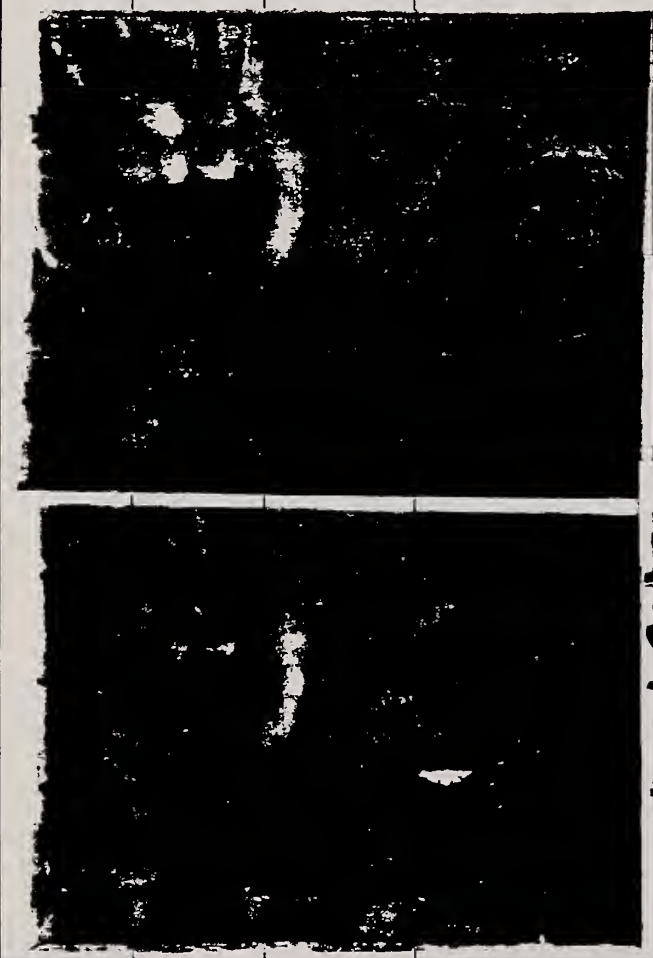
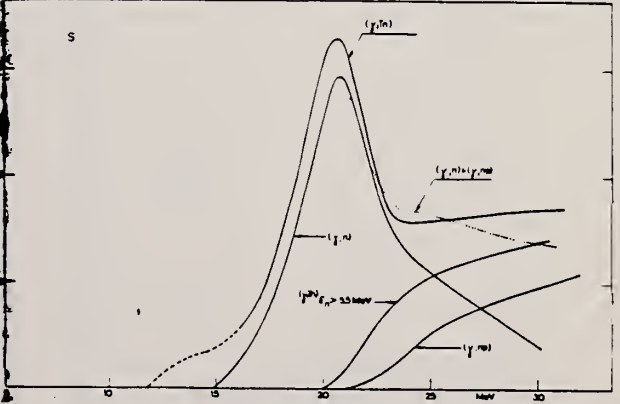
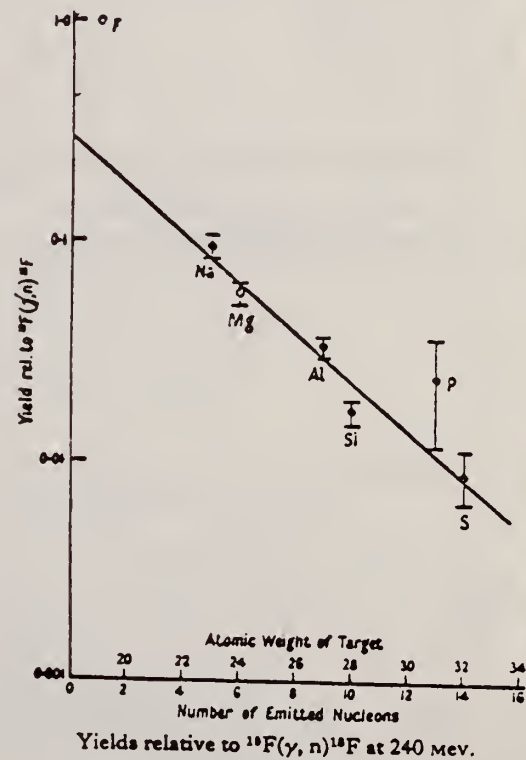
Reaction	E or ΔE	E ₀	Γ	∫σdE	Jπ	Notes
(γ,n)	Bremss. 31					Detection of annihilation radiation of β ⁺ from 3-sec S ³¹ .
(γ,np)						Annihilation radiation of β ⁺ from p ³⁰ (T _{1/2} = 2.5 min).
(γ,xn)						Threshold detector using reaction Si ²⁸ (n,p)Al ²⁸ ; E _n > 5.5 MeV.
(γ,xn). all energies						1 - meter cube H ₂ O tank containing Geiger counters surrounded by Rh powder.
						
						

Fig. 2. Cross sections for the photoreactions of fig. 1.

METHOD					REF. NO.	
Synchrotron; proton-neutron cross section; radioactivity					60 Wa 2	
REACTION	RESULT	EXCITATION ENERGY	SOURCE		DETECTOR	
			TYPE	RANGE	TYPE	RANGE
G, 7P6N	ABX	0-240	C	240	ACT-I	

NVB

$$\sigma = (0.03 \pm 0.01) 10^{-27} \text{ cm}^2 / \text{equivalent quantum}$$



G.R. Bishop, G.A. Proca
J. Phys. Radium 22, 541 (1961)

ELEM. STM.		
S	32	16
REF. NO.	61 B1 1	
	NVB	

METHOD

Linac

REACTION	RESULT	EXCITATION ENERGY	SOURCE		DETECTOR		ANGLE
			TYPE	RANGE	TYPE	RANGE	
E, E/	FMF	0-4	D	150	MAG-D		135

Transition to second excited state (3.81 MeV) is certainly not E2, but is perhaps E0.

MULTIPOLARITY

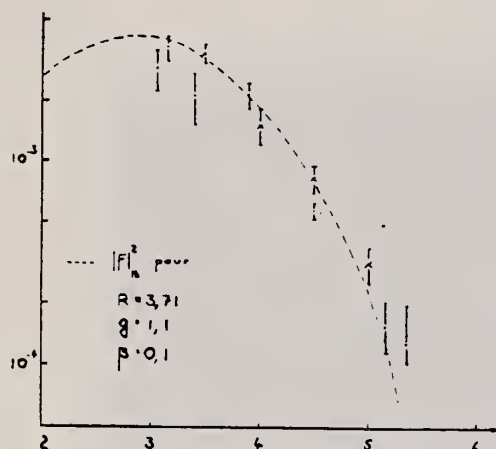


FIG. 3. — $|F(q)|^2 = f(qR)$ niveau 2+.
 $|F(q)|_{th} = \sqrt{\beta_2} |j_2(qR) \cdot \exp(-q^2 g^2/2)|$.

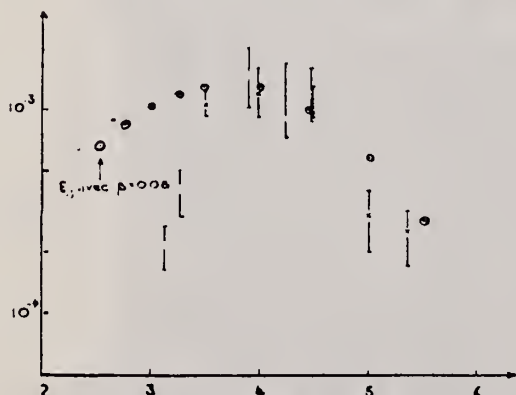


FIG. 4. — $|F(q)|^2 = f(qR)$, deuxième niveau.

Method Cockraft-Walton; photon spectra, angular distributions; NaI

Ref. No. 62 Be 4
JHH

Reaction	E or ΔE	E_0	Γ	$\int \sigma dE$	$J\pi$	Notes
$P^{31}(p, \gamma)$	0.355	9.185			1^\pm	Angular distribution data in tables 1, 2 and 3.
	0.440	9.267			1^\pm	
	0.540	9.367			2^\pm	

TABLE 1

The γ -intensities in the direction of the proton beam and angular distribution coefficients from the resonance at $E_0 = 355$ keV

γ -energy (MeV)	Transition	Rel. int. ^{a)}	$a_1 a_2$	$a_0 a_2$
9.185	9.185 \rightarrow 0	0.17	0.26 ± 0.10	-0.13 ± 0.15
6.945	9.185 \rightarrow 2.24	0.18	0.03 ± 0.06	not determined
3.6		0.12		
2.24	2.24 \rightarrow 0	0.34 ± 0.1		

^{a)} 1 unit rel. int. = $(0.85 \pm 0.09) \times 10^{-18}$ γ proton for thick $Ca(PO_3)_2$ target. The accuracy of the values is about 10%, if not stated otherwise.

TABLE 2

The γ -intensities in the direction of the proton beam and angular distribution coefficients from the resonance at $E_0 = 440$ keV

γ -energy (MeV)	Transition	Rel. int. ^{a)}	$a_1 a_2$	$a_0 a_2$
9.267	9.267 \rightarrow 0	1	-0.02 ± 0.02	0.037 ± 0.046
7.027	9.267 \rightarrow 2.24	0.61	-0.04 ± 0.03	not determined
4.797	9.267 \rightarrow 4.47	1.2		
4.47	4.47 \rightarrow 0	0.07 ± 0.03		
2.23	4.47 \rightarrow 2.24			
2.24	2.24 \rightarrow 0	2.7		

^{a)} 1 unit rel. int. = $(0.85 \pm 0.09) \times 10^{-18}$ γ proton for thick $Ca(PO_3)_2$ target. The accuracy of the values is about 10%, if not stated otherwise.

TABLE 3

The γ -intensities in the direction of the proton beam and angular distribution coefficients from the resonance at $E_0 = 540$ keV

γ -energy (MeV)	Transition	Rel. int. ^{a)}	$a_1 a_2$	$a_0 a_2$
9.367	9.367 \rightarrow 0	0.079 ± 0.027		
7.127	9.367 \rightarrow 2.24	6.6	0.35 ± 0.02	0.042 ± 0.028
4.06	6.30 \rightarrow 2.24	1.2		
3.067	9.367 \rightarrow 6.30	1.2		
2.24	2.24 \rightarrow 0	7.5		
1.5		0.4 ± 0.5		
2.3				

^{a)} 1 unit rel. int. = $(0.85 \pm 0.09) \times 10^{-18}$ γ proton for thick $Ca(PO_3)_2$ target. The accuracy of the values is about 10%, if not stated otherwise.

TABLE 6

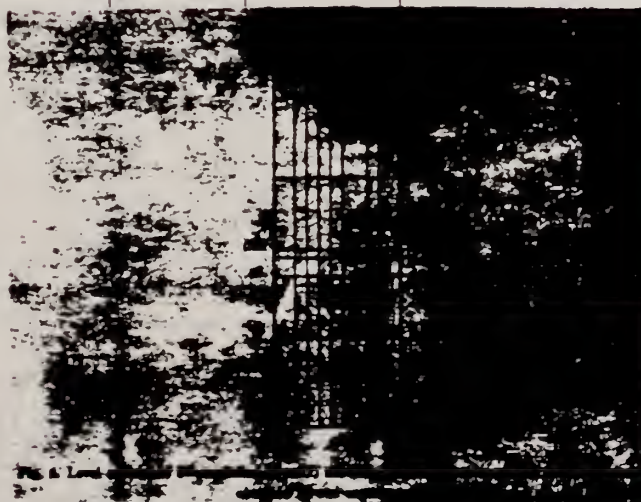
The first three resonances in the $P^{31}(p, \gamma)^{32}S$ reaction

$(E_0 \pm \delta)$ (keV)	Γ (keV)	$\frac{\Gamma_{\gamma}}{\Gamma_{\text{meas.}}}$	$\left(\frac{\Gamma_{\gamma}}{\Gamma_{\text{meas.}}}\right)$ (theor. ^{a)}	I^b	Intensity ^{a)} ($\times 10^{11} \gamma/p$)
355	≤ 3	0.93	2.3	1^\pm	0.30 ^{a)}
440	≤ 3	1.65	2.3	1^\pm	2.18
540	≤ 5	$(1.2 \pm 0.4) \times 10^{-1}$	10^{-2}	2^\pm	6.82

^{a)} In the Weisskopf-approximation

^{b)} Intensity of the γ -radiation from the disintegration of the 9 MeV levels, measured in the direction of the proton beam, for $Ca(PO_3)_2$ target. Experimental accuracy about 10%.

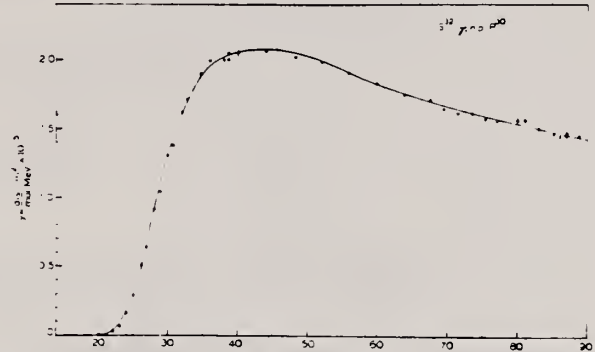
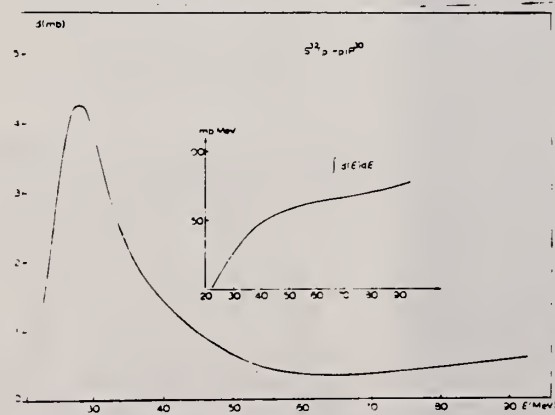
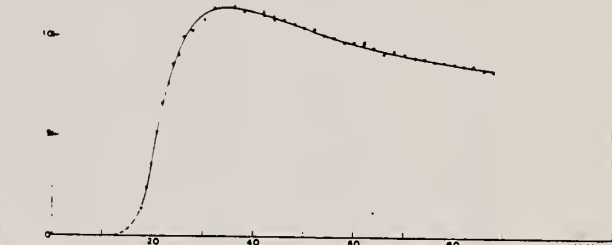
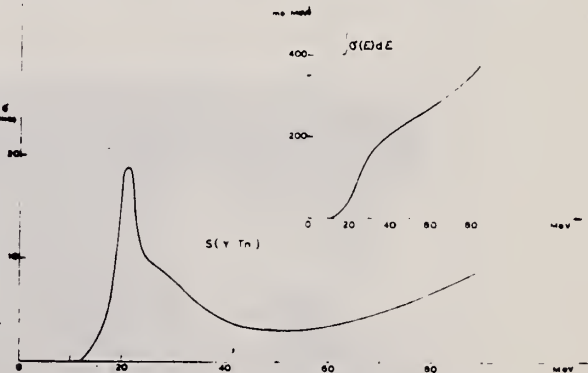
^{c)} The yield of $E_0 = 355$ keV resonance is uncertain on account of unknown cascades.



Elem. Sym.	A	Z
S	32	16

Method 100 MeV electron synchrotron; activation, NaI coinc. for annihilation radiation of β^+ from P^{30} ; BF_3 prop. counters.

Ref. No.
62 Bo 3 JHH

Reaction	E or ΔE	E_0	Γ	$\int \sigma dE$	$J\pi$	Notes <u>965</u>
$S^{32}(\gamma, np)$ $S^{32}(\gamma, xn)$	Bremss. 30-90					For figure 6, neutron multiplicity was not known but a rough estimate based on Levinger and Bethe (Phys. Rev. <u>85</u> , 577 (1952)) is 1.6.
<div style="display: flex; justify-content: space-between;"> <div style="width: 48%;">  <p>Fig. 1. The $S^{32}(\gamma, np)P^{30}$ yield. The normalization is obtained by comparison with the $Cu^{64}(\gamma, n)$ reaction measured in ref 4)</p> </div> <div style="width: 48%;">  <p>Fig. 3. The $S^{32}(\gamma, np)P^{30}$ cross section and integrated cross section.</p> </div> </div> <div style="display: flex; justify-content: space-between;"> <div style="width: 48%;">  <p>Fig. 5. The $S(\gamma, Tn)$ yield normalized to the data of ref 4)</p> </div> <div style="width: 48%;">  <p>Fig. 8. The $S(\gamma, Tn)$ cross section and integrated cross section.</p> </div> </div>						

Ref 5: Bergman and Brown - Phys. Rev. 96, 83 (1954)
Ref 8: Cook - Phys. Rev. 106, 300 (1957)

Method 4 MeV electron Van de Graaff; brems.; nuclear resonance scattering, ring scatterer; NaI

Ref. No.
62 ~~Bo~~ JHR

Reaction	E or ΔE	E ₀	Γ	Σ δE	Γ ₀	Notes
$S^{32}(\gamma, \gamma)$	Brems. 0 - 4					Detector at 110°.

TABLE 1
Mean lifetimes of excited states deduced from the resonance scattering of bremsstrahlung

Nucleus	%	Energy (MeV)	Spins	ϵ	Γ_0/Γ	$W'(\theta)$	$\tau \times 10^{12} \pm 35\%$ (sec)
Fl^{19}	100	1.46	$\frac{1}{2}^+ - \frac{1}{2}^+$	3	0.13	(1)	0.23 ϵ
Na^{23}	100	2.06	$\frac{1}{2}^+ - \frac{1}{2}^+$	3	0.1	0.79	> 0.04
		2.39	$\frac{1}{2}^+ - \frac{1}{2}^+$	3	0.53	(1)	> 1.6 ϵ
		2.64	$\frac{1}{2}^+ - \frac{1}{2}^+$	3	0.6	(1)	> 0.3 ϵ
		2.70	$\frac{1}{2}^+ - \frac{1}{2}^+$	3	(0.1)	(1)	> 0.008 ϵ
		2.95	$\frac{1}{2}^+ - \frac{1}{2}^+$	3	0.46	(1)	0.03 ϵ
Al^{27}	100	2.73	$\frac{1}{2}^+ - \frac{1}{2}^+$	1	≤ 0.3	0.91	> 0.23
		2.98	$\frac{1}{2}^+ - \frac{1}{2}^+$	1	0.216	1	2.2×10^{-4}
Si^{28}	4.71	1.25	$\frac{1}{2}^+ - \frac{1}{2}^+$	2	1	0.58	1.5
		2.43	$\frac{1}{2}^+ - \frac{1}{2}^+$	2	(1)	0.88	0.2
P^{31}	100	1.26	$\frac{1}{2}^+ - \frac{1}{2}^+$	2	1	0.88	2.2
		2.23	$\frac{1}{2}^+ - \frac{1}{2}^+$	2	1	0.79	4.5
		3.13	$\frac{1}{2}^+ - \frac{1}{2}^+$	2	(1)	0.58	0.2
		3.29	$\frac{1}{2}^+ - \frac{1}{2}^+$	3	3	0.79	> 1.8(Γ_0/Γ) ³
		3.41	$\frac{1}{2}^+ - \frac{1}{2}^+$	3	3	(1)	> 1.3(Γ_0/Γ) ³
		3.51	$\frac{1}{2}^+ - \frac{1}{2}^+$	2	3	0.38	0.02(Γ_0/Γ) ³
S^{32}	95	3.78	$0^+ - 2^+$	3	3	(1)	> 0.6(Γ_0/Γ) ³
Si^{28}	4.2	2.127	$0^+ - 2^+$	3	1	0.63	> 1.0
Cl^{35}	75.5	1.22	$\frac{1}{2}^+ - \frac{1}{2}^+$	3	1	(1)	6 ϵ
		1.76	$\frac{1}{2}^+ - \frac{1}{2}^+$	3	(1)	(1)	4 ϵ
		2.7(2.65)	$\frac{1}{2}^+ - \frac{1}{2}^+$	3	3	(1)	0.31(Γ_0/Γ) ³
		3.01	$\frac{1}{2}^+ - \frac{1}{2}^+$	3	3	(1)	0.37(Γ_0/Γ) ³
Cl^{36}	75.5	3.1	$\frac{1}{2}^+ - \frac{1}{2}^+$	3	3	(1)	> 0.74(Γ_0/Γ) ³
		3.17	$\frac{1}{2}^+ - \frac{1}{2}^+$	3	3	(1)	> 1.54(Γ_0/Γ) ³
Cl^{37}	24.5	0.838	$\frac{1}{2}^+ - \frac{1}{2}^+$	3	1	(1)	> 13 ϵ
		1.72	$\frac{1}{2}^+ - \frac{1}{2}^+$	3	3	(1)	> 0.3(Γ_0/Γ) ³
K^{39}	93	2.53	$\frac{1}{2}^+ - \frac{1}{2}^+$	3	1	(1)	> 1.6 ϵ
		2.52	$\frac{1}{2}^+ - \frac{1}{2}^+$	3	1	(1)	> 1.5 ϵ
		3.02	$\frac{1}{2}^+ - \frac{1}{2}^+$	3	1	(1)	0.37 ϵ
		3.60	$\frac{1}{2}^+ - \frac{1}{2}^+$	3	1	(1)	> 0.7 ϵ
		3.88(3.94)	$\frac{1}{2}^+ - \frac{1}{2}^+$	3	3	(1)	0.14(Γ_0/Γ) ³
		4.06-4.12	$\frac{1}{2}^+ - \frac{1}{2}^+$	3	3	(1)	> 0.2(Γ_0/Γ) ³
Ca^{40}	96	3.90	$0^+ - 2^+$	3	1	0.63	> 0.46
Cu^{63}	69	1.33	$\frac{1}{2}^+ - \frac{1}{2}^+$	2	(1)	0.8	44 > τ > 11

The factor ϵ equals $(2I+1)(2I_0+1)^{-1}$

TABLE 2
Comparison of mean lifetime measurements

Nucleus	Energy	%	Spins	ϵ	Γ_0/Γ	$W'(\theta)$	$\tau \times 10^{12}$ sec	
							This work	Other
Lu^{175}	3.56	7	$1^+ - 0$	$\frac{1}{2}$	(1)	1	0.012	0.0073 ± 0.0015 ⁽¹⁾
B^{11}	2.14	81	$\frac{1}{2}^+ - (\frac{1}{2})^-$	$\frac{1}{2}$	1	1	0.53	0.47 ± 0.06 ⁽²⁾
Al^{27}	2.21	100	$\frac{1}{2}^+ - \frac{1}{2}^+$	$\frac{1}{2}$	(1)	1	3.2	2.7 ± 0.3 ⁽³⁾
Al^{27}	1.01	100	$\frac{1}{2}^+ - \frac{1}{2}^+$	$\frac{1}{2}$	0.98	1	520	170 ± 50 ⁽⁴⁾
Si^{28}	1.78	92	$0^+ - 2^+$	5	1	0.63	88	73 ± 23 ⁽⁵⁾
Si^{28}	2.24	96	$0^+ - 2^+$	5	1	0.63	26	16 ± 16 ⁽⁶⁾
Mg^{24}	1.37	78.6	$0^+ - 2^+$	5	1	0.63	220	185 ± 40 ⁽⁷⁾
Mg^{24}	1.61	25	$\frac{1}{2}^+ - \frac{1}{2}^+$	$\frac{1}{2}$	(1)	1	3.6	2.5 ± 0.6 ⁽⁸⁾
Cu^{63}	0.963	69	$\frac{1}{2}^+ - \frac{1}{2}^+$	$\frac{1}{2}$	1	0.93	230	72 ± 18 ⁽⁹⁾
Cu^{63}	0.67	69	$\frac{1}{2}^+ - \frac{1}{2}^+$	$\frac{1}{2}$	1	1	100	90 ± 15 ⁽¹⁰⁾
							31	± 3 ⁽¹¹⁾

The factor ϵ equals $(2I+1)(2I_0+1)^{-1}$.

METHOD					REF. NO.	
Linac					62 F1 3	JDM
REACTION	RESULT	EXCITATION ENERGY	SOURCE		DETECTOR	
			TYPE	RANGE	TYPE	RANGE
G ₂ N	RLY	16-28	C	32	TPF-D	1-12

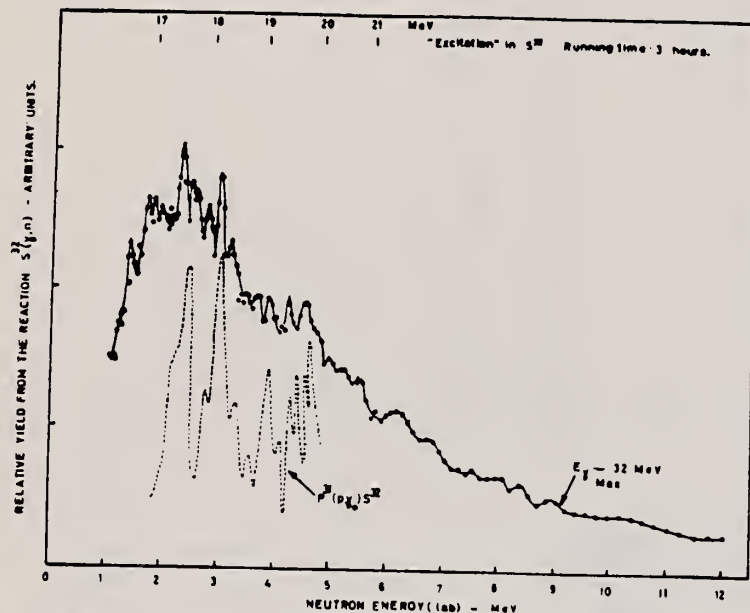


Fig. 2. Energy spectrum of photoneutrons from the reactions $S^{32}(\gamma, n)S^{31}$.

Method Betatron; neutron yield; radioactivity; NBS chamber

Ref. No.	NVB
62 Ku 1	

Reaction	E or ΔE	E_0	Γ	$\int \sigma dE$	$J\pi$	Notes
$S^{32}(\gamma, n)$	Bremss. 12-27	20.5 16.2 17.0	6.3	$\int_{12}^{27} = 86 \text{ MeV-mb}$		$\sigma_{\text{max}} = 13.6 \text{ mb}$ Γ - width of giant resonance

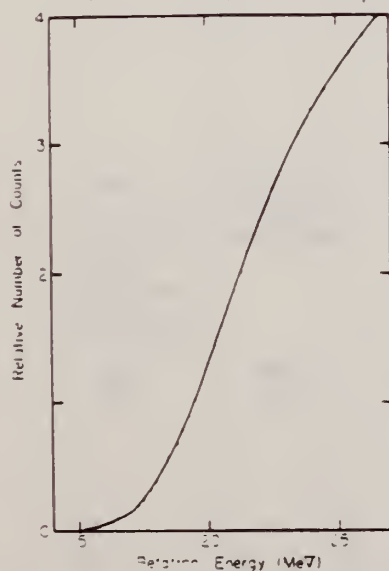


Fig. 6. The activation curve of the reaction $S^{32}(\gamma, n)S^{31}$.

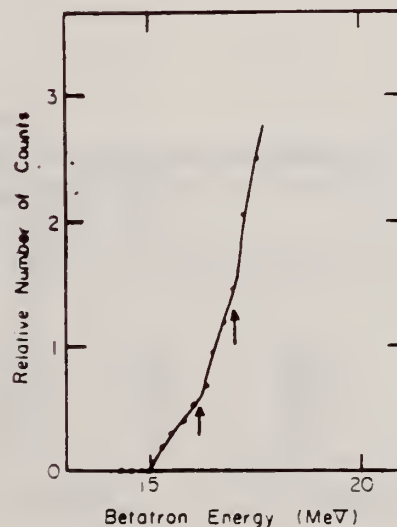


Fig. 7. The activation curve of the reaction $S^{32}(\gamma, n)S^{31}$ near the threshold. Arrows indicate breaks in the curve.

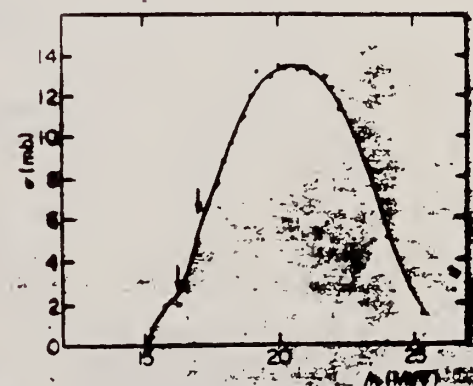


Fig. 10. Cross section of the reaction $S^{32}(\gamma, n)S^{31}$. Arrows indicate the breaks in the activation curve.

REACTION	RESULT	EXCITATION ENERGY	SOURCE		DETECTOR		ANGLE
			TYPE	RANGE	TYPE	RANGE	
G,N	SPC	15-30	C	30	EMU-D	0-15	DST

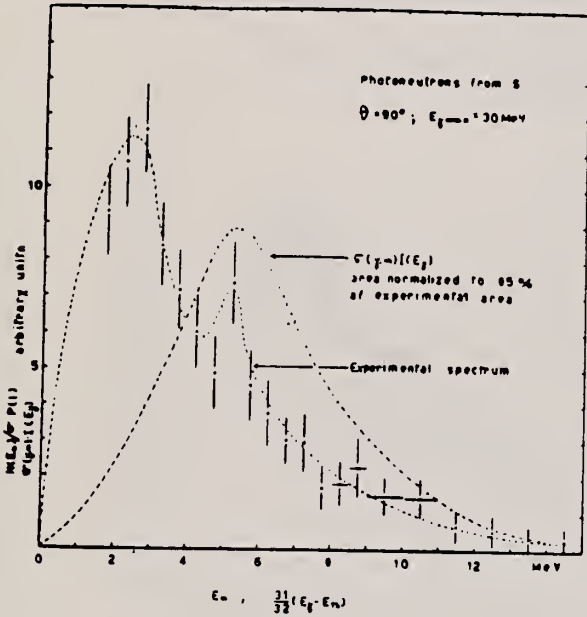


Fig. 1

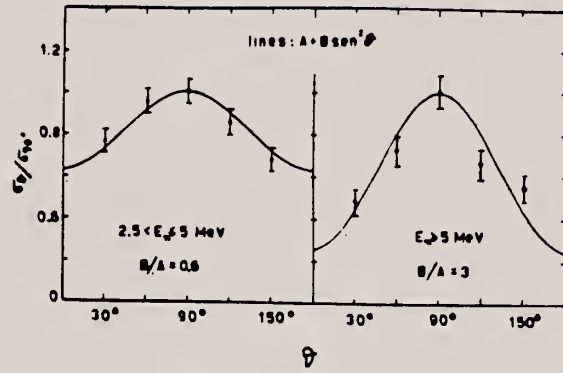


Fig. 2

Table 1

Reaction in S ³²	Threshold Energy (MeV)	E _σ max (MeV)	∫ ₀ ^{30 MeV} σ dE (MeV-barns)	yield
				yield (γ, n) + (γ, np) with 30 MeV bremsstrahlung
(γ, n)	15.1	21	0.093	85%
(γ, np)	21.2	>30	0.028	15%
(γ, 2n)	28.0			

Elem. Sym.	A	Z
S	32	16

Method Betatron; BF_3 counters; Al thin-wall ion chamber monitor

Ref. No.
62 Mu 2
NVB

Reaction	E or ΔE	E ₀	Γ	∫σdE	Jπ	Notes
S ³² (γ,n)	Bremss. 12.5-24	15.7 16.8 17.9 18.75 19.7		22.5 ∫ ₀ ^{22.5} = 60±5 MeV-mb		Suggested correspondence with observed proton energy peaks.

Table. Characteristic constants of both reaction.

p ₃₂		S ₃₂	
E _{res} (MeV)	σ _{res} (mb)	E _{res} (MeV)	σ _{res} (mb)
13.5	6		
14.6	8		
15.8	14	15.7	7
(17)	(17)	16.8	10
17.5	21	17.9	20
19.0	22	18.75	11
20.3	22	19.7	16

∫ ₀ ^{22.5} σ(γ, n) dE	∫ ₀ ^{22.5} σ(γ, n) dE
= 120±10 Mev-mb	= 60±5 Mev-mb

Ref 3: M. Kimura, et al: to be published.

Fig. 2. Cross section for S³²(γ, n) reaction, in which solid line was deduced from yield curve smoothing method and dotted line was deduced from running integral smoothing method. — — — indicate P³²(p, γ) excitation function as a function of E_γ (MeV) obtained by Kimura, et al.²

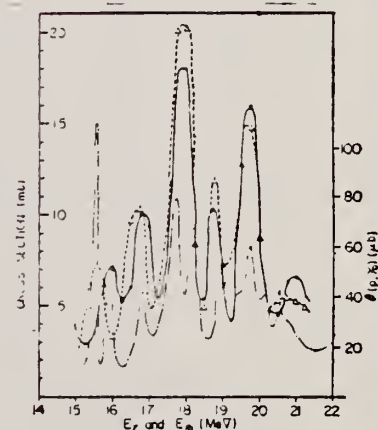


Fig. 2. Cross section for $\text{S}^{32}(\gamma, n)$ reaction, in which solid line was deduced from yield curve smoothing method and dotted line was deduced from running integral smoothing method. --- indicate $\text{P}^{32}(p, \gamma)$ excitation function as a function of E_0 (MeV) obtained by Kimura, et al.

Elem. Sym.	A	Z
S	32	16

Method 550 kev Cockcroft-Walton accelerator; NaI

Ref. No.
62 Ne 1
JHH

Reaction	E or ΔE	E_0	Γ	$\int \sigma dE$	$J\pi$	Notes
$P^{31}(p,\gamma)S^{32}$	340-460 KeV	355 keV 440 keV			1^+ 1^+	$E_{\gamma_0} = 9.183 \text{ MeV}$ $E_{\gamma_0} = 9.267 \text{ MeV}$

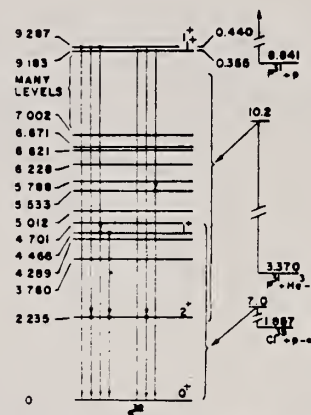


Fig. 1. Energy level diagram of S^{32} nucleus. Gamma ray transitions indicated were observed in the present experiment. Spin and parity assignments to the 4.46 MeV, 9.18 MeV, and 9.26 MeV levels were made on the basis of the present work.

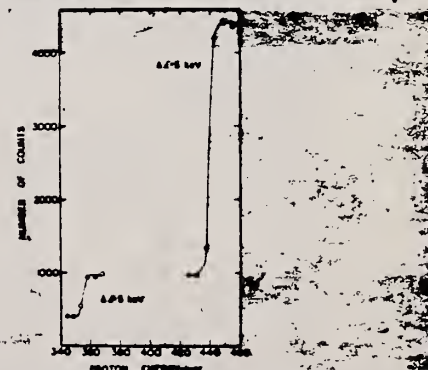


Fig. 2. Yield curves for gamma radiation from proton bombardment of thick phosphorus targets. Yield at the two resonances were measured in separate runs.

Method

Linné (Standard Mark II) - counter telescope

Ref. No.

652a1**35**

Reaction	E or ΔE	E_0	Γ	$\int \sigma dE$	$J\pi$	Notes
(e,e')	41.5		eV			Inelastic electron scattering cross section at 180° ($\text{cm}^2/\text{sr} \times 10^{-32}$) 1.3±30% 1.7±30% 2.6±30% The rel. widths correspond to transitions from the 0^+ state to 1^+ excited states.
		5.7	0.76	0.24		
		8.5	3.5	0.51		
		11.4	14.2	1.11		

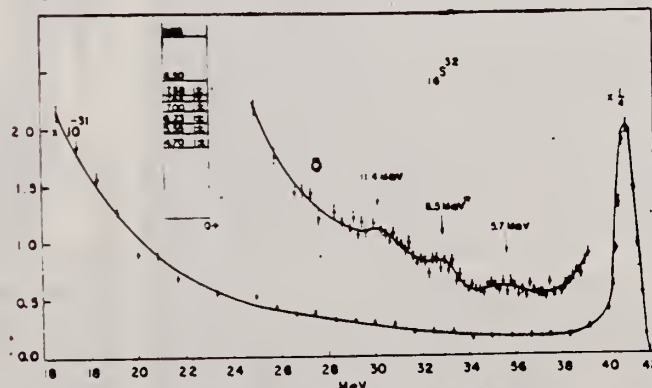


Fig. 15. Spectrum of 41.5 MeV electrons scattered from a sulphur target at 180°.

Elem. Sym.	A	Z
S	32	16
Ref. No.		JHH
63 Ch 1		

Method
Inverse; NaI

Reaction	E or ΔE	E_0	Γ	$\int \sigma dE$	$J\pi$	Notes
$p^{31}(p,\gamma)$	0.355 0.440	9.21 9.29			1^+ 1^+	Isotropic angular distributions.

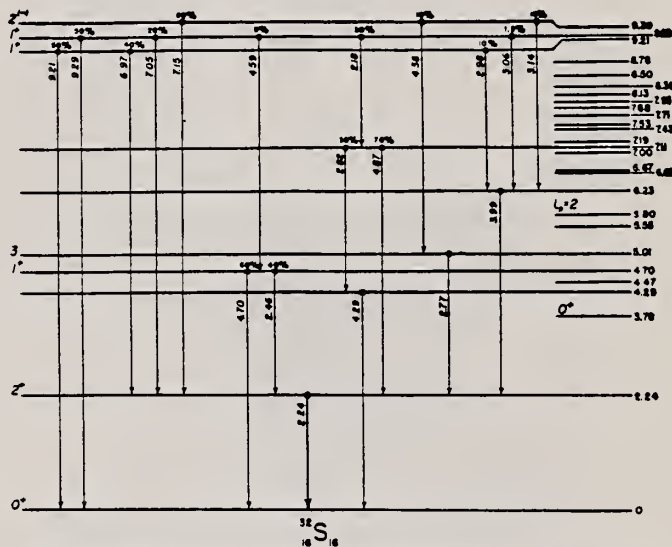


Fig. 3. Decay scheme for the 9.21, 9.29 and 9.39 MeV levels of ^{32}S . Known levels, which do not appear to participate in these cascades, are shown only at the right-hand edge. The spin assignments for the 2.24, 3.78, 5.01 and 5.80 MeV levels are taken from ref. 4). Branching ratios are accurate to not worse than a factor of two. Some weak branches may have been missed.

References

- 1) E. B. Nelson, R. R. Carlson and L. D. Schlenker, Nuclear Physics 31 (1962) 65
- 2) P. R. Chagnon and P. A. Treado, Bull. Am. Phys. Soc. 7 (1962) 301
- 3) S. L. Andersen, in Proc. Rutherford Jubilee Int. Conf., ed. by J. B. Birks (Heywood Newnes, London, 1961) p. 261
- 4) P. M. Endt and C. van der Leun, Nuclear Physics 34 (1962) 1

TABLE I

Thick-target (Zn, p) yields and widths for the three resonances

E_0 (keV, lab.)	355	440	540
E_r (MeV)	9.21	9.29	9.39
E_r (MeV)	9.21	6.97	All
γ (10^{-18} photon/proton)	0.40	0.14	0.80
$(2J-1) \Gamma_p \Gamma_\gamma \Gamma$ (eV)	0.006	0.005	0.012
$\Gamma_p \Sigma \Gamma_\gamma \Gamma$ (eV)		0.004	0.045

By the procedure outlined in ref. 1) one readily obtains the quantity $(2J-1) \Sigma \Gamma_p \Gamma_\gamma \Gamma$ in which Γ_p and Γ_γ are partial particle and radiation widths, the sum being taken over partial waves, channel spins and multiplicities contributing to each resonant capture and subsequent radiation process. The last line is calculated using the resonance spins found in this work. The yields, and consequently the widths, are uncertain to about $\pm 20\%$.

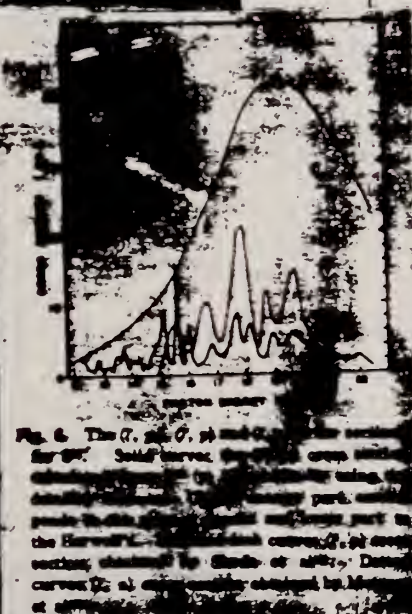
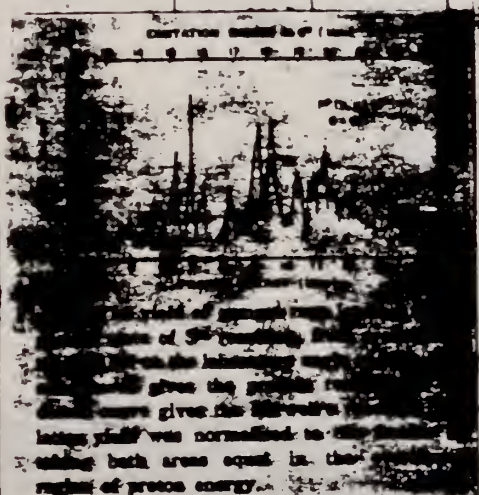
Ref. M. Kimura, K. Shoda, N. Mutsuro, M. Sugawara, K. Abe,
K. Kageyama, M. Mishina, A. Ono, T. Ishizuka, S. Mori,
N. Kawamura, T. Nakagawa, E. Tanaka
J. Phys. Soc. Japan 18, 477 (1963)

Elem. Sym.	A	Z
S	32	16

Method Cyclotron; inverse; NaI spectrometer

Ref. No.	
63 K1 2	NVB

Reaction	E or ΔE	E_0	Γ	$\int \sigma dE$	$J\pi$	Notes
$p^{31}(p, \gamma)S^{32}$	8-14	17-22		$\int_{12.5}^{22.5} \sigma(\gamma, p) dE_{\gamma} =$ $= 34 \text{ MeV-mb}$		Detectors at 90° , 45° .



ELEM. SYM.	A	Z
S	32	16
REF. NO.		NVB
63 Sp 1		

METHOD Van de Graaff; inverse; NaI spectrometer

REACTION	RESULT	EXCITATION ENERGY	SOURCE		DETECTOR		ANGLE
			TYPE	RANGE	TYPE	RANGE	
P,G	NØX	9 - 10	D	0 - 1	NAI-D		DST
		(9.48, 9.94)		(642 - 1116)			
				keV			

$$E_p = 642, \Gamma_\gamma = 9.5 \times 10^{-5} \Gamma_{\gamma w}(E_1)$$

G-WIDTH, J-PI

$$E_\gamma = 1116, \Gamma_\gamma = \begin{cases} 1.6 \times 10^{-2} \Gamma_{\gamma w}(M1) \\ 3.1 \times 10^{-4} \Gamma_{\gamma w}(E1) \end{cases}$$

where, $\Gamma_{\gamma w}$ = Weisskopf width, $\Gamma_{\gamma w}(E1) = 0.11A^{2/3} E_\gamma^3$ eV.

$$\Gamma_{\gamma w}(M1) = 0.021 E_\gamma^3 \text{ eV.}$$

In Figure 10, $W(\theta) = 1 - (0.20 \pm 0.02)P_2(\cos \theta)$; in Figure 12, $W(\theta) = 1 - (0.17 \pm 0.02)P_2(\cos \theta)$

$$E_p = 642 \text{ keV}, J^\pi = 1^-, E_\gamma = 9.48 \text{ MeV}$$

$$E_p = 1116 \text{ keV}, J^\pi = 1^\pm, E_\gamma = 9.94 \text{ MeV}$$

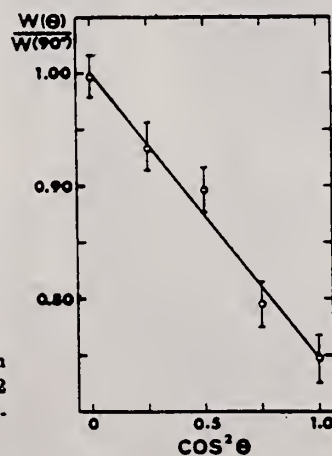


Fig. 10. Experimental angular distribution function of the 9.48 MeV transition at the 642 keV resonance. The curve has not been corrected for the solid angle of the detector.

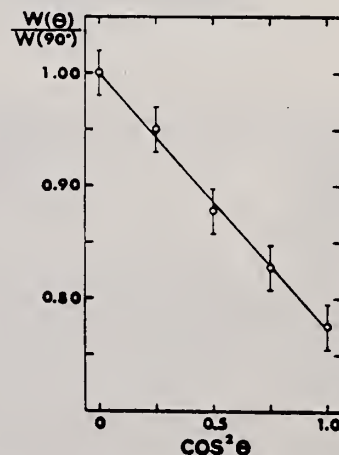


Fig. 12. Experimental angular distribution function of the 9.94 MeV transition at the 1116 keV resonance. The curve has not been corrected for the solid angle of the detector.

METHOD
Linac; Faraday cup/SEM monitor

[Page 1 of 5]

REF. NO.
64 Lo 1

JOC

REACTION	RESULT	EXCITATION ENERGY	SOURCE		DETECTOR		ANGLE
			TYPE	RANGE	TYPE	RANGE	
$E, E/$	FMF	0 - 9	D	120-180	MAG-D		DST

J-PI

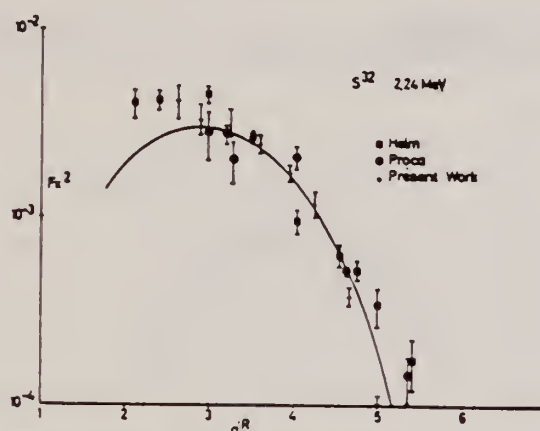


Fig. 3. The experimental form factors obtained for the level at 2.24 MeV. The results of Helm ¹⁾ (squares) and of Bishop and Proca ²⁾ (open circles) are included for comparison. The full line represents the expression $F_1 = j_1(qR)\exp(-q^2 R^2)$ multiplied by the normalizing factor $\beta_1 = (6.26) \cdot 10^{-4}$.

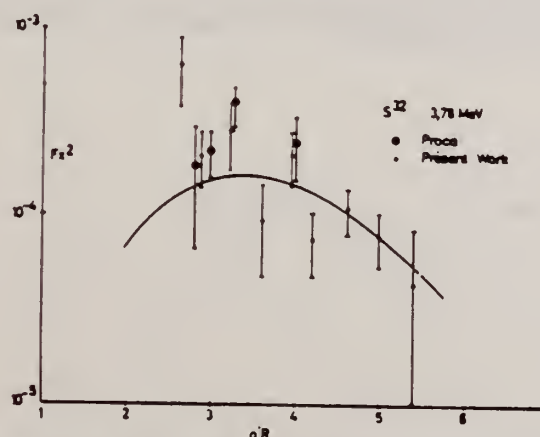


Fig. 4. The experimental form factors obtained for the level at 3.78 MeV. The results of Bishop and Proca ²⁾ (large circles) are included for comparison. The full line represents $F_0 = [1 - j_0(qR)]^2 \exp(-q^2 R^2)$ multiplied by the normalizing factor $\beta_0 = 3.17 \cdot 10^{-4}$.

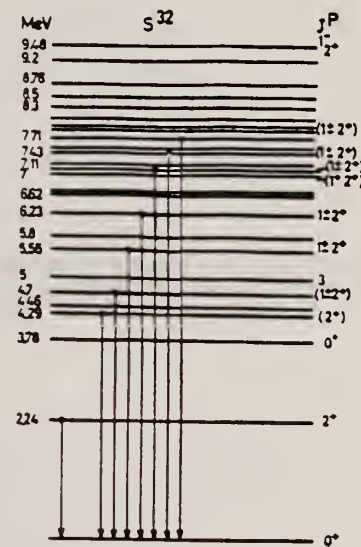


Fig. 1. The decay scheme of S^{32} . All excitation energies are given in MeV.

METHOD
Linac; Faraday cup/SEM monitor

[Page 2 of 5]

REACTION	RESULT	EXCITATION ENERGY	SOURCE		DETECTOR		ANGLE
			TYPE	RANGE	TYPE	RANGE	

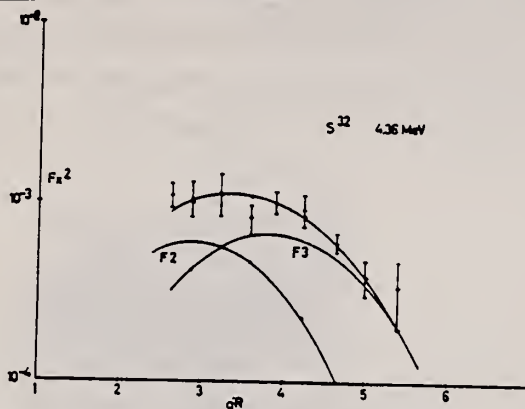


Fig. 5. The experimental form factors obtained for the peak observed at 4.36 ± 0.1 MeV. The full lines represent the expressions F_2 and $F_3 = j_3^2(qR) \exp(-q^2 g^2)$ multiplied by their respective normalizing factor $\beta_2 = 1.25 \cdot 10^{-3}$ and $\beta_3 = 3.74 \cdot 10^{-3}$.

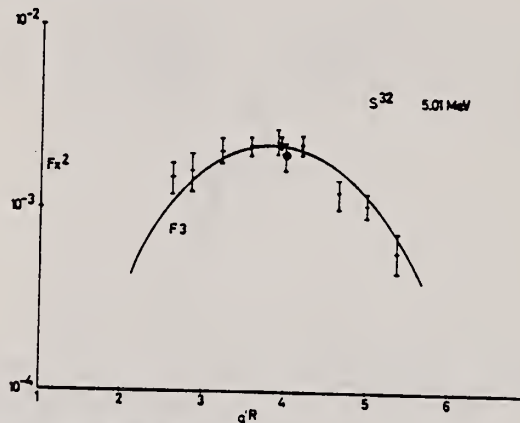


Fig. 6. The experimental form factors obtained for the level at 5.01 MeV. The full line represents the expression F_3 multiplied by the normalizing factor $\beta_3 = 1.26 \cdot 10^{-3}$.

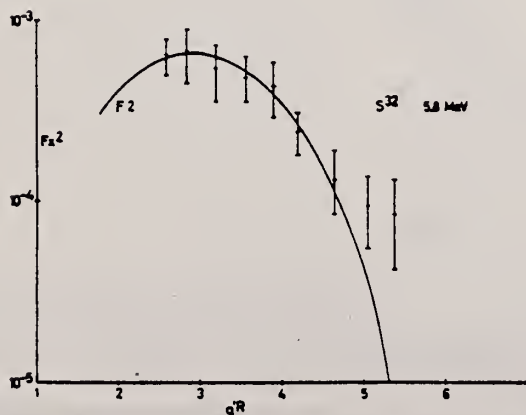


Fig. 7. The experimental form factors obtained for the level at 5.8 MeV. The full line represents the expression F_3 multiplied by $\beta_3 = 1.34 \cdot 10^{-3}$.

METHOD

Linac; Faraday cup/SEM monitor

[Page 3 of 5]

REF. NO.

64 Lo 1

JOC

REACTION	REACTANT	EXCITATION ENERGY	SOURCE		DETECTOR		ANGLE
			TYPE	RANGE	TYPE	RANGE	

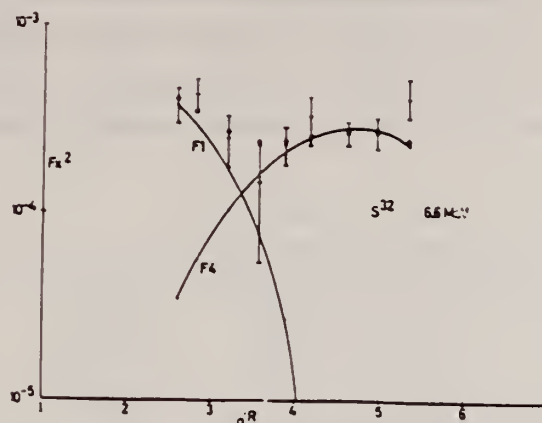


Fig. 8. The experimental form factors for the peak observed at 6.6 ± 0.2 MeV. The full lines represent the expressions $\beta_1 F_1$ and $\beta_4 F_4$ with $F_1 = j_1^2(qR) \exp(-q^2 a^2)$, $\beta_1 = 3.68 \cdot 10^{-3}$ and $\beta_4 = 4.42 \cdot 10^{-3}$.

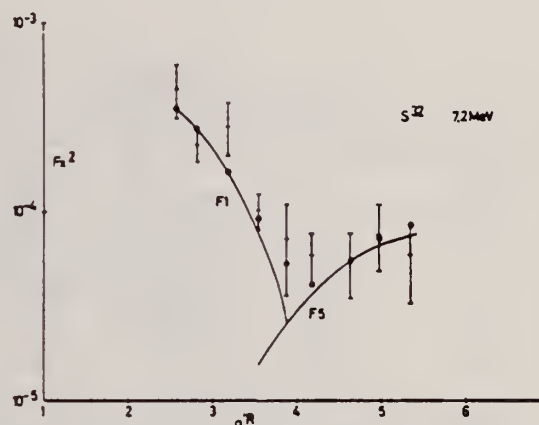


Fig. 9. The experimental form factors observed for the peak at 7.2 ± 0.1 MeV. The full lines represent respectively the expressions $\beta_1 F_1$ and $\beta_5 F_5$ with $\beta_1 = 3.35 \cdot 10^{-3}$ and $\beta_5 = 3.35 \cdot 10^{-3}$.

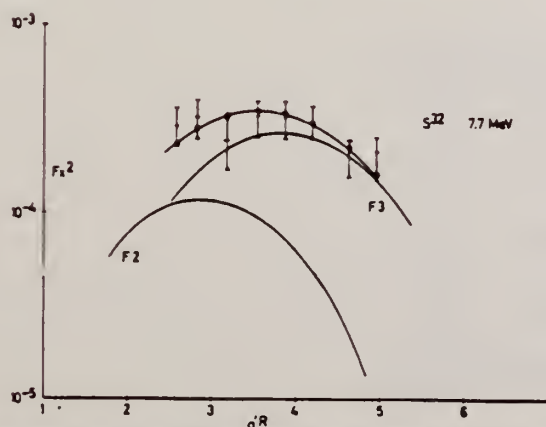


Fig. 10. The experimental form factors observed for the peak at 7.7 ± 0.2 MeV. The full lines represent respectively the expressions $\beta_2 F_2$ and $\beta_3 F_3$ where $\beta_2 = 2.5 \cdot 10^{-3}$ and $\beta_3 = 1.52 \cdot 10^{-3}$.

METHOD

Linac; Faraday cup/SEM monitor

[Page 4 of 5]

REF. NO.

64 Lo 1

JOC

REACTION	RESULT	EXCITATION ENERGY	SOURCE		DETECTOR		ANGLE
			TYPE	RANGE	TYPE	RANGE	

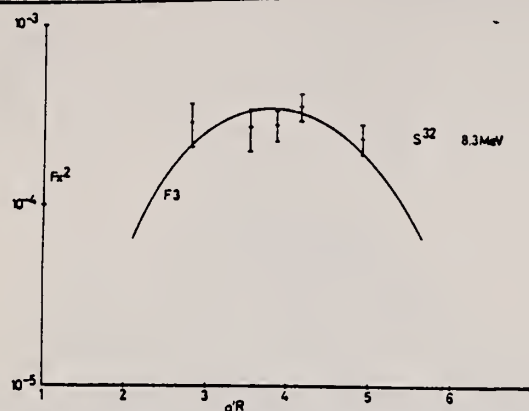


Fig. 11. The experimental form factors observed for the peak at 8.3 ± 0.2 MeV. The full line represents the expression $\beta_2 F_2$ where $\beta_2 = 1.93 \cdot 10^{-2}$.

TABLE 2

Analysis of the peak at 4.3 MeV as described in the text

Multipole $E\lambda$	$\beta_\lambda \times 10^{-2}$	Reduced transition probability	P	$B(E\lambda \uparrow)/B_{sp}$
E3	(5.4 ± 0.6)	$(21.6 \pm 2.5)(-76) \text{ cm}^2$	23	5
{ E2 E3	(1.25 ± 0.1)	$(39.8 \pm 3)(-52) \text{ cm}^2$	6.7	1.3
	(3.74 ± 0.44)	$(15 \pm 1.7)(-76) \text{ cm}^2$		
{ E2 E4	(2.1 ± 0.25)	$(67.5 \pm 8)(-52) \text{ cm}^2$	4.58	2.2
	(6.33 ± 0.75)	$(3.18 \pm 0.37)(-100) \text{ cm}^2$		

The value of P is to be compared with 7 for the case of a single E3 transition and 6 for the other two hypotheses.

TABLE 3

Analysis of the peak at 6.6 MeV

Multipole $E\lambda$	$\beta_\lambda \times 10^{-2}$	Reduced transition probability	P	$B(E\lambda \uparrow)/B_{sp}$
{ E1 E4	(0.368 ± 0.045)	$(9.4 \pm 1)(-27) \text{ cm}^2$	6.98	0.5
	(4.42 ± 0.55)	$(22.2 \pm 2.7)(-101) \text{ cm}^2$		
{ E1 E5	(0.432 ± 0.054)	$(11 \pm 1.4)(-27) \text{ cm}^2$	6.7	0.56
	(16.3 ± 2)	$(10.3 \pm 1.2)(-125) \text{ cm}^{10}$		
{ E2 E4	(0.46 ± 0.06)	$(14.7 \pm 1.8)(-52) \text{ cm}^2$	19.5	0.5
	(3.69 ± 0.47)	$(18.5 \pm 2.3)(-101) \text{ cm}^2$		
{ E2 E5	(0.599 ± 0.075)	$(19 \pm 2.4)(-52) \text{ cm}^2$	10.8	0.6
	(13.4 ± 1.7)	$(8.4 \pm 1)(-125) \text{ cm}^{12}$		

The value of P is to be compared with 7 so that the combinations E2, E4 and E2, E5 are most improbable.

METHOD				REF. NO.	
Linac; Faraday cup/SEM monitor				64 Lo 1	
[Page 5 of 5]				JOC	
REACTION	RESULT	EXCITATION ENERGY	SOURCE		ANGLE
			TYPE	RANGE	

TABLE 4
Analysis of the peak at 7.2 MeV

Multipole $E\lambda$	$\beta_1 \times 10^{-3}$	Reduced transition probability	P	$B(E\lambda \uparrow)/B_{sp}$
E1	(0.297 ± 0.04)	$(7.56 \pm 1) (-27) \text{ cm}^2$	4.7	0.38
E4	(1.01 ± 0.14)	$(5.07 \pm 0.7) (-101) \text{ cm}^2$		0.87
E1	(0.335 ± 0.047)	$(8.55 \pm 1) (-27) \text{ cm}^2$	6.99	0.4
E5	(3.35 ± 0.47)	$(2.1 \pm 0.3) (-125) \text{ cm}^{10}$		2.6

The value of P is to be compared with 7.

TABLE 5
Analysis of the peak at 7.7 MeV

Multipole $E\lambda$	$\beta_1 \times 10^{-3}$	Reduced transition probability	P	$B(E\lambda \uparrow)/B_{sp}$
E0	0.066 ± 0.008		3.27	
E3	(1.95 ± 0.25)	$(7.8 \pm 1) (-76) \text{ cm}^2$	8.4	1.8
E2	(0.25 ± 0.03)	$(7.99 \pm 1) (-52) \text{ cm}^2$	4.47	0.2
E3	(1.52 ± 0.2)	$(6.1 \pm 0.76) (-76) \text{ cm}^2$		1.4
E2	(0.557 ± 0.072)	$(17.8 \pm 2.3) (-52) \text{ cm}^2$	2.49	0.57
E4	(2.89 ± 0.38)	$(14.5 \pm 1.9) (-101) \text{ cm}^2$		2.5
E2	(0.664 ± 0.85)	$(21.2 \pm 2.7) (-52) \text{ cm}^2$	3.56	0.7
E5	(9.89 ± 1.3)	$(6.2 \pm 0.5) (-125) \text{ cm}^{10}$		7.8

The value of P is to be compared with 7 for a single transition and 6 for a doublet.

METHOD

Van de Graaff; Si(α, γ)S, $P^{31}(p, \gamma)S^{32}$

[Page 1 of 2]

REF. NO.

64 Sm 1

NVB

J-PI, WIDTHS

At 642.1 keV resonance, the (p, γ_0) angular distribution is $W(\theta) = 1 - (0.273 \pm 0.015)P_2(\cos\theta)$

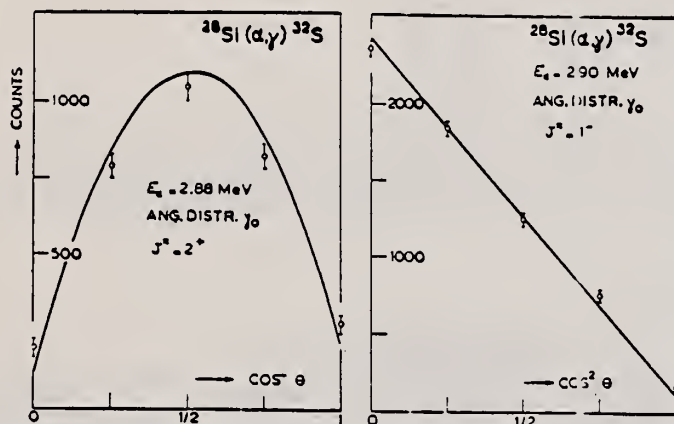


Fig. 3. Angular distributions of γ_0 at the 2.878 and 2.904 MeV $^{28}\text{Si}(\alpha, \gamma)^{32}\text{S}$ resonances measured with a $10 \times 10 \text{ cm}$ NaI crystal at 10 cm from the target. The curves correspond to the theoretical expressions for $J^\pi = 2^+$ and 1^- , respectively.

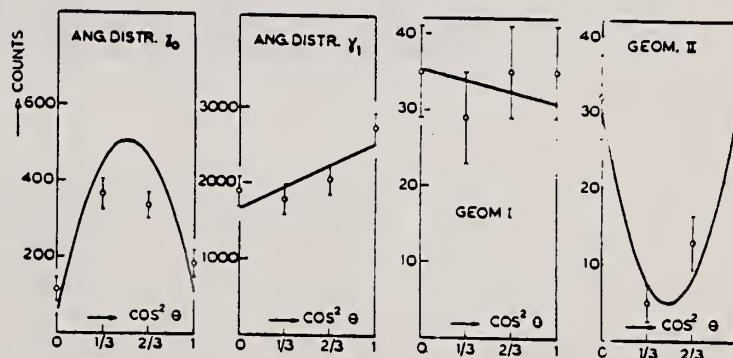


Fig. 4. Angular distributions of γ_0 and γ_1 , and angular correlations of the cascade (π) \rightarrow (1) \rightarrow (0) in geometries I and II, as measured at the 3.162 MeV $^{28}\text{Si}(\alpha, \gamma)^{32}\text{S}$ resonance. The curves correspond to the theoretical expressions for resonance spin 2^+ and $E2/M1$ amplitude ratio of γ_1 $\approx +0.10$. Two $10 \times 10 \text{ cm}$ NaI crystals were used, both at 10 cm from the target.

METHOD

Van de Graaff; $\text{Si}(\alpha, \gamma)\text{S}$, $\text{P}^{31}(\text{p}, \gamma)\text{S}^{32}$

[Page 2 of 2]

REF. NO.

64 Sm 1

NVB

REACTION	RESULT	EXCITATION ENERGY	SOURCE		DETECTOR		ANGLE
			TYPE	RANGE	TYPE	RANGE	

TABLE I

Resonances in the $^{28}\text{Si}(\alpha, \gamma)^{32}\text{S}$ reaction					
1 $E_{\alpha}(\text{MeV})$	2 $E_{\alpha}(\text{MeV})$ ($Q = 6.946 \text{ MeV}$)	3 Observed γ transitions	4 $\Gamma_{\gamma 0}/\Gamma_{\gamma 0}$	5 $(2J+1)\Gamma_{\alpha}\Gamma_{\gamma}/\Gamma(\text{eV})$ (*)	6 J^{π}
2.618	9.236	γ_1 , 2.24	< 0.1	0.3	1^{-}
2.878	9.464	γ_0 , γ_1 , 2.24	1.5	0.4	2^{+}
2.904	9.487	γ_0	> 5	0.7	1^{-}
3.162	9.713	γ_0 , γ_1 , 4-5.5†)	0.15	0.2**)	2^{+}
all $\pm 4 \text{ keV}$					
2.51, 2.24					

*) Only γ_0 and γ_1 are included in the yields.**) At this resonance the total strength is $\approx 0.3 \text{ eV}$.

†) see text.

J-PI, WIDTHS

TABLE II

$^{31}\text{P}(\text{p}, \gamma)^{32}\text{S}$ resonances, corresponding to $^{28}\text{Si}(\alpha, \gamma)^{32}\text{S}$ resonances of table I						
$E_p(\text{keV})$	$E_{\alpha}(\text{keV})$ ($Q = 8862.6 \text{ keV}$)	J	$(2J+1)(\Gamma_{\gamma 0} + \Gamma_{\gamma 1})$ $\times \Gamma_p \Gamma_{\gamma} (\text{eV})$	$(2J+1)\Gamma_p \Gamma_{\gamma}/\Gamma$ (eV)	Observed γ transitions	Corresponding (α, γ) resonance (MeV)
386			< 0.00015	< 0.00015	none	2.618
618.9 ± 1.0	9462		0.003	0.003	γ_0, γ_1	2.878
642.1 ± 1.0	9485	1	0.19	0.23	γ_0 ; see text	2.904
875.5 ± 1.4	9711		0.02	0.03	γ_0, γ_1	3.162

TABLE III

Comparison of yield measurements of $^{31}\text{P}(\text{p}, \gamma)^{32}\text{S}$ resonances by different authors. (All strengths in eV).					
Resonance energy (keV)	Measured quantity	Present work	Other authors		
			(a)	(b)	(c)
440	$(2J+1)(\Gamma_p/\Gamma) \times \Gamma_{\gamma 0}$	0.042	0.067	0.052	
540	$(2J+1)(\Gamma_p/\Gamma) \times \Gamma_{\gamma 1}$	0.25	0.25		
812	$(2J+1)(\Gamma_p/\Gamma) \times \Gamma_{\gamma 1}$	0.5			1.8
820	$(2J+1)(\Gamma_p/\Gamma) \times \Gamma_{\gamma 0}$	0.17			0.36

(a) Chagnon and Treado, ref. 10.

(b) Ter Veld and Brinkman, ref. 11.

(c) Paul *et al.*, ref. 12.

TABLE IV

Radiative widths in ^{32}S								
$E_{\alpha}(\text{MeV})$	$\Gamma_{\gamma}(\text{eV})$	$\Gamma_{\gamma 0}(\text{eV})$	type of γ_0	$\Gamma_{\gamma 0}(\text{eV})$	type of γ_1	$ M ^2(E2)$	$ M ^2(E1)$	$ M ^2(M1)$
9.236	> 0.1			> 0.1	E1		$> 3.10^{-4}$	
9.464	0.08	0.06	E2	0.02	M1*)	0.07		3.10^{-30}
9.487	0.37	0.30	E1				3.10^{-4}	
9.713	> 0.06	> 0.01	E2	> 0.05	M1	> 0.01		$> 5.10^{-8}$

*) The E2/M1 mixing ratio of γ_1 for this level was not actually measured, but is assumed to be small. The value of $|M|^2(M1)$ for this level thus may be considered as an upper limit.

REF.

U. Amaldi, Jr., G. Campos Venuti, G. Cortellessa, G. Fronterotta,
A. Reale, P. Salvadori
Rend. Acc. Naz. Lincei 39, 470 (1965)

ELEM. SYM.	A	Z
S	32	16

METHOD

REF. NO.	
65 Am 2	egf

REACTION	RESULT	EXCITATION ENERGY	SOURCE		DETECTOR		ANGLE
			TYPE	RANGE	TYPE	RANGE	
E, E/P	RLY	0-120	D	500-630	MAG-D	408	51

Table gives parameters of Maxwellian distributions used to fit data.

100 MEV P COINC

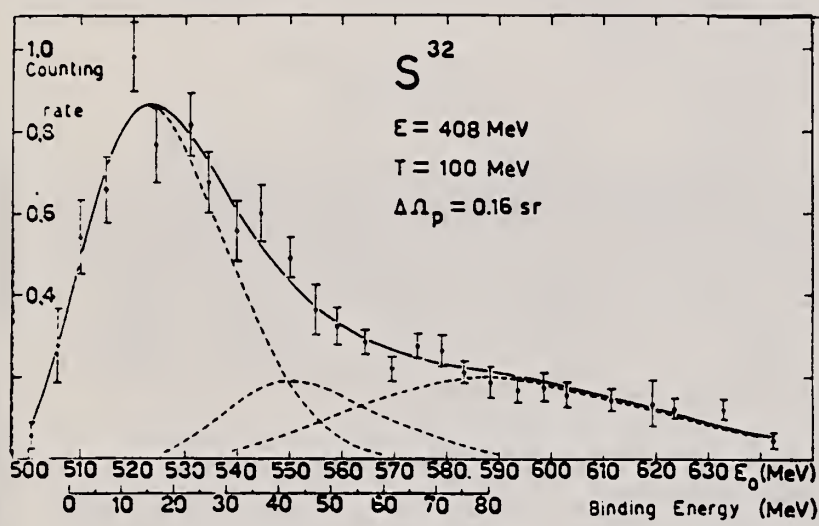


Fig. 1.

TABLE I.

h (counting rate)	σ (MeV)	x_0 (MeV)
0.84 ± 0.13	27.5 ± 3	523.2 ± 2.2
0.23 ± 0.08	31 ± 11	553 ± 7
0.17 ± 0.04	59 ± 17	593 ± 9

TABLE III.

Possible attribution	Binding Energy (MeV)
2s-1d	15.0 ± 2.2
1p	44 ± 7
1s	72 ± 9

METHOD

[Page 1 of 2]

REF. NO.

65 De 1

EGF

REACTION	RESULT	EXCITATION ENERGY	SOURCE		DETECTOR		ANGLE
			TYPE	RANGE	TYPE	RANGE	
P,G	ABX	10 - 21	D	2-12	NAI-D	10-22	DST

Fit angular distribution to $A+B\sin^2\theta+C\sin^2\theta\cos\theta+D\sin^2\theta\cos^2\theta$.

See article for detailed results as function of energy.

Sees some effect of E2 absorption.

82+

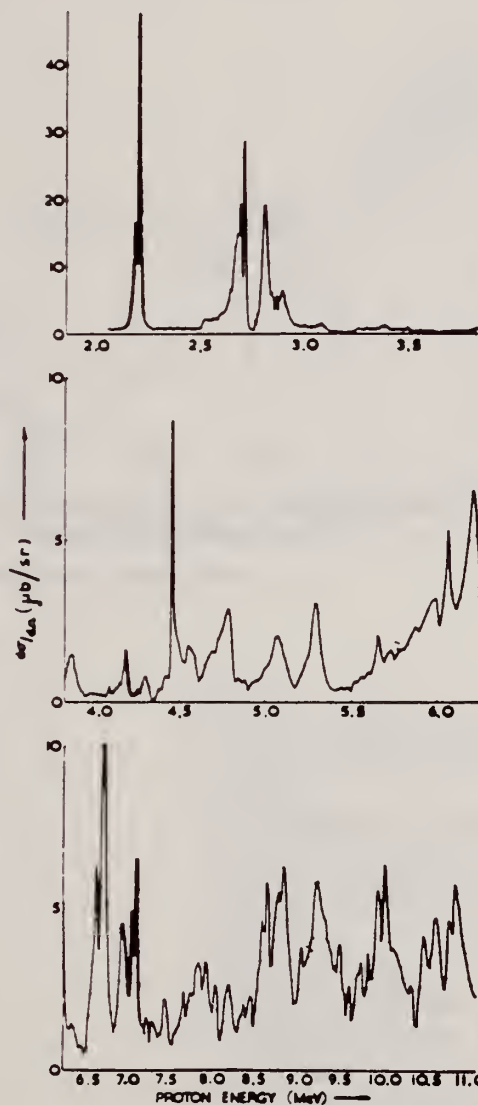


Fig. 3. Excitation function at 90°; yield in (μb/sr) against proton energy in centre of mass (MeV).

REACTION	RESULT	EXCITATION ENERGY	SOURCE		DETECTOR		ANGLE
			TYPE	RANGE	TYPE	RANGE	

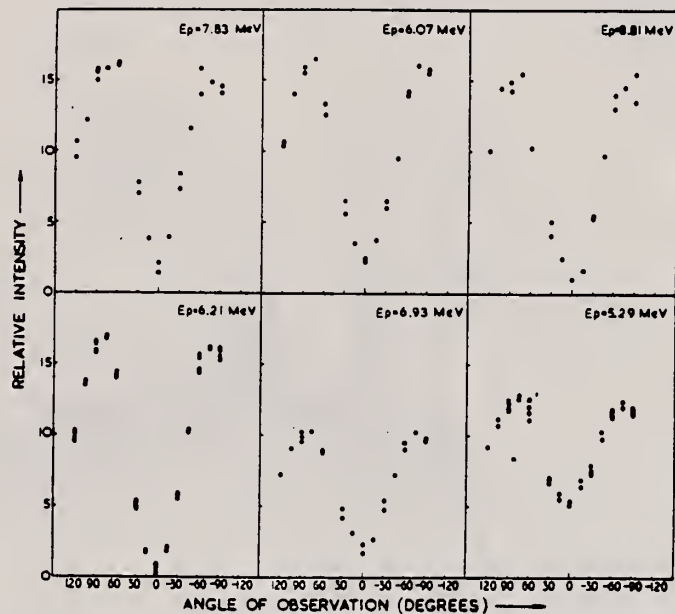


Fig. 4. Typical angular distributions.

METHOD

Radioactivity yield curve

REF. NO.

65 Th 1

EGF

REACTION	RESULT	EXCITATION ENERGY	SOURCE		DETECTOR		ANGLE
			TYPE	RANGE	TYPE	RANGE	
G,N	ABX	THR - 22	C	15 - 22	ACT-I		4PI

Absolute yield based on comparison with Al^{27} yield at 21.8 MeV. Al^{27} yield normalized to Barber, George and Reagan C^{12} .

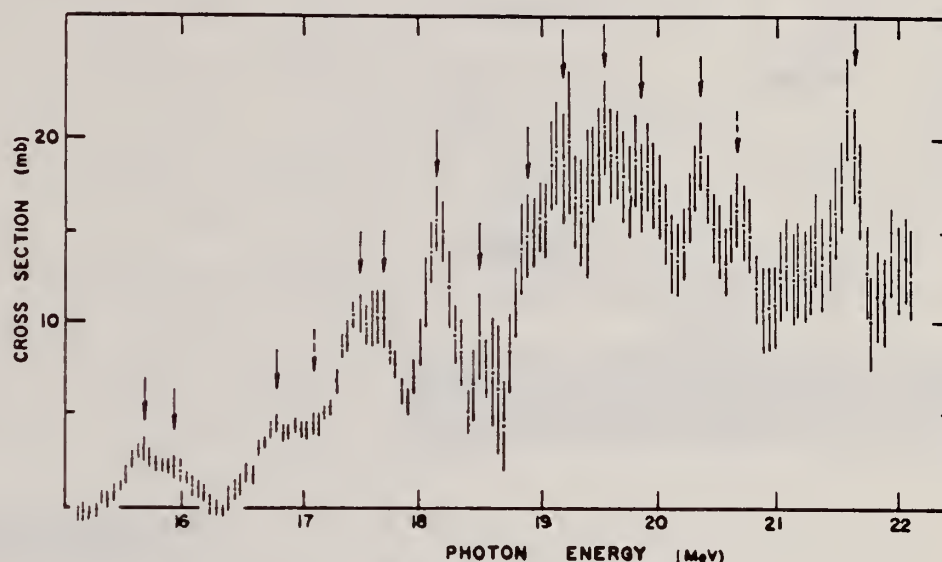
Fig. 1. Cross section for the $S^{32}(\gamma, n)S^{31}$ reaction.

Table 1
Structure in the $S^{32}(\gamma, n)S^{31}$ cross section.

E (MeV)	$\int \sigma dE$ (MeV · mb)	E (MeV)	$\int \sigma dE$ (MeV · mb)
15.7	0.8	18.5	2.0
16.0	0.6	18.9	5.5
16.8	2.0	19.2	6.5
(17.1)	0.8	19.55	7.0
17.5	2.5	19.9	7.5
17.7	2.5	20.3	7.5
18.2	4.5	(20.65)	4.0
		21.3	6.5

Table 2
Integrated cross sections for the reaction $S^{32}(\gamma, n)S^{31}$.

E (MeV)	$\int \sigma(E) dE$ (MeV · mb)	Reference
22.1	64 ± 7	This experiment
22	65 ± 5	[9]
22.5	60 ± 6	[10]
23	67	[11]
22	44	[8]

References

1. F.W.K. Firk, Nucl. Phys. 52 (1964) 437.
2. N. Mutsuro, private communication 1963.
3. N. Tanner, Nucl. Phys. 52 (1964) 29.
4. J.E.E. Baglin and B.M. Spicer, Nucl. Phys. 54 (1964) 549.
5. M.N. Thompson, J.M. Taylor, B.M. Spicer and J.E.E. Baglin, Nucl. Phys. (to be published).
6. A.S. Penfold and J.E. Leiss, Analysis of Photo-Cross Sections, University of Illinois press (1958).
7. W. Barber, W. George and D. Reagan, Phys. Rev. 98 (1955) 73.
8. L.N. Bolen and W.D. Whitehead, Phys. Rev. 132 (1963) 2251.
9. G. Bonazzola, O. Borello, S. Costa and S. Ferroni, Nucl. Phys. 34 (1962) 637.
10. N. Mutsuro, K. Kageyama, M. Mishina, T. Nakagawa, E. Tanaka and M. Kimura, Journ. Phys. Soc. Jap. 17 (1962) 1673.
11. R.W.H. Haslam, R.G. Summers-Gill and E.H. Crosby, Can. Journ. Phys. 30 (1952) 257.

METHOD				REF. NO.	
Betatron; NBS chamber monitor				65 Va 3	NVB
REACTION	RESULT	EXCITATION ENERGY	SOURCE		ANGLE
			TYPE	RANGE	
G, NP	ABX	50 - 300	C	50-300	4PI

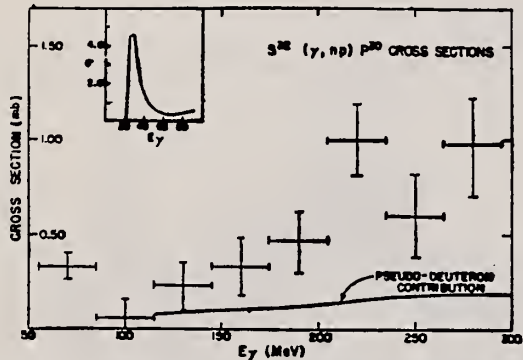


FIG. 2. Cross sections for the $S^{32}(\gamma, np)P^{30}$ reaction. The data points are the results from the present study. The insert shows the normalized low-energy results of Bonazzoni *et al.* (Ref. 13). The solid line shows the calculated contribution to the cross section from events associated with quasi-deuteron absorption processes.

TABLE I. Integrated cross sections for the $S^{32}(\gamma, np)P^{30}$, $Ca^{40}(\gamma, np)K^{39}$, and $Zn^{66}(\gamma, np)Cu^{64}$ reactions.

E_{max} (MeV)	$\int_0^{E_{max}} \sigma dE$ (MeV mb)		
	$S^{32}(\gamma, np)P^{30}$	$Ca^{40}(\gamma, np)K^{39}$	$Zn^{66}(\gamma, np)Cu^{64}$
50	64 ± 2	31 ± 1	128 ± 3
100	79 ± 5	35 ± 5	160 ± 7
140	81 ± 6	35 ± 7	160 ± 20
200	107 ± 8	43 ± 9	270 ± 30
250	150 ± 10	72 ± 11	370 ± 45
300	190 ± 12	88 ± 14	400 ± 60

ELEM. SYM.	A	Z
S	32	16

METHOD

Linac; S.E.M. Monitor; NBS Ionization Chamber

[Page 1 of 2]

REF. NO.

66 B1 1

JDM

REACTION	RESULT	EXCITATION ENERGY	SOURCE		DETECTOR		ANGLE
			TYPE	RANGE	TYPE	RANGE	
G ₂ N	ABX	20 - 200	C	20 - 200	BF3-I		4PI

TABLE I. - In this Table are given the cross-sections measured in millibarn averaged over the energy ranges indicated in column 1. The contributions from the internal (I) and external (E) counters add together to give the total (T) cross-section.

		¹² C	²⁷ Al	S
Thres. ÷ 40 MeV	T	3.66	10.15	7.15
	E		0.80	0.70
	I	3.28	9.35	6.45
(40 ÷ 80) MeV	T	2.52	7.80	6.78
	E		1.35	1.48
	I	1.58	6.45	5.30
(80 ÷ 120) MeV	T	2.55	7.70	6.12
	E		1.87	2.27
	I	1.42	5.83	3.73
(120 ÷ 160) MeV	T	2.80	9.18	6.58
	E		3.00	2.66
	I	1.44	6.18	2.92
(160 ÷ 200) MeV	T	3.18	13.40	12
	E		3.25	3.60
	I	1.70	8.15	8.6

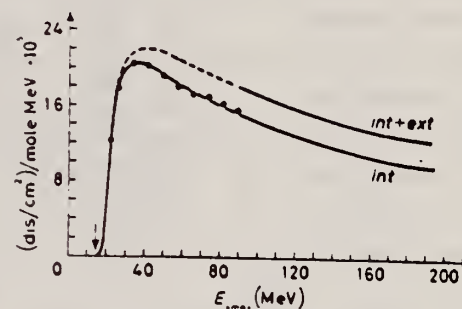


Fig. 5. - Sulphur yield.

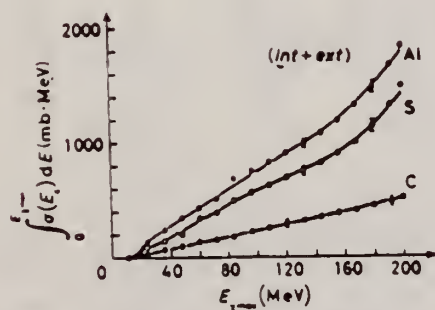


Fig. 9. - Total neutron integral cross-sections.

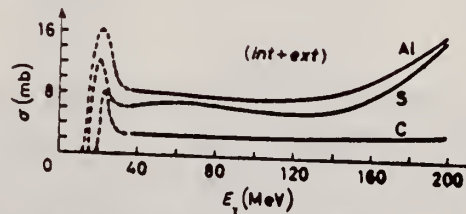


Fig. 10. - Total neutron differential cross-sections.

REACTION	RESULT	EXCITATION ENERGY	SOURCE		DETECTOR		ANGLE
			TYPE	RANGE	TYPE	RANGE	

TABLE II. - In this table the data from Table I are treated, as discussed in the text to give cross-sections corresponding to photoneutrons in the approximate energy ranges (0÷15) MeV and above 15 MeV. Thus the result a) corresponds to the relation $a = I - 0.4E$, and b) corresponds to $b = 1.4 \cdot E$.

	¹² C	²⁷ Al	S
Thres. ÷ 40 MeV	a) 3.13	9.03	6.17
	b) 0.53	1.12	0.98
(40 ÷ 80) MeV	a) 1.20	5.91	4.71
	b) 1.32	1.89	2.07
(80 ÷ 120) MeV	a) 0.97	5.08	3.35
	b) 1.58	2.62	3.35
(120 ÷ 160) MeV	a) 0.90	4.98	1.46
	b) 1.90	4.20	5.12
(160 ÷ 200) MeV	a) 1.11	6.05	6.95
	b) 2.07	7.35	5.05

a) = $I - 0.4E$, I = int. counter.
b) = $E \cdot 1.4$, E = ext. counter.

TABLE IV. - The total absorption cross-section for γ -rays is calculated by dividing the total neutron production cross-section by the neutron multiplicity. The result is given in the first column under each element and, for comparison, in the second column the value of b is inserted from Table II.

	¹² C		²⁷ Al		S	
(40 ÷ 80) MeV	2.2	1.3	0.0	1.9	5.2	2.1
(80 ÷ 120) MeV	1.8	1.6	4.7	2.6	3.7	3.4
(120 ÷ 160) MeV	1.8	1.9	4.6	4.2	3.4	5.1
(160 ÷ 200) MeV	1.7	2.1	5.7	7.4	5.1	5.1

TABLE VI.

	$\sigma_{int}^{(14)}$ 0 ÷ 35	$\sigma_{int}^{(14)}$ 35 ÷ 140	$\sigma_{int}^{(14)}$	$\sigma_{int}^{(16)}$	$\sigma_{int}^{(B.L.)}$
1	2	3	4	5	6
C	144	220	364 ± 40	373	252
Al	344	590	934 ± 100	840	567
S	466	382	848 ± 90	990	670

REF. P. Holmberg Comm. Phys.-Math. Ed. Soc. Sc. Fennica 31, 1 (1966)			ELEM. SYM.	A	Z
			S	32	16
METHOD			REF. NO. 66 Ho 1		JDM
REACTION	RESULT	EXCITATION ENERGY	SOURCE		ANGLE
			TYPE	RANGE	
P,G	SPC	10	D	1	55
			DETECTOR		
			TYPE	RANGE	
			NAI-D	1 - 10	

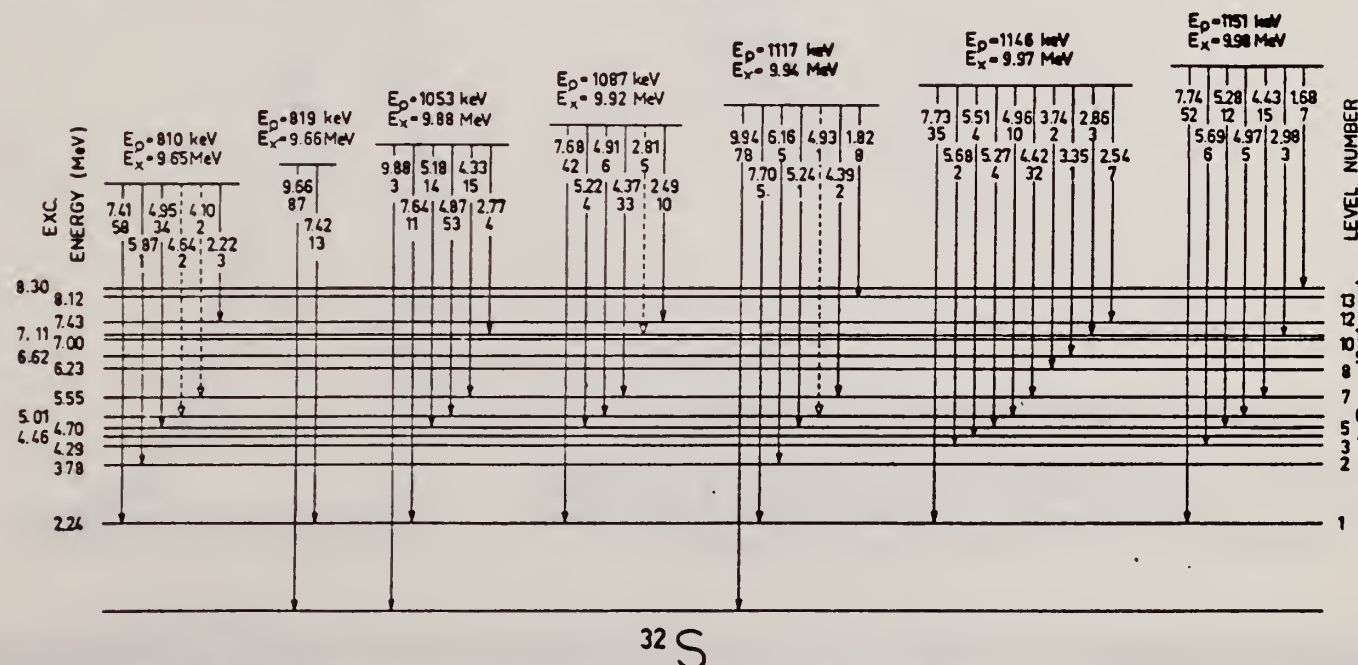
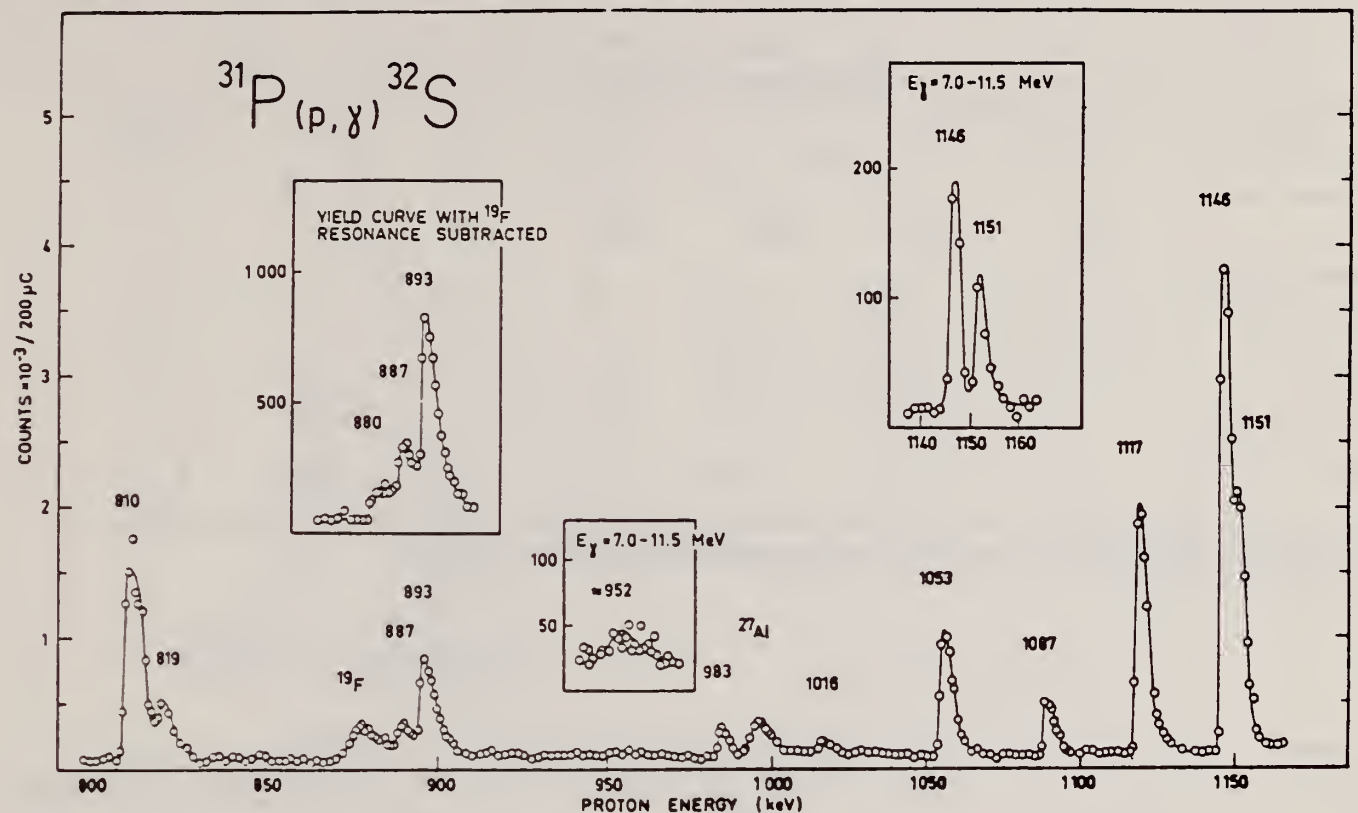


Fig. 9 The decay of resonance states excited in the $^{31}\text{P}(p,\gamma)^{32}\text{S}$ reaction as found in the present investigation.

ELEMENT	A	Z
S	32	16
REF. NO.		JDM
66 Ho 3		

METHOD

Betatron

REACTION	RESULT	EXCITATION ENERGY	SOURCE		DETECTOR		ANGLE
			TYPE	RANGE	TYPE	RANGE	
G,A	SPC	THR-31	C	31	SCD-D	3-13	130

TABLE I
Experimental data and results

Element	Mg	Al	S	Ni	Cu	Zn	Error (%)
target thickness (mg/cm ²)	0.81	1.54	0.80	2.50	2.68	3.00	5 ^{a)}
dose (r)	6190	25400	23200	3880	5840	4220	10
yield absolute (10 ⁶ /mole · r) for $E_m > 3.16$ MeV	0.61	0.93	1.46	1.65	0.92	2.42	11 ^{a)}
yield relative to Ni	0.36	0.56	0.88	1	0.55	1.43	5 ^{a)}
$Y_{\gamma,2}/Y_{\gamma,tot}(\%)$	9.6	11.4	12.4	7.0	3.2	^{b)}	
nuclear temp. θ (MeV)	1.43	1.48	1.46	1.04		0.91	10
level density parameter a (MeV ⁻¹)	5.1	4.8	4.9	8.6		10.8	10

^{a)} For S, the error of the target thickness has been 10 %, of the absolute yield 14 % and of the relative yield 10 %.

^{b)} For Zn $\sigma_{\gamma,tot}$ is not known.

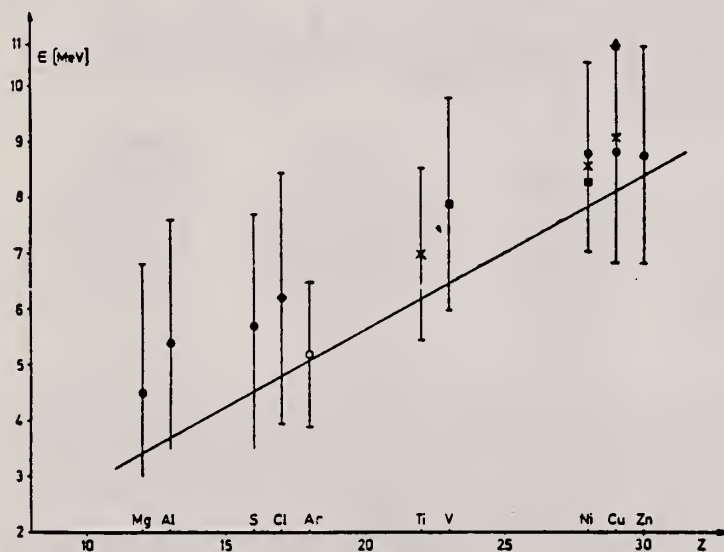


Fig. 4. Position of the peaks in different photoalpha spectra plotted against Z of the target nuclei. \times : Scheer *et al.*¹⁶⁾, \blacksquare : Kregar and Povh⁸⁾, \blacktriangle : Meneghetti and Vitale⁵⁾, \blacklozenge : Erdős *et al.*¹⁾, \circ : Komar *et al.*⁷⁾, \bullet : this work. The signs show the position of the maximum, the bars give the widths at half maximum. The curve shows the height of the Coulomb barrier.

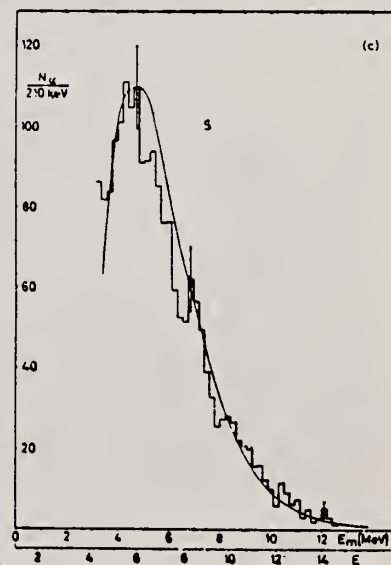


Fig. 3 (c)

elem. sym.		
S	32	16
REF. NO.		
67 An 2		egf

METHOD			SOURCE		DETECTOR		ANGLE
REACTION	RESULT	EXCITATION ENERGY	TYPE	RANGE	TYPE	RANGE	
G,XN	ABX	THR-26	C	13-26	BF3-I		4PI

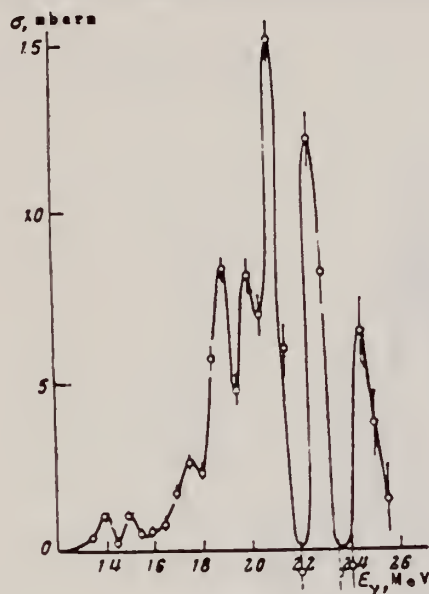


Fig.4

Fig.4. Total cross section for the (γ, n) reaction on ^{32}S .

REF.

ELEM. SYM.

A

Z

J. M. Loiseaux, J. M. Maison, and M. Langevin
J. de Physique 28, 11 (1967)

S

32

16

METHOD

REF. NO.

67 Lo 1

JOC

REACTION	RESULT	EXCITATION ENERGY	SOURCE		DETECTOR		ANGLE
			TYPE	RANGE	TYPE	RANGE	
G ₂ G/	ABX	14-32	C	34	NAI-D		DST

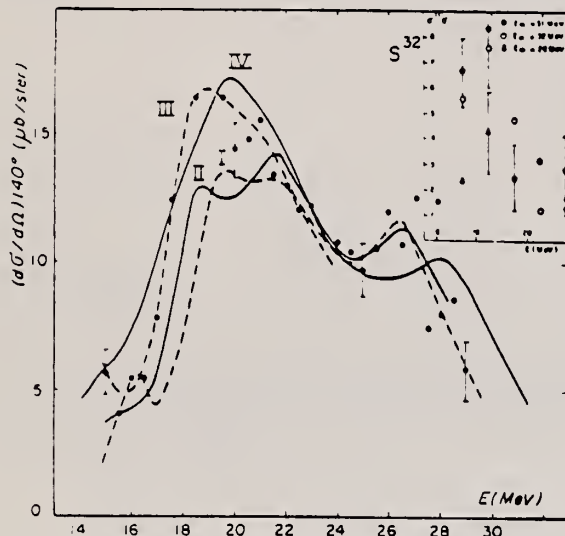


FIG. 8. — ^{32}S Section efficace différentielle de diffusion à 140° déterminée à $E_m = 25$ MeV (courbe I), $E_m = 28$ MeV (courbe II), $E_m = 32$ MeV (courbe III), $E_m = 34$ MeV (courbe IV).

$\sigma' - \frac{d\sigma}{d\Omega}$: contribution de la diffusion inélastique entre 16 et 22 MeV.

REF. D. V. Webb, B. M. Spicer, and H. Arenhovel
Phys. Rev. 164, 1397 (1967)

ELEM. SYM.	A	Z
S	32	16

METHOD	REF. NO.	
	67 We 1	HMG

REACTION	RESULT	EXCITATION ENERGY	SOURCE		DETECTOR		ANGLE
			TYPE	RANGE	TYPE	RANGE	
G,N	ABX	THR-32	C	20-32	ACT-I		4PI

$\int_{th}^{31.5} \sigma dE = 138 \pm 9 \text{ MeV mb.}$

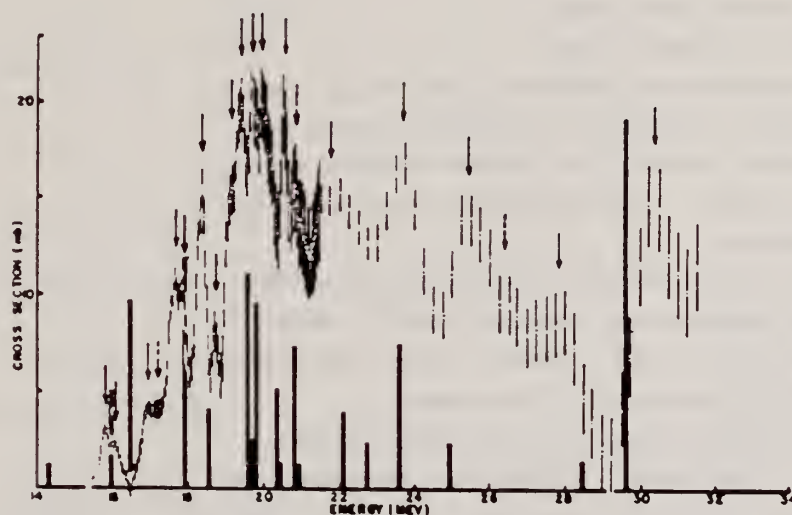


FIG. 1. The experimental cross section for the $S^{32}(\gamma,n)$ reaction, together with the predictions of the collective-correlations theory.

METHOD

REF. NO.

67 We 2

EGF

REACTION	RESULT	EXCITATION ENERGY	SOURCE		DETECTOR		ANGLE
			TYPE	RANGE	TYPE	RANGE	
G,N	ABX	20-32	C	20-32	ACT-I		4PI

The Sulphur Photoneutron Cross Section^{*}

D. V. Webb and B. M. Spicer

University of Melbourne, Australia

and

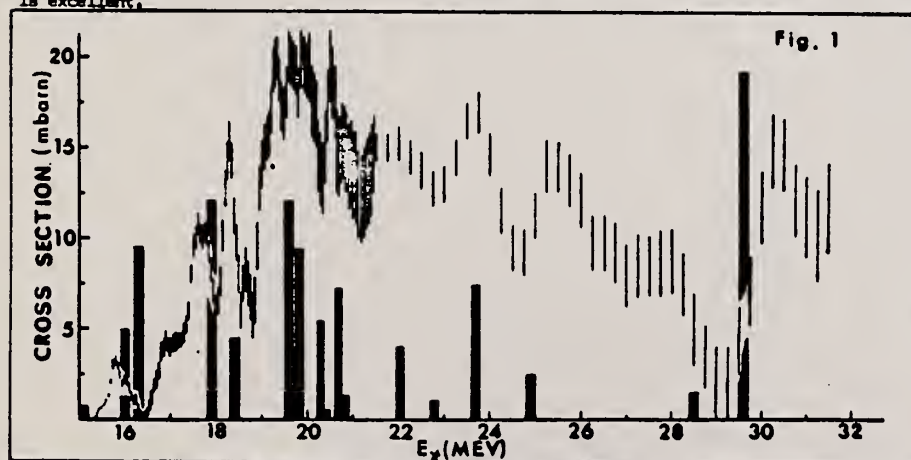
H. Arenhovel and W. Greiner

University of Frankfurt, Germany

The $S^{32}(\gamma, n)$ cross section has been measured from threshold to 22 MeV¹⁾ in 50 keV steps, and from 20 MeV to 32 MeV in 250 keV steps. The yield of S^{31} was measured by counting the annihilation radiation from the 2.6 second s^{+} -activity. The yield curve was analysed by the Leiss-Penfold method to give the cross section. Considerable structure is indicated even in the poorer resolution part of the measurement.

The particle-hole calculation²⁾ of the dipole states of S^{32} predicts the giant resonance maximum to be at about 19 MeV, in good agreement with the experimental result. In addition, strongly absorbing states are predicted at 22 and 29 MeV. However, there is far more structure in the experimental cross section than can be explained on this simple basis.

Consequently, the experimental data has been compared with a calculation of the giant resonance structure, including collective correlations. The dipole states were treated in the particle-hole framework, and the surface vibration phonons within the collective model. The coupling of the particle-hole states with the surface phonons is then treated in particle-hole language. The parameters for the collective quadrupole oscillator were taken from the low energy spectrum of S^{32} , while the strength of the residual interaction in the particle-hole framework remained as a free parameter. The agreement with experiment is shown in Fig. 1 and is excellent.



^{*}Supported in part by a grant from the U.S. Army Research Office.

References: 1) M. N. Thompson et al: Phys. Letters 14 (1965) 223.

2) B. M. Spicer: Aust.J.Phys. 18 (1965) 1.

U.S. DEPARTMENT OF COMMERCE
 NATIONAL BUREAU OF STANDARDS

REF.

B. C. Cook, D. W. Anderson, T. J. Englert
Phys. Letters 26B, 341 (1968)

ELEM. SYM.

A

Z

S

32

16

METHOD

REF. NO.

68 Co 1

HMG

REACTION	RESULT	EXCITATION ENERGY	SOURCE		DETECTOR		ANGLE
			TYPE	RANGE	TYPE	RANGE	
G, N	RLX	THR- 65	C	13- 65	ACT-I		4PI

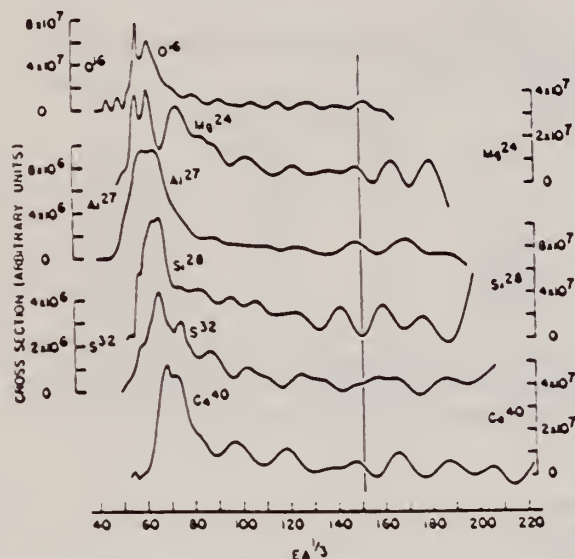


Fig. 1. Cross section for elements in the s-d shell as a function of $EA^{1/2}$. The vertical line is only an aid to the eye. Universal curves expected for the hydrodynamical model are not evident.

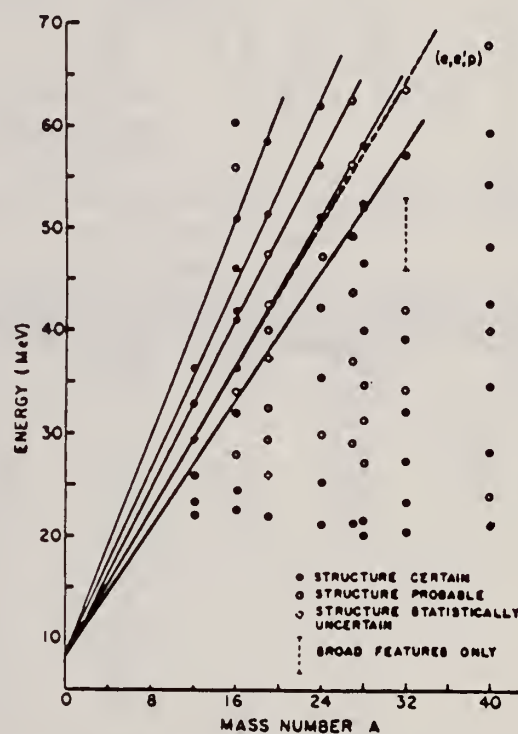


Fig. 2. A dependence of structure. A qualitative estimate for the statistical validity for structure is also indicated. The solid straight lines have the form $mA + 8$ MeV while the dashed line represents the position of the 1s level as determined from (e,e'p) experiments.

REF.

L. Meyer-Schutzmeister, Z. Vager, R. E. Segel and P. P. Singh
Nucl. Phys. **A108**, 180 (1968)

ELEM. SYM.

A

Z

S

32

16

METHOD

REF. NO.

[Page 1 of 2]

68 Me 1

EGF

REACTION	RESULT	EXCITATION ENERGY	SOURCE		DETECTOR		ANGLE
			TYPE	RANGE	TYPE	RANGE	
$A_{\alpha}G$	ABX	13-18	D	7-12	NAT-D	10-18	DST

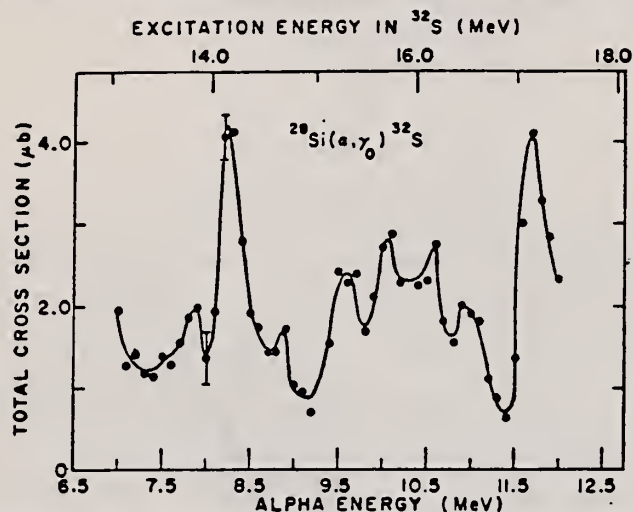


Fig. 15. The absolute cross section for the reaction $^{28}\text{Si}(\alpha, \gamma)^{32}\text{S}$ as a function of the energy of the incident α -beam. It was calculated on the assumption that the angular distributions had a $\sin^2 \theta$ dependence (typical for an electric-dipole transition) over the entire studied energy region. The SiO target had a thickness of $520 \mu\text{g}/\text{cm}^2$.

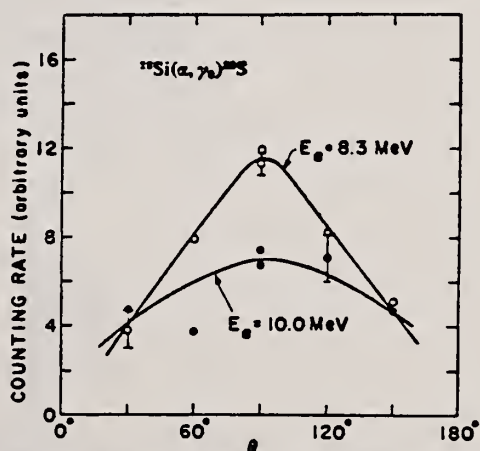


Fig. 16. The angular distribution of the $^{28}\text{Si}(\alpha, \gamma)^{32}\text{S}$ reaction at $E_{\alpha} = 8.3$ and 10.3 MeV.

METHOD

REF. NO.

[Page 2 of 2]

68 Me 1

EGF

REACTION	RESULT	EXCITATION ENERGY	SOURCE		DETECTOR		ANGLE
			TYPE	RANGE	TYPE	RANGE	

TABLE 1

The averaged absolute cross sections $\sigma(\alpha, \gamma_0)$ and $\sigma(\alpha, \gamma_1)$ for the reactions $^{24}\text{Mg}(\alpha, \gamma_0)$, $^{24}\text{Mg}(\alpha, \gamma_1)$, $^{26}\text{Mg}(\alpha, \gamma_0)$ and $^{28}\text{Si}(\alpha, \gamma_0)$

ΔE_x (MeV)	$^{24}\text{Mg}(\alpha, \gamma)^{28}\text{Si}$		$^{26}\text{Mg}(\alpha, \gamma_0)^{30}\text{Si}$		$^{28}\text{Si}(\alpha, \gamma_0)^{32}\text{S}$	
	$\sigma(\alpha, \gamma_0)$ (μb)	$\sigma(\alpha, \gamma_1)$ (μb)	ΔE_x (MeV)	$\sigma(\alpha, \gamma_0)$ (μb)	ΔE_x (MeV)	$\sigma(\alpha, \gamma_0)$ (μb)
14.65-16.65	8.5	5.0	14.1-16.1	6.1	13.1-15.5	1.7
16.65-18.65	12.9	6.1	16.1-18.1	9.7	15.5-17.5	2.2
18.65-20.65	11.0	8.6	18.1-20.1	4.6		
20.65-22.65	2.1	5.6	20.1-22.1	1.0		
14.65-22.65	8.6	6.3	14.1-22.1	5.3	13.1-17.5	1.9

The cross sections in the first four rows were obtained from the data in figs. 3-6 and 15 by averaging over the indicated ≈ 2 MeV ranges of excitation energy E_x in the product nucleus (^{28}Si , ^{30}Si or ^{32}S). The last line gives the average for the entire energy range that was studied.

TABLE 3

The cross sections $\sigma(\gamma, \alpha_0)$ for the α -decay of the nuclei ^{28}Si , ^{30}Si and ^{32}S

Target nucleide	ΔE (MeV)	$\sigma(\gamma, \alpha_0)$ (mb)	$\sigma(\gamma, p_0)$ (mb)	$\frac{\sigma(\gamma, \alpha_0)}{\sigma(\gamma, p_0)}$	$\gamma^2(\alpha_0)/\gamma^2(p_0)$	
					$l = 1$	$l = 3$
^{28}Si	16.65-18.65	1.01	6.2	0.16	0.35	0.12
	18.65-20.65	0.94	11.7	0.080	0.095	0.041
	20.65-22.65	0.22	9.6	0.023	0.019	0.011
	16.65-22.65	0.72	9.2	0.08		
^{30}Si	14.1-16.1	0.43				
	16.1-18.1	0.69				
	18.1-20.1	0.35				
	18.1-20.1	0.35				
	20.1-22.1	0.08				
	14.1-22.1	0.38				
^{32}S	13.1-15.5	0.20	1.7	0.12		
	15.5-17.5	0.27	2.1	0.13		
	17.5-19.5		3.0			
	13.1-17.5	0.23	1.9	0.12		

The averages were taken over ≈ 2 MeV wide energy regions ΔE and over the total studied energy region of the giant dipole resonance. These cross sections were obtained by detailed balance from the α -capture in ^{24}Mg , ^{26}Mg and ^{28}Si . For comparison, the average cross sections $\sigma(\gamma, p_0)$ over the same energy regions ΔE for the reactions $^{28}\text{Si}(\gamma, p_0)^{27}\text{Al}$ and $^{32}\text{S}(\gamma, p_0)^{31}\text{P}$ are also presented. These likewise were obtained by detailed balance from the inverse reactions as measured by Singh *et al.* ⁴⁾ and by Dearnaley *et al.* ⁵⁾. For the calculation, we assumed an isotropic angular distribution for the $^{28}\text{Si}(\gamma, p_0)$ reaction, a $\sin^2 \theta$ distribution for $^{32}\text{S}(\gamma, p_0)$. In addition, the ratios $\sigma(\gamma, \alpha_0)/\sigma(\gamma, p_0)$ are given for both ^{28}Si and ^{32}S and also the calculated reduced width $\gamma^2(\alpha_0)/\gamma^2(p_0)$ for an orbital-angular-momentum transfer of $l = 1$ and of $l = 3$ in the decay of ^{28}Si .

METHOD

REF. NO.

[Page 1 of 2]

68 Sh 3

egf

REACTION	RESULT	EXCITATION ENERGY	SOURCE		DETECTOR		ANGLE
			TYPE	RANGE	TYPE	RANGE	
G, XP	SPC	17-20	D	17, 20	EMU-D	2-14	DST

Table II. Anisotropic factor B/A of angular distributions determined by least-squares fits with $A+B\sin^2\theta$.

^{25}S					
$(E_{\gamma\text{max}}=17.0\text{ MeV})$		$(E_{\gamma\text{max}}=24.0\text{ MeV})$		$(\text{Curve } D \text{ in Fig. 3})$	
$E_{\gamma}(\text{MeV})$	B/A	$E_{\gamma}(\text{MeV})$	B/A	$E_{\gamma}(\text{MeV})$	B/A
4.0-5.1	0.9 ± 0.1	3.6-5.2	0.2 ± 0.1	3.6-5.2	0.1 ± 0.1
5.1-5.7	2.4 ± 0.7	5.2-6.0	0.7 ± 0.1	5.2-6.0	0.5 ± 0.2
5.7-7.1	$\infty^{(1)}$	6.0-7.2	0.8 ± 0.2	6.0-7.2	0.4 ± 0.2
7.1 \leq	$\infty^{(1)}$	7.2-7.7	0.6 ± 0.2	7.7-9.0	1.1 ± 0.2
4.0 \leq	2.8 ± 0.4	7.7-9.0	1.1 ± 0.2	9.0-10.3	2.7 ± 1.2
		9.0-10.8	2.7 ± 1.2	10.8 \leq	$\infty^{(1)}$
		10.8 \leq	$\infty^{(1)}$		
		3.6 \leq	0.7 ± 0.1		

⁽¹⁾ The notation ∞ indicates that the distribution is almost $\sin^2\theta$. It is used when the result has stronger maximum than that of $1+10\sin^2\theta$.

Table III. Anisotropic factor B/A of angular distributions estimated for the groups of strong transitions.

	Assumed residual Energy (MeV)	E_{γ} (MeV)	B/A	Used data ⁽¹⁾
^{22}Na	1.27	18.8-20.5	0.5 ± 0.4	20.5
	3.3	20.8-22.1	$\infty^{(1)}$	D
	7.0	22.1-24	$\infty^{(1)}$	24.0
^{31}P		20.7-22.7	1.5 ± 0.3	D
	0	15.7-21	$\infty^{(1)}$	24.0, 19.0
	7.0	17.4-20.2	0.5 ± 0.6	D
^{32}S		20.2-22.7	1.3 ± 1.3	D
	0	14-20	$\infty^{(1)}$	(p, γ)
		14-14.8	2.4 ± 0.7	17.0
		14.8-16.2	$\infty^{(1)}$	17.0
		16.2-17.1	$\infty^{(1)}$	17.0
	5.0	19.2-20.1	0.5 ± 0.2	D
		20.1-21.3	0.4 ± 0.2	D
^{40}Ca	0	17.1-20.5	1.5 ± 0.2	20.5
	2.8	17.4-19.9	2.6 ± 0.3	20.5
	6.0	17.2-18.7	0.05 ± 0.09	20.5
		18.7-20.5	0.6 ± 0.1	20.5

- a) The numerical number indicates the maximum energy of the bremsstrahlung irradiated for the data. D shows the difference between the two distributions. (p, γ) shows the inverse reaction data.
b) The notation ∞ indicates that the distribution is almost $\sin^2\theta$, i.e., the result has stronger maximum than $1+10\sin^2\theta$.

REF. K. Shoda, K. Abe, T. Ishizuka, N. Kawamura, M. Oyama,
and Baik-Nung Sung
J. Phys. Soc. Japan 25, 664 (1968)

ELEM. SYM.	A	Z
S	32	16

METHOD

REF. NO.	egf
68 Sh 3	

[Page 2 of 2]

REACTION	RESULT	EXCITATION ENERGY	SOURCE		DETECTOR		ANGLE
			TYPE	RANGE	TYPE	RANGE	

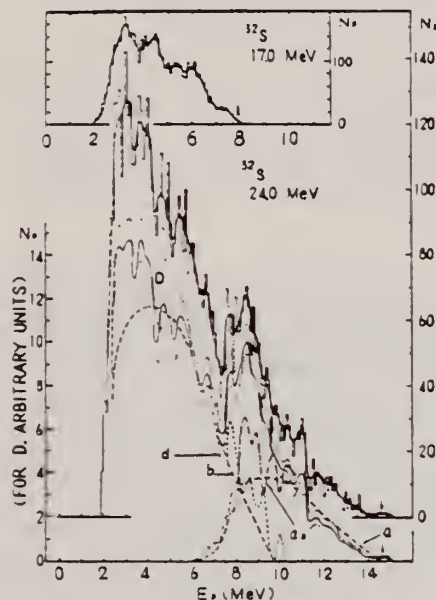


Fig. 3. Energy distributions of photoprotons from ^{32}S irradiated with 17.0 MeV 24.0 MeV bremsstrahlung. See also the caption of Fig. 1 for curves *D*, *a* and *b*. Here *a* and *b* correspond to the ground and 5.0 MeV state of residual nucleus respectively. Curve *a*₀ is the component spectrum on residual ground state calculated from the $^{31}\text{P}(p, \gamma)^{32}\text{S}$ reaction.¹⁰ Curve *d* is a difference spectrum between *a*₀ and *D*.

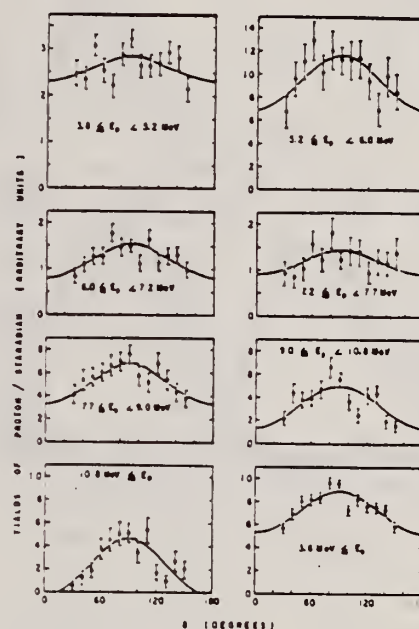


Fig. 7. Angular distributions of photoprotons from ^{32}S irradiated with 24.0 MeV bremsstrahlung. Curves from least-squares fits are shown. (See also Table II.)

REF.

S.V. Dementii, M.G. Afanas'ev, E.M. Arkatov, V.G. Vlasenko,
V.O. Gol'dshtein, E.L. Kuplennikov and V.I. Startsev
Ukr. Fiz. Zhur. 14, 1911 (1969)

ELEM. SYM. A Z

S

32

16

METHOD

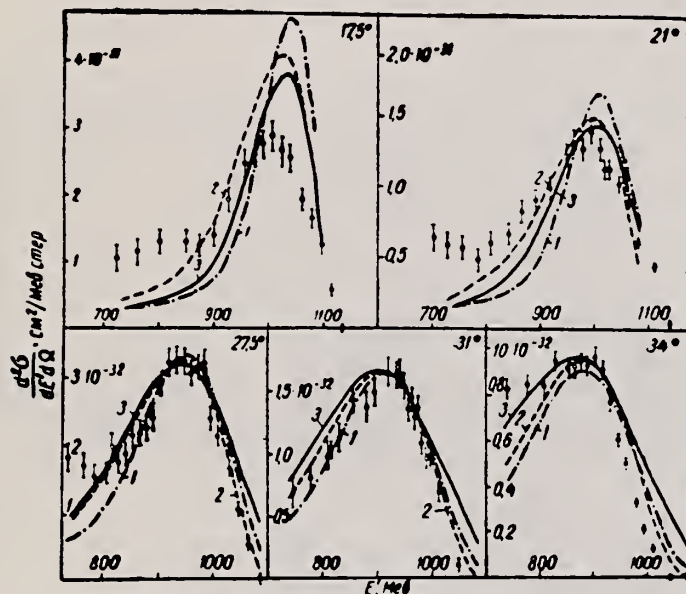
REF. NO.

69 De 8

egf

REACTION	RESULT	EXCITATION ENERGY	SOURCE		DETECTOR		ANGLE
			TYPE	RANGE	TYPE	RANGE	
E, E/	ABX	0-200	D	999	MAG-D		DST

999=1.11 GEV, QUASI-EL



3615 QUASI-ELASTIC SCATTERING OF 1115-MeV ELECTRONS BY NUCLEONS OF ^{23}S NUCLEI. Dementii, S. V.; Afanas'ev, N. G.; Arkatov, I. M.; Vlasenko, V. G.; Gol'dshtein, V. A.; Kuplennikov, E. L.; Startsev, V. I. (Kharkov Inst. of Physics and Tech.). Ukr. Fiz. Zh.; 14: 1911-12 (Nov 1969). (In Russian).

Previously, it was shown that inelastic scattering of electrons on ^{12}C and ^{28}Si nuclei at large excitation energies of the first continuum in the electron spectrum can be described by the mechanism of quasi-elastic scattering on intra-nuclear nucleons. Data obtained for scattering of 1115-MeV electrons on ^{23}S nuclei in the region of the quasi-elastic continuum at 17.5, 21, 27.5, 31, and 34° were analyzed. It was observed that the mean square radius of the distribution of the charge in ^{23}S nucleus $\langle Z^2 \rangle^N = 2.5 \pm 0.2f$, obtained on the basis of the quasi-elastic method, differed 20% from the $\langle Z^2 \rangle^N = 3.12f$ magnitude obtained by the method of elastic electron scattering. A similar discrepancy (13%) was observed earlier in the case of ^{12}C and ^{28}Si radii calculated according to the quasi-elastic electron scattering and elastic electron scattering. (R.V.J.)

METHOD

REF. NO.

69 Gu 3

hmg

REACTION	RESULT	EXCITATION ENERGY	SOURCE		DETECTOR		ANGLE
			TYPE	RANGE	TYPE	RANGE	
E, E/	FMF	13-31	D	120-200	MAG-D		DST

Table I. Absolute differential cross sections and form factor for the giant resonance for S^{32} . The integration of the spectra was carried out between the limits 13 and 31 MeV

θ , deg	E , MeV	$d\sigma/d\Omega$, cm ² /sr	q , F ⁻¹	q' , F ⁻¹	$F_A^2(q)$	$V_L(q)$ $V_T(q)$
20	100.1	$(7.21 \pm 2.88) \cdot 10^{-28}$	0.34	0.35	$(2.01 \pm 0.81) \cdot 10^{-2}$	1.71
30	98.9	$(1.85 \pm 0.33) \cdot 10^{-28}$	0.50	0.51	$(2.24 \pm 0.48) \cdot 10^{-2}$	1.67
40	100.0	$(7.02 \pm 1.40) \cdot 10^{-28}$	0.66	0.67	$(3.24 \pm 0.65) \cdot 10^{-2}$	1.54
50	109.3	$(2.22 \pm 0.33) \cdot 10^{-28}$	0.81	0.83	$(2.57 \pm 0.39) \cdot 10^{-2}$	1.37
60	109.1	$(6.23 \pm 1.12) \cdot 10^{-28}$	0.96	0.98	$(1.55 \pm 0.28) \cdot 10^{-2}$	1.18
60	122.0	$(2.84 \pm 0.65) \cdot 10^{-28}$	0.57	0.59	$(2.65 \pm 0.8) \cdot 10^{-2}$	1.15

Table III. Fine structure of S^{32} giant resonance

Our data (e.s.)	Total absorption		Reaction (γ, n) [1]	Reaction (γ, p) [1]	Particle-hole theory [2]	Dynamic collective theory [4]
	[1]	[1]				
	< 15				11.24 13.42 13.99	14.3
16.6 ± 0.2	16.7	16.0	16.0 16.8	15.2 15.6	14.75	16.0 16.6
	(17.5)		17.5	17.6	17.44	
18.2 ± 0.2	18.1			18.1 18.8	18.34	18.0 18.6
19.8 ± 0.2	19.6	19.7	19.0 19.6	19.6		19.5 19.8
21.0 ± 0.1	21.6	21.0	20.5 21.5	20.4		20.3 20.8
22.6 ± 0.2	22.4			22.0		22.1 22.7 23.6
24.6 ± 0.2	23.5		23		23.97	25
	25.4		27			28.4
29.8 ± 0.2	30					29.7

Note. The level energies are given in MeV

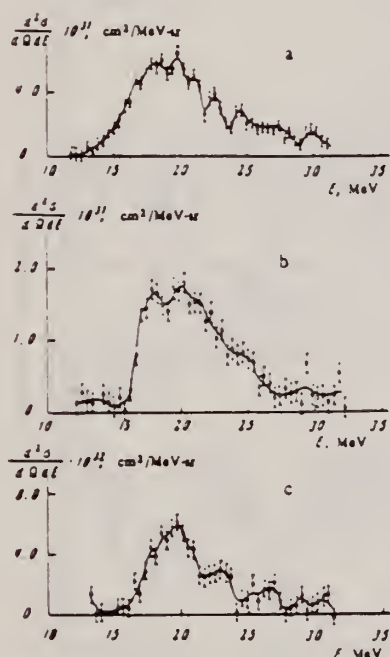


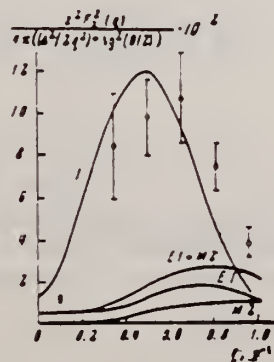
FIG. 1. Energy spectra of electrons inelastically scattered with excitation of the giant resonance in S^{32} . Initial electron energy is $E_0 = 200$ MeV; a - $\theta = 40^\circ$, $q = 131$ MeV/c; b - $\theta = 50^\circ$, $q = 161$ MeV/c; c - $\theta = 60^\circ$, $q = 190$ MeV/c.

Table II. Parameters obtained from analysis of data on excitation of giant resonance in S^{32}

Parameters	Heim's model	Liquid-drop model	Model-independent method
χ^2	2.7	4.8	0.6
n	3	3	4
$B(E1, 0^+ \rightarrow 1^-)$, $e^2 \beta^2$	5.0 ± 0.6	5.3 ± 1.1	3.6 ± 0.5
Γ , keV	139 ± 1.6	14.7 ± 2.9	10.0 ± 1.4
G	2.5 ± 0.3	2.6 ± 0.5	1.8 ± 0.3
C_1 , MeV		1393 ± 278	
B_1 , MeV sec ⁻²		$(1.51 \pm 0.31) \cdot 10^{-43}$	
β_1^d		0.15 ± 0.02	
$\langle f \parallel r \parallel i \rangle$, F			1.89 ± 0.13
$\langle f \parallel r^2 \parallel i \rangle$, F ²			22.0 ± 3.9
trans, F			3.41 ± 0.19

Note. χ^2 is the criterion of quality of fit, n is the number of degrees of freedom, $B(E1, 0^+ \rightarrow 1^-)$ is the reduced transition probability, Γ and G are the radiative width and the collectiveness of the transition, C_1 and B_1 are the oscillator parameters of the nucleus, β_1^d is the deformation parameter $\langle f \parallel r \parallel i \rangle$ and $\langle f \parallel r^2 \parallel i \rangle$ are the transition matrix elements, and R_{trans} is the transition radius of the nucleus.

FIG. 2. The quantity $z^2 F_A^2(q)/4\pi [(\Delta^2/2q^2) + \lg^2(\theta/2)]$ for the S^{32} giant resonance, as a function of momentum transfer. Points: \circ - our data; point in lower left corner - photon point. [6]



B.S. Dolbilkin, A.I. Isakov, V.I. Korin, et al., Yad. Fiz. 8, 1080 (1968) [Sov. J. Nucl. Phys. 8, 625 (1969)].

[OVER]

³L.L. Hill and H. Überall, Phys. Letters 24B, 364 (1967).

⁴D. V. Webb, B. M. Spicer, and H. Arenhövel, Phys. Rev. 164, 1397 (1967).

⁹J.M. Wyckoff, B. Ziegler, H.W. Koch, and R. Uhlig Phys. Rev. 137, B576 (1965).

¹⁰V.G. Shevchenko, Proc. of the Intern. Conf. on Electromagnetic Interactions, Dubna, 2, 1967, p.206

¹¹M. Kimura, K. Shoda, and N. Mutsuro, et al., J. Phys. Soc. Japan 18, 477 (1963).

METHOD

REF. NO.

[Page 1 of 4]

69 Ma 5

egf

REACTION	RESULT	EXCITATION ENERGY	SOURCE		DETECTOR		ANGLE
			TYPE	RANGE	TYPE	RANGE	
P,G	ABX	18-21	D	9-12	NAI-D	15-25	DST

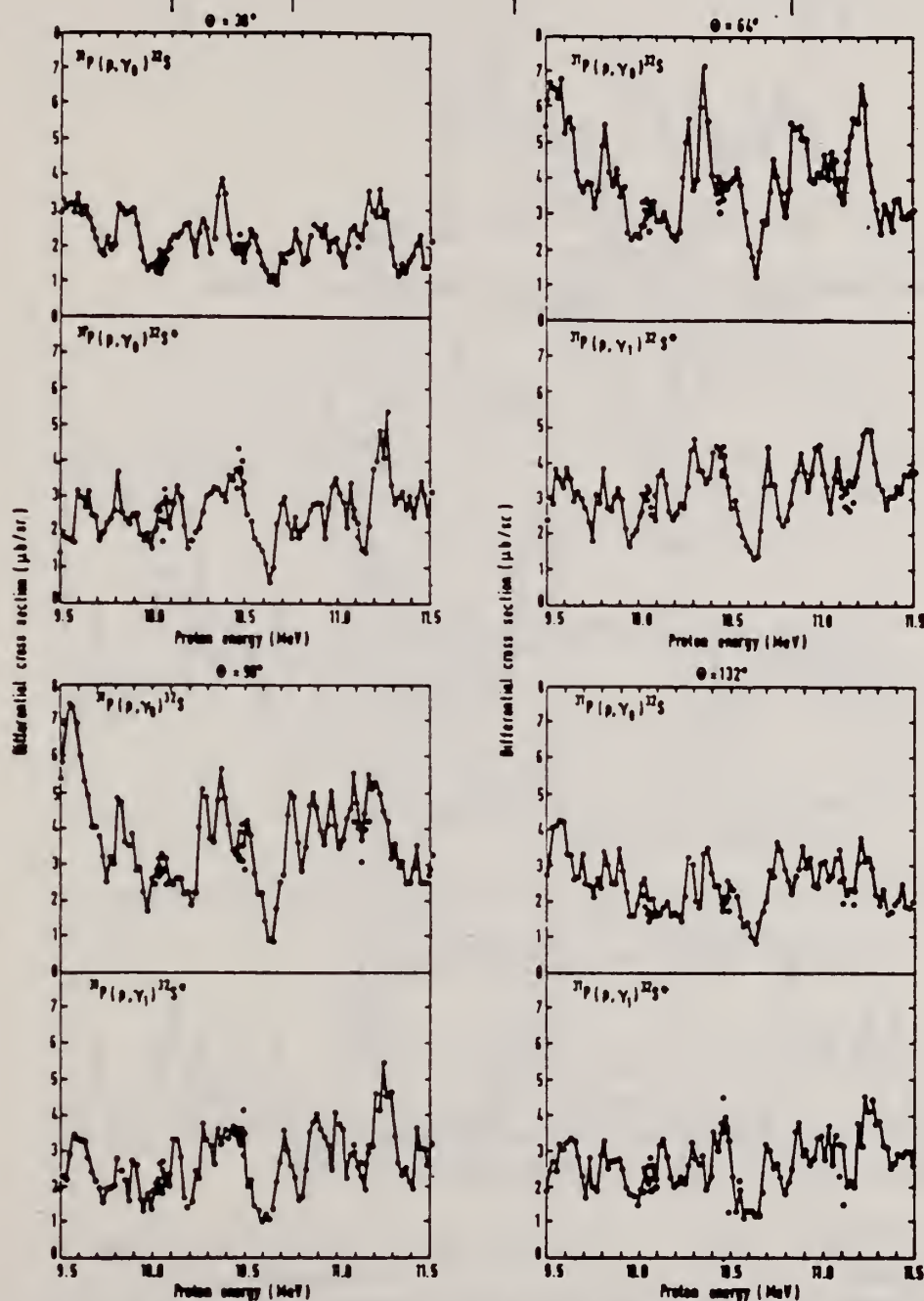


Fig. 3. (a) Excitation functions for the reactions $^{21}\text{P}(p, \gamma_0)^{22}\text{S}$ and $^{21}\text{P}(p, \gamma_1)^{22}\text{S}$ at $\theta = 30^\circ, 64^\circ, 98^\circ$ and 132° obtained with $12.5 \text{ cm} \times 15 \text{ cm}$ NaI(Tl) crystals.

[over]

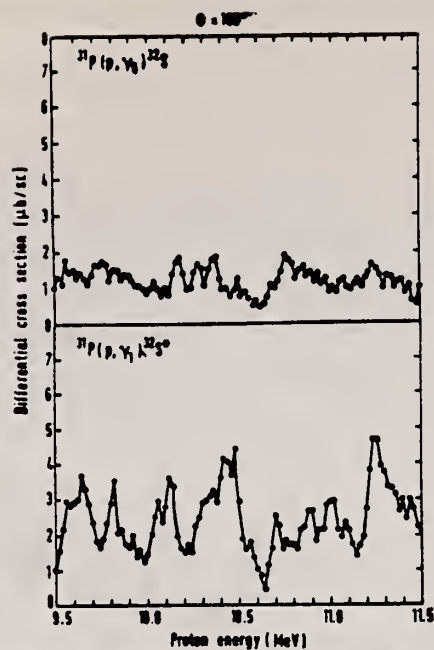


Fig. 3. (b) Excitation functions for the reactions $^{31}\text{P}(p, \gamma_0)^{32}\text{S}$ and $^{31}\text{P}(p, \gamma_1)^{32}\text{S}$ at $\theta = 160^\circ$ taken with the 24×30 cm NaI(Tl) crystal.

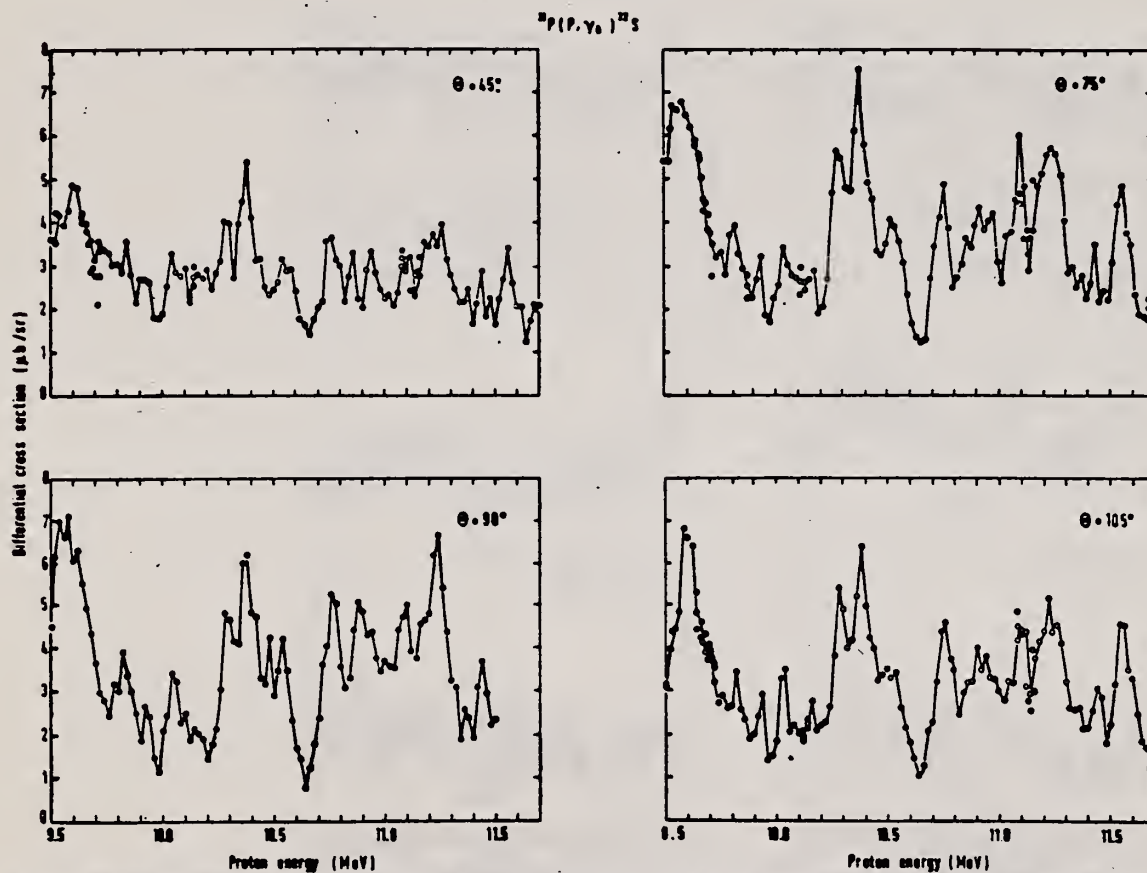


Fig. 4. Excitation functions for the reaction $^{31}\text{P}(p, \gamma_0)^{32}\text{S}$ at $\theta = 45^\circ, 75^\circ, 90^\circ$ and 105° obtained with 12.5×15 cm NaI(Tl) crystals.

METHOD

REF. NO.

[Page 3 of 4]

69 Ma 5

egf

REACTION	RESULT	EXCITATION ENERGY	SOURCE		DETECTOR		ANGLE
			TYPE	RANGE	TYPE	RANGE	

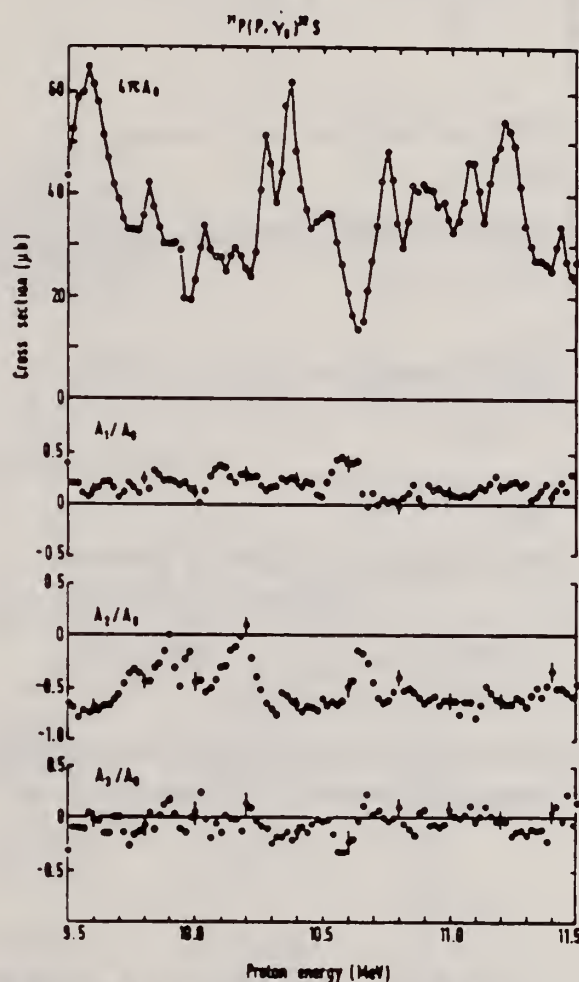


Fig. 6. The integrated cross section $4\pi A_0$ and coefficients A_i/A_0 for the reaction $^{11}\text{P}(p, \gamma_0)^{12}\text{S}$ obtained from fitting the angular distributions to the series $W(\theta) = \sum_{i=0}^3 A_i P_i(\cos \theta)$.

[over]

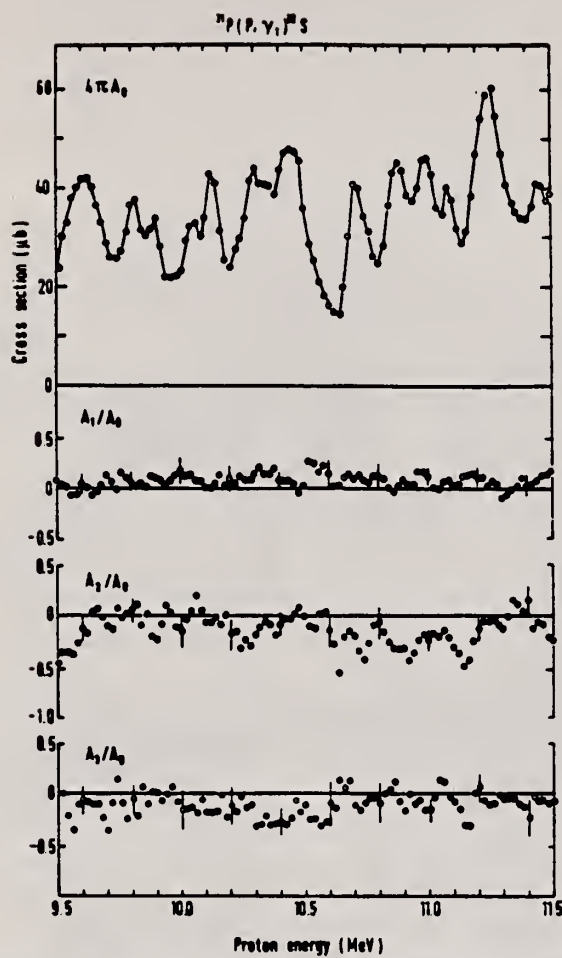


Fig. 7. The integrated cross section $4\pi A_0$ and coefficients A_i/A_0 for the reaction $^{31}\text{P}(p, \gamma)^{32}\text{S}$ obtained from fitting the angular distributions to the series $W(\theta) = \sum_{i=0}^3 A_i P_i(\cos \theta)$.

REF. NO.

69 P1 1

HMG

METHOD

REACTION	RESULT	EXCITATION ENERGY	SOURCE		DETECTOR		ANGLE
			TYPE	RANGE	TYPE	RANGE	
P,G	LFT	4-11	D	1-2	SCD-D	0-10	DST
				(1.248-1.583)			(55,90)

Lifetime measurements for ground state decays were made for levels at: 4.280, 4.694, 5.006, 5.544 MeV.

³²S BRANCHING RATIOS

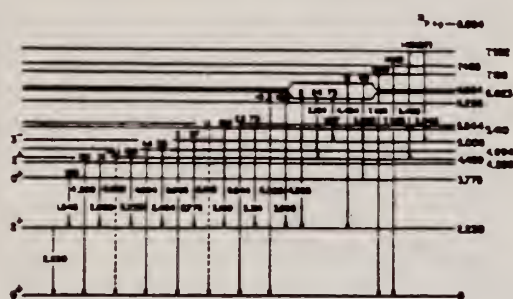


FIG. 5. Summary of the measured branching ratio for the low-lying states in ³²S.

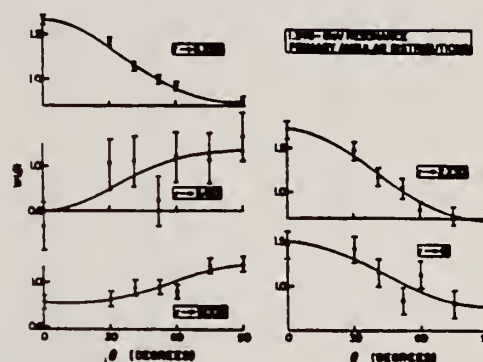


FIG. 6. Primary angular distributions measured at the 1.248-MeV resonance. Solid curves are least-squares fits to Eq. (4).

TABLE II. Summary of lifetime measurements.

Level (MeV)	Present results		Other (psec)
	P(γ)	τ (psec)	
3.775	0.052±0.015	0.52 _{-0.10} ^{+0.20}	1.00 ^a
4.280	0.726±0.008	0.029±0.002	0.074 ^a 0.035 _{-0.008} ^{+0.008} b
4.694	0.103±0.009	0.53±0.05	0.49 ^a
5.006	0.022±0.010	1.50 _{-0.70} ^{+0.80}	0.75 ^a 0.66 _{-0.18} ^{+0.20} b
5.410	0.415±0.011	0.097±0.005	0.19 ^a
5.544	0.640±0.174	0.043±0.035	0.064±0.001 ^b
6.226	0.380±0.092	0.11 _{-0.08} ^{+0.08}	0.064±0.007 ^a
6.623	0.145±0.025	0.37±0.08	0.57 _{-0.27} ^{+0.30} b
6.664	0.57±0.05	0.054 _{-0.008} ^{+0.012}	
7.952	>0.94	<0.01	

^a Reference 23.

^b Reference 24.

²³ R. Ollerhead, T. Alexander, and O. Hausser, *Phys. Rev. Lett.* **13**, 87 (1968).

²⁴ H. Evans, B. Castel, J. Montague, R. Paulson, and W. Zuk, *Phys. Rev. Lett.* **13**, 87 (1968).

TABLE I. Summary of branching ratios in percent of total γ decay from resonant state.

Final state (MeV)	1.248 MeV ($E^* = 10.073$)		1.438 MeV ($E^* = 10.257$)		1.556 MeV ($E^* = 10.371$)		1.583 MeV ($E^* = 10.398$)	
	a	b	a	b	a	b	a	b
0	2	2	<0.1	...	<0.5	1	<0.5	...
2.230	29	32	1	<1	11	10	<1	<1
4.280	2	4			40	35	2	3
4.459			9	10			1	8
4.694	2	3			11	5	...	3
5.006	14	12	5	10	2	5	7	10
5.410	4	...			12	...		
5.544	...	3			4	10		
6.226	47	42	...	4	3	4	...	3
6.623			76	60	...	15	85	58
6.664					13	...		
7.11	...	2	...	1	...	8	...	5
7.188					1	...		
7.43			...	4	...	8	...	5
7.485					2	...		
7.952			9	...			4	...
8.30			...	4			...	5

Present work.

Reference 10.

¹⁰S. Anderson, Physica Norvegica 1, 247 (1965)

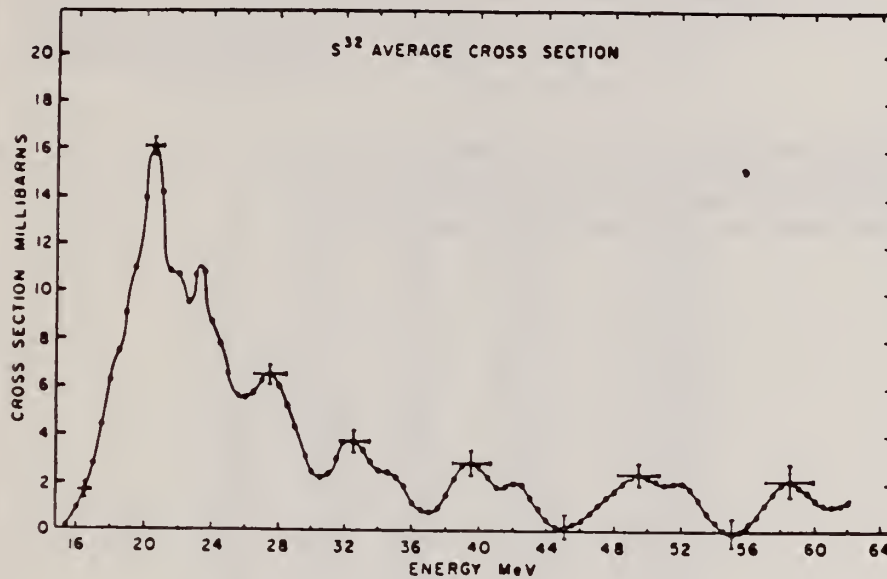
METHOD

REF. NO.

70 An 3

egf

REACTION	RESULT	EXCITATION ENERGY	SOURCE		DETECTOR		ANGLE
			TYPE	RANGE	TYPE	RANGE	
G,XN	ABX	15-62	C	16-62	ACT-I		4PI



284+ S16 (G,N + G,2N)

Fig. 4. The least-structure cross-section solution for the reactions $^{32}\text{S}(\gamma, n)^{31}\text{S}$ and $^{32}\text{S}(\gamma, 2n)^{30}\text{S}$ is shown. The cross section is most accurately represented by $\sigma = 1.0 \sigma_n + 0.8 \sigma_{2n}$ since the experimental timing cycle was less efficient for accumulating ^{30}S yield than for ^{31}S yield because of the half-life differences.

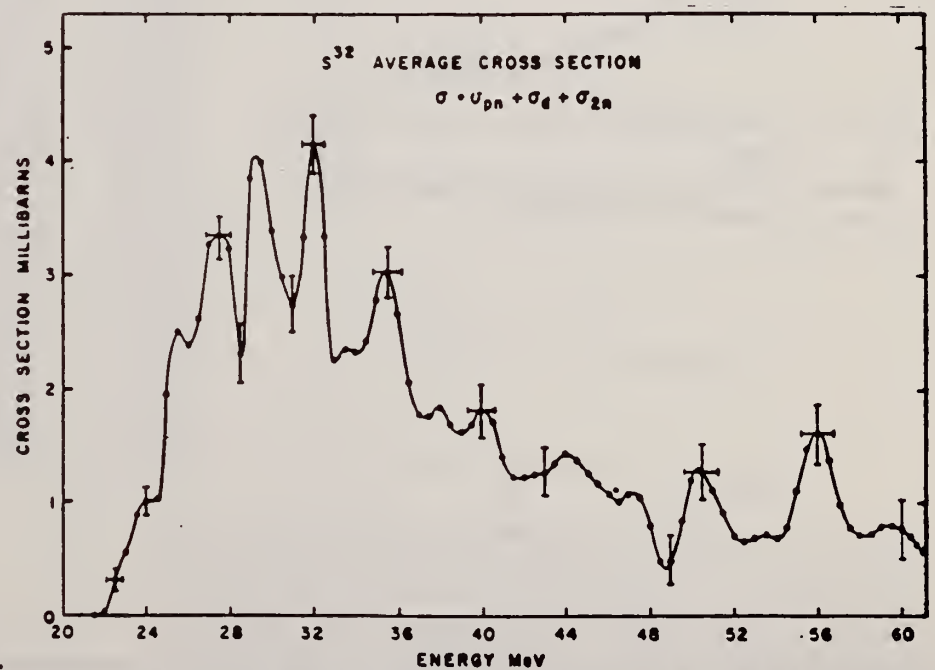


Fig. 5. The least-structure cross-section solution for the reactions $^{32}\text{S}(\gamma, pn)^{30}\text{P}$, $^{32}\text{S}(\gamma, d)^{30}\text{P}$ and $^{32}\text{S}(\gamma, 2n)^{30}\text{S}$ is shown.

REF. B.S. Ishkhanov, I.M. Kapitonov, E.V. Lazutin, I.M. Piskarev,
V.S. Sopov, V.G. Shevchenko
Yad. Fiz. 12, 224 (1970)
Sov. J. Nucl. Phys. 12, 121 (1971)

ELEM. SYM.	A	Z
S	32	16
REF. NO.		hmg
70 Is 2		

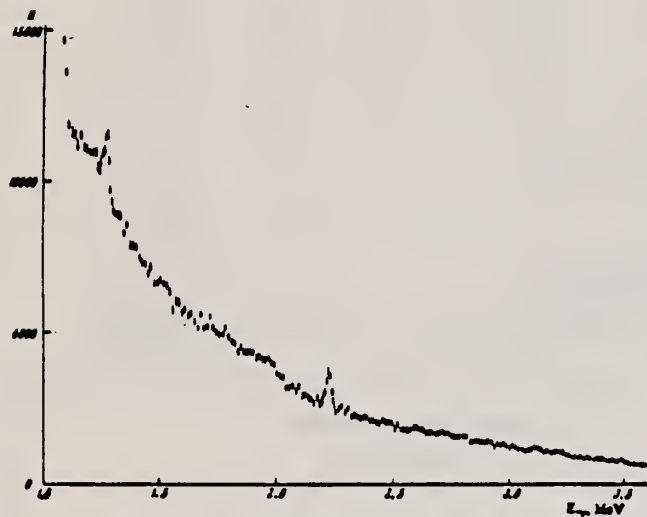
METHOD

REF. NO.	hmg
70 Is 2	

REACTION	RESULT	EXCITATION ENERGY	SOURCE		DETECTOR		ANGLE
			TYPE	RANGE	TYPE	RANGE	
G, PG	SPC	THR-32	C	32	SCD-D	0-4	135
G, NG	SPC	THR-32	C	32	SCD-D	0-4	135

LEVELS: 1.26, 2.23

The 35-MeV betatron at the Nuclear Physics Institute, Moscow State University, has been used in conjunction with a Ge(Li) detector of volume 20 cm³ to obtain γ -ray spectra from the reactions $S^{32}(\gamma, p\gamma')$ and $S^{32}(\gamma, n\gamma')$. Peaks are observed in the spectrum at γ -ray energies of 1.26 and 2.23 MeV. The absolute values of the integrated cross sections in these peaks are respectively 40 and 90 MeV-mb.



Spectrum of γ rays from the reactions $S^{32}(\gamma, p\gamma')$ and $S^{32}(\gamma, n\gamma')$.
The energy scale corresponds to the photopeak.

REACTION	RESULT	EXCITATION ENERGY	SOURCE		DETECTOR		ANGLE
			TYPE	RANGE	TYPE	RANGE	
$E, E/$	ABX	4	D	58,59	MAG-D		105
		(3.78)		(58.38, 59.19)			

Tabelle 3. Experimentelle Parameter und Meßwerte. E_0 , θ Primärenergie, Streuwinkel im Laborsystem. q unelastischer Impulsübertrag. σ/σ_E gemessenes Verhältnis von unelastischem zu elastischem differentiellen Wirkungsquerschnitt; in Klammer ist der statistische Fehler in % angegeben. $d\sigma/d\Omega$ unelastischer differentieller Wirkungsquerschnitt; wegen der Fehlerangaben vgl. Text. Die Meßwerte für Si und S sind als Ergebnisse für ^{28}Si und ^{32}S aufzufassen (vgl. Text)

$$4 = 3.78 \text{ O}^+$$

	E_0 (MeV)	θ (°)	q^2 (fm $^{-2}$)	σ/σ_E (10 $^{-4}$)	$d\sigma/d\Omega$ (10 $^{-33}$ cm 2 /ster.)
^{12}C 7,65 MeV	59,58	117,04	0,231	14,90 (0,6)	24,69 \pm 1,60
	56,94	129,02	0,231	13,79 (1,0)	13,68 \pm 0,96
	54,12	141,11	0,229	14,98 (0,7)	8,15 \pm 0,55
	52,75	153,15	0,231	15,24 (1,0)	6,62 \pm 0,47
	51,90	165,05	0,231	15,78 (1,8)	1,16 \pm 0,09
	51,18	104,98	0,145	5,80 (0,7)	28,80 \pm 1,69
	47,90	117,04	0,145	5,51 (0,7)	17,19 \pm 1,01
	45,48	129,02	0,145	5,97 (1,2)	11,14 \pm 0,71
	43,57	141,11	0,143	5,95 (1,1)	6,09 \pm 0,38
	42,54	153,15	0,145	5,82 (1,4)	2,67 \pm 0,18
	37,51	104,98	0,074	1,41 (1,4)	15,38 \pm 1,07
	35,08	117,04	0,073	1,33 (1,6)	9,14 \pm 0,57
	33,39	129,02	0,073	1,44 (1,7)	5,89 \pm 0,37
	32,04	141,11	0,073	1,39 (2,0)	3,11 \pm 0,21
	31,36	153,15	0,073	1,39 (3,2)	1,39 \pm 0,11
^{24}Mg 6,44 MeV	59,01	116,94	0,232	5,53 (2,2)	28,28 \pm 2,24
	55,81	129,03	0,231	5,41 (1,5)	16,65 \pm 1,20
	53,64	140,95	0,231	5,65 (1,6)	9,51 \pm 0,70
	52,14	153,00	0,231	5,17 (2,1)	3,95 \pm 0,32
	36,98	104,96	0,074	0,59 (2,6)	25,08 \pm 1,78
	34,59	116,94	0,074	0,56 (3,2)	15,09 \pm 1,16
	32,87	129,03	0,074	0,58 (2,8)	9,37 \pm 0,68
	31,72	140,95	0,074	0,58 (3,1)	5,10 \pm 0,39
	30,86	153,00	0,074	0,68 (5,5)	2,69 \pm 0,27
	58,38	116,94	0,232	5,61 (1,9)	38,70 \pm 2,68
^{28}Si 4,98 MeV	55,12	129,03	0,231	5,27 (0,9)	21,98 \pm 1,34
	52,87	141,11	0,231	5,58 (1,3)	12,72 \pm 0,81
	51,28	153,00	0,230	5,69 (1,9)	6,00 \pm 0,42
	49,93	104,96	0,145	2,05 (1,6)	49,60 \pm 3,13
	49,97	104,96	0,146	2,10 (1,4)	50,68 \pm 3,09
	46,77	116,94	0,146	2,23 (2,2)	33,90 \pm 2,31
	44,28	129,03	0,146	2,14 (2,0)	19,48 \pm 1,29
	42,44	141,11	0,146	2,20 (1,7)	10,98 \pm 0,70
	41,23	153,00	0,145	2,45 (2,1)	5,64 \pm 0,38
	41,37	153,00	0,146	2,48 (2,5)	5,67 \pm 0,40
	36,28	104,96	0,074	0,53 (4,5)	32,51 \pm 2,90
	36,26	104,96	0,074	0,56 (4,0)	34,35 \pm 2,89
	33,98	116,94	0,074	0,55 (4,3)	21,28 \pm 1,83
	32,17	129,03	0,074	0,52 (4,0)	11,98 \pm 1,00
^{32}S 3,78 MeV	30,87	141,11	0,073	0,59 (5,3)	7,54 \pm 0,73
	29,96	153,00	0,073	0,66 (5,7)	3,89 \pm 0,39
	30,09	153,00	0,074	0,60 (5,0)	3,52 \pm 0,33
	58,38	116,94	0,225	0,48 (25)	3,30 \pm 1,00
^{40}Ca 3,35 MeV	59,19	104,96	0,210	0,32 (37)	5,17 \pm 3,36
	58,80	104,96	0,209	0,27 (45)	4,40 \pm 3,30

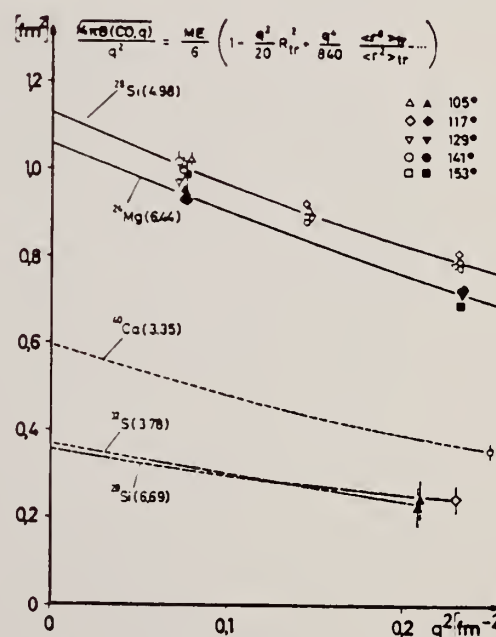


Fig. 3. Meßergebnisse für Monopolübergänge in ^{24}Mg (6,44 MeV), ^{28}Si (4,98 und 6,69 MeV), ^{32}S (3,78 MeV) und ^{40}Ca (3,35 MeV) als Funktion von q^2 . Die eingezeichneten Meßpunkte und die zugehörigen Kurven gelten für eine Auswertung mit f_c , x_1 und x_2 nach Modell I. Für ^{28}Si (4,98) sind nur die aus σ/σ_E und D_{BA}^{exp} berechneten longitudinalen Anteile aufgetragen (vgl. S.1), wobei die Meßpunkte bei gleicher Impulsübertragung und gleichem Streuwinkel (vgl. Tabelle 3) zusammengefaßt wurden. Die gestrichelten Kurven zeigen die Extrapolation nach $q=0$ mit vorgegebenem Übergangsradius

METHOD

REF. NO.

70 Th 1

egf

REACTION	RESULT	EXCITATION ENERGY	SOURCE		DETECTOR		ANGLE
			TYPE	RANGE	TYPE	RANGE	
G,XG	ABX	THR-29	C	29	SCD-D	1-4	125

1st excited states of ^{31}S and ^{31}P is 120 ± 30 Mev-mb
 2nd excited states of ^{31}S and ^{31}P is 90 ± 20 MeV-mb

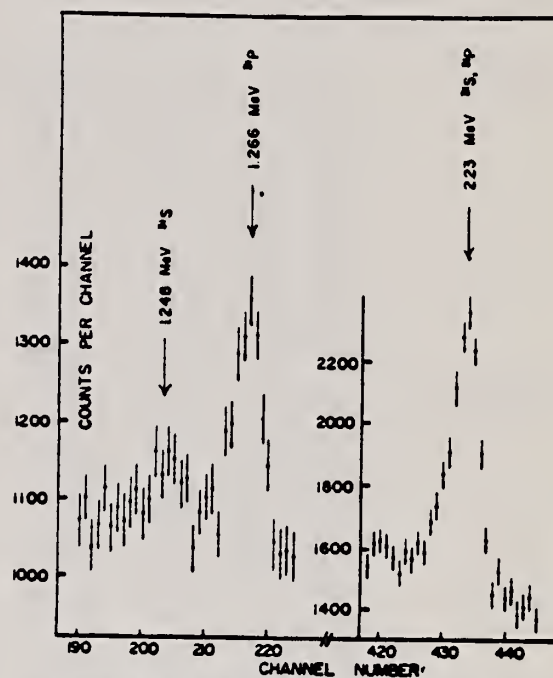


Fig. 2. Spectrum of de-excitation γ -rays following photodisintegration of ^{32}S .

E. Bramania
NucI. Phys. A175, 17 (1971)

ELEM. SYM.	A	Z
S	32	16

METHOD

REF. NO.

71 Br 1

egf

REACTION	RESULT	EXCITATION ENERGY	SOURCE		DETECTOR		ANGLE
			TYPE	RANGE	TYPE	RANGE	
G, NP	ABX	19-30	C	19-30	ACT-I		4PI

814

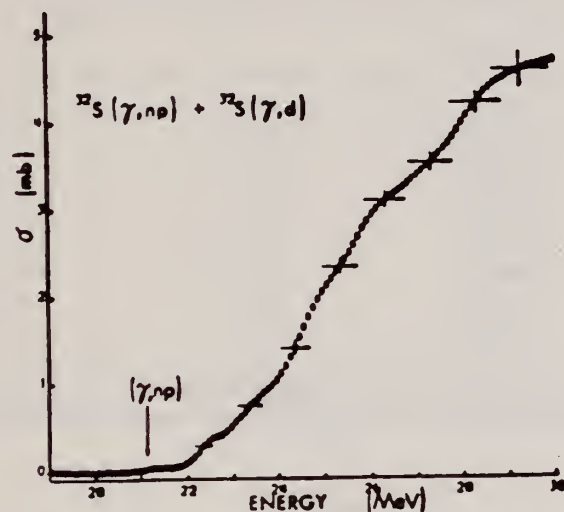


Fig. 4. The experimental $(\gamma, np) + (\gamma, d)$ cross section in ^{32}S .



2

32

16

REF. NO.

71 Ch 1

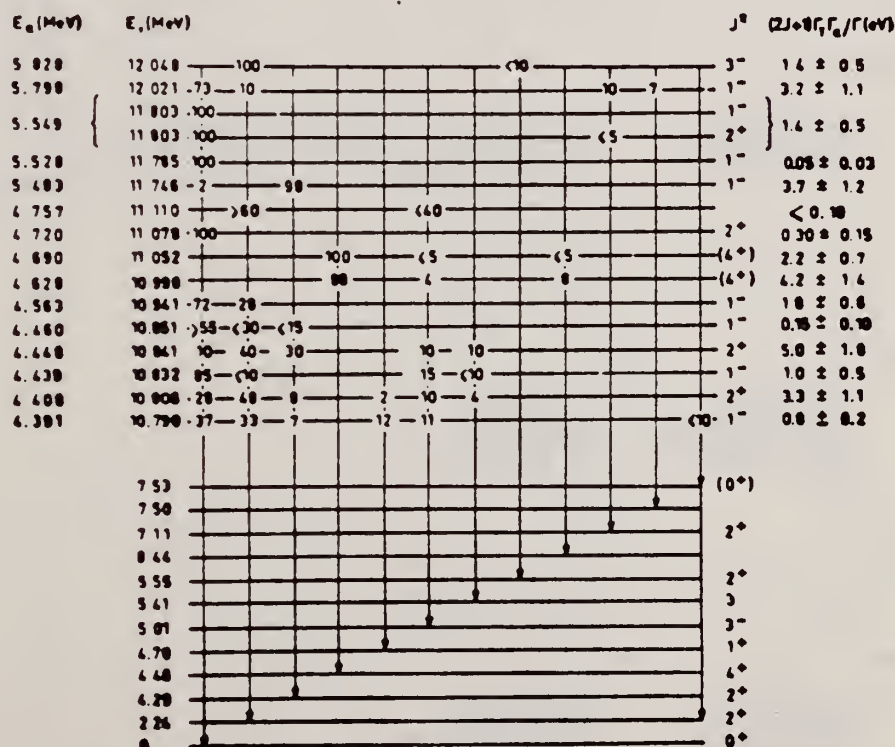
egf

REACTION	RESULT	EXCITATION ENERGY	SOURCE		DETECTOR		ANGLE
			TYPE	RANGE	TYPE	RANGE	
A ₁ G	LFT	10-12	D	4-6	SCD-D		DST

J-PI

$E_{\pi_1} \rightarrow E_{\pi_2}$ (MeV)	$J^{\pi_1} \rightarrow J^{\pi_2}$	$E1$	
		Γ_1 (meV)	$ M ^2 \times 10^3$
10.79 \rightarrow 0	$1^- \rightarrow 0^+$	70 ± 35	0.08 ± 0.04
10.79 \rightarrow 2.24	$1^- \rightarrow 2^+$	$60 \pm 30^*)$	$0.13 \pm 0.07^*)$
10.83 \rightarrow 0	$1^- \rightarrow 0^+$	290 ± 130	0.34 ± 0.15
10.85 \rightarrow 0	$1^- \rightarrow 0^+$	22 ± 13	0.02 ± 0.01
10.94 \rightarrow 0	$1^- \rightarrow 0^+$	400 ± 100	0.45 ± 0.12
10.94 \rightarrow 2.24	$1^- \rightarrow 2^+$	$170 \pm 80^*)$	$0.37 \pm 0.19^*)$
11.75 \rightarrow 0	$(1^-) \rightarrow 0^+$	20 ± 10	0.02 ± 0.01
11.75 \rightarrow 4.29	$(1^-) \rightarrow 2^+$	$1150 \pm 390^*)$	$4.0 \pm 1.4^*)$
11.78 \rightarrow 0	$1^- \rightarrow 0^+$	15 ± 10	0.015 ± 0.010
12.02 \rightarrow 0	$1^- \rightarrow 0^+$	800 ± 300	0.7 ± 0.3
12.03 \rightarrow 2.24	$3^- \rightarrow 2^+$	$200 \pm 70^*)$	$0.3 \pm 0.1^*)$

^{a)} Dans ces cas, il y a deux solutions pour δ . On a utilisé les plus petites valeurs de δ ; les autres solutions, qui donnent $|M|^2(M2) \geq 20$ u.w. sont moins probables.



(over)

TABLEAU I

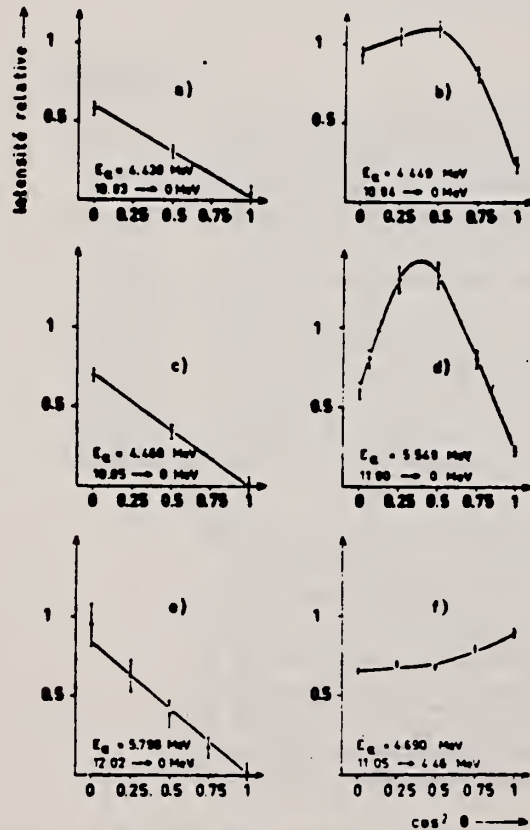
Moment angulaire total des niveaux résonnants et mélange de multipolarité des transitions observées

$E_{\gamma} \rightarrow E_x$ (MeV)	A_2	A_4	$J_i \rightarrow J_f$	δ°
10.79 \rightarrow 0 ⁺	-0.92 ± 0.04		$1^- \rightarrow 0^+$	
10.79 \rightarrow 2.24	0.3 ± 0.2		$1^- \rightarrow 2^+$	0.3 ± 0.2 (ou 1.4 ± 1.2)
10.81 \rightarrow 0 ⁺)	0.4 ± 0.1	-1.2 ± 0.2	$2^+ \rightarrow 0^+$	
10.81 \rightarrow 2.24	0.25 ± 0.10	-0.40 ± 0.18	$2^+ \rightarrow 2^+$	0.19 ± 0.06
10.83 \rightarrow 0	-1.0 ± 0.1		$1^- \rightarrow 0^+$	
10.84 \rightarrow 0 ⁺)	-0.30 ± 0.04	-0.64 ± 0.05	$2^+ \rightarrow 0^+$	
10.84 \rightarrow 2.24	1.1 ± 0.1	0.05 ± 0.10	$2^+ \rightarrow 2^+$	-0.54 ± 0.15
10.84 \rightarrow 4.29	1.1 ± 0.1	-0.08 ± 0.15	$2^+ \rightarrow 2^+$	-0.60 ± 0.12
10.85 \rightarrow 0	-1.1 ± 0.1		$1^- \rightarrow 0^+$	
10.94 \rightarrow 0	-1.10 ± 0.05		$1^- \rightarrow 0^+$	
10.94 \rightarrow 2.24	-0.1 ± 0.2		$1^- \rightarrow 2^+$	0.00 ± 0.18 (ou 3.0 ± 1.5)
10.94 \rightarrow 4.46	0.21 ± 0.07	0.14 ± 0.10	$(4^+) \rightarrow 4^+$	0.30 ± 0.06
			$(3^-) \rightarrow 4^+$	0.24 ± 0.06
			$(5^-) \rightarrow 4^+$	-0.26 ± 0.04
11.05 \rightarrow 4.46	0.14 ± 0.07	0.15 ± 0.08	$(4^+) \rightarrow 4^+$	0.34 ± 0.08
			$(3^-) \rightarrow 4^+$	0.20 ± 0.07
			$(5^-) \rightarrow 4^+$	-0.23 ± 0.04
11.08 \rightarrow 0	0.6 ± 0.3	-1.8 ± 0.4	$2^+ \rightarrow 0^+$	
11.75 \rightarrow 0	-1.0 ± 0.1		$1^- \rightarrow 0^+$	
11.75 \rightarrow 4.29	0.15 ± 0.02		$(1^-) \rightarrow 2^+ \text{ *)}$	0.21 ± 0.02 (ou 1.8 ± 0.1)
11.78 \rightarrow 0	-0.95 ± 0.06		$1^- \rightarrow 0^+$	
11.80 \rightarrow 0 ⁺)	0.40 ± 0.15	-1.4 ± 0.2	$2^+ \rightarrow 0^+$	
			$1^- \rightarrow 0^+$	
12.02 \rightarrow 0	-1.1 ± 0.1		$1^- \rightarrow 0^+$	
12.05 \rightarrow 2.24	-0.4 ± 0.04	0.08 ± 0.06	$3^- \rightarrow 2^+$	-0.03 ± 0.02

) La distribution angulaire est perturbée par les résonances 1^- voisines.) Au maximum de cette résonance, on a une contribution de 60 % de la résonance à 10.83 MeV pour les γ_0 .*) La distribution correspond à 78 % d'une transition $2^+ \rightarrow 0^+$ et 22 % d'une transition $1^- \rightarrow 0^+$.

*) Discussion sect. 4.

*) Les phases sont données suivant la convention de Rose et Brink.

Fig. 3. Distributions angulaires de rayonnements γ .

REF.

N.V. Goncharov, A.I. Derebchinskii, O.P. Kononov, S.G. Tonapetyan,
and V.M. Khvorostyan
Yad. Fiz. 14, 31 (1971)
Sov. J. Nucl. Phys. 14, 18 (1972)

ELEM. SYM.

A

Z

S

32

16

METHOD

REF. NO.

71 Go 2

hmg

REACTION	RESULT	EXCITATION ENERGY	SOURCE		DETECTOR		ANGLE
			TYPE	RANGE	TYPE	RANGE	
G, PI+	RLY	150-500	C	500	CCH-D		DST

PI/PI+ YIELD RATIO

Measurements are reported of the relative yield of π^+ mesons and the π^+/π^- yield ratio for mesons with energy 40 ± 10 MeV emitted in the angular range $\theta_{lab} = 50-160^\circ$ in photon-induced reactions with $E_{max} = 500$ MeV with light and medium nuclei. The charged π -meson detector was a 34-cm Freon bubble chamber with a tube for the beam. The π^+/π^- yield ratio for He^4 , Li^7 , C^{12} , Si^{28} , S^{32} , Ca^{40} , and Nb^{93} was found to be respectively 0.94 ± 0.14 , 2.15 ± 0.31 , 1.22 ± 0.21 , 1.25 ± 0.15 , 1.0 ± 0.13 , 1.11 ± 0.13 , and 1.53 ± 0.25 . It was established that the π^+ -meson yield follows a $ZA^{-1/3}$ law.

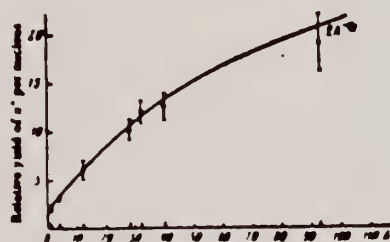
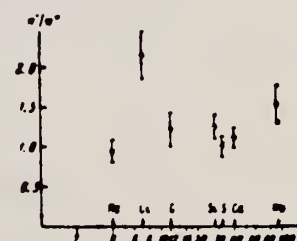


FIG. 2. Relative yield of π^+ mesons per nucleus as a function of mass number A.

FIG. 3. π^+/π^- yield ratio as a function of mass number A.





S

32

16

METHOD

REF. NO.

72 Co 2

egf

REACTION	RESULT	EXCITATION ENERGY	SOURCE		DETECTOR		ANGLE
			TYPE	RANGE	TYPE	RANGE	
P,G	LFT	9-11	D	0-2	SCD-D		55

J-PI

TABLE I

Energies and strengths of $^{31}\text{P}(p,\gamma)^{32}\text{S}$ resonances for $E_p < 2.03$ MeV

E_p (keV)		$(2J+1)\Gamma_p\Gamma_\gamma/\Gamma$ (eV)		E_p (keV)		$(2J+1)\Gamma_p\Gamma_\gamma/\Gamma$ (eV)	
present experiment	ref. ^{1a)}	present experiment ^{b)}	ref. ^{1a)}	present experiment	ref. ^{1a)}	present experiment ^{b)}	ref. ^{1a)}
	354.8 ± 0.4	0.003	0.012	1400.1 ± 0.6	1400.1 ± 0.7	1.3	
	439.4 ± 0.5	0.25	0.14	1402.9 ± 0.8		5.0	
	541.4 ± 0.6	1.0	0.30	1411.4 ± 0.6		2.0	
	618.9 ± 1.0	0.06	0.007	1438.3 ± 0.7	1437.7 ± 0.7	11	14
	642.4 ± 0.7	0.52 ± 0.08 ^{a)}	0.52 ± 0.08 ^{a)}	1473.1 ± 0.6	1470.1 ± 0.7	2.4	2.3
	811.3 ± 0.5	2.2	2.7	1556.6 ± 0.6	1555.5 ± 0.8	9	11
	821.0 ± 1.0	0.43		1582.9 ± 0.6	1583.1 ± 0.8	8	12
	874.3 ± 0.5	0.29	0.07	1698.9 ± 1.0	1697 ± 2	0.9	
	887.8 ± 0.5	0.18	0.10	1746.9 ± 1.0	1742 ± 2	2.9	2
	894.5 ± 0.5	0.7		1764.2 ± 1.0	1760 ± 2	0.9	
	983.8 ± 1.0	0.18		1796.1 ± 1.0	1792 ± 2	1.1	
1056.5 ± 0.6	1053.7 ± 0.5	1.1		1891.5 ± 1.0	1890 ± 2	2.2	50
1089.6 ± 0.6	1089.1 ± 0.5	0.38		1896.0 ± 1.0		2.5	
1120.7 ± 0.6	1117.4 ± 0.5	3.0	2.3	1954.0 ± 1.0	1949 ± 2	7	7
1150.5 ± 0.6	1148.2 ± 0.5	3.9	6.0	1977.1 ± 1.0	1972 ± 2	3.9	4
1155.1 ± 0.6		1.5		1983.6 ± 1.0	1978 ± 2	8	11
1251.4 ± 0.6	1247.8 ± 0.6	11	9.2	1990.9 ± 1.0	1985 ± 2	5.3	8
	1379.4 ± 0.7			2026.6 ± 1.0	2020 ± 2	15	28

^{a)} Ref. ^{1a)}.^{b)} Errors of the order of 30 %.¹E.B. Paul, H.E. Gove & G.A. Bartholomew, Phys. Rev. **99** (1955) 1339⁵P.R. Chagnon & P.A. Treado, Nucl. Phys. **40** (1963) 195⁷L.K. ter Veld & H. Brinkman, Nucl. Phys. **40** (1963) 438¹⁰P.M. Endt & C. van der Leun, Nucl. Phys. **A105** (1967) 1¹⁵G.A.P. Engelbertink & P.M. Endt, Nucl. Phys. **88** (1966) 12

(over)

TABLE 3
Gamma decay of $^{31}\text{P}(p, \gamma)^{32}\text{S}$ resonances for $E_p < 2.1$ MeV.
Percentages in brackets imply uncertainties regarding the excitation of the levels

Resonances			γ -decay (in %) to E_x (MeV) in ^{32}S													other levels
E_p *) (keV)	E_r *) (keV)	$J^{\pi c}$	0 0 ⁺	2.23 2 ⁺	3.78 0 ⁺	4.28 2 ⁺	4.46 4 ⁺	4.70 1 ⁺	5.01 3 ⁻	5.41 3 ⁺	5.55 2 ⁺	5.80 1 ⁻	6.22 2 ⁻	6.62 4 ⁻	E_x (%)	
355	9209	1 ^d	38	35	6						5	5	11		7.12(18), 7.54(7)	
439	9290	1 ⁺ *)	40	20				13					2		8.13(1)	
541	9389	2 ⁻	2	63		2		2	9		1	2	17	1		
619	9464	2 ⁺	51	22				(27)							7.12(4.5)	
642	9487	1 ⁻	82			9.5			3.5			0.5				
811	9651	2 ⁺ *)	0.1	61				38		0.9					7.19(4)	
821	9660	1 ^d	74	15	2			3			2					
874	9712	2 ⁺	7	59				34								
888	9725	2 ⁻ , 3, 4 ⁻							40					14	46	
895	9731	1 ⁻ , 2 ⁺	3	18		24		5	4		3	19	18		7.12(2), 8.13(4)	
984	9818	2 ⁺ , 3 ⁻	0.4	19		9	1.6		52			3	6		7.12(9)	
1057	9888	1, 2	1	10		5		5			9				7.00(24), 7.12(46)	
1090	9920		< 0.5	46		2				(3)	31				6.85(10), 7.12(8)	
1121	9950	1	77	9	3	2		(2)							8.13(7)	
1151	9979	3 ⁻	< 0.3	32			6		8	7	26		4	5	6.85(5), 7.12(3)	
															7.48(4)	
1155	9984	2 ⁺	< 0.5	64		2		19	1	1	12		0.4	0.6		
1251	10077	2 ⁻	2	34		2		(1)	12	4			45			
1400	10221	2 ⁺	0.5	10		6	5	25		3.5	6				7.12(44)	
1403	10224	3 ⁻		11			18	4	63						7.12(4)	
1411	10232	2 ⁺	7	9	2	11	3	7	4				2		7.00(48), 7.12(3), 7.54(4)	
1438	10258	4 ⁻		1			11		4					77	6.76(3), 7.95(4)	
1473	10292	2 ⁺	2	36		2			25	2			31		8.13(2)	
1557	10372	2 ⁺	0.5	12		43		8	1.5	13	2		2		6.67(14), 7.19(2), 7.48(2)	
1583	10398	4 ⁽⁻⁾		1		2	1.8		5.6					84	6.76(2.4), 7.70 (0.3), 7.95(2.9)	
1699	10510	1, 2, 3 ⁻	5	25		15		8		8					7.12(39)	
1747	10557	1 ⁻ , 2 ⁽⁺⁾	40	60												
1764	10574	2 ⁺ (3 ⁻)	7	44			16			33						
1796	10604	1 ⁻ , 2	19	6					8	10	39	5			7.12(10), 8.13(3)	
1892	10697	2 ⁺	70	5	3	10	1	2	3		2	3			7.54(0.5), 7.70 (0.5)	
1896	10701	1 ⁻ , 2 ⁺	84	5	4			3				4				
1954	10757	2 ⁺ , 3, 4 ⁺		2			70				19					
1977	10780	1 ⁻ , 2 ⁺	9	60		21		2		4					7.00(4)	
1984	10786	1 ⁻ , 2 ⁺	54	16	2	3	(1)	11			13					
1991	10793	1 ⁻ , 2 ⁽⁺⁾	23	49		9		5	10						7.12(4)	
2027	10828	1 ⁻ , 2 ⁺	24	37	2	22		2	6	3		3			7.12(1)	

*) Ref. 1^o) and present experiment, table 1.

*) As computed with $Q = 8864.9 \pm 0.9$ keV from the present experiment and E_p in table 1.

*) Present experiment unless otherwise indicated, see subsect. 4.1 and table 10.

*) Refs. 3, 7).

*) Ref. 3).

*) Ref. 1).

METHOD

REF. NO.

72 Es 1

hmg

REACTION	RESULT	EXCITATION ENERGY	SOURCE		DETECTOR		ANGLE
			TYPE	RANGE	TYPE	RANGE	
P,G	LFT	6-8	D	3-6	SCD-D		UKN
		(5.550)		(3.371)			

LEVEL IS 5.550 MEV

TABLE IV. $M1$ and $E2$ decay strengths of the $\frac{1}{2}^+$, $\frac{3}{2}^+$ level of ^{32}Cl and their comparison with the theoretical predictions.

Transition $J_i, T_i \rightarrow J_f, T_f$	Energy $E_i - E_f$ (MeV)	Branching (%)	Possible multipolarities	$M1$ Strength (10^{-2} W.u.)		$E2$ strength (W.u.)	
				Present experiment	Theory (Ref. 17)	Present experiment	Theory (Ref. 17)
$\frac{1}{2}^+, \frac{1}{2}^- \rightarrow \frac{1}{2}^+, \frac{1}{2}^-$	5.550 - 0.810	>88	$M1$	15 ± 4	9.2
$\frac{1}{2}^+, \frac{1}{2}^- \rightarrow \frac{1}{2}^+, \frac{1}{2}^-$	5.550 - 0	<12	$M1, E2$	<1.4	0.7	<1.8	0.2

The residual activity between bursts of a mechanically chopped beam has been used to measure the yield of the reaction $^{32}\text{S}(p, \gamma)^{32}\text{Cl}$ systematically in the bombarding energy range $E_p = 3.36$ to 5.41 MeV. Two $T = \frac{1}{2}$ states in ^{32}Cl at $E_x = 3.371 \pm 0.005$ MeV, $E_x = 5.550 \pm 0.007$ MeV and at $E_p = 5.282 \pm 0.006$ MeV, $E_x = 7.402 \pm 0.006$ MeV have been located with the resonance strengths $(2J + 1)\Gamma_p \Gamma_\gamma / \Gamma = 0.76 \pm 0.18$ and 1.50 ± 0.37 eV, respectively. Each of these resonances was narrower than the estimated 2-keV spread in the proton beam. These two states are interpreted as the analogs of the ground and the second excited state of ^{32}P with J^π values $\frac{1}{2}^+$ and $\frac{3}{2}^+$, respectively. γ decay of the lower resonance, investigated with a Ge(Li) detector, shows >88% and <12% branchings to the first excited state and ground state of ^{32}Cl , respectively. The $M1$ strengths of these transitions are compared with those obtained from β analog transitions and with the theoretical predictions based on the many-particle shell-model calculations.

ELEM. SYM.	A	Z
S	32	16
REF. NO.	72 Th 7	
	hvm	

REACTION	RESULT	EXCITATION ENERGY	SOURCE		DETECTOR		ANGLE
			TYPE	RANGE	TYPE	RANGE	
G,NG	ABX	13- 26	C	14- 28	SCD-D		150
G,PG	ABX	13- 26	C	14- 28	SCD-D		150

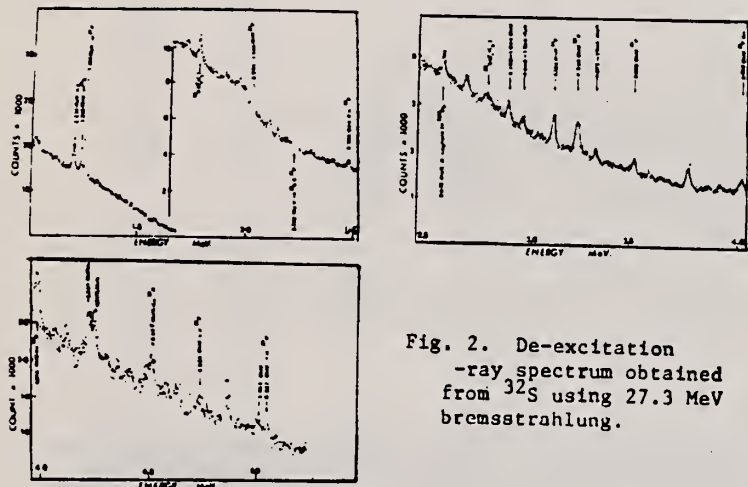


Fig. 2. De-excitation ray spectrum obtained from ^{32}S using 27.3 MeV bremsstrahlung.

The scale for the cross section was obtained by reference to that for the photodisintegration of ^{16}O to the 6.30 MeV state in ^{15}N , as measured by Caldwell et al (5). Their results, at 90° were corrected using the data of Baglin et al (6) to give a value at 150° suitable for the calibration. For the intercalibration an homogenous mixture of sulphur and water was irradiated at 28 MeV. The ratio of the number of γ -rays from the 2.233 MeV states in ^{31}P and ^{31}S to the number from the 6.30 MeV state in ^{15}N set the calibration. This normalization took into account the differences in shape of the two photo-cross sections.

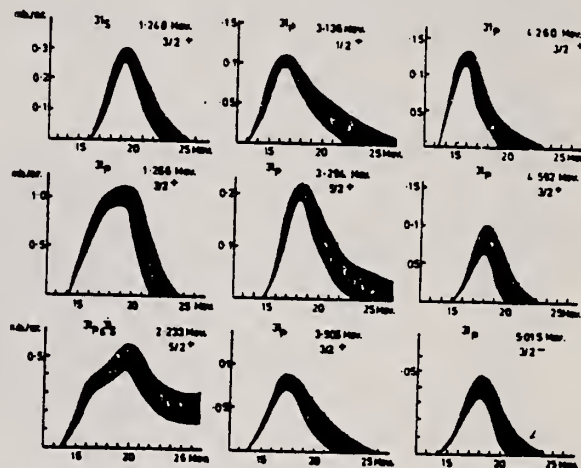


Fig. 3. Cross sections to some excited states.

Table 1. Summary of results

1 Residual state MeV J^π	2 $\int_{0.1}^{0.2} \frac{d\sigma}{d\Omega} d\Omega$ MeV mb/sr	3 Region of strength MeV	4 Orbits best represented used by any of all which will result in this residual state	5 Predicted giant resonance states with large components of any of these orbits
^{32}S				
1.268 $3/2^+$	3.9 ± 0.9	15-20	$(2s_{1/2} d_{3/2})^2$ with 2p or 1f nucleon	No strongly excited states
2.233 $5/2^+$	3.5 ± 0.7	15-25	$(d_{3/2} 2s_{1/2} d_{3/2})$ with 2p or 1f nucleon	States at ~20 MeV and ~25 MeV
2.294 $1/2^+$	0.4 ± 0.2	14-21	$(2s_{1/2} d_{3/2})^2$ with 2p nucleon	No strongly excited states
2.294 $5/2^+$	1.1 ± 0.3	18-21	$(2s_{1/2} d_{3/2})^2$ with 2p or 1f nucleon	States at ~18-21 MeV
2.414 $7/2^+$	1.9 ± 0.7	N.C.	$(2s_{1/2} d_{3/2})^2$ with 1f nucleon	No strongly excited states
3.905 $3/2^+$	0.8 ± 0.2	14-19	$(2s_{1/2} d_{3/2})^2$ with 2p or 1f nucleon	States at ~14-19 MeV
4.190 $5/2^+$	0.6 ± 0.2	N.C.	No satisfactory basic config	
4.260 $3/2^+$	0.6 ± 0.2	14-19	" " " " " "	
4.582 $3/2^+$	0.5 ± 0.2	18-19	" " " " " "	
5.075 $3/2^+$	2.0 ± 0.6	18-20	" " " " " "	
5.254 $1/2^+$	0.6 ± 0.2	N.C.	" " " " " "	
5.557 $3/2^+$	0.2 ± 0.1	N.C.	" " " " " "	
5.988 $3/2^+$	0.4 ± 0.2	N.C.	" " " " " "	
^{32}S				
1-205 $3/2^+$	1.4 ± 0.6	18-20	$(1f_7/2 3s_{1/2})$ with 2p or 1f nucleon	No strongly excited states

N.C. no cross section shape measured. @ indicates 2-233 MeV state in ^{32}S

ELEM. SYM.	A	Z
S	32	16
REF. NO.		
73 Be 10		hmg

METHOD			SOURCE		DETECTOR		ANGLE
REACTION	RESULT	EXCITATION ENERGY	TYPE	RANGE	TYPE	RANGE	
G,N	ABX	15- 32	D	15- 32	BF3-I		4PI
G,PN	ABX	20- 30	D	20- 30	BF3-I		4PI
G,2N	ABX	28- 32	D	28- 32	BF3-I		4PI

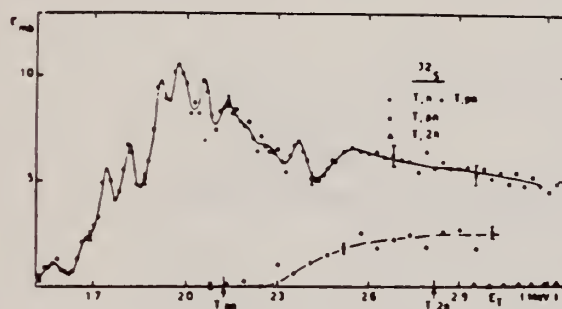


Fig. 5 Partial photoneutron cross sections $\sigma(\gamma, n)$, $\sigma(\gamma, pn)$ and $\sigma(\gamma, 2n)$ of ^{32}S .

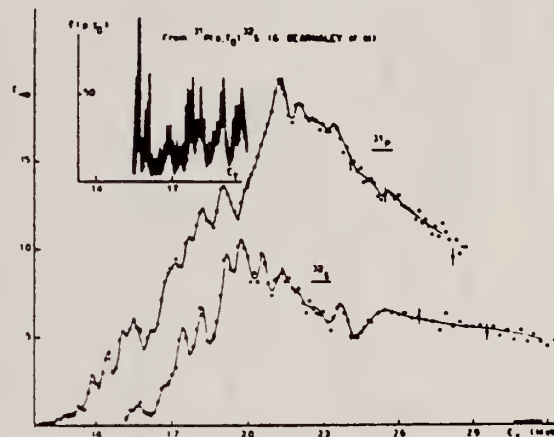


Fig. 6 Comparison of ^{31}P and ^{32}S photoneutron cross sections with $^{31}\text{P}(p, \gamma_0)^{32}\text{S}$ measured by Dearnaley.⁹

⁹ G. Dearnaley et al., Nucl. Phys. **64**, 177 (1965)

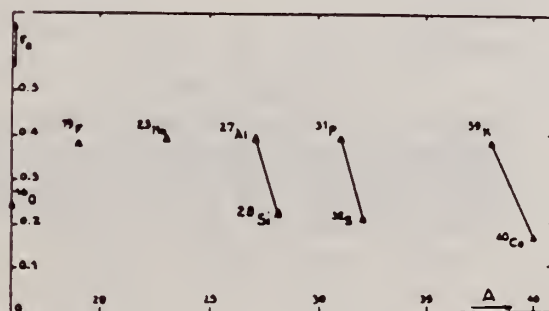


Fig. 13 Integrated photoneutron cross-sections for s-d shell nuclei.

REF. V. di Napoli, F. Salvetti, M.L. Terranova, H.G. de Carvalho,
and J.B. Martins
Phys. Rev. C8, 206 (1973)

ELEM. SYM.	A	Z
S	32	16

METHOD	REF. NO.
	73 D1 4

hmg

REACTION	RESULT	EXCITATION ENERGY	SOURCE		DETECTOR		ANGLE
			TYPE	RANGE	TYPE	RANGE	
G, SPL	ABY	THR-999	C	999	AGI-I		4PI

999 = 1 GEV

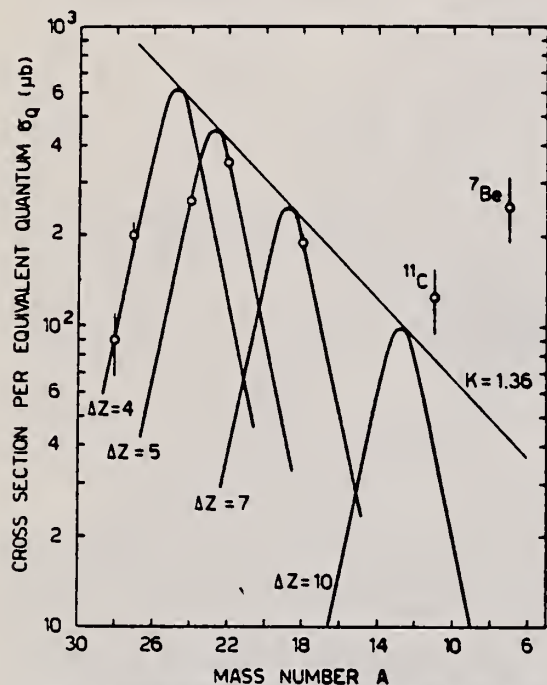


FIG. 2. Yields of radionuclides observed in a thin sulfur target irradiated with 1-GeV bremsstrahlung versus the mass number. ΔZ is the difference between the atomic number of the target nucleus ($Z=16$) and the atomic number of the produced radionuclide.

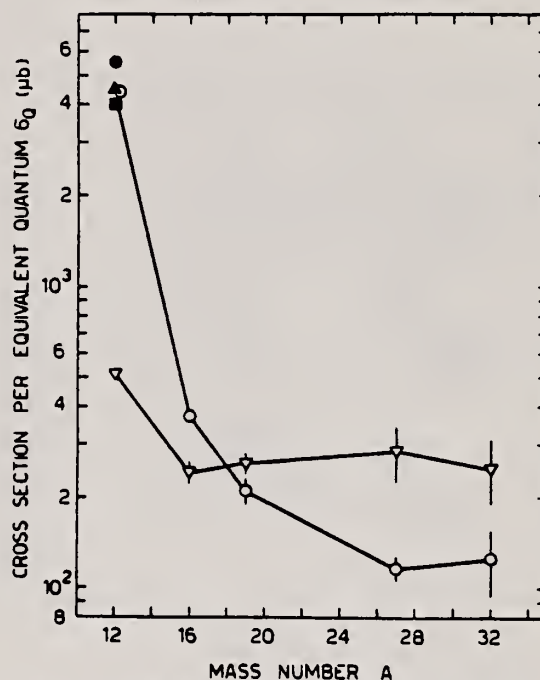


FIG. 3. Yields of ^{11}C and ^7Be versus the mass number of the target nucleus. Filled circle: ^{11}C , Ref. 18. Filled triangle: ^{11}C , Ref. 17. Filled square: ^{11}C , Ref. 8. Open circles: ^{11}C , present work. Reversed open triangles: ^7Be , present work.

- ⁸G. Anderson et al., Nucl. Phys. A197, 44 (1972).
¹⁶V. di Napoli et al., Nuovo Cimento 55B, 95 (1968).
¹⁷A. Masaike, J. Phys. Soc. Japan 19, 427 (1964).

REF.

B.S. Ishkhanov and V.G. Shevchenko
PICNS-73, Vol. I, p. 511 Asilomar

ELEM. SYM.

A

Z

S

32

16

METHOD

REF. NO.

73 Is 3

hmg

REACTION	RESULT	EXCITATION ENERGY	SOURCE		DETECTOR		ANGLE
			TYPE	RANGE	TYPE	RANGE	
G,N	RLX	16- 21	C	16- 21	BF3-I		4PI

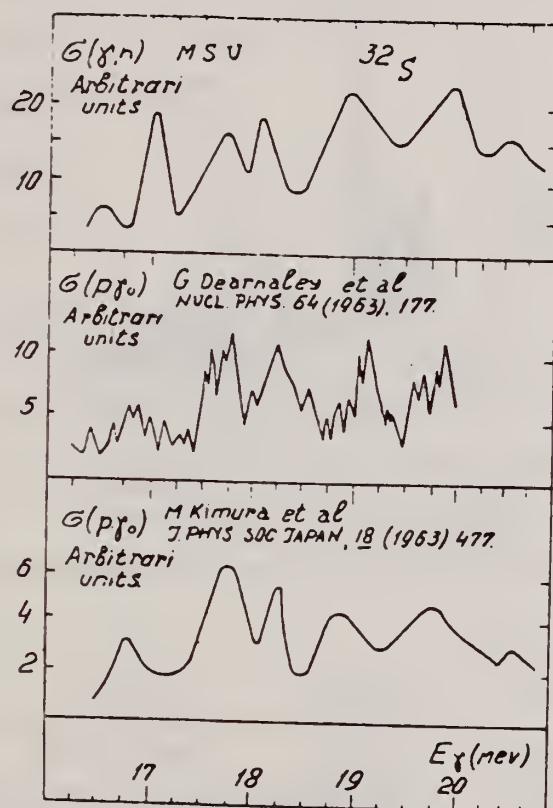


Fig.2. Comparison of our cross section of reaction $^{32}\text{S}(\gamma, n)$ (upper figure) with the cross sections of reaction (p, γ_0) obtained in papers ⁷ (middle figure) and ⁸ (lower figure)

ELEM. SYM.	A	Z
S	32	16
REF. NO.		
73 Lo 4		hmg

METHOD					REF. NO.		
					73 Lo 4	hmg	
REACTION	RESULT	EXCITATION ENERGY	SOURCE		DETECTOR		ANGLE
			TYPE	RANGE	TYPE	RANGE	
G,N	ABX	16- 32	C	16- 32	TOF-D		90

GD AND EXCIT STATE

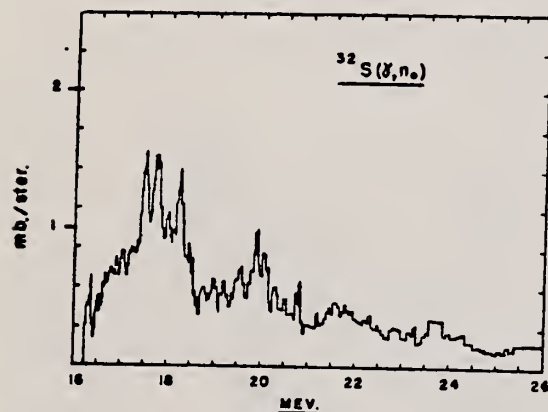


Figure 1: ^{32}S differential ground state cross section at 90° as a function of excitation energy.

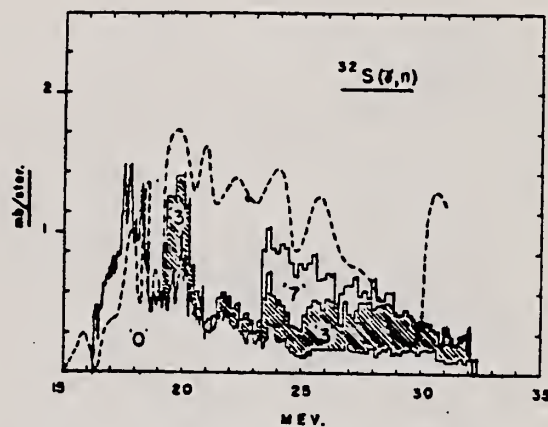


Figure 3: ^{32}S total differential cross section at 90° as a function of excitation energy. See text.

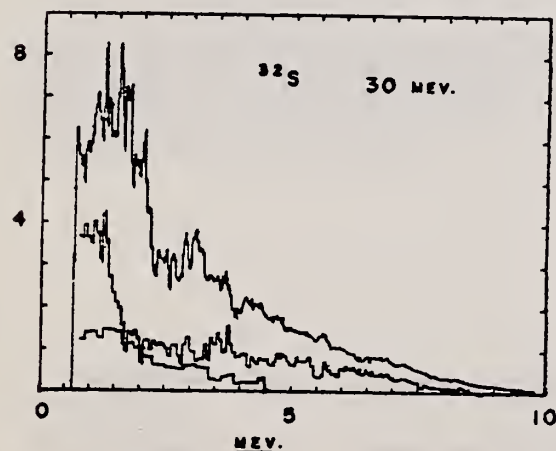


Figure 2: Photoneutron energy spectra generated in the analysis of the 30 MeV measurement. See text.

Table 1

Integrated partial cross sections in the decay of ^{32}S

Configuration (in ^{31}S)	Excitation in ^{31}S	Measured strength		Theoretical Calculation ³⁾
		MeV-nb	%	
$(d_{5/2})^{-1} 2_1^+$ $(d_{5/2})^{-1} 0_2^+$ $(d_{5/2})^{-1} 2_2^+$	0 MeV	53	53	13%
	3 MeV	31	32	34%
	7 MeV	15	15	53%
Total		99	100	

METHOD

REF. NO.

73 Ve 6

egf

REACTION	RESULT	EXCITATION ENERGY	SOURCE		DETECTOR		ANGLE
			TYPE	RANGE	TYPE	RANGE	
P, G	LFT	10- 11	D	1- 2	NAI-D		DST

TABLEAU 1

Energies et forces des résonances de la réaction $^{31}\text{P}(p, \gamma)^{32}\text{S}$ dans le domaine $E_p = 1.24-1.60$ MeV

E_p (keV)			$(2J+1)\Gamma_p\Gamma_\gamma/\Gamma$ (eV)		
nos résultats ^{a)}	réf. ¹¹⁾	réf. ¹²⁾ ^{b)}	nos résultats ^{c)}	réf. ¹¹⁾ ^{d)}	réf. ¹²⁾ ^{e)}
1247.4	1251.4 ± 0.6	1248	11.8	11	9.2
1279.1			0.25		
1399.3 ± 0.8	1400.1 ± 0.6	1398	1.3	1.3	1.8
1401.9	1402.9 ± 0.8	1401	3.8	5	5.8
1405.1		1404	0.25 ^{c)}		
1410.6 ± 0.8	1411.4 ± 0.6	1409	1.0	2	1.5
1437.3	1438.3 ± 0.7	1437	8.3	11	20
1469.0		1468	0.15		
1472.1	1473.1 ± 0.6	1471	1.5	2.4	2.4
1474.3		1474	0.38 ^{c)}		
1514.7			2.2		
1555.4	1556.6 ± 0.6	1553	8.7	9	11
1581.1	1582.9 ± 0.6	1583	7.9	8	15.2
1585.2 ^{f)}					

^{a)} ±1.5 keV sauf pour $E_p = 1399$ et 1411 keV (voir paragraphe 3.3).^{b)} ±1 keV.^{c)} Précision 20% sauf pour les résonances à $E_p = 1405$ et 1474 keV où la précision est estimée à 40%.^{d)} Précision 30%.^{e)} Précision 40%.^{f)} L'énergie de cette résonance est déduite de l'étude de la réaction $^{31}\text{P}(p, p)^{31}\text{P}$ (paragraphe 5.8).

TABLEAU 3

Energies d'excitation (keV) de quelques niveaux du noyau ^{32}S

Nos résultats	Réf. ¹¹⁾	Réf. ¹²⁾	Réf. ²²⁾	Réf. ²⁴⁾
2231.1 ± 1.0	2230.5 ± 0.3		2230.4 ± 1.6	2230.5 ± 1.5
3778.1 ± 1.4	3778.2 ± 1.8		3776.3 ± 3.2	3778.7 ± 2.5
4280.8 ± 1.0	4282.2 ± 1.0		4279.6 ± 2.0	4281.5 ± 1.5
4696.0 ± 1.0	4695.3 ± 0.4		4694.4 ± 1.8	4694.2 ± 1.5
5007.8 ± 1.4	5006.5 ± 1.0			
5413.8 ± 1.4	5412.6 ± 1.0			
5550.3 ± 1.7	5548.8 ± 1.4		5548.7 ± 2.0	5548.0 ± 2.0
7000.8 ± 1.4	7003.7 ± 1.0		6998.0 ± 2.8	7000.5 ± 2.5
7112.8 ± 1.4	7116.5 ± 1.0	7114 ± 2		7112 ± 4
7536.0 ± 1.4	7535.5 ± 1.0	7535 ± 5		

est $Q = 8863.9 \pm 1.4$ keV, en excellent accord avec la valeur expérimentale de Coetzee *et al.* ¹¹⁾ $Q = 8864.9 \pm 0.9$ keV et la valeur donnée dans la table de masses 1971 de Wapstra *et al.* ²⁴⁾ $Q = 8863.9 \pm 0.8$ keV.

(over)

TABLEAU 2

Rapports d'embranchement des niveaux résonnants de la réaction $^{31}\text{P}(p, \gamma)^{32}\text{S}$

E_p (MeV)	$E_x^*)$ (MeV)	J^π	0 0 ⁺	2.23 2 ⁺	3.78 0 ⁺	4.28 2 ⁺	4.46 4 ⁺	4.70 1 ⁺	5.01 3 ⁻	5.41 3 ⁺	5.55 2 ⁺	5.78 1 ⁻	6.22 2 ⁻	6.41 0 ⁻	6.62 4 ⁻	6.67 (1,2) ⁺⁺	Autres niveaux ^{c)}
1.247	10.072	2 ⁻	1.8	28		1.6		0.9	12	4		50					7.11(0.7), 8.13(0.3) 8.30(0.4), 8.50(0.2)
1.279	10.102	2, 3, 4		46		14	18		12	6	4						7.11(39)
1.399	10.219	3 ⁺		12		7	8	22		4	8						
1.402	10.222	3 ⁻		12			22		66								
1.411	10.230	1 ⁺	7	7	2	11		8		5	4		5				7.00(41), 7.11(6) 7.54(4)
1.437	10.256	4 ⁻		0.6			8		4	0.4				1	75		6.76(3.2), 7.35(1.0) 7.70(0.5), 7.95(6.4)
1.469	10.287	3 ⁻		11			15		74								
1.472	10.289	2 ⁻	2.2	32		1.5			19	1.5		1.6	36			2.3	7.00(1.5), 8.13(2.4)
1.515	10.331	1 ⁻	12	61				15			6						8.13(6)
1.555 ^{a)}	10.369	2 ⁺	< 0.5	11		40		11	2	12	4		3			13	7.19(1), 7.49(2)
1.581	10.395	4 ⁻		0.5			1.3		5.8				0.7		83		6.76(2.3), 6.85(1.0) 7.70(0.5), 7.95(4.9)
1.585 ^{a)}	10.399	0 ⁻ ^{a)}										76					8.13(24)

^{a)} Les énergies d'excitation des niveaux résonnants sont données avec une précision de 2 keV.^{b)} Réf. ²³⁾.^{c)} Les valeurs $J^\pi = (2^-, 3^\pm, 4^+)$, $(3^-, 4^+, 5^-)$, $(3^\pm, 4^+)$ et $(3, 4)^-$ sont attribuées respectivement aux niveaux $E_x = 6.41, 6.76, 6.85$ et 7.95 MeV (paragraphe 5.4 et 5.8); les valeurs $J^\pi = 1^+$ et 2^+ ont été attribuées aux niveaux $E_x = 7.19$ MeV [réf. ¹¹⁾] et 7.49 MeV [réf. ³⁴⁾], respectivement; les valeurs $(J^\pi, T) = (1^+, 1)$, $(2^+, 1)$, $(0^+, 1)$ et $(1^+, 1)$ ont été attribuées respectivement aux niveaux $E_x = 7.00, 7.11, 7.54$ et 8.13 MeV [réf. ¹⁹⁾]. Les spins et parités des niveaux $E_x = 7.35, 7.70$ et 8.30 MeV ne sont pas connus.^{d)} Les rapports d'embranchement de cette résonance sont ceux de la réf. ⁴⁾.^{e)} Voir paragraphes 3.2 et 5.8. Il n'est pas sûr que toutes les transitions aient été observées.

- 5) C.J. Piluso, G.C. Salzman et D.K. McDaniels, Phys. Rev. 181 (1969) 1555
- 11) W.F. Coetzee, M.A. Mever et D. Reitmann, Nucl. Phys. A185 (1972) 644
- 12) F. Leccia et al., J. De Phys. 33 (1972) 451
- 19) A. Graue, L. Herland, J.R. Lien, et E.R. Cosman, Nucl. Phys. A120 (1968) 513
- 22) A.J. Armini, J.W. Sunier et J.R. Richardson, Phys. Rev. 165 (1968) 1194
- 23) C. Detraz et al., Nucl. Phys. A203 (1973) 444
- 24) A.H. Wapstra et N.B. Gove, Nucl. Data A9 (1971) 267
- 34) D. Castera, these de 3e cycle, Université de Bordeaux, 1970

ELEM. SYM.	A	Z
S	32	16
REF. NO.		
74 Fo 5		egf

METHOD			SOURCE		DETECTOR		ANGLE
REACTION	RESULT	EXCITATION ENERGY	TYPE	RANGE	TYPE	RANGE	
G,A	ABX	12- 18	D	6- 12	NAI-D		DST

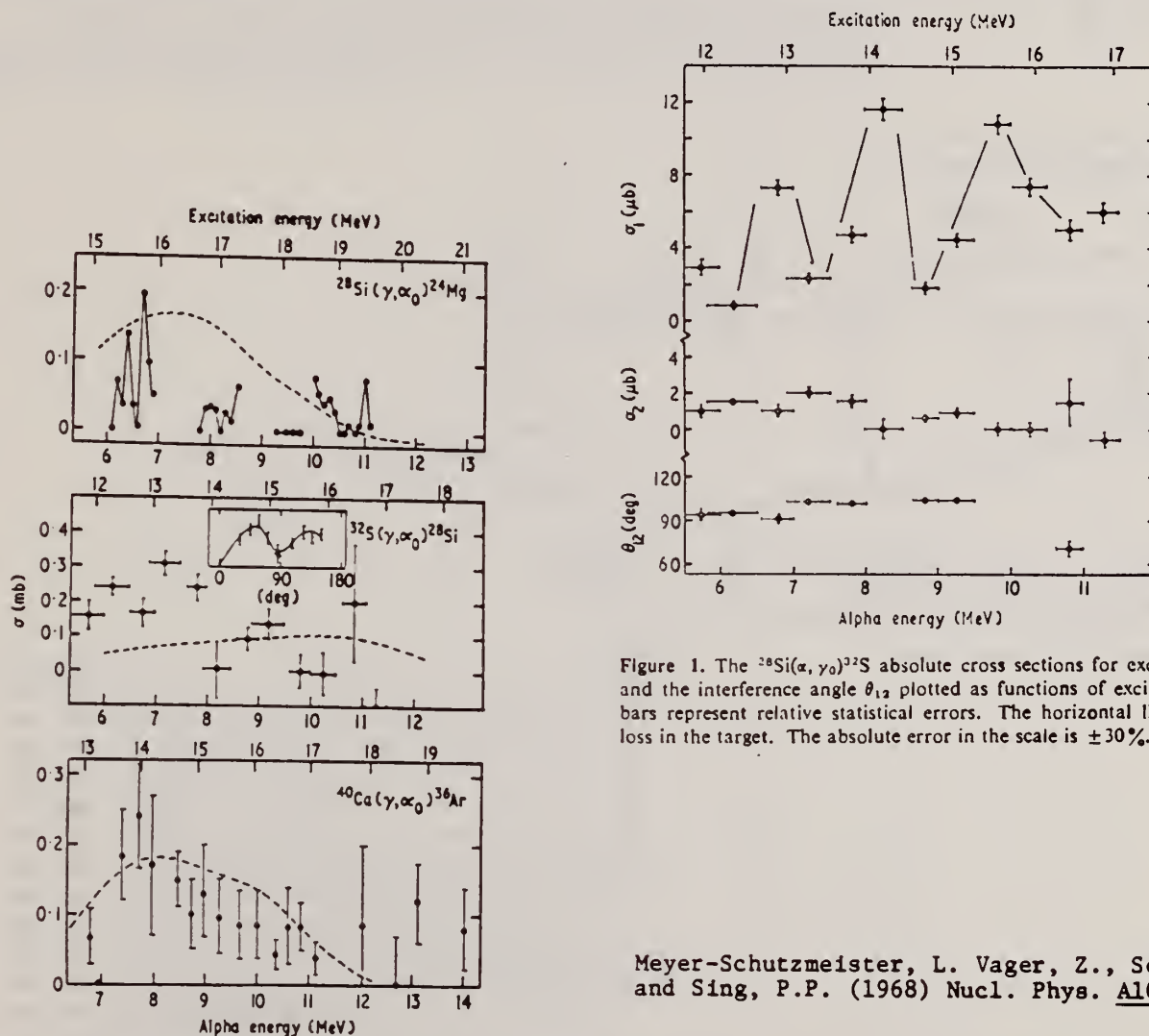


Figure 1. The $^{28}\text{Si}(\alpha, \gamma)^{28}\text{Si}$ absolute cross sections for exciting 1^- and 2^+ states and the interference angle θ_{12} plotted as functions of excitation energy. The error bars represent relative statistical errors. The horizontal lines indicate the energy loss in the target. The absolute error in the scale is $\pm 30\%$.

Meyer-Schutzmeister, L. Vager, Z., Segel, R.E., and Sing, P.P. (1968) Nucl. Phys. A108, 180.

Figure 2. Cross sections for exciting 2^+ states obtained by the (α, γ) reaction and inverted using the principle of detailed balance. The bars indicate the relative errors where known. The $^{24}\text{Mg}(\gamma, \alpha_0)^{24}\text{Mg}$ points were calculated from angular distributions measured by Meyer-Schutzmeister *et al* (1968). The $^{40}\text{Ca}(\gamma, \alpha_0)^{36}\text{Ar}$ data are taken from Watson *et al* (1973). The absolute errors in the cross section scales are $\pm 30\%$. The insert shows an angular distribution measured at $E_\alpha = 6.5$ MeV. The full curve represents the fit obtained using equation (1). The broken curves are calculated cross sections using a γ -ray strength that exhausts 100% of the $15A(2^+)$.

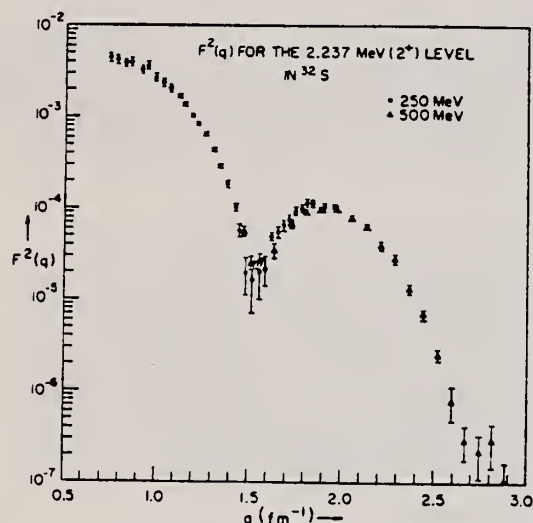
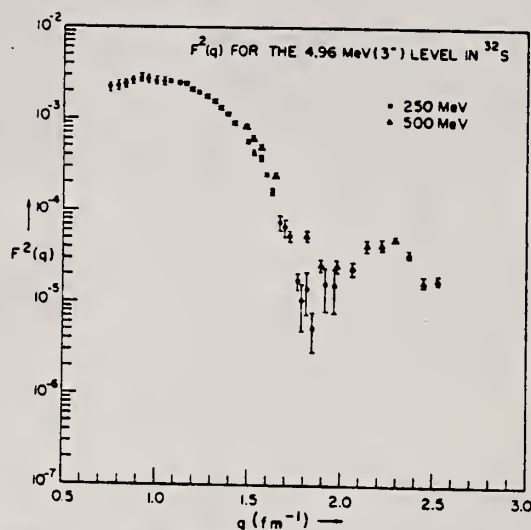
METHOD

REF. NO.

74 L1 2

hmg

REACTION	RESULT	EXCITATION ENERGY	SOURCE		DETECTOR		ANGLE
			TYPE	RANGE	TYPE	RANGE	
E, E/	FMF	2, 5	C	250, 500	MAG-D		DST
		(2.237, 4.96)					

Detailed elastic scattering data tables for
 ^{24}Mg , ^{27}Al , ^{28}Si , and ^{32}S .2 LEVELS 2.237, 4.96 MEVFIG. 13. Experimental form factor of the 2.237-MeV (2^+) level in ^{32}S .FIG. 14. Experimental form factor of the 4.96-MeV (3^-) level in ^{32}S .

REF. V.Y. Kostin, E.G. Kopanets, A.A. Koval, A.N. Lvov,
V.Y. Migaleny, S.P. Tsytko
Ukr. Fiz. Zh. 20, 1787 (1975)

ELEM. SYM.	A	Z
S	32	16

METHOD

REF. NO.	hmg
75 Ko 13	

REACTION	RESULT	EXCITATION ENERGY	SOURCE		DETECTOR		ANGLE
			TYPE	RANGE	TYPE	RANGE	
P, G	LFT	10- 12	D	1- 3	SCD-D		DST
				(1.8-3.0)			

The reaction $^{31}\text{P}(p, \gamma)^{32}\text{S}$ was studied in the range of $E_p = 1800-3000$ keV. The excitation, function γ -ray spectra and angular correlations were measured. The strengths of resonances, decay schemes, quantum characteristics and probabilities of electromagnetic transitions in the ^{32}S nucleus were determined.

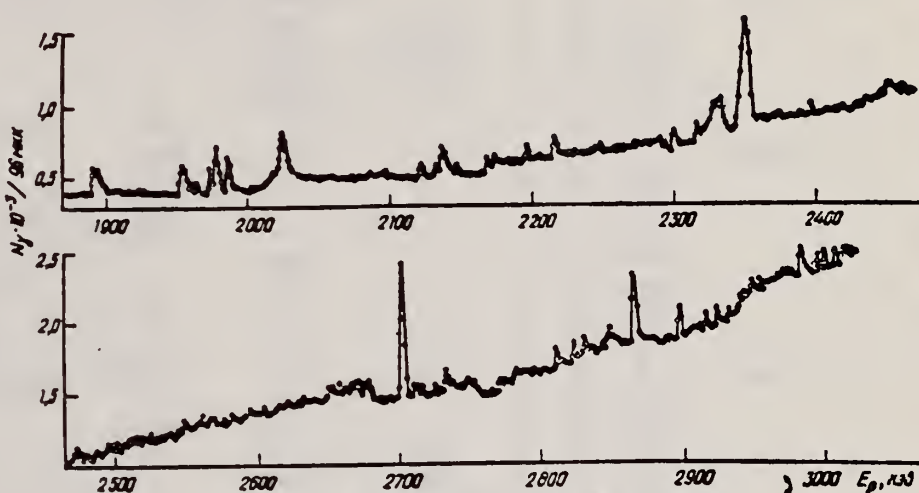


Рис. 1. Функция возбуждения реакции $^{31}\text{P}(p, \gamma)^{32}\text{S}$.

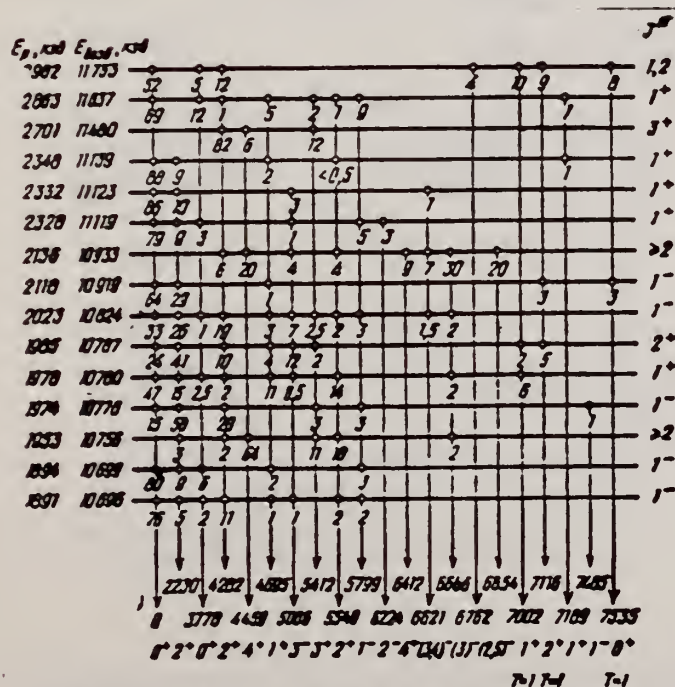


Рис. 2. Схем распада резонансных уровней ядра ^{32}S .

(over)

Таблица 6

E_f , кэВ	J_f^{π}	E_f , кэВ	J_f^{π}	T_f	$ M(M1) ^2 \cdot 10^4$, ед. Вайскопфа	$ M(E2) ^2$, ед. Вайскопфа	$ M(E1) ^2 \cdot 10^4$, ед. Вайскопфа	$ M(M2) ^2$, ед. Вайскопфа
10696	1 ⁻	0	0 ⁺	0	—	—	15±5	
		3778	0 ⁺	0	—	—	1,6±0,8	
10699	1 ⁻	0	0 ⁺	0	—	—	13±4	
		3778	0 ⁺	0	—	—	3,5±1,2	
10776	1 ⁻	0	0 ⁺	0	—	—	2,1±0,8	
10780	1 ⁺	0	0 ⁺	0	4,9±1,5	—	—	
		2230	2 ⁺	0	3,1±1,3	—	—	
		3778	0 ⁺	0	0,9±0,3	—	—	
		4282	2 ⁺	0	0,3±0,2	0,5±0,3	—	
		5549	2 ⁺	0	1,6±0,7	15±5	—	
		7002	1 ⁺	1	15±4	—	—	
10787	2 ⁺	0	0 ⁺	0	—	0,3±0,1	—	
		2230	2 ⁺	0	0,3±0,1	1,4±0,4	—	
		4282	2 ⁺	0	0,5±0,2	1,0±0,3	—	
		4695	1 ⁺	0	0,04±0,02	0,8±0,4	—	
	2 ⁻	7116	2 ⁺	1	5±2	0,07±0,03	—	
	1 ⁻	5006	3 ⁻	0	—	—	8±3	(2,5±1,2) · 10 ⁻²
10824	1 ⁻	0	0 ⁺	0	—	—	20±6	
		2230	2 ⁺	0	—	—	32±8	
		4282	2 ⁺	0	—	—	53±19	
		4695	1 ⁺	0	—	—	10±5	
		5006	3 ⁻	0	—	9±4	—	
		5412	3 ⁺	0	—	—	—	80±60
		5549	2 ⁺	0	—	—	11±7	
		5799	1 ⁻	0	6±4	—	—	
10919	1 ⁻	0	0 ⁺	0	—	—	6,5±2,2	
		2230	2 ⁺	0	—	—	6±2	(1,8±0,6) · 10 ⁻²
		7535	0 ⁺	0	—	—	10±4	
11119	1 ⁺	0	0 ⁺	0	6±2	—	—	
		2230	2 ⁺	0	1,3±0,7	0,03±0,02	—	
		3778	0 ⁺	0	1,0±0,6	—	—	
		5006	3 ⁻	0	—	—	—	15±7
		5799	1 ⁻	0	—	—	1,0	
		6224	2 ⁻	0	—	—	8,4±4,2	
11123	1 ⁺	0	0 ⁺	0	7,4±2,1	—	—	
		2230	2 ⁺	0	2,0±1	0,02±0,01	—	
		5006	3 ⁻	0	—	—	—	50
11139	1 ⁺	0	0 ⁺	0	50±18	—	—	
		2230	2 ⁺	0	10±4	0,19±0,09	—	
		4695	1 ⁺	0	5,5±3,5	0,38±0,20	—	
11480	3 ⁺	4282	2 ⁺	0	3,1±0,8	20±5	—	
		4459	4 ⁺	0	1,7±0,6	0,6±0,2	—	
		5412	3 ⁺	0	3,2±0,8	4,4±1,2	—	
11637	1 ⁺	0	0 ⁺	0	7,7±2,3	—	—	
		3778	0 ⁺	0	4,3±1,8	—	—	
		4695	1 ⁺	0	2,6±1,1	—	—	
		5799	1 ⁻	0	—	—	24±12	

REF. V.M. Asaturyan, E.O. Grigoryan, G.A. Vartapetyan, A.S. Danagulyan,
N.A. Demekhina & A.G. Khudaverdyan
Sov. J. Nucl. Phys. 25, 601 (1977)
Yad. Fiz. 25, 1133 (1977)

ELEM. SYM.	A	Z
S	32	16

METHOD

REF. NO.

77 As 10

hmg

REACTION	RESULT	EXCITATION ENERGY	SOURCE		DETECTOR		ANGLE
			TYPE	RANGE	TYPE	RANGE	
G,Be7 G,C11	ABY	THR*5	C	2*5	SCD-D		UKN
G,N13 G,F18				(4.5)			
G,Na22 G,Na24							

Photonuclear reactions in the targets ^{27}Al , ^{28}Si , ^{31}P , ^{32}S , and ^{40}Ca have been studied for maximum bremsstrahlung energies of 2, 2.4, 3, and 4.5 GeV. The yields of the residual nuclei ^7Be , ^{11}C , ^{13}N , ^{18}F , ^{22}Na , and ^{24}Na were measured by means of a germanium-lithium semiconductor detector with a sensitive volume of 30 cm³. In discussion of the results we took into account the contribution of the low energy part of the bremsstrahlung spectrum. Comparison of the measured yields with estimates calculated by Rudstam's formula permitted us to conclude that there is a difference in the mechanism of formation of the light fragments ^7Be , ^{11}C , and ^{13}N from that of the other residual nuclei ^{18}F , ^{22}Na , and ^{24}Na .

*GEV 5=4.5 GEV

TABLE II.

Residual nucleus	Reaction yields, mb/O					Normalized yields	$\sigma_{\text{exp}}/\sigma_{\text{theor}}$
	$E_{\gamma, \text{max}} = 1 \text{ GeV}$	2 GeV	2.4 GeV	3 GeV	4.5 GeV		
Al target							
^{24}Na	0.85 ± 0.02	0.81	0.81	0.87	0.87	0.98	0.56
^{22}Na	0.743 ± 0.02		1.02 ± 0.15		1.07 ± 0.1	0.668	0.98
^{18}F	0.27 ± 0.005	0.39 ± 0.02		0.4 ± 0.02	0.39 ± 0.01	0.288	1.6
^{13}N		0.021 ± 0.004		0.025 ± 0.005	0.022 ± 0.004	0.0127	2.54
^{11}C	0.117 ± 0.013	0.104 ± 0.015		0.12 ± 0.02	0.107 ± 0.015	0.081	$3.3 \cdot 10^2$
^7Be	0.39 ± 0.05		0.37 ± 0.08		0.3 ± 0.08	0.246	$1.5 \cdot 10^2$
Si target							
^{24}Na	0.31 ± 0.04	0.274 ± 0.024	0.27 ± 0.02	0.39 ± 0.02	0.25 ± 0.02	0.34	0.43
^{22}Na	0.17 ± 0.02		1.22 ± 0.2		1.22 ± 0.1	1.17	2.30
^{18}F	0.2 ± 0.01	0.38 ± 0.03		0.38 ± 0.02	0.38 ± 0.02	0.36	2.80
^{13}N		0.033 ± 0.01		0.037 ± 0.01	0.039 ± 0.01	0.0247	7.36
^{11}C		0.108 ± 0.02		0.115 ± 0.028	0.121 ± 0.027	0.107	$1.3 \cdot 10^2$
^7Be			0.388 ± 0.05		0.32 ± 0.04	0.291	$6.2 \cdot 10^2$
P target							
^{24}Na	0.31 ± 0.02				0.35 ± 0.02	0.438	0.72
^{22}Na	0.35 ± 0.02				0.35 ± 0.04	0.421	2.08
^7Be					0.35 ± 0.02	0.286	$8.91 \cdot 10^2$
S target							
^{24}Na	0.34 ± 0.04	0.25 ± 0.02	0.25 ± 0.02	0.34 ± 0.02	0.27 ± 0.02	0.417	1.1
^{22}Na	0.35 ± 0.04				0.44 ± 0.02	0.508	3.88
^{18}F	0.19 ± 0.04	0.38 ± 0.04		0.25 ± 0.04	0.27 ± 0.04	0.284	4.73
^{13}N		0.047 ± 0.02		0.063 ± 0.02	0.068 ± 0.02	0.054	$2.88 \cdot 10^2$
^{11}C	0.122 ± 0.013	0.161 ± 0.028		0.142 ± 0.028	0.13 ± 0.02	0.128	$1.23 \cdot 10^2$
^7Be	0.25 ± 0.02		0.38 ± 0.02		0.34 ± 0.04	0.344	1.19
Cl target							
^{24}Na	0.22 ± 0.01	0.38 ± 0.02		0.3 ± 0.02	0.38 ± 0.02	0.297	1.8
^{18}F	0.35 ± 0.02	0.21 ± 0.04				0.18	7.82
K target							
^{24}Na	0.08 ± 0.005	0.1 ± 0.01		0.125 ± 0.012	0.15 ± 0.015	0.16	2
^{18}F	0.09 ± 0.005	0.11 ± 0.05				0.1	7.58
Ca target							
^{24}Na	0.78 ± 0.008	0.098 ± 0.01		0.09 ± 0.01	0.12 ± 0.012	0.117	2.2
^{22}Na	0.05 ± 0.005				0.21 ± 0.02	0.21	6.37
^7Be					0.245 ± 0.023	0.23	$1.5 \cdot 10^2$

Data for Cl and K targets previously published in Reference 11.

¹¹G. A. Vartapetyan *et al.*, Yad. Fiz. 17, 685 (1973) [Sov. J. Nucl. Phys. 17, 350 (1973)].

REF. V. Ya. Kostin, E.G. Kopanets, A.A. Koval, A.N. L'vov,
V.Ya. Migalenyay, S.P. Tsytko
Izv. Akad. Nauk SSSR 41, 151 (1977)
Bull. Acad. Sci. 41, 124 (1977)

ELEM. SYM.	A	Z
S	32	16
REF. NO.		
77 Ko 9		egf

METHOD

REACTION	RESULT	EXCITATION ENERGY	SOURCE		DETECTOR		ANGLE
			TYPE	RANGE	TYPE	RANGE	
P,G	NOX	10	D	1	SCD-D		DST

The angular distributions of γ -rays from the decay of the resonance states of ^{32}S (9950, 9979, 10,372, and 10,756 keV) in the $^{31}\text{P}(p,\gamma)^{32}\text{S}$ reaction have been determined. The probable spin values of these states are: 1, 1, 2, and (2), respectively.

9.95 MEV

Table 1

Angular Distributions of γ -Rays from the Decay of Resonance States of ^{32}S

E_p , keV	E_{γ} , keV	I^{π}	P_0	E_f , keV	I_f^{π}	$a_1 \pm \Delta a_1$	$a_2 \pm \Delta a_2$	δ
1121	9950	1	1 ± 0.00 -0.05	0	0+	0.032 ± 0.166	0.211 ± 0.171	0
				2230	2+	0.761 ± 0.039	-0.161 ± 0.102	0.7 ± 0.1
				8126	1+	0.299 ± 0.038	0.093 ± 0.038	0.10 ± 0.06
1151	9979	1	0.65 ± 0.05	2230	2+	-0.003 ± 0.041	0.102 ± 0.043	0.1 ± 0.1 $\pi\pi\pi$
				5549	2+	-0.339 ± 0.035	0.038 ± 0.035	2.84 ± 0.91 -5.3 ± 1.8
1557	10 372	2+	0.70 ± 0.05	2230	2+	0.479 ± 0.041	-0.024 ± 0.043	-0.08 ± 0.03
				4282	2+	0.544 ± 0.033	-0.068 ± 0.034	-0.08 ± 0.02
				4695	1+	-0.276 ± 0.035	-0.171 ± 0.036	-0.10 ± 0.10
				5412	3+	0.140 ± 0.09	0.009 ± 0.010	2.84 ± 0.53
				6668	(2)	0.438 ± 0.031	-0.037 ± 0.032	0.72 ± 0.26
1953	10 756	(2)	0.00 ± 0.05 -0.05	4459	4+	-0.19 ± 0.04	0.04 ± 0.04	-0.45 ± 0.15
				5412	2+	0.23 ± 0.07	0.00 ± 0.10	0.48 ± 0.12
				5549	2+	-0.20 ± 0.09	-0.03 ± 0.03	0.86 ± 0.11

* P_0 is the probability of population of a substate of a resonance level with total angular momentum component $I_3 = 0$.

ELEM. SYM.	A	Z
S	32	16
METHOD		REF. NO.
		77 Ro 2
		egf

REACTION	RESULT	EXCITATION ENERGY	SOURCE		DETECTOR		ANGLE
			TYPE	RANGE	TYPE	RANGE	
A, G	LFT	8- 11	D	2- 4	SCD-D		55

Abstract: The γ -decays of eleven resonances in the $^{33}\text{Si}(x, \gamma)^{32}\text{S}$ reaction below $E_x = 3.83$ MeV have been studied using a large Ge(Li) detector. Results for branching ratios differ considerably from previous NaI work. The previous discrepancy in radiative strengths for the 2.61 MeV resonance is explained by this data. The strengths of the first five resonances at $E_x = 1.77, 1.99, 2.19, 2.37$ and 2.42 MeV appear to be $(39 \pm 13)\%$ lower than previously reported. Spin-parities of 1^- , 2^+ and 2^+ have been assigned to the levels at 8.50, 8.69 and 8.86 MeV respectively. The radiative width of the $E_x = 1.467$ MeV, $J^\pi = 3^-$ resonance in the $^{31}\text{P}(p, \gamma)^{32}\text{S}$ reaction has also been measured.

TABLE 2

A comparison of radiative strengths measured here and in previous experiments (in c.m. units)

E_x (MeV)	$\omega\gamma = (2J+1)\Gamma_\gamma/\Gamma$ (meV)		
	present $\pm 20\%$	Toevs ^{a)}	Smulders ^{b)}
1.77	16	22 ± 6	
1.99	12	18 ± 5	
2.19	16	36 ± 12	
2.37	52	82 ± 20	
2.42	64	120 ± 30	
2.61	540	540 ± 130	520
2.88	720		670
2.90	830		860
3.16	630		450
3.74	8.1 eV		11 ± 3 eV ^{c)}
3.81	2.3 eV		3.0 ± 1.2 eV ^{c)}

^{a)} Changed to c.m. units.

^{b)} The original values have been changed to take into account all decay branches reported here compared to those reported in table 1 of ref. ²⁾. Assumed to be c.m.

^{c)} Ref. ³⁾ based on ref. ²⁾.

²⁾ P.J.M. Smulders, Physica 30, 1197 (1964)

³⁾ J. Vernotte et al., Nucl. Phys. A124, 350 (1969)

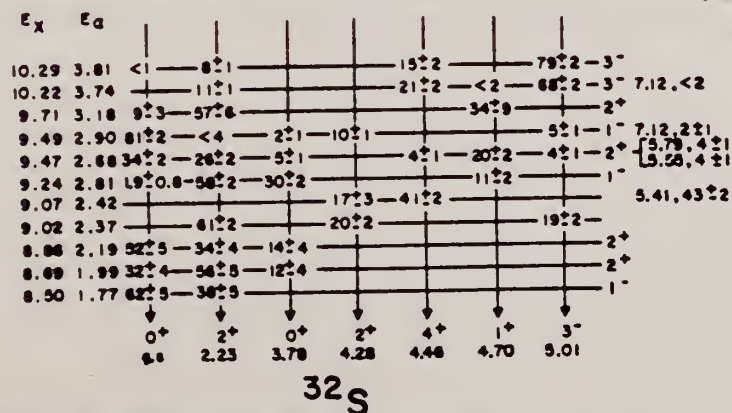


Fig. 3. The γ -decay schemes obtained from a Ge(Li) detector at 55° to the incident beam. The known $2^+ \rightarrow 0^+$ branches have been corrected to take into account angular distribution effects.

ELEM. SYM.	A	Z
S	32	16
REF. NO.		77 Th 2
		egf

Remarks: Deexcitation G-Rays

REACTION	RESULT	EXCITATION ENERGY	SOURCE		DETECTOR		ANGLE
			TYPE	RANGE	TYPE	RANGE	
G,NG	ABX	17- 27	C	16- 27	SCD-D		150
G,PG	ABX	11- 27	C	16- 27	SCD-D		150

Abstract: Cross sections and integrated cross sections for photodisintegration of ^{32}S to specific residual states in ^{31}P and ^{31}S have been measured. Comparison with spectroscopic factors for nucleon pickup reactions on ^{32}S leading to the same residual states are made. It is concluded that the creation and decay of the dipole state in ^{32}S is predominantly a single-nucleon interaction.

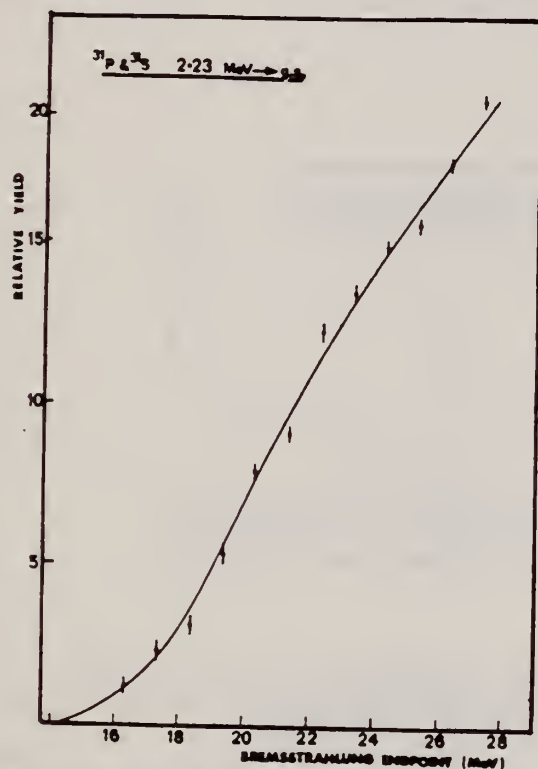


Fig. 2. A typical curve drawn through the yield of deexcitation γ -rays from the 2.32 MeV levels of ^{31}S and ^{31}P .

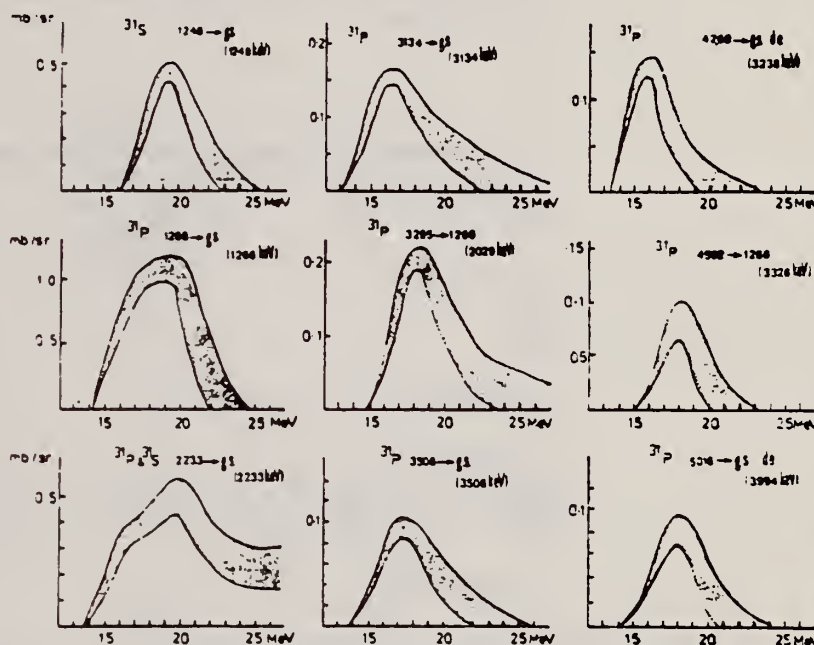


Fig. 3. Cross sections for photoreactions producing γ -rays of the energies indicated.

(OVER)

TABLE 1
Integrated cross sections for reaction to various residual states

Residual level (MeV)	J^π	$\int_0^{26} \sigma \frac{d\sigma}{d\Omega} \Big _{150^\circ} dE$ (MeV · mb/sr)	Residual level (MeV)	J^π	$\int_0^{26} \sigma \frac{d\sigma}{d\Omega} \Big _{150^\circ} dE$
³¹P			³¹S		
g.s.	$\frac{1}{2}^+$	3.3 ^{a)}	g.s.	$\frac{1}{2}^+$	3.7 ^{a)}
1.266	$\frac{3}{2}^+$	3.8 ± 1.0	1.248	$\frac{3}{2}^+$	1.9 ± 0.2
2.234	$\frac{5}{2}^+$	2.0 ± 0.3 ^{b)}	2.232	$\frac{3}{2}^+$	1.0 ± 0.3 ^{b)}
3.134	$\frac{1}{2}^+$	0.9 ± 0.1	3.08	$\frac{1}{2}^+$	weak
3.295	$\frac{5}{2}^+$	1.0 ± 0.1	3.351		0.15 ± 0.1
3.414	$\frac{7}{2}^+$	0.26 ± 0.05			
3.506	$\frac{3}{2}^+$	0.8 ± 0.2	²⁸Si		
4.190	$\frac{5}{2}^+$	0.5 ± 0.1	1.788	2 ⁺	0.6 ± 0.2
4.260	$\frac{3}{2}^+$	1.0 ± 0.4	4.168	4 ⁺	0.3 ± 0.1
4.592	$\frac{5}{2}^+$	0.4 ± 0.1			
5.015	$\frac{3}{2} (\frac{1}{2}^-)$	(0.7 ± 0.3)			
5.015	$\frac{1}{2} (\frac{3}{2}^+)$				
5.253	$\frac{1}{2}^+$	0.4 ± 0.1			
5.557	$\frac{3}{2}^+$	0.3 ± 0.15			
5.988	$(\frac{1}{2}, \frac{3}{2})$	(0.3 ± 0.2)			

^{a)} The procedure used to obtain the ground-state cross sections is discussed in the text.

^{b)} Calculated assuming that the 2.23 MeV levels in ³¹P and ³¹S are populated in the same ratio as the first excited states.

TABLE 2
Comparison of residual state population with single-nucleon pickup spectroscopic factors

Residual state in ³¹ P MeV	J^π	$\int_0^{26} \sigma \frac{d\sigma}{d\Omega} \Big _{150^\circ} dE$ (MeV · mb/sr)	Pickup spectroscopic factors S_p for ³² S(d, ³ He) ³¹ P ^{a)}
2s_{1/2} hole states			
g.s.	$\frac{1}{2}^+$	3.3	2.2
5.25	$\frac{1}{2}^+$	0.4	0.4
6.41	$\frac{1}{2}^+$		0.6
d_{3/2} hole states			
1.266	$\frac{3}{2}^+$	3.8	1.4
d_{5/2} hole states			
2.234	$\frac{5}{2}^+$	2.0	3.0
3.294	$\frac{5}{2}^+$	1.0	1.1
4.190	$\frac{5}{2}^+$	0.5	1.1
4.78	$\frac{5}{2}^+$		0.46
p-shell hole states			
5.99	$(\frac{1}{2}, \frac{3}{2}^-)$	(0.3)	
		$\Sigma = 11.3$	1.0 ± 0.4
Other levels populated			
3.134	$\frac{1}{2}^+$	0.9	Stripping spectroscopic factors (2J+1)S _p from ³⁰ Si(³ He, d) ³¹ P ^{b)}
3.414	$\frac{7}{2}^+$	0.26	
3.506	$\frac{3}{2}^+$	0.8	0.07
4.260	$\frac{3}{2}^+$	1.0	0.03
4.592	$\frac{3}{2}^+$	0.4	0.11
5.015	?	0.7	?
5.557	$\frac{3}{2}^+$	0.3	
		$\Sigma = 4.4$	0.1

^{a)} Ref. ²⁴).

^{b)} Ref. ¹⁵).

¹⁵ A.C. Wolff and H.G. Leighton, Nucl. Phys. **A140**, 319 (1970)

²⁶ G.Th. Kaschl, G. Mairle, U. Schmidt-Rohr, G.J. Wagner and P. Turek, Nucl. Phys. **A136**, 286 (1969)

REF. V. Di Napoli, J. B. Martins, G. Rosa, F. Salvetti, O. A. P. Tavares,
M. L. Terranova and H. G. De Carvalho
J. Inorg. Nucl. Chem. 40, 1619 (1978)

ELEM. SYM.	A	Z
S	32	16

METHOD

REF. NO.

78 Di 10

hg

REACTION	RESULT	EXCITATION ENERGY	SOURCE		DETECTOR		ANGLE
			TYPE	RANGE	TYPE	RANGE	
G,C11	ABY	30(30.93)-999	C	300-999	ACT-I		4PI
G,Be7	ABY	28(28.59)-999	C	300-999	ACT-I		4PI

Abstract—Mean cross sections for the photoproduction of ^7Be and ^{11}C from ^{19}F , ^{27}Al , ^{28}Si and ^{32}S targets, ^7Be from $^{10,11}\text{B}$, and ^{11}C from ^{14}N and ^{16}O targets have been measured using bremsstrahlung beams in the energy range 0.3–1.0 GeV. The results have been compared with previous measurements and an excellent agreement has been found. In most cases, the values obtained turned out to be much larger than those expected from a simple spallation mechanism. A fragmentation and/or a fission-like process has been suggested in explaining the mechanism of such reactions.

999=1 GEV

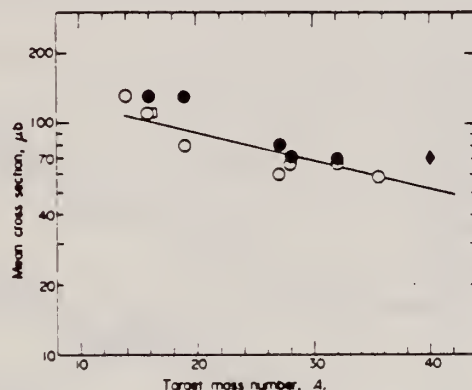


Fig. 1. Mean cross sections per photon, σ_0 , of ^{11}C photoproduction vs the target mass number A . Experimental data are taken from: ●, Ref. [9]; □, Ref. [13]; ♦, Ref. [2]; ○, present work. The straight line is a least squares fit of the experimental points.

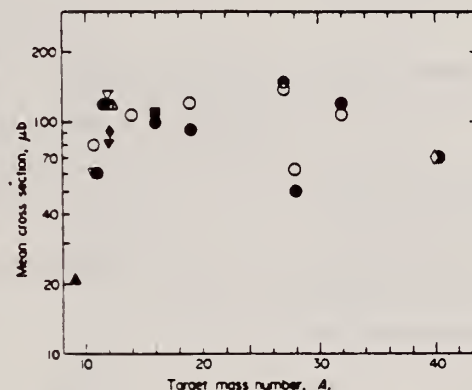


Fig. 2. The same as in Fig. 1 for ^7Be photoproduction. Experimental data are taken from: ▲, Refs. [6,7]; ▽, Ref. [8]; ●, Ref. [9]; △, Ref. [10]; ♦, Ref. [11]; ▼, Ref. [12]; □, Ref. [13]; ■, Ref. [14]; ○, Ref. [2]; ○, present work.

Table 1. Cross sections per equivalent quantum of ^{11}C photoproduction

E_0 (GeV)	Cross Section, σ_0 (μb)					
	^{14}N	^{16}O	^{19}F	^{27}Al	^{28}Si	^{32}S
0.30	520±30	200±20	110±20	28±10	35±10	45±10
0.32	520±30	210±20	120±20	30±10	42±10	50±10
0.35	530±30	230±20	125±20	38±10	45±10	60±10
0.40	530±30	230±20	130±20	42±10	52±10	65±10
0.48	550±30	255±20	150±20	60±10	70±10	80±10
0.55	570±30	260±20	160±20	60±10	78±10	85±10
0.65	600±30	290±20	180±20	70±10	85±10	98±10
0.75	620±30	300±20	180±20	79±10	95±10	110±10
0.90	650±30	320±20	190±20	90±10	110±10	120±10
1.00	680±30	330±20	210±20	100±10	115±10	125±10

Table 2. Cross sections per equivalent quantum of ^7Be photoproduction

E_0 (GeV)	Cross Section, σ_0 (μb)						
	$^{10,11}\text{B}$	^{14}N	^{16}O	^{19}F	^{27}Al	^{28}Si	^{32}S
0.30	150±20	200±20	113±20	152±20	40±20	20±20	50±20
0.32	160±20	200±20	120±20	150±20	45±20	30±20	54±20
0.35	160±20	210±20	130±20	159±20	42±20	30±20	60±20
0.40	175±20	226±20	145±20	170±20	98±20	20±20	70±20
0.48	190±20	245±20	163±20	186±20	100±20	50±20	140±20
0.55	200±20	260±20	187±20	200±20	93±20	48±20	90±20
0.65	220±20	280±20	197±20	214±20	140±20	68±20	130±20
0.75	225±20	300±20	215±20	227±20	180±20	70±20	130±20
0.90	240±20	318±20	230±20	245±20	186±20	88±20	165±20
1.00	250±20	330±20	242±20	260±20	200±20	97±20	190±20

(OVER)

Table 3. Comparison between experimentally determined and calculated cross sections of ^7Be and ^{11}C photo-production and indication of the dominant reaction channels

Target Nucleus	Product Nucleus	Nominal Nucleon Loss, ΔA	$\Delta A/A_t$ (%)	$\bar{\sigma}_{\text{exp}}^{(*)}$ (μb)	$\bar{\sigma}_{\text{CMD}}^{(**)}$ (μb)	$\frac{\bar{\sigma}_{\text{exp}}}{\bar{\sigma}_{\text{CMD}}}$	Apparent Threshold (Exp.) E_{th} (MeV)	Possible Mechanism of Production
$^{10,11}\text{B}$	^7Be	(3), 4	(30), 36	67	28	2	≤ 50	Spallation
^{12}C	^7Be	5	42	110	20	5	≤ 50	Spallation
^{14}N	^7Be	7	50	108	12	9	≤ 50	Fission Spallation
^{14}N	^{11}C	3	21	130	60	2	≤ 50	Spallation
^{16}O	^7Be	9	56	107	8	13	$50 < E_{\text{th}} < 200$	Fission Fragmentation
^{16}O	^{11}C	5	31	117	33	3	≤ 50	Spallation
^{19}F	^7Be	12	63	106	5	21	$50 < E_{\text{th}} < 200$	Fission Fragmentation
^{19}F	^{11}C	8	42	105	16	7	$50 < E_{\text{th}} < 200$	Fission Fragmentation Spallation
^{27}Al	^7Be	20	74	142	2	71	> 200	Fragmentation
^{27}Al	^{11}C	16	59	70	5	14	$50 < E_{\text{th}} < 200$	Fission Fragmentation
^{28}Si	^7Be	21	75	56	2	28	> 200	Fragmentation
^{28}Si	^{11}C	17	61	68	4	17	$50 < E_{\text{th}} < 200$	Fission Fragmentation
^{32}S	^7Be	25	78	114	2	57	≈ 200	Fragmentation
^{32}S	^{11}C	21	66	68	3	23	$50 < E_{\text{th}} < 200$	Fission Fragmentation
$^{35,37}\text{Cl}$	^{11}C	24, (26)	69, (70)	59	3	20	$50 < E_{\text{th}} < 200$	Fission Fragmentation
^{40}Ca	^7Be	33	83	70	1	70	> 200	Fragmentation
^{40}Ca	^{11}C	29	73	70	2	35	> 200	Fragmentation

(*) Mean values of the different measurements (see Figs. 1 and 2).

(**) Calculated values according to Ref. [5].

REF. V.V. Varlamov, B.S. Ishkhanov, I.M. Kapitonov, Zh.L. Kocharova &
V.I. Shvedunov
Yad. Fiz 28, 590 (1978)
Sov. J. Nucl. Phys. 28, 302 (1978)

ELEM. SYM.	A	Z
S	32	16

METHOD	REF. NO.
	78 Va 3

ANGLE
hmg

REACTION	RESULT	EXCITATION ENERGY	SOURCE		DETECTOR		ANGLE
			TYPE	RANGE	TYPE	RANGE	
G,P	ABX	11-30	C	17-30	SCD-D		90

TABLE II. Probabilities of formation of ^{31}P nucleus in various states.

State of ^{31}P nucleus, MeV	Probability, %	State of ^{31}P nucleus, MeV	Probability, %
0	5±0.5	4.8	13±1
1.27	13±1	8.9	15±2
2.23	9±1	9.5	20±2
3.3	11±1	12.5	14±2

Spectra of photoprotons from ^{32}S have been measured in a bremsstrahlung beam. The bremsstrahlung end-point energy was varied over the range 17-30 MeV with a step of no more than 1 MeV. Distributions of the fraction of transitions to various states of the final nucleus ^{31}P have been calculated and the partial photoproton cross sections corresponding to these transitions have been determined. From these data we have obtained for ^{32}S information on the probability of electric dipole excitations in the various shells, the magnitude of the configuration splitting of the giant dipole resonance, and the contribution of configurations of the one-particle-one-hole type to formation of the giant dipole resonance. A comparison with the results of theoretical calculations is made.

TABLE III. Probabilities of decay (in %) to various levels of the ^{31}P final nucleus for different portions of the giant resonance of the ^{32}S nucleus.

E_f , MeV	E_γ , MeV				E_f , MeV	E_γ , MeV			
	17.4-17.6	17.6-18.3	18.3-19.0	19.0-20.0		17.4-17.6	17.6-18.3	18.3-19.0	19.0-20.0
0	16	7	2	1	4.8	17	22	12	6
1.27	30	22	11	7	8.9				
2.23	13	12	8	6	9.5				
3.3	22	15	9	7	12.5				

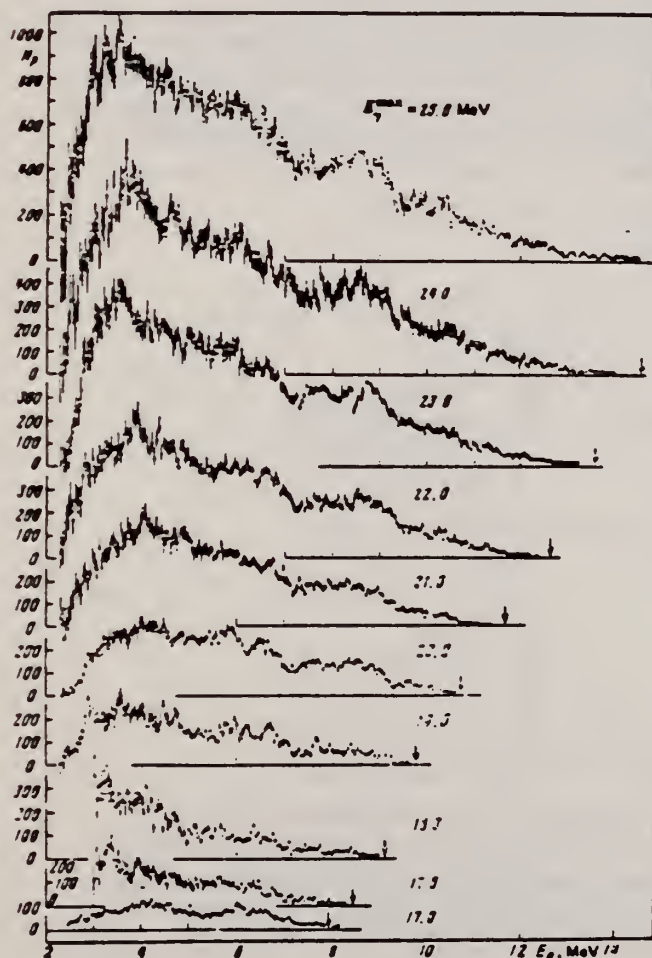


FIG. 1. Spectra of photoprotons for $E_\gamma^{\text{max}} = 17.0, 17.6, 18.3, 19.0, 20.0, 21.0, 22.0, 23.0, 24.0$, and 25.0 MeV.

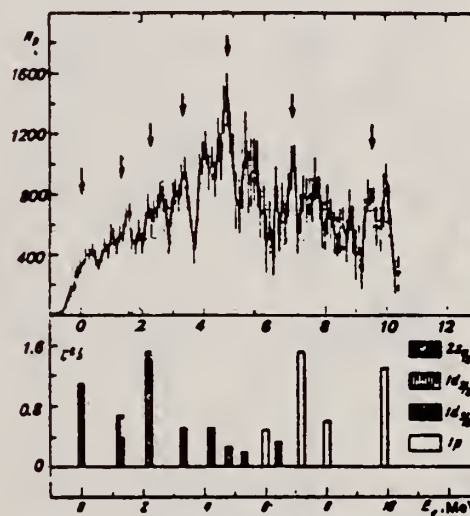


FIG. 4. Comparison of the distribution of the fraction of transitions to various states of the ^{31}P final nucleus, obtained in the present work for $E_\gamma^{\text{max}} = 17-24$ MeV (upper figure) with the data of the $^{32}\text{S}(d, ^3\text{He})^{31}\text{P}$ reaction²⁸ (lower figure). The vertical scale in the lower figure gives values of the spectroscopic factors of the ^{31}P levels.

(OVER)

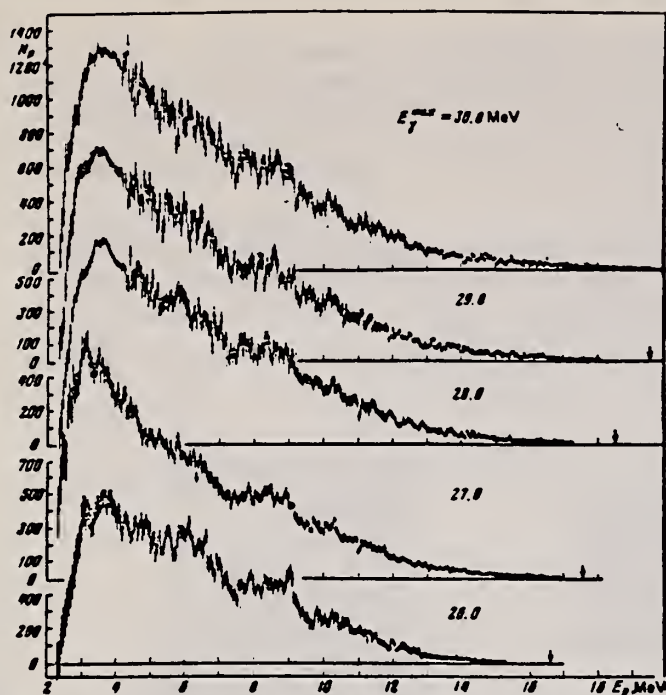


FIG. 2. Spectra of photoprotons for $E_\gamma = 26.0, 27.0, 28.0, 29.0,$ and 30.0 MeV.

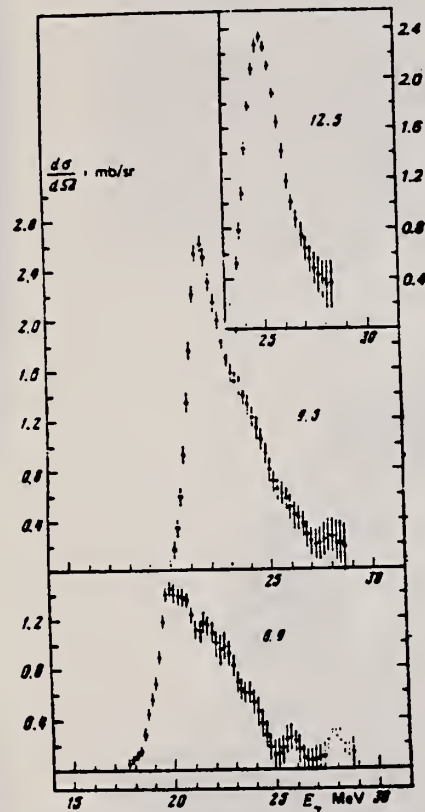


FIG. 6. Cross sections for the reaction $^{32}\text{S}(\gamma, p)^{31}\text{P}$ with formation of the final nucleus in states with energy $6.9, 9.3,$ and 12.5 MeV (from bottom to top).

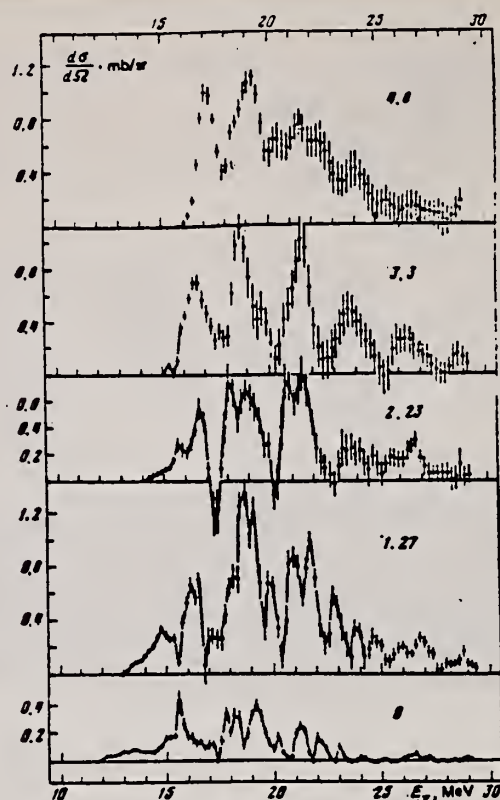


FIG. 5. Cross sections for the reaction $^{32}\text{S}(\gamma, p)^{31}\text{P}$ with formation of the final nucleus in the ground state and in the states with energies $1.27, 2.23, 3.3,$ and 4.8 MeV (from bottom to top).

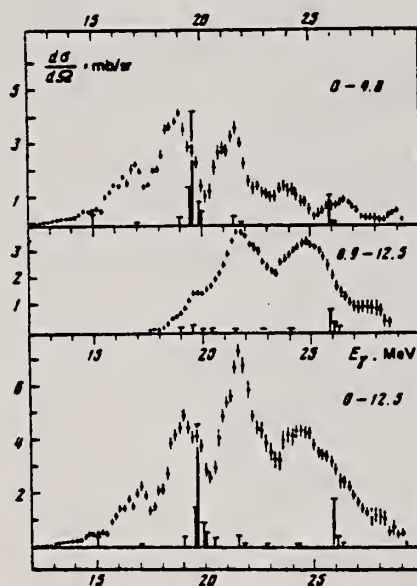


FIG. 7. Sums of partial photoproton cross sections for the ^{32}S nucleus: combined cross section with formation of the final nucleus in states with energy $0-4.8$ MeV (upper figure), combined cross section with formation of the final nucleus in states with energy $6.9-12.5$ MeV (center figure), total cross section for the reaction $^{32}\text{S}(\gamma, p)^{31}\text{P}$ (lower figure). The vertical columns are theoretical results.

REF. E. Kuhlmann, J.R. Calarco, V.K.C. Cheng, D.G. Mavis, J.R. Hall,
S.S. Hanna
Phys. Rev. C20, 5 (1979)

ELEM. SYM.	A	Z
S	32	16
REF. NO.		hg
79 Ku 6		

METHOD			SOURCE		DETECTOR		ANGLE
REACTION	RESULT	EXCITATION ENERGY	TYPE	RANGE	TYPE	RANGE	
A,G	ABX	11-21	D	5-16	NAI-D		DST

E2 STRENGTH, SEE 79KU5

Excitation functions and angular distributions of the reactions $^{28,30}\text{Si}(\alpha, \gamma_0)$ were used to study the distribution of E2 strength in the energy regions 11-21 MeV of $^{32,34}\text{Si}$, as well as to probe the importance of isospin in the decay of the E1 giant resonance in these nuclei. It was found that the E2 strength in the (γ, α_0) channel is widely distributed and accounts for about 12% of the energy weighted isoscalar sum rule in each nucleus. Together with the E2 strength observed in lower resonances, about 45% of the sum rule is accounted for in ^{32}S and 34% in ^{34}S , where the measurements on the lower resonances are incomplete. The spreading of the E2 strength can be attributed to the mixing of πp - πh configurations into the basic $1p$ - $1h$ excitations of the E2 resonance, and the large E2 strength is attributed to the presence of a direct or semidirect component in the (γ, α_0) process. A comparison of the E1 strengths in the (γ, α_0) channel of the giant dipole resonances in $^{32,34}\text{S}$ indicates that isospin conservation is important in these reactions. The relative weakness of the E1 (γ, α_0) strength in ^{34}S compared to the E2 strength is attributed to the relative purity of the $1p$ - $1h$ character of the E1 resonance as compared to that of the E2 resonance.

[NUCLEAR REACTIONS $^{28}\text{Si}(\alpha, \gamma_0)$, $E = 5-16$ MeV; $^{30}\text{Si}(\alpha, \gamma_0)$, $E = 4-15$ MeV; measured $\sigma(E, E_\gamma, \Theta_\gamma)$. $^{32,34}\text{S}$ deduced E1, E2 strengths. Enriched targets.]

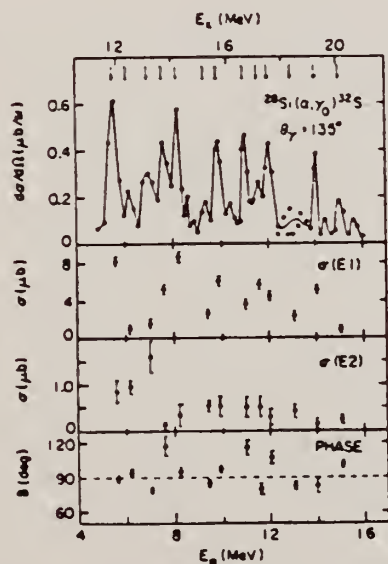


FIG. 1. Top: excitation function at $\theta = 135^\circ$ for the reaction $^{28}\text{Si}(\alpha, \gamma_0)^{32}\text{S}$. The arrows indicate energies at which angular distributions were measured. Middle: the extracted E1 and E2 total cross sections for the (α, γ_0) reaction. Bottom: the E2 phase δ relative to the E1 phase.

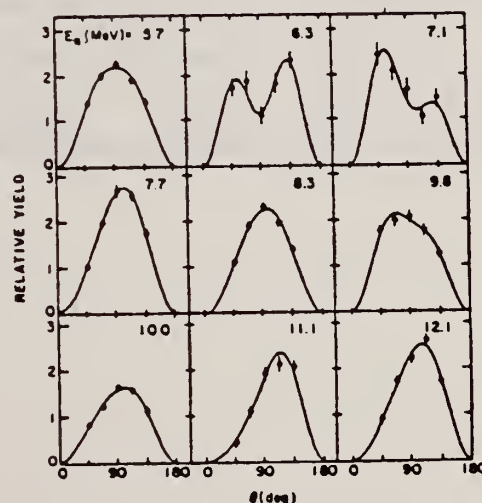


FIG. 2. Typical angular distributions for the reaction $^{28}\text{Si}(\alpha, \gamma_0)^{32}\text{S}$. The solid lines are fits obtained with Eq. (10).
(1)

(over)

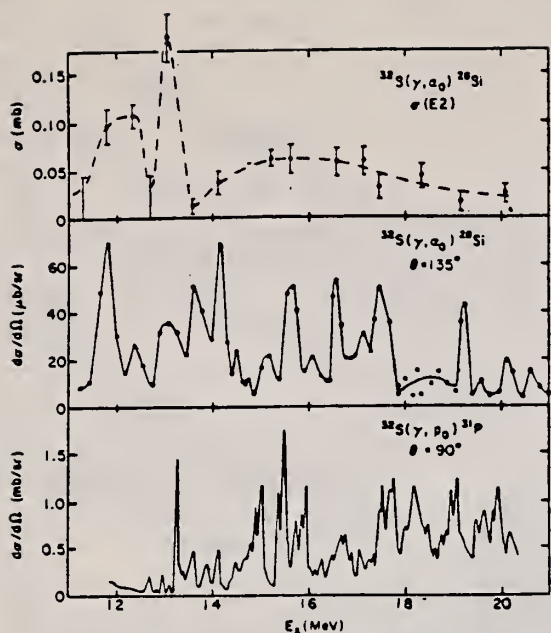


FIG. 3. Top: the total E2 cross section converted by detailed balance to that for $^{32}\text{S}(\gamma, \alpha_0)^{28}\text{Si}$. Middle: the total differential cross section at $\theta = 135^\circ$ converted to $^{32}\text{S}(\gamma, \alpha_0)^{28}\text{Si}$. Bottom: the total differential cross section at $\theta = 90^\circ$ for $^{32}\text{S}(\gamma, p_0)^{31}\text{P}$ obtained by detailed balance from $^{31}\text{P}(p, \gamma_0)^{32}\text{S}$ (Ref. 14).

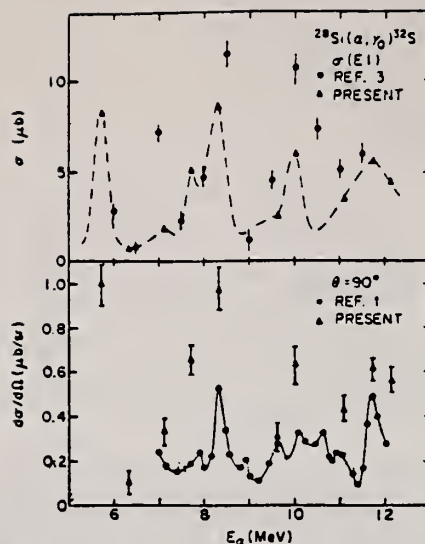
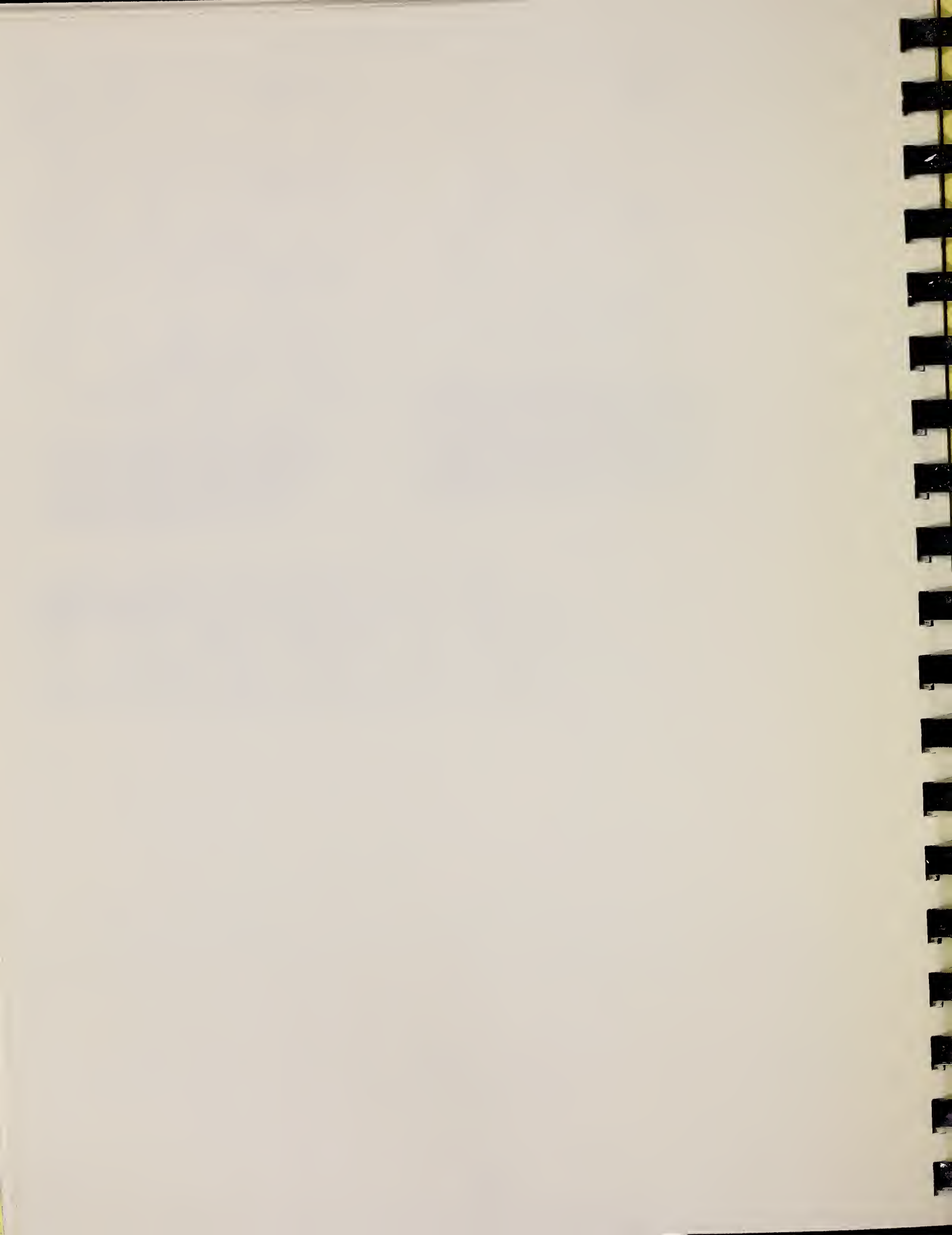


FIG. 4. Top: the E1 cross sections derived from $^{28}\text{Si}(\alpha, \gamma_0)^{32}\text{S}$ in the present work compared with those of Ref. 3. The dashed line is included to guide the eye and follows roughly the (α, γ_0) excitation curve. Bottom: the 90° yields in $^{28}\text{Si}(\alpha, \gamma_0)^{32}\text{S}$ obtained by adjusting the 135° measurements by the measured angular distributions in the present work compared with the 90° yield curve of Ref. 1.

TABLE II. Integrated E1 and E2 strengths in $^{32}\text{S}(\gamma, \alpha_0)^{28}\text{Si}$ and $^{31}\text{S}(\gamma, \alpha_0)^{30}\text{Si}$ and total integrated E2 strengths based on a Hauser-Feshbach calculation.

Nucleus	ΔE_x (MeV)	$\int \sigma(E1) dE$ (% sum rule)	$\int \sigma(E2)/E^2 dE$ (% sum rule)	ΔE_x (MeV)	$\int \sigma_{\text{tot}}^{\text{CN}}(E2)/E^2 dE$ (% sum rule)
^{32}S	11.6 - 20.3	0.88	11.6	0 - 20.3	≈ 150
^{31}S	11.1 - 19.3	3.2	12.6	0 - 19.3	≈ 370



S
A=33

S
A=33

S
A=33

REF. I. Bergqvist, J. A. Biggerstaff, J. H. Gibbons, W. M. Good
Phys. Rev. 158, 1049 (1967)

ELEM. SYM.	A	Z
S	33	16

METHOD

REF. NO.	
67 Be 7	egf

REACTION	RESULT	EXCITATION ENERGY	SOURCE		DETECTOR		ANGLE
			TYPE	RANGE	TYPE	RANGE	
N,G	LFT	8-9	D	0-1	NAI-D	0-7	90

SOURCE 30,111 KEV

TABLE VIII. Gamma rays from $^{35}\text{S}(\text{n},\gamma)^{36}\text{S}$; $E_n=30\text{ KeV}$, $J^\pi=\frac{1}{2}^-$.

E_γ (MeV) ^a	I_γ (per 100 captures)	Assignments	$J_i^\pi \rightarrow J_f^\pi$	Γ_γ (meV)	$1000 M ^2$
8.7	8 ± 2	$C \rightarrow 0$	$\frac{1}{2}^- \rightarrow \frac{1}{2}^+$	40	0.09
7.8	60 ± 4	$C \rightarrow 0.84$	$\frac{1}{2}^- \rightarrow \frac{1}{2}^+$	300	0.9
6.7	6 ± 2	$C \rightarrow 1.97$	$\frac{1}{2}^- \rightarrow \frac{1}{2}^+$	30	0.1
6.4	10 ± 3	$C \rightarrow 2.31$	$\frac{1}{2}^- \rightarrow \frac{1}{2}^+$	50	0.3
5.5	8 ± 4	$(C \rightarrow 3.22)$	$(\frac{1}{2}^- \rightarrow \frac{1}{2}^-)$	(40)	(1)
4.8	10 ± 4				
0.84	90 ± 10	$0.84 \rightarrow 0$	$\frac{1}{2}^+ \rightarrow \frac{1}{2}^+$		

^a Additional weak lines are evident in the energy region from 1 to 4.2 MeV.

TABLE IX. Gamma rays from $^{35}\text{S}(\text{n},\gamma)^{36}\text{S}$;
 $E_n=111\text{ keV}$, $J^\pi=\frac{1}{2}^+$.

E_γ (MeV)	I_γ (per 100 captures)	Assignment	$J_i^\pi \rightarrow J_f^\pi$
8.71	21 ± 2	$C \rightarrow 0$	$\frac{1}{2}^+ \rightarrow \frac{1}{2}^+$
(8.3)		$^{35}\text{S}(\text{n},\gamma)?$	
7.91	19 ± 3	$C \rightarrow 0.84$	$\frac{1}{2}^+ \rightarrow \frac{1}{2}^+$
5.53	30 ± 4	$C \rightarrow 3.22$	$\frac{1}{2}^+ \rightarrow \frac{1}{2}^-$
(4.1-5.0) ^a	~ 20		
(3.8)	(≤ 5)		
3.40	10 ± 5	$\{ (4.21 \rightarrow 0.84)$ $(5.71 \rightarrow 2.31)$	
3.22	18 ± 8	$3.22 \rightarrow 0$	$\frac{1}{2}^- \rightarrow \frac{1}{2}^+$
3.0	10 ± 5	$C \rightarrow 5.71$	$\frac{1}{2}^+ \rightarrow (\frac{1}{2})^-$
2.38	31 ± 5	$3.22 \rightarrow 0.84$	$\frac{1}{2}^- \rightarrow \frac{1}{2}^+$

^a Unresolved structure.

Pelekhov, *Atlas of Gamma-Ray Spectra from Radiation Capture of Thermal Neutrons* (Pergamon Press, Inc., New York, 1959).

ELEM. SYM.	A	Z
S	33	16
REF. NO.	78 Ok 2	
	hg	

METHOD			SOURCE		DETECTOR		ANGLE
			TYPE	RANGE	TYPE	RANGE	
A,G	RLY	9-11	D	3-4	SCD-D		DST

Highly excited levels of ^{33}S populated by α -particle capture in ^{29}Si have been investigated for $E_x = 1.962$ MeV to 4.287 MeV. Excitation curves measured with Ge(Li) and BF_3 detectors are reported. More than fifty resonances can be identified with levels in ^{33}S . (α, γ) angular distributions measured on five strong resonances have yielded J^π values $1/2^+$, $3/2^+$, $5/2^-$, $5/2^-$, $5/2^-$ and $3/2^+$ respectively, for the $E_x = 10.054$, 10.466, 10.523, 10.721, 10.758 and 10.776 MeV levels in ^{33}S . Elastic scattering experiments have been performed and the J^π assignments are found to be consistent with the l -values inferred from the elastic scattering data. Decay schemes from the above ^{33}S levels have been proposed. A new level at 9.245 MeV is also suggested and the J^π values for the 4.425 and 2.87 MeV states are shown to be consistent with $7/2^+$ and $3/2^+$ assignment, respectively.

JPI, 3 LEVELS

Nuclear Reactions $^{29}\text{Si}(\alpha, \gamma)$ and $^{29}\text{Si}(\alpha, \alpha)$, $E_\alpha = 1.962 - 4.287$ MeV. Measured relative $\sigma(E)$. Deduced J^π and E_γ of ^{33}S levels. New ^{33}S level at $E_x = 9.245$ MeV. Enriched targets.

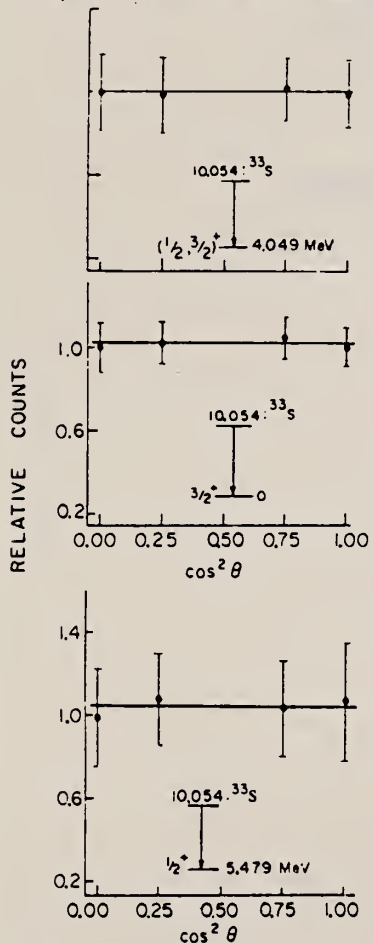


Fig. 4. Measured angular distributions of three transitions at 3.343 MeV E_x resonance in $^{29}\text{Si}(\alpha, \gamma)^{33}\text{S}$ reaction. The solid line in each figure gives the theoretical angular distribution for the assigned resonance spin

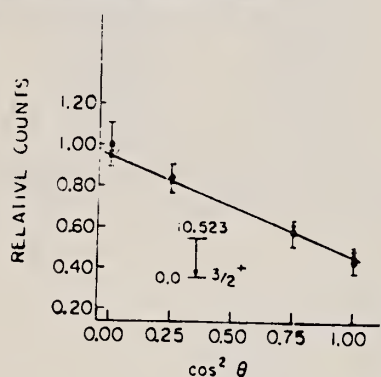


Fig. 6. Measured angular distributions of transitions at 3.845 MeV E_x resonance. The fit with a compound $J = 5/2$ shows minimum χ^2 values for all three transitions

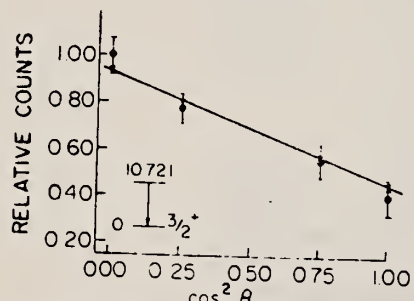


Fig. 7. Measured angular distribution of transition at 4.091 MeV E_x resonance

Table 1. Summary of spins and parities, multipoles, mixing ratio and values of χ^2 as obtained from $^{29}\text{Si}(\alpha, \gamma)^{33}\text{S}$ reaction at the 3.845 MeV incident α -particle energy

Final state	Initial J	Multipole	Mixing ratio	χ^2
$3/2^-(3.22 \text{ MeV})$	$3/2$	$E1$ or $M1$	—	0.209
	$5/2$	$E2/M1$	0.126	0.020
$3/2^-(4.21 \text{ MeV})$	$3/2$	$E1$ or $M1$	—	0.148
	$5/2$	$E2/M1$	0.211	0.036
$3/2^+(g.s.)$	$3/2$	$E1$ or $M1$	—	0.401
	$5/2$	$E1$ or $M1$	—	0.004

S
A=34

S
A=34

S
A=34

Ref. E.C. Booth, K.A. Wright
Nuclear Phys. **35**, 472 (1962)

Elem. Sym.	A	Z
S	34	16
Ref. No.		JHH
62		

Method 4 MeV electron Van de Graaff; brems.; nuclear resonance scattering, ring scatterer; NaI

Reaction	E or ΔE	E_0	Γ	$\int \sigma dE$	$J\pi$	Notes
$S^{34} (\gamma, \gamma)$	Brems. 0 - 4					

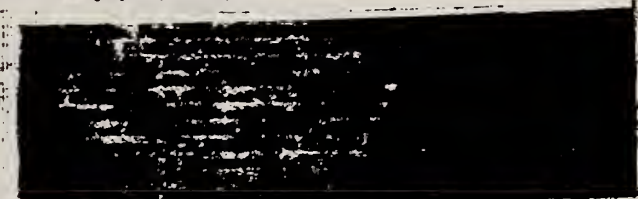
Table 3
Mean lifetimes of excited states deduced from the resonance scattering of bremsstrahlung

Nucleus	%	Energy (MeV)	Spin	Γ	$\Gamma_d \Gamma$	Γ^2	$\tau \times 10^{-12}$ sec
^{27}Al	100	1.46	$3^+ - 1^+$	7	0.15	(17)	0.36
^{28}Al	100	2.08	$3^+ - 1^+$	8	0.1	(9)	0.08
		2.08	$1^+ - 0^+$	7	0.05	(11)	0.15
		2.64	$2^+ - 0^+$	7	0.0	(11)	0.35
		2.70	$2^+ - 0^+$	7	0.11	(11)	0.10
		2.80	$2^+ - 0^+$	7	0.08	(11)	0.08
^{41}Ar	100	2.73	$1^+ - 0^+$	1	5.0	0.94	0.33
		2.80	$1^+ - 0^+$	1	0.10	1	2.2×10^{-2}
^{46}Ca	4.71	1.35	$1^+ - 0^+$	1	1	0.05	1.0
		1.43	$1^+ - 0^+$	1	1	0.05	0.5
^{70}Ge	100	1.80	$1^+ - 0^+$	1	1	0.05	0.5
		2.20	$0^+ - 0^+$	1	1	0.75	4.0
		2.13	$0^+ - 0^+$	1	1	0.05	0.2
		2.20	$0^+ - 0^+$	1	1	0.75	$> 1.0 \times 10^{-11}$
		2.41	$0^+ - 0^+$	1	1	1	$> 1.0 \times 10^{-11}$
		2.61	$0^+ - 0^+$	1	1	0.05	$> 0.05 \times 10^{-11}$
^{88}Sr	90	2.70	$0^+ - 0^+$	1	1	1	$> 0.05 \times 10^{-11}$
^{90}Sr	4.5	2.127	$0^+ - 0^+$	1	1	0.05	> 1.0
^{92}Sr	74.0	1.32	$0^+ - 0^+$	1	1	1	0.5
		1.70	$0^+ - 0^+$	1	1	1	0.5
		2.73 (5.6)	$0^+ - 0^+$	1	1	1	$> 0.05 \times 10^{-11}$
^{94}Zr	73.0	0.91	$0^+ - 0^+$	1	1	1	$> 0.7 \times 10^{-11}$
		0.94	$0^+ - 0^+$	1	1	1	$> 1.0 \times 10^{-11}$
		1.17	$0^+ - 0^+$	1	1	1	$> 1.0 \times 10^{-11}$
^{96}Zr	96	1.73	$0^+ - 0^+$	1	1	1	$> 0.05 \times 10^{-11}$
		2.00	$0^+ - 0^+$	1	1	1	> 1.0
		2.00	$0^+ - 0^+$	1	1	1	> 1.0
		2.00	$0^+ - 0^+$	1	1	1	> 1.0
		2.00	$0^+ - 0^+$	1	1	1	> 1.0
		2.00 (5.6)	$0^+ - 0^+$	1	1	1	$> 0.05 \times 10^{-11}$
		4.00 (5.12)	$0^+ - 0^+$	1	1	1	$> 0.05 \times 10^{-11}$
^{98}Zr	90	2.00	$0^+ - 0^+$	1	1	0.05	> 0.05
^{100}Zr	90	1.20	$0^+ - 0^+$	1	1	0.0	> 0.05

Table 2
Comparison of mean lifetime measurements

Nucleus	Energy	%	Spin	Γ	$\Gamma_d \Gamma$	Γ^2	$\tau \times 10^{-12}$ sec	
							This work	Other
^{27}Al	2.60	7	$1^+ - 0^+$	1	(1)	1	0.013	0.0073 \pm 0.0015 ^(a)
								-0.0013
								0.0106 \pm 0.001 ^(b)
^{41}Ar	2.14	81	$1^+ - 0^+$	1	1	1	0.53	0.47 \pm 0.05 ^(a)
^{46}Ca	2.31	100	$1^+ - 0^+$	1	(1)	1	2.3	2.7 \pm 0.3 ^(a)
^{70}Ge	1.01	100	$1^+ - 0^+$	1	0.00	1	330	170 \pm 50 ^(a)
^{92}Sr	1.70	92	$0^+ - 0^+$	5	1	0.63	85	70 \pm 23 ^(a)
^{94}Zr	2.34	94	$0^+ - 0^+$	5	1	0.63	30	~10 ^(a)
^{96}Zr	1.87	78.3	$0^+ - 0^+$	5	1	0.60	230	165 \pm 60 ^(a)
^{98}Zr	1.41	28	$0^+ - 0^+$	1	(1)	1	2.6	2.6 \pm 0.9 ^(a)
^{100}Zr	0.905	90	$0^+ - 0^+$	1	1	0.05	300	75 \pm 13 ^(a)
^{100}Zr	0.67	90	$0^+ - 0^+$	1	1	1	100	52 \pm 3 ^(a)

The factor g equals $(M+1)(M_g+1)^{-1}$.



METHOD

[Page 1 of 3]

REF. NO.

65 Mc 2

EGF

REACTION	RESULT	EXCITATION ENERGY	SOURCE		DETECTOR		ANGLE
			TYPE	RANGE	TYPE	RANGE	
A ₂ G	RLY	11-12	D	3-4	NAI-D	0-12	DST

Strengths normalized to 2.904 MeV level taken to be:

$$(2J+1) \frac{\Gamma_{\alpha} \Gamma_{\gamma}}{\Gamma} = 0.7 \text{ eV.}$$

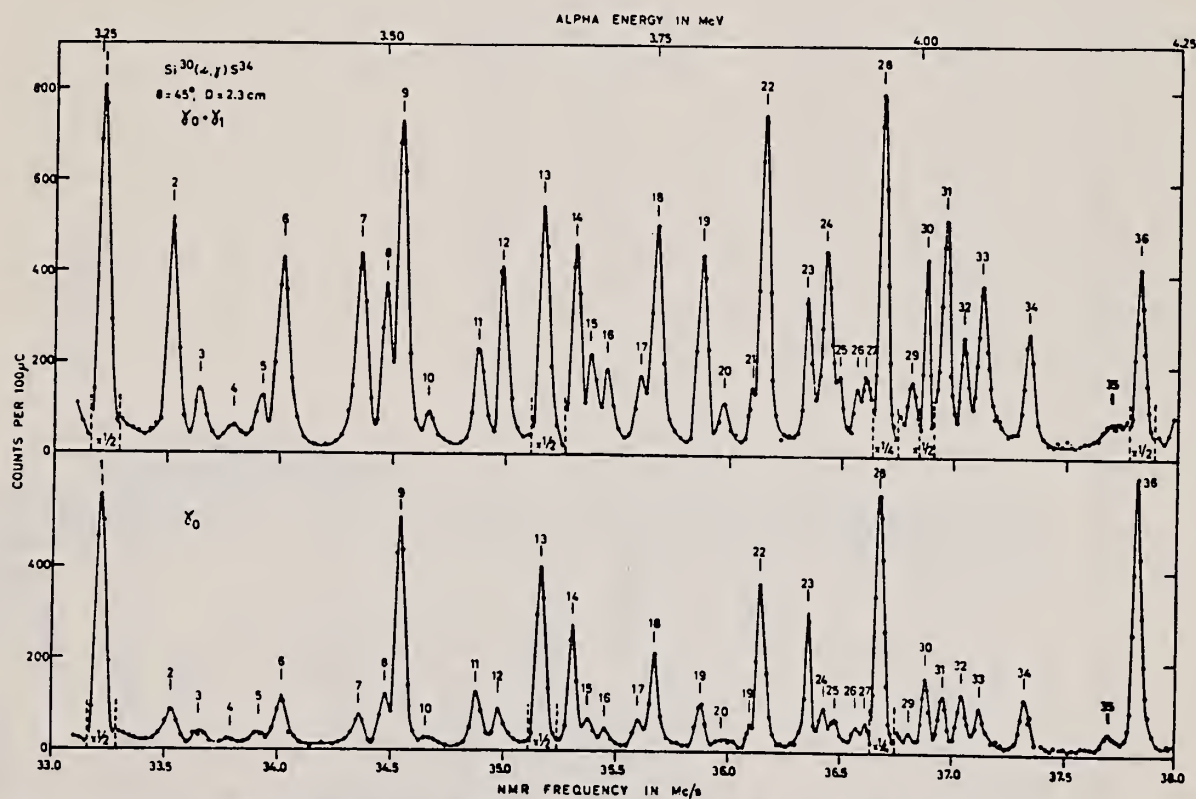


Fig. 1. Yield curve of the $^{30}\text{Si}(\alpha, \gamma)^{34}\text{S}$ reaction in the $E_{\alpha} = 3.25\text{--}4.25$ MeV region.

METHOD

REF. NO.

[Page 2 of 3]

65 Mc 2

EGF

REACTION	RESULT	EXCITATION ENERGY	SOURCE		DETECTOR		ANGLE
			TYPE	RANGE	TYPE	RANGE	

$^{84}\text{Si}(\alpha, \gamma)^{88}\text{S}$ REACTION

117

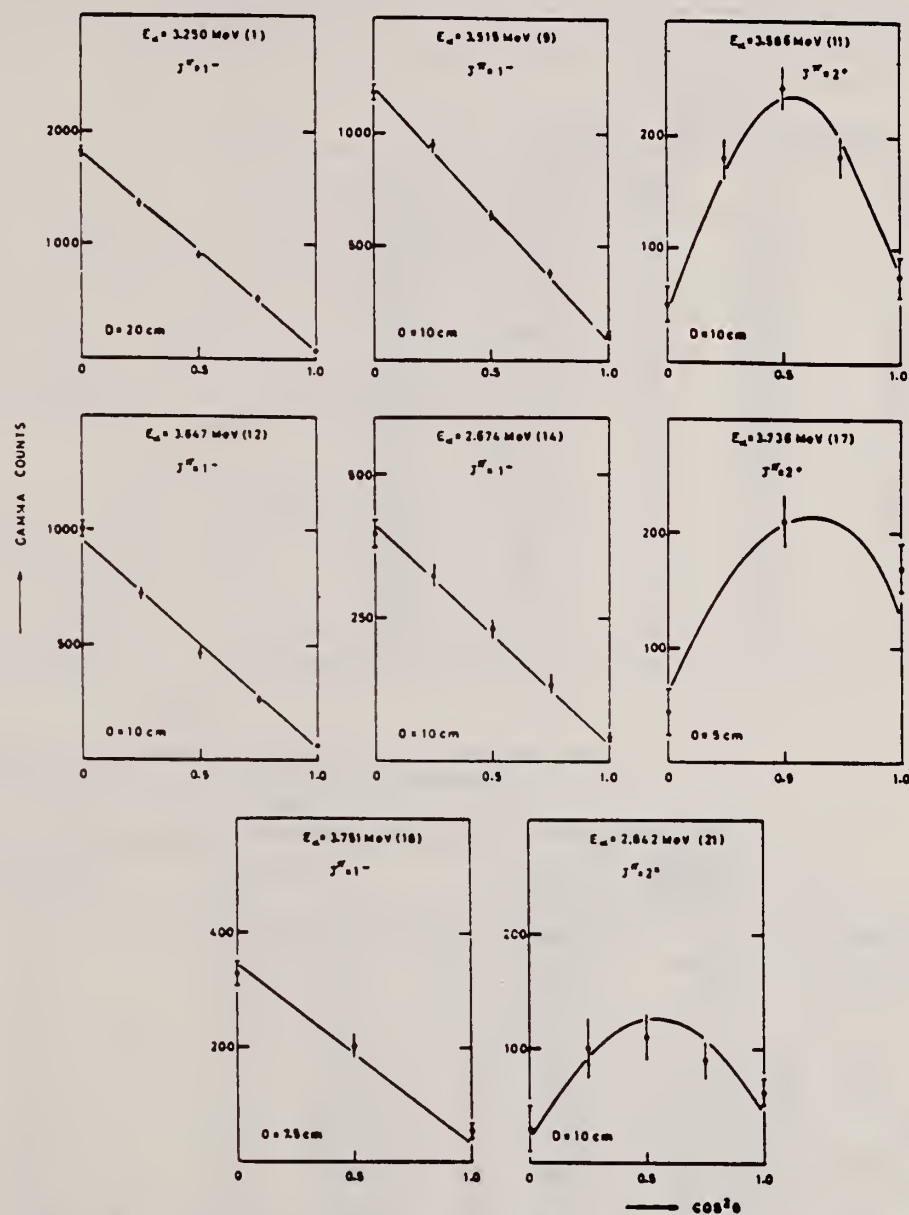


Fig. 2. Measured angular distributions of γ , at resonances 1, 9, 11, 13, 14, 17, 18 and 21. The solid line in each figure is the theoretical angular distributions for the assigned spin values, as modified for the detector size.

METHOD

REF. NO.

[Page 3 of 3]

65 Mc 2

EGF

REACTION	RESULT	EXCITATION ENERGY	SOURCE		DETECTOR		ANGLE
			TYPE	RANGE	TYPE	RANGE	

TABLE 1
Resonances in the $^{30}\text{Si}(\alpha, \gamma)^{34}\text{S}$ reaction

Resonance number	$E_x(\text{lab})$ (MeV)	$^{34}\text{S}^*$ (MeV)	Resonance number	$E_x(\text{lab})$ (MeV)	$^{34}\text{S}^*$ (MeV)
1	3.250	10.784	19	3.795	11.265
2	3.313	10.840	20	3.814	11.282
3	3.338	10.862	21	3.843	11.307
4	3.368	10.888	22	3.853	11.316
5	3.392	10.909	23	3.894	11.352
6	3.408	10.924	24	3.908	11.365
7	3.480	10.987	25	3.918	11.373
8	3.503	11.007	26	3.940	11.393
9	3.515	11.018	27	3.948	11.400
10	3.540	11.040	28	3.961	11.411
11	3.586	11.081	29	3.993	11.440
12	3.609	11.101	30	4.007	11.452
13	3.647	11.134	31	4.024	11.467
14	3.674	11.158	32	4.043	11.484
15	3.690	11.172	33	4.058	11.497
16	3.706	11.186	34	4.106	11.539
17	3.736	11.213	35	4.160	11.614
18	3.751	11.226	36	4.220	11.640

All values ± 5 keV.TABLE 2
Spins and parities, main modes of decay and resonance strengths of ground state transitions in ^{34}S

Resonance number	E_x (MeV)	J^π	Main decay				$(2J+1)\Gamma_{\gamma_0}\Gamma_d/\Gamma$ (eV)	Γ_γ (eV)
			γ_0	γ_1	γ_2	γ_d		
1	3.250	1 ⁻	1	0.2	0.05		7.2	3
9	3.515	1 ⁻	1	0.14	0.17		3.9	1.7
11	3.586	2 ⁺	1	0.44	0.47		0.5	0.2
13	3.647	1 ⁻	1	0.18	0.09		6.2	2.6
14	3.674	1 ⁻	1	0.17	1.3		2.1	1.7
17	3.736	(2 ⁺)	1	1.5	3.1	13	0.2	0.2
18	3.751	1 ⁻	1	0.15	4.1		1.2	2.8
21	3.843	2 ⁺	1	0.38	0.67		0.2	0.08
22	3.853	1 ⁻	1	0.65	0.48		3.1	2.2
23	3.894	1 ⁻	1	0.49	2.8		0.8	1.4
24	3.908	(2 ⁺)	1	17	7.4		0.1	1.5
25	3.918	2 ⁺	1	0.89	2.7	7	0.1	0.1
28	3.961	1 ⁻	1	0.19	0.05		10.7	4.4
32	4.043	1 ⁻	1	0.46	0.56	13	0.9	0.6
34	4.106	1 ⁻	1	0.96	1.6	26	0.9	1.0
36	4.220	1 ⁻	1	0.25	0.20	7.5	4.7	2.3

METHOD

Alpha capture

REF. NO.

67 W1 1

EGF

REACTION	RESULT	EXCITATION ENERGY	SOURCE		DETECTOR		ANGLE
			TYPE	RANGE	TYPE	RANGE	
A ₉ G	LFT	11-12	D	4-5	NAI-D	1-12	DST

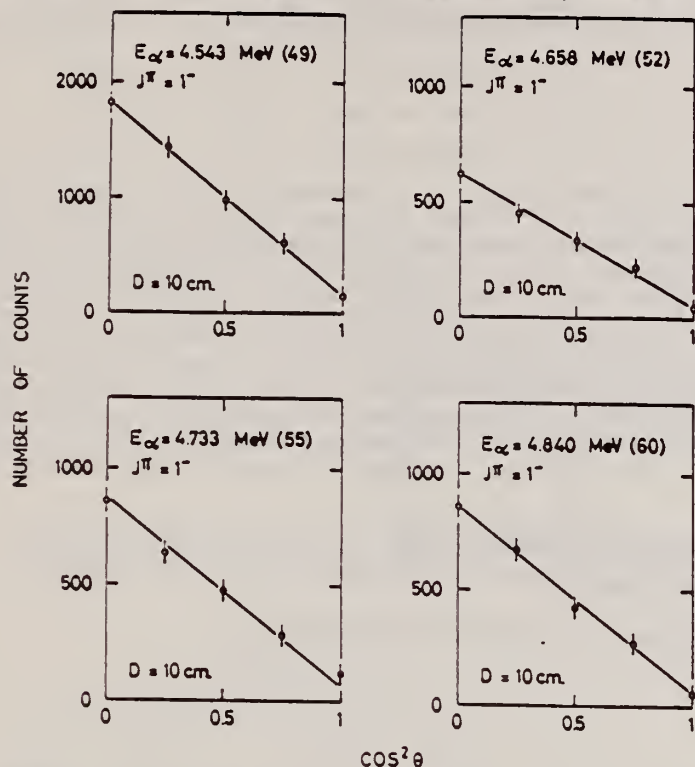


Fig. 3. Measured angular distributions of γ_0 at resonances 49, 52, 55 and 60. The solid line in each figure is the theoretical angular distribution, as modified for the detector size.

TABLE 4
Properties of some levels of ³⁴S

Resonance number	E_x (lab) (MeV)	Main decay mode	Partial resonance strength (eV)	J^π	Mixing parameters for γ_1 -transition	Radiative widths in Weisskopf units			
						$ M ^2(E1) \times 10^4$	$ M ^2(E2)$	$ M ^2(M1)$	$ M ^2(M2)$
2	3.313	γ_1	2.1	3 ⁻	-0.024 ± 0.017	0.56			0.028
6	3.408	γ_1	1.3	1 ⁻	0.154 ± 0.070	0.78			1.58
7	3.480	γ_1	1.5	2 ⁺	0.078 ± 0.032		0.005	0.023	
8	3.503	γ_1	0.94	2 ⁺	-0.52 ± 0.22		0.11	0.011	
12	3.609	γ_1	1.7	3 ⁻	0.062 ± 0.001	0.42			0.13
19	3.795	γ_1	1.6	2 ⁺	0.18 ± 0.15		0.023	0.021	
24	3.908	γ_1	2.0	3 ⁻	0.022 ± 0.006	0.45			0.017
31	4.005	γ_1	2.4	3 ⁻	0.037 ± 0.002	0.52			0.054
32	4.023	γ_1	1.2	1 ⁻	-0.13 ± 0.07	0.58			0.75
34	4.060	γ_1	0.74	(1 ⁻)	-0.058 ± 0.016	0.37			0.095
40	4.293	γ_1	0.63	1 ⁻	-0.080 ± 0.080	0.29			0.14
48	4.531	γ_1	2.1	(3 ⁻)	0.005 ± 0.021	0.39			
49	4.543	γ_0	5.2	1 ⁻		1.26			
50	4.571	γ_1	1.9	3 ⁻	0.031 ± 0.004	0.36			0.024
52	4.658	γ_0	2.1	1 ⁻		0.50			
55	4.733	γ_0	1.5	1 ⁻		0.36			
60	4.840	γ_0	3.5	1 ⁻		0.81			

REF. U.E.P. Berg, K. Bangert, G. Junghans, R. Stock and
K. Wienhard
Nucl. Phys. A306, 178 (1978)

ELEM. SYM.	A	Z
S	34	16
REF. NO.		
78 Be 3		rs

METHOD

REACTION	RESULT	EXCITATION ENERGY	SOURCE		DETECTOR		ANGLE
			TYPE	RANGE	TYPE	RANGE	
G,G	LFT	7- 11	C	18	SCD-D		125

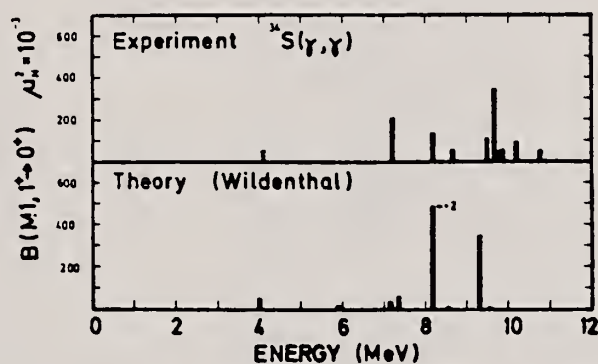


Fig. 3. Comparison of experimental (upper part of the figure) and theoretical (lower part) $B(M1)$ values for ^{34}S .

TABLE 2
Results from the $^{34}\text{S}(\gamma, \gamma)$ experiment

Transition energy (MeV)	J^π	I_γ (MeV · mb)	Γ_0^a (eV)	Mean lives (fs)	$B(M1)^c$ (μ_N^2)
7.220 ± 0.002	$(1, 2^+)$	0.204 ± 0.061	0.92 ± 0.28 1.09 ± 0.33^b	0.72 0.61 ^{b)}	(0.212)
7.781 ± 0.002	1^-	0.109 ± 0.015	0.57 ± 0.09	1.15	
8.185 ± 0.003	$(1, 2^+)$	0.148 ± 0.042	0.86 ± 0.28	0.77	0.136
8.385 ± 0.003	1^-	0.081 ± 0.025	0.49 ± 0.15	1.34	
8.511 ± 0.003	1^-	0.082 ± 0.014	0.52 ± 0.09	1.27	
8.657 ± 0.007	$(1, 2^+)$	0.063 ± 0.039	0.41 ± 0.25	1.60	0.055
9.478 ± 0.004	$(1, 2^+)$	0.145 ± 0.052	1.13 ± 0.49	0.58	0.115
9.640 ± 0.004	$(1, 2^+)$	0.448 ± 0.088	3.61 ± 0.72	0.18	0.349
9.711 ± 0.005	$(1, 2^+)$	0.061 ± 0.017	0.50 ± 0.14	1.32	0.047
9.860 ± 0.007	$(1, 2^+)$	0.075 ± 0.018	0.63 ± 0.15	1.04	0.057
10.171 ± 0.005	$(1, 2^+)$	0.124 ± 0.031	1.11 ± 0.28	0.59	0.092
10.786 ± 0.013	$(1, 2^+)$	0.074 ± 0.014	0.75 ± 0.14	0.88	0.052

^{a)} Assuming $\Gamma_0/\Gamma = 1$ and $J = 1$.

^{b)} Calculated under the assumption of an E2 transition.

^{c)} Assuming $J^\pi = 1^+$.

REF. E. Kuhlmann, J.R. Calarco, V.C. Cheng, D.G. Mavis, J.R. Hall,
S.S. Hanna
Phys. Rev. C20, 5 (1979)

ELEM. SYM.	A	Z
S	34	16
REF. NO.		hg
79 Ku 6		

METHOD

REACTION	RESULT	EXCITATION ENERGY	SOURCE		DETECTOR		ANGLE
			TYPE	RANGE	TYPE	RANGE	
A,G	ABX	11-21	D	4-15	NAI-D		DST

Excitation functions and angular distributions of the reactions $^{28,30}\text{Si}(\alpha, \gamma)$ were used to study the distribution of E2 strength in the energy regions 11-21 MeV of $^{32,34}\text{Si}$, as well as to probe the importance of isospin in the decay of the E1 giant resonance in these nuclei. It was found that the E2 strength in the (γ, α_0) channel is widely distributed and accounts for about 12% of the energy weighted isoscalar sum rule in each nucleus. Together with the E2 strength observed in lower resonances, about 45% of the sum rule is accounted for in ^{32}S and 34% in ^{34}S , where the measurements on the lower resonances are incomplete. The spreading of the E2 strength can be attributed to the mixing of $np-nh$ configurations into the basic $1p-1h$ excitations of the E2 resonance, and the large E2 strength is attributed to the presence of a direct or semidirect component in the (γ, α_0) process. A comparison of the E1 strengths in the (γ, α_0) channel of the giant dipole resonances in $^{32,34}\text{S}$ indicates that isospin conservation is important in these reactions. The relative weakness of the E1 (γ, α_0) strength in ^{34}S compared to the E2 strength is attributed to the relative purity of the $1p-1h$ character of the E1 resonance as compared to that of the E2 resonance.

E2 STRENGTH, SEE 79KU5

[NUCLEAR REACTIONS $^{28}\text{Si}(\alpha, \gamma)$, $E = 5-16$ MeV; $^{30}\text{Si}(\alpha, \gamma)$, $E = 4-15$ MeV; measured $\sigma(E, E_\gamma, \Theta_\gamma)$. $^{32,34}\text{S}$ deduced E1, E2 strengths. Enriched targets.]

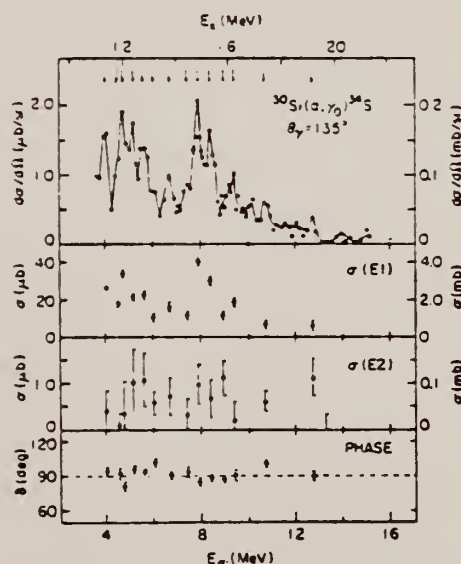


FIG. 5. Top: excitation function at $\theta = 135^\circ$ for the reaction $^{28}\text{Si}(\alpha, \gamma)^{32}\text{S}$. The arrows indicate energies at which angular distributions were measured. Middle: the extracted E1 and E2 total cross sections for the (α, γ) reaction. Bottom: the E2 phase δ relative to the E1 phase. The ordinate scale given on the right refers to the inverse reaction $^{32}\text{S}(\gamma, \alpha_0)^{28}\text{Si}$.

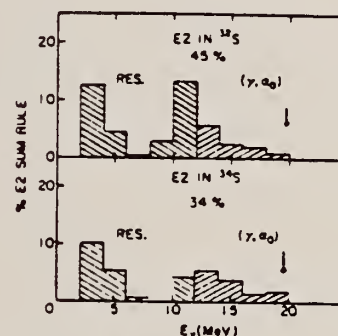


FIG. 6. The E2 strength in ^{32}S and ^{34}S integrated over 2 MeV intervals (in percentage of the isoscalar E2 sum rule) in the bound states and low-lying resonances (Ref. 21) up to $E_\alpha = 12$ MeV and in the α_0 -decay channel (this work) above 12 MeV. The region from 8-10 MeV in ^{34}S is unstudied.

S
A=36

S
A=36

S
A=36

REF. A. A. Koval, E. G. Kopanets, Yu. S. Korda, L. N. Sukhotin and
S. P. Tsytko
Izv. Akad. Nauk Fiz. 30, 416 (1966)
Bull. Acad. Sci. USSR-Phys. 30, 423 (1966)

ELEM. SYM.	A	Z
S	36	16
REF. NO.		
66 Ko 4		JOC

METHOD			REF. NO.		
			66 Ko 4		JOC
REACTION	RESULT	EXCITATION ENERGY	SOURCE		ANGLE
			TYPE	RANGE	
P, G	NOX	10-11	D	1-2	DST

Table 3

Angular distribution coefficients

SPINS

E_p, keV	a_1	a_2	E_p, keV	a_1	a_2
1421	$0,515 \pm 0,028$	$-0,369 \pm 0,042$	1921	$-0,326 \pm 0,007$	$0,013 \pm 0,012$
1468	$0,199 \pm 0,003$	$0,189 \pm 0,083$	1939	$0,210 \pm 0,013$	$0,230 \pm 0,002$
1499	$0,062 \pm 0,046$	$-0,046 \pm 0,076$	1979	$0,191 \pm 0,084$	$0,370 \pm 0,140$
1744	$-0,572 \pm 0,044$	$0,038 \pm 0,061$	2014	$0,389 \pm 0,039$	$0,066 \pm 0,058$
1806	$-0,380 \pm 0,015$	$-0,459 \pm 0,025$	2083	$0,448 \pm 0,008$	$0,122 \pm 0,085$
1846	$0,426 \pm 0,039$	$-0,534 \pm 0,064$			

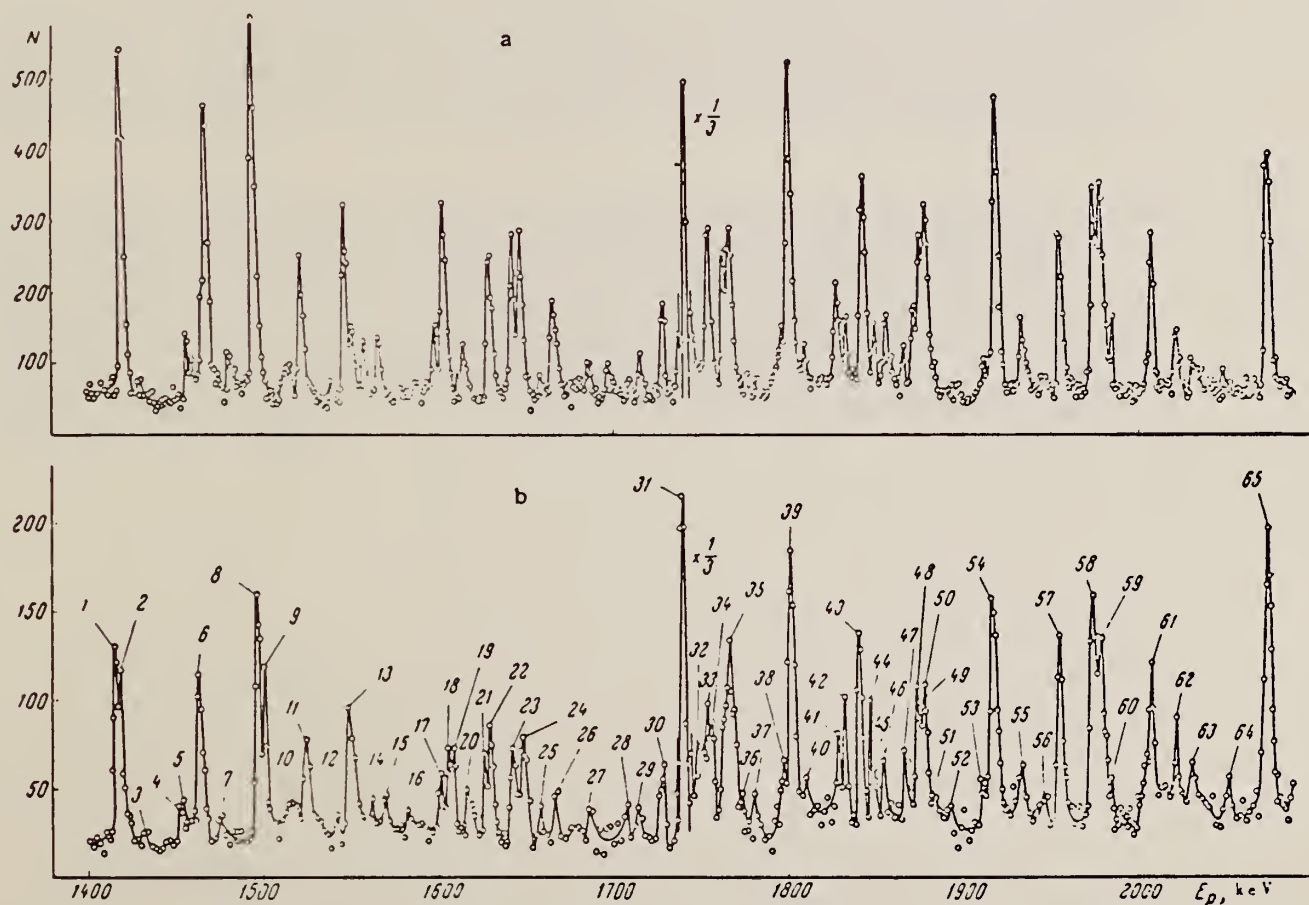


Fig. 1. Excitation functions for the $S^{36}(p, \gamma)Cl^{37}$ reaction (the vertical scale is laid off in the number of pulses per 625 μC): a - case when the monitor recorded γ rays with $E_\gamma \geq 7.5$ MeV, b - case of recording only the transitions to the ground state. The detector was mounted at an angle of 90° relative to the proton beam.

CHLORINE

Z=17

Chlorine was first prepared in 1774 by K. W. Scheele; he heated manganese dioxide with hydrochloric acid and observed the release of a gas "most oppressive to the lungs". Guided by the prevailing phlogiston theory, Scheele considered this novel substance to be "dephlogisticated muriatic acid".

Sir Humphry Davy established the elementary nature of the gas and called it chlorine. The word is derived from the Greek *chloros*, meaning greenish-yellow. Because he was unable to decompose the gas, Davy hypothesized that it was an element and further determined that hydrochloric acid contains only hydrogen and the new element, chlorine. This was in direct contradiction to Lavoisier's theory that all acids contain oxygen. Davy's views eventually prevailed and chlorine was accepted as an element.

P. Erdos, P. Jordan and P. Stoll
Helv. Phys. Acta 28, 322 (1955)

C1

17

METHOD

REF. NO.

55 Er 1

EGF

REACTION	RESULT	EXCITATION ENERGY	SOURCE		DETECTOR		ANGLE
			TYPE	RANGE	TYPE	RANGE	
G, A	ABY	THR-31	C	32	EMU-I		4PI

Betatron run at 31.5 MeV.

$\text{Cl}(\gamma, \alpha)\text{P}$ 13 ± 2 MeV-mb.

ELEM. SYM.	A	Z
Cl		17
REF. NO.		
66 Be 3		JDM

METHOD

Nuclear Resonance Scattering using N,G reactions.

REACTION	RESULT	EXCITATION ENERGY	SOURCE		DETECTOR		ANGLE
			TYPE	RANGE	TYPE	RANGE	
G,G	RLX	5 - 10	D	5 - 10	NAI-D	5 - 10	135

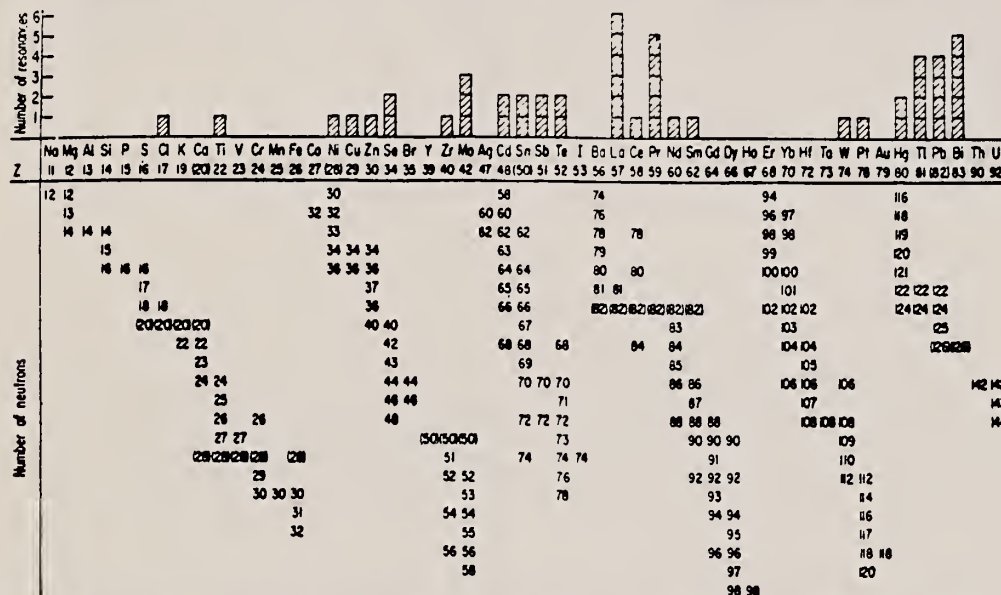


FIG. 3. Histogram of distribution of observed resonances among the different targets. The atomic number is given directly beneath the chemical symbol followed by the neutron numbers of the naturally occurring isotopes. Magic numbers are shown in brackets.

TABLE III. List of effective cross sections.

Scatterer	Energy (MeV)	Gamma source	δ (mb)	Scatterer	Energy (MeV)	Gamma source	δ (mb)
Sm ¹⁴⁴	8.997	Ni	100	Sn	7.01	Cu	110
Pr ¹⁴¹	8.881	Cr	9	Nd	6.867	Co	30
La	8.532	Ni	6	Pr ¹⁴¹	6.867	Co	3
Te	8.532	Ni	3*	Te	6.7	Ni	...
Cu	8.499	Cr	24	La	6.54	Ag	12
Zr	8.496	Se	3050	La	6.474	Co	110
Zn	8.119	Ni	13	Mo	6.44	Hg	25*
Se	7.817	Ni	50	La	6.413	Ti	72
Se	7.76	K	90	Mo	6.413	Ti	10
Sb	7.67	V	...	Ti	6.413	Ti	25
Cd	7.64	Fe	40*	W	6.3	Ti	...
Ni	7.64	Fe	7*	Sb	6.31	Hg	6*
Pr ¹⁴¹	7.64	Fe	12*	Ti	6.31	Hg	2*
Ti	7.64	Fe	370*	Sn	6.27	Ag	75
La	7.634	Cu	7	Pb ²⁰⁸	6.15	Gd	...
Mo	7.634	Cu	11	Te	5.8	Ni	...
Bi ²⁰⁹	7.634	Cu	4	La	6.12	Cl	35
Te	7.528	Ni	66*	Pr ¹⁴¹	6.12	Cl	110
Bi ²⁰⁹	7.416	Se	100	Pt	5.99	Hg	40*
Bi ²⁰⁹	7.300	As	80*	Ti	5.99	Hg	5*
Pb ²⁰⁸	7.285	Fe	4100	Pb ²⁰⁸	5.9	Sr	...
Cl ³⁵	7.285	Fe	34	Ce	5.646	Co	17
Pr ¹⁴¹	7.185	Se	80	Bi ²⁰⁹	5.646	Co	55
Ti	7.16	Cu	120	Pb ²⁰⁸	5.53	Ag	70
La	7.15	Mn	50	Hg	5.44	Hg	75*
Bi ²⁰⁹	7.149	Ti	2000	Hg	4.903	Co	385

- * High-energy component of a complex spectrum.
- * A broad scattered spectrum with no observable peak structure.
- * There are actually two lines of energies 7.647 and 7.633 MeV having equal intensities in the iron capture gamma spectrum. The cross section has therefore been corrected, although there is no possibility at present of deciding which line is responsible for each resonance.
- * Is probably an independent level in the complex spectrum of Ni γ rays on Te.
- * Rough estimate.
- * May be inelastic component from 7.528 level in Te.
- * The relative line intensities in this case are due to Groshev and co-workers.
- * No line is known for the source at this energy.
- * Difficult to resolve among the many source lines present at this energy.

METHOD

REF. NO.

69 No 1

egf

REACTION	RESULT	EXCITATION ENERGY	SOURCE		DETECTOR		ANGLE
			TYPE	RANGE	TYPE	RANGE	
G, NA24	ABY	104-999	C	100-999	ACT-I		4PI

999 = 1.2 GEV



FIG. 2. Cross sections as a function of gamma-ray energy.

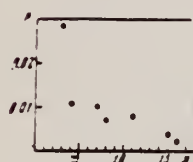


FIG. 3. Dependence of P on number of nucleons which have left the nucleus.

Table I

Reaction	Nucleons emitted	Threshold, MeV	Target	Distribution of isotopes, %
Al ²⁷ -> Na ²⁴	2p, n	31	Al	100
Si ²⁸ -> Na ²⁴	3p, n	43	Si	92.27
P ³¹ -> Na ²⁴	4p, 3n	60	P	100
S ³² -> Na ²⁴	5p, 3n	78	S	95.02
Cl ³⁵ -> Na ²⁴	6p, 5n	101	NH ₄ Cl	75.1
K ³⁹ -> Na ²⁴	8p, 7n	140	K ₂ ClO ₄	93.04
Ca ⁴⁰ -> Na ²⁴	9p, 7n	148	CaO	98.97

*The threshold was calculated as the binding energy of the emitted nucleons.

Table II. Cross sections for reactions in the saturation region

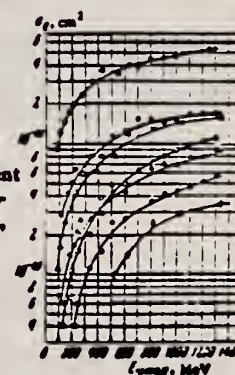
Reaction	$\sigma_{\text{ex}}, \text{cm}^2$	Reaction	$\sigma_{\text{ex}}, \text{cm}^2$
Al ²⁷ -> Na ²⁴	185 ± 20	Cl ³⁵ -> Na ²⁴	94 ± 7
Si ²⁸ -> Na ²⁴	72 ± 4	K ³⁹ -> Na ²⁴	15 ± 5
P ³¹ -> Na ²⁴	71 ± 8	Ca ⁴⁰ -> Na ²⁴	23 ± 5
S ³² -> Na ²⁴	52 ± 6		

According to the photomesonic mechanism, the cross section for the reaction can be written in the form

$$\sigma = \sigma_0 A P. \quad (1)$$

Here σ_0 is the total cross section for interaction of the photon with a free nucleon with inclusion of the nucleon motion in the nucleus (σ_0 , as has been shown by Roos and Peterson,^[6] depends only weakly on photon energy for $E_\gamma > 300$ MeV); A is the number of nucleons in the nucleus, and P is the probability that the reaction will proceed by a given channel.

FIG. 1. Cross section σ_0 per equivalent photon as a function of maximum bremsstrahlung energy. Points: O - Al, \odot - Si, Δ - P, \triangle - S, \square - Cl, \boxplus - K, \diamond - Ca.



REF.

A. Järund, B. Friberg, and B. Forkman
Z. Physik 262, 15 (1973)

ELEM. SYM.

A

Z

Cl

17

METHOD

REF. NO.

73 Ja 3

egf

REACTION	RESULT	EXCITATION ENERGY	SOURCE		DETECTOR		ANGLE
			TYPE	RANGE	TYPE	RANGE	
G, NA24	ABY	THR-999	C	100-999	ACT-I		4PI

999±1 GEV

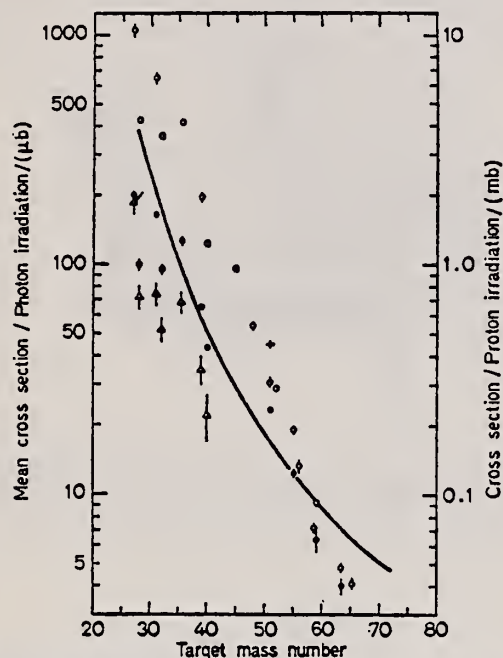


Fig. 7. Mean cross sections for ^{24}Na production as a function of target mass number. Present work filled circles. Noga *et al.* [3] open triangles, Kumbartzki *et al.* [13] cross and Korteling *et al.* [1] 400 MeV protons open circles. The solid line gives the mean cross sections calculated by Jonsson *et al.* [17]

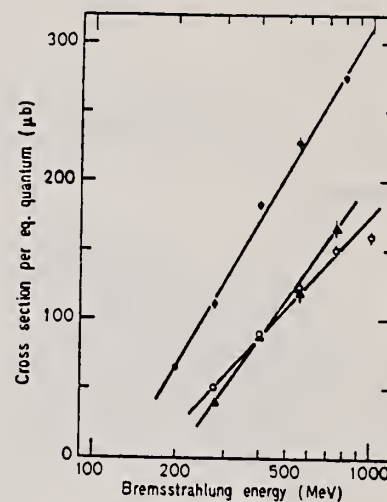


Fig. 3

Fig. 3. The determined yields for the reactions $^{31}\text{P} \rightarrow ^{24}\text{Na}$ (filled circles), $^{32}\text{S} \rightarrow ^{24}\text{Na}$ (open circles) and $^{35,37}\text{Cl} \rightarrow ^{24}\text{Na}$ (filled triangles)

¹Korteling, R.G. *et al.*, J. Inorg. Nucl. Chem. 29, 2863 (1967).

³Noga, V.I. *et al.*, Sov. J. Nucl. Phys. 9, 637 (1969).

¹³Kumbartzki, G. *et al.*, Nucl. Phys. A176, 23 (1971).

¹⁷Jonsson, G.G. *et al.*, LUNP7212, Oct. 1972, to be published in Physica Scripta.

A. Veyssiere, H. Beil, R. Bergere, P. Carlos, A. Lepretre, and
A. De Miniac
Nucl. Phys. A227, 513 (1974)

Cl

17

METHOD

REF. NO.

74 Ve 1

egf

REACTION	RESULT	EXCITATION ENERGY	SOURCE		DETECTOR		ANGLE
			TYPE	RANGE	TYPE	RANGE	
* G,N	ABX	10- 28	D	10- 28	BF3-I		4PI
** G,2N	ABX	17- 28	D	17- 28	BF3-I		4PI

* 895+

** 896

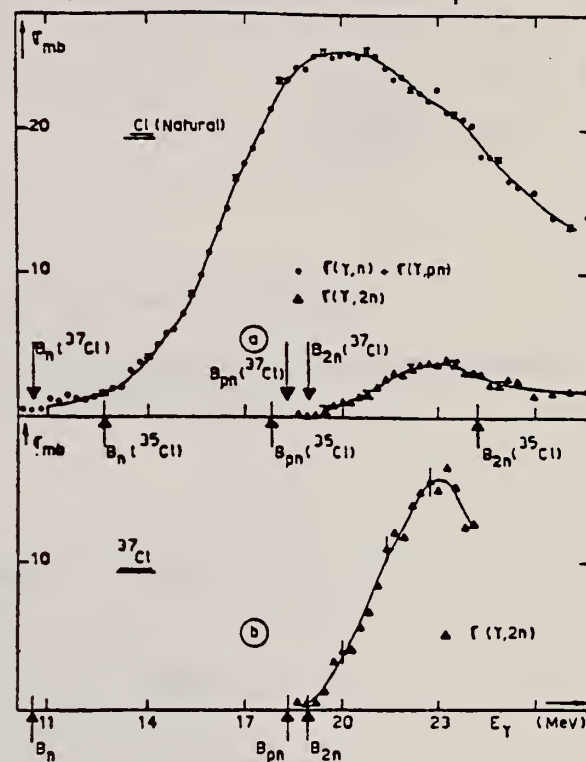


Fig. 9. (a) Photonuclear cross sections $[\sigma(\gamma, n) + \sigma(\gamma, pn)]$ and $\sigma(\gamma, 2n)$ for natural Cl. (b) Partial photoneutron cross sections $\sigma(\gamma, 2n)$ of ^{37}Cl .

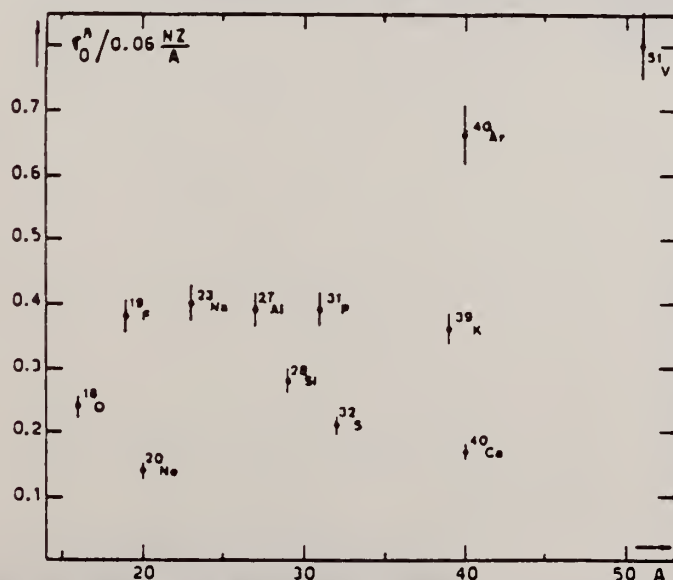


Fig. 22. Ratio of experimental integrated photoneutron cross section σ_0^* over the Thomas, Reiche and Kuhn sum rule $[0.06 \frac{NZ}{A}]$. Numerical values and upper integration limits E_M are taken from table 3. Also $\Delta\sigma_0^* = \pm 7\%$ for all nuclei.

(over)
U.S. DEPARTMENT OF COMMERCE
NATIONAL BUREAU OF STANDARDS

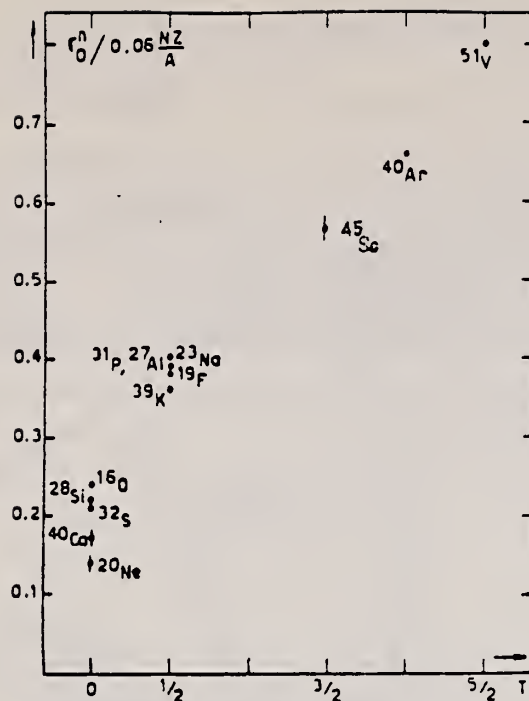


Fig. 24. The $[\sigma_0^n/(0.06 NZ/A)]$ ratio as a function of isospin T . Possible overall errors of $\pm 7\%$ are to be applied to all nuclei shown.

TABLE 3
Experimental integrated photoneutron cross sections $\sigma_0^n = \int_0^{E_M} \sigma_{Tn}(E) dE$ compared with the classical sum rule $[0.06 NZ/A]$ of Thomas, Reich and Kuhn

	$T = 0$					$T = \frac{1}{2}$					$T = \frac{3}{2}$	$T = 2$	$T = \frac{5}{2}$
Nucleus	^{16}O	^{20}Ne	^{28}Si	^{32}S	^{40}Ca	^{19}F	^{23}Na	^{27}Al	^{31}P	^{39}K	^{45}Sc	^{40}Ar	^{51}V
σ_0^n (MeV · mb)	58 ± 4	42 ± 3	94 ± 7	98 ± 7	100 ± 7	108 ± 7	137 ± 9	158 ± 10	182 ± 12	210 ± 14	383 ± 25	393 ± 28	602 ± 42
$\sigma_0^n/(0.06 NZ/A)$	0.24	0.14	0.22	0.21	0.17	0.38	0.40	0.39	0.39	0.36	0.57	0.66	0.8
E_M (MeV)	30	26.7	30	30	29.5	29	30	30	29	30	28.1	26.7	28

REF.

V. di Napoli, G. Rosa, F. Salvetti, M. L. Terranova,
H. G. de Carvalho, J. B. Martins, O. A. P. Tavares
J. Inorg. Nucl. Chem. 37, 1101 (1975)

ELEM. SYM.

A

Z

Cl

17

METHOD

REF. NO.

75 Di 4

egf

REACTION	RESULT	EXCITATION ENERGY	SOURCE		DETECTOR		ANGLE
			TYPE	RANGE	TYPE	RANGE	
G,F18	ABY	THR-999	C	300-999	ACT-I		4PI
G,NA22	ABY	THR-999	C	300-999	ACT-I		4PI
G,NA24	ABY	THR-999	C	300-999	ACT-I		4PI

999 = 1 GEV

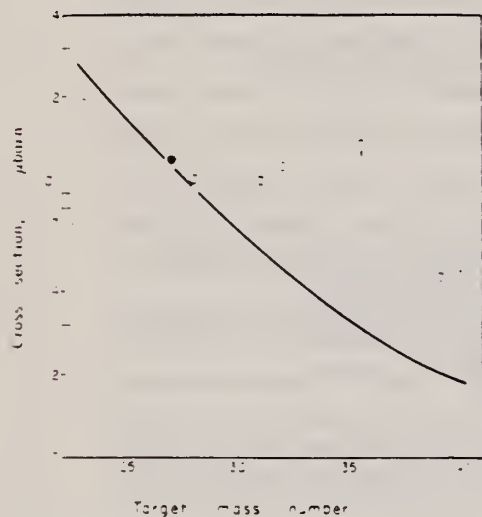


Fig. 2. Mean absolute cross section of ^{18}F photoproduction vs the target mass number. Open triangle: energy range 0.15-0.72 GeV, Ref. [18]. Filled circle: energy range 0.3-1 GeV, Ref. [3]. Open circles: present work. The curve has been calculated by means of Eqn (1).

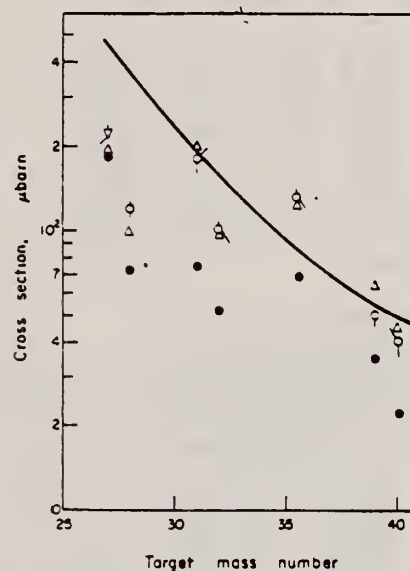


Fig. 4. Mean absolute cross section of ^{22}Na photoproduction vs the target mass number. Filled circles: energy range 0.1-1 GeV, Ref. [20]. Reversed open triangle: energy range 0.3-1 GeV, Ref. [8]. Open triangles: energy range 0.25-1 GeV, Ref. [19]. Open circles: present work. The curve has been calculated by means of Eqn (1).

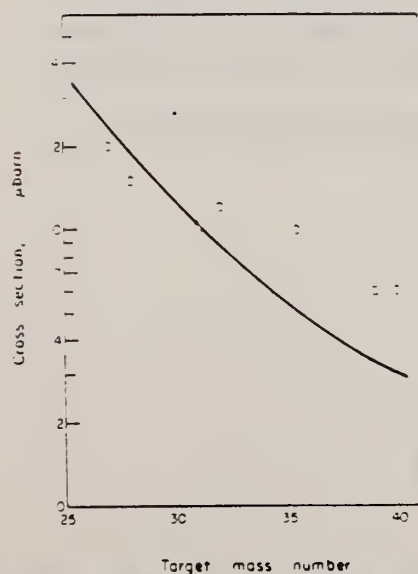


Fig. 3. Mean absolute cross section of ^{22}Na photoproduction vs the target mass number. The curve has been calculated by means of Eqn (1).

Table 2. Cross-section per equivalent quantum $\sigma_0(\mu\text{b})$ of photoproduction of ^{18}F

Target nucleus	Bremsstrahlung maximum energy $E_0(\text{GeV})$				
	0-30	0-40	0-55	0-75	1-00
^{23}Na	590 ± 30	640 ± 30	720 ± 30	780 ± 30	830 ± 30
^{27}Al	116 ± 7	172 ± 6	202 ± 6	245 ± 5	270 ± 5
^{28}Si	80 ± 10	110 ± 10	145 ± 10	170 ± 10	200 ± 10
^{31}P	60 ± 10	90 ± 10	130 ± 10	150 ± 10	180 ± 10
^{32}S	55 ± 10	90 ± 10	125 ± 10	160 ± 10	190 ± 10
^{37}Cl	185 ± 20	230 ± 20	270 ± 20	310 ± 20	350 ± 20
^{39}K	35 ± 5	50 ± 5	65 ± 5	75 ± 5	90 ± 5
^{40}Ca	5 ± 2	20 ± 3	35 ± 5	45 ± 5	60 ± 5

*The results for ^{27}Al have already been published (see [3]) and are reported for comparison.

(over)

Table 3. Cross-section per equivalent quantum $\sigma_Q(\mu b)$ of photoproduction of ^{23}Na

Target nucleus	Bremsstrahlung maximum energy E_0 (GeV)				
	0.30	0.40	0.55	0.75	1.00
^{27}Al	490 \pm 20	560 \pm 20	667 \pm 20	690 \pm 20	745 \pm 20
^{28}Si	290 \pm 20	330 \pm 20	380 \pm 20	430 \pm 20	470 \pm 20
^{31}P	230 \pm 20	250 \pm 20	290 \pm 20	330 \pm 20	350 \pm 20
^{32}S	206 \pm 10	240 \pm 10	280 \pm 10	320 \pm 10	350 \pm 10
$^{35,37}\text{Cl}$	230 \pm 10	260 \pm 10	290 \pm 10	320 \pm 10	350 \pm 10
^{39}K	30 \pm 3	50 \pm 5	65 \pm 5	80 \pm 5	100 \pm 5
^{40}Ca	5 \pm 2	20 \pm 3	45 \pm 5	60 \pm 5	60 \pm 5

Table 4. Cross-section per equivalent quantum $\sigma_Q(\mu b)$ of photoproduction of ^{24}Na

Target nucleus	Bremsstrahlung maximum energy E_0 (GeV)				
	0.30	0.40	0.55	0.75	1.00
$^{27}\text{Al}^a$	370 \pm 10	440 \pm 10	500 \pm 20	550 \pm 20	660 \pm 20
^{28}Si	100 \pm 10	140 \pm 10	160 \pm 10	210 \pm 10	240 \pm 10
^{31}P	100 \pm 20	160 \pm 20	200 \pm 20	270 \pm 20	310 \pm 20
^{32}S	120 \pm 10	160 \pm 10	180 \pm 10	210 \pm 10	240 \pm 10
$^{35,37}\text{Cl}$	65 \pm 10	100 \pm 10	140 \pm 10	190 \pm 10	220 \pm 10
^{39}K	20 \pm 5	35 \pm 5	55 \pm 5	65 \pm 5	80 \pm 5
^{40}Ca	12 \pm 3	25 \pm 5	35 \pm 5	50 \pm 5	60 \pm 5

^aThe results for ^{27}Al have already been published (see [8]) and are reported for comparison.

Table 5. Mean absolute cross-section $\bar{\sigma}_i(\mu b)$ in the energy range 0.3–1 GeV

Target nucleus	Produced radionuclide		
	^{18}F	^{22}Na	^{24}Na
^{23}Na	190 \pm 30		
$^{27}\text{Al}^a$	120 \pm 10	200 \pm 20	220 \pm 20
^{28}Si	100 \pm 10	150 \pm 20	120 \pm 10
^{31}P	100 \pm 20	150 \pm 20	180 \pm 20
^{32}S	100 \pm 10	120 \pm 10	100 \pm 10
$^{35,37}\text{Cl}$	135 \pm 20	100 \pm 10	130 \pm 10
^{39}K	45 \pm 5	60 \pm 5	50 \pm 5
^{40}Ca	46 \pm 5	60 \pm 5	40 \pm 5

^aThe results for the photoproduction of ^{18}F and ^{24}Na from ^{27}Al have already been published (Ref. [3] and [8], respectively).

- V. di Napoli and M. L. Terranova, *J. inorg. nucl. Chem.* **36**, 3633 (1974).
- V. di Napoli, A. M. Lacerenza, F. Salvetti, S. M. Terenzi, H. G. de Carvalho and J. B. Martins, *J. inorg. nucl. Chem.* **35**, 1419 (1973).
- C. M. Lederer, J. M. Hollander and I. Perlman, *Table of Isotopes*, 6th Edn Wiley, New York (1967).
- R. G. Korteling and A. A. Caretto, Jr., *J. inorg. nucl. Chem.* **29**, 2863 (1967).
- R. G. Korteling and A. A. Caretto, Jr., *Phys. Rev. C* **1**, 193 (1970).
- R. G. Korteling and A. A. Caretto, Jr., *Phys. Rev. C* **1**, 1960 (1970).
- V. di Napoli, A. M. Lacerenza, F. Salvetti, H. G. de Carvalho and J. B. Martins, *Lett. Nuovo Cimento* **1**, 835 (1971).
- I. Halpern, R. J. Debs, J. T. Eisinger, A. W. Fairhall and H. G. Richter, *Phys. Rev.* **97**, 1327 (1955).
- C. B. Fulmer, K. S. Toth, I. R. Williams, T. H. Handley, C. F. Dell, E. L. Callis, T. M. Jenkins and J. M. Wyckoff, *Phys. Rev. C* **2**, 1371 (1970).
- G. J. Kumbartzki, U. Kim and C. K. Kwan, *Nucl. Phys. A* **160**, 237 (1970).
- G. J. Kumbartzki and U. Kim, *Nucl. Phys. A* **176**, 23 (1971).
- K. Lindgren and G. G. Jonsson, *Nucl. Phys. A* **197**, 71 (1972).
- C. E. Roos and V. Z. Peterson, *Phys. Rev.* **124**, 1610 (1961).
- T. A. Gabriel and R. G. Alsmiller, Jr., *Phys. Rev.* **182**, 1035 (1969).
- G. G. Jonsson and K. Lindgren, *Phys. Scr.* **7**, 49 (1973).
- G. Rudstam, *Z. Naturf.* **21a**, 1027 (1966).
- A. Masaike, *J. phys. Soc. Japan* **19**, 427 (1964).
- A. Järund, B. Friberg and B. Forkman, Private communication to G. G. Jonsson and K. Lindgren, quoted in Ref. [16]; see also A. Järund, B. Friberg and B. Forkman, University of Lund Report No. LUNP-7303, 1973 (unpublished).
- V. I. Noga, Yu. N. Ranyuk and P. V. Sorokin, *Yad. Fiz.* **9**, 1152 (1969) (transl.: *Sov. J. Nucl. Phys.* **9**, 673 (1969)).
- T. Methasiri and S. A. E. Johansson, *Nucl. Phys. A* **167**, 97 (1971).
- J. R. Nix and E. Sassi, *Nucl. Phys.* **81**, 61 (1966).
- W. D. Myers and W. J. Swiatecki, *Nucl. Phys.* **81**, 1 (1966).

REF.

A. S. Danagulyan, N. A. Demekhina
 Yad. Fiz. 24, 681 (1976)
 Sov. J. Nucl. Phys. 24, 355 (1976)

ELEM. SYM.

A

Z

Cl

17

METHOD

REF. NO.

76 Da 4

hmg

REACTION	RESULT	EXCITATION ENERGY	SOURCE		DETECTOR		ANGLE
			TYPE	RANGE	TYPE	RANGE	
G, NA24	ABX	THR* 5	C	2* 5	ACT-I		4PI

*ENERGY, GEV

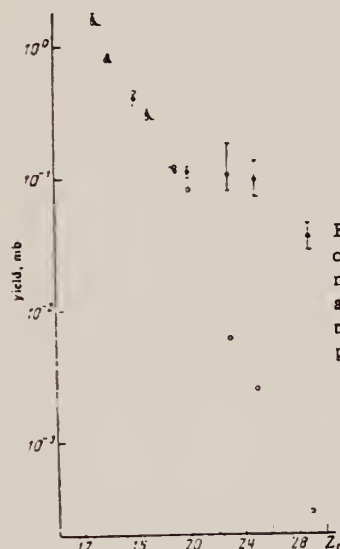


FIG. 2. Yield values and theoretical values according to the modified Rudstam formula as a function of the target charge number Z_t . Points: ●—experiment, ○—theory.

TABLE I. Experimental yields and reaction cross sections obtained in the measurements at the Erevan electron accelerator.

Target nucleus	Reaction yield, mb					Reaction cross section, mb
	$E_{\gamma \text{ max}}, \text{ GeV}$					
	2	3	4	4.5	5	
^{27}Al	0.81 ± 0.08	0.87		0.87		0.07213 ± 0.0346
^{28}Si	0.27 ± 0.02	0.28		0.29		0.0267 ± 0.013
^{32}S	0.24 ± 0.02	0.22		0.27		0.0323 ± 0.0155
^{35}Cl	0.28 ± 0.03	0.30		0.28		—
^{39}K	0.1 ± 0.01	0.125		0.15		0.06 ± 0.0288
^{40}Ca	0.098 ± 0.01	0.09		0.115		0.035 ± 0.0168
^{51}V	0.083 ± 0.02	0.094 ± 0.02	0.048 ± 0.02		0.062 ± 0.025	0.019
^{55}Mn	0.079 ± 0.02	0.075 ± 0.02	0.087 ± 0.017		0.088 ± 0.015	0.01076 ± 0.0056
^{63}Cu	0.029 ± 0.008	0.037 ± 0.007	0.036 ± 0.007		0.034 ± 0.007	0.00547 ± 0.0028

Note. The reaction cross sections have been calculated in the $1/E$ approximation of the bremsstrahlung spectrum.

CL
A=34

CL
A=34

CL
A=34

ELEM. SYM.	A	Z
Cl	34	17
METHOD		REF. NO.
71 Sn 1		hmg

REACTION	RESULT	EXCITATION ENERGY	SOURCE		DETECTOR		ANGLE
			TYPE	RANGE	TYPE	RANGE	
HE,NG	LFT	1,2	D	8	DSA-D		0
		(.461,.666)		(8.3)			

LEV. .461, .666

TABLE IV. Lifetime analysis.

Transition (keV)	D_m (mil) ^a	v/c (%)	Uncorrected τ (psec) ^b	Final τ (psec) ^c
461 \rightarrow 0	0.58 ± 0.07	0.647 ± 0.008	7.61 ± 0.92	7.1 ± 0.7
	0.48 ± 0.08	0.612 ± 0.007	6.61 ± 1.10	
666 \rightarrow 0	1.04 ± 0.10	0.639 ± 0.008	13.66 ± 1.37	12.8 ± 1.0
	0.90 ± 0.11	0.606 ± 0.005	12.57 ± 1.54	
1230 \rightarrow 461	1.55 ± 0.15	0.647 ± 0.015	20.34 ± 1.97	19.4 ± 1.4
1230 \rightarrow 666	1.42 ± 0.14	0.645 ± 0.011	18.64 ± 1.844	

^aIn units of 10^{-3} inches.

^bComputed from the relation $\tau = D_m/v$, in units of 10^{-12} sec.

^cIncluding geometry, solid-angle, counter-efficiency, and velocity-distribution corrections (see text).

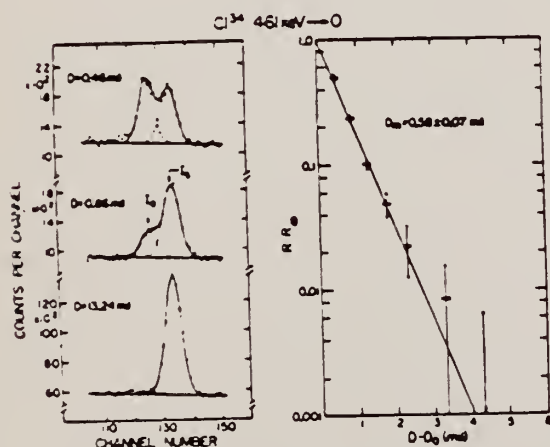


FIG. 4. γ -ray spectra and lifetime curve for the 461-keV \rightarrow 0 transition. The left portion of the figure displays the γ -ray spectra in the region of the 461 \rightarrow 0 transition, measured at three different plunger displacements D . The right portion of the figure is a logarithmic lifetime plot of $R - R_0$ vs $D - D_0$, with $R_0 = 0.018 \pm 0.005$. The curves through the data points represent least-squares fits to the data as described in the text.

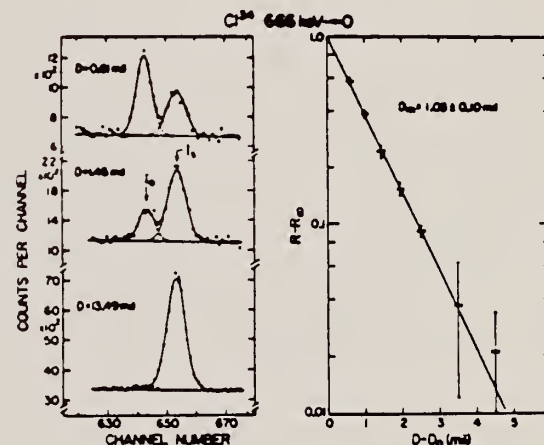


FIG. 5. γ -ray spectra and lifetime curves for the 666-keV \rightarrow 0 transition. The figure details are similar to the description given in the caption of Fig. 4, with $R_0 = 0.028 \pm 0.007$.

(over)

TABLE VI. A comparison of the experimental $B(M1)$ and $B(E2)$ reduced transition strengths in Cl^{34} , deduced from the present lifetime and branching ratio measurements, expressed in units of Weisskopf estimate B_W . [See Ref. 16. For completeness, we note: $B(M1)_W = 1.79 \mu_N^2$ and for $A = 34$, $B(E2)_W = 6.54 e^2 \text{F}^4$.]

Transition (keV)	ω^*, T_i	ω^*, \tilde{T}_i	$[B(M1) \times 10^2] / B(M1)_W$	$B(E2) / B(E2)_W$	$\kappa(E2/M1)^a$
461—0	(1 ⁺ , 0)	(0 ⁺ , 1)	4.5 ± 0.4		
461—147		(3 ⁺ , 0)		<27.	
666—0	(1 ⁺ , 0)	(0 ⁺ , 1)	0.83 ± 0.06		
666—147		(3 ⁺ , 0)		<2.5	
1230—0	(2 ⁺ , 0)	(0 ⁺ , 1)		<0.1	
1230—147		(3 ⁺ , 0)	$0.006^{+0.024}_{-0.004}$	$1.0^{+0.1}_{-0.1}$	2.2 ± 1.8
1230—461		(1 ⁺ , 0)	$0.05^{+0.03}_{-0.02}$	$4.4^{+1.0}_{-1.0}$	1.2 ± 0.5
1230—666		(1 ⁺ , 0)	0.32 ± 0.03	5.4 ± 2.7	0.37 ± 0.09

^aReferences 2 and 3. Note also that the uncertainties in the reduced strengths for the mixed transitions arise predominantly from the large uncertainties in the mixing ratios and are thus directly correlated. For example, if the 1230—461 transition has a $B(M1)$ of 0.08×10^{-2} W.u., then the $B(E2)$ must be 2.2 W.u.

²F. Brandolini, I. Filosofo, C. Signorini, and M. Morando, Nucl. Phys. A149, 401 (1970).

³F. Brandolini, R. G. R. Engmann, and C. Signorini, Nucl. Phys. A149, 411 (1970).

¹⁶D. H. Wilkinson, in Nuclear Spectroscopy, edited by F. Ajzenberg-Selove (Academic Press Inc., New York, 1960), Pt. B, p. 859 ff.

CL
A=35

CL
A=35

CL
A=35

Ref. R. Basile, C. Schuhl, W. Sebaoun
Compt. Rend. 241, 387 (1955)

Elem. Sym.	A	Z
Cl	35	17

Method 22 MeV betatron; neutron yield; radioactivity

Ref. No.
55 Ba 3
EGF

Reaction	E or ΔE	E_0	Γ	$\int \sigma dE$	$J\pi$	Notes
$Cl^{35}(\gamma, n)$	Bremss 22					$E_{th}(\gamma, n) = 12.79 \pm 0.07$ MeV See Table for breaks near threshold.



Fig. 2. — Courbe d'absorption de neutrons $^{35}Cl, n, \gamma$ (Basile, Schuhl, Sebaoun).

Les résultats expérimentaux sont représentés sur la figure 2 en fonction de l'énergie.

$E - E_0$ (MeV)...	-	0.34	0.72	0.98	1.24	1.50
		± 0.04	± 0.04	± 0.04	± 0.04	± 0.04
E (MeV).....	12.79	13.13	13.51	13.72	13.89	14.00
	± 0.07	± 0.07	± 0.07	± 0.07	± 0.07	± 0.07

E , énergie des neutrons; E_0 , seuil de la réaction $^{35}Cl, n, \gamma$, soit 12.79 ± 0.07 MeV.

METHOD			REF. NO.		
Betatron			55 Bo 2		
REACTION	RESULT	EXCITATION ENERGY	SOURCE		ANGLE
			TYPE	RANGE	
G,N	ABX	13-21	C	13-21	4PI

2-18

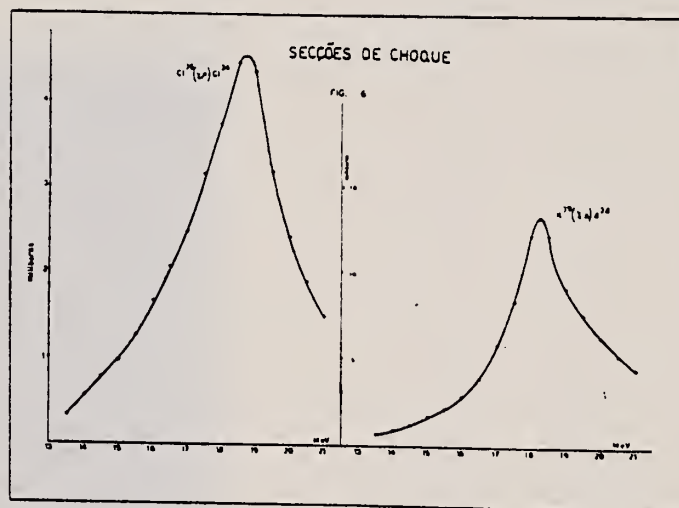


Fig. 6

Elementos	Limiar (Threshold)	E_M	σ_M	$\sigma_{int.}$	Largura	Δ GOLDBERG E LETTE LOPEZ, 1955
Cl	$12,35 \pm 0,035$ Mev	18,75 Mev	7,4 milibarn	$0,026 \text{ mb} \times \text{Mev}$	3,3 Mev	4,45 Mev
K	$13 \pm 0,15$ Mev	18,25 Mev	13,8 milibarn	$0,041 \text{ mb} \times \text{Mev}$	2,6 Mev	4,2 Mev

M.D. DeSouza Santos, J. Goldemberg, R.R. Pieroni, E. Silva,
O.A. Borello, S.S. Villaca, J.L. Lopes
Int. Conf. Peaceful Uses of Atomic Energy II (UN, NY), 169 (1955)

ELEM. SYM.	A	Z
C1	35	17

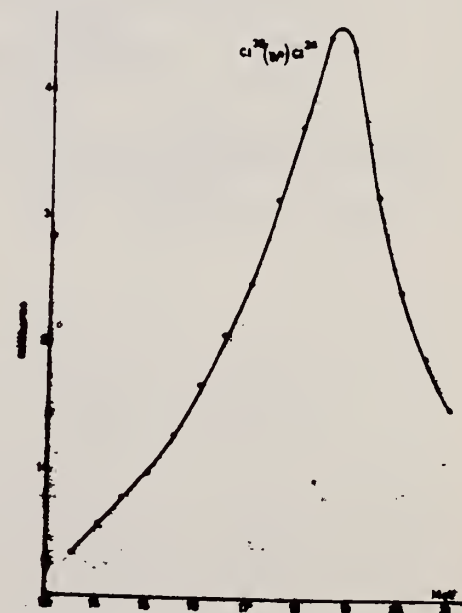
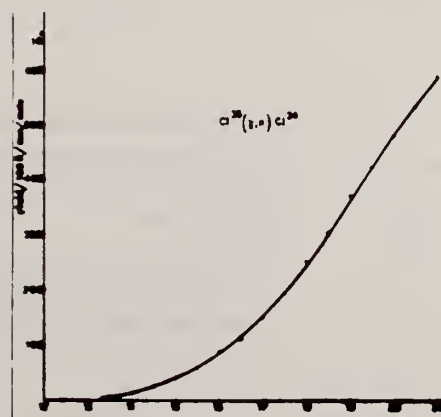
METHOD	Betatron; neutron yield; radioactivity; r-chamber	REF. NO.	55 De 1	EGF
--------	---	----------	---------	-----

REACTION	RESULT	EXCITATION ENERGY	SOURCE		DETECTOR		ANGLE
			TYPE	RANGE	TYPE	RANGE	
G,N	ABX	13-21	C	13-21	ACT-I		4PI

(γ, n) threshold 12.35 ± 0.035 MeV

THRESHOLD

$$\int \sigma dE = 0.02 \text{ MeV-b}$$



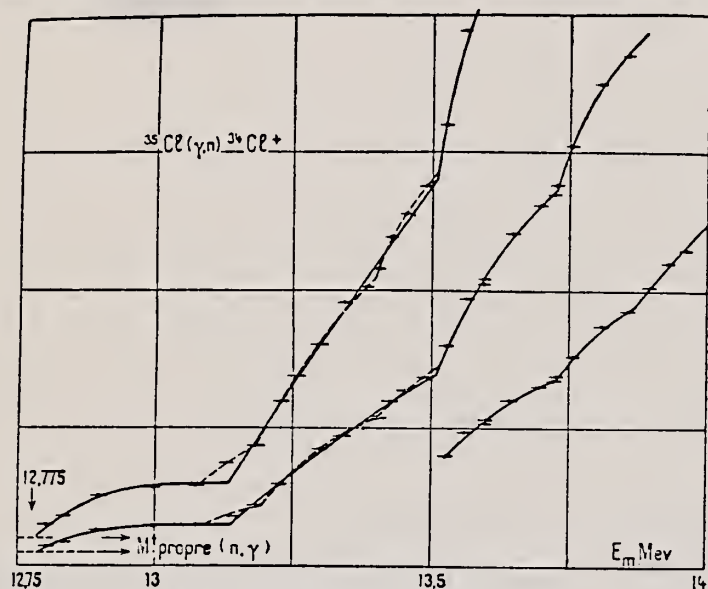
METHOD

REF. NO.

57 Ba 3

JOC

REACTION	RESULT	EXCITATION ENERGY	SOURCE		DETECTOR		ANGLE
			TYPE	RANGE	TYPE	RANGE	
G,N	RLY	12-14	C	12-14	ACT- I		4PI

BREAKSFig. 7. — Courbe d'activation de ^{35}Cl .

Les mesures sont consignées dans le tableau suivant (fig. 7) :

Seuil (MeV)	Energie des discontinuités (MeV)					
12.79 ± 0.07	13,13	(13,37)	13,51	13,72	13,89	14,1
Ecart entre les discontinuités (keV)						
340	240	140	210	170	210	

Énergie en MeV des raies (*)	12,79	13,13	(13,37)	13,51	13,72	13,89	14,1
$\sigma(V)dV$ en u. a . . .	1,15	3,8		2,29	7,4	5,17	3,58

(*) Etant donnée la forme de la courbe d'activation, il semble évident qu'il existe des discontinuités plus faibles entre celles qui ont été mises en évidence.

ELEM. SYM.	A	Z
Cl	35	17
REF. NO.		egf
59 Fe 1		

REACTION	RESULT	EXCITATION ENERGY	SOURCE		DETECTOR		ANGLE
			TYPE	RANGE	TYPE	RANGE	
G,N	ABX	10- 30	C	12- 30	ACT-I		4PI *
G,N	ABX	16- 30	C	19- 30	THR-I		4PI **

* ISOMER RATIO
 ** SI(NP)DETC

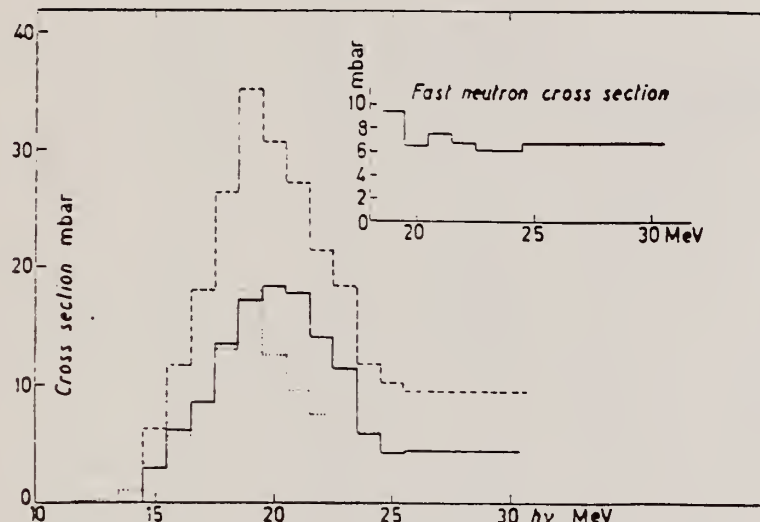


Fig. 2. - Cross sections from $^{35}\text{Cl}(\gamma, n)^{34}\text{Cl}$ ground and isomeric state calculated with the Penfold-Leisa method (--- isomeric state; — ground state, - - - g.s.+i.s.). The inset shows the fast neutron cross section in natural chlorine.

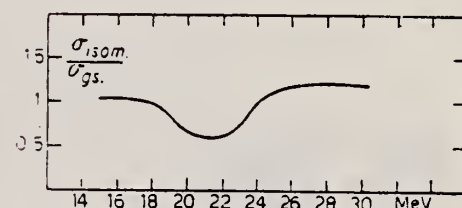


Fig. 3. - Branching ratio (b.r.) i.s./g.s. as a function of γ -ray energy.

TABLE I.

	Γ (MeV)	σ_{peak} (mb)	E_{peak} (MeV)	$\int_0^{30} \sigma dE$ (MeV-mb)
$^{35}\text{Cl}(\gamma, n)^{34}\text{Cl}$ g.s.	6	18.3	20	141
$^{35}\text{Cl}(\gamma, n)^{34}\text{Cl}$ i.s.	5	18	19	125
$^{35}\text{Cl}(\gamma, n)^{34}\text{Cl}$ (g.s.+i.s.)	6.5	35.2	19.5	266

Method	Ref. No.
Betatron; activation; NaI for annihilation radium from Cl^{34} positrons.	61 Sa 1 JHH

Reaction	E or ΔE	E_0	Γ	$\int \sigma dE$	$J\pi$	Notes
(γ, n)	12 - 14					$E_{\gamma} \text{ thresh.} = 12.66 \pm 0.04 \text{ MeV.}$ "Break" at 12.75 MeV corresponds to threshold of Schull [Nuovo Cimento <u>4</u> , Suppl., 1162 (1956)]. Refer Table II.

TABLE II. Thresholds (in Mev) of the $\text{P}^{31}(\gamma, n)\text{P}^{30}$ and $\text{Cl}^{35}(\gamma, n)\text{Cl}^{34}$ reactions compared to the results of other groups.

References	$\text{P}^{31}(\gamma, n)\text{P}^{30}$	$\text{Cl}^{35}(\gamma, n)\text{Cl}^{34}$
Our results ^a	12.23 \pm 0.04	12.66 \pm 0.04
Schull ^b	12.33 \pm 0.05	12.79 \pm 0.05
Chidley <i>et al.</i> ^c	12.50 \pm 0.05	
Wapstra (mass data) ^d	12.40 \pm 0.08	12.71 \pm 0.12
Everling (mass data) ^e	12.316 \pm 0.02	12.57 \pm 0.04

^a These results are given in the laboratory system. In the center-of-mass system the results will not decrease more than 3 kev.

^b See reference 2.

^c Can. J. Phys. **36**, 407 (1956).

^d Physica **21**, 367 (1955).

^e Nuclear Phys. **15**, 342 (1960).

Ref 2: Schull, Suppl. Nuovo cimento 4, 1162 (1956)

Elem. Sym.	A	Z
Cl	35	17
Ref. No. 62 Bq 5		
JHH		

Method 4 MeV. electron Van de Graaff; brems.; nuclear resonance scattering, ring scatterer; NaI

Reaction	E or ΔE	E_0	Γ	$\int \sigma dE$	$J\pi$	Notes
$Cl^{35}(\gamma, \gamma)$	Brems. 0 - 4					

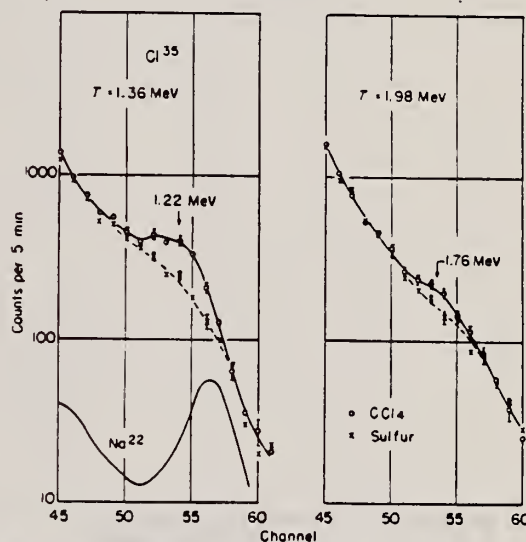


Fig. 4. Resonance fluorescence from the 1.22 MeV and 1.76 MeV states of Cl^{35} . The Na^{22} peak is at 1.28 MeV.

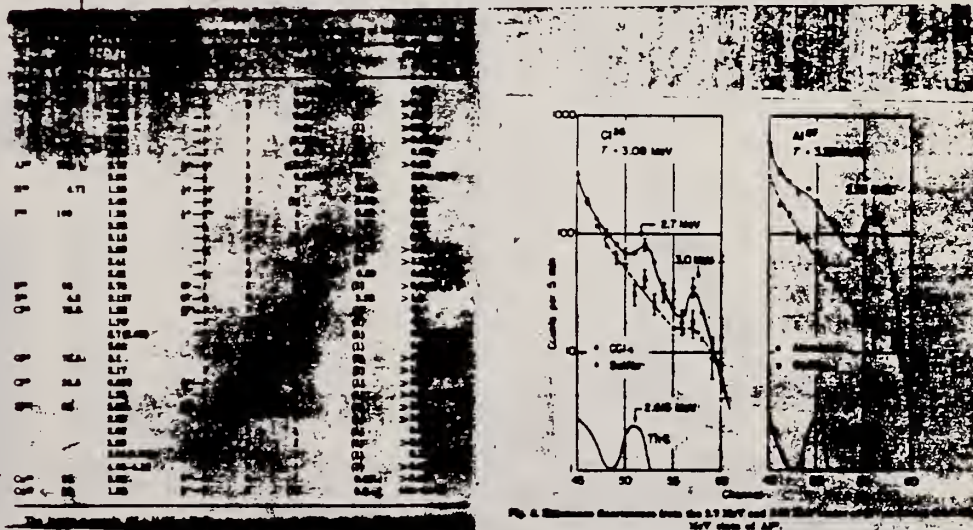


Fig. 5. Resonance fluorescence from the 3.08 MeV and 3.18 MeV states of Cl^{35} . The Th^{232} peak is at 2.6 MeV.

Method Betatron; neutron yield; radioactivity; NBS chamber

Ref. No.	NVB
62 Ku 1	

Reaction	E or ΔE	E_0	Γ	$\int \sigma dE$	$J\pi$	Notes
$Cl^{35}(\gamma, n)$	Bremss. 12-27	19.8 13.8 14.1 15.1 16.2 17.6 18.2	6.5 MeV	$\int_{12}^{27} = 93 \text{ MeV-mb}$		$\sigma_{\max} = 13.5 \text{ mb}$ $\Gamma = \text{width of giant resonance}$

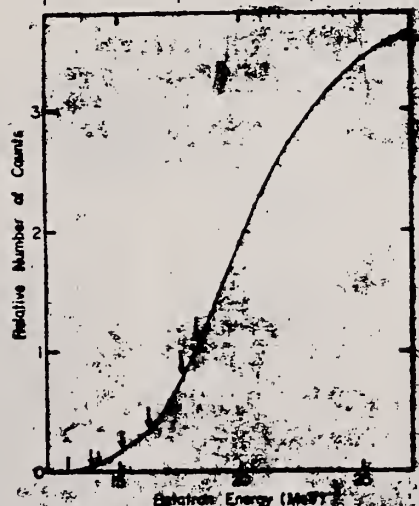


Fig. 4. The activation curve of the reaction $Cl^{35}(\gamma, n)Cl^{35}$. Arrows indicate breaks in the curve.

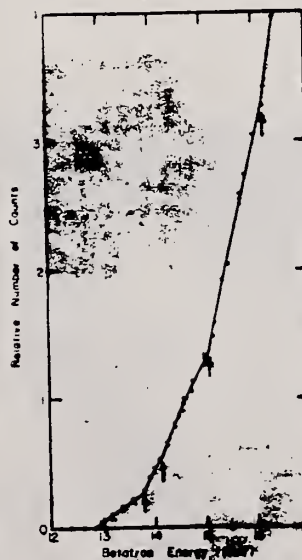


Fig. 5. The activation curve of the reaction $Cl^{35}(\gamma, n)Cl^{35}$ near the threshold. Arrows indicate breaks in the curve.

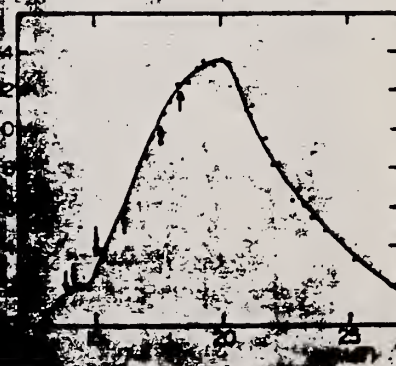


Fig. 6. The activation curve of the reaction $Cl^{35}(\gamma, n)Cl^{35}$. Arrows indicate breaks in the curve.

REF.

J.H. Hough and W.L. Mouton
Nucl. Phys. 76, 248 (1966)

ELEM. SYM.

A

Z

Cl

35

17

METHOD

1.4 MeV Linac; self-absorption

REF. NO.

66 Ho 2

JDM

REACTION	RESULT	EXCITATION ENERGY	SOURCE		DETECTOR		ANGLE
			TYPE	RANGE	TYPE	RANGE	
G,G	LFT	1	C	1	NAI-D	0 - 1	117

TABLE I
Mean lifetimes

Nucleus	State (MeV)	Spin	Mean lifetime (psec) (Hough and Mouton)	Mean lifetime (psec) (Other workers)	Ref.
²⁷ Al	1.01	½	0.5 ^{+0.5} _{-0.2}	5.2 ± 1.7	¹⁾
				0.041 ^{+0.029} _{-0.016}	²⁾
				1.7 ^{+1.2} _{-0.5}	³⁾
³¹ P	1.26	½	0.73 ^{+0.19} _{-0.12}	0.46 ± 0.23	⁴⁾
				0.22 ± 0.07	⁵⁾
				0.96 ^{+0.50} _{-0.21}	¹⁾
				0.72 ^{+0.13} _{-0.10}	⁶⁾
³⁵ Cl	1.22	½	0.13 ^{+0.03} _{-0.02}	0.30 ± 0.10	⁷⁾

REF. E. G. Kopanets, Yu. S. Korfa, A. A. Koval, L. N. Sukhoton, and S. P. Tsytko J. Nucl. Phys. (USSR) <u>6</u> , 233 (1967) Sov. J. Nucl. Phys. <u>6</u> , 170 (1968)			ELEM. SYM.	A	Z
			Cl	35	17
METHOD			REF. NO. 67 Ko 2		HMG
REACTION	RESULT	EXCITATION ENERGY	SOURCE		ANGLE
			TYPE	RANGE	
P,G	LFT	8	D	2.0	DST
		(8.385)		(2.079)	

J-PI

For ground state transition

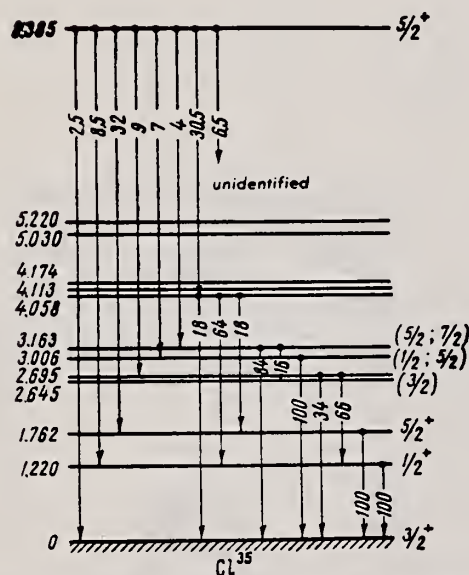
$$W(\theta) = 1 + a_2 P_2 + a_4 P_4$$

$$a_2 = -.828 \pm .220$$

$$a_4 = .715 \pm .326$$

Table III

E_γ , MeV	I^π	$\frac{\sigma_T = \frac{(2I+1) \cdot \Gamma_\gamma}{\Gamma_\gamma \Gamma_p}}{2\Gamma}$, eV	Γ_γ , eV	Type of transition	$ M ^2$
8.4	$\left\{ \begin{array}{l} 5/2^+ \\ 5/2^+ \end{array} \right.$	4	0.0146	M1	0.0012
		4	0.054	E2	0.044
6.6	$\left\{ \begin{array}{l} 5/2^+ \\ 5/2^+ \end{array} \right.$	4	0.0044	E2	0.013
		4	0.216	M1	0.034
1.76	$\left\{ \begin{array}{l} 5/2^+ \\ 5/2^+ \end{array} \right.$		0.0012	M1	0.0105
			0.00013	E2	1.5

Fig. 4. Decay scheme of the 8.385-MeV resonance level of Cl³⁵.

METHOD					REF. NO.	
					67 Wa 1	HMG
REACTION	RESULT	EXCITATION ENERGY	SOURCE		DETECTOR	
			TYPE	RANGE	TYPE	RANGE
P,G	LFT	8.0	D	2.0	SCD-D	4PI
		(7.84)		(1.512)		

TABLE I. A summary of results from the angular-correlation measurements. The transition speeds are given in Weisskopf units. The values in parentheses are allowed by the angular-correlation measurements but generally correspond to unreasonable transition speeds.

Transition	Branching ratio	Multipole mixing ratio	$ M ^2(L)$	$ M ^2(L+1)$
7.84 \rightarrow 0	0.22	-0.02 ± 0.03 (3.6 ± 0.26)	$E1 = 2.1 \times 10^{-4}$ ($E1 = 1.4 \times 10^{-4}$)	$M2 = 0.1 \pm 0.1$ $M2 = 140$
7.84 \rightarrow 1.22	0.34	-0.06 ± 0.03 (3.1 ± 0.3)	$E1 = 5.5 \times 10^{-4}$ ($E1 = 5.5 \times 10^{-4}$)	$M2 = 1 \pm 0.5$ $M2 = 520$
7.84 \rightarrow 4.17	0.29	0.05 ± 0.03	$M1 = 1.0$	$E2 = 0.7 \pm 0.6$
4.17 \rightarrow 0	0.51	-0.06 ± 0.03 (-3.08 ± 0.30)
4.17 \rightarrow 1.22	0.43	-0.11 ± 0.04 (2.27 ± 0.30)
7.54 \rightarrow 3.16	0.97	0.07 ± 0.02	$M1 = 1.6$	$E2 = 1.4 \pm 0.5$
3.16 \rightarrow 0	0.90	-0.16 ± 0.01

ELEM. SYM.	A	Z
C1	35	17
REF. NO.		
72 Hu 5		egf

METHOD					REF. NO.	
					72 Hu 5	
REACTION	RESULT	EXCITATION ENERGY	SOURCE		DETECTOR	
			TYPE	RANGE	TYPE	RANGE
P,G	ABY	7- 8	D	1- 2 (.7-2.1)	NAI-D	55

TABLE I
Energie et force des résonances de la réaction $^{34}\text{S}(p,\gamma)^{35}\text{Cl}$

E_p (keV)	$(2J+1)I_p^2/I^2$ (eV)	E_γ (keV)	$2(J+1)I_p^2/I^2$ (eV)
716.0±0.7	0.2	1598.9±1.3	0.8
754.1±0.7	0.5	1647.3±1.2	1.2
831.5±0.8	0.4	1665.2±1.2	1.5
848.2±0.7	1.1	1673.7±1.1	2.7
880.5±0.8	0.4	1679.7±1.1	4.1
889.0±0.8	1.3	1684.3±1.3	4.5
928.2±0.9	1.4	1714.0±1.1	0.9
1020.4±0.8	3.2	1717.9±1.1	3.5
1054.9±1.0	0.4	1756.0±1.0	1.6
1112.2±1.0	0.3	1776.7±1.1	2.5
1165 ^{b)}	(0.6)	1787.7±1.1	4.2
1183.2±1.1	0.2	1794.8±1.3	1.2
1213.7±1.0	21±3 ^{c)}	1829.1±1.3	2.4
1225.6±1.0	1.5	1839.0±1.2	2.1
1266.5±1.0	3.2	1862.7±1.3	0.8
1285.5±1.1	1.2	1893.2±1.1	8.0
1323.7±1.2	0.5	1901.8±1.1	6.2
1339.8±1.1	1.5	1928.2±1.3	1.9
1353.7±1.1	2.5	1955.9±1.3	1.8
1362.4±1.2	0.4	1964.1±1.4	1.6
1375.7±1.1	3.7	1970.0±1.3	2.4
1415.6±1.2	1.3	1975.6±1.3	2.9
1449.0±1.1	1.5	1986.0±1.3	4.0
1453.6±1.2	0.8	2006.7±1.2	4.2
1469.6±1.2	1.5	2010.5±1.3	1.0
1510 ^{b)}	(11)	2073.5±1.2	14.1
1542.3±1.3	0.5	2080.0±1.4	0.6
1554.9±1.2	1.6	2096.6±1.2	6.4
1574.4±1.2	1.4	2101.0±1.4	3.6

^{a)} Les erreurs sur les forces sont de l'ordre de 50 % pour les résonances faibles (< 1 eV), et 30 % pour les résonances fortes.

^{b)} Doublet de résonances, voir texte.

^{c)} Réf. ²⁷⁾.

(over)

Résonances			Décroissances γ , en pourcentages, vers E_x (MeV)/ J^π															Autres niveaux E_x (%)
$E_p^a)$ (keV)	$E_x^b)$ (keV)	$J^\pi^c)$	0 $\frac{1}{2}^+$	1.22 $\frac{1}{2}^+$	1.76 $\frac{1}{2}^+$	2.65 $\frac{3}{2}^+$	2.69 $\frac{3}{2}^+$	3.00 $\frac{1}{2}^+$	3.16 $\frac{1}{2}^-$	3.92 $\frac{1}{2}^-$	3.94 $\frac{1}{2}^+$	3.97 $\frac{1}{2}^+$	4.06 $\frac{1}{2}^-, \frac{1}{2}^-$	4.11	4.17	4.18 $\frac{1}{2}^-$		
716	7063	$\frac{1}{2}, \frac{1}{2}$	48	18	16	3	6	2	6				1					
754	7100	$\frac{1}{2}^+, \frac{3}{2}, \frac{1}{2}^+$	11	67	4		13	3		2							6.10(4)	
832	7175	$\frac{1}{2}, \frac{3}{2}, \frac{1}{2}^+$	40	16			4			2		10	24				4.85(2), 5.01(1)	
848	7192	$\frac{1}{2}^+, d)$		72						5		2	3			15	5.21(6), 5.40(1), 5.85(1)	
881	7223	$\frac{3}{2} d)$	58		8		10	3		1					7		5.68(2), 6.10(3)	
889	7231	$\frac{1}{2}^+ d)$	93	2		2	2										1	
928	7269	$\frac{1}{2} d)$	69	23			1					1	1			0.5	4.84(1), 5.01(1.5), 5.40(0.5), 5.75(1.5)	
1020	7358	$\frac{1}{2} e)$	10	70	10			0.5		0.5		3	3			1	4.84(1), 5.01(0.5), 5.65(0.5), 4.35(10)	
1055	7392	$\frac{1}{2}^+, \frac{3}{2}, \frac{1}{2}^+$				10		14	49		8			9				
1112	7448	$\frac{1}{2}^+, \frac{3}{2}, \frac{1}{2}$		73	4		8	10		5								
1165	7499	$\frac{1}{2}, \frac{3}{2}$			7	55		13			25							
1166	7500	$\frac{1}{2}, \frac{3}{2}$		20									70				6.10(10)	
1183	7517	$\frac{1}{2}^+, \frac{3}{2}, \frac{1}{2}$			20	3			68		2						4.35(2), 5.59(3), 5.60(2)	
1214	7546	$\frac{1}{2}^+ f)$	0.2		0.3	0.5		1.8	95								4.77(1.5), 5.59(0.2), 5.64(0.5)	
1226	7558	$\frac{1}{2}, \frac{3}{2}$	36	36			21			1			5			1		
1267	7598	$\frac{1}{2} g)$	31	1	2	1.5	19	9	4				1.5		2	2	4.63(2), 4.77(1), 4.84(2), 4.88(2), 5.16(2)	
1285	7616	$\frac{1}{2}^-, \frac{1}{2}$	80		10				3				1			3	5.21(3)	
1324	7653	$\frac{1}{2}, \frac{3}{2}$	57									2	32			1	4.84(3), 5.65(1), 5.68(1), 6.10(3)	
1340	7669	$\frac{1}{2}, \frac{3}{2}$	2		57	14		8	4						4		4.35(6), 4.88(1), 5.16(4)	
1354	7683	$\frac{1}{2}, \frac{3}{2}$	72	1				9					6		5	2	5.21(0.5), 5.40(2), 5.60(2), 5.75(0.5)	
1362	7691	$\frac{1}{2}, \frac{3}{2}$	96					2					1				5.60(1)	
1376	7704	$\frac{1}{2}^+, \frac{3}{2}$	88	1		4		1						1			4.84(1), 5.65(4)	
1416	7743	$\frac{1}{2}^+, \frac{3}{2}, \frac{1}{2}$			2	43			18		12			5			4.77(1), 4.88(19)	
1449	7775	$\frac{1}{2}, \frac{3}{2}$	16	13	46	2	7	4					1			7	4.77(2), 4.84(2)	
1454	7780	$\frac{1}{2}, \frac{3}{2}$			20	9			5	10			1	3	40		4.35(2), 4.77(7), 5.21(1), 5.40(1), 5.59(1)	
1470	7795	$\frac{1}{2}, \frac{3}{2}$	85	9													4.85(0.5), 5.01(2), 5.40(2), 5.65(1), 5.75(0.5)	
1513	7834	$h)$	27	27				4					2		3	35	5.21(1), 6.10(1)	
1542	7866	$\frac{1}{2}^+, \frac{3}{2}, \frac{1}{2}$	62	12	18										4		5.01(4)	
1555	7878	$\frac{1}{2}, \frac{3}{2}, \frac{1}{2}^+$	9		31		30	10		2			1	4			4.63(1), 4.84(3), 5.65(9)	
1574	7897	$\frac{1}{2}^-, \frac{3}{2}$	3		77				4				2		6	8		
1599	7921	$\frac{1}{2}, \frac{3}{2}, \frac{1}{2}^+$	48	28	1		12			1		1	1		6	2		
1647	7968	$\frac{1}{2}, \frac{3}{2}, \frac{1}{2}^+$			21	22		5	13					2	6		4.35(8), 4.77(6), 4.88(9), 5.21(3), 5.59(2), 5.64(3)	
1665	7985	$\frac{1}{2}, \frac{3}{2}, \frac{1}{2}^+$	36	62													5.65(1), 6.10(1)	
1674	7993	$\frac{1}{2}^-, \frac{3}{2}$	87		1				6							3	5.40(3)	
1680	7999	$\frac{1}{2}^+, \frac{3}{2}, \frac{1}{2}$	1		76	2					2				8		4.77(8), 5.64(3)	
1684	8004	$\frac{1}{2}, \frac{3}{2}, \frac{1}{2}^+$	60		20			3	17									
1714	8033	$\frac{1}{2}, \frac{3}{2}$	2	56	5		5						11			15	5.80(6)	
1718	8036	$\frac{1}{2}^+, \frac{3}{2}, \frac{1}{2}^+$	9	6	17		61	3					4					
1756	8073	$\frac{1}{2}, \frac{3}{2}, \frac{1}{2}$	1		53			2						2	7		4.77(4), 4.88(2), 5.16(1), 5.21(7), 5.59(11), 5.64(10)	
1777	8093	$\frac{1}{2}, \frac{1}{2}^+$	40		9	17	5		5	3			2				4.77(1), 4.84(3), 5.16(2), 5.21(1), 5.60(6), 5.64(5), 5.80(1)	
1788	8104	$\frac{1}{2}, \frac{1}{2}^+$	40	35	3		8	8				3	0.5			1	4.84(0.5), 4.85(0.5), 5.60(0.5)	
1795	8111	$\frac{1}{2}^+, \frac{3}{2}, \frac{1}{2}^+$	26	32	6		17					5			5		5.60(3), 6.49(6)	
1829	8144	$\frac{1}{2}, \frac{3}{2}$	63	15			3			3		1	3			9	5.01(2), 5.68(1)	
1839	8154	$\frac{1}{2}, \frac{3}{2}$	4			50		4	9					7	8		5.21(8), 5.59(7), 5.64(3)	
1863	8177	$\frac{1}{2}, \frac{3}{2}, \frac{1}{2}$	8		68		3	4	8								4.63(9)	
1893	8207	$\frac{1}{2} i)$	76	3	16		1	1		1			2					
1902	8215	$\frac{1}{2} i)$	47				4	5	44									
2073	8382	$\frac{1}{2} j)$	3		34	5	1	25		24				8				

^{a)} Nos résultats (voir tableau 1).
indication contraire.

^{d)} Réf. 1).

^{b)} Calculées avec la valeur $Q = 6367.4 \pm 1.6$ keV mesurée dans ce travail.

^{e)} Réfs. 7, 8).

^{f)} Réfs. 4, 7).

^{g)} Réf. 8).

^{h)} Résonance double (voir paragraphes 3.3 et 4.4).

ⁱ⁾ Réf. 15).

^{j)} Réf. 18).

REF.

E. Woly nec, G. Moscati, J. R. Moreira, O. D. Goncalves,
M. N. Martins
Phys. Rev. C11, 1083 (1975)

ELEM. SYM.

A

Z

Cl

35

17

METHOD

REF. NO.

75 Wo 2

hmg

REACTION	RESULT	EXCITATION ENERGY	SOURCE		DETECTOR		ANGLE
			TYPE	RANGE	TYPE	RANGE	
G,N	RLY	19- 38	C	19- 38	ACT-I		4PI

RATIO (G,N)/(E,N)

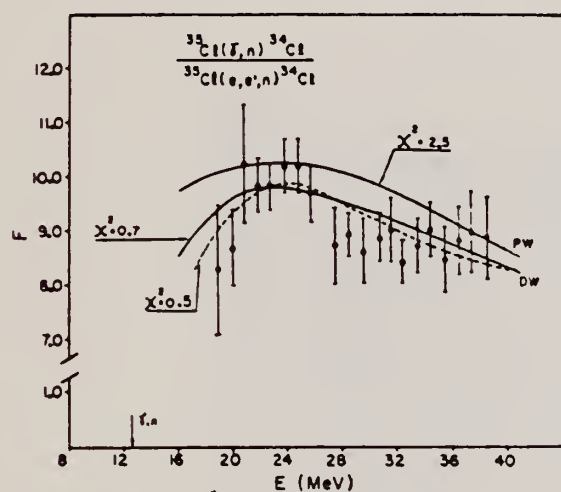


FIG. 3. Measured F for $^{35}\text{Cl}(\gamma, n)$. Dashed curve is a polynomial fit to the points. Full curves are F_{PW} and F_{DW} predictions.

$$F_{PW}^{(E)} = (N_r / Z_r^2 r_e^2 N_r)$$

$$\times \frac{\int_0^{E_1 - m_e} \sigma_\gamma(\omega) \phi(E_1, \omega, Z_r) (d\omega/\omega)}{\int_0^{E_1 - m_e} \sigma_\gamma(\omega) N_{PW}^{E_1}(E_1, \omega) (d\omega/\omega)}, \quad (10)$$

$$F_{DW}^{(E)} = (N_r / Z_r^2 r_e^2 N_r)$$

$$\times \frac{\int_0^{E_1 - m_e} \sigma_\gamma(\omega) \phi(E_1, \omega, Z_r) (d\omega/\omega)}{\int_0^{E_1 - m_e} \sigma_\gamma(\omega) N_{DW}^{E_1}(E_1, \omega, Z_r) (d\omega/\omega)}, \quad (11)$$

ELEM. SYM.	A	Z
Cl	35	17
METHOD		REF. NO.
		76 Sp 10
		egf

REACTION	RESULT	EXCITATION ENERGY	SOURCE		DETECTOR		ANGLE
			TYPE	RANGE	TYPE	RANGE	
P,G	LFT	8- 9	D	2- 3	SCD-D		55

Abstract: The yield curve of the reaction $^{34}\text{S}(p, \gamma)^{34}\text{Cl}$ has been measured over the energy range $E_p = 1.95$ –2.91 MeV. Proton energies and strengths of 84 resonances are given. The decay schemes of 38 selected resonances have been studied, and for these branching ratios and spin limits are presented. The proton energy of the well known $J^\pi = \frac{7}{2}^-$ analogue resonance has been measured as $E_p = 1211.45 \pm 0.09$ keV. The reaction Q-value is $Q = 6371.6 \pm 0.4$ keV.

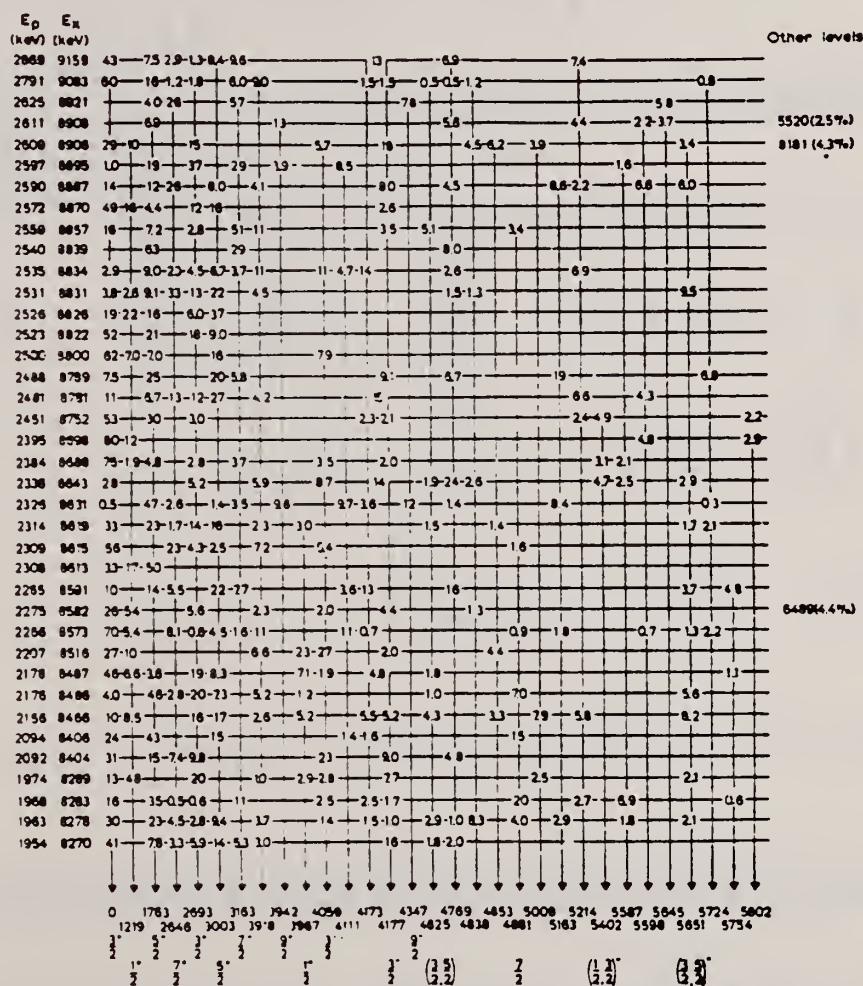


Fig. 4. Decay schemes and branching ratios (%) of 38 of the resonances observed for $E_p > 1.95$ MeV in $^{34}\text{S}(p, \gamma)^{34}\text{Cl}$. Spins and parities of the bound states have been taken from ref. 1⁶). Errors in the branchings b are typically 10%, for $b > 50\%$ to 25% for $b \approx 10\%$. Weak branchings ($b \approx 1\%$) have errors 50%.

(over)

TABLE I

Resonances observed in the reaction $^{34}\text{S}(p, \gamma)^{35}\text{Cl}$ for $E_p > 1.95$ MeV

No.	E_p (keV)	E_γ (keV)	$(2J+1)F_p F_\gamma / F^2$ (eV)	J^π	E_p (keV)	E_γ (keV)
1	1954.4	8270.1	0.6	$\frac{1}{2}^+$		8271 \pm 4
2	1962.9	8278.4	0.7	$\frac{1}{2}^+, \frac{3}{2}^+, \frac{5}{2}^-$		
3	1967.9	8283.2	0.4	$\frac{1}{2}^+, \frac{3}{2}^+, \frac{5}{2}^-$		8292 ^{b)}
4	1973.8 \pm 0.3	8289.1 \pm 0.5	0.9	$\frac{1}{2}^+, \frac{3}{2}^+, \frac{5}{2}^-$	1985 \pm 2	
5	1983.7	8298.7	0.6	$\frac{1}{2}^+, \frac{3}{2}^+, \frac{5}{2}^-$		
6	1984.5	8299.4	0.9	$\frac{1}{2}^+, \frac{3}{2}^+, \frac{5}{2}^-$		
7	2005.0 \pm 0.3	8319.5 \pm 0.5	2.7	$\frac{1}{2}^+$	2071 \pm 2	8321 \pm 4
8	2070.4	8382.9	6.1	$\frac{1}{2}^+$		
9	2076.9	8389.1	0.4	$\frac{1}{2}^+$		
10	2092.4	8404.2	0.7	$\frac{1}{2}^+, \frac{3}{2}^+, \frac{5}{2}^-$	2094 \pm 3	8399 \pm 4
11	2093.9	8405.7	2.3	$\frac{1}{2}^+, \frac{3}{2}^+, \frac{5}{2}^-$	2100 \pm 3	
12	2097.5	8409.2	1.4	$\frac{1}{2}^+, \frac{3}{2}^+, \frac{5}{2}^-$	2109 \pm 3	
13	2106.6	8418.0	0.5	$\frac{1}{2}^+$		
14	2120.6	8431.6	1.0	$\frac{1}{2}^+$	2125 \pm 2	8429 \pm 4
15	2125.2	8436.1	0.5	$\frac{1}{2}^+$		
16	2155.6	8465.6	0.9	$\frac{1}{2}^+, \frac{3}{2}^+, \frac{5}{2}^-$		
17	2176.4	8485.8	2.1	$\frac{1}{2}^+, \frac{3}{2}^+, \frac{5}{2}^-$	2177 \pm 3	8482 \pm 4
18	2178.0	8487.4	1.9	$\frac{1}{2}^+, \frac{3}{2}^+, \frac{5}{2}^-$	2179 \pm 3	
19	2199.1	8507.9	0.3	$\frac{1}{2}^+$		8505 \pm 5
20	2207.1	8515.6	0.5	$\frac{1}{2}^+$	2207 \pm 2	
21	2227.3	8535.3	0.1	$\frac{1}{2}^+$		8532 \pm 4
22	2266.4	8573.2	2.9	$\frac{1}{2}^+, \frac{3}{2}^+, \frac{5}{2}^-$		8568 \pm 4
23	2275.3	8581.9	1.0	$\frac{1}{2}^+, \frac{3}{2}^+, \frac{5}{2}^-$		
24	2280.7	8587.1	0.1	$\frac{1}{2}^+, \frac{3}{2}^+, \frac{5}{2}^-$		
25	2285.0	8591.3	0.7	$\frac{1}{2}^+, \frac{3}{2}^+, \frac{5}{2}^-$		
26	2307.7	8613.4	1.0	$\frac{1}{2}^+, \frac{3}{2}^+, \frac{5}{2}^-$		8617 \pm 4
27	2309.4	8615.0	2.4	$\frac{1}{2}^+, \frac{3}{2}^+, \frac{5}{2}^-$		
28	2314.0	8619.5	3.8	$\frac{1}{2}^+$		
29	2326.3 \pm 0.3	8631.4 \pm 0.5	2.7	$\frac{1}{2}^+$		
30	2338.0	8642.8	0.9	$\frac{1}{2}^+, \frac{3}{2}^+, \frac{5}{2}^-$		
31	2384.1	8687.6	2.2	$\frac{1}{2}^+, \frac{3}{2}^+, \frac{5}{2}^-$		
32	2386.3	8689.7	0.7	$\frac{1}{2}^+, \frac{3}{2}^+, \frac{5}{2}^-$		
33	2395.1	8698.3	0.6	$\frac{1}{2}^+, \frac{3}{2}^+, \frac{5}{2}^-$		8698 ^{b)}
34	2404.8	8707.7	0.2	$\frac{1}{2}^+, \frac{3}{2}^+, \frac{5}{2}^-$		
35	2416.5	8719.0	0.5	$\frac{1}{2}^+, \frac{3}{2}^+, \frac{5}{2}^-$		8721 \pm 4
36	2450.7	8752.3	1.7	$\frac{1}{2}^+, \frac{3}{2}^+, \frac{5}{2}^-$		
37	2467.3	8768.4	0.3	$\frac{1}{2}^+, \frac{3}{2}^+, \frac{5}{2}^-$		
38	2473.4	8774.4	0.6	$\frac{1}{2}^+, \frac{3}{2}^+, \frac{5}{2}^-$		
39	2480.5	8781.2	1.7	$\frac{1}{2}^+, \frac{3}{2}^+, \frac{5}{2}^-$		
40	2488.1	8788.6	1.2	$\frac{1}{2}^+, \frac{3}{2}^+, \frac{5}{2}^-$		8786 \pm 4
41	2496.6	8799.8	1.7	$\frac{1}{2}^+, \frac{3}{2}^+, \frac{5}{2}^-$		
42	2522.8	8822.4	0.7	$\frac{1}{2}^+, \frac{3}{2}^+, \frac{5}{2}^-$		
43	2526.2	8825.7	3.7	$\frac{1}{2}^+, \frac{3}{2}^+, \frac{5}{2}^-$		
44	2531.4	8830.6	2.1	$\frac{1}{2}^+, \frac{3}{2}^+, \frac{5}{2}^-$		
45	2535.3	8834.5	0.7	$\frac{1}{2}^+, \frac{3}{2}^+, \frac{5}{2}^-$		8840 \pm 4
46	2540.5	8839.5	1.5	$\frac{1}{2}^+, \frac{3}{2}^+, \frac{5}{2}^-$		
47	2559.0	8857.5	4.6	$\frac{1}{2}^+, \frac{3}{2}^+, \frac{5}{2}^-$		
48	2571.9	8870.0	1.0	$\frac{1}{2}^+, \frac{3}{2}^+, \frac{5}{2}^-$		

^{a)} All ± 0.5 keV unless otherwise indicated.^{b)} All ± 0.7 keV unless otherwise indicated.^{c)} Yields normalized to $(2J+1)F_p F_\gamma / F^2 = 9.7 \pm 0.7$ eV at $E_p = 1211$ keV (see text). Errors range from $\pm 20\%$ for the strongest resonances to $\pm 50\%$ for strengths < 1 eV.^{d)} Deduced from decay schemes unless otherwise indicated.^{e)} $^{34}\text{S}(p, p)^{34}\text{S}$ [ref. ⁹⁾].^{f)} $^{32}\text{S}(\alpha, p)^{35}\text{Cl}$ [ref. ¹⁶⁾] unless otherwise indicated.^{g)} Ref. ²¹⁾.^{h)} Assignment uncertain in ref. ¹⁶⁾.ⁱ⁾ $F = 3.1 \pm 0.3$ keV.^{j)} $F = 2.0 \pm 0.4$ keV.⁹⁾ W. Bruynestyn, thesis, University of Utrecht (1971).¹⁶⁾ J. D. Goss et al., Phys. Rev. C7 (1973) 1871.²¹⁾ J. Kuperus, Physica 30 (1964) 899.

TABLE I (continued)

No.	E_p (keV)	E_γ (keV)	$(2J+1)F_p F_\gamma / F^2$ (eV)	J^π	E_p (keV)	E_γ (keV)
49	2587.9	8885.6	0.4	$\frac{1}{2}^+, \frac{3}{2}^+, \frac{5}{2}^-$		8888 \pm 4
50	2589.9	8887.5	1.4	$\frac{1}{2}^+, \frac{3}{2}^+, \frac{5}{2}^-$		
51	2597.4	8894.8	1.2	$\frac{1}{2}^+, \frac{3}{2}^+, \frac{5}{2}^-$		
52	2609.2	8906.3	1.0	$\frac{1}{2}^+, \frac{3}{2}^+, \frac{5}{2}^-$		
53	2611.3	8908.3	1.5	$\frac{1}{2}^+, \frac{3}{2}^+, \frac{5}{2}^-$		
54	2624.6	8921.2	1.1	$\frac{1}{2}^+, \frac{3}{2}^+, \frac{5}{2}^-$		
55	2638.5	8934.7	1.0	$\frac{1}{2}^+, \frac{3}{2}^+, \frac{5}{2}^-$		8957 \pm 4
56	2658.8	8954.4	2.4	$\frac{1}{2}^+, \frac{3}{2}^+, \frac{5}{2}^-$		
57	2663.8	8959.3	1.2	$\frac{1}{2}^+, \frac{3}{2}^+, \frac{5}{2}^-$		
58	2688.6	8983.4	2.2	$\frac{1}{2}^+, \frac{3}{2}^+, \frac{5}{2}^-$		
59	2690.9	8985.7	0.6	$\frac{1}{2}^+, \frac{3}{2}^+, \frac{5}{2}^-$		
60	2695.3	8989.9	0.7	$\frac{1}{2}^+, \frac{3}{2}^+, \frac{5}{2}^-$		
61	2699.4	8993.9	2.3	$\frac{1}{2}^+, \frac{3}{2}^+, \frac{5}{2}^-$		
62	2703.8	8998.2	1.7	$\frac{1}{2}^+, \frac{3}{2}^+, \frac{5}{2}^-$		8997 \pm 4
63	2708.3	9002.5	0.6	$\frac{1}{2}^+, \frac{3}{2}^+, \frac{5}{2}^-$		
64	2727.1 ¹⁾	9020.8	0.8	$\frac{1}{2}^+, \frac{3}{2}^+, \frac{5}{2}^-$		
65	2732.4	9025.9	1.1	$\frac{1}{2}^+, \frac{3}{2}^+, \frac{5}{2}^-$		9027 \pm 4
66	2738.0	9031.4	2.6	$\frac{1}{2}^+, \frac{3}{2}^+, \frac{5}{2}^-$		
67	2741.3	9034.5	0.4	$\frac{1}{2}^+, \frac{3}{2}^+, \frac{5}{2}^-$		
68	2746.6	9039.7	0.8	$\frac{1}{2}^+, \frac{3}{2}^+, \frac{5}{2}^-$		
69	2757.0	9049.8	3.2	$\frac{1}{2}^+, \frac{3}{2}^+, \frac{5}{2}^-$		9086 \pm 4
70	2791.0 \pm 0.4	9082.9 \pm 0.6	16.0	$\frac{1}{2}^+, \frac{3}{2}^+, \frac{5}{2}^-$		
71	2798.3	9090.0	0.7	$\frac{1}{2}^+, \frac{3}{2}^+, \frac{5}{2}^-$		
72	2809.4	9100.7	1.2	$\frac{1}{2}^+, \frac{3}{2}^+, \frac{5}{2}^-$		
73	2810.6	9101.9	2.1	$\frac{1}{2}^+, \frac{3}{2}^+, \frac{5}{2}^-$		
74	2817.8	9108.9	0.5	$\frac{1}{2}^+, \frac{3}{2}^+, \frac{5}{2}^-$		9109 \pm 5
75	2820.5	9111.5	0.5	$\frac{1}{2}^+, \frac{3}{2}^+, \frac{5}{2}^-$		9131 ^{g)}
76	2834.9	9125.5	1.2	$\frac{1}{2}^+, \frac{3}{2}^+, \frac{5}{2}^-$		
77	2846.3 ¹⁾	9136.6	0.2	$\frac{1}{2}^+, \frac{3}{2}^+, \frac{5}{2}^-$		
78	2849.6	9139.8	1.9	$\frac{1}{2}^+, \frac{3}{2}^+, \frac{5}{2}^-$		
79	2867.5	9157.1	2.0	$\frac{1}{2}^+, \frac{3}{2}^+, \frac{5}{2}^-$		
80	2869.0	9158.6	6.7	$\frac{1}{2}^+, \frac{3}{2}^+, \frac{5}{2}^-$		9160 \pm 4
81	2875.3	9164.8	0.4	$\frac{1}{2}^+, \frac{3}{2}^+, \frac{5}{2}^-$		9165 ^{g)}
82	2896.9	9185.7	0.9	$\frac{1}{2}^+, \frac{3}{2}^+, \frac{5}{2}^-$		
83	2901.6	9190.3	0.9	$\frac{1}{2}^+, \frac{3}{2}^+, \frac{5}{2}^-$		9194 \pm 4
84	2907.1	9195.6	4.0	$\frac{1}{2}^+, \frac{3}{2}^+, \frac{5}{2}^-$		

REF. E.G. Kopanets, A.A. Koval, V. Ya. Kostin, L.P. Korda, P.M. Tutakin
S.P. Tsytko
Izv. Akad. Nauk SSSR 41, 1688 (1977)
Bull. Acad. Sci. 41, 128 (1977)

ELEM. SYM.	A	Z
Cl	35	17
REF. NO.		
77 Ko 8		egf

METHOD					REF. NO.		
					77 Ko 8		egf
REACTION	RESULT	EXCITATION ENERGY	SOURCE		DETECTOR		ANGLE
			TYPE	RANGE	TYPE	RANGE	
P,G	NOX	7	D	1	SCD-D		DST

Measurements of the angular distributions of γ -rays have been performed for the resonances at $E_p = 1019, 1267, 1285, 1340, 1354$, and 1376 keV. The most probable values of the spins of the resonance states were obtained: $I = 3/2$ ($E_p = 1019, 1267$ keV), $5/2$ ($1340, 1376$ keV). The values of the mixing coefficients for the multipolarities of the γ -transitions have been determined.

4 STATES,
7.6-7.7 MEV

Results of Analysis of the Distribution of γ -Rays Emitted in the $^{35}\text{S}(\text{p},\gamma)^{36}\text{Cl}$ Reaction

E_{γ} keV	E_{exp} keV	E_{down} keV	$I_{\gamma}^{n_{down}}$	$a_1 \pm \Delta a_1$	$a_2 \pm \Delta a_2$	I_{res}	$\delta \pm \Delta \delta$
1019	7358	1219	$1/2^+$	-0.25 ± 0.11	0.31 ± 0.11	$1/2$	-0.05 ± 0.03 or 2.5 ± 0.3
		1763	$3/2^+$	-0.20 ± 0.24	0.92 ± 0.25	$1/2$	-0.01 ± 0.10 or > 2.5
		0	$3/2^+$	-0.56 ± 0.03	-0.05 ± 0.02	$1/2$	1.8 ± 0.5
1267	7598	1763	$3/2^+$	0.30 ± 0.09	-0.17 ± 0.09	$1/2$	0.19 ± 2.2
		2894	$3/2^+$	0.33 ± 0.01	-0.05 ± 0.01	$1/2$	-5.3 ± 0.9 or 0.01 ± 0.05
		3003	$3/2^+$	0.42 ± 0.03	-0.10 ± 0.03	$1/2$	0.85 ± 0.42
		3163	$1/2^-$	0.19 ± 0.02	0.08 ± 0.02	$1/2$	-0.25 ± 0.15
1285	7618	0	$1/2^+$	-0.57 ± 0.03	0.27 ± 0.03	$1/2$	2.2 ± 0.3
		1763	$3/2^+$	-0.11 ± 0.03	-0.06 ± 0.03	$1/2$	0.48 ± 0.11
		1763	$3/2^+$	-0.40 ± 0.09	0.07 ± 0.08	$1/2$	0.86 ± 0.14
1340	7669	2648	$1/2^-$	0.33 ± 0.08	-0.12 ± 0.08	$1/2$	0.28 ± 2.2
		3003	$3/2^+$	0.52 ± 0.01	-0.18 ± 0.01	$1/2$	-1.4 ± 0.5
		0	$3/2^+$	0.18 ± 0.11	-0.04 ± 0.11	$1/2$	< -3.5
		3003	$3/2^+$	-0.16 ± 0.12	0.08 ± 0.13	$1/2$	-0.26 ± 0.11
1354	7683	4173		0.01 ± 0.14	0.23 ± 0.16	-	0.01 ± 0.07
		0	$1/2^+$	-0.63 ± 0.04	0.15 ± 0.03	$1/2$	0.48 ± 0.32
		2648	$1/2^-$	-0.18 ± 0.17	0.41 ± 0.18	$1/2$	-
1376	7704	5651	$(3/2)^+$	0.14 ± 0.15	-0.39 ± 0.17	$1/2$	0.1 ± 0.1
							-1.01 ± 0.10 or > 13 < -2 or > 13

REF. A.A. Koval, E.G. Kopanets, V.Ya. Kostin, L.P. Korda, P.M. Tutakin,
S.P. Tsytko
Izv. Akad. Nauk SSSR 41, 1658 (1977)
Bull. Acad. Sci. 41, 104 (1977)

ELEM. SYM.	A	Z
Cl	35	17
REF. NO.		
77 Ko 10		hg

METHOD			SOURCE		DETECTOR		ANGLE
REACTION	RESULT	EXCITATION ENERGY	TYPE	RANGE	TYPE	RANGE	
P,G	NOX	7	D	1	SCD-D		DST
		(7.546)		(1.214)			

LEV 7.546 J-PI B(ML)

The angular distributions of γ -rays from the reaction involving the radiation capture of protons by ^{35}S nuclei are measured at four resonance energies $E_p = 1055, 1183, 1214, \text{ and } 1416 \text{ keV}$.

Table 1

E_p , keV	E_{γ} , keV	Transition	I_{res}	I_f^*	Z^{min}
1055	7392	Res. - 3.00 {	$1/2$	$1/2^+$	50.90
		$1/2$	$1/2^-$	0.32	
		Res. - 3.16 {	$1/2$	$1/2^-$	11.88
		$1/2$	$1/2^-$	0.77	
1183	7517	Res. - 1.76 {	$1/2$	$1/2^+$	61.90
		$1/2$	$1/2^-$	8.15	
		Res. - 3.16 {	$1/2$	$1/2^-$	2.78
		$1/2$	$1/2^-$	0.30	
1214	7546	Res. - 0 {	$1/2$	$1/2^+$	52.20
		$1/2$	$1/2^-$	12.22	
		Res. - 3.00 {	$1/2$	$1/2^+$	11.90
		$1/2$	$1/2^-$	3.69	
1416	7743	Res. - 3.16 {	$1/2$	$1/2^-$	14.80
		$1/2$	$1/2^-$	9.70	
		Res. - 2.65 {	$1/2$	$1/2^+$	4.45
		$1/2$	$1/2^-$	1.71	
		Res. - 3.16 {	$1/2$	$1/2^-$	168.00
		$1/2$	$1/2^-$	37.80	
		Res. - 3.04 {	$1/2$	$1/2^+$	5.71
		$1/2$	$1/2^-$	0.34	

Table 2

E_{le} , keV	Transition	I_1^*	I_f^*	$\delta \pm \Delta \delta$	$ 3f(\sigma_L) ^2$, Weissk. units			
					M1	M2	E1	E2
7392	Res. - 3.00 {	$1/2^+(-)$	$1/2^+$	0.011 ± 0.013	-	-	$9 \cdot 10^{-4}$	-
	Res. - 3.16 {	$1/2^+(-)$	$1/2^-$	0.280 ± 0.250	0.014	-	-	0.230
7517	Res. - 1.76 {	$1/2^+(-)$	$1/2^+$	0.008 ± 0.022	-	0.050	$3.14 \cdot 10^{-4}$	-
	Res. - 3.16 {	$1/2^+(-)$	$1/2^-$	0.101 ± 0.200	0.010	-	-	-
7546	Res. - 0 {	$1/2^-$	$1/2^+$	0.102 ± 0.200	-	1.400	-	-
	Res. - 3.00 {	$1/2^-$	$1/2^+$	0.055 ± 0.043	-	-	$7 \cdot 10^{-4}$	-
	Res. - 3.16 {	$1/2^-$	$1/2^-$	0.081 ± 0.100	1.400	-	-	-
7743	Res. - 2.65 {	$1/2^+(-)$	$1/2^+$	0.103 ± 0.000	-	-	$7 \cdot 10^{-4}$	-
	Res. - 3.16 {	$1/2^+(-)$	$1/2^-$	0.183 ± 0.081	0.014	-	-	0.081
	Res. - 3.94 {	$1/2^+(-)$	$1/2^+$	-0.163 ± 0.170	-	-	$5 \cdot 10^{-4}$	-

ELEM. SYM.	A	Z
CL	35	17
METHOD		REF. NO.
		78 Di 10
		hg

REACTION	RESULT	EXCITATION ENERGY	SOURCE		DETECTOR		ANGLE
			TYPE	RANGE	TYPE	RANGE	
G,C11	ABY	31(31.25)-999	C	300-999	ACT-I		4PI

Abstract—Mean cross sections for the photoproduction of ^7Be and ^{11}C from ^{19}F , ^{27}Al , ^{28}Si and ^{32}S targets, ^7Be from ^{10}B , and ^{11}C from ^{14}N and ^{16}O targets have been measured using bremsstrahlung beams in the energy range 0.3–1.0 GeV. The results have been compared with previous measurements and an excellent agreement has been found. In most cases, the values obtained turned out to be much larger than those expected from a simple spallation mechanism. A fragmentation and/or a fission-like process has been suggested in explaining the mechanism of such reactions.

999=1 GEV

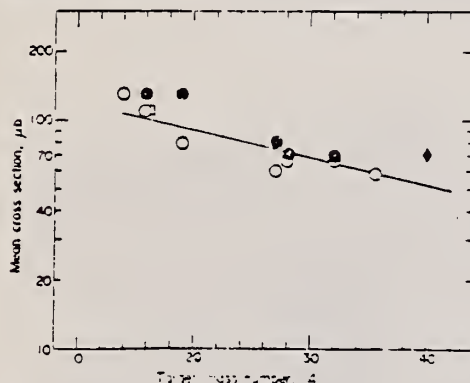


Fig. 1. Mean cross sections per photon, σ_p , of ^{11}C photoproduction vs the target mass number A . Experimental data are taken from: \bullet , Ref. [9]; \square , Ref. [13]; \blacklozenge , Ref. [2]; \circ , present work. The straight line is a least squares fit of the experimental points.

Table 3. Comparison between experimentally determined and calculated cross sections of ^7Be and ^{11}C photoproduction and indication of the dominant reaction channels

Target Nucleus	Product Nucleus	Nominal Nucleon Loss, n	$\Delta A/A_t$ ($\times 10^3$)	$\sigma_{\text{exp}}^{(*)}$ (μb)	$\sigma_{\text{CMO}}^{(**)}$ (μb)	$\sigma_{\text{exp}}/\sigma_{\text{CMO}}$	Apparent Threshold (E_{th}) (MeV)	Possible Mechanism of Production
$^{10,11}\text{B}$	^7Be	(3)	(30), 16	67	28	2	≤ 50	Spallation
^{12}C	^7Be	5	42	110	20	5	≤ 50	Spallation
^{14}N	^7Be	7	50	108	12	9	≤ 50	Fission Spallation
^{14}N	^{11}C	3	21	130	60	2	≤ 50	Spallation
^{16}O	^7Be	9	56	107	8	13	$50 < E_{\text{th}} < 200$	Fission Fragmentation
^{16}O	^{11}C	5	31	117	33	3	≤ 50	Spallation
^{19}F	^7Be	12	63	106	5	21	$50 < E_{\text{th}} < 200$	Fission Fragmentation
^{19}F	^{11}C	8	42	105	16	7	$50 < E_{\text{th}} < 200$	Fission Fragmentation Spallation
^{27}Al	^7Be	20	74	142	2	71	> 200	Fragmentation
^{27}Al	^{11}C	16	59	70	5	14	$50 < E_{\text{th}} < 200$	Fission Fragmentation
^{28}Si	^7Be	21	75	56	2	28	> 200	Fragmentation
^{28}Si	^{11}C	17	61	68	4	17	$50 < E_{\text{th}} < 200$	Fission Fragmentation
^{32}S	^7Be	25	78	114	2	57	≈ 250	Fragmentation
^{32}S	^{11}C	21	66	68	3	23	$50 < E_{\text{th}} < 200$	Fission Fragmentation
$^{35,37}\text{Cl}$	^{11}C	24, (26)	67, (70)	59	3	20	$50 < E_{\text{th}} < 200$	Fission Fragmentation
^{40}Ca	^7Be	33	83	70	1	70	> 200	Fragmentation
^{40}Ca	^{11}C	29	73	70	2	35	> 200	Fragmentation

(*) Mean values of the different measurements (see Figs. 1 and 2).

(**) Calculated values according to Ref. [5].

Table 1. Cross sections per equivalent quantum of ^{11}C photoproduction

E_0 (GeV)	^{14}N	^{16}O	^{19}F	^{27}Al	^{28}Si	^{32}S	$^{35,37}\text{Cl}$
0.30	520:30	200:20	110:20	28:10	35:10	45:10	30:10
0.32	520:30	210:20	120:20	30:10	42:10	50:10	30:10
0.35	530:30	230:20	125:20	38:10	45:10	60:10	40:10
0.40	530:30	230:20	130:20	42:10	52:10	65:10	50:10
0.48	550:30	255:20	150:20	60:10	70:10	80:10	60:10
0.55	570:30	260:20	160:20	60:10	78:10	85:10	60:10
0.65	600:30	290:20	180:20	70:10	85:10	98:10	75:10
0.75	620:30	300:20	180:20	79:10	95:10	110:10	85:10
0.90	650:30	320:20	190:20	90:10	110:10	120:10	95:10
1.00	680:30	330:20	210:20	100:10	115:10	125:10	100:10

REACTION	RESULT	EXCITATION ENERGY	SOURCE		DETECTOR		ANGLE
			TYPE	RANGE	TYPE	RANGE	
G,G	LFT	8	D	8	NAI-D		82
		(8.21)		(8.21)			

Data is a combination for the doublet at proton energy of 1.89 MeV (1891, 1993 KeV)

RESONANCE ABSORPTION

Abstract: Parameters of selected levels in ^{35}Cl have been determined by means of several techniques, including proton elastic scattering studies, angular distribution measurements, calibration of the excitation energies by a cascade crossover method and resonance absorption experiments. For the $E_p = 1375, 1683$ and 2791 keV resonances we found $J^\pi = \frac{1}{2}^+$, while the assignments for the $E_p = 1354, 1893, 1974$ and 2541 keV resonances were $\frac{1}{2}^-$, $\frac{1}{2}^+$, $\frac{1}{2}^-$ and $\frac{3}{2}^+$, respectively. The parity of the $E_p = 1891$ keV resonance is positive, a $J = \frac{1}{2}$ assignment is tentatively made for this level. Values for the proton width were determined. The excitation energies of these resonances and also of 18 bound levels were measured with sub-keV precision. The absolute resonance strength in the $E_p = 1891$ keV resonance has been determined to be 4.1 ± 0.5 eV, in agreement with recent thick-target γ -ray yield measurements.

E

NUCLEAR REACTIONS $^{34}\text{S}(p, \gamma)$, (p, p) , $E = 1.4\text{--}2.8$ MeV; measured $\sigma(E, E_p, \theta)$. ^{35}Cl deduced levels J, π, Γ , levels, resonance strength. Enriched targets.

TABLE 3

Characteristic data of the resonance absorption experiments with the $E_p = 1.89$ MeV resonance in $^{34}\text{S}(p, \gamma)^{35}\text{Cl}$ and a CCl_4 absorber

Quantity	Long absorber case	Short absorber case
$n (\times 10^{23} \text{ cm}^{-2})$	4.57	2.20
$\lambda^2 (\times 10^{-23} \text{ cm}^2)$	22.82	22.82
A_γ (eV)	19.6 ± 2.8	9.3 ± 1.5
W_γ (keV)	0.29 ± 0.04	0.27 ± 0.05
$n\sigma_0$	0.41 ± 0.06	0.20 ± 0.03
$S = (2J_\gamma + 1) \frac{\Gamma_p \Gamma_\gamma}{\Gamma} \text{ (eV)}$	4.3 ± 0.7	4.0 ± 0.7
χ^2/df	0.97	0.40

Rows 3 to 7 contain the results of separate gauss fits to the data (W_γ is the FWHM of the gaussian instrumental function).

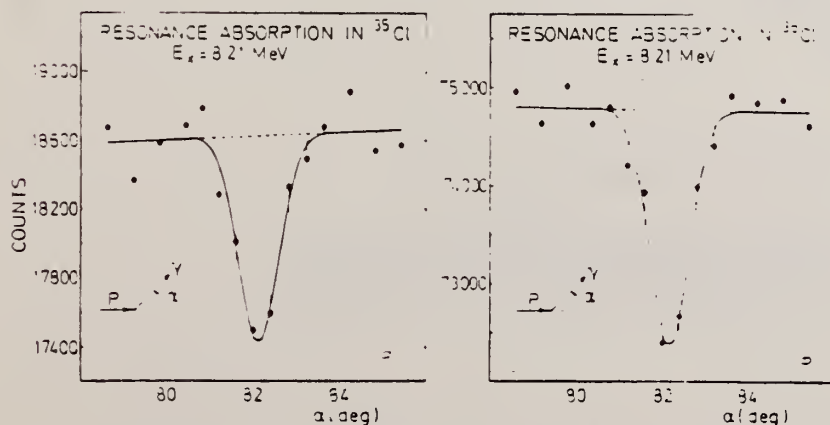


Fig. 13. Transmission intensity as function of angle α , with (a) the long absorber assembly and (b) the short absorber. The solid line represents the best fit to the data with a gaussian instrumental function.

(OVER)

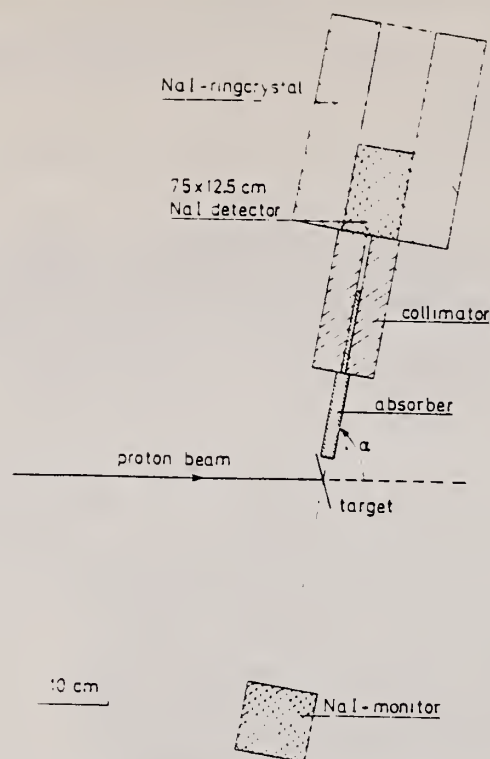


Fig. 11. Projection on the reaction plane of the experimental set-up used for the resonance absorption experiments. In the vertical plane the collimator has a wider opening in order to increase the counting rate.

176

W. Biesiot et al. ^{35}Cl

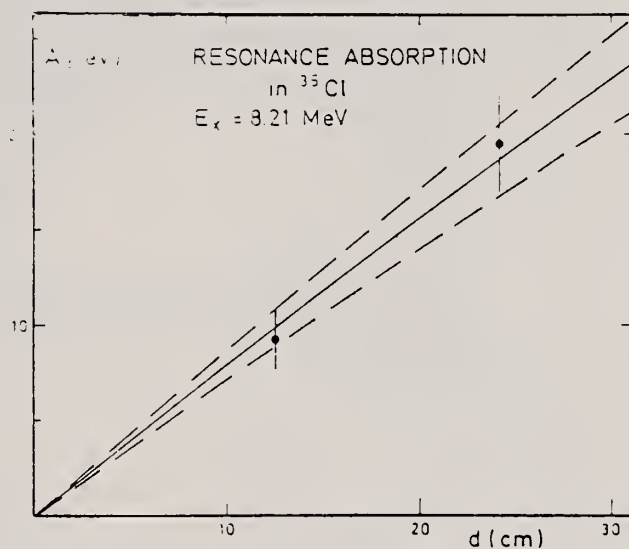


Fig. 14. The absorption integral A_1 as a function of absorber length d . The data points represent values obtained from separate fits to the data. The solid line gives the relation between A_1 and d resulting from a simultaneous fit to the data (see text). The dotted lines indicate the associated standard deviation. The solid lines show little curvature because of the small values of $\mu\sigma_n$ corresponding to the absorber lengths used.

CL
A=36

CL
A=36

CL
A=36

METHOD reactor; inverse; NaI

REF. NO.

59 Se 1

NVB

REACTION	RESULT	EXCITATION ENERGY	SOURCE		DETECTOR		ANGLE
			TYPE	RANGE	TYPE	RANGE	
N,G	SPC	9 (8.55 MeV)	C	0	NAI-D		90

G-WIDTH

Radiation width:

$$\Gamma_{\gamma} = 0.009 \text{ eV}$$

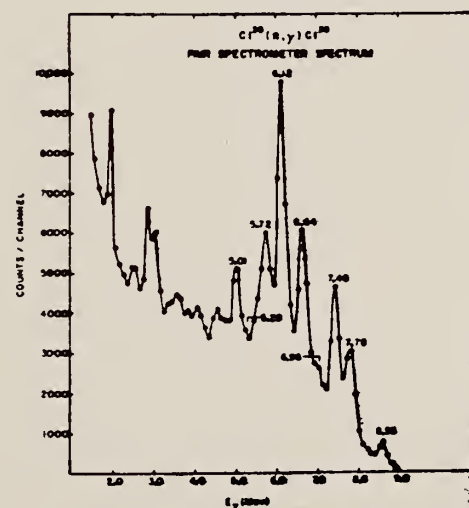


FIG. 1. Three-crystal pair spectrometer spectrum of gamma rays following thermal neutron capture in C^{13} . The energy scale is that of reference 2.

² Groshev, Adyasevich, and Demidov, *Proceedings of the International Conference on the Peaceful Uses of Atomic Energy*, 1955 (United Nations, New York, 1956).

REF. I. Bergqvist, J. A. Biggerstaff, J. H. Gibbons, W. M. Good
Phys. Rev. 158, 1049 (1967)

ELEM. SYM.	A	Z
Cl	36	17
REF. NO.		egf
67 Be 7		

METHOD			SOURCE		DETECTOR		ANGLE
REACTION	RESULT	EXCITATION ENERGY	TYPE	RANGE	TYPE	RANGE	
N,G	LFT	8-9	D	0-1	NAI-D	0-7	90

SOURCE 25,50 KEV

TABLE X. Gamma rays from $^{36}\text{Cl}(n,\gamma)^{36}\text{Cl}$; $E_n \approx 25$ keV.

E_γ (MeV)	I_γ relative to $C \rightarrow 0$	Assignment	J_f^*
8.60	1.0	$C \rightarrow 0$	2^+
7.78	1.2	$C \rightarrow 0.79$	$(0, 2)^+$
7.44	0.6	$C \rightarrow 1.16$	2^+
7.00	0.2	$C \rightarrow 1.60$	2^+
6.65	0.8	$C \rightarrow 1.95, 1.96$	$(1^+, 2^-)$
6.2	0.3	$C \rightarrow 2.5$ (3 levels)	
5.9	0.4	$C \rightarrow 2.68$	
5.6	0.5		
5.0	0.5		
4.6	~ 0.2		
4.1	~ 0.3		
3.6	~ 0.4		
2.9	~ 0.4		
2.6	~ 0.2		
1.94	~ 0.5	$1.95, 1.96 \rightarrow 0$	$[(1^+, 2^-) \rightarrow 2^+]$

* Unresolved structure.

TABLE XI. Gamma rays from $^{36}\text{Cl}(n,\gamma)^{36}\text{Cl}$; $E_n \approx 50$ keV.

E_γ (MeV)	I_γ relative to $C \rightarrow 0$	Assignment	J_f^*
8.60	1.0	$C \rightarrow 0$	2^+
7.78	6.1	$C \rightarrow 0.79$	$(0, 2)^+$
7.44	1.4	$C \rightarrow 1.16$	2^+
7.00	2.0	$C \rightarrow 1.60$	2^+
6.65	2.3	$C \rightarrow 1.95, 1.96$	$(1^+, 2^-)$
[6.4]		$[C \rightarrow 1, 2]^*$	
6.2	4.5	$C \rightarrow 2.5$ (3 levels)	
[5.7]		$[C \rightarrow 3]^*$	
[5.1]		$[C \rightarrow 4, 5]^*$	
[4.5]		$[C \rightarrow 6, 7]^*$	
4.1			
3.6			
3.4		$(\text{Na}^{35}(n,\gamma)?)$	
2.9			
2.7			
1.94	6.7	$1.95, 1.96 \rightarrow 0$	$(1^+, 2^-) \rightarrow 2^+$
1.58	3.3		$2^+ \rightarrow 2^+$

* Transitions due to $^{35}\text{Na}(n,\gamma)$, $E_{n\gamma} = 54$ keV.
* Unresolved structure.

CL
A=37

CL
A=37

CL
A=37

METHOD					REF. NO.	
Betatron; neutron threshold; ion chamber					60 Ge 3	NVB
REACTION	RESULT	EXCITATION ENERGY	SOURCE		DETECTOR	
			TYPE	RANGE	TYPE	RANGE
G,N	NØX	THR	C THR		BF3-I	4 PI

THRESHOLD

TABLE I. Summary and comparison of neutron separation energies inferred from present threshold measurements with values predicted from mass data and reaction energies. All energies are expressed in the center-of-mass system in Mev.

Reaction	No. runs	Present results	Other results	Method	Reference
$\text{Cl}^{37}(\gamma, n)\text{Cl}^{36}$	1	10.307 ± 0.037	10.322 ± 0.023 10.316 ± 0.004	LSA mass data	h g

g C. F. Giese and J. L. Benson, Phys. Rev. 110, 712 (1958).
 h P. M. Endt et al., Phys. Rev. 109, 1002 (1957).

Elem. Sym.	A	Z
Cl	37	17
Ref. No.		JHH
62 B 6		

Method 4 MeV electron Van de Graaff; brems.; nuclear resonance scattering, ring scatterer; NaI

Reaction	E or ΔE	E_0	Γ	$\int \sigma dE$	$J\pi$	Notes
$Cl^{37}(\gamma, \gamma)$	Brems. 0 - 4					

TABLE 3
Mean lifetimes of excited states deduced from the resonance scattering of bremsstrahlung

Nucleus	%	Energy (MeV)	Spin	Γ	Γ/Γ_0	$\tau \times 10^{12} \pm 50\%$ sec.
Cl^{35}	100	1.05	$1^+ \rightarrow 1^-$	0.13	(1)	0.34e
Na^{24}	100	1.00	$1^+ \rightarrow 0^+$	0.1	0.79	> 0.06
		1.30	$1^+ \rightarrow 0^+$	0.63	(1)	> 1.5e
		2.64	$1^+ \rightarrow 0^+$	0.8	(1)	> 0.3e
		2.70	$1^+ \rightarrow 0^+$	0.11	(1)	> 0.008e
		2.80	$1^+ \rightarrow 0^+$	0.44	(1)	0.10e
Al^{27}	100	2.73	$1^+ \rightarrow 0^+$	0.8	0.91	> 0.22
		3.06	$1^+ \rightarrow 0^+$	0.316	(1)	1.2 - 1e-1
Si^{28}	4.71	1.79	$1^+ \rightarrow 0^+$	0	0.48	1.5
		2.43	$1^+ \rightarrow 0^+$	0	0.48	0.9
P^{31}	100	1.96	$1^+ \rightarrow 0^+$	0	0.48	2.3
		2.23	$1^+ \rightarrow 0^+$	0	0.79	4.5
		3.13	$1^+ \rightarrow 0^+$	0	0.48	0.9
		3.29	$1^+ \rightarrow 0^+$	0	0.79	> 1.4e (f _{av}) ^{1/2}
		3.41	$1^+ \rightarrow 0^+$	0	0.88	> 1.3e (f _{av}) ^{1/2}
		3.51	$1^+ \rightarrow 0^+$	0	0.88	> 0.8e (f _{av}) ^{1/2}
Si^{29}	56	3.79	$0^+ \rightarrow 0^+$	0	(1)	> 0.4e (f _{av}) ^{1/2}
Si^{30}	4.3	1.197	$0^+ \rightarrow 0^+$	0	0.63	> 1.0
Cl^{37}	79.2	1.35	$1^+ \rightarrow 1^-$	0	(1)	4e
		1.79	$1^+ \rightarrow 1^-$	0	(1)	4e
		2.71 (0.68)	$1^+ \rightarrow 1^-$	0	(1)	0.31e (f _{av}) ^{1/2}
Cl^{35}	79.5	3.01	$1^+ \rightarrow 1^-$	0	(1)	> 0.25e (f _{av}) ^{1/2}
Cl^{37}	24.6	0.630	$1^+ \rightarrow 1^-$	0	(1)	> 10e
		1.73	$1^+ \rightarrow 1^-$	0	(1)	> 0.4e (f _{av}) ^{1/2}
K^{39}	99	1.63	$1^+ \rightarrow 1^-$	0	(1)	> 1.5e
		1.63	$1^+ \rightarrow 1^-$	0	(1)	> 1.5e
		3.05	$1^+ \rightarrow 1^-$	0	(1)	> 0.7e
		3.06	$1^+ \rightarrow 1^-$	0	(1)	> 0.7e
		3.66 (2.84)	$1^+ \rightarrow 1^-$	0	(1)	> 0.1e (f _{av}) ^{1/2}
Ca^{40}	99	4.05-4.12	$1^+ \rightarrow 1^-$	0	(1)	> 0.3e (f _{av}) ^{1/2}
Ca^{42}	99	2.90	$0^+ \rightarrow 0^+$	0	0.63	> 0.4e
Ca^{44}	99	1.33	$1^+ \rightarrow 1^-$	0	(1)	4e > 1.1

The factor γ equals $(M + 1)/M_0 + 1$

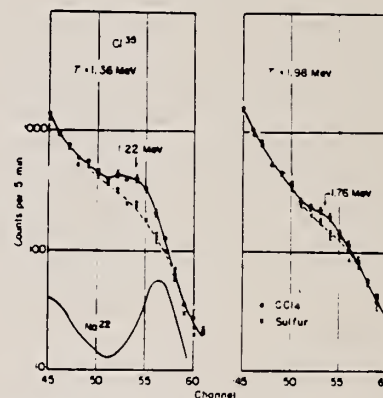


Fig. 4. Resonance fluorescence from the 1.22 MeV and 1.78 MeV states of Cl^{35} . The Na^{24} peak is at 1.28 MeV.

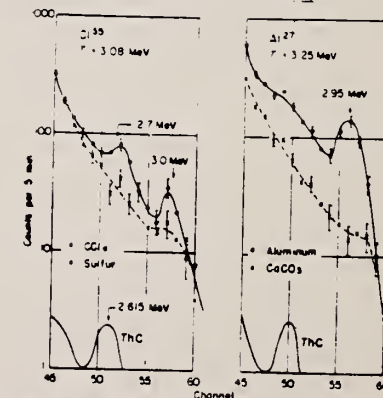


Fig. 5. Resonance fluorescence from the 2.7 MeV and 3.01 MeV states of Cl^{37} and from the 3.01 MeV state of Al^{27} .

REF. Yu. P. Ievlev, A. A. Koval, E. G. Kopanets, Yu. S. Korda,
L. N. Sukhotin, and S. P. Tsytko
Uk. Fiz. Zhur. 12, 743 (1967)

ELEM. SYM.	A	Z
Cl	37	17
REF. NO.		egf
67 Ie 1		

REACTION	RESULT	EXCITATION ENERGY	SOURCE		DETECTOR		ANGLE
			TYPE	RANGE	TYPE	RANGE	
P, G	LFT	9-10	D	1-2	NAI-D	9-10	55
		(9.78-9.988)		(1.42-1.63)			

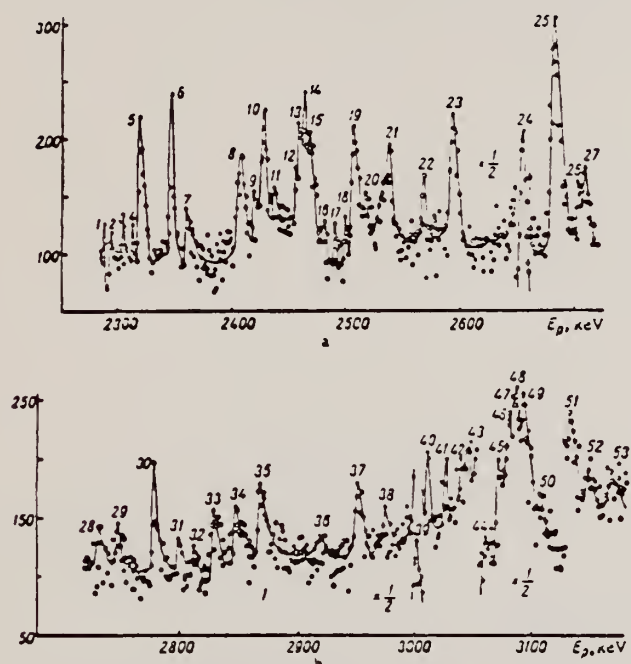


FIGURE 1. Excitation function of the reaction $S^{35}(p, \gamma)Cl^{36}$. The monitor was set at 55° to the proton beam for recording the γ quanta emitted in the transition to the ground state:
(a) $E_p = 2300-2700$ keV; (b) $E_p = 2700-3200$ keV.

TABLE 2. Matrix elements of the radiative transitions of Cl^{37} into the ground state in Weisskopf units

E_p keV	E_{γ} MeV	E_{γ} MeV	$2\pi\omega_{\gamma} = (2\pi)^{-1} \hbar^{-1} E_{\gamma}^2 T_{\gamma}^2$ eV	J_i	T_{γ} eV	Transition	Radiative width, eV	W_{γ}
1421	9.781	9.8	1.66	$7/2^+$	0.21	E2	0.21	0.35
1468	9.827	9.8	1.18	$3/2^+$	0.30	E2	0.01	0.017
						M1	0.29	0.015
1864	10.195	10.2	1.86	$7/2^+$	0.23	E2	0.23	0.38
						E2	0.25	0.42
1921	10.268	10.3	1.08	$3/2^+$	0.27	M1	0.02	0.001
1979	10.324	10.3	1.22	$5/2^+$	0.20	E2	0.20	0.33
						E2	0.01	0.017
2014	10.358	10.4	1.08	$5/2^+$	0.18	M1	0.17	0.008
2083	10.426	10.4	1.88	$3/2^+$	0.47	E2	0.001	0.002
						M1	0.469	0.008

REF.

A. Veyssiere, H. Beil, R. Bergere, P. Carlos, A. Lepretre, and
A. De Miniac
Nucl. Phys. **A227**, 513 (1974)

Cl

37

17

METHOD

REF. NO.

74 Ve 1

egf

REACTION	RESULT	EXCITATION ENERGY	SOURCE		DETECTOR		ANGLE
			TYPE	RANGE	TYPE	RANGE	
* G, 2N	ABX	18- 24	D	18- 24	BF3-I		4PI

898*

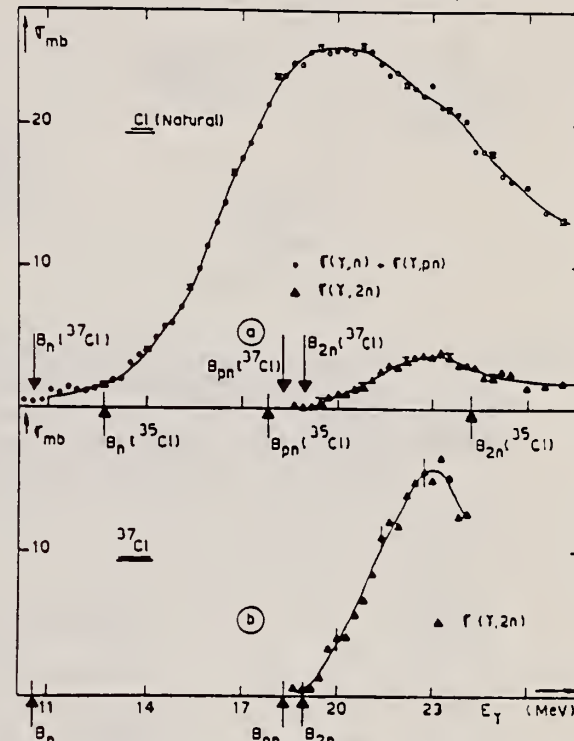


Fig. 9. (a) Photonuclear cross sections $[\sigma(\gamma, n) + \sigma(\gamma, pn)]$ and $\sigma(\gamma, 2n)$ for natural Cl. (b) Partial photoneutron cross sections $\sigma(\gamma, 2n)$ of ^{37}Cl .

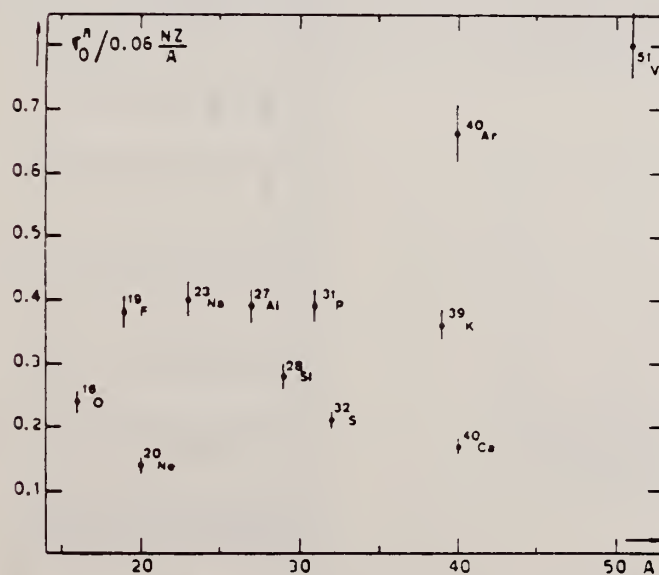


Fig. 22. Ratio of experimental integrated photoneutron cross section σ_0^* over the Thomas, Reiche and Kuhn sum rule $[0.06 NZ/A]$. Numerical values and upper integration limits E_M are taken from table 3. Also $\Delta\sigma_0^* = \pm 7\%$ for all nuclei.

(over)

U.S. DEPARTMENT OF COMMERCE
NATIONAL BUREAU OF STANDARDS

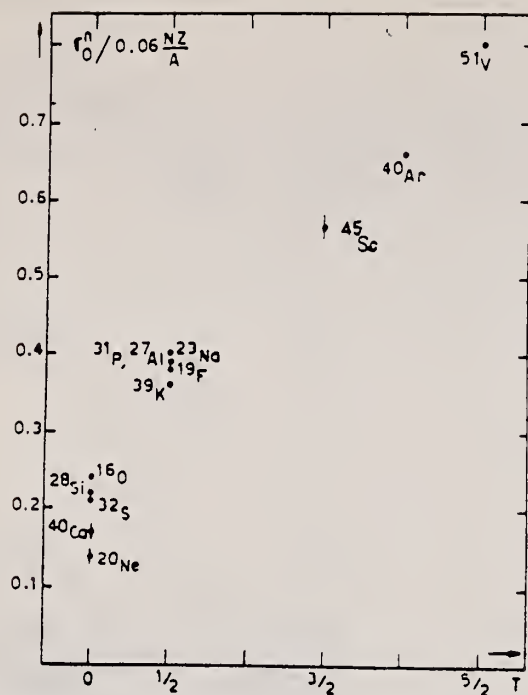


Fig. 24. The $[\sigma_0^n / (0.06 NZ/A)]$ ratio as a function of isospin T . Possible overall errors of $\pm 7\%$ are to be applied to all nuclei shown.

TABLE 3
Experimental integrated photoneutron cross sections $\sigma_0^n = \int_0^{E_M} \sigma_{Tn}(E) dE$ compared with the classical sum rule $[0.06 NZ/A]$ of Thomas, Reich and Kuhn

	$T = 0$					$T = \frac{1}{2}$					$T = \frac{3}{2}$	$T = 2$	$T = \frac{5}{2}$
Nucleus	^{16}O	^{20}Ne	^{28}Si	^{32}S	^{40}Ca	^{19}F	^{23}Na	^{27}Al	^{31}P	^{39}K	^{45}Sc	^{40}Ar	^{51}V
σ_0^a (MeV · mb)	58 ± 4	42 ± 3	94 ± 7	98 ± 7	100 ± 7	108 ± 7	137 ± 9	158 ± 10	182 ± 12	210 ± 14	383 ± 25	393 ± 28	602 ± 42
$\sigma_0^a/(0.06NZ/A)$	0.24	0.14	0.22	0.21	0.17	0.38	0.40	0.39	0.39	0.36	0.57	0.66	0.8
E_M (MeV)	30	26.7	30	30	29.5	29	30	30	29	30	28.1	26.7	28

ELEM. SYM.	A	Z
Cl	37	17
REF. NO.		hg
78 Di 10		

METHOD					REF. NO.		hg
					78 Di 10		
REACTION	RESULT	EXCITATION ENERGY	SOURCE		DETECTOR		ANGLE
			TYPE	RANGE	TYPE	RANGE	
G,C11	ABY	34(34.90)-999	C	300-999	ACT-I		4PI

Abstract—Mean cross sections for the photoproduction of ^7Be and ^{11}C from ^{19}F , ^{27}Al , ^{28}Si and ^{35}S targets, ^7Be from ^{10}B and ^{12}C from ^{14}N and ^{16}O targets have been measured using bremsstrahlung beams in the energy range 0.3–1.0 GeV. The results have been compared with previous measurements and an excellent agreement has been found. In most cases, the values obtained turned out to be much larger than those expected from a simple spallation mechanism. A fragmentation and/or a fission-like process has been suggested in explaining the mechanism of such reactions.

999=1 GEV

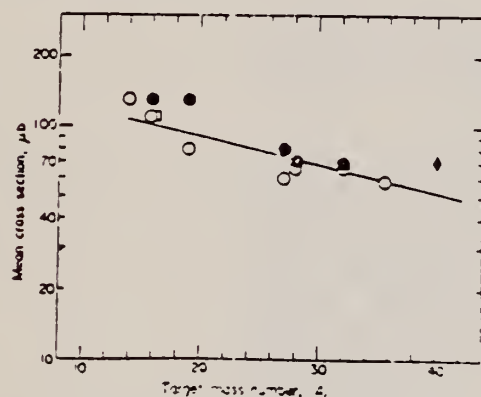


Fig. 1. Mean cross sections per photon, σ_p , of ^{11}C photoproduction vs the target mass number A . Experimental data are taken from: ● Ref. [9]; □ Ref. [13]; ♦ Ref. [2]; ○ present work. The straight line is a least squares fit of the experimental points.

Table 3. Comparison between experimentally determined and calculated cross sections of ^7Be and ^{11}C photoproduction and indication of the dominant reaction channels

Target Nucleus	Product Nucleus	Nominal Nuclear Loss, λ	$\Delta A/A$ ($\times 10^3$)	$\bar{\sigma}_{exp}$ (°) (μb)	$\bar{\sigma}_{CMO}$ (°°) (μb)	$\bar{\sigma}_{exp}/\bar{\sigma}_{CMO}$	Apparent Threshold (Exp.) E_{th} (MeV)	Possible Mechanism of Production
^{10}B	^7Be	(3)	(30), 36	67	28	2	≤ 50	Spallation
^{12}C	^7Be	5	42	110	20	5	≤ 50	Spallation
^{14}N	^7Be	7	50	108	12	9	≤ 50	Fission Spallation
^{16}O	^{11}C	3	21	130	60	2	≤ 50	Spallation
^{16}O	^7Be	9	56	107	8	13	$50 < E_{th} < 200$	Fission Fragmentation
^{16}O	^{11}C	5	31	117	33	3	≤ 50	Spallation
^{19}F	^7Be	12	63	106	5	21	$50 < E_{th} < 200$	Fission Fragmentation
^{19}F	^{11}C	8	42	105	16	7	$50 < E_{th} < 200$	Fission Fragmentation Spallation
^{27}Al	^7Be	20	74	142	2	71	> 200	Fragmentation
^{27}Al	^{11}C	16	59	70	5	14	$50 < E_{th} < 200$	Fission Fragmentation
^{28}Si	^7Be	21	75	56	2	28	> 200	Fragmentation
^{28}Si	^{11}C	17	61	68	4	17	$50 < E_{th} < 200$	Fission Fragmentation
^{32}S	^7Be	25	78	114	2	57	> 200	Fragmentation
^{32}S	^{11}C	21	66	68	3	23	$50 < E_{th} < 200$	Fission Fragmentation
$^{35,37}\text{Cl}$	^{11}C	24, (26)	69, (70)	59	3	20	$50 < E_{th} < 200$	Fission Fragmentation
^{40}Ca	^7Be	33	83	70	1	70	> 200	Fragmentation
^{40}Ca	^{11}C	29	73	70	2	35	> 200	Fragmentation

(°) Mean values of the different measurements (see Figs. 1 and 2).

(°°) Calculated values according to Ref. [10].

Table 1. Cross sections per equivalent quantum of ^{11}C photoproduction

E_0 (GeV)	^{14}N	^{16}O	^{19}F	^{27}Al	^{28}Si	^{32}S	$^{35,37}\text{Cl}$
0.30	520:30	200:20	110:20	28:10	35:10	45:10	30:10
0.32	520:30	210:20	120:20	30:10	42:10	50:10	30:10
0.35	530:30	230:20	125:20	38:10	45:10	60:10	40:10
0.40	530:30	230:20	130:20	42:10	52:10	65:10	50:10
0.48	550:30	255:20	150:20	60:10	70:10	80:10	60:10
0.55	570:30	260:20	160:20	70:10	78:10	85:10	60:10
0.65	600:30	290:20	180:20	70:10	85:10	98:10	75:10
0.75	620:30	300:20	180:20	79:10	95:10	110:10	85:10
0.90	650:30	320:20	190:20	90:10	110:10	120:10	95:10
1.00	680:30	330:20	210:20	100:10	115:10	125:10	100:10

ARGON

Z=18

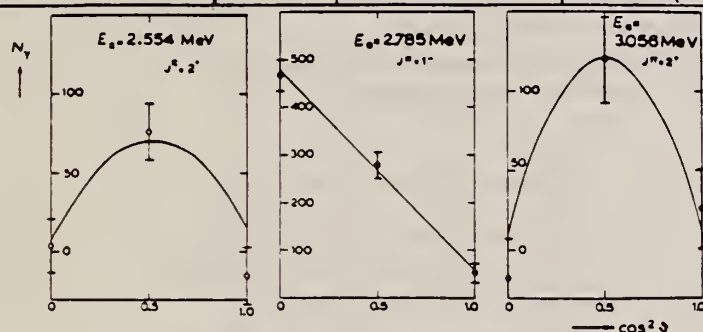
In 1785, Cavendish published a paper describing an experiment in which nitrogen and oxygen were completely removed from the air. He found a residue and estimated the amount to be not more than 1/120 of the total nitrogen. This experiment was forgotten for over a century.

In 1894, Lord Rayleigh was doing an accurate redetermination of the densities of the principal gases; he found the density of atmospheric nitrogen to be always 0.5% greater than that of nitrogen derived from chemical sources. The difference, much larger than the experimental error, could be only attributed to a contaminant in the nitrogen derived from the atmosphere. Sir William Ramsay (1852-1916) and Lord Rayleigh showed that the contaminant was proportional to the volume of air used. They called this new gas argon (from the Greek, *argos*, "inactive") because it is chemically inert. The discovery of argon has been spoken of as the "Triumph of the Fourth Decimal Place".

AR
A=36

The isolation of argon was of profound scientific importance because it formed the starting point for many great developments in chemistry and atomic physics. It lead directly to the discovery of other noble gases and completed, in form at least, the periodic classification of the elements.

METHOD					REF. NO.		
$S^{32}_{(u,\gamma)}Ar^{36}$ $Cl^{35}_{(p,\gamma)}Ar^{36}$					64 Er 1		JOC
Van de Graaff							
REACTION	RESULT	EXCITATION ENERGY	SOURCE		DETECTOR		ANGLE
			TYPE	RANGE	TYPE	RANGE	
A,G	RLY	8 - 10	D	2-3	NAI-D		DST
				(2.2 - 3.2)			
P,G	RLY	8 - 10	D	0-1	NAI-D		
				(0.4 - 1.0)			



J-PI, WIDTHS

Fig. 2. Ground-state angular distributions measured at three $^{32}S(\alpha, \gamma)^{36}Ar$ resonances; distance target-crystal, $D = 10$ cm. The solid curves give the theoretical angular distributions, including solid angle attenuation, for the assigned spins.

TABLE 1

Resonances in the reaction $^{32}S(\alpha, \gamma)^{36}Ar$; energies, spins and parities, strengths, main decay and the corresponding $^{35}Cl(p, \gamma)^{36}Ar$ resonances

E_α (MeV)	$^{36}Ar^*$ (MeV)	J^π	$(2J+1)\Gamma_\alpha\Gamma_\gamma/\Gamma$ (eV)	Main decay	$^{35}Cl(p, \gamma)^{36}Ar$ resonances (E_p in keV)
2.554	8.911	2^+	0.03	γ_0	
2.785	9.117	1^-	0.3	γ_0	
3.056	9.357	2^+	0.05	γ_0	873
3.161	9.451		0.15	γ_1	968
3.182	9.464		0.05	$\gamma_0\gamma_1$	986
all ± 0.005			all $\pm 30\%$		

TABLE 3

Resonances in the reaction $^{35}Cl(p, \gamma)^{36}Ar$; energies, comparison with literature values and strengths

Resonance number	E_p (keV)				$^{36}Ar^*$ (MeV)	$(2J+1)\Gamma_p\Gamma_\gamma/\Gamma$ (eV)
	this work	ref. 10)	ref. 11)	ref. 11)		
1	444.0	445.9		444.1 ± 0.5	8.938	0.3
2	522.2				9.014	0.04
3	533.0	533.8		532.9 ± 0.6	9.025	0.7
4	575.4	575.9		575.2 ± 0.6	9.065	0.6
5	643.1	644.2		643.2 ± 0.7	9.131	0.6
6	656.0	656.8		656.0 ± 0.7	9.143	0.4
7	704.5				9.190	(0.2)
8	733.4	734.6	736		9.219	2.4
9	754.3	755.4			9.239	0.5
10	762.4				9.247	0.6
11	772.6				9.257	0.4
12	817.0	818.2	819		9.300	1.9
13	859.7	861.4	861		9.341	16
14	873.3				9.355	0.5
15	883.5	885.7	883		9.365	3
16	891.6	893.0	890		9.372	3
17	897.6	899.2	896		9.378	6
18	958.6				9.438	0.2
19	968.0				9.447	0.5
20	985.9				9.464	2.5
	all ± 1.0	all ± 1.5	all ± 5			all $\pm 30\%$

REACTION	RESULT	EXCITATION ENERGY	SOURCE		DETECTOR		ANGLE
			TYPE	RANGE	TYPE	RANGE	
P,G	RLX	12-19	D	4-12	NAI-D	10-20	DST

Giant Dipole Resonance in Ar³⁶†

L. Meyer-Schutzmeister, D. S. Gemmell, R. C. Bearse, and N. G. Puttaswamy
 Argonne National Laboratory, Argonne, Illinois

and

R. E. Segel

Argonne National Laboratory, Argonne, Ill. and Northwestern University, Evanston, Ill.

The radiative capture of protons by Cl³⁵ has been studied over the range $4 \leq E_p \leq 12$ MeV which covers the excitation region $12.4 \leq E_x \leq 19.2$ MeV in Ar³⁶. The experiments were performed in a manner similar to the others previously reported by the Argonne group.¹⁾ Figure 1 shows a yield curve taken in 25-keV steps with a 1.5 mgm/cm² BaCl₂ target; the Cl³⁵ enrichment was about 99%. Most of the yield curve in Fig. 1 was taken at 45° to the incident beam, but the portion from 7.0 to 8.5 MeV was taken at 90° and an adjustment was made for the gamma-ray angular distribution. The yield curve is dominated by the onset of the giant resonance but, because of the comparatively low Q and also because the giant resonance appears to come at a higher energy in Ar³⁶ than in neighboring nuclides, the beam energy was not high enough to reach the peak of the giant resonance. There is a great deal of fine structure but, at least in the giant-resonance region, the direct-interaction component contributes most of the cross section.

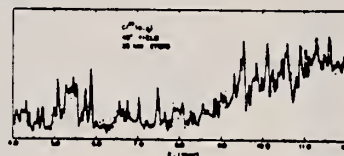


Fig. 1. Yield curve, taken in 25-keV steps, for the Cl³⁵(p, γ)Ar³⁶ reaction.

The γ_1 yield curve is qualitatively similar to that obtained for γ_0 except that the γ_1 yield is still rising at the high-energy end. This indicates that the peak of the γ_1 giant resonance has not yet been reached. The integrated (γ_0, γ_1) yield, obtained by detailed balance, is 0.060 MeV-b which is about 11% of the dipole sum [taken as $(2\pi^2 e^2 / Mc)(NZ/A)$].

Angular distributions were taken every 100 keV over the entire range; some samples are shown in Fig. 2. The angular distributions show marked variations below the giant-resonance region but then settle down to the usual near-invariance at higher energy. The greater yield in the forward direction, indicative of E1-E2 interference, is quite marked.

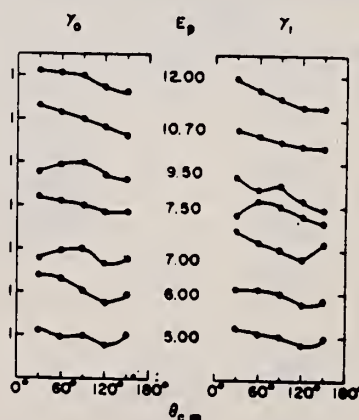


Fig. 2. Typical angular distributions observed for Cl³⁵(p, γ)Ar³⁶, Ar³⁶*

METHOD

REF. NO.

69 Ho 1

egf

REACTION	RESULT	EXCITATION ENERGY	SOURCE		DETECTOR		ANGLE
			TYPE	RANGE	TYPE	RANGE	
G,XP	ABY	THR- 33	C	24-33	SCI-D	3-14	90

Tabelle 1. Daten zu den einzelnen Reaktionen. Die Werte für den integrierten Wirkungsquerschnitt wurden unter der Annahme ausschließlicher Grundzustandsübergänge berechnet. Für ^{23}Na und ^{39}K als Ausnahme s. Text

Tar-get	Anreiche-rungsgrad	(γ, p)-Schwelle MeV	Druck oder Dicke	End-energie MeV	Zahl gemess. Protonen	Ausbeute $\mu\text{b}/\text{MeV sr}$	$^{32.5} \int \sigma(E) dE$ MeVmb	Figur
^{18}O	99	16,0	230 Torr	32,5	36074	58 ± 7	38 ± 6	1, 2
^{20}Ne	90,9	12,8	450 Torr	28,0	3175	$7,4 \pm 1$	—	—
			610 Torr	32,5	6293	$14,9 \pm 2$	61 ± 11	5, 6
^{22}Ne	99,9	15,3	240 Torr	24,0	1960	$2,3 \pm 0,4$	—	4, 5
				28,0	4790	$3,6 \pm 0,6$	—	4, 5
				32,5	5210	$6,7 \pm 0,9$	45 ± 8	4, 5
^{23}Na	100	8,8	65 μ	24,0	14182	$6,3 \pm 1,0$	—	7
			60 μ	32,5	11152	$12,8 \pm 2,0$	117 ± 30	7
^{36}Ar	99	8,5	250 Torr	32,5	45173	57 ± 6	270 ± 40	8, 10
^{40}Ar	99,6	12,5	230 Torr	32,5	29359	$14,2 \pm 15$	104 ± 15	9, 11
^{39}K	93,1	6,4	80 μ	24,0	24230	$17,4 \pm 2,8$	—	12
			90 μ	32,5	24941	$41,9 \pm 6,7$	405 ± 100	12
^{84}Kr	99	10,7	170 Torr	32,5	35515	$12,7 \pm 2,0$	80 ± 20	14
Kr	natürl.	10	170 Torr	32,5	13570	$12,5 \pm 2,0$	75 ± 20	13
Xe	natürl.	9	150 Torr	32,5	7553	$7,6 \pm 0,9$	40 ± 7	15

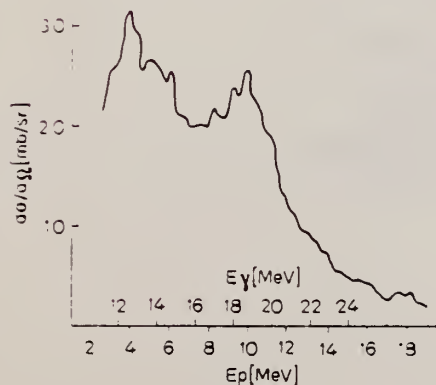


Fig. 10

Fig. 10. Aus Fig. 8 berechneter (γ, p)-Wirkungsquerschnitt für ^{36}Ar

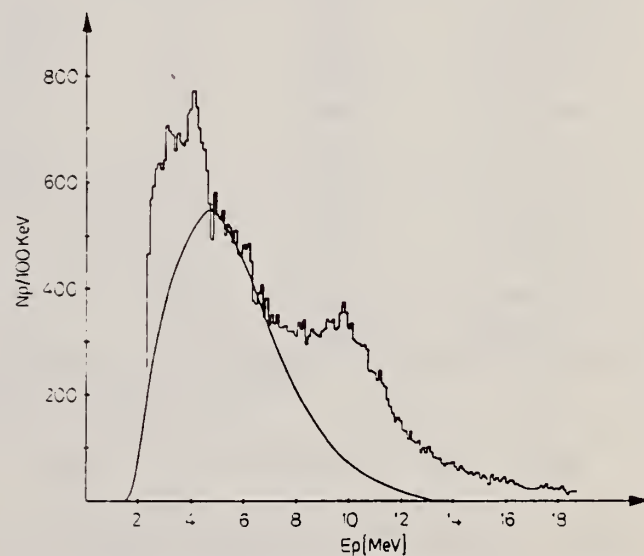


Fig. 8 Histogramm: Energieverteilung der Photoprotonen aus ^{36}Ar . Kurve: Berechnetes Verdampfungsspektrum, beides für $E_0 = 32,5$ MeV

ELEM. SYM.	A	Z
Ar	36	18
REF. NO.		
70 Ke 1		egf

METHOD						REF. NO.	egf
						70 Ke 1	
REACTION	RESULT	EXCITATION ENERGY	SOURCE		DETECTOR		ANGLE
			TYPE	RANGE	TYPE	RANGE	
P,G	RLX	14-20	D	6-12	NAI-D	10-22	90

244

$$\int \sigma(\gamma, p_0) \, 38/36 \approx 1/3 \text{ (or both)}$$

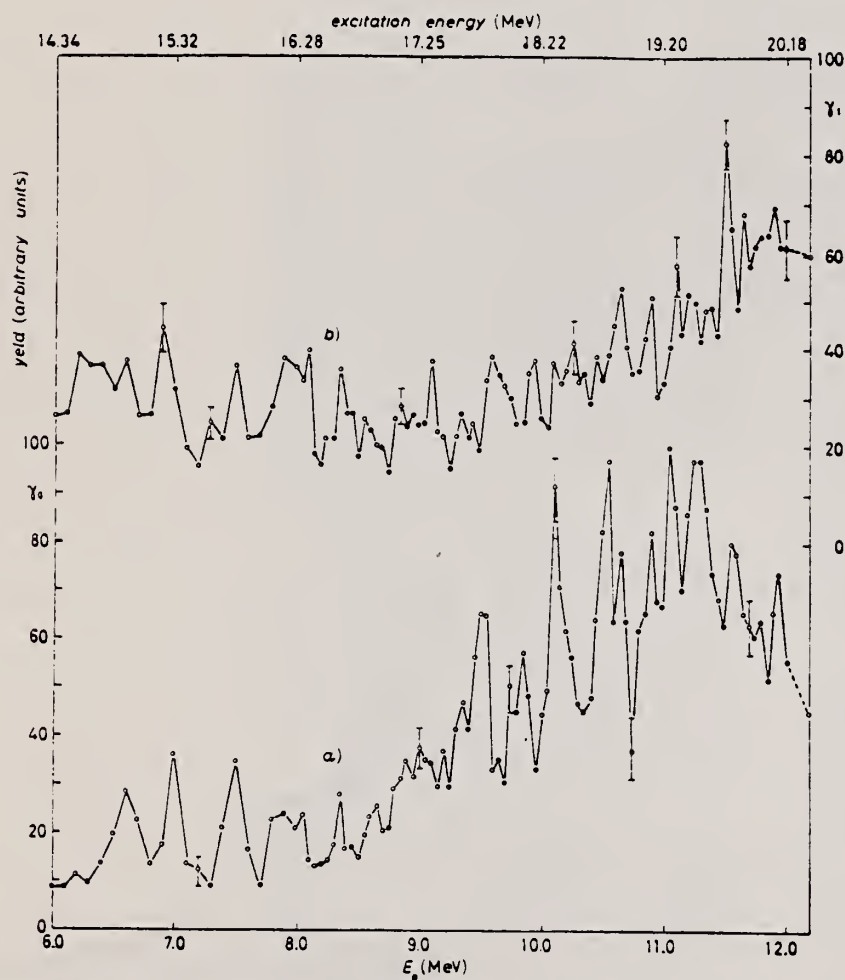


Fig. 1. - The observed differential cross-sections for $^{36}\text{Cl}(p, \gamma)^{36}\text{Ar}$ at 90° : a) $\sigma_{900}(^{36}\text{Cl}(p, \gamma)^{36}\text{Ar})$; b) $\sigma_{900}(^{36}\text{Cl}(p, \gamma)^{36}\text{Ar})$.

ELEM. SYM.	A	Z
Ar	36	18
METHOD	REF. NO.	
	72 Fa 1	hmg

REACTION	RESULT	EXCITATION ENERGY	SOURCE		DETECTOR		ANGLE
			TYPE	RANGE	TYPE	RANGE	
E, E/	ABX	7-13	D	39, 56	MAG-D		180
				(39. 2, 56. 2)			

J-PI, G-WIDTH, 8 LEV

Magnetic transitions in ^{40}Ar have been investigated by 180° electron scattering from an isotopically enriched gaseous target at energies of 39 and 56 MeV. As in the case of ^{32}S , considerable fragmentation of the magnetic dipole strength is evident. Magnetic dipole transitions are observed at 10.05 and 11.25 MeV with ground-state transition widths of 6.2 and 8.9 eV, respectively. A magnetic quadrupole transition is observed at 8.44 MeV with a ground-state transition width of 10.6×10^{-3} eV. Two possible magnetic quadrupole transitions and one possible magnetic dipole transition are observed at 7.46, 11.58, and 12.09 MeV, respectively. Ambiguous results were obtained as to the multipolarity of two transitions at 9.27 and 10.55 MeV. The experimental results are discussed in terms of the theory of Kurath.

TABLE I. Differential cross sections, spin and parity, transition radius, and radiation width for energy levels in ^{40}Ar , including DWBA corrections.

Level energy (MeV)	$(d\sigma/d\Omega)_{\text{M}}$ (10^{-34} cm ² /sr)	$(d\sigma/d\Omega)_{\text{E}}$ (10^{-34} cm ² /sr)	J^π	R (fm)	Γ_0 (eV)
7.46 ± 0.05	27 ± 6	29 ± 9	(2 ⁻)	4.0 ^{+0.7} _{-0.7}	3.3 ^{+1.3} _{-1.3} × 10 ⁻³
8.44 ± 0.04	45 ± 7	47 ± 13	2 ⁻	4.0 ^{+0.7} _{-0.7}	10.6 ^{+9.3} _{-9.3} × 10 ⁻³
9.27 ± 0.04	38 ± 8	62 ± 14	(1 ⁺)	2.0 ^{+0.4} _{-0.4}	1.8 ^{+0.7} _{-0.7}
			(2 ⁻)	4.9 ^{+0.7} _{-0.7}	3.0 ^{+1.3} _{-1.3} × 10 ⁻³
10.05 ± 0.06	41 ± 8	117 ± 17	1 ⁺	3.3 ^{+0.7} _{-0.7}	6.2 ^{+1.9} _{-1.9}
10.55 ± 0.06	33 ± 9	51 ± 19	(1 ⁺)	1.9 ^{+0.4} _{-0.4}	2.2 ^{+0.9} _{-0.9}
			(2 ⁻)	5.0 ^{+0.7} _{-0.7}	5.1 ^{+1.3} _{-1.3} × 10 ⁻³
11.25 ± 0.06	38 ± 9	114 ± 23	1 ⁺	3.4 ^{+0.7} _{-0.7}	8.9 ^{+1.9} _{-1.9}
11.58 ± 0.06	42 ± 9	48 ± 21	(2 ⁻)	4.5 ^{+0.7} _{-0.7}	6.9 ^{+1.3} _{-1.3} × 10 ⁻³
12.09 ± 0.07	42 ± 10	71 ± 27	(1 ⁺)	2.3 ^{+0.4} _{-0.4}	5.0 ^{+0.9} _{-0.9}

^a If the data and equations yield $R^2 < 0$, the lower limit of R is taken to be zero.

(over)

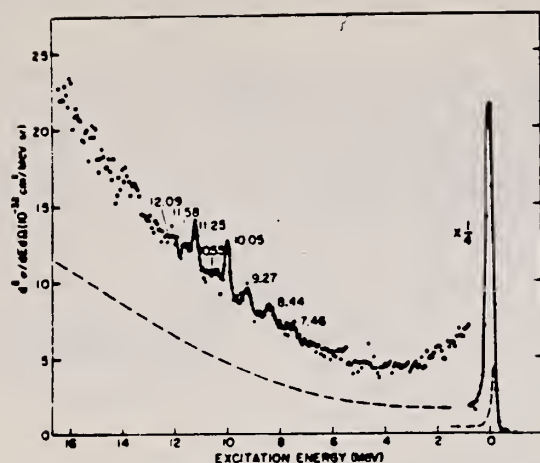


FIG. 1. Differential cross section for 180° scattering of 39.2-MeV electrons from ^{36}Ar . If the ordinate is regarded as arbitrary counting rate, the dashed curve gives a comparison of the counting rate resulting from the two Havar foils (target chamber evacuated) with that resulting from the chamber-filled condition; it is not a cross-section curve.

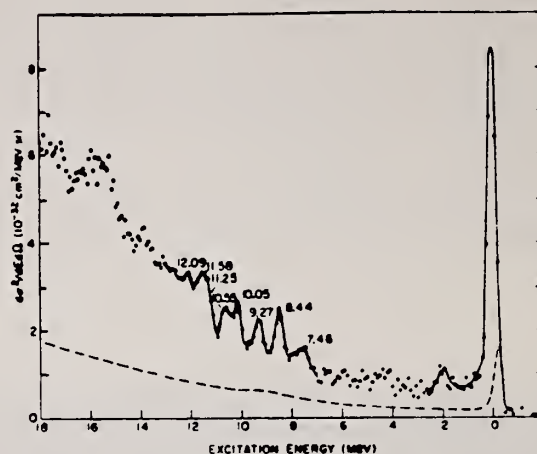


FIG. 2. Differential cross section for 180° scattering of 56.2-MeV electrons from ^{36}Ar . If the ordinate is regarded as arbitrary counting rate, the dashed curve gives a comparison of the counting rate resulting from the two Havar foils (target chamber evacuated) with that resulting from the chamber-filled condition; it is not a cross-section curve.

Errata

Decay of a New Isomer in ^{154}Tb to High-Spin Levels in ^{154}Gd . L. L. Riedinger, D. C. Sousa, E. G. Funk, and J. W. Mihelich [Phys. Rev. C 4, 1352 (1971)]. The following by-line was inadvertently omitted: Research supported in part by the U. S. Atomic Energy Commission. The FN accelerator is supported by the National Science Foundation.

States in ^{36}Ar Excited by 180° Electron Scattering. L. W. Fagg, W. L. Bendel, E. C. Jones, Jr., L. Cohen, and H. F. Kaiser [Phys. Rev. C 5, 120 (1972)]. The ninth line in the first column of page 123 should read: "... that, with the filling of the $d_{5/2}$ shell at ^{36}Si , there."

ELEM. SYM.	A	Z
Ar	36	18
REF. NO.		
77 F1 5		egf

METHOD

REACTION	RESULT	EXCITATION ENERGY	SOURCE		DETECTOR		ANGLE
			TYPE	RANGE	TYPE	RANGE	
E,E/	ABX	2,4	D	65,115	MAG-D		DST

Abstract: The low-lying level structure of ^{36}Ar and ^{40}Ar has been investigated using the technique of inelastic electron scattering. Data were collected at the National Bureau of Standards Linear Accelerator with incident electron energies between 65 and 115 MeV and scattering angles of 92.5° and 110° . The data span a range of momentum transfer squared between 0.29 and 0.92 fm^{-2} . Tassie model and Helm model analyses have been applied to data for levels at 1.97 and 4.18 MeV in ^{36}Ar and at 1.46, 2.52, 3.21 and 3.68 MeV in ^{40}Ar . A 2^+ assignment to the 3.21 MeV state in ^{40}Ar is suggested. Transition strengths, transition radii, and mean lifetimes for these states are computed and compared with results of previous experiments.

1.97, 4.18 MeV

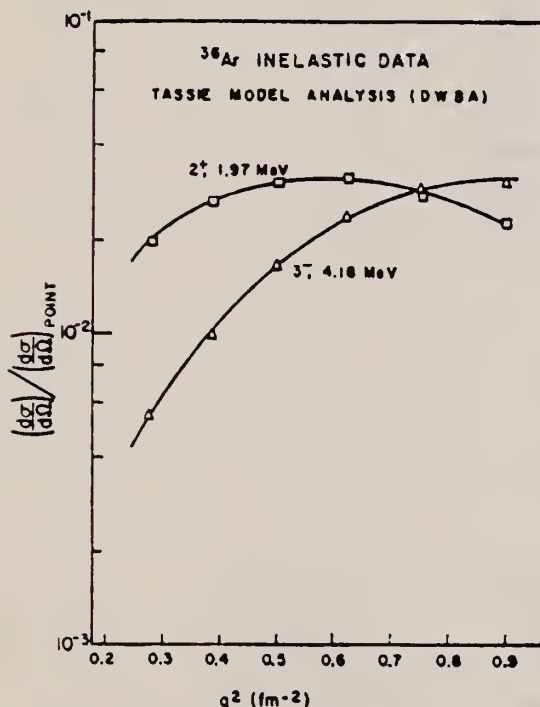


Fig. 1. The ratio of the ^{36}Ar experimental differential cross section to the Coulomb corrected point differential cross section as a function of momentum transfer squared. The smooth curves represent the best fit of the Tassie model to the data.

TABLE I
 ^{36}Ar inelastic scattering cross section

Incident energy (MeV)	Scattering angle (deg)	Elastic scattering ^{a)} cross section ($\mu\text{b/sr}$)	Inelastic scattering cross section (nb/sr)	
			1.97 MeV(2^+)	4.18 MeV(3^-)
115.74	110.29	0.712	201 ± 4	273 ± 9
105.61	110.44	2.462	292 ± 8	309 ± 5
95.58	110.44	6.988	405 ± 8	311 ± 6
85.32	110.36	17.82	513 ± 17	281 ± 7
75.13	110.33	41.12	587 ± 22	225 ± 5
64.97	110.33	89.05	579 ± 28	171 ± 10

TABLE 3
Tassie model parameters ^{a)}

Nucleus	ω (MeV)	J^π	$B(EL)\dagger$ (fm ^{2L})	c_{ir} (fm)	t_{ir} (fm)	χ_r^2	ν	R (fm)	$(R_{ir}/R_{ir}^0)^b$
⁴⁰ Ar	1.46	2 ⁺	382 ± 13	2.23 ± 0.12	3.21 ± 0.08	2.84	4	5.21 ± 0.29	1.07 ± 0.06
	2.52	2 ⁺	63.2 ± 11.5	3.09 ± 0.42	3.48 ± 0.39	0.99	4	5.94 ± 0.83	1.22 ± 0.17
	3.21	2 ⁺	29.3 ± 4.0	2.03 ± 0.47	2.95 ± 0.28	1.22	4	4.72 ± 1.07	0.97 ± 0.22
	3.68	3 ⁻	8750 ± 1020	3.25 ± 0.69	2.15 ± 0.46	0.78	4	4.97 ± 1.04	0.91 ± 0.19
³⁶ Ar	1.97	2 ⁺	280 ± 16	3.62 ± 0.18	1.76 ± 0.30	0.56	3	4.36 ± 0.24	0.92 ± 0.05
	4.18	3 ⁻	11300 ± 470	4.10 ± 0.25	1.23 ± 0.36	0.68	3	4.58 ± 0.26	0.87 ± 0.05

^{a)} DWBA approximation.

^{b)} $R_{ir}^2 = \langle J^\pi || r^{L+2} || 0^+ \rangle / \langle J^\pi || r^L || 0^+ \rangle$; R_{ir}^0 calculated using ground-state values of c and t .

TABLE 4
Helm model parameters

Nucleus	ω (MeV)	J^π	$B(CL)$ (fm ^{2L})	R_{ir} (fm)	χ_r^2	ν
⁴⁰ Ar	1.46	2 ⁺	334 ± 44	4.44 ± 0.11	7.9	5
	2.52	2 ⁺	45 ± 24	4.98 ± 0.38	1.3	5
	3.21	2 ⁺	29 ± 17	4.19 ± 0.50	1.2	5
	3.68	3 ⁻	10800 ± 2900	4.80 ± 0.26	1.0	5
³⁶ Ar	1.97	2 ⁺	330 ± 40	4.42 ± 0.10	1.2	5
	4.18	3 ⁻	16200 ± 2000	4.79 ± 0.15	0.4	5

TABLE 5
Transition strengths from present work

Nucleus	ω (MeV)	J^π	$ M ^2$ (W.u.)	$\Gamma_{J^\pi \rightarrow J^\pi_{g.s.}}$ (eV)
⁴⁰ Ar	1.46	2 ⁺	9.4 ± 0.3	(4.10 ± 0.14) × 10 ⁻⁴
	2.52	2 ⁺	1.6 ± 0.3	(1.04 ± 0.19) × 10 ⁻³
	3.21	2 ⁺	0.72 ± 0.10	(1.61 ± 0.22) × 10 ⁻³
	3.68	3 ⁻	13.2 ± 1.5	(4.30 ± 0.30) × 10 ⁻⁶
³⁶ Ar	1.97	2 ⁺	7.9 ± 0.5	(1.34 ± 0.08) × 10 ⁻³
	4.18	3 ⁻	21.0 ± 0.9	(1.35 ± 0.06) × 10 ⁻³

AR
A=38

AR
A=38

AR
A=38

Ar	38	18
REF. NO. 64 Er 1		JOC

METHOD $S^{34}(\alpha, \gamma)Ar^{38}$			SOURCE		DETECTOR		ANGLE
REACTION	RESULT	EXCITATION ENERGY	TYPE	RANGE	TYPE	RANGE	
A, G	RLY	9 - 10	D	2-3	NAI-D		DST
				(2.2 - 3.2)			

J-PI, WIDTHS

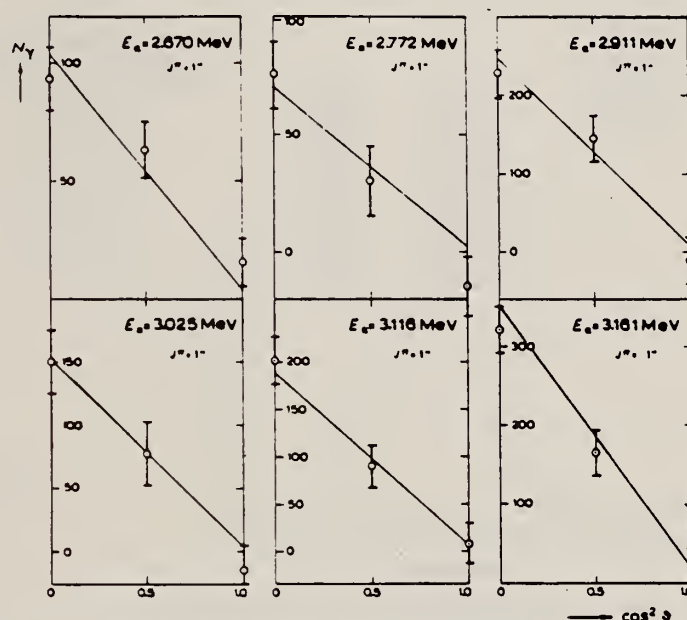


Fig. 3. Ground-state angular distributions measured at six $^{34}S(\alpha, \gamma)^{38}Ar$ resonances. The solid curves give the calculated distributions for the assigned spin values, taking into account the solid angle attenuation.

TABLE 2
Resonances in the reaction $^{34}S(\alpha, \gamma)^{38}Ar$; energies, spins and parities, strengths and main decay

E_a (MeV)	$^{38}Ar^*$ (MeV)	J^π	$(2J+1)\Gamma_\alpha\Gamma_\gamma/\Gamma$ (eV)	Main decay
2.670	9.602	1^-	4.0	%
2.772	9.693	1^-	1.5	%
2.911	9.817	1^-	0.3	%
3.025	9.919	1^-	4.5	%
3.116	10.001	1^-	3.0	%
3.161	10.041	1^-	4.5	%
all ± 0.005			all $\pm 30\%$	

METHOD	Electrostatic generator; $S^{34}(\alpha, \gamma)A^{38}$	REF. NO.	64 Ph 1	JOC
--------	---	----------	---------	-----

REACTION	RESULT	EXCITATION ENERGY	SOURCE		DETECTOR		ANGLE
			TYPE	RANGE	TYPE	RANGE	
A,G	RLY	9 - 11	D	3 - 4	NAI-D		DST
				(3.0 - 3.6)			

J-PI, WIDTHS

TABLE 1
Resonances observed in the $S^{34}(\alpha, \gamma)A^{38}$ reaction

E_R	(MeV) ^a	Γ (MeV)	J^π	E_{exc} ^b
2.670 ± 0.005			1 ⁻	9.601 ± 0.008
2.772 ± 0.005			1 ⁻	9.698 ± 0.008
2.911 ± 0.005			1 ⁻	9.817 ± 0.008
3.025 ± 0.005	3.03 ± 0.010	≲ 0.002	1 ⁻	9.920 ± 0.008
3.116 ± 0.005	3.12 ± 0.010	≲ 0.002	1 ⁻	10.001 ± 0.008
3.161 ± 0.005	3.17 ± 0.010	≲ 0.002	1 ⁻	10.043 ± 0.008
	3.29 ± 0.010	≲ 0.002	1 ⁻	10.16 ± 0.012
	3.34 ± 0.010	≲ 0.002	1 ⁻	10.20 ± 0.012
	3.40 ± 0.010	≲ 0.002	1 ⁻	10.26 ± 0.012
	3.49 ± 0.010	≲ 0.002	1 ⁻	10.34 ± 0.012
	3.55 ± 0.010	≲ 0.002	1 ⁻	10.39 ± 0.012
	3.60 ± 0.010	≲ 0.002	1 ⁻	10.43 ± 0.012

TABLE 3
Radiative widths of the 10.34 MeV level

E_γ (MeV)	Γ_γ (eV)	M^2 ($\times 10^{-3}$)
10.34	0.52	0.62
8.17	0.16	0.38
6.33	0.065	0.34
5.74	0.076	0.53

METHOD

REF. NO.

65 Eh 1

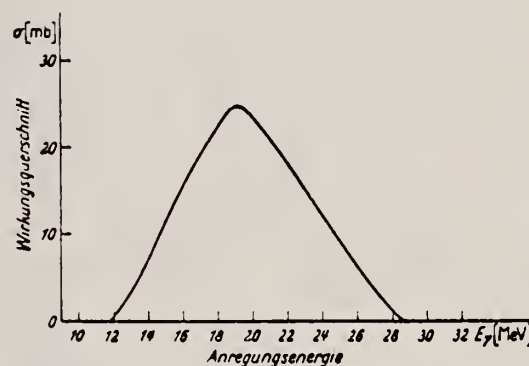
EGF

REACTION	RESULT	EXCITATION ENERGY	SOURCE		DETECTOR		ANGLE
			TYPE	RANGE	TYPE	RANGE	
G,N	ABY	THR - 31	C	18 - 31	ACT-I		4PI

Tabelle 1

E_0 MeV	Ausbeute $Y(E_0)$ $Ar^{40}(\gamma, n) + Ar^{40}(\gamma, p)$ $\mu b/MeV$	Ausbeute $Y(E_0)$ $Ar^{38}(\gamma, n)$ $\mu b/MeV$	E_0 MeV	Ausbeute $Y(E_0)$ $Ar^{40}(\gamma, n) + Ar^{40}(\gamma, p)$ $\mu b/MeV$	Ausbeute $Y(E_0)$ $Ar^{38}(\gamma, n)$ $\mu b/MeV$
18,1	$299 \pm 17\%$	$131 \pm 25\%$	26,4	$510 \pm 3\% *$	$303 \pm 3\% *$
20,1	$418 \pm 10\%$	$217 \pm 12\%$	28,6	$535 \pm 2\%$	$330 \pm 3\%$
22,1	$547 \pm 7\%$	$286 \pm 9\%$	30,7	$516 \pm 2\%$	$337 \pm 3\%$
24,3	$563 \pm 3\%$	$322 \pm 4\%$			

* Da die Ergebnisse der Bestrahlung bei 26,4 MeV für beide Isotope zu klein ausfallen, das Verhältnis der Ausbeute beider Isotope jedoch mit den Werten bei anderen Endenergien übereinstimmt, scheint bei dieser Bestrahlung ein Fehler bei der Kammerjustierung unterlaufen zu sein.

Fig. 6. Energieabhängigkeit des Wirkungsquerschnittes für die Reaktion $Ar^{38}(\gamma, n)$

REF. K. G. Kernbach
Lettere al Nuovo Cimento III, 461 (1970)

ELEM. SYM.	A	Z
Ar	38	18

METHOD

REF. NO.

70 Ke 1

egf

REACTION	RESULT	EXCITATION ENERGY	SOURCE		DETECTOR		ANGLE
			TYPE	RANGE	TYPE	RANGE	
P, G	RLX	14-22	D	4-12	NAI-D	10-22	90

$\int \sigma(\gamma, p_0) \ 38/36 \approx 1/3$ (or both)

245

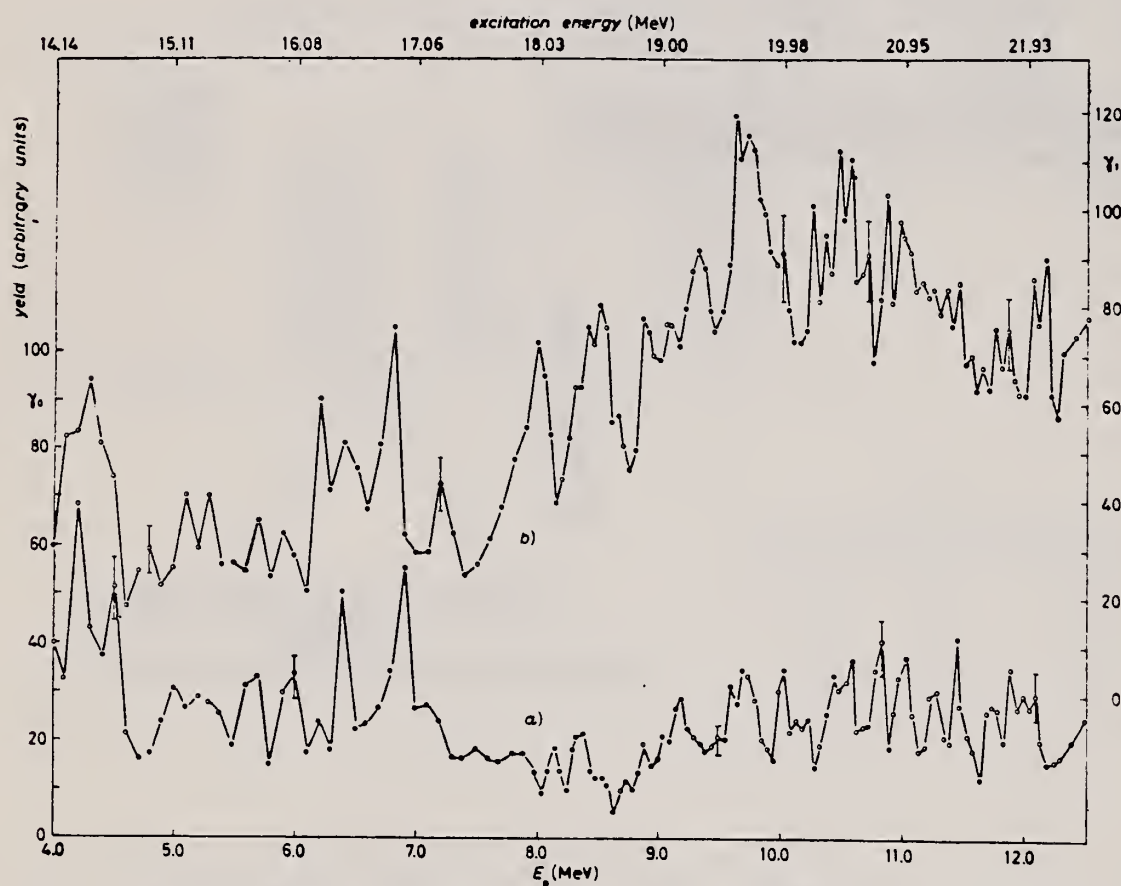


Fig. 2. - The observed differential cross-sections for $^{36}\text{Cl}(p, \gamma)^{36}\text{Ar}$ at 90° : a) $\sigma_{000}(^{36}\text{Cl}(p, \gamma)^{36}\text{Ar})$; b) $\sigma_{001}(^{36}\text{Cl}(p, \gamma)^{36}\text{Ar})$.

REF.

A. Chevallier, E. Bozek, J. Chevallier, A. Pape, R. Armbruster
Nucl. Phys. A191, 201 (1972)

ELEM. SYM.

A

Z

Ar

38

18

METHOD

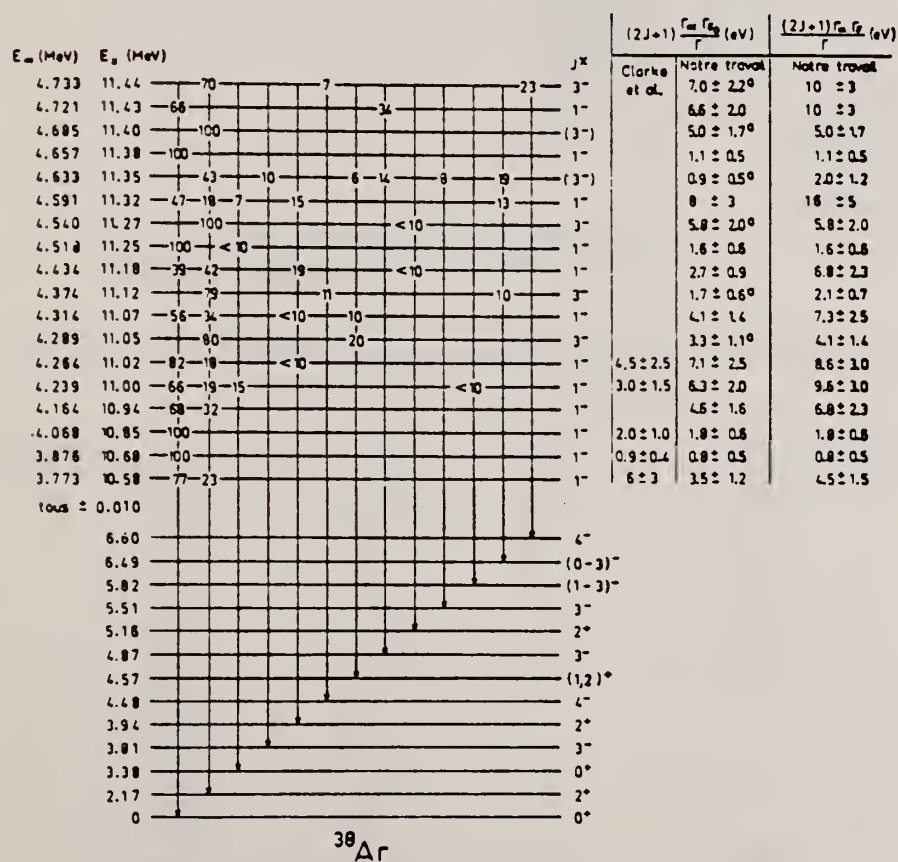
REF. NO.

72 Ch 1

egf

REACTION	RESULT	EXCITATION ENERGY	SOURCE		DETECTOR		ANGLE
			TYPE	RANGE	TYPE	RANGE	
A,G	ABX	10-12	D	4-5	NAI-D		DST
		(10.58-11.44)					

J-PI, 12 LEVELS

Fig. 2. Niveaux observés dans la réaction $^{34}\text{S}(\alpha, \gamma)^{38}\text{Ar}$ (a) les quantités indiquées correspondent ici aux rayonnements γ_1 .

(over)

TABLEAU I

Coefficients A_2 et A_4 des distributions angulaires γ_0 et γ_1 ; coefficient de mélange de multipolarité des transitions γ_1 ; limites inférieures des transitions électriques dipolaires observées dans ^{38}Ar

$E_i \rightarrow E_f$ (MeV)	A_2	A_4	$J_i^{(\pi)}$	$\delta^{(b)}$	E_i	
					Γ_1 (eV) ^(a)	$ M_1 ^2 \times 10^2$ (u.W.)
10.58 \rightarrow 0	-0.91 ± 0.07		1 ⁻		1.1 ± 0.4	0.12 ± 0.05
10.68 \rightarrow 0	-0.88 ± 0.11		1 ⁻		0.3 ± 0.2	0.04 ± 0.03
10.85 \rightarrow 0	-0.89 ± 0.07		1 ⁻		0.6 ± 0.2	0.06 ± 0.02
10.94 \rightarrow 0	-0.93 ± 0.10		1 ⁻		1.6 ± 0.5	0.16 ± 0.05
11.00 \rightarrow 0	-0.90 ± 0.05		1 ⁻		2.1 ± 0.7	0.21 ± 0.07
11.02 \rightarrow 0	-0.90 ± 0.05		1 ⁻		2.3 ± 0.9	0.23 ± 0.09
11.02 \rightarrow 2.17	$+0.2 \pm 0.2$		1 ⁻	-0.3 ± 0.2	0.5 ± 0.3	0.09 ± 0.05
11.05 \rightarrow 2.17	-0.30 ± 0.06	$+0.15 \pm 0.07$	3 ⁻	-0.07 ± 0.03	0.5 ± 0.2	0.09 ± 0.04
11.07 \rightarrow 0	-1.01 ± 0.10		1 ⁻		1.4 ± 0.5	0.14 ± 0.05
11.07 \rightarrow 2.17	-0.4 ± 0.5		1 ⁻	-0.0 ± 0.2	0.8 ± 0.3	0.16 ± 0.05
11.12 \rightarrow 2.17	-0.25 ± 0.08	$+0.22 \pm 0.08$	3 ⁻	-0.11 ± 0.04	0.2 ± 0.1	0.05 ± 0.02
11.18 \rightarrow 0	-0.78 ± 0.09		1 ⁻		0.9 ± 0.3	0.08 ± 0.03
11.18 \rightarrow 2.17	-0.1 ± 0.2		1 ⁻	-0.00 ± 0.03	1.0 ± 0.4	0.17 ± 0.07
11.25 \rightarrow 0	-0.9 ± 0.2		1 ⁻		0.55 ± 0.20	0.05 ± 0.02
11.27 \rightarrow 2.17	-0.48 ± 0.07	$+0.17 \pm 0.07$	3 ⁻	-0.02 ± 0.03	0.8 ± 0.3	0.14 ± 0.05
11.32 \rightarrow 0	-0.91 ± 0.16		1 ⁻		2.4 ± 0.8	0.22 ± 0.08
11.32 \rightarrow 2.17	$+0.1 \pm 0.5$		1 ⁻	$+0.2 \pm 0.2$	0.9 ± 0.3	0.15 ± 0.06
11.38 \rightarrow 0	-0.96 ± 0.15		1 ⁻		0.4 ± 0.2	0.035 ± 0.015
11.40 \rightarrow 2.17 ^(c)	-0.4 ± 0.3	$+0.4 \pm 0.2$	(3 ⁻)	-0.23 ± 0.15	0.7 ± 0.2	0.12 ± 0.04
11.43 \rightarrow 0	-0.80 ± 0.10		1 ⁻		1.8 ± 0.6	0.16 ± 0.05
11.44 \rightarrow 2.17	-0.42 ± 0.08	$+0.15 \pm 0.10$	3 ⁻	-0.02 ± 0.03	1.0 ± 0.3	0.17 ± 0.05

^(a) $J^\pi_i = 0^+$ ou 2^+ pour $E_i(^{38}\text{Ar}^*) = 0$ et 2.17 MeV respectivement.

^(b) Le signe de δ est déterminé selon la convention de Rose et Brink.

^(c) En supposant $\Gamma_\alpha > \Gamma_\beta$ et $\Gamma_\alpha > \Gamma_\gamma$.

^(d) Les calculs ont été faits pour le spin 3⁻, qui est plus probable.

ELEM. SYM.	A	Z
Ar	38	18
REF. NO.	79 Si 9	
	hg	

REACTION	RESULT	EXCITATION ENERGY	SOURCE		DETECTOR		ANGLE
			TYPE	RANGE	TYPE	RANGE	
A,G	LFT	9-11	D	2-4	SCD-D		DST
		(9.598-10.334)		(2.669-3.481)			

The reaction $^{34}\text{S}(\alpha, \gamma)^{38}\text{Ar}$ has been investigated in the energy range $E_\alpha = 2.0\text{--}3.5\text{ MeV}$. Eighteen resonance levels were found, nine of which have not been previously reported; six of the new levels have $J > 1$. The excitation energy, J^π , decay scheme, mixing ratio, and transition strength for decays from the resonances were deduced.

J-PI, G-WIDTH

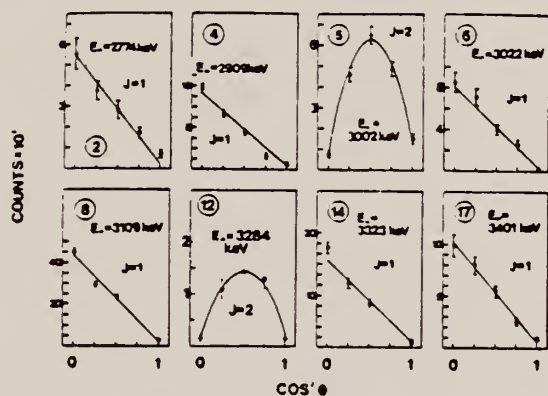


FIG. 5. Angular distributions for ground state decay of $^{34}\text{S}(\alpha, \gamma)^{38}\text{Ar}$ resonances. The circled numbers refer to resonance numbers given in Table I.

TABLE I. Resonances in the $^{34}\text{S}(\alpha, \gamma)^{38}\text{Ar}$ reaction

Resonance	Present work			Literature values			Reference
	E_α (keV)	J^π	$\omega\gamma^*$ (eV)	E_α (keV)	J^π	$\omega\gamma$ (eV)	
1	2669 ± 5	1^-	$1.71 \pm 0.34^\dagger$	2670	1^-	4.0 ± 1.2	2
2	2774 ± 5	1^-	1.3 ± 0.3	2772	1^-	1.5 ± 0.5	2
3	2894 ± 5	3^-	0.3				
4	2909 ± 5	1^-	0.3	2911	1^-	0.3 ± 0.1	2
5	3002 ± 5	2^+	0.6				
6	3022 ± 5	1^-	$2.62 \pm 0.56^\dagger$	3025	1^-	4.5 ± 1.5	2
7	3066 ± 5	2^+	0.2				
8	3109 ± 10	1^-	1.7 ± 0.4	3116	1^-	3.0 ± 1.0	2
9	3155 ± 5	1^-	2.0 ± 0.5	3161	1^-	4.5 ± 1.5	2
10	3173 ± 5		0.04				
11	3196 ± 5	3^-	0.6				
12	3284 ± 10	2^+	0.3				
13	3311 ± 5	3^-	2.4 ± 0.6				
14	3323 ± 10	1^-	4.9 ± 1.2	3324	1^-	8 ± 4	3
15	3364 ± 10		0.04				
16	3394 ± 10		< 0.04				
17	3401 ± 10	1^-	2.6 ± 0.6	3408	1^-	2.7 ± 1.4	3
18	3491 ± 10	1^-	1.6 ± 0.4	3498	1^-	2.1 ± 1.1	3

All $\pm 5\text{ keV}$

*Error is $\pm 50\%$ when not indicated.
†Absolute strength measurement.

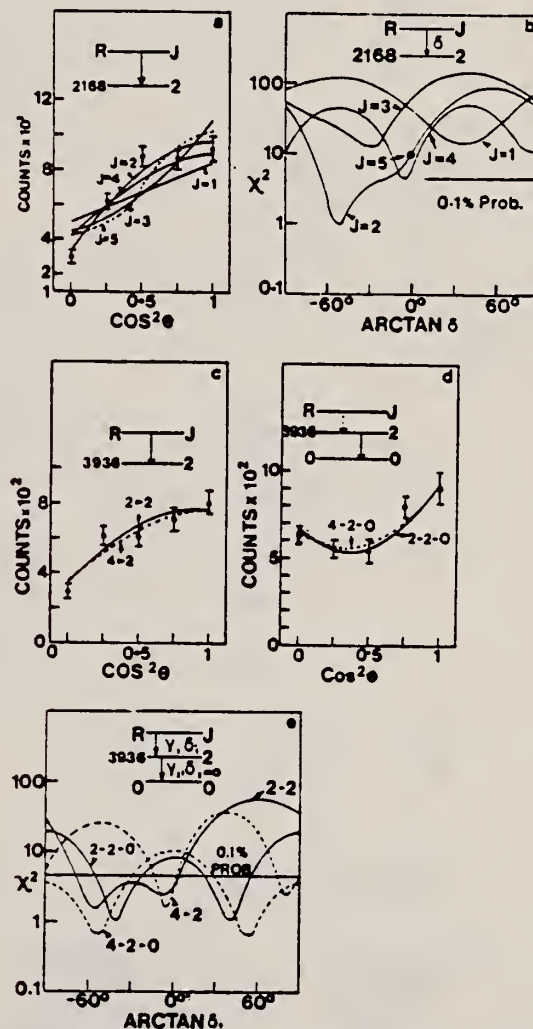
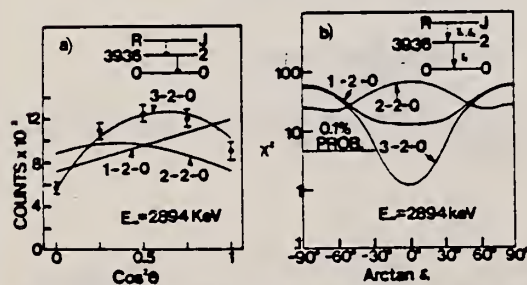


FIG. 7. Angular distributions and χ^2 used to assign spin to resonance 7 at $E_\alpha = 3066\text{ keV}$.

(over)

TABLE 3. Transition strengths

Resonance energy E_R (keV)	Transition $E_R \rightarrow E_f$ (keV)	$J_R \rightarrow J_f$	Mixing ratio	$ M ^2$			(Wu)
				$E1 \times 10^{-3}$	$M1 \times 10^{-3}$	$E2 \times 10^{-3}$	
2669	9 598 \rightarrow 0	$1^- \rightarrow 0^+$		0.84 ± 0.17			
2774	9 692 \rightarrow 0	$1^- \rightarrow 0^+$		0.30 ± 0.09			
	3377	0^+		0.68 ± 0.19			
	3936	2^+	-0.07 ± 0.12 -0.09	0.38 ± 0.11			< 1.3
2894	9 799 \rightarrow 3936	$3^- \rightarrow 2^+$		0.17			
2909	9 813 \rightarrow 0	$1^- \rightarrow 0^+$		0.12			
	3377	0^+		0.04			
3002	9 896 \rightarrow 0	$2^+ \rightarrow 0^+$				25	
	2168	2^+	0.27 ± 0.06		3.3	13	
	3810	3^-	0.11 ± 0.07	0.14			$0.03 < M2 < 0.54$
	3936	2^+	-0.84 ± 0.21 -0.27		1.3	80	
	4566	2^+	-0.18 ± 0.13		4.7	18	
3022	9 914 \rightarrow 0	$1^- \rightarrow 0^+$		1.2 ± 0.3			
3066	9 953 \rightarrow 2168	$2^+ \rightarrow 2^+$	-1.19 ± 0.08 -0.30		0.7	60	
	3810	3^-	-0.07 ± 0.12 -0.09	0.07			
	3936	2^+	-1.43 ± 0.32 -0.37		0.7	150	
3109	9 992 \rightarrow 0	$1^- \rightarrow 0^+$		0.74 ± 0.17			
3155	10 033 \rightarrow 0	$1^- \rightarrow 0^+$		0.86 ± 0.22			
3196	10 070 \rightarrow 2168	$3^- \rightarrow 2^+$		0.08			
	3936	2^+	0.02 ± 0.04	0.03			
			2.90 ± 1.11 -0.54	0.003			3
	4480	4^-	0.27 ± 0.20 -0.10		3	30	
			2.90 ± 0.83 -0.94		0.4	300	
	4566	2^+	0.09 ± 0.04	0.2			0.2
	6212	2^+	-0.05 ± 0.08	0.3			
3284	10 148 \rightarrow 0	$2^+ \rightarrow 0^+$				6	
	2168	2^+	0.05 ± 0.04		5		
3311	10 172 \rightarrow 2168	$3^- \rightarrow 2^+$	-0.05 ± 0.04	0.43 ± 0.10			
	3936	2^+	0	0.27 ± 0.09			
	4480	4^-	0.14 ± 0.05 $+0.81$ -0.60		21 ± 6 1 ± 0.5	43 ± 12 2100 ± 900	
	4566	2^+	0.04 ± 0.05 -0.08	0.24 ± 0.07			
3323	10 183 \rightarrow 0	$1^- \rightarrow 0^+$		2.0 ± 0.5			
3401	10 253 \rightarrow 0	$1^- \rightarrow 0^+$		0.77 ± 0.18			
	3377	0^+		0.58 ± 0.13			
3491	10 334 \rightarrow 0	$1^- \rightarrow 0^+$		0.49 ± 0.11			
	3377	0^+		0.21 ± 0.05			

*Error is $\sim 50\%$ when not indicated.FIG. 6. Angular distributions and χ^2 used to assign spin to resonance 3.

AR
A=40

AR
A=40

AR
A=40

REF.

B. M. Spicer
Phys. Rev. 100, 791 (1955)

ELEM. SYM.

A

Z

Ar

40

18

METHOD

REF. NO.

55 Sp 3

JOC

REACTION	RESULT	EXCITATION ENERGY	SOURCE		DETECTOR		ANGLE
			TYPE	RANGE	TYPE	RANGE	
G,P	SPC	THR - 23	C	23	EMU-D		DST

$$Y = 6.6 \times 10^8 \text{ protons/mole/R}$$

Ang. dist. fitted to $a + b \sin^2\theta(1 + c \cos\theta)$.

TABLE II. Values of a , b , and c for the angular distributions.

Distributions	a	b	c
All protons	39	266	1
Protons $e_p < 3$ Mev	2	160	0.5
Protons $e_p > 3$ Mev	45	96	2
Protons $e_p > 4$ Mev	10	52	2

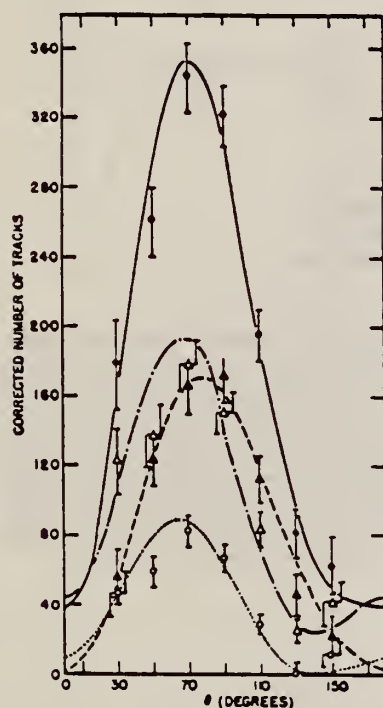


FIG. 3. Angular distributions of photoprotons from argon.
— all protons, --- protons of energy less than 3 Mev, protons of energy greater than 3 Mev, protons of energy greater than 4 Mev.

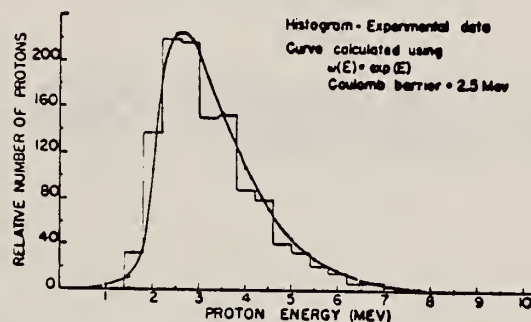


FIG. 1. Energy distribution of photoprotons from argon.

R. H. Helm
Phys. Rev. 104, 1466 (1956)

Ar

40

18

METHOD

REF. NO.

56 He 3

hmg

REACTION	RESULT	EXCITATION ENERGY	SOURCE		DETECTOR		ANGLE
			TYPE	RANGE	TYPE	RANGE	
E, E/	FMF	1-7	D	187	MAG-D		DST

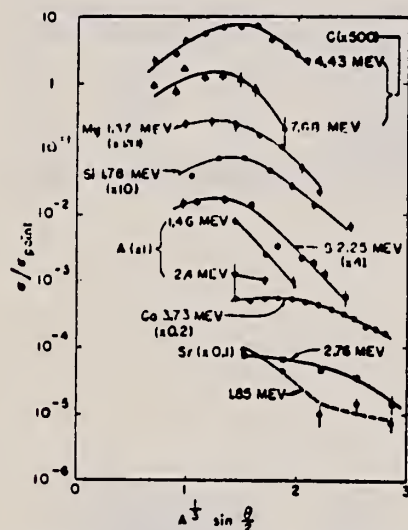


FIG. 3. Inelastic angular distributions (observed cross section divided by Feshbach point-charge cross sections). The results of Hahn *et al.* (reference 8) for Ca and of Fregeau and Hofstadter (reference 11) are included for comparison.

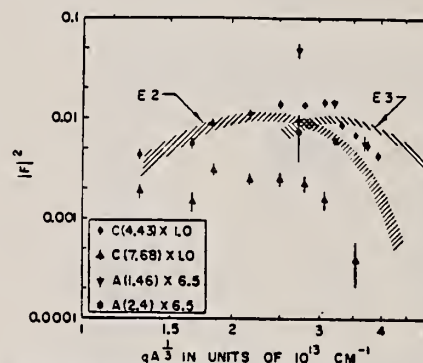


FIG. 8. Comparison of carbon (reference 11) and argon inelastic data to the "universal curves." The shaded areas, arbitrarily normalized, represent the envelopes of the experimental points of Fig. 7. E2 refers to quadrupole and E3 to octupole transitions. It is evident that the known quadrupole cases (4.43 Mev) deviates somewhat from the "universal curve" of the heavier elements, while the C (7.68 Mev) would, if appropriately normalized, fit the "universal curve" almost as well as the 4.43 Mev. The argon data are normalized to make the 2.4 Mev fall on the E2 curve, although it could equally well fit the E3 or possibly the monopole curves. The A (1.46 Mev) curve clearly has too steep a slope to fit either the E2 or E3, and therefore is very probably a monopole.

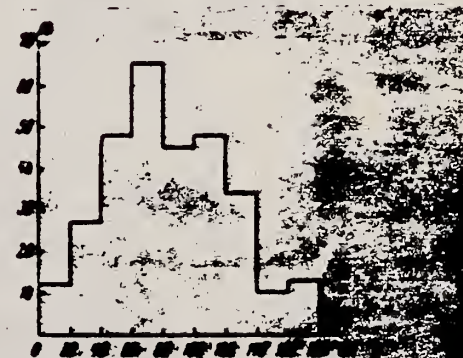
Ref. A.P. Komar, I.P. Iavor
Zhur. Eksp. i Teoret. Fiz. 31, 531 (1956); Soviet Phys. JETP
4, 432 (1957)

Elem. Sym.	A	Z
A	40	18

Method
Synchrotron; cloud chamber.

Ref. No.	JHH
56 Ko 1	

Reaction	E or ΔE	E_0	Γ	$\int \sigma dE$	$J\pi$	Notes
$A^{40}(\gamma, p)$	Bremss. 90					Protons counted in energy range $E_p = 2-10$ MeV.



Angular distribution of photoprotons from A^{40}
number of proton tracks θ - angle between the γ -
beam and direction of ejected proton

A. P. Komar and I. P. Iavor
 J. Exptl. Theoret. Phys. (USSR) 31, 531 (1956)
 Soviet Phys. JETP 4, 432 (1957)

Ar

40

18

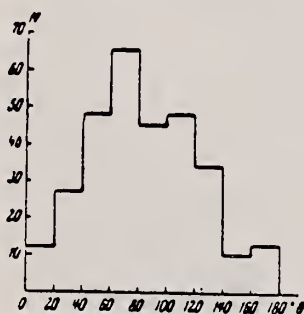
METHOD

REF. NO.

57 Ko 2

EGF

REACTION	RESULT	EXCITATION ENERGY	SOURCE		DETECTOR		ANGLE
			TYPE	RANGE	TYPE	RANGE	
G,XP	NOX	THR - 90	C	90	CCH-D	2-110	DST



Angular distribution of photoprotons from A^{40} . N — number of proton tracks; θ — angle between the γ -beam and direction of ejected proton.

Method 15 MeV betatron; proton spectra and angular distribution; cloud chamber

Ref. No.
58 Gu 1
EH

Reaction	E or ΔE	E_0	Γ	$\int \sigma dE$	$J\pi$	Notes
$A^{40}(\gamma, p)$	Bremss. 15	0.71 0.84				Angular distribution is pair $\sin^2\theta$ which can only take place if final Cl^{39} is $1/2^+$. Such a state is at 0.8 MeV.

Fig. 4. Winkelverteilung für die beiden Protonengruppen mit Energien von 0,713 und 0,837 MeV

Fig. 2. Energieverteilung von 597 Protonen aus der Reaktion $A^{40}(\gamma, p)Cl^{39}$. Schraffiert: Elchprotonen aus der Reaktion $N^{14}(mib, p)Cl^{14}$

Fig. 3. Winkelverteilung von 1218 Protonen aus der Reaktion $A^{40}(\gamma, p)Cl^{39}$. Die geronnene Anzahl von Protonen im Winkelintervall ist jeweils angegeben. Die ausgezogene Kurve entspricht einer reinen $\sin^2\theta$ -Verteilung, die gestrichelte einer Verteilung der Form $2 + 3 \sin^2\theta$. Alle drei Kurven sind auf gleiche Gesamtzahl von Protonen normiert

Ref. I.P. Iavor
Zhur. Eksp. i Teoret. Fiz. 34, 1420 (1958); Soviet Phys. JETP 7,
983 (1958)

Elem. Sym.	A	Z
A	40	18

Method 70 MeV synchrotron; cloud chamber; ionization chamber

Ref. No.	
58 Ia 1	EH

Reaction	E or ΔE	E_0	Γ	$\int \sigma dE$	$J\pi$	Notes
$A^{40}(\gamma, xp)$	Bremss. 70					Angular distribution curve has form: $I(\theta) = A + B (\sin \theta + p \sin \theta \cos \theta)^2$ where, $A = 27; B = 30; p = 0.5.$

Fig. 2. Angular distribution of photoprotons from argon with energies of 2 to 15 Mev. The histogram is the result of analysis of 406 proton tracks. The number of tracks shown has been referred to unit solid angle.

Fig. 3. Energy distribution of photoprotons from argon. 1 - distribution calculated from the theory of the direct photo effect; 2 - distribution calculated from the statistical theory of nuclear reactions; 3 - total theoretical energy distribution of photoprotons; histogram - experimental results.

Reaction	Number of cases	Energy (Mev)
$^{40}Ar(\gamma, p)$	474	2.0 - 15.0
$^{40}Ar(\gamma, n)$	120	0.0 - 1.0
$^{40}Ar(\gamma, \alpha)$	10	0.0 - 1.0
$^{40}Ar(\gamma, \beta)$	10	0.0 - 1.0

¹⁰ Ferguson, Halpern, Nathans, and Yergin, Phys. Rev. 95, 776 (1954).

Elem. Sym.	A	Z
A	40	18

Ref. No.	
59 Br 1	EH

Reaction	E or ΔE	E_0	Γ	$\int \sigma dE$	$J\pi$	Notes
$A^{40}(\gamma, p)$	Bremss. 34			$\int^{28} = 160 \text{ MeV-mb}$		$C^{12}(\gamma, n)$ used as standard for $\int \sigma dE$
$A^{40}(\gamma, np)$				$\int^{28} = 35 \text{ MeV-mb}$		

Method
31 MeV Betatron; emulsions

Ref. No.	
59 Em 2	EH

Reaction	E or ΔE	E_0	Γ	$\int \sigma dE$	$J\pi$	Notes
$A(\gamma, p)$	Bremss. 23					90° spectrum. The peak in "proton" spectra at 2.5 MeV (Coulomb barrier 5 MeV) observed by others is really α particles; obtain (γ, α) cross section; peak ~ 16 MeV $\frac{d\sigma}{dr} \sim 5\text{mb/ster}$
$A(\gamma, \alpha)$	26					
	30					

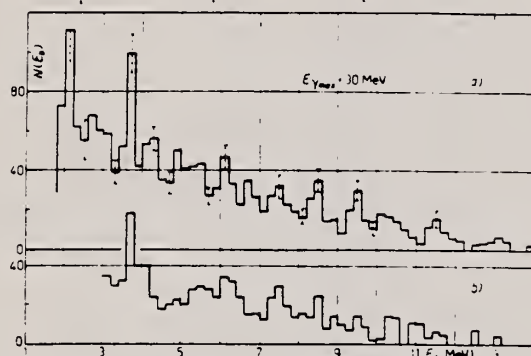


Fig. 2. - Comparison of spectra obtained at 30 MeV peak bremsstrahlung, at different times and in different experimental conditions.

Fig. 3. - Comparison of fields in unities of (charged particles/atom/R/D) at $90^\circ < \theta < 110^\circ$. $\cdot 10^{10}$: argon \blacksquare for all accepted tracks; \triangle for tracks with a total range $> 75 \mu\text{m}$ of emulsion; \circ for tracks with a total range $< 75 \mu\text{m}$ of emulsion; oxygen \diamond for all accepted tracks. Nitrogen \square for all accepted tracks

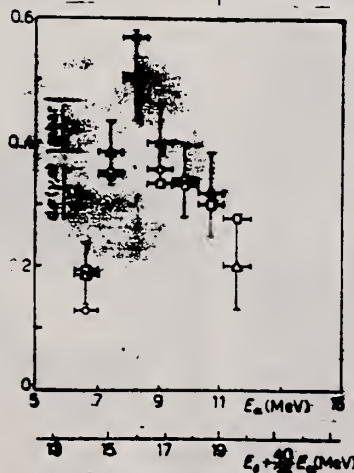
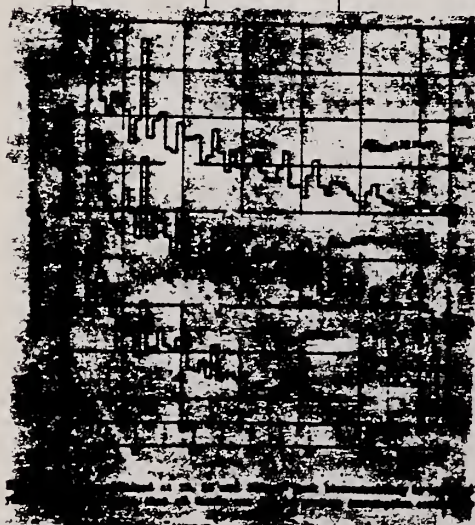
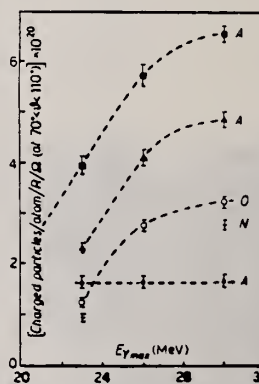
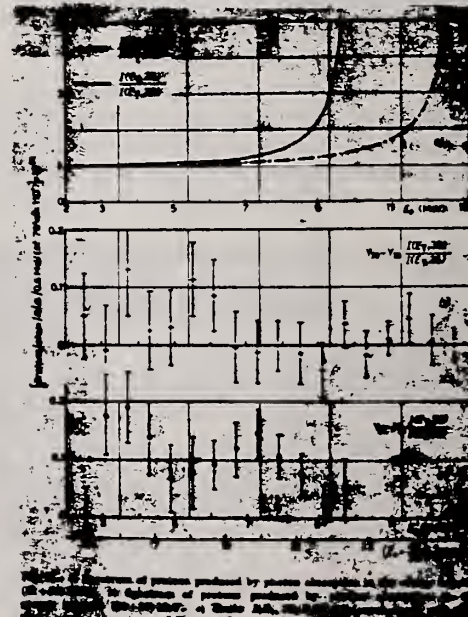


Fig. 4. - Photoalpha cross-section in argon as a function of alpha particle energy. Points \triangle , \diamond , \square refer to $E_{\gamma, \text{max}} = 23, 26, 30$ MeV irradiations respectively.



Ref. A.S. Penfold, E.L. Garwin
Phys. Rev. 114, 1139 (1959)

Elem. Sym.	A	Z
Ar	40	18

Method Betatron; activation

Ref. No.	JHH
59 Pe 1	

Reaction	E or ΔE	E_0	Γ	$\int \sigma dE$	$J\pi$	Notes
$Ar^{40}(\gamma, p)$	Bremss. 14-44	23.5				
$Ar^{40}(\gamma, np)$		27.5				
$Ar^{40}(\gamma, n)$		16.5				
$Ar^{40}(\gamma, 2n)$		20				
$Ar^{40}(\sigma_t)$		23.5	10.3 MeV	$\int_0^{23} = 470 \pm 70$ MeV-mb ($\pm 15\%$) $\int_0^{40} = 900 \pm 180$ MeV-mb ($\pm 20\%$)		Re-analysis of data of McPherson, Pederson and Katz [Can. J. Phys. <u>32</u> , 593 (1954)] $\sigma_{max}(E = 23.5 \text{ MeV}) = 86 \text{ mb}$

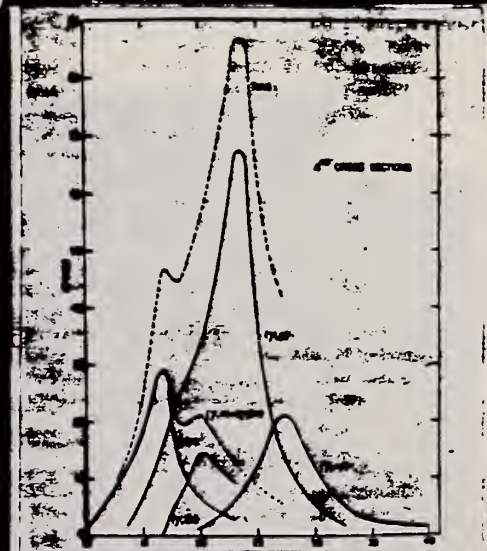
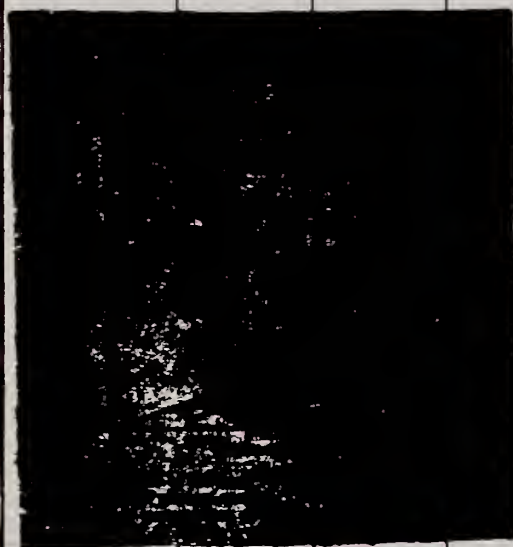




FIG. 3. The photo-neutron reaction cross sections of Ar^{40} plotted as a function of photon energy.

Ref. H.G. Dosch, K.H. Lindenberg, P. Brix
Nuclear Phys. 18, 615 (1960)

Elem. Sym.	A	Z
Ar	40	18

Method 35 MeV betatron; activation; methane flow β counter.

Ref. No.	
60 Do 1	JHH

Reaction	E or ΔE	E ₀	Γ	∫σdE	Jπ	Notes
(γ, p)	Bremss. 30 34			$\int_0^{33} = 100 \pm 15 \text{ MeVmb}$		Data as referenced to C ¹² (γ, n) and Cu ⁶³ (γ, n) in Table 3; compared with other measurements in Table 4.
(γ, np)				$\int_0^{33} = 25 \pm 10 \text{ MeVmb}$		
						
						
Ref 9:		Harber, George and Reagan, Phys. Rev. <u>98</u> , 73 (1958)				
Ref 11:		Herman and Brown, Phys. Rev. <u>96</u> , 83 (1954)				
Ref. 3:		Brix, Kording, Lindenberg, Z. Physik <u>154</u> , 569 (1959).				
Ref. 4:		Penfold and Garwin, Phys. Rev. <u>114</u> , 1139 (1959)				
Ref 13:		Iavor, Soviet JETP <u>34</u> , 983 (1958)				
Ref 17:		Golden Zaffarano and Martin, private communication and Bull Am. Phys. Soc <u>5</u> , 57 (1960).				
Ref 18:		Gorbunow and Spiridonov, Soviet JETP <u>6</u> , 16 (1958).				

Ref. R.W. Fast, P.A. Flournoy, R.S. Tickle, W.D. Whitehead Phys. Rev. <u>118</u> , 535 (1960)						Elem. Sym. Ar	A 40	Z 18
Method 70 MeV Synchrotron; B F ₃ ctrs.						Ref. No. 60 Fa 1		JH
Reaction	E or ΔE	E ₀	Γ	∫ σ dE	J π	Notes		
(γ, n)	~10-50	21	10	0.392 ²⁵ MeV 10 MeV-barns 0.598 ⁵⁰ 10 MeV-barns		σ _{max} (21 MeV) = 41 mb. No correction for neutron multiplicity hence tail (σ = 6 mb at 40 MeV) pro- bably too high, as well as being not statistically significant.		

E. Finckh, U. Hegel
Z. Physik 162, 154 (1961)

ELEM. SYM.	A	Z
A	40	18
REF. NO.		NVB
61 F1 1		

METHOD					
Betatron; proton yield; CsI; $C^{12}(\gamma, n)C^{11}$ monitor					
REACTION	RESULT	EXCITATION ENERGY	SOURCE		ANGLE
			TYPE	RANGE	
G, P	RLY	0 - 35	C	35	90
		(0 - 34.5)		(34.5)	

$$\frac{\text{Yield of } A(\gamma, p)}{\text{Yield of } C^{12}(\gamma, n)C^{11}} = 2.45 \pm 14\%$$

REF.

A.P. Komar, B.A. Bochagov, G.E. Solyakin
 Dokl. Akad. Nauk SSSR 141, 1339 (1961); Soviet Phys.
 Doklady 6, 1088 (1962)

ELEM. SIM.

A

40

18

METHOD

Synchrotron; alpha spectrum; multigrid ion chamber

REF. NO.

61 Ko 1

NVB

REACTION	RESULT	EXCITATION ENERGY	SOURCE		DETECTOR		ANGLE
			TYPE	RANGE	TYPE	RANGE	
G,A	SPC	10 - 17	C	70	ION-D	3-12	90

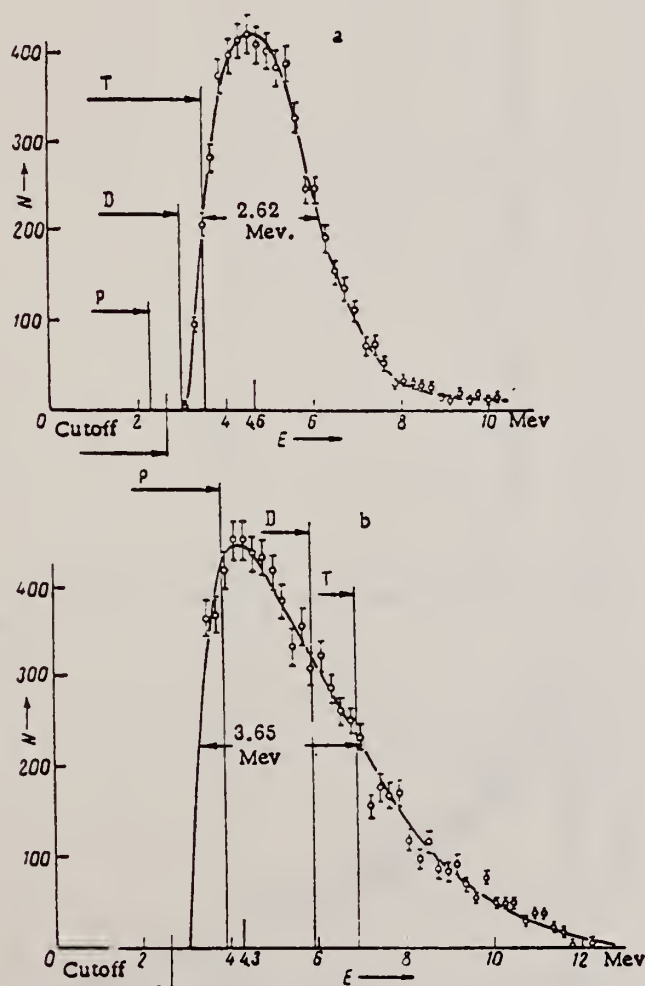


Fig. 2. Energy spectra of α particles produced in the photodisintegration of argon. a) At a pressure of 1 atm; b) 3 atm.

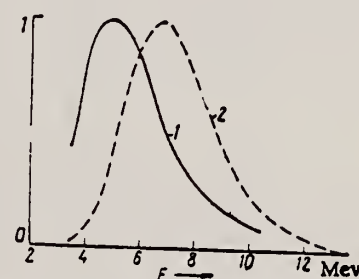


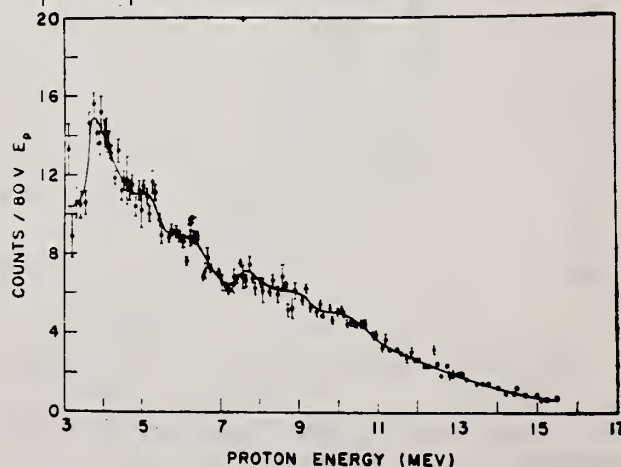
Fig. 3. Comparison of the experimental energy distribution of α particles and the energy distribution calculated from statistical theory for the reaction $A^{40}(\gamma, \alpha)S^{36}$. 1) Experimental spectrum; 2) calculated spectrum.

Ref. W. R. Dodge, W. C. Barber
Phys. Rev. 127, 1746 (1962)

Elem. Sym.	A	Z
Ar	40	18
Ref. No.		BG
62Do1		

Method
Magnetic analysis of proton spectrum produced by electron bombardment

Reaction	E or ΔE	E_0	Γ	$\int \sigma dE$	$J\pi$	Notes
(e,p)	30	$E_p = 3.6 \pm .1$		See notes		<p>Correspondence between (e,pe') reaction and (γ,p) reaction. Assumed electron has associated with it a virtual photon spectrum. Electron production yields were analyzed by use of E1 virtual photon spectrum to obtain $\sigma(\gamma,p)$.</p> <p>62 MeV-mb $\int_{E_p=3.1}^{E_p=15.25} \sigma(\gamma,p) dE_\gamma < 110 \text{ MeV-mb}$</p>



Ref. W.C. Barber, J. Goldemberg, G.A. Peterson, Y. Torizuka
Nuclear Phys. 41, 461 (1963)

Elem. Sym.	A	Z
Ar	40	18

Method Linac (Stanford Mark II); counter telescope; magnet

Ref. No.	BG
63 Ba 1	

Reaction	E or ΔE	E_0	Γ	$\int \sigma dE$	$J\pi$	Notes
$\text{Ar}^{40}(e, e)$	41.5					<p>No resonances</p> <p>Ground state 0^+</p> <p>Detector at 180°</p>

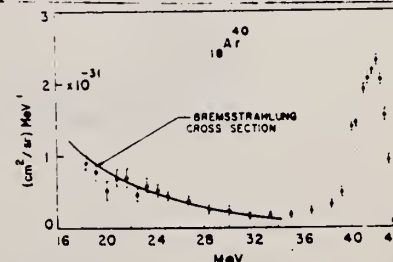


Fig. 16. Spectrum of 41.5 MeV electrons scattered from an Ar^{40} gas target at 180°

REACTION	RESULT	EXCITATION ENERGY	SOURCE		DETECTOR		ANGLE
			TYPE	RANGE	TYPE	RANGE	
G ₂ N+P	ABY	THR - 31	C	18 - 31	ACT-I		4PI

Tabelle 1

E_0 MeV	Ausbeute $Y(E_0)$ $\text{Ar}^{40}(\gamma, n) + \text{Ar}^{40}(\gamma, p)$ $\mu\text{b/MeV}$	Ausbeute $Y(E_0)$ $\text{Ar}^{38}(\gamma, n)$ $\mu\text{b/MeV}$	E_0 MeV	Ausbeute $Y(E_0)$ $\text{Ar}^{40}(\gamma, n) + \text{Ar}^{40}(\gamma, p)$ $\mu\text{b/MeV}$	Ausbeute $Y(E_0)$ $\text{Ar}^{38}(\gamma, n)$ $\mu\text{b/MeV}$
18,1	$299 \pm 17\%$	$131 \pm 25\%$	26,4	$510 \pm 3\% *$	$303 \pm 3\% *$
20,1	$418 \pm 10\%$	$217 \pm 12\%$	28,6	$535 \pm 2\%$	$330 \pm 3\%$
22,1	$547 \pm 7\%$	$286 \pm 9\%$	30,7	$516 \pm 2\%$	$337 \pm 3\%$
24,3	$563 \pm 3\%$	$322 \pm 4\%$			

* Da die Ergebnisse der Bestrahlung bei 26,4 MeV für beide Isotope zu klein ausfallen, das Verhältnis der Ausbeute beider Isotope jedoch mit den Werten bei anderen Endenergien übereinstimmt, scheint bei dieser Bestrahlung ein Fehler bei der Kammerjustierung unterlaufen zu sein.

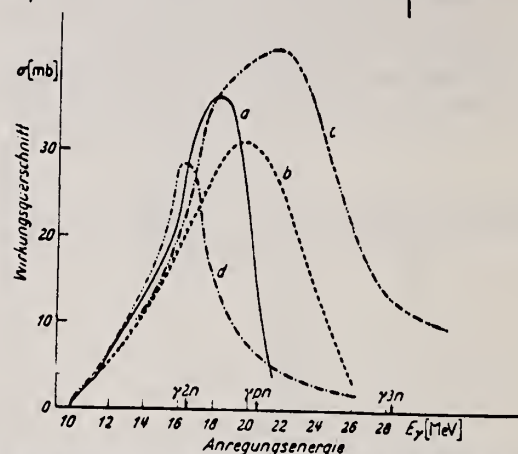


Fig. 4. Energieabhängigkeit des Wirkungsquerschnittes der Reaktion $\text{Ar}^{40}(\gamma, n)$, a) nach dieser Arbeit, d) nach PENFOLD und GARWIN⁴; Energieabhängigkeit des Wirkungsquerschnittes für Neutronenemission b) nach FERGUSON et al.⁵, c) nach FAST et al.¹⁰

Tabelle 2

Reaktion	Schwelle ²⁰ MeV	Resonanz- maximum MeV	Resonanz- breite MeV	$\int \sigma(E) dE$ MeVmb	Herkunft der Daten
1. $\text{Ar}^{40}(\gamma, n)$	9,875	18,5	5	200 ± 40	Fig. 5, Kurve a
2. $\text{Ar}^{40}(\gamma, p)$	12,523	23,5	5	100 ± 15	Fig. 5, Kurve b
3. $\text{Ar}^{40}(\gamma, 2n)$	16,460	22,5	6	130 ± 30	Fig. 5, Kurve c
4. $\text{Ar}^{40}(\gamma, pn)$	20,593	27,5	6	22 ± 3	Fig. 5, Kurve d
5. $\text{Ar}^{40}(\gamma, \alpha)$	6,809	—	—	5	IAVOR ³
6. $\text{Ar}^{40}(\gamma, 2p)$	22,810	—	—	1	IAVOR ³
7. $\text{Ar}^{40}(\gamma, 3n)$	28,3	—	—	—	—
8. $\text{Ar}^{40}(\gamma \text{ abs})$	—	19	10	450 ± 60	—

* Der Wert von 0,05 ergibt sich für den Nachbarkern Ca^{40} nach einer Abschätzung entsprechend den Rechnungen von MORINAGA¹⁹.

¹⁹ MORINAGA, H.: Phys. Rev. 97, 1185 (1955).

²⁰ Nuclear Data Tables, USAEC, Washington, 1961.

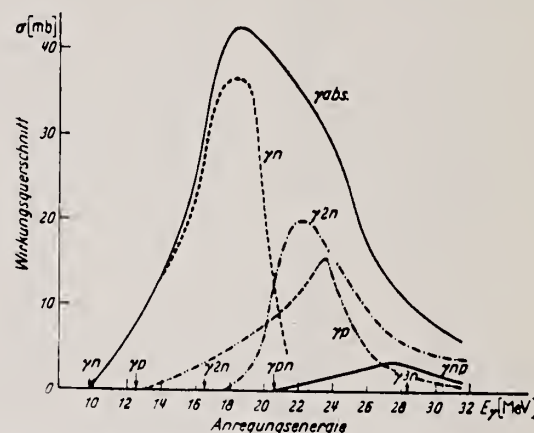


Fig. 5. Energieabhängigkeit der Partialwirkungsquerschnitte zum Kernphotoeffekt am Ar^{40} . a) $\sigma(\gamma, n)$ diese Arbeit. b) $\sigma(\gamma, p)$ nach PENFOLD und GARWIN⁴, normiert nach DOSCH et al.⁷. c) $\sigma(\gamma, 2n)$ nach GL (1). Nähere Erläuterungen im Text. d) $\sigma(\gamma, pn)$ nach PENFOLD und GARWIN⁴, normiert nach DOSCH et al.⁷. e) σ_{abs} als Summe von a) bis d) nach GL (2).

METHOD

Sources: 9.17 MeV $C^{13}(p,\gamma)$, 17.64 MeV $Li^7(p,\gamma)$

[Page 1 of 2]

REF. NO.

65 Re 1

EGF

REACTION	RESULT	EXCITATION ENERGY	SOURCE		DETECTOR		ANGLE
			TYPE	RANGE	TYPE	RANGE	
G,P	ABX	9.17	D	9.17	CCH-D		4PI
G,A	ABX	9.17	D	9.17	CCH-D		4PI

2.29 α peak corresponds to g.s. transition $\sigma = 31 \pm 6 \mu b$

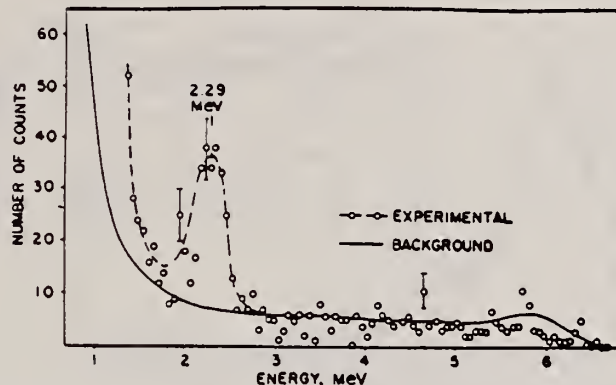


Fig. 1. The photodisintegration of ^{40}Ar at 9.17 MeV showing the photoalpha peak. The background, shown normalized to the same running time, was obtained with the proton energy off the target resonance.

TABLE I
Experimental results at 17.71 MeV

Spectrum peak	Reaction	Remarks	Q value (MeV)	Cross section (mb)
A	$^{40}Ar(\gamma, \alpha)^{36}S$	to ground state of ^{36}S	-6.6 ± 0.4	0.08 ± 0.05
B	$^{40}Ar(\gamma, \alpha)^{36}S$	to excited state(s) of ^{36}S at ≈ 3.5 MeV	-10.1 ± 0.1	0.35 ± 0.06
C	$^{40}Ar(\gamma, \alpha)^{36}S$	to excited state(s) of ^{36}S at ≈ 4.7 MeV	-11.3 ± 0.1	0.40 ± 0.08
	$^{40}Ar(\gamma, \alpha)^{36}S$	total cross section		0.83 ± 0.16 (± 0.09)
D	$^{40}Ar(\gamma, p)^{39}Cl$	to ground state of ^{39}Cl	-12.46 ± 0.1	1.15 ± 0.2
	$^{40}Ar(\gamma, p)^{39}Cl$	to excited states of ^{39}Cl at ≈ 0.5 MeV	-12.99 ± 0.1	1.26 ± 0.2
F, G	$^{40}Ar(\gamma, p)^{39}Cl$	to excited states of ^{39}Cl		4.75 ± 1.0
	$^{40}Ar(\gamma, p)^{39}Cl$	total cross section		7.16 ± 1.26 (± 0.56)

The uncertainties in brackets are estimated on the assumption that the efficiency of the gamma counter is known exactly.

REACTION	RESULT	EXCITATION ENERGY	SOURCE		DETECTOR		ANGLE
			TYPE	RANGE	TYPE	RANGE	

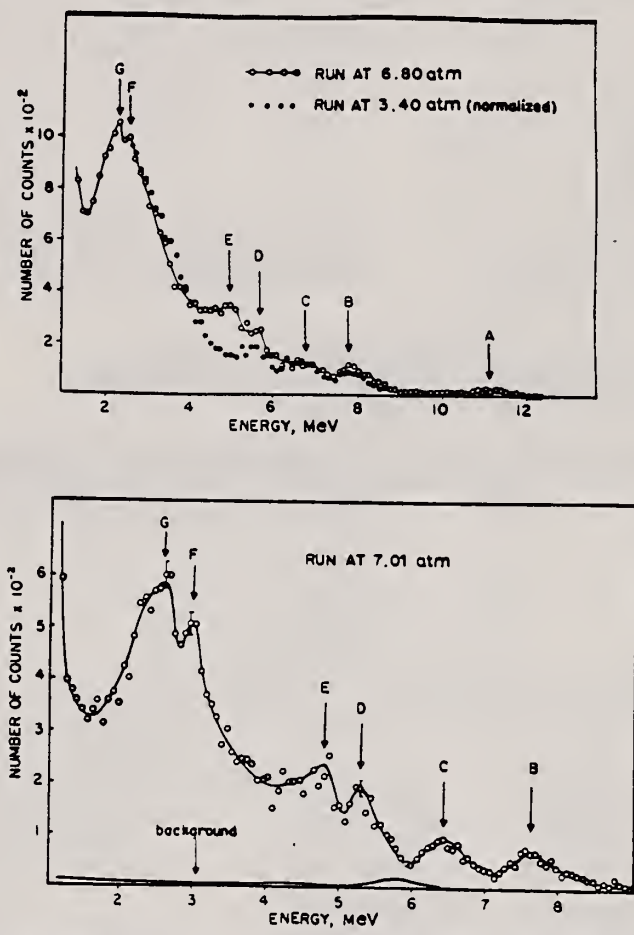


Fig. 2. The photodisintegration of ⁴⁰Ar at 17.71 MeV. The group at A and the peaks B and C we attribute to photoalpha particles leaving ³⁶S in its ground and lower excited states, respectively. Peaks D and E and the group G, F are identified with proton transitions to the ground, first and higher excited states of ³⁹Cl.

REF. R. Wendling and R. Kosiek Z. fur Physik <u>192</u> , 502 (1966)				ELEM. SYM. Ar		A 40		Z 18	
METHOD f				REF. NO. 66 We 2				EGF	
REACTION	RESULT	EXCITATION ENERGY	SOURCE		DETECTOR		ANGLE		
			TYPE	RANGE	TYPE	RANGE			
G,A	ABX	7-33	C	33	SCD-D	4-16	90		
				(32.5)					

Tabelle

Element	Dicke (mg/cm ²)	Gesamt- auflösung (keV)	Gesamtzahl gemessener α-Teilchen	Ausbeute (μb/MeV · ster)	Ausbeute 10 ⁴ Nα Mol · r	E _{max} (exp) (MeV)	E _{max} (McV)
Al	2,35	770	14600	1,3 ± 0,2	3,5 ± 0,6	(≈ 3,5)	3,5
Ar	200 Torr	480	5200	3,0 ± 0,5	8,3 ± 1,3	5,2	3,5
Se	3,72	790	12200	0,28 ± 0,04	0,76 ± 0,12	9,2	4,5
Ag	3,12	670	3150	0,12 ± 0,02	0,33 ± 0,05	11,8	6,5

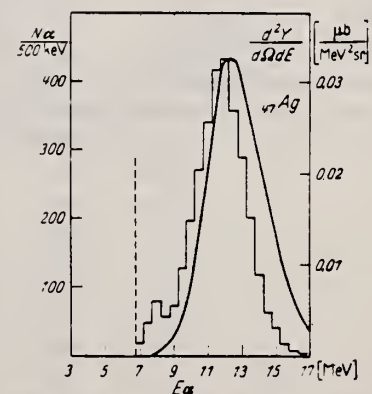
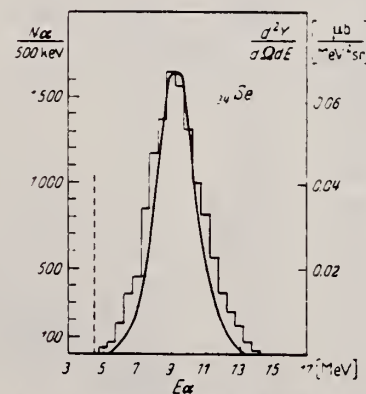
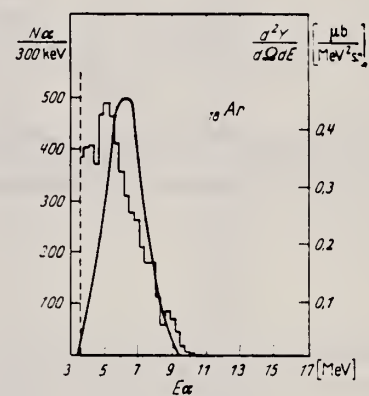
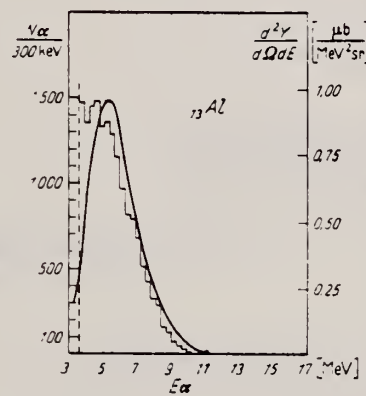


Fig. 1. a Histogramm: Gemessene Energieverteilung und differentielle Ausbeute der Photo-α-Teilchen.
b Kurve: Berechnetes Spektrum. Nähere Angaben im Text

METHOD					REF. NO.		egf
					69 Ho 1		
REACTION	RESULT	EXCITATION ENERGY	SOURCE		DETECTOR		ANGLE
			TYPE	RANGE	TYPE	RANGE	
G,XP	ABY	THR- 33	C	24-33	SCI-D	3-14	90

500

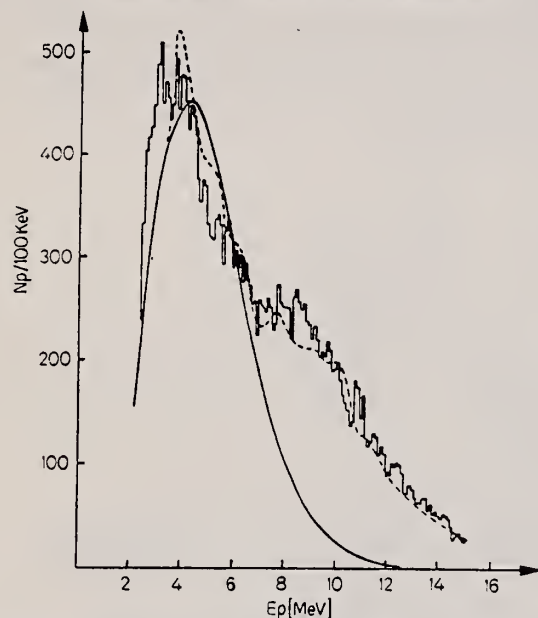


Fig. 9. Histogramm: Energieverteilung der Photoprotonen aus ^{40}Ar für $E_0 = 32,5$ MeV. Kurve gestrichelt: Ergebnis der $(e, e'p)$ -Messung von DODGE und BARBER³ für $E_0 = 70$ MeV. Kurve ausgezogen: Berechnetes Verdampfungsspektrum für $E_0 = 32,5$ MeV

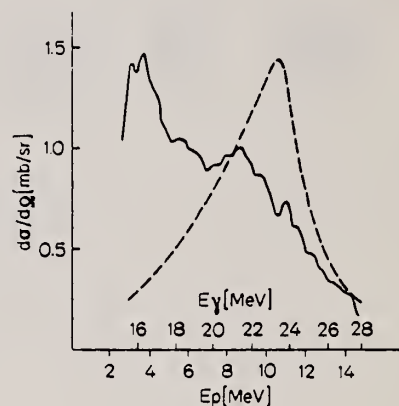


Fig. 11

Fig. 11. Aus Fig. 9 berechneter (γ, p) -Wirkungsquerschnitt für ^{40}Ar . Gestrichelte Kurve: (γ, p) -Wirkungsquerschnitt nach PENFOLD und GARWIN

Tabelle 1. Daten zu den einzelnen Reaktionen. Die Werte für den integrierten Wirkungsquerschnitt wurden unter der Annahme ausschließlicher Grundzustandsübergänge berechnet. Für ^{23}Na und ^{39}K als Ausnahme s. Text

Tar-get	Anreiche-rungsgrad	(γ, p) -Schwelle MeV	Druck oder Dicke	End-energie MeV	Zahl geness. Protonen	Ausbeute $\mu\text{b/MeV sr}$	$\int \sigma(E) dE$ 32.5 MeVmb	Figur
^{16}O	99	16,0	230 Torr	32,5	36074	58 ± 7	38 ± 6	1, 2
^{20}Ne	90,9	12,8	450 Torr	28,0	3175	$7,4 \pm 1$	—	—
			610 Torr	32,5	6293	$14,9 \pm 2$	61 ± 11	5, 6
^{22}Ne	99,9	15,3	240 Torr	24,0	1960	$2,3 \pm 0,4$	—	4, 5
				28,0	4790	$3,6 \pm 0,6$	—	4, 5
				32,5	5210	$6,7 \pm 0,9$	45 ± 8	4, 5
^{23}Na	100	8,8	65 μ	24,0	14182	$6,3 \pm 1,0$	—	7
			60 μ	32,5	11152	$12,8 \pm 2,0$	117 ± 30	7
^{36}Ar	99	8,5	250 Torr	32,5	45173	57 ± 6	270 ± 40	8, 10
^{40}Ar	99,0	12,5	230 Torr	32,5	29559	$14,2 \pm 15$	104 ± 15	9, 11
^{39}K	93,1	6,4	80 μ	24,0	24230	$17,4 \pm 2,8$	—	12
			90 μ	32,5	24941	$41,9 \pm 6,7$	405 ± 100	12
^{84}Kr	99	10,7	170 Torr	32,5	35515	$12,7 \pm 2,0$	80 ± 20	14
Kr	natürl.	10	170 Torr	32,5	13570	$12,5 \pm 2,0$	75 ± 20	13
Xe	natürl.	9	150 Torr	32,5	7553	$7,6 \pm 0,9$	40 ± 7	15

REF.

K.H. Lokan, N.K. Sherman, R.W. Gellie, J.W. Jury, J.I. Lodge,
and R.G. Johnson
Phys. Rev. Letters 28, 1526 (1972)

ELEM. SYM. A Z

Ar

40

18

METHOD

REF. NO.

72 Lo 2

hmg

REACTION	RESULT	EXCITATION ENERGY	SOURCE		DETECTOR		ANGLE
			TYPE	RANGE	TYPE	RANGE	
G,N	ABX	10-13	D	13	TOF-D		90
		(10.4-12.6)		(12.6)			

TABLE I. Transition strengths for excited states of ^{40}Ar .

Excitation Energy (MeV)	Area of Resonance (MeV-mb/ster)	$g_{\gamma_0}^a$ (eV)	$\Gamma_{\gamma_0}^b$ (eV)
10.393	(0.075)	(11.3)	(7.5)
10.418	(0.064)	(9.6)	(6.4)
10.451	(0.033)	(5.0)	(3.3)
10.481	(0.033)	(5.0)	(3.4)
10.573	0.047	7.3	4.9
10.593	0.052	8.1	5.4
10.640	0.059	9.3	6.2
10.680	0.044	7.0	4.6
10.725	0.044	7.0	4.7
10.762	0.080	12.8	8.5
10.813	0.072	11.7	7.8
10.92	0.080	13.2	8.8
11.05	0.031	5.2	3.5
11.09	0.066	11.2	7.5
11.20	0.042	7.3	4.8
11.26	0.034	6.0	4.0
11.34	0.050	8.9	5.9
11.43	0.062	11.2	7.4
11.51	0.083	15.2	10.1
11.67	0.023	4.4	3.0
11.71	0.018	3.5	2.3
11.81	0.060	11.5	7.7
11.90	0.047	9.2	6.2
12.06	0.045	9.1	6.0
(12.16)	(0.042)	(8.7)	(5.8)
12.27	0.022	4.6	(3.1)
12.41	(0.02)	(4.5)	(3.0)

^a Assuming angular distribution $1 + \frac{1}{2} \sin^2 \theta$.

^b Assuming $g = \frac{1}{2}$.

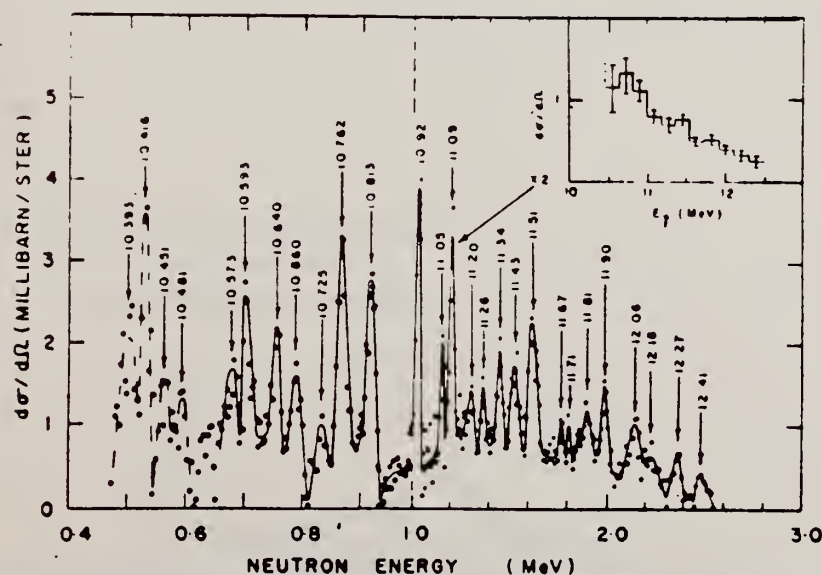


FIG. 2. Differential cross section at 90° for the reaction $^{40}\text{Ar}(\gamma, n)^{40}\text{Ar}$. Note the change of scale at a neutron energy of 1 MeV. The inset shows the same cross section plotted as a function of photon energy, and averaged over 200-keV intervals.

U.S. DEPARTMENT OF COMMERCE
NATIONAL BUREAU OF STANDARDS

REF. R. Bergere, H. Beil, P. Carlos, A. Lepretre, A. Veyssiere
 PICNS-73, Vol. I, p. 525 Asilomar

ELEM. SYM.	A	Z
Ar	40	18

METHOD	REF. NO.	
	73 Be 10	hmg

REACTION	RESULT	EXCITATION ENERGY	SOURCE		DETECTOR		ANGLE
			TYPE	RANGE	TYPE	RANGE	
G, SN	ABX	11- 27	D	11- 27	BF3-I		4PI
G, 2N	ABX	16- 27	D	16- 27	BF3-I		4PI

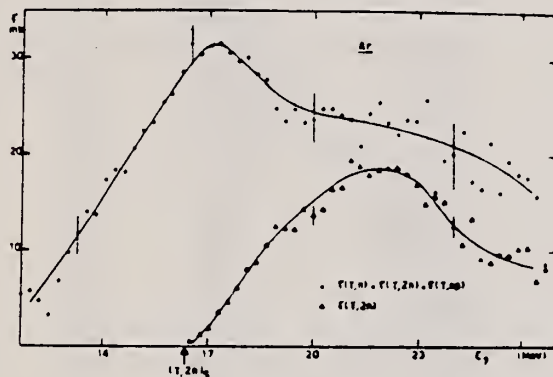


Fig. 11 Partial photoneutron $\sigma(\gamma, n) + \sigma(\gamma, pn)$ and $\sigma(\gamma, 2n)$ cross sections of ^{40}Ar .

ELEM. SYM.	A	Z
Ar	40	18
REF. NO.		
73 Ju 1		hmg

METHOD					REF. NO.	
					73 Ju 1	hmg
REACTION	RESULT	EXCITATION ENERGY	SOURCE		DETECTOR	
			TYPE	RANGE	TYPE	RANGE
G, XN	ABX	10- 23	C	13- 23	TOF-D	

$$\int_0^{23} \tau(\gamma, xn) dE = (260 \pm 60) \text{ MeV-mb.}$$

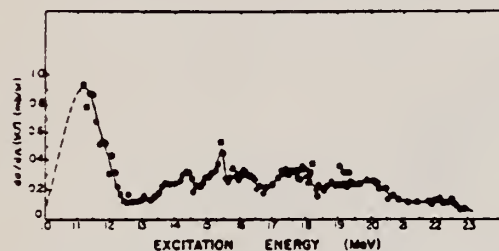


FIG. 5. Ground state neutron cross section over the entire region studied. Data have been averaged over 200 keV intervals. The data are a collage of results obtained using 11 different end-point energies. Statistical errors are approximately the diameter of the circles.

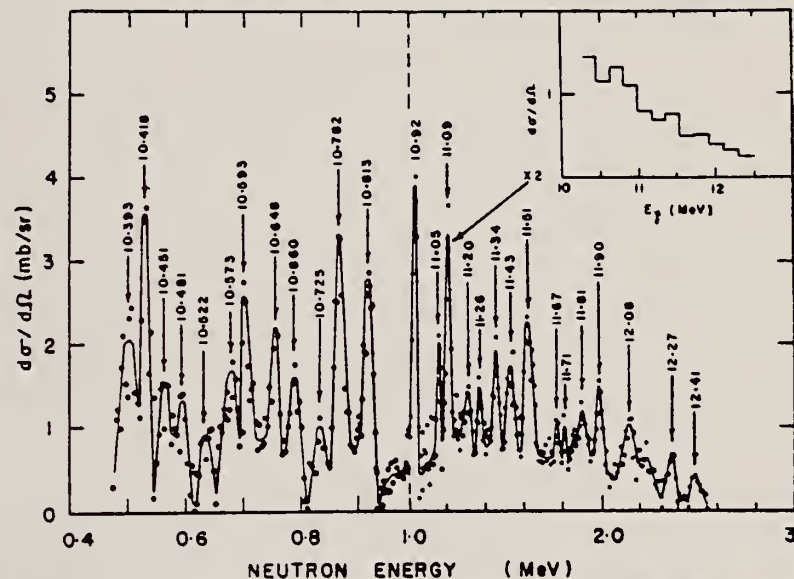


FIG. 4. The 90° differential photoneutron cross section for the reaction $^{40}\text{Ar}(\gamma, n)^{39}\text{Ar}$ in the low energy region. Note changes in both vertical and horizontal scales.

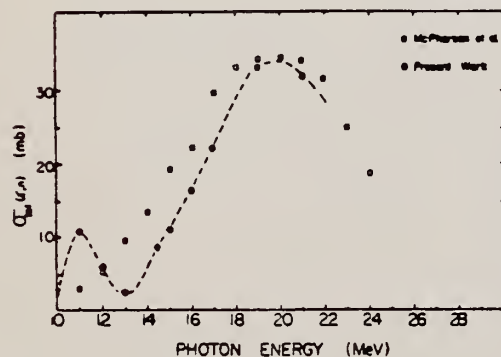


FIG. 9. The total photoneutron cross section for ^{40}Ar .

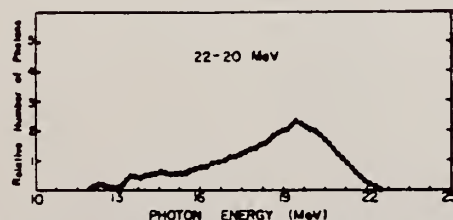


FIG. 7. An example of a photon difference spectrum obtained by subtracting two bremsstrahlung intensity distributions.

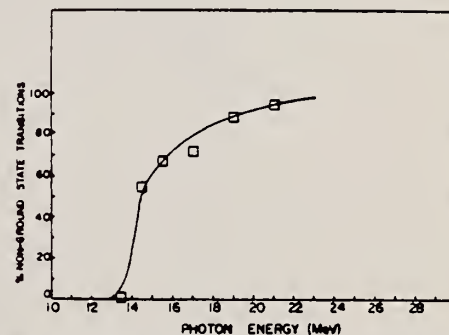


FIG. 8. The energy dependence of the relative number of non-ground state transitions from excited states in ^{40}Ar . 100% means that all photoneutrons are emitted during decays to excited states of ^{39}Ar .

REF.

A. Veyssiere, H. Beil, R. Bergere, P. Carlos, A. Lepretre, and
A. De Miniac
Nucl. Phys. **A227**, 513 (1974)

ELEM. SYM.

A

C

Ar

40

18

METHOD

REF. NO.

74 Ve 1

egf

REACTION	RESULT	EXCITATION ENERGY	SOURCE		DETECTOR		ANGLE
			TYPE	RANGE	TYPE	RANGE	
G,N *	ABX	10- 27	D	10- 27	BF3-I		4PI
G,2N **	ABX	16- 27	D	16- 27	BF3-I		4PI

* 899+

** 900

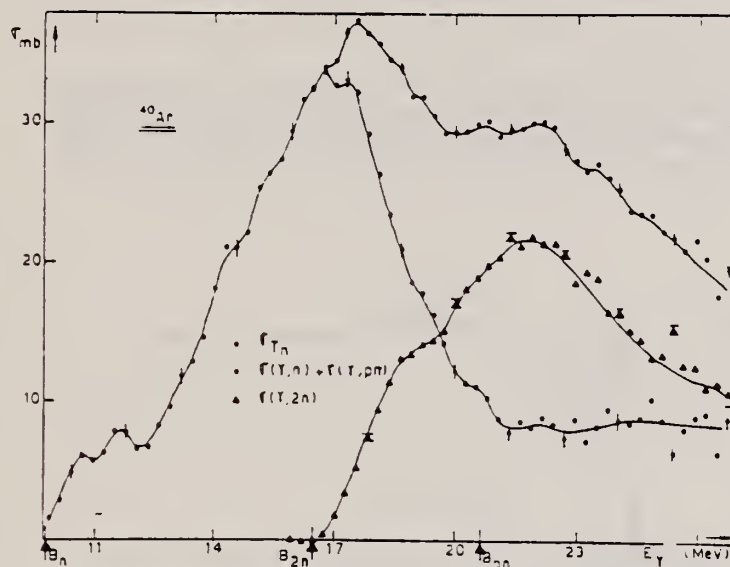


Fig. 12. Photoneutron cross sections σ_{Tn} , $[\sigma(\gamma, n) + \sigma(\gamma, pn)]$ and $\sigma(\gamma, 2n)$ of ^{40}Ar .

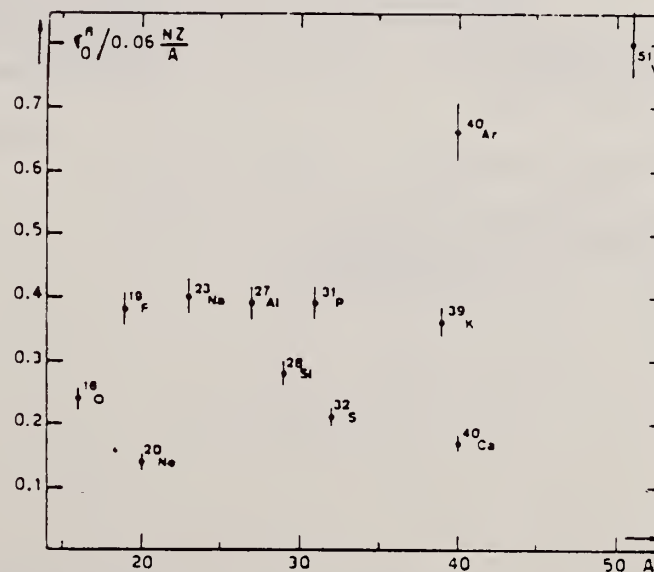


Fig. 22. Ratio of experimental integrated photoneutron cross section σ_0^* over the Thomas, Reiche and Kuhn sum rule $[0.06 NZ/A]$. Numerical values and upper integration limits E_M are taken from table 3. Also $\Delta\sigma_0^* = \pm 7\%$ for all nuclei.

FORM NBS-418
(REV. 7-14-64)
USCOMM-OC 26010-P64

DEPT OF COMMERCE
BUREAU OF STANDARDS

(over)

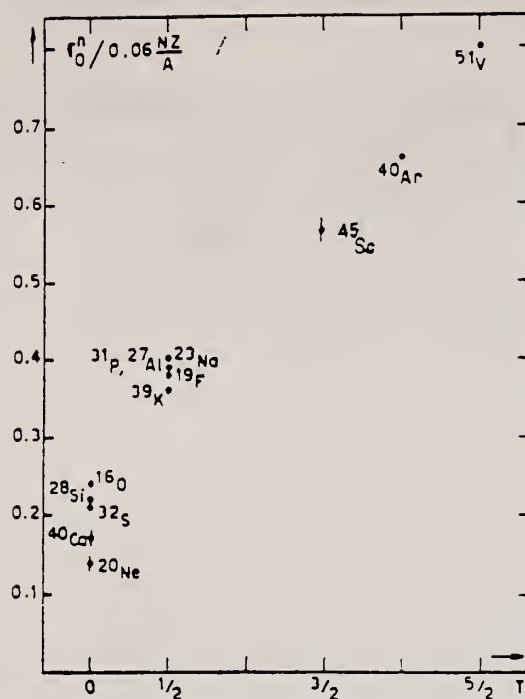


Fig. 24. The $[\sigma_0^n / (0.06 NZ/A)]$ ratio as a function of isospin T . Possible overall errors of $\pm 7\%$ are to be applied to all nuclei shown.

TABLE 3
Experimental integrated photoneutron cross sections $\sigma_0^n = \int_0^{E_N} \sigma_{Tn}(E) dE$ compared with the classical sum rule $[0.06 NZ/A]$ of Thomas, Reich and Kuhn

	$T = 0$					$T = \frac{1}{2}$					$T = \frac{3}{2}$	$T = 2$	$T = \frac{5}{2}$
Nucleus	^{16}O	^{20}Ne	^{28}Si	^{32}S	^{40}Ca	^{19}F	^{23}Na	^{27}Al	^{31}P	^{39}K	^{43}Sc	^{40}Ar	^{51}V
σ_0^n (MeV · mb)	58 ± 4	42 ± 3	94 ± 7	98 ± 7	100 ± 7	108 ± 7	137 ± 9	158 ± 10	132 ± 12	210 ± 14	383 ± 25	393 ± 28	602 ± 42
$\sigma_0^n / (0.06 NZ/A)$	0.24	0.14	0.22	0.21	0.17	0.38	0.40	0.39	0.39	0.36	0.57	0.66	0.8
E_N (MeV)	30	26.7	30	30	29.5	29	30	30	29	30	28.1	26.7	28

REF.

I.I. Chkalov, H.G. Shevchenko, A.Yu. Buki, A.A. Khomich,
A.S. Litvinenko, and V.N. Polishchuk
Yad. Fiz. 22, 893 (1975)
Sov. J. Nucl. Phys. 22, 464 (1976)

ELEM. SYM.	A	Z
Ar	40	18
REF. NO.		hmg
75 Ch 4		

METHOD

REACTION	RESULT	EXCITATION ENERGY	SOURCE		DETECTOR		ANGLE
			TYPE	RANGE	TYPE	RANGE	
$E, E/$	SPC	0- 35	D	151,164	MAG-D		DST

Experimental results are presented of a study of the fine structure of the giant resonance in the nuclei ^{20}Ne and ^{40}Ar by the method of inelastic scattering of electrons. A correlation is observed between the energy positions of the maxima of the fine structure of the giant resonance in the nuclei ^{20}Ne and ^{40}Ar , on the one hand, and the positions of the discrete levels in the respective nuclei ^{19}F and ^{39}Ar , on the other.

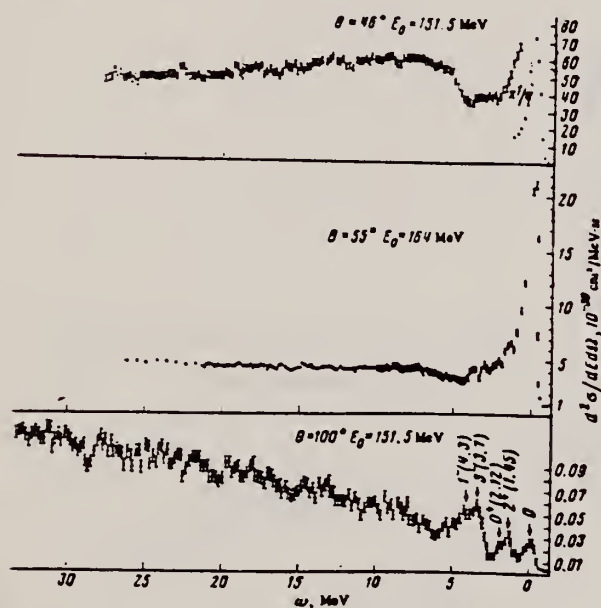
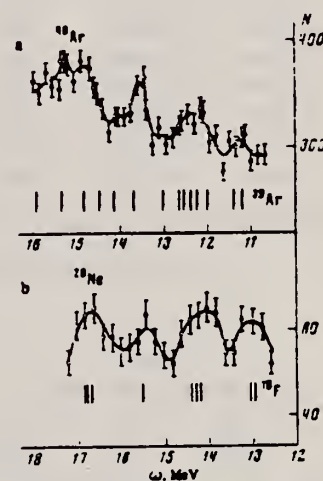
FIG. 2. Spectra of electrons scattered by ^{40}Ar .

FIG. 3. Fine structure of the giant resonance in the nuclei ^{40}Ar (a) and ^{20}Ne (b) at $\theta = 100^\circ$ and $E_0 = 152$, and the discrete-level schemes of the nuclei ^{39}Ar and ^{19}F .

ELEM. SYM.	A	Z
Ar	40	18
REF. NO.		
77 Fi 5		egf

METHOD					REF. NO.		
					77 F1 5	egf	
REACTION	RESULT	EXCITATION ENERGY	SOURCE		DETECTOR		ANGLE
			TYPE	RANGE	TYPE	RANGE	
E,E/	ABX	1- 3	D	65,115	MAG-D		DST

Abstract: The low-lying level structure of ^{36}Ar and ^{40}Ar has been investigated using the technique of inelastic electron scattering. Data were collected at the National Bureau of Standards Linear Accelerator with incident electron energies between 65 and 115 MeV and scattering angles of 92.5° and 110° . The data span a range of momentum transfer squared between 0.29 and 0.92 fm^{-2} . Tassie model and Helm model analyses have been applied to data for levels at 1.97 and 4.18 MeV in ^{36}Ar and at 1.46, 2.52, 3.21 and 3.68 MeV in ^{40}Ar . A 2^+ assignment to the 3.21 MeV state in ^{40}Ar is suggested. Transition strengths, transition radii, and mean lifetimes for these states are computed and compared with results of previous experiments.

1.46, 2.52, 3.21, 3.68

TABLE 2
 ^{40}Ar inelastic scattering cross sections

Incident energy (MeV)	Scattering angle (deg)	Elastic scattering ^{a)} cross section ($\mu\text{b/sr}$)	Inelastic scattering cross section (nb/sr)			
			1.46 MeV (2^+)	2.52 MeV (2^+)	3.21 MeV ($1^+, 2^+$)	3.68 MeV (3^-)
115.80	110.29	0.607	196 ± 4^b	9.3 ± 1.1^b	26.5 ± 1.6^b	181 ± 7
105.49	110.08	2.289	280 ± 9	14.7 ± 3.6	25.9 ± 6.2	197 ± 16
95.56	110.08	6.532	366 ± 10	24.4 ± 3.9	40.3 ± 4.1	202 ± 12
85.36	110.30	16.43	498 ± 16	43.9 ± 6.4	56.0 ± 5.8	190 ± 9
75.22	110.30	38.32	648 ± 77	70.1 ± 15.3	47.9 ± 16.1	188 ± 23
64.94	110.30	85.12	586 ± 32	54.8 ± 12.8	46.6 ± 15.6	124 ± 18
85.25	92.98	72.07	1127 ± 24	112 ± 10	113 ± 12	277 ± 15

^{a)} Phase-shift analysis of Fermi two-parameter fit to the elastic data with $c = 3.532 \text{ fm}$ and $r = 2.373$.

^{b)} Corrected for cell leakage ($< 1\%$ correction).

TABLE 3
Tassie model parameters ^{a)}

Nucleus	ω (MeV)	J^π	$B(EL)^\dagger$ (fm^{2L})	c_α (fm)	t_α (fm)	X_ν^2	ν	R (fm)	$(R_u/R_u^0)^b$
^{40}Ar	1.46	2^+	382 ± 13	2.23 ± 0.12	3.21 ± 0.08	2.84	4	5.21 ± 0.29	1.07 ± 0.06
	2.52	2^+	63.2 ± 11.5	3.09 ± 0.42	3.48 ± 0.39	0.99	4	5.94 ± 0.83	1.22 ± 0.17
	3.21	2^+	29.3 ± 4.0	2.03 ± 0.47	2.95 ± 0.28	1.22	4	4.72 ± 1.07	0.97 ± 0.22
	3.68	3^-	8750 ± 1020	3.25 ± 0.69	2.15 ± 0.46	0.78	4	4.97 ± 1.04	0.91 ± 0.19
^{36}Ar	1.97	2^+	280 ± 16	3.62 ± 0.18	1.76 ± 0.30	0.56	3	4.36 ± 0.24	0.92 ± 0.05
	4.18	3^-	11300 ± 470	4.10 ± 0.25	1.23 ± 0.36	0.68	3	4.58 ± 0.26	0.87 ± 0.05

^{a)} DWBA approximation.

^{b)} $R_u^0 = \langle J^\pi || r^{L+1} || 0^+ \rangle / \langle J^\pi || r^L || 0^+ \rangle$; R_u^0 calculated using ground-state values of c and r .

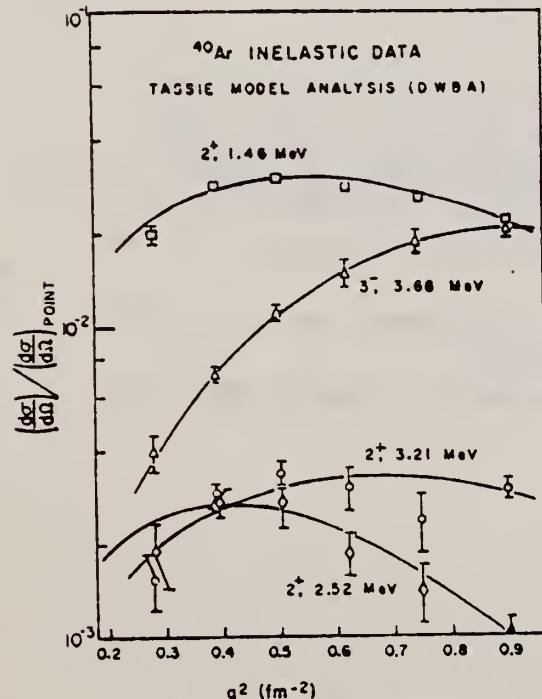


Fig. 2. The ratio of the ^{40}Ar experimental differential cross section to the Coulomb corrected point differential cross section as a function of momentum transfer squared. The smooth curves represent the best fit of the Tassie model to the data.

USCOMM-NBS-DC

TABLE 4
Helm model parameters

Nucleus	ω (MeV)	J^π	$B(CL)$ (fm ²⁴)	R_{ex} (fm)	χ^2	ν
⁴⁰ Ar	1.46	2 ⁺	334 ± 44	4.44 ± 0.11	7.9	5
	2.52	2 ⁺	45 ± 24	4.98 ± 0.38	1.3	5
	3.21	2 ⁺	29 ± 17	4.19 ± 0.50	1.2	5
	3.68	3 ⁻	10800 ± 2900	4.80 ± 0.26	1.0	5
³⁶ Ar	1.97	2 ⁺	330 ± 40	4.42 ± 0.10	1.2	5
	4.18	3 ⁻	16200 ± 2000	4.79 ± 0.15	0.4	5

TABLE 7
Mean lifetimes of ⁴⁰Ar levels

ω (MeV)	Present work ^{a)} (ps)	⁴⁰ Ar(e, e') ⁴⁰ Ar ^{b)} (ps)	⁴⁰ Ar(p, p'γ) ⁴⁰ Ar ^{c)} (ps)	³⁷ Cl(α, pγ) ⁴⁰ Ar ^{d)} (ps)	⁴⁰ Ar + heavy ions ^{e)} (ps)
1.46	1.61 ± 0.06			1.2 ± 0.4 ^{f)}	1.2 ± 0.3 ^{g)}
				2.5 ± ^{1.8} _{1.3} ^{g)}	1.9 ± 0.3 ^{g)}
2.52	0.28 ± 0.05	0.33 ± 0.06	0.54 ± 0.10	0.27 ± 0.07 ^{f)}	
3.21	0.05 ± 0.01		< 0.21		

^{a)} Tassie model analysis. Branching ratios from Endt and Van der Leun, ref. ⁸⁾, used where necessary.

^{b)} Ref. ³⁾.

^{c)} Ref. ¹²⁾, DSA.

^{d)} Ref. ¹³⁾, DSA.

^{e)} Ref. ¹⁴⁾, DSA.

^{f)} Ref. ²⁰⁾, Coulomb excitation.

^{g)} Ref. ⁹⁾, Coulomb excitation.

- ³R.H. Helm, Phys. Rev. 104, 1466 (1956)
- ¹²A.R. Poletti and D.J. Beale, Bull. Am. Phys. Soc. 17, 92 (1972)
- ¹³A.N. James, P.R. Alderson, D.C. Bailey, P.E. Car, J.L. Durell, M.W. Greene and J.F. Sharpey-Schafer, Nucl. Phys. A172, 401 (1971)
- ¹⁴W.M. Curie, L.G. Earwaker, J. Martin and A.K. Sen Gupta, J. of Phys. A3, 73 (1970)
- ²⁰G.M. Gusinskii, K.I. Etokhina and I. Kh. Lemberg, Yad. Fiz. 2, 794 (1965); Sov. J. Nucl. Phys. 2, 567 (1966)
- ⁹K. Nakai, J.L. Quebert, F.S. Stephens and R.M. Diamond, Phys. Rev. Lett. 24, 903 (1970)

ELEM. SYM.	A	Z
Ar	40	18
METHOD		REF. NO.
		79 Ya 1
		hg

REACTION	RESULT	EXCITATION ENERGY	SOURCE		DETECTOR		ANGLE
			TYPE	RANGE	TYPE	RANGE	
G,P	RLY	12-65	C	25-65	ACT-I		4PI
		12.5-65					
G,2P	RLY	22-65					
		22.8-65					

In order to prepare the ^{39}Cl and ^{38}S , the production rates by the $^{40}\text{Ar}(\gamma, p)^{39}\text{Cl}$ and $^{40}\text{Ar}(\gamma, 2p)^{38}\text{S}$ reactions were determined as a function of the maximum bremsstrahlung energy up to 65 MeV, and the optimum irradiation conditions for producing them were established. Then an isotonic saline solution for injection and small amounts of sodium chloride were labeled with the ^{39}Cl at a high specific activity by the use of a recirculatory argon-gas target system.

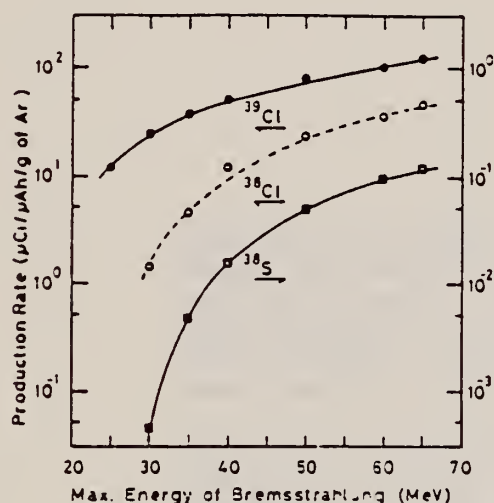


FIG. 2 The production rates of radionuclides on argon target as a function of the maximum energy of bremsstrahlung.

POTASSIUM

Z=19

Potassium (from potash + ium) was recognized as an element in 1807 by Sir Humphry Davy when he electrolysed potash and produced shiny droplets of the reactive metal. It was the first element discovered by electrolytic separation and soon led to the discovery of the alkaline earth metals by a similar method. The alkaline earth metals themselves were destined to become powerful tools in the search for other metals.

K

Jeremiah, in the Old Testament, refers to "wash yourself with lye and use much soap". Both the lye and soap are products of potash. The preparation of potash was the subject of the first United States patent issued to Samuel Hopkins. In the early years of the colonization of America, large areas of woods were burned to obtain the ashes containing potassium carbonate.

K

Elem. Sym.	A	Z
K		19
Ref. No.	59 Em 1	
	EH	

Method Emulsions; bremsstrahlung

Reaction	E or ΔE	E_0	Γ	$\int \sigma dE$	$J\pi$	Notes
(γ, xn)	31					<p>Neutron spectrum measured at 60°, 90°, and 120°. 90° neutron yield same for K at Ca for $E_n > 2$ MeV.</p> <p>Calculated spectrum of form $F(E_n) = \text{const. } E_n \exp. (-E_n/T)$ with $T = 1.1$ MeV are normalized to data at 2 MeV in 90° spectrum.</p>

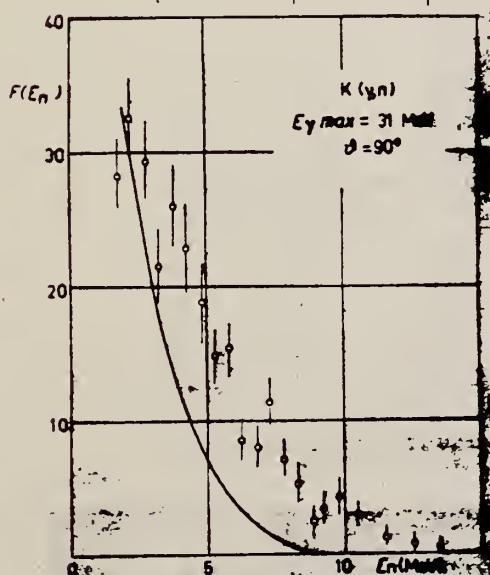


Fig. 4. - Photoneutron spectrum from K at $\theta \sim 90^\circ$.

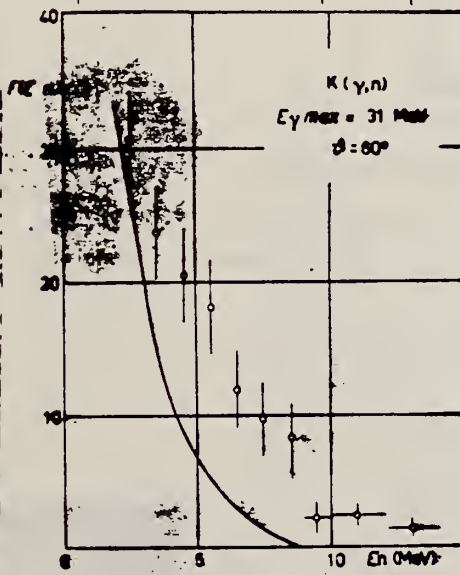


Fig. 5. - Photoneutron spectrum from K at $\theta \sim 60^\circ$.

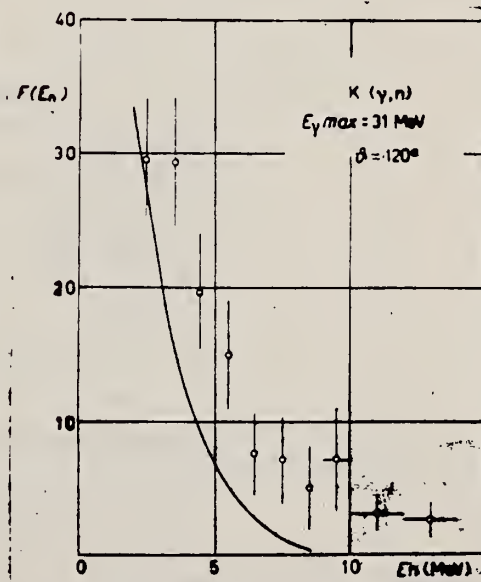


Fig. 6. - Photoneutron spectrum from K at $\theta \sim 120^\circ$.

Elem. Sym.	A	Z
K		19
Ref. No.		NVB
61 To 1		

Method 25 MeV betatron; photon scattering; NaI(Tl) spectrometer;
ion chamber.

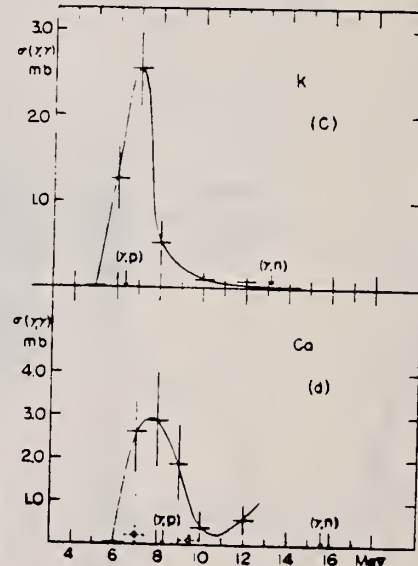
Reaction	E or ΔE	E_0	Γ	$\int \sigma dE$	$J\pi$	Notes
K(γ, γ)	Bremss. 5-12	7.0				Detector at 120° Table II from J. Phys. Soc. Japan <u>18</u> 17-22 (1963)

References

- 1) E. G. Fuller and E. Hayward: Phys. Rev. **101** (1956) 692.
- 2) see E. Segre: *Experimental Nuclear Physics*, vol. 1, p. 346.
- 3) J. S. Levin and D. J. Hughes: Phys. Rev. **101** (1956) 1328.
- 4) K. Reibel and A. K. Mann: Phys. Rev. **118** (1960) 701.

Table II. The correction of the energy scale.

Energy in Ref. 1	should be read
4.0 Mev	4.4 Mev
6.0	6.6
8.0	8.8
10.0	11.0
12.0	13.2
14.0	15.4



The figure contains two plots of the photon-photon cross-section $\sigma(\gamma, \gamma)$ in millibarns (mb) as a function of photon energy in Mev. The upper plot, labeled 'K (C)', shows a prominent peak at approximately 8 Mev and a secondary, smaller peak at about 12 Mev. The lower plot, labeled 'Ca (d)', shows a similar pattern with a main peak around 8 Mev and a smaller one around 12 Mev. In both plots, vertical arrows point to specific energy values on the x-axis, which correspond to the particle threshold energies for various nuclear reactions as detailed in the accompanying text.

...the experiment used monochromatic γ -rays.

...The arrows indicate the positions of the particle threshold energies of ...

...The arrows indicate the positions of the particle threshold energies of ...

...The arrows indicate the positions of the particle threshold energies of ...

...The arrows indicate the positions of the particle threshold energies of ...

Ref. S. Costa, F. Ferrero, S. Ferroni, B. Minetti, C. Molino R. Malvano Phys. Letters <u>6</u> , 226 (1963)						Elem. Sym. K A Z 19
Method 100 MeV Synchrotron; 4π neutron detector; calculated integrated cross sections - fitted with polynomial of degree η						Ref. No. 63 Co 3 EGF
Reaction	E or ΔE	E_0	Γ	$\int \sigma dE$	$J\pi$	Notes
(γ, xn)						$\sigma_b = \int \frac{\sigma(E)}{E} dE$ gets $\langle \vec{v}_p \cdot \vec{v}_n - \vec{v}_n \cdot \vec{v}_{n1} \rangle$ $= (Rc^2 - R_p^2 - \frac{3}{\pi^2} \frac{tr \cdot c}{e^2} \sigma_b \frac{A-1}{A^2}) \times \frac{2}{A-2}$ See "Boron" for plots of this and $\int \sigma dE / 60 \text{ NZ/A}$.

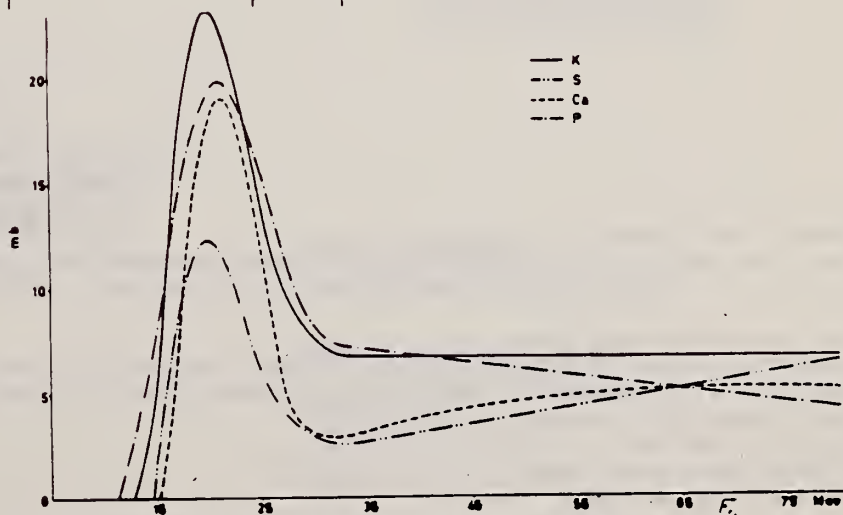


Fig. 1. Photonuclear cross sections for several light elements versus γ -ray energy.

METHOD

REF. NO.

69 No 1

egf

REACTION	RESULT	EXCITATION ENERGY	SOURCE		DETECTOR		ANGLE
			TYPE	RANGE	TYPE	RANGE	
G, NA24	ABY	140-999	C	100-999	ACT-I		4PI

999 = 1.2 GEV

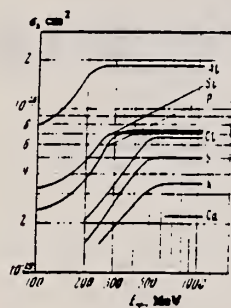


FIG. 2. Cross sections as a function of ray energy.

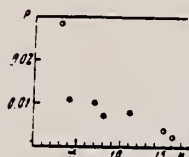


FIG. 3. Dependence of P on number of nucleons which have left the nucleus.

Table I

Reaction	Nucleons emitted	Threshold, MeV	Target	Distribution of isotopes, %
Al ²⁷ → Na ²⁴	2p, n	31	Al	100
Si ²⁸ → Na ²⁴	3p, n	43	Si	92.27
P ³¹ → Na ²⁴	4p, 3n	60	P	100
S ³² → Na ²⁴	5p, 3n	76	S	95.02
Cl ³⁵ → Na ²⁴	6p, 3n	104	NH ₄ Cl	75.4
K ³⁹ → Na ²⁴	8p, 7n	140	K ₂ CO ₃	91.06
Ca ⁴⁰ → Na ²⁴	9p, 7n	148	CaO	98.97

*The threshold was calculated as the binding energy of the emitted nucleons.

Table II. Cross sections for reactions in the saturation region

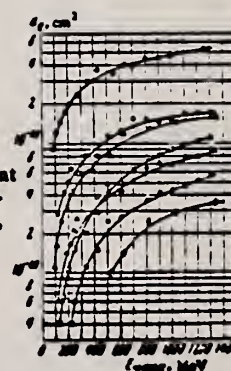
Reaction	σ_{γ} , 10^{-24} cm ²	Reaction	σ_{γ} , 10^{-24} cm ²
Al ²⁷ → Na ²⁴	185 ± 20	Cl ³⁵ → Na ²⁴	68 ± 7
Si ²⁸ → Na ²⁴	72 ± 8	K ³⁹ → Na ²⁴	35 ± 5
P ³¹ → Na ²⁴	71 ± 8	Ca ⁴⁰ → Na ²⁴	22 ± 5
S ³² → Na ²⁴	52 ± 6		

According to the photomesonic mechanism, the cross section for the reaction can be written in the form

$$\sigma = \sigma_0 A P, \quad (1)$$

Here σ_0 is the total cross section for interaction of the photon with a free nucleon with inclusion of the nucleon motion in the nucleus (σ_0 , as has been shown by Roos and Peterson,^[6] depends only weakly on photon energy for $E_{\gamma} > 300$ MeV); A is the number of nucleons in the nucleus, and P is the probability that the reaction will proceed by a given channel.

FIG. 1. Cross section σ_0 per equivalent photon as a function of maximum bremsstrahlung energy. Points: O - Al, O - Si, Δ - P, Δ - S, □ - Cl, ■ - K, ○ - Ca.



REACTION	RESULT	EXCITATION ENERGY	SOURCE		DETECTOR		ANGLE
			TYPE	RANGE	TYPE	RANGE	
E, E/	FMF	3,7 (3.6, 6.5)	D	99-227	MAG-D	99-227	DST

Table 4

B(EL) 3.6, 6.5

Characteristics of transitions excited by high-energy electrons in
 ^{23}Na and ^{39}K

Method	Parameters and method of determination	2,03 MeV ^{23}Na ($\lambda=2$)	3,6 MeV ^{39}K ($\lambda=3$)	6,5 MeV ^{39}K ($\lambda=1$)
1	$\beta_\lambda, 10^{-2}$	$11,6 \pm 2,5$	$13,1 \pm 2,8$	$3,40 \pm 0,69$
	$B(E\lambda, I_i \rightarrow I_f) e^2 \text{ fermi}^{2\lambda}$	107 ± 23	11800 ± 2500	$14,3 \pm 2,9$
	G	$13,7 \pm 3,0$	19 ± 4	$6,4 \pm 1,3$
2	$A_\lambda, \text{ fermi}^{\lambda-2}$	$1,55 \pm 0,10$	$1,39 \pm 0,04$	$1,79 \pm 0,15$
	$B_\lambda, \text{ fermi}^2$	$0,45 \pm 0,07$	$0,34 \pm 0,09$	$0,79 \pm 0,17$
	$B(E\lambda, I_i \rightarrow I_f), e^2 \text{ fermi}^{2\lambda}$	80 ± 11	6300 ± 400	$8,5 \pm 1,5$
	$R_{\text{trans}}, \text{ fermi}$	$10,2 \pm 1,4$ $3,93 \pm 0,57$	10 ± 1 $4,38 \pm 0,08$	$3,8 \pm 0,7$ $3,89 \pm 0,22$

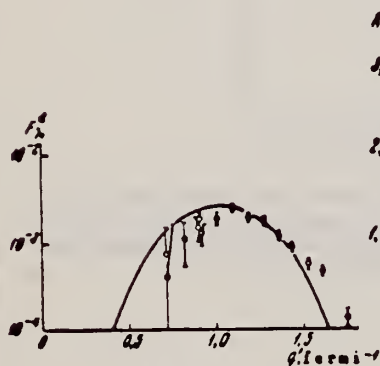


Fig. 5

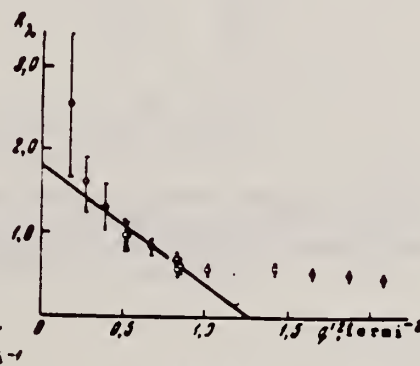


Fig. 6

Fig. 5. Squared form factor as a function of momentum transfer q' for the "inelastic" peak at 3.6 ± 0.2 MeV for ^{39}K . The curve was calculated with Eq. (11) for $\beta_\lambda = 0.131$ and $\lambda = 3$.

Fig. 6. Experimental dependence of R_λ on q'^2 for the "inelastic" peak at 6.5 ± 0.3 MeV for ^{39}K ($\lambda = 1$). The straight line is a least squares fit to the first nine points.

[over]

Table 2

Squared form factors for inelastic scattering of electrons with
excitation of levels in ^{23}Na and ^{39}K

2.08 MeV ^{23}Na		3.6 MeV ^{39}K		6.5 MeV ^{39}K	
q , fermi $^{-1}$	$F_{\lambda}^2 \cdot 10^{-4}$	q , fermi $^{-1}$	$F_{\lambda}^2 \cdot 10^{-4}$	q , fermi $^{-1}$	$F_{\lambda}^2 \cdot 10^{-4}$
0.41	13.9 ± 13.9	0.72	7.43 ± 7.95	0.41	77.5 ± 22.9
0.51	26.3 ± 18.7	0.72	4.18 ± 11.12	0.52	45.4 ± 14.1
0.61	24.2 ± 14.7	0.82	10.9 ± 5.5	0.62	43.1 ± 15.1
0.71	32.4 ± 9.4	0.91	18.5 ± 3.3	0.72	23.9 ± 5.7
0.71	22.0 ± 10.3	0.91	14.6 ± 4.4	0.72	23.3 ± 7.8
0.80	45.8 ± 10.8	0.92	12.6 ± 3.3	0.82	18.2 ± 4.1
0.90	70.3 ± 9.1	1.01	18.4 ± 2.4	0.91	6.7 ± 2.0
0.90	31.0 ± 8.9	1.10	24.7 ± 2.4	0.91	11.4 ± 2.8
0.99	46.3 ± 5.0	1.19	18.9 ± 1.7	0.92	9.2 ± 2.4
1.08	31.2 ± 2.9	1.28	17.0 ± 1.7	1.01	7.5 ± 1.9
1.17	20.8 ± 1.7	1.37	11.8 ± 1.2	1.19	6.3 ± 1.5
1.26	14.5 ± 1.2	1.44	8.66 ± 0.87	1.28	4.45 ± 1.09
1.35	11.1 ± 0.9	1.53	5.50 ± 0.75	1.37	3.78 ± 0.88
1.41	7.46 ± 0.67	1.61	4.56 ± 0.52	1.44	2.77 ± 0.57
1.45	7.20 ± 0.50	1.75	1.35 ± 0.35		
1.48	5.52 ± 0.51				
1.51	5.71 ± 0.43				
1.54	4.43 ± 0.35				
1.73	1.37 ± 0.15				
1.86	1.11 ± 0.14				
1.98	0.91 ± 0.12				
2.08	1.67 ± 0.20				

REACTION	RESULT	EXCITATION ENERGY	SOURCE		DETECTOR		ANGLE
			TYPE	RANGE	TYPE	RANGE	
G,NA24	ABY	THR-999	C	100-999	ACT-I		4PI

999=1 GEV

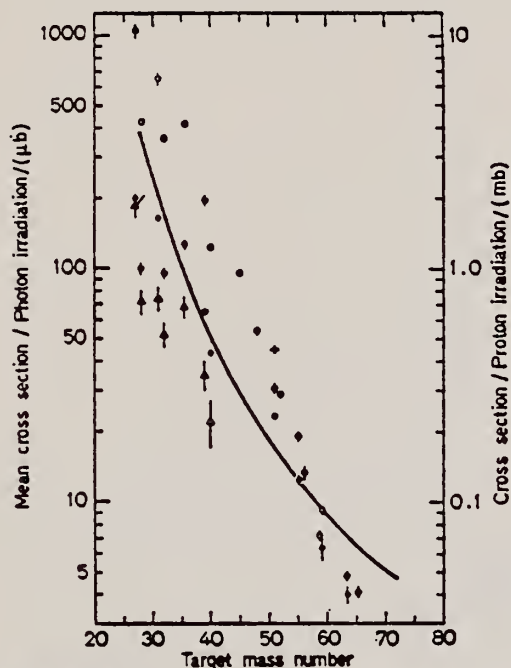


Fig. 7. Mean cross sections for ^{24}Na production as a function of target mass number. Present work filled circles. Noga *et al.* [3] open triangles, Kumbartzki *et al.* [13] cross and Korteling *et al.* [1] 400 MeV protons open circles. The solid line gives the mean cross sections calculated by Jonsson *et al.* [17]

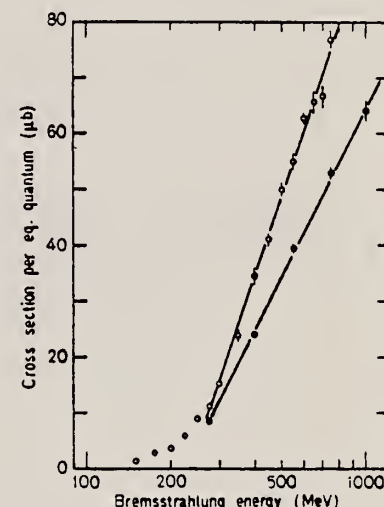


Fig. 4

Fig. 4. The determined yields for the reactions $^{39,40,41}\text{K} \rightarrow ^{24}\text{Na}$ (open circles) and $^{40, \dots}\text{Ca} \rightarrow ^{24}\text{Na}$ (filled circles)

¹Korteling, R.G. *et al.*, J. Inorg. Nucl. Chem. 29, 2863 (1967).

³Noga, V.I. *et al.*, Sov. J. Nucl. Phys. 9, 637 (1969).

¹³Kumbartzki, G. *et al.*, Nucl. Phys. A176, 23 (1971).

¹⁷Jonsson, G.G. *et al.*, LUNP7212, Oct. 1972, to be published in Physica Scripta.

REF.

A. Veyssiere, H. Beil, R. Bergere, P. Carlos, A. Lepretre, and
A. De Miniac
Nucl. Phys. A227, 513 (1974)

ELEM. SYM.	A	Z
K		19
REF. NO.		
74 Ve 1	egf	

REACTION	RESULT	EXCITATION ENERGY	SOURCE		DETECTOR		ANGLE
			TYPE	RANGE	TYPE	RANGE	
G,N *	ABX	13- 32	D	13- 32	BF3-I		4PI
G,ZN **	ABX	30- 32	D	30- 32	BF3-I		4PI
G,NP ***	ABX	18- 29	D	18- 29	BF3-I		4PI

* 904
** 902
*** 903

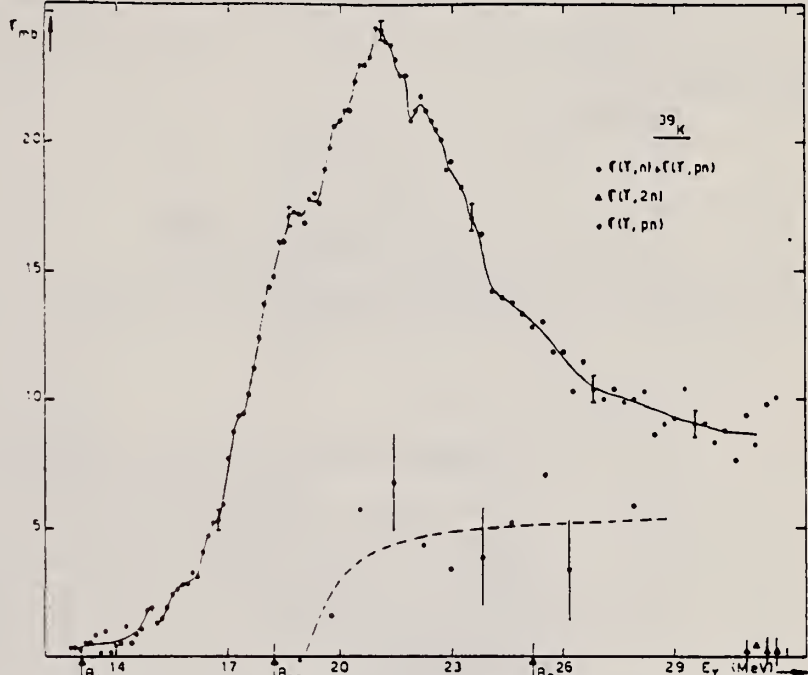


Fig. 10. Partial photoneutron cross sections $[\sigma(\gamma, n) + \sigma(\gamma, pn)]$, $\sigma(\gamma, pn)$ and $\sigma(\gamma, 2n)$ of ^{39}K .

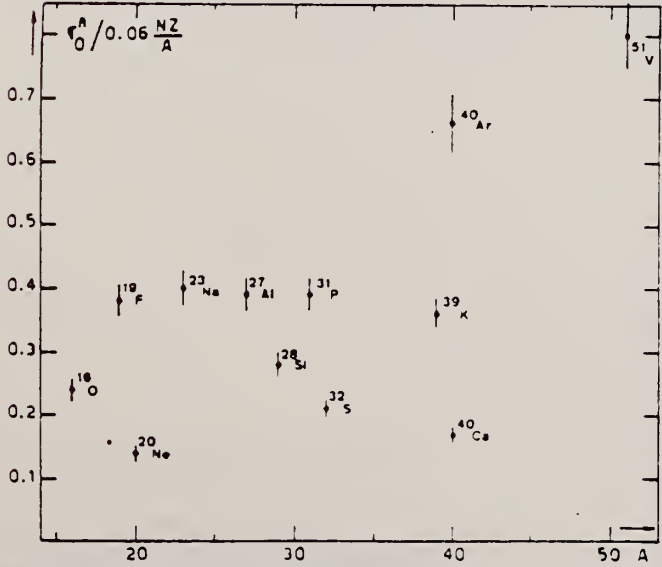


Fig. 22. Ratio of experimental integrated photoneutron cross section σ_0^N over the Thomas, Reiche and Kuhn sum rule $[0.06 NZ/A]$. Numerical values and upper integration limits E_M are taken from table 3. Also $\Delta\sigma_0^N = \pm 7\%$ for all nuclei.

(over)

U.S. DEPARTMENT OF COMMERCE
NATIONAL BUREAU OF STANDARDS

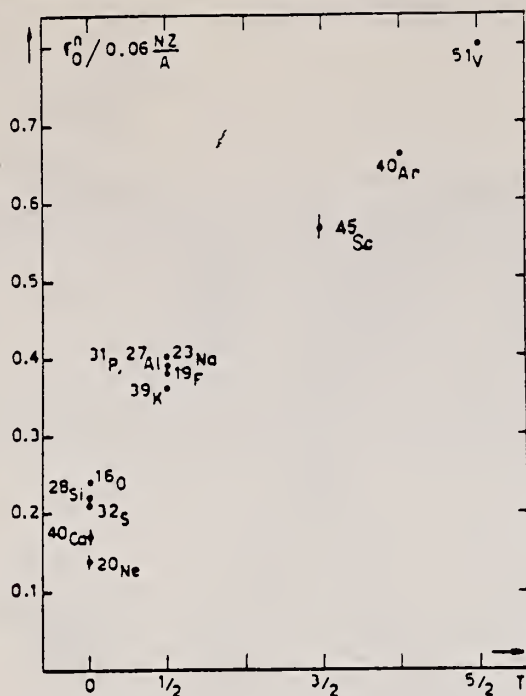


Fig. 24. The $\{\sigma_0^n/(0.06 NZ/A)\}$ ratio as a function of isospin T . Possible overall errors of $\pm 7\%$ are to be applied to all nuclei shown.

TABLE 3
Experimental integrated photoneutron cross sections $\sigma_0^n = \int_0^{E_M} \sigma_{Tn}(E) dE$ compared with the classical sum rule $[0.06 NZ/A]$ of Thomas, Reich and Kuhn

	$T = 0$					$T = \frac{1}{2}$					$T = \frac{3}{2}$	$T = 2$	$T = \frac{5}{2}$
Nucleus	^{16}O	^{20}Ne	^{28}Si	^{32}S	^{40}Ca	^{19}F	^{23}Na	^{27}Al	^{31}P	^{39}K	^{45}Sc	^{40}Ar	^{51}V
σ_0^n (MeV · mb)	58 ± 4	42 ± 3	94 ± 7	98 ± 7	100 ± 7	108 ± 7	137 ± 9	158 ± 10	182 ± 12	210 ± 14	383 ± 25	393 ± 28	602 ± 42
$\sigma_0^n/(0.06 NZ/A)$	0.24	0.14	0.22	0.21	0.17	0.38	0.40	0.39	0.39	0.36	0.57	0.66	0.8
E_M (MeV)	30	26.7	30	30	29.5	29	30	30	29	30	28.1	26.7	28

REF.

V. di Napoli, G. Rosa, F. Salvetti, M. L. Terranova,
H. G. De Carvalho, J. B. Martins, O. A. P. Tavares
J. Inorg. Nucl. Chem. 37, 1101 (1975)

ELEM. SYM.

A

Z

K

19

METHOD

REF. NO.

75 Di 4

egf

REACTION	RESULT	EXCITATION ENERGY	SOURCE		DETECTOR		ANGLE
			TYPE	RANGE	TYPE	RANGE	
G,F18	ABY	THR-999	C	300-999	ACT-I		4PI
G,NA22	ABY	THR-999	C	300-999	ACT-I		4PI
G,NA24	ABY	THR-999	C	300-999	ACT-I		4PI

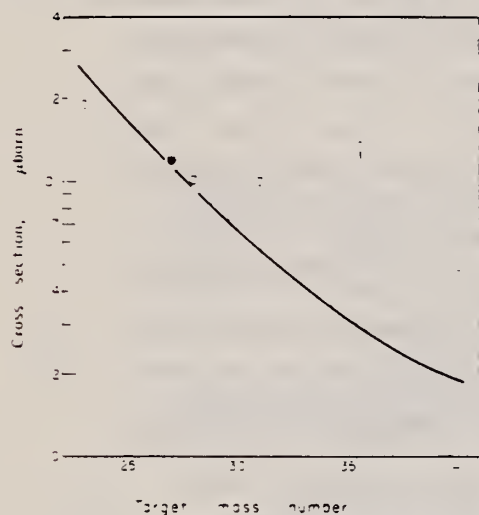


Fig. 2. Mean absolute cross section of ^{18}F photoproduction vs the target mass number. Open triangle: energy range 0.15-0.72 GeV, Ref. [18]. Filled circle: energy range 0.3-1 GeV, Ref. [3]. Open circles: present work. The curve has been calculated by means of Eqn (1).

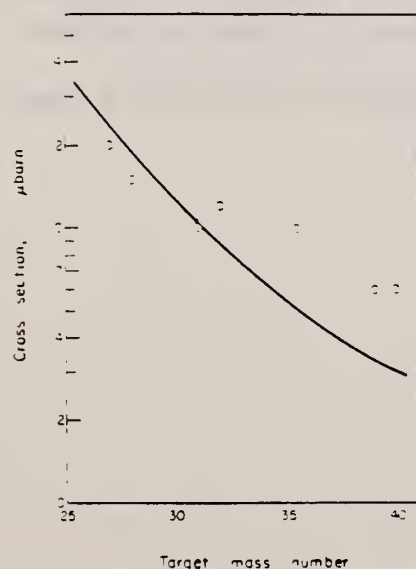


Fig. 3. Mean absolute cross section of ^{22}Na photoproduction vs the target mass number. The curve has been calculated by means of Eqn (1).

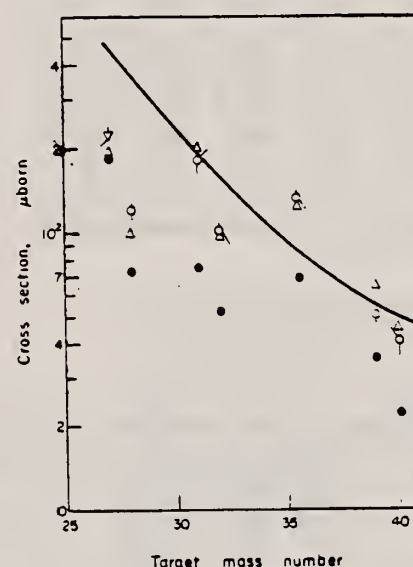


Fig. 4. Mean absolute cross section of ^{24}Na photoproduction vs the target mass number. Filled circles: energy range 0.1-1 GeV, Ref. [20]. Reversed open triangle: energy range 0.3-1 GeV, Ref. [8]. Open triangles: energy range 0.25-1 GeV, Ref. [19]. Open circles: present work. The curve has been calculated by means of Eqn (1).

Table 2. Cross-section per equivalent quantum $\sigma_0(\mu\text{b})$ of photoproduction of ^{18}F

Target nucleus	Bremsstrahlung maximum energy $E_0(\text{GeV})$				
	0-30	0-40	0-55	0-75	1-00
^{23}Na	590 ± 30	640 ± 30	720 ± 30	780 ± 30	830 ± 30
$^{27}\text{Al}^a$	116 ± 7	172 ± 6	202 ± 6	245 ± 5	270 ± 5
^{28}Si	80 ± 10	110 ± 10	145 ± 10	170 ± 10	200 ± 10
^{31}P	60 ± 10	90 ± 10	130 ± 10	150 ± 10	180 ± 10
^{32}S	55 ± 10	90 ± 10	125 ± 10	160 ± 10	190 ± 10
$^{35,37}\text{Cl}$	185 ± 20	230 ± 20	270 ± 20	310 ± 20	350 ± 20
^{39}K	35 ± 5	50 ± 5	65 ± 5	75 ± 5	90 ± 5
^{40}Ca	5 ± 2	20 ± 3	35 ± 5	45 ± 5	60 ± 5

^aThe results for ^{27}Al have already been published (see[3]) and are reported for comparison.

(over)

Table 3. Cross-section per equivalent quantum $\sigma_Q(\mu b)$ of photoproduction of ^{23}Na

Target nucleus	Bremsstrahlung maximum energy E_0 (GeV)				
	0.30	0.40	0.55	0.75	1.00
^{27}Al	490 ± 20	560 ± 20	667 ± 20	690 ± 20	745 ± 20
^{28}Si	290 ± 20	330 ± 20	380 ± 20	430 ± 20	470 ± 20
^{31}P	230 ± 20	250 ± 20	290 ± 20	330 ± 20	350 ± 20
^{32}S	206 ± 10	240 ± 10	280 ± 10	320 ± 10	350 ± 10
$^{35,37}\text{Cl}$	230 ± 10	260 ± 10	290 ± 10	320 ± 10	350 ± 10
^{39}K	30 ± 3	50 ± 5	65 ± 5	80 ± 5	100 ± 5
^{40}Ca	5 ± 2	20 ± 3	45 ± 5	60 ± 5	60 ± 5

Table 4. Cross-section per equivalent quantum $\sigma_Q(\mu b)$ of photoproduction of ^{23}Na

Target nucleus	Bremsstrahlung maximum energy E_0 (GeV)				
	0.30	0.40	0.55	0.75	1.00
$^{27}\text{Al}^a$	370 ± 10	440 ± 10	500 ± 20	550 ± 20	660 ± 20
^{28}Si	100 ± 10	140 ± 10	160 ± 10	210 ± 10	240 ± 10
^{31}P	100 ± 20	160 ± 20	200 ± 20	270 ± 20	310 ± 20
^{32}S	120 ± 10	160 ± 10	180 ± 10	210 ± 10	240 ± 10
$^{35,37}\text{Cl}$	65 ± 10	100 ± 10	140 ± 10	190 ± 10	220 ± 10
^{39}K	20 ± 5	35 ± 5	55 ± 5	65 ± 5	80 ± 5
^{40}Ca	12 ± 3	25 ± 5	35 ± 5	50 ± 5	60 ± 5

^aThe results for ^{27}Al have already been published (see [8]) and are reported for comparison.

Table 5. Mean absolute cross-section $\bar{\sigma}_a(\mu b)$ in the energy range 0.3–1 GeV

Target nucleus	Produced radionuclide		
	^{18}F	^{22}Na	^{24}Na
^{23}Na	190 ± 30		
$^{27}\text{Al}^a$	120 ± 10	200 ± 20	220 ± 20
^{28}Si	100 ± 10	150 ± 20	120 ± 10
^{31}P	100 ± 10	100 ± 20	180 ± 20
^{32}S	110 ± 10	120 ± 10	100 ± 10
$^{35,37}\text{Cl}$	135 ± 20	100 ± 10	130 ± 10
^{39}K	45 ± 5	60 ± 5	50 ± 5
^{40}Ca	46 ± 5	60 ± 5	40 ± 5

^aThe results for the photoproduction of ^{18}F and ^{24}Na from ^{27}Al have already been published (Ref. [3] and [8], respectively).

2. V. di Napoli and M. L. Terranova, *J. inorg. nucl. Chem.* **36**, 3633 (1974).
3. V. di Napoli, A. M. Lacerenza, F. Salvetti, S. M. Terenzi, H. G. de Carvalho and J. B. Martins, *J. inorg. nucl. Chem.* **35**, 1419 (1973).
4. C. M. Lederer, J. M. Hollander and I. Perlman, *Table of Isotopes*, 6th Edn Wiley, New York (1967).
5. R. G. Korteling and A. A. Caretto, Jr., *J. inorg. nucl. Chem.* **29**, 2863 (1967).
6. R. G. Korteling and A. A. Caretto, Jr., *Phys. Rev. C* **1**, 193 (1970).
7. R. G. Korteling and A. A. Caretto, Jr., *Phys. Rev. C* **1**, 1960 (1970).
8. V. di Napoli, A. M. Lacerenza, F. Salvetti, H. G. de Carvalho and J. B. Martins, *Lett. Nuovo Cimento* **1**, 835 (1971).
9. I. Halpern, R. J. Debs, J. T. Eisinger, A. W. Fairhall and H. G. Richter, *Phys. Rev.* **97**, 1327 (1955).
10. C. B. Fulmer, F. S. Toth, I. R. Williams, T. H. Handley, C. F. Dell, E. L. Jallis, T. M. Jenkins and J. M. Wyckoff, *Phys. Rev. C* **2**, 1371 (1970).
11. G. J. Kumbartzki, U. Kim and C. K. Kwan, *Nucl. Phys.* **A160**, 237 (1970).
12. G. J. Kumbartzki and U. Kim, *Nucl. Phys.* **A176**, 23 (1971).
13. K. Lindgren and G. G. Jonsson, *Nucl. Phys.* **A197**, 71 (1972).
14. C. E. Roos and V. Z. Peterson, *Phys. Rev.* **124**, 1610 (1961).
15. T. A. Gabriel and R. G. Alsmüller, Jr., *Phys. Rev.* **182**, 1035 (1969).
16. G. G. Jonsson and K. Lindgren, *Phys. Scr.* **7**, 49 (1973).
17. G. Rudstam, *Z. Naturf.* **21a**, 1027 (1966).
18. A. Masaike, *J. phys. Soc. Japan* **19**, 427 (1964).
19. A. Järund, B. Friberg and B. Forkman, Private communication to G. G. Jonsson and K. Lindgren, quoted in Ref. [16]; see also A. Järund, B. Friberg and B. Forkman, University of Lund Report No. LUNP-7303, 1973 (unpublished).
20. V. I. Noga, Yu. N. Ranyuk and P. V. Sorokin, *Yad. Fiz.* **9**, 1152 (1969) (transl.: *Sov. J. Nucl. Phys.* **9**, 673 (1969)).
21. T. Methasiri and S. A. E. Johansson, *Nucl. Phys.* **A167**, 97 (1971).
22. J. R. Nix and E. Sassi, *Nucl. Phys.* **81**, 61 (1966).
23. W. D. Myers and W. J. Swiatecki, *Nucl. Phys.* **81**, 1 (1966).

REF. A. S. Danagulyan, N. A. Demekhina
Yad. Fiz. 24, 681 (1976)
Sov. J. Nucl. Phys. 24, 355 (1976)

ELEM. SYM.	A	Z
K		19
REF. NO.		
76 Da 4		hmg

METHOD		REF. NO.			
		76 Da 4		hmg	
REACTION	RESULT	EXCITATION ENERGY	SOURCE		ANGLE
			TYPE	RANGE	
G, NA24	ABX	THR* 5	C	2* 5	4PI

*ENERGY, GEV

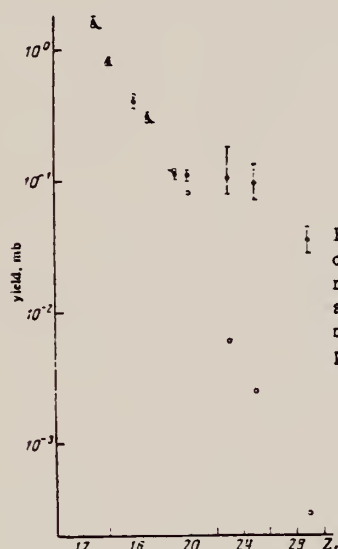


FIG. 2. Yield values and theoretical values according to the modified Rudstam formula as a function of the target charge number Z_t . Points: ●—experiment, ○—theory.

TABLE I. Experimental yields and reaction cross sections obtained in the measurements at the Erevan electron accelerator.

Target nucleus	Reaction yield, mb					Reaction cross section, mb
	E_T range, GeV					
	2	3	4	4.5	5	
^{27}Al	0.81±0.06	0.87		0.87		0.07213±0.0346
^{28}Si	0.27±0.02	0.28		0.29		0.0287±0.013
^{29}S	0.24±0.02	0.22		0.27		0.0323±0.0155
Cl	0.28±0.03	0.30		0.28		—
^{35}K	0.1±0.01	0.125		0.13		0.08±0.0288
^{40}Ca	0.068±0.01	0.09		0.115		0.035±0.0108
^{41}V	0.085±0.02	0.094±0.02	0.098±0.02		0.082±0.025	0.019
^{51}Mn	0.079±0.02	0.075±0.02	0.087±0.017		0.088±0.015	0.01078±0.0058
Cu	0.029±0.006	0.037±0.007	0.1136±0.007		0.034±0.007	0.00547±0.0029

Note. The reaction cross sections have been calculated in the $1/E$ approximation of the bremsstrahlung spectrum.

K
A=37

K
A=37

K
A=37

REF. D. R. Goosman and R. W. Kavanagh
Phys. Rev. 161, 1156 (1967)

ELEM. SYM.	A	Z
K	37	19
REF. NO.		HMG
67 Go 2		

METHOD

REACTION	RESULT	EXCITATION ENERGY	SOURCE		DETECTOR		ANGLE
			TYPE	RANGE	TYPE	RANGE	
P,G	LFT	2 -4	D	0-6	SCD-D	0-6	DST

J-PI

[See reverse side for Table]

TABLE VII. Levels in ^{92}K below 5.5-MeV excitation energy. The symbol ω means $J+\frac{1}{2}$.

Excitation energy (keV)	Proton energy (keV)	J^π, T	T (keV) or $\tau_{1/2}$	$\nu = 4.3$ (μ)	$\omega T_p/T^*$ (meV)	$\omega T_p/T^*$ (eV)	T_p (keV)	T_p^* (eV)	T_p^* (meV)	Reactions ^b
0	...	$\frac{1}{2}^+$	$1.23 \pm 0.02 \text{ sec}^c$	B, E, F, G
1368 \pm 3	...	$(\frac{1}{2}^+)$	B, I
1390 \pm 2	...	$\frac{1}{2}^-$	$9.6 \pm 1.4 \text{ nsec}$	B, I, F
2169 \pm 5	321 \pm 5	$(\frac{1}{2}^-)$	B, E, F, G
2278 \pm 9	433 \pm 9	G
2750 \pm 1	918 \pm 1 ^e	$\frac{1}{2}^+$	$\leq 0.8^e$	≤ 57	208 ± 30	69 ± 10	A, F, G
3083 \pm 4	1260 \pm 4	$(\frac{1}{2}^-)$	$(\leq 0.016 \pm 0.003)$	(≤ 1.5)	13 ± 2	(4.3 ± 0.7)	A, D, F
3311 \pm 4	1494 \pm 4	$\frac{1}{2}^-$	2.2 ± 0.3	0.22	31 ± 4	...	2.2 ± 0.3	...	15 ± 2	A, D, F
(3408 \pm 20)	(1686 \pm 20)	8 \pm 3	A
3623 \pm 15	1815 \pm 15	$\frac{1}{2}^+, \frac{1}{2}^+, \frac{1}{2}^+$	14 \pm 3	A, H
3944 \pm 10	2042 \pm 10	$\frac{1}{2}^+, \frac{1}{2}^+, \frac{1}{2}^+$	21 \pm 6	A, H
3962 \pm 15	2163 \pm 15	...	$\leq 10 \pm 4$	0.34	70 \pm 21 ^e	...	$\leq 10 \pm 4$	A, D
4127 \pm 15 ^f	2184 \pm 15	$\frac{1}{2}^-, \frac{1}{2}^-, \frac{1}{2}^+$	A, H
4281 \pm 20	2333 \pm 15 ^f	$\frac{1}{2}^+, \frac{1}{2}^+, \frac{1}{2}^+$	23 \pm 12	A
4417 \pm 5	2491 \pm 20	170 \pm 50	A, (H) ¹
4435 \pm 5	2631 \pm 5	$\frac{1}{2}^-$	113 \pm 34	A, C, (H)
4523 \pm 20	2649 \pm 5	$\frac{1}{2}^+$	29 \pm 23	A, D
4585 \pm 13	2740 \pm 20	$\frac{1}{2}^+$	0.5 ± 0.3^k	0.0005	700 \pm 210	...	0.5 ± 0.3^k	...	29 ± 23	A, D
4659 \pm 10	2804 \pm 13	$\frac{1}{2}^+$	90^h	0.24	90^h	...	700 \pm 210	A, H
4721 \pm 10	2880 \pm 10	$\frac{1}{2}^+, \frac{1}{2}^+, \frac{1}{2}^+$	53 \pm 20	A, C, D
4833 \pm 13	3059 \pm 13	$\frac{1}{2}^+, \frac{1}{2}^+$	98 \pm 42	A, C, D
5018 \pm 3	3240 \pm 3	$\frac{1}{2}^+, \frac{1}{2}^+, \frac{1}{2}^+$	0.20 ± 0.08^k	0.002	52 \pm 21	...	0.20 ± 0.08^k	...	16 ± 5^m	A, C, D
5048 \pm 3	3280 \pm 3	$\frac{1}{2}^+, \frac{1}{2}^+, \frac{1}{2}^+$	0.60 ± 0.15^m	0.004	33 \pm 17	...	0.60 ± 0.15^m	...	1.6 ± 0.3^m	A, C, D, (H) ¹
5116 \pm 5 ^a	3348 \pm 5 ^a	$\frac{1}{2}^+, \frac{1}{2}^+, \frac{1}{2}^+$	0.04 ± 0.02^m	0.0003	110 \pm 50	...	0.04 ± 0.02^m	...	0.42 ± 0.14^m	A, C, D, (H) ¹
5127 \pm 4	3359 \pm 4	$\frac{1}{2}^+$	0.2 ± 0.1^k	0.0001	50 \pm 30	...	0.2 ± 0.1^k	...	50 ± 30	A, D
5207 \pm 8	3444 \pm 8	$\frac{1}{2}^-$	0.5 ± 0.2^k	0.036	180 \pm 80	...	0.5 ± 0.2^k	...	200 ± 110	A, C, D
5258 \pm 5	3496 \pm 5	$\frac{1}{2}^+$	139 \pm 60	A, C
5318 \pm 6	3558 \pm 6	$\frac{1}{2}^+$	48 \pm 24	A, C
5339 \pm 9	3580 \pm 9	C
5415 \pm 6	3658 \pm 6	A, C
5449 \pm 6	3693 \pm 6	A, C
5468 \pm 6	3713 \pm 6	$\frac{1}{2}^+$	A, C

^a Does not include possible (β, β') contributions to lower proton-unstable states.
^b The reaction code is: A: $^{92}\text{Ar}(^{37}\text{Ar})^{92}\text{K}$; B: $^{92}\text{Ar}(^{37}\text{Ar})^{92}\text{K}$; C: $^{92}\text{Ar}(^{37}\text{Ar})^{92}\text{K}$; D: $^{92}\text{Ar}(^{37}\text{Ar})^{92}\text{K}$; E: $^{92}\text{Ar}(^{37}\text{Ar})^{92}\text{K}$; F: $^{92}\text{Ar}(^{37}\text{Ar})^{92}\text{K}$; G: $^{92}\text{Ar}(^{37}\text{Ar})^{92}\text{K}$; H: $^{92}\text{Ar}(^{37}\text{Ar})^{92}\text{K}$; I: either or both of reactions E and G.
^c Reference 19.
^d Reference 24.
^e This level is from the allowed decay of ^{92}Ca (Ref. 3).
^f This level is from the allowed decay of ^{92}Ca (Ref. 3).
^g This level is the unresolved sum for the 3962- and 3982-keV levels.
^h Reference 25.
ⁱ This is not established by Fig. 2 alone, but also appears in the decay of ^{92}Ca (Ref. 3).
^j $5/2^+$ (Ref. 3).
^k This level is from the data of Ref. 25. See Sec. V.7 for explanation.
^l Reference 23.
^m Assuming $J = 3/2$. Multiply by 2/3 for $J = 5/2$.
ⁿ This level was found by Ref. 25 but the energy is here determined from its proximity to the 5127-keV level.
^o This spin results from this report or that of Ref. 23, in conjunction with that of Ref. 25.

K
A=39

K
A=39

K
A=39

METHOD

Betatron /

REF. NO.

55 Bo 2

NVB

REACTION	RESULT	EXCITATION ENERGY	SOURCE		DETECTOR		ANGLE
			TYPE	RANGE	TYPE	RANGE	
G,N	ABX	13-21	C	13-21	ACT-I		4PI

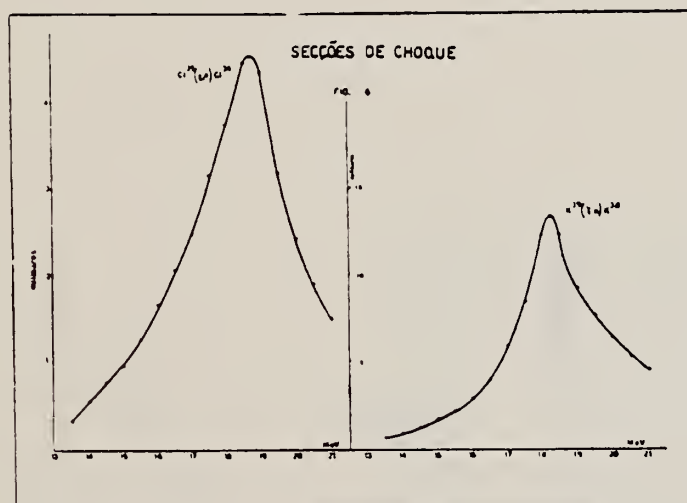


Fig. 6

Elementos	Limiar (Threshold)	E_M	σ_M	$\sigma_{int.}$	Largura	Δ GOLDEMBERG & LEITE LOPEZ, 1955
Cl	12.33 ± 0.035 Mev	18.75 Mev	7.4 milibarn	$0.026 \text{ mb} \times \text{Mev}$	3.3 Mev	4.45 Mev
K	13 ± 0.15 Mev	18.25 Mev	13.8 milibarn	$0.041 \text{ mb} \times \text{Mev}$	2.6 Mev	4.2 Mev

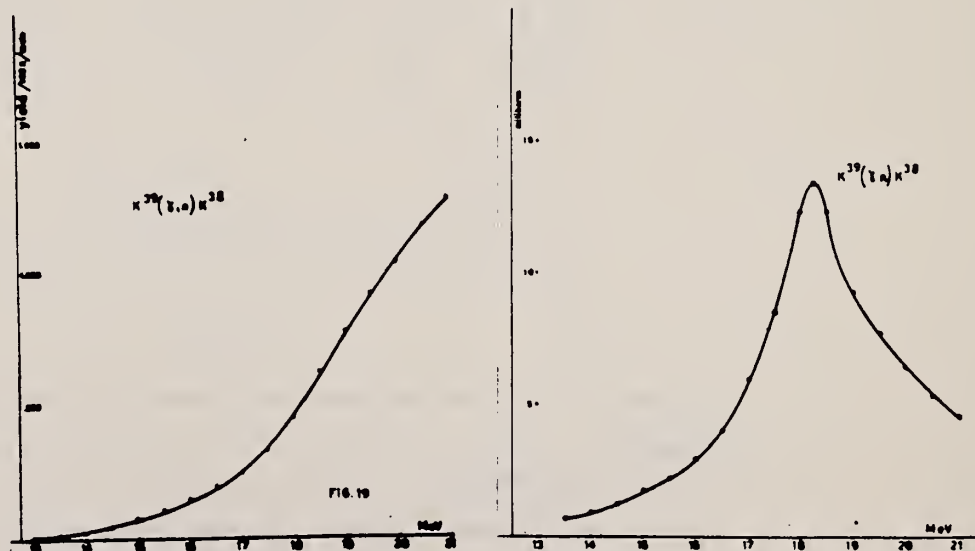
METHOD Betatron; neutron yield; radioactivity; r-chamber

REACTION	RESULT	EXCITATION ENERGY	SOURCE		DETECTOR		ANGLE
			TYPE	RANGE	TYPE	RANGE	
G,N	ABX	13-21	C	13-21	ACT-I		4PI

threshold (γ, n) = 13.00 MeV

THRESHOLD

$$\int \sigma dE = 0.04 \text{ MeV-b}$$



J. Schmouker, P. Erdos, P. Jordan and P. Stoll
 J. Phys. Radium 16, 169 (1955)

K

39

19

METHOD

REF. NO.

55 Sc 2

EGF

REACTION	RESULT	EXCITATION ENERGY	SOURCE		DETECTOR		ANGLE
			TYPE	RANGE	TYPE	RANGE	
G,NA	ABY	THR- 32	C	32	ACT-I		4PI

Betatron run at 31.5 MeV. Yields measured relative to $^{65}\text{Cu}(\gamma, n)^{64}\text{Cu} = 1.4 \text{ barn-MeV}$
 $^{63}\text{Cu}(\gamma, n)^{62}\text{Cu} = 0.7 \text{ barn-MeV}$
 $\sigma \text{ } ^{39}\text{K}(\gamma, n)^{34}\text{Cl} = 0.3 \pm 0.25 \text{ MeV-mb}$

Ref. P. Erdos, P. Scherrer, P. Stoll
Helva. Phys. Acta 30, 639 (1957)

Elem. Sym.	A	Z
K	39	19
Ref. No. 57 Er 1		EGF

Method Betatron; α yield; radioactivity; $\text{Cu}^{65}(\gamma, n)$ reaction

Reaction	E or ΔE	E_0	Γ	$\int \sigma dE$	$J\pi$	Notes
$\text{K}^{39}(\gamma, n\alpha)$	Bremss. 32			0.3 ± 0.25 MeV-mb		Based on yield measurement.

Method **KI detector; Li (p,γ) source**

Ref. No.	EH
58 Ke 1	

Reaction	E or ΔE	E ₀	Γ	∫σdE	Jπ	Notes
(γ,p)	17.6					

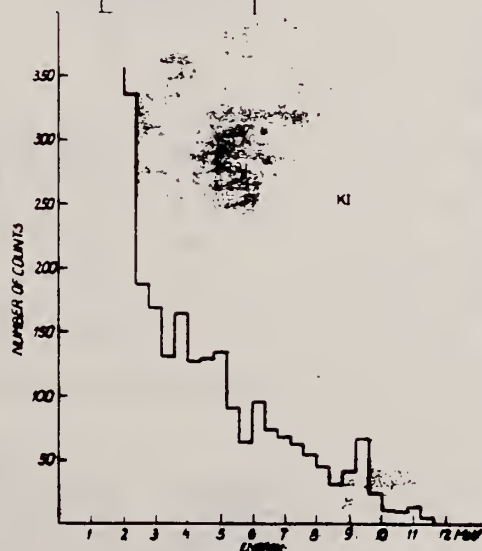


Fig. 7. Pulse spectrum of KI crystal.



TABLE I

Nucleus	N ₀	σ ₀ (b)	N _γ	N _{sp}	σ(γ,p)(mb)	σ(17.6)(mb)
¹¹ Na ²³	4.2 × 10 ⁶	10.7	1176 ± 96	240	2.4 ± 1.1	3.6 ± 1.5
¹² C ¹²	3.8 × 10 ⁶	11.8	3578 ± 98	230	10 ± 3.5	15 ± 5.8
¹⁴ N ¹⁴	1.7 × 10 ⁶	20.8	130 ± 10	10	1.5 ± 0.6	1.5 ± 0.6
¹⁶ O ¹⁶	1.7 × 10 ⁶	20.8	130 ± 10	10	1.5 ± 0.6	1.5 ± 0.6

Elem. Sym.	A	Z
K	39	19
Ref. No. 58 Op 2		
KH		

Method $\text{Li}(p, \gamma)$; proton spectra; Geiger counter; spectrometer
(monitor) (detector)

Reaction	E or ΔE	E_0	Γ	$\int \sigma dE$	$J\pi$	Notes
$\text{K}^{39}(\gamma, p)$	Bremss. 17.6					$\sigma(\gamma, p) = > 11 \text{ mb}$

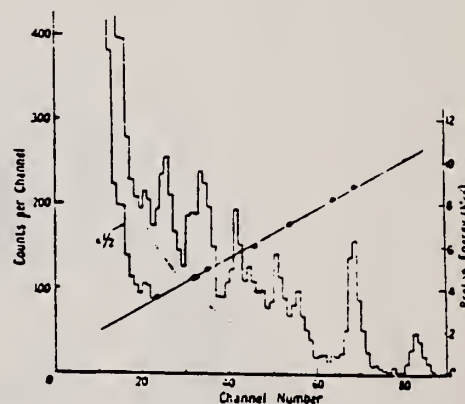


Figure 3. $^{39}\text{K}(\gamma, p)$ spectrum and proton calibration curve.

Table 2†									
Group energy	10-5	8-81	7-33	6-75	6-44	5-70	4-78	4-55	3-8
Excitation of ^{39}A	0	2-16	3-75	4-3	5-1	5-4	6-3	6-6	7-3
Cross section (mbn)	0-9	2-4	1-0	1-4	2-4	1-2	0-5	1-3	0-8

† The group at 2.5 mev (see text) corresponding to a level at 8.6 mev is not included in table 2.

METHOD					REF. NO.	
Betatron; neutron threshold; ion chamber					60 Ge 3	NVB
REACTION	RESULT	EXCITATION ENERGY	SOURCE		DETECTOR	
			TYPE	RANGE	TYPE	RANGE
G,N	NX	THR	C	THR	ACT-I	4PI

THRESHOLD

TABLE I. Summary and comparison of neutron separation energies inferred from present threshold measurements with values predicted from mass data and reaction energies. All energies are expressed in the center-of-mass system in Mev.

Reaction	No. runs	Present results	Other results	Method	Reference
$K^{20}(\gamma, n)K^{20}$ (to 7.7-min state)	1	$\leq 13.125 \pm 0.038$	13.089 ± 0.033 13.087 ± 0.011	LSA mass data	^a ^b

^a C. F. Gleason and J. L. Benson, Phys. Rev. 110, 712 (1958).
^b P. M. Endt et al., Phys. Rev. 105, 1002 (1957).

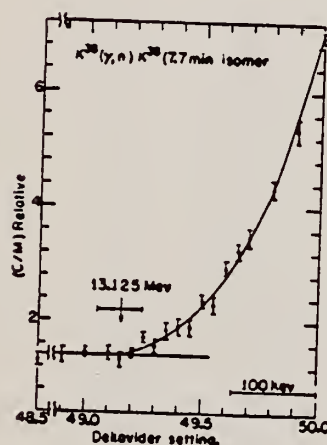


FIG. 7. Activation curve for the reaction $K^{20}(\gamma, n)K^{20}$ (7.7-min state) from 12.95 Mev to 13.35 Mev.

Elem. Sym.	A	Z
K	39	19
Ref. No.		
60 Ho 1		JHH

Method
Betatron; activation; proportional counter.

Reaction	E or ΔE	E_0	Γ	$\int \sigma dE$	$J \pi$	Notes
(γ, d) (γ, np)	Bremss. 20-25					Activation of Ar ³⁷ (34 days). K and L x-rays (2.8 and 0.25 kev) from electron capture in Ar ³⁷ counted.

Y-axis: NUMBER OF REACTIONS / MOLE · ROENTGEN
X-axis: DOSE, ROENTGEN

FORM NBS-418
(8-1-63)
USCOMM-DC 18886-P63

U.S. DEPARTMENT OF COMMERCE
NATIONAL BUREAU OF STANDARDS

Ref. E.C. Booth, K.A. Wright
Nuclear Phys. 35, 472 (1962)

Elem. Sym.	A	Z
K	39	19

Method 4 MeV electron Van de Graaff; brems.; nuclear resonance scattering, ring scatterer; NaI

Ref. No.	JHH
62 Bq 6	

Reaction	E or ΔE	E_0	Γ	$\int \sigma dE$	$J\pi$	Notes
$K^{39}(\gamma, \gamma)$	Brems. 0 - 4					

FORM NBS-418
(8-1-63)
USCOMM-DC 18886-P68

U.S. DEPARTMENT OF COMMERCE
NATIONAL BUREAU OF STANDARDS

Method Betatron; β^+ radioactivity, NaI for annihilation quanta; photon-difference method.

Ref. No.	JHH
62 Go 3	

Reaction	E or ΔE	E_0	Γ	$\int \sigma dE$	$J\pi$	Notes
$K^{39}(\gamma, n)$	Bremss. 14-24					

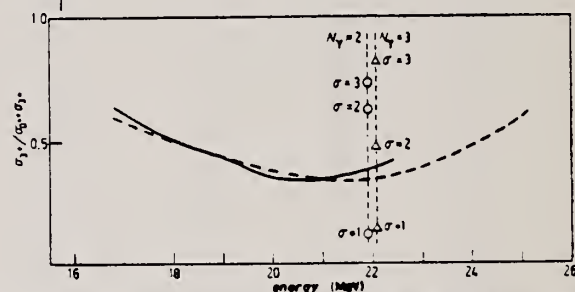


Fig. 5. - $\sigma_2/(\sigma_2 + \sigma_1)$ ratio as a function of energy for the potassium and chlorine elements. --- Cl (Turin), — K (S. Paulo).

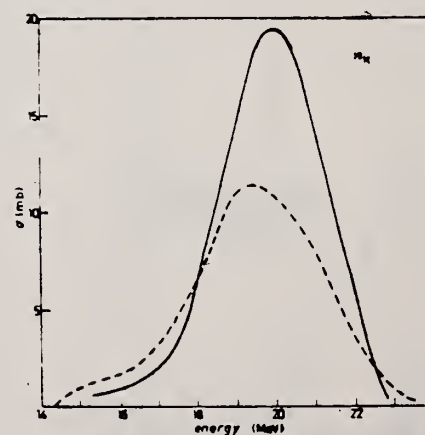


Fig. 2. - Cross sections obtained by the photo difference method for the $^{39}K(\gamma, n)^{38}K$ (3^+ , 0^+) reactions. --- 3^+ (7.70 min), — 0^+ (0.96 s).

Ref. K. Shoda, H. Niizeki, N. Fujiwara, A. Okiguchi, A. Watanabe,
M. Midera
J. Phys. Soc. Japan 17, 1083 (1962)

Elem. Sym.	A	Z
K	39	19

Method Betatron; proton spectrum; nuclear emulsion

Ref. No.	NVB
62 Sh 9	

Reaction	E or ΔE	E_0	Γ	$\int \sigma dE$	$J\pi$	Notes
$K^{39}(\gamma, p)$	Bremss. 24					

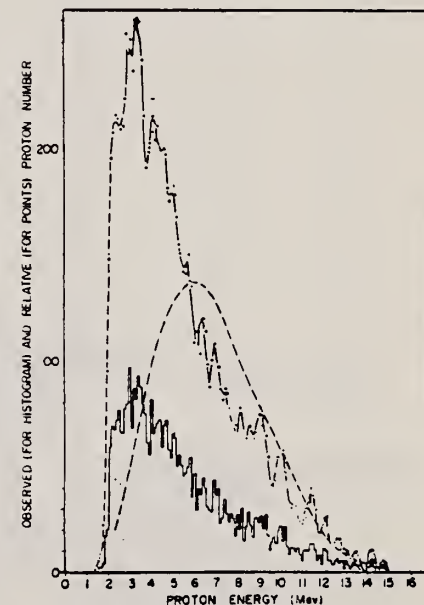


Fig. 1. The energy distribution of photoprotons from K^{39} . The histogram is a measured distribution. The solid line is a smoothed distribution. The broken line is a calculated curve using the statistical model with the Weiskopf level density $\omega = C \exp [2\sqrt{0.91 E}] \text{ Mev}^{-1}$ and a classical Coulomb barrier height of 6.02 Mev.

Ref. **W.C.Barber, J.Goldenberg, G.A.Petersen, Y.Turkin**

Nuclear Phys. 41, 461 (1963); erratum to be published (as of 9/3/63)

Elem. Sym.	A	Z
K	39	19

Method

Lins (Stanford Mark II) - counter telescope

Ref. No.

6381

B G

Reaction	E or ΔE	E_0	Γ	$\int \sigma dE$	$J\pi$	Notes
(e,e')	41.5	no resonances				ground state $3/2^+$

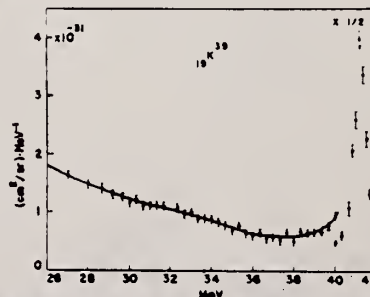


Fig. 17. Spectrum of 41.5 MeV electrons scattered from a potassium target at 180°.

METHOD			SOURCE		DETECTOR		ANGLE
REACTION	RESULT	EXCITATION ENERGY	TYPE	RANGE	TYPE	RANGE	
G,N	ABX	THR - 70	C	12- 70	ACT-I		4PI

Measured Isomer production ratio.
 Isomer ratio $R = .55 \pm .18$ $E_\gamma = 35$.
 Spin cut off $\sigma = 1.65 \pm 0.35$

ISOMER RATIO

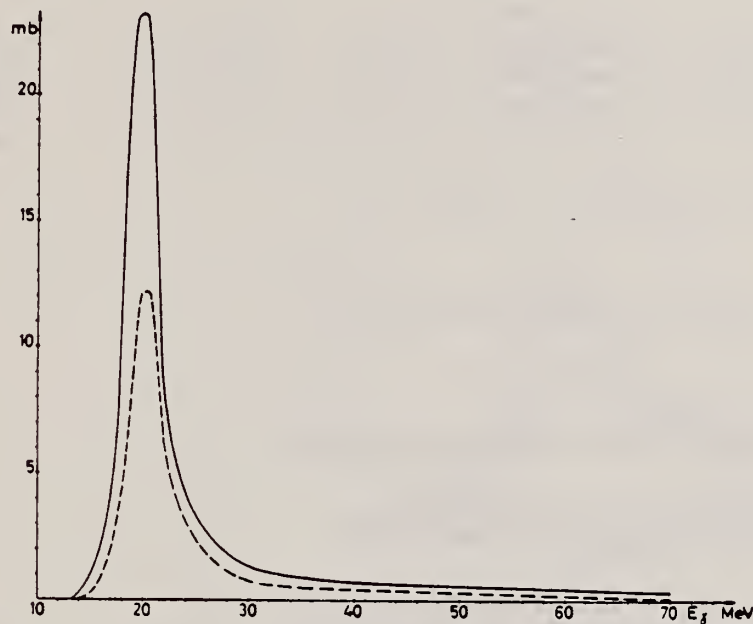


Fig. 1. (γ, n) reaction in ^{40}K , total (solid line) and 0^+ state (dashed line) cross sections.

TABLE I
 Spins and half-lives of isomeric states

Target nucleus	Spin of isomeric states	Half-life	Modes of decay (used for detection)	Detection method
^{40}K	0^+	0.95 sec	β^+ (100 %)	γ - γ fast-slow coincidence (resolving time 0.2 and 2 μsec)
$J = \frac{1}{2}$	3^+	7.7 min	β^+ (> 99 %)	γ - γ coincidence
^{96}Zr	$\frac{1}{2}^-$	4.3 min	γ (93 %) β^+ (1.7 %)	NaI (well type) spectrometer centered on the 0.588 MeV γ ray line γ - γ coincidence
$J = 0$	$\frac{1}{2}^+$	79 h	β^+ (30 %)	γ - γ coincidence
^{96}Mo	$\frac{1}{2}^-$	66 sec	γ (57 %) β^+ (38 %)	NaI (well type) spectrometer centered on the 0.658 MeV γ ray line γ - γ coincidence
$J = 0$	$\frac{1}{2}^+$	16 min	β^+ (94 %)	γ - γ coincidence

METHOD

REF. NO.

65 Co 3

JOC

REACTION	RESULT	EXCITATION ENERGY	SOURCE		DETECTOR		ANGLE
			TYPE	RANGE	TYPE	RANGE	
G, N	ABX	THR-80	C	80	ACT-I		4PI
G, NP	ABX	THR-80	C	80	ACT-I		4PI

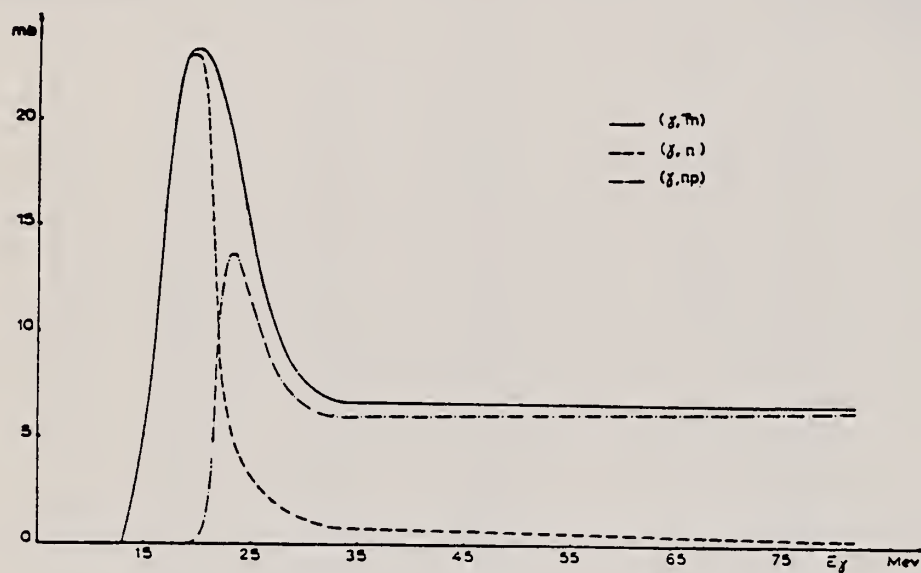


Fig. 4.

Sezioni d'urto per i processi $K^{39}(\gamma, n)K^{38}$ (tratto pieno) e $K^{39}(\gamma, np)K^{38}$. La scala delle energie è stata opportunamente dilatata fino a 30 MeV per rappresentare meglio la regione della risonanza gigante.

REF. J. M. Loiseaux, J. M. Maison, and M. Langevin
J. de Physique 28, 11 (1967)

ELEM. SYM.	A	Z
K	39	19

METHOD

REF. NO.

67 Lo 1

JOC

REACTION	RESULT	EXCITATION ENERGY	SOURCE		DETECTOR		ANGLE
			TYPE	RANGE	TYPE	RANGE	
G, G/	ABX	14-32	C	34	NAI-D		DST

TABLEAU I

COEFFICIENT a DES DISTRIBUTIONS ANGULAIRES

$$W(\theta) = 1 + a \cos^2 \theta$$

^{16}O	$a(19-25 \text{ MeV}) = 1 \pm 0,1$				
^{23}Na	$a(15-18 \text{ MeV}) = 0,1 \pm 0,1$	$a(18,5-23 \text{ MeV}) = 0,4 \pm 0,15$	$a(25-30 \text{ MeV}) = 0,85 \pm 0,2$		
^{24}Mg	$a(16,5-20 \text{ MeV}) = 0,3 \pm 0,1$	$a(20-25 \text{ MeV}) = 0,5 \pm 0,1$	$a(25,5-32 \text{ MeV}) = 0,5 \pm 0,1$		
^{28}Si	$a(15-17,5 \text{ MeV}) = 0,87 \pm 0,1$	$a(18-23 \text{ MeV}) = 0,7 \pm 0,1$	$a(25,5-32 \text{ MeV}) = 0,5 \pm 0,1$		
^{39}K	$a(14,5-18,5 \text{ MeV}) = 0,5 \pm 0,1$	$a(19-24,5 \text{ MeV}) = 1 \pm 0,1$	$a(25-32 \text{ MeV}) = 1 \pm 0,1$		

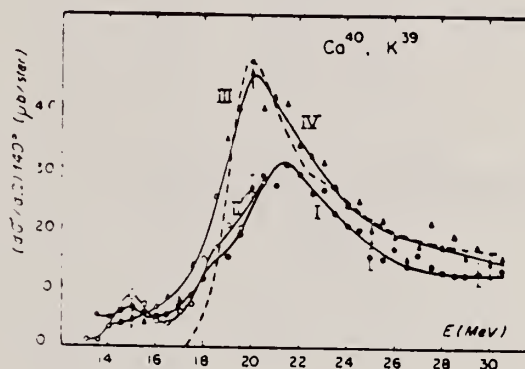


FIG. 9.

Sections efficaces différentielles de diffusion pour ^{39}K déterminée à $E_m = 22 \text{ MeV}$ (courbe II) et $E_m = 32 \text{ MeV}$ (courbe I).

Section efficace différentielle de diffusion pour ^{40}Ca déterminée à $E_m = 32 \text{ MeV}$ (courbe III) et prévue par la relation de dispersion (courbe IV).

METHOD						REF. NO.	
/						69 Ho 1	
REACTION	RESULT	EXCITATION ENERGY	SOURCE		DETECTOR		ANGLE
			TYPE	RANGE	TYPE	RANGE	
G,XP	ABY	THR- 33	C	24-33	SCI-D	3-14	90

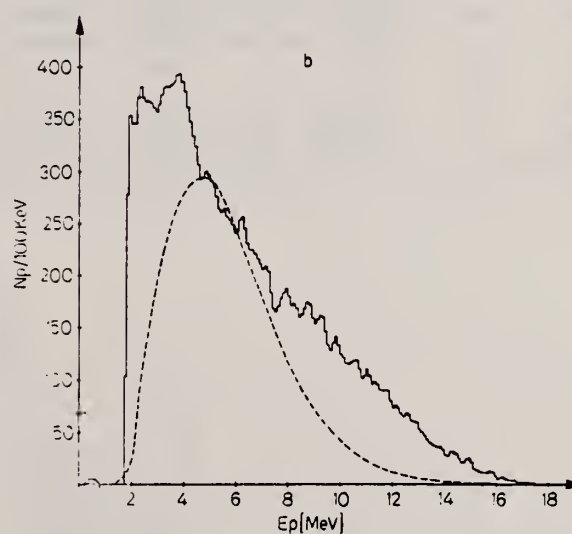
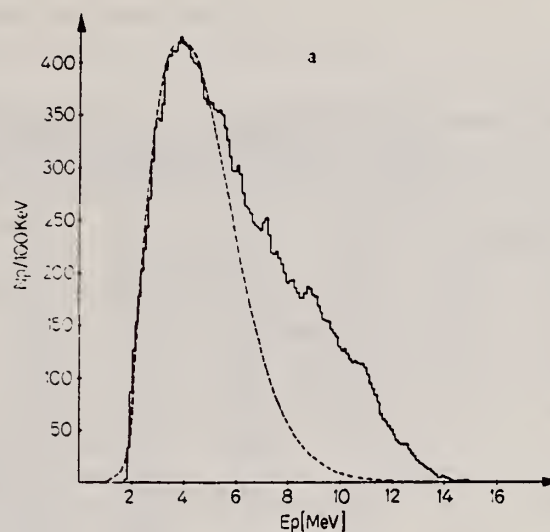


Fig. 12a u. b. Energieverteilung der Photoprotonen aus ^{39}K für a $E_0 = 24$ MeV und b $E_0 = 32,5$ MeV. Kurven: Berechnete Verdampfungsspektren

[over]

Tabelle 1. Daten zu den einzelnen Reaktionen. Die Werte für den integrierten Wirkungsquerschnitt wurden unter der Annahme ausschließlicher Grundzustandsübergänge berechnet. Für ^{23}Na und ^{39}K als Ausnahme s. Text

Tar- get	Anreiche- rungsgrad %	(γ, p)- Schwelle MeV	Druck oder Dicke	End- energie MeV	Zahl gemess. Protonen	Ausbeute $\mu\text{b}/\text{MeV sr}$	$\int_{32,5}^{\infty} \sigma(E) dE$ MeVmb	Figur
^{18}O	99	16,0	230 Torr	32,5	36074	58 ± 7	38 ± 6	1, 2
^{20}Ne	90,9	12,8	450 Torr	28,0	3175	$7,4 \pm 1$	—	—
			610 Torr	32,5	6293	$14,9 \pm 2$	61 ± 11	5, 6
^{22}Ne	99,9	15,3	240 Torr	24,0	1960	$2,3 \pm 0,4$	—	4, 5
				28,0	4790	$3,6 \pm 0,6$	—	4, 5
				32,5	5210	$6,7 \pm 0,9$	45 ± 8	4, 5
^{23}Na	100	8,8	65 μ	24,0	14182	$6,3 \pm 1,0$	—	7
			60 μ	32,5	11152	$12,8 \pm 2,0$	117 ± 30	7
^{30}Ar	99	8,5	250 Torr	32,5	45173	57 ± 6	270 ± 40	8, 10
^{40}Ar	99,6	12,5	230 Torr	32,5	29559	$14,2 \pm 15$	104 ± 15	9, 11
^{39}K	93,1	6,4	80 μ	24,0	24230	$17,4 \pm 2,8$	—	12
			90 μ	32,5	24941	$41,9 \pm 6,7$	405 ± 100	12
^{84}Kr	99	10,7	170 Torr	32,5	35515	$12,7 \pm 2,0$	80 ± 20	14
Kr	natürl.	10	170 Torr	32,5	13570	$12,5 \pm 2,0$	75 ± 20	13
Xe	natürl.	9	150 Torr	32,5	7553	$7,6 \pm 0,9$	40 ± 7	15

METHOD /

REF. NO.

69 We 1

egf

REACTION	RESULT	EXCITATION ENERGY	SOURCE		DETECTOR		ANGLE
			TYPE	RANGE	TYPE	RANGE	
G,N	RLX	13-29	C	13-29	ACT-I		4PI

182 TO 123 KEV ISOMER

THE ^{39}K PHOTONEUTRON CROSS SECTION TO THE ISOMERIC STATE OF ^{38}K

D. V. Webb, E. G. Muirhead and B. M. Spicer, School of Physics, University of Melbourne, Parkville, Victoria 3052, Australia.

Preliminary results are presented of a measurement of the $^{39}\text{K}(\gamma, n)^{38\text{m}}\text{K}$ cross section. The 0^+ ($T = 1$) isomeric state at 123 KeV in ^{38}K decays by positron emission with a half life of 0.95 secs. The decays are counted by detecting the annihilation γ -quanta, either singly or in coincidence. Yield curves were measured for both singles and coincidence counts from below threshold (13.2 MeV) to 29 MeV, in steps of 200 KeV, and were analysed separately by the Leiss-Penfold method with a bin width of 800 KeV.

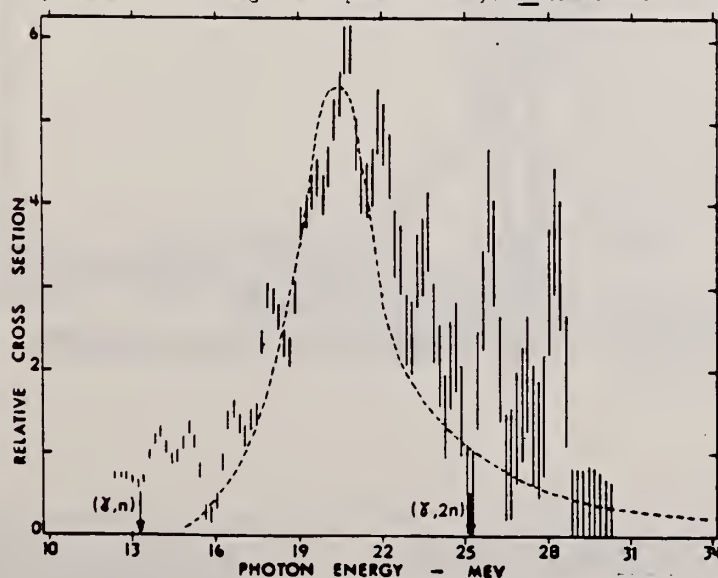
The 'singles' cross section is shown in the figure; the coincidence data clearly reproduces seven peaks seen below 22 MeV. Although an absolute cross section has not been assigned, the envelope grossly smoothed is consistent with the coarser resolution data of Costa et al (Nucl.Phys. 72 (1965) 158), whose result is represented by the dotted curve in the figure.

Since the ^{39}K ground state is a $3/2^+$ ($T = 1/2$) state, the dipole states are $1/2^-$, $3/2^-$, $5/2^-$ ($T = 1/2$ or $3/2$). Isospin geometrical factors indicate that the absorption strength will be divided among the $T = 3/2$ and $T = 1/2$ states approximately in the ratio 3:2. However, it should be noted that the isomeric state is equally accessible from $T = 3/2$ and $T = 1/2$ states by neutron emission. Thus the strong expectation is that the structure observed in this reaction reflects that of the total γ -ray absorption cross section.

The dipole states are expected to have a 2 hole - 1 particle structure, and can be visualized as a 1^- ($T = 1$) particle hole excitation in a ^{40}Ca core coupled to a $1d_{3/2}$ hole. One expects, therefore, to find some relationship between the energies of the structure in the giant resonances of ^{40}Ca and ^{39}K . Energies of peaks in the (γ, n) cross sections are as follows:

^{40}Ca	15.9	17.8	18.5	18.9	19.2	19.6	19.9	20.8	21.7	22.3	24.1	25.4	MeV
^{39}K	16.6	17.9					19.5	20.7	22.0		23.5	25.8	MeV

The $^{40}\text{Ca}(\gamma, n)$ data is that of Baglin and Spicer (Nucl.Phys. 54 (1964) 549).



REF. K. Kayser, W. Collin, P. Filss, S. Guldbakke, G. Nolte,
H. Reich, J. O. Trier, W. Witschel
Z. Physik 239, 447 (1970)

ELEM. SYM.	A	Z
K	39	19
REF. NO.		
70 Ka 2		egf

METHOD			SOURCE		DETECTOR		ANGLE
REACTION	RESULT	EXCITATION ENERGY	TYPE	RANGE	TYPE	RANGE	
G,N	ABX	15-120	C	15-140	ACT-I		4PI

Investigation of the Photo Nuclear Reactions $^{12}\text{C}(\gamma, n)$, $^{12}\text{C}(\gamma, 2n)$, $^{39}\text{K}(\gamma, n)$ and $^{40}\text{Ca}(\gamma, np)$ up to the Meson Threshold

In order to obtain data on the photon absorption process between the giant resonance and the meson threshold the cross sections of the reactions $^{12}\text{C}(\gamma, n)^{12}\text{C}$, $^{12}\text{C}(\gamma, 2n)^{10}\text{C}$, $^{39}\text{K}(\gamma, n)^{38}\text{K}$, and $^{40}\text{Ca}(\gamma, np)^{38}\text{K}$ have been determined by the analysis of yield curves at the 140 MeV electron synchrotron of the PTB.

Though the (γ, n) cross sections grow small with increasing photon energy they are different from zero up to energies of 60 MeV and above. The cross section of the reaction $^{12}\text{C}(\gamma, 2n)$ is extremely small; its highest value amounts to 0.15% of the highest value of the $^{12}\text{C}(\gamma, n)$ reaction. The measured $^{40}\text{Ca}(\gamma, np)$ cross section is of the order predicted by the naive quasi-deuteron model. The integrated cross sections of the above reactions up to 140 MeV are 85 ± 7 , 0.90 ± 0.10 , 139 ± 16 , and 76 ± 7 MeV mb respectively.

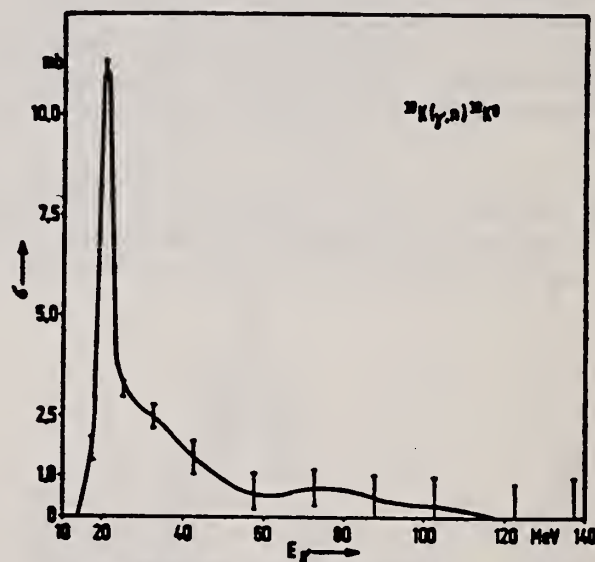


Fig. 5. Wirkungsquerschnitt der Reaktion $^{39}\text{K}(\gamma, n)^{38}\text{K}$

METHOD

REF. NO.

70 Pe 1

egf

REACTION	RESULT	EXCITATION ENERGY	SOURCE		DETECTOR		ANGLE
			TYPE	RANGE	TYPE	RANGE	
E, E/	ABX	0-6	D	60	MAG-D	54-60	DST

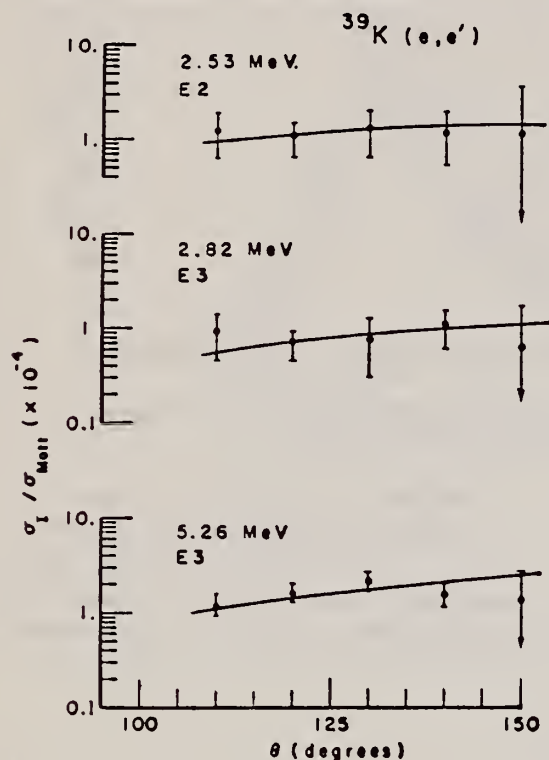


Fig. 4. The measured angular distributions for populating the 2.53 MeV ($\frac{1}{2}^+$), 2.82 MeV ($\frac{1}{2}^-$) and 5.26 MeV states of ^{39}K are compared to DWBA predictions. The values of $B(EL)$ obtained from this comparison are listed in table 2.

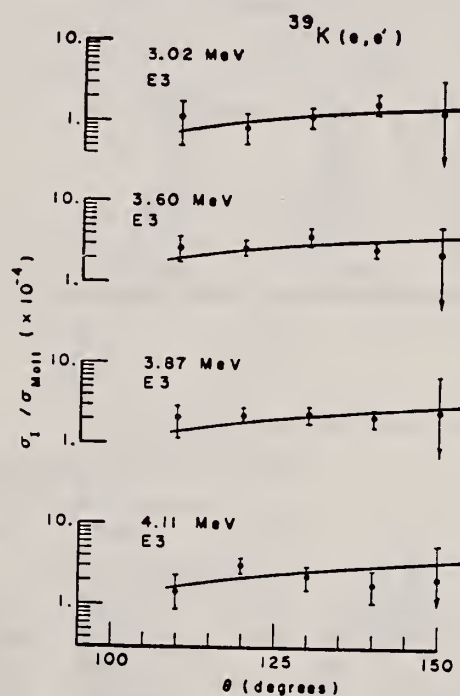


Fig. 5. The measured angular distributions for populating the strongly excited states of ^{39}K are compared to the DWBA predictions for octupole excitations. The values of $B(E3)$ obtained from this comparison are listed in table 2.

[over]

TABLE 2
Result of the present work for ^{39}K

E_x (MeV)	EL	$B(EL)\dagger$ ($e^2 \cdot \text{fm}^{2L}$)	(s.p.u.)	χ^2 ($f=4$)
2.51 ± 0.02	E2	22.1 ± 5.3	0.56	0.24
2.82 ± 0.03	E3	2480 ± 530	3.9	0.89
3.02 ± 0.02	E3	3410 ± 550	5.4	1.43
3.60 ± 0.03	E3	8500 ± 790	13.4	4.40
3.87 ± 0.03	(E3)	6650 ± 650	10.5	3.31
4.11 ± 0.03	(E3)	7610 ± 950	12.0	7.02
5.26 ± 0.06	(E3)	5280 ± 440	8.3	4.23

The measured excitation energy, assumed multipolarity, and the normalization transition strengths $B(EL)\dagger$ are presented. We also list the enhancements over the single-particle estimate for the transition rate and the χ^2 of the comparison between our data and the DWBA prediction.

TABLE 3
Comparison of experimental values $B(E2)$ and $B(E3)$ for ^{39}K and ^{40}Ca

		$(\alpha, \alpha')^a, ^d)$	$(p, p')^b)$	$(e, e')^c)$
^{40}Ca	3.73 MeV (3^-)	$B(E3)\dagger = 24.4$	31.2	32
	3.90 MeV (2^+)	$B(E2)\dagger = 3.2$	1.9	1.8
^{39}K	2.53 MeV ($\frac{1}{2}^+$)	$B(E2)\dagger = 0.35$		0.56
	2.82 MeV ($\frac{3}{2}^-$)	$B(E3)\dagger = 1.0$		3.9
	3.02 MeV ($\frac{3}{2}^-$)	2.3		5.4
	3.60 MeV ($\frac{3}{2}^-$)	6.3		13.4
	3.87 MeV ($\frac{3}{2}^-$)	4.8		10.5
	4.11 MeV ($\frac{3}{2}^-$)	5.1		12.0
	5.26 MeV ($?^-$)	2.2		8.3
Ratios to the ^{40}Ca E3 strength				
	(α, α')	(weak coupling)	(e, e')	
	3.02	9.4 %	14.3 %	17.0 %
	3.60	25.8	35.7	42.3
	3.87	19.7	28.5	33.1
	4.11	20.9	21.5	37.9
		75.8 %	100.0 %	130.3 %

^{a)} Ref. ¹⁵⁾.

^{b)} Ref. ¹⁶⁾.

^{c)} Ref. ¹⁸⁾.

^{d)} Ref. ⁴⁾.

All values are quoted as ratios to the single-particle estimate. Only the DWBA results of ref. ⁴⁾ are used.

TABLE 1
Observed cross sections for the scattering of 60.2 MeV electrons to the levels of ^{39}K presented as the ratio to the Mott point-charge prediction

θ	109.7°	119.7°	129.7°	139.8°	149.8°	E_x (MeV)
σ_i/σ_M ($\times 10^{-4}$)	1.24 ± 0.64	1.02 ± 0.37	1.29 ± 0.67	1.22 ± 0.71	1.10 ± 2.50	2.53
	0.92 ± 0.47	0.69 ± 0.22	0.73 ± 0.43	1.11 ± 0.51	0.58 ± 1.21	2.88
	1.11 ± 0.63	0.80 ± 0.30	1.11 ± 0.28	1.75 ± 0.47	1.24 ± 2.32	3.02
	2.70 ± 0.93	2.69 ± 0.35	3.66 ± 0.76	2.63 ± 0.51	2.42 ± 2.68	3.60
	2.04 ± 0.88	2.25 ± 0.30	2.38 ± 0.55	2.11 ± 0.40	2.55 ± 4.22	3.87
	1.41 ± 0.72	3.06 ± 0.43	2.21 ± 0.63	1.83 ± 0.79	2.13 ± 3.52	4.11
	1.19 ± 0.16	1.74 ± 0.31	2.23 ± 0.34	1.60 ± 0.37	1.32 ± 1.41	5.26
q_0 (fm^{-1})	0.479	0.508	0.543	0.564	0.580	

ELEM. SYM.	A	Z
K	39	19
REF. NO.		
71 We 1		egf

METHOD			SOURCE		DETECTOR		ANGLE
REACTION	RESULT	EXCITATION ENERGY	TYPE	RANGE	TYPE	RANGE	
G,N	ABX	13-30	C	13-30	ACT-I		4PI

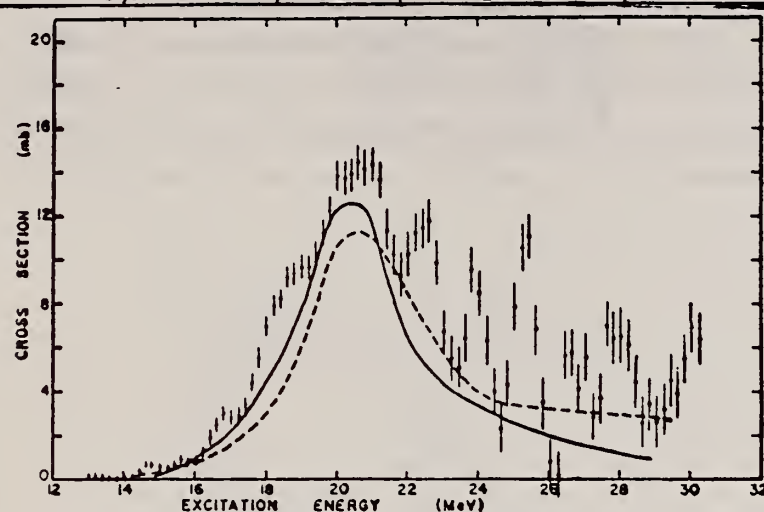


Fig. 4. Comparison of the present "singles" measurement with that of Costa *et al.* (solid line) and Kayser *et al.* (dashed line), [ref. ^{1,2}].

¹ S. Costa, F. Ferrero, S. Ferroni, L. Pasqualini and E. Silva, Nucl. Phys. 72, 158 (1965).

² K. Kayser (Physikalisch-Technische Bundesanstalt) private communication.

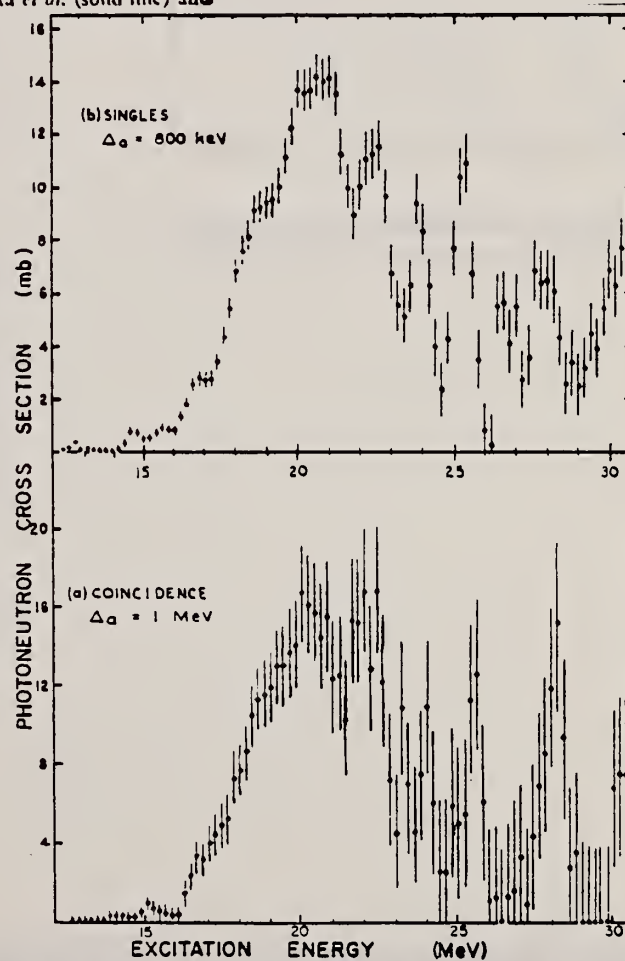


Fig. 3. Cross sections of the $^{39}\text{K}(\gamma, n)^{38}\text{K}$ reaction derived from (a) the "coincidence" yield curve analysed in 1 MeV intervals, and (b) "singles" yield curve analysed in 800 keV intervals.

REF. R. Bergare, H. Beil, P. Carlos, A. Lepretre, A. Veyssiere
PICNS-73, Vol. I, p. 525 Asilomar

ELEM. SYM.	A	Z
K	39	19
REF. NO.		
73 Be 10		hmg

METHOD

REACTION	RESULT	EXCITATION ENERGY	SOURCE		DETECTOR		ANGLE
			TYPE	RANGE	TYPE	RANGE	
G,N	ABX	12- 31	D	12- 31	BF3-I		4PT
G,PN	ABX	19- 29	D	19- 29	BF3-I		4PT
G,2N	ABX	31- 32	D	31- 32	BF3-I		4PT

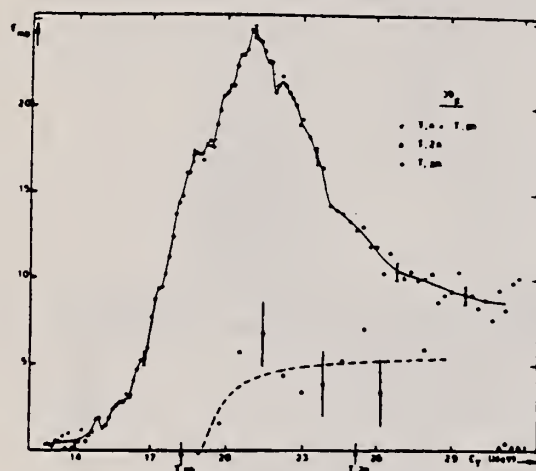


Fig. 7 Partial photoneutron cross sections $\sigma(\gamma,n)$ $\sigma(\gamma,pn)$ and $\sigma(\gamma,2n)$ of ^{39}K .

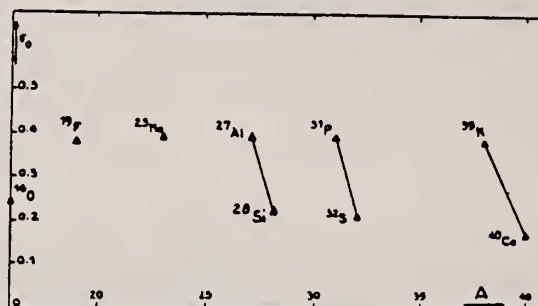


Fig. 13 Integrated photoneutron cross-sections for s-d shell nuclei.

V.G. Vlasenko, N.G. Afanas'ev, V.A. Gol'dshtein, S.V. Dementii,
E.L. Kuplennikov, V.I. Ogurtsov, and V.I. Startsev
Yad. Fiz. 17, 1124 (1973); Sov. J. Nucl. Phys. 17, 585 (1973)

K

39

19

METHOD

/

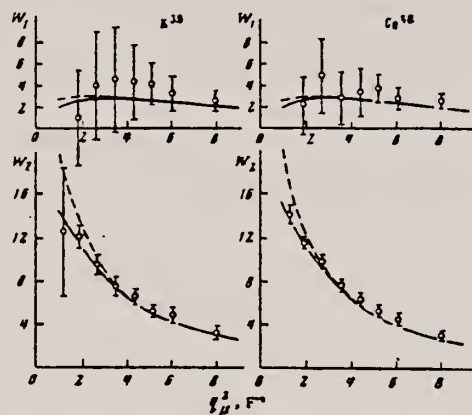
REF. NO.

73 V1 8

hmg

REACTION	RESULT	EXCITATION ENERGY	SOURCE		DETECTOR		ANGLE
			TYPE	RANGE	TYPE	RANGE	
E, E/	FMF	30-180	D	550-999	MAG-D		DST

999=1.15 GEV



Inelastic electromagnetic form factors for K^{39} and Ca^{40} .

REF. D. V. Webb, G. A. Peterson, W. L. Bendel, E. C. Jones, Jr.,
L. W. Fagg
Phys. Rev. C12, 330 (1975)

ELEM. SYM.	A	Z
K	39	19

METHOD					REF. NO.	
					75 We 1	hmg
REACTION	RESULT	EXCITATION ENERGY	SOURCE		DETECTOR	
			TYPE	RANGE	TYPE	RANGE
E, E/	ABX	2	D	50,61	MAG-D	180
		(2.523)		(50.98,60.65)		

Maximum $\Gamma(M1) = .11$ meV

2.523 LEVEL

TABLE L Inelastic electron scattering cross sections for the 2.523 MeV $\frac{1}{2}^+$ state.

Total incident energy (MeV)	Cross section ratio (2.523/2.814)	Inelastic momentum transfer (fm ⁻¹)	Cross section (10 ⁻³⁴ cm ² /sr)
60.65	0.891	0.601	2.2 ± 0.5
50.98	0.823	0.503	3.1 ± 0.9

ELEM. SYM.	A	Z
K	39	19
METHOD	REF. NO.	
	81 Gr 3	
	hg	

REACTION	RESULT	EXCITATION ENERGY	SOURCE		DETECTOR		ANGLE
			TYPE	RANGE	TYPE	RANGE	
E, E/	ABX	2	D	40-66	MAG-D		DST
		(2.523)					

Abstract: The mixed E2 M1 transitions from the $\frac{1}{2}^+$ ground states to the first excited $\frac{1}{2}^+$ states in ^{39}K and ^{41}K were studied by low momentum transfer inelastic electron scattering. The E2 contribution dominates the cross section and $B(E2)^\dagger$ values for ^{39}K of $18.9 \pm 1.8 \text{ e}^2 \cdot \text{fm}^4$ and for ^{41}K of $23.9 \pm 4.2 \text{ e}^2 \cdot \text{fm}^4$ were obtained. Together with the measured lifetimes of these states $B(M1)^\dagger$ values for the I -forbidden $d_{3/2} \rightarrow s_{1/2}$ transition are deduced to be $0.015 \pm 0.006 \mu_K^2$ in ^{39}K and $0.067 \pm 0.006 \mu_K^2$ in ^{41}K .

2=2.523 MEV B(E2)

E NUCLEAR REACTIONS $^{39,41}\text{K}(e, e')$, $E = 40-66 \text{ MeV}$; measured $\sigma(E_e, \theta)$; $^{39,41}\text{K}$ levels deduced $B(E2)$, $B(M1)$.

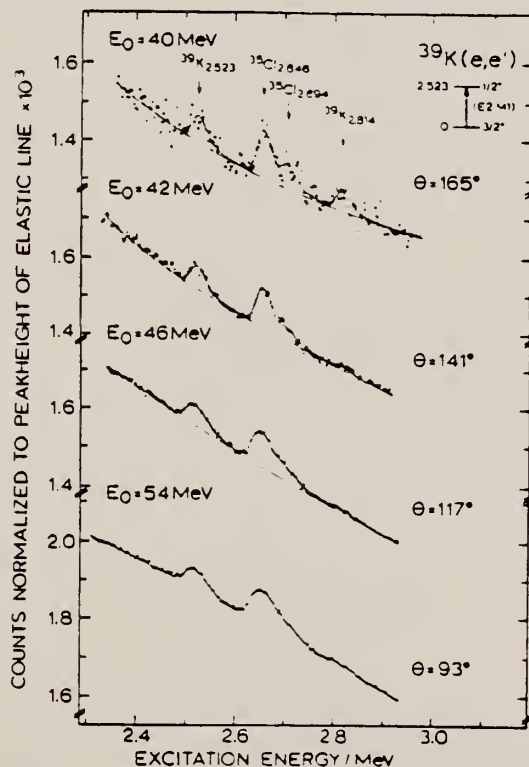


Fig. 1. Spectra of inelastically scattered electrons on a KC1 target taken at various scattering angles and bombarding energies but at the same momentum transfer $q = 0.39 \text{ fm}^{-1}$ for the excitation of the $J^\pi = \frac{1}{2}^+$ state at $E_x = 2.523 \text{ MeV}$ in ^{39}K . The various lines are sitting on the radiative tail of the elastic lines from K and Cl and the decomposition of the spectra into various lines is also shown.

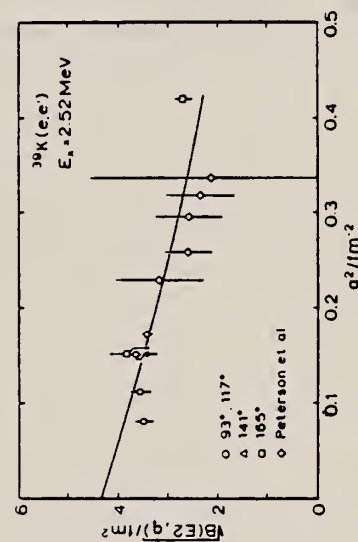


Fig. 3 The square root of the reduced longitudinal transition probability (note that we write $B(E2)$ instead of $B(C2)$) for the $\frac{1}{2}^+ \rightarrow \frac{1}{2}^+$ transition in ^{39}K as a function of the square of the momentum transfer. Data from ref. 3) are combined with the data from the present experiment. A model calculation employing eq. (1) of the main text is compared with the data points.

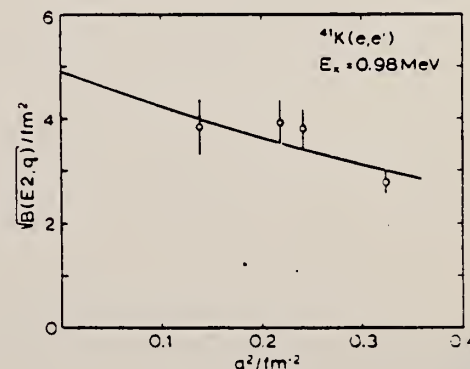


Fig. 4 The same as in fig. 3 but for the $\frac{1}{2}^+ \rightarrow \frac{1}{2}^+$ transition in ^{41}K .

(OVER)

TABLE 1

Square of the momentum transfer, bombarding energy, scattering angle, experimental and theoretical cross sections and Coulomb correction factors for the transition from the ground state to the first excited state at $E_i = 2.523$ MeV in ^{39}K

q^2 (fm^{-2})	E_0 (MeV)	θ°	$(d\sigma/d\Omega)$ (10^{-6} fm^2)			f_C^{-1}
			exp	theory C2 + E2	theory C2	
0.081	40.0	93	3.29 ± 0.34	4.07	4.04	0.75
0.112	40.0	117	1.97 ± 0.24	2.16	2.12	0.75
0.151	54.1	93	6.37 ± 0.28	5.99	5.91	0.79
0.151	46.2	117	3.00 ± 0.19	2.56	2.49	0.78
0.151	41.9	141	0.84 ± 0.08	0.90	0.84	0.76
0.151	39.9	165	0.152 ± 0.032	0.17	0.12	0.76
0.172	49.4	117	2.74 ± 0.19	2.73	2.65	0.79
0.420	65.9	165	0.168 ± 0.022	0.26	0.12	0.90

TABLE 4

Summary of the results on the E2 and M1 strength for the ground to first excited state transition in ^{39}K and ^{41}K , respectively, and comparison with other measurements

Nucleus	E_i (MeV)	$B(E2, k) \uparrow (\text{e}^2 \cdot \text{fm}^4)$				$B(M1, k) \uparrow / \mu_N^2$ present work
		present work	ref. ⁵⁾	ref. ⁷⁾	ref. ⁸⁾	
^{39}K	2.523	18.9 ± 1.8	22 ± 5			0.015 ± 0.006
^{41}K	0.980	23.9 ± 4.2		22 ± 7	6.0 ± 0.9	0.067 ± 0.006

K
A=41

K
A=41

306

K
A=41

METHOD

Van de Graaff; inverse; NaI spectrometer

Page 1 of 2

REF. NO.

63 Ko 2

NVB

REACTION	RESULT	EXCITATION ENERGY	SOURCE		DETECTOR		ANGLE
			TYPE	RANGE	TYPE	RANGE	
P,G	RLY	9	D	0-1	NAI-D		DST
			(750-1450 keV)				

SEP ISOTPS

A⁴⁰ target prepared with mass spectrometer.

In Table III, numbers are relative yields.

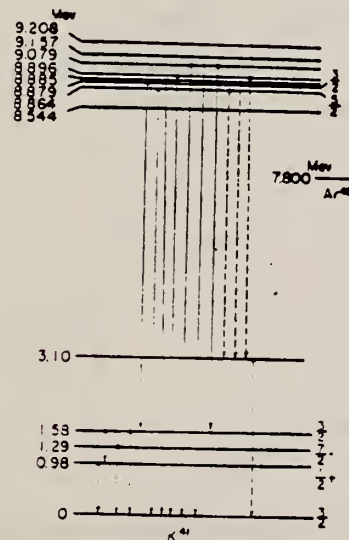


Fig. 7. Level scheme of K^{41} . Excitation energies and gamma-ray decay scheme in K^{41} are illustrated.

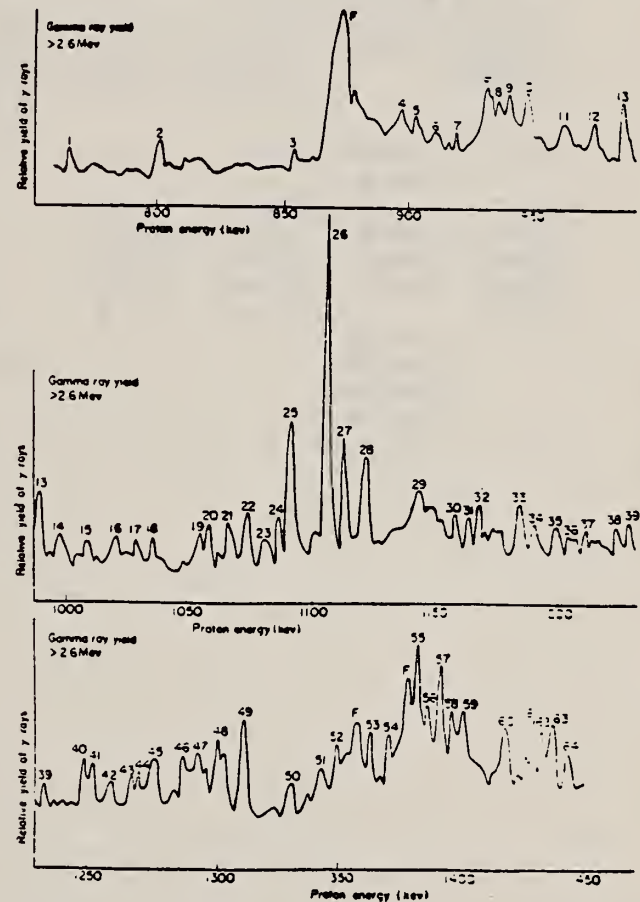


Fig. 3 The excitation curve of the reaction $Ar^{40}(p, n)K^{40}$. The peaks marked F are due to the $Fe(p, n)Co^{56}$ reaction.

(SEE PAGE 2 FOR TABLES)

K

41

19

METHOD

Page 2 of 2

REF. NO.

63 Ko 2

REACTION	RESULT	EXCITATION ENERGY	SOURCE		DETECTOR		ANGLE
			TYPE	RANGE	TYPE	RANGE	

Table III. Angular distributions of 8.9 Mev, 7.2 Mev and 1.58 Mev γ -rays.

	0°	30°	60°	90°
8.9 Mev at resonance 25	1.00 \pm 0.10			2.00 \pm 0.20
7.2 Mev at resonance 26	1.00 \pm 0.10	0.93 \pm 0.10	0.76 \pm 0.10	0.74 \pm 0.10
1.58 Mev	1.00 \pm 0.10	1.00 \pm 0.10	0.97 \pm 0.10	1.00 \pm 0.10

Table II. Gamma-rays observed at the 1091 Kev, 1106 Kev, 1112 Kev, 1123 Kev, 1311 Kev and 1391 Kev (peaks 25, 26, 27, 28, 49 and 57)

1091 Kev	1106 Kev	1112 Kev	1123 Kev	1311 Kev	1391 Kev	Transition
8.9 \pm 0.08Mev		8.9 \pm 0.08Mev	8.9 \pm 0.08Mev	9.0 \pm 0.08Mev	9.0 \pm 0.08Mev	resonance level →0
			7.6 \pm 0.08			resonance level →1.3 Mev
7.2 \pm 0.08	7.2 \pm 0.08Mev	7.2 \pm 0.08	7.2 \pm 0.08			resonance level →1.58 Mev
	6.1 \pm 0.08					(resonance level →3.1 Mev)
5.9 \pm 0.08		5.9 \pm 0.08	5.9 \pm 0.08			
5.5 \pm 0.08	5.6 \pm 0.08	5.5 \pm 0.08	5.5 \pm 0.08			
4.2 \pm 0.08	4.5 \pm 0.08	4.2 \pm 0.08	4.2 \pm 0.08			
3.7 \pm 0.08	3.8 \pm 0.08	3.7 \pm 0.08	3.7 \pm 0.08			
3.1 \pm 0.08		3.1 \pm 0.08	3.1 \pm 0.08			(3.1 Mev→0)
	1.58 \pm 0.02					1.58 Mev→0
	1.29 \pm 0.02			1.30 \pm 0.02		1.30 Mev→0
	0.98 \pm 0.02					0.98 Mev→0
	0.60 \pm 0.02					1.58 Mev →0.98 Mev

REF. I. Blomqvist, G. Nydahl and B. Forkman
Nucl. Phys. A162, 193 (1971)

ELEM. SYM.	A	Z
K	41	19
REF. NO.		egf
71 B1 1		

REACTION	RESULT	EXCITATION ENERGY	SOURCE		DETECTOR		ANGLE
			TYPE	RANGE	TYPE	RANGE	
G,PI+	ABY	150-700	C	150-700	ACT-I		4PI

SEE 68 NY 1

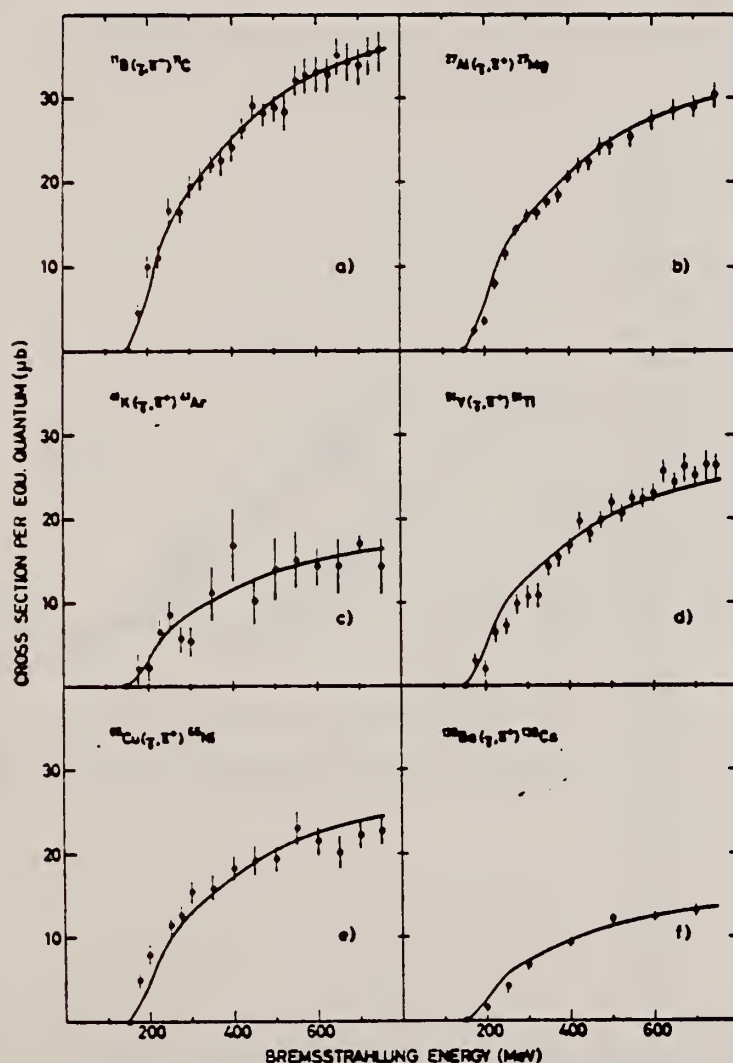


Fig. 2. Absolute yields for all but one of the measured reactions.

ELEM. SYM.	A	Z
K	41	19

METHOD	REF. NO.	
	81 Gr 3	hg

REACTION	RESULT	EXCITATION ENERGY	SOURCE		DETECTOR		ANGLE
			TYPE	RANGE	TYPE	RANGE	
E ₀ E/	ABX	1 (.980)	D	40-66	MAG-D		DST

Abstract: The mixed E2 M1 transitions from the $\frac{1}{2}^+$ ground states to the first excited $\frac{3}{2}^+$ states in ^{39}K and ^{41}K were studied by low momentum transfer inelastic electron scattering. The E2 contribution dominates the cross section and $B(E2)^\dagger$ values for ^{39}K of $18.9 \pm 1.8 \text{ e}^2 \cdot \text{fm}^4$ and for ^{41}K of $23.9 \pm 4.2 \text{ e}^2 \cdot \text{fm}^4$ were obtained. Together with the measured lifetimes of these states $B(M1)^\dagger$ values for the l -forbidden $d_{3/2} \rightarrow s_{1/2}$ transition are deduced to be $0.015 \pm 0.006 \mu_K^2$ in ^{39}K and $0.067 \pm 0.006 \mu_K^2$ in ^{41}K .

1=.980 KEV, B(E2)

E NUCLEAR REACTIONS $^{39,41}\text{K}(e, e')$, $E = 40\text{--}66 \text{ MeV}$, measured $\sigma(E_e, 0)$, $^{39,41}\text{K}$ levels deduced $B(E2)$, $B(M1)$.

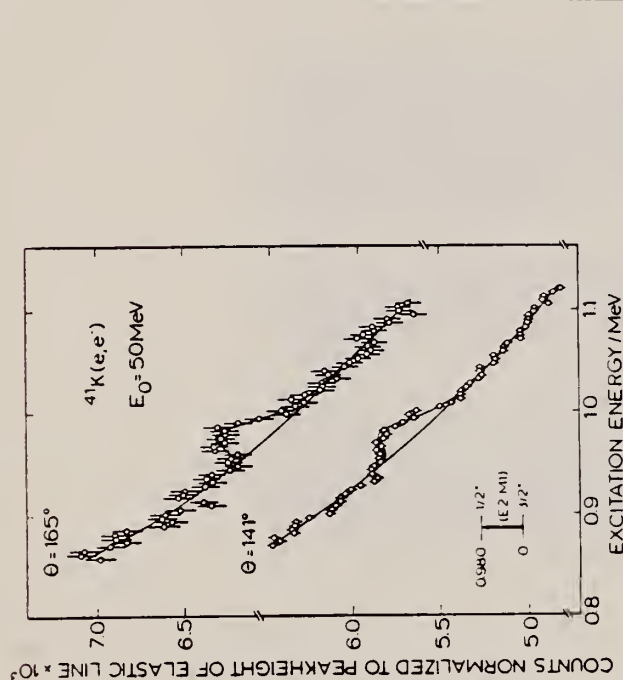


Fig. 2 Spectra of inelastically scattered electrons on a KCl target enriched to 98% in ^{41}K . Note the very strong radiative tail due to the elastic lines from K and Cl on which the line corresponding to the excitation of the $J^\pi = \frac{3}{2}^+$ state at $E_x = 0.980 \text{ MeV}$ is sitting.

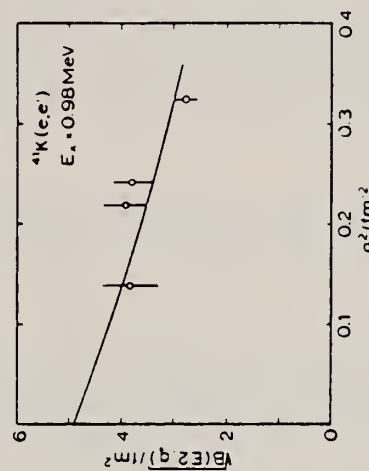


Fig. 4 The same as in fig. 3 but for the $\frac{3}{2}^+ \rightarrow \frac{1}{2}^+$ transition in ^{41}K .

TABLE 4

Summary of the results on the E2 and M1 strength for the ground to first excited state transition in ^{39}K and ^{41}K , respectively, and comparison with other measurements

Nucleus E_x (MeV)	$B(E2, A) [e^2 \text{ fm}^4]$			$B(M1, A) [\mu_K^2]$	
	present work	ref. 3)	ref. 7)	ref. 8)	present work
^{39}K 2.523	18.9 ± 1.8	22 ± 5			0.015 ± 0.006
^{41}K 0.980	23.9 ± 4.2		22 ± 7	6.0 ± 0.9	0.067 ± 0.006

TABLE 3

The same as in table 1 but for the transition from the ground state to the first excited state at $E_x = 0.980 \text{ MeV}$ in ^{41}K

$q^2 (\text{fm}^{-2})$	$E_0 (\text{MeV})$	θ°	$(d\sigma/d\Omega) (10^{-3} \text{ fm}^2)$			f_c^{-1}
			exp	theory C2 + E2	theory C2	
0.139	39.6	141	0.99 ± 0.27	1.065	1.057	0.76
0.219	49.5	141	1.54 ± 0.30	1.26	1.245	0.80
0.242	49.5	165	0.220 ± 0.043	0.192	0.176	0.80
0.324	60.1	141	1.08 ± 0.16	1.279	1.258	0.85

CALCIUM

Z=20

Although the metal itself was unknown to the early civilizations, calcium (from the Latin, *calx* "lime") compounds were used extensively. The Romans used a lime mortar prepared by the burning of limestone; the Egyptians employed gypsum (calcium sulfate) as a plaster in Tut-ankh-Amen's tomb. A particularly beautiful lamp made of calcite (calcium carbonate) was also found in the tomb.

CA

In the early history of chemistry, the nonmetallic substances that were insoluble in water and unchanged by fire were called earths. Lime and magnesia showed alkaline reactions and, therefore, were called alkaline earths.

Davy, after his successful isolation of sodium and potassium, was the first to obtain a relatively pure form of metallic calcium from its rare earth oxide. Following the suggestions of Berzelius, Davy (in 1808) prepared an amalgam with lime. The amalgam was then distilled to drive out the mercury; the residue, a silvery-white metal, was calcium.

CA

REACTION	RESULT	EXCITATION ENERGY	SOURCE		DETECTOR		ANGLE
			TYPE	RANGE	TYPE	RANGE	
G,PI+	ABY	140-250	C	250	MAG-D		90
G,PI-	ABY	140-250	C	250	MAG-D		90

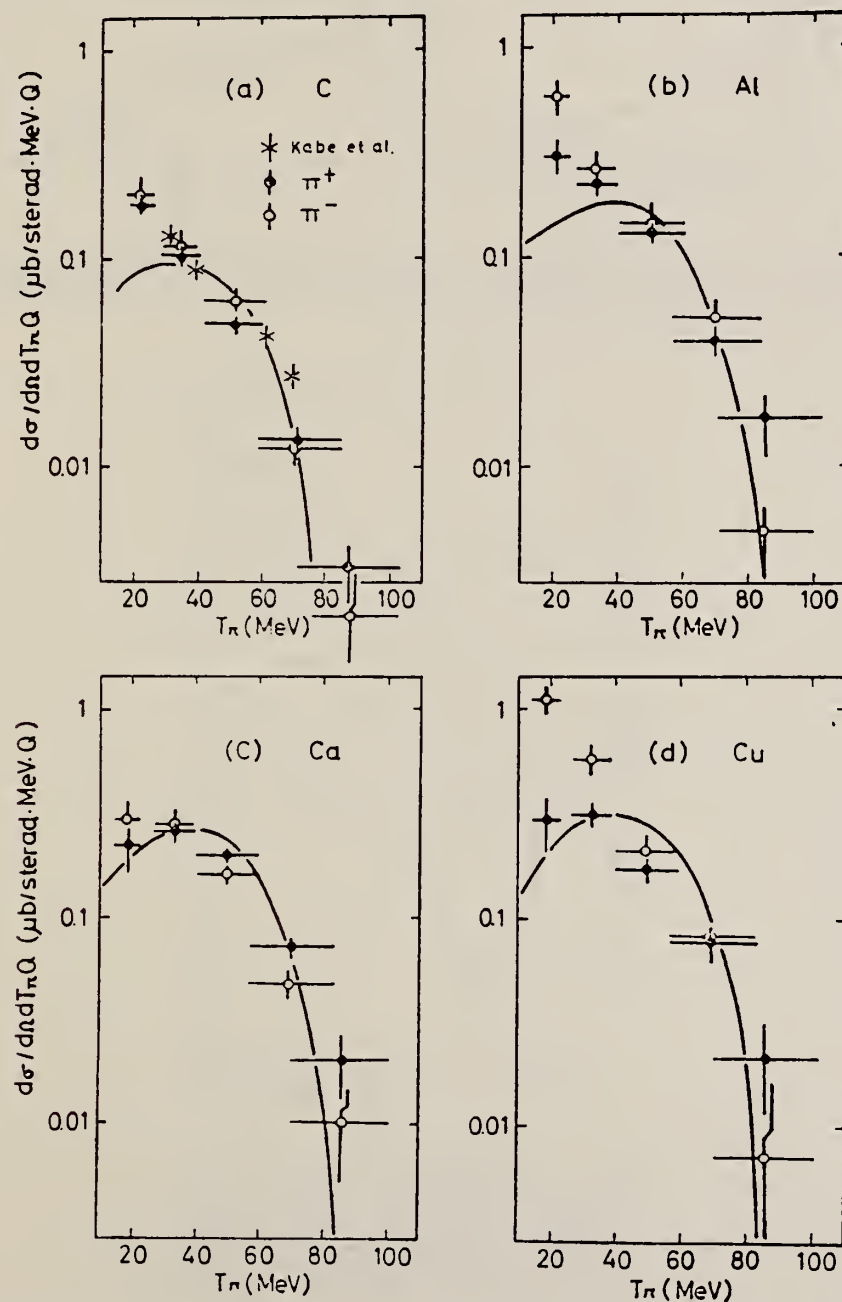


Fig. 2. The energy spectra of photoproduced π^- from C, Al, Ca, and Cu at 90° in the laboratory system by 250-MeV bremsstrahlung. The data of Ca are normalized to $0.26 \mu\text{b sterad}^{-1} \text{MeV}^{-1} Q^{-1}$ for π^+ at 35 MeV. The solid curves are the calculated spectra of π^+ by a theoretical model.

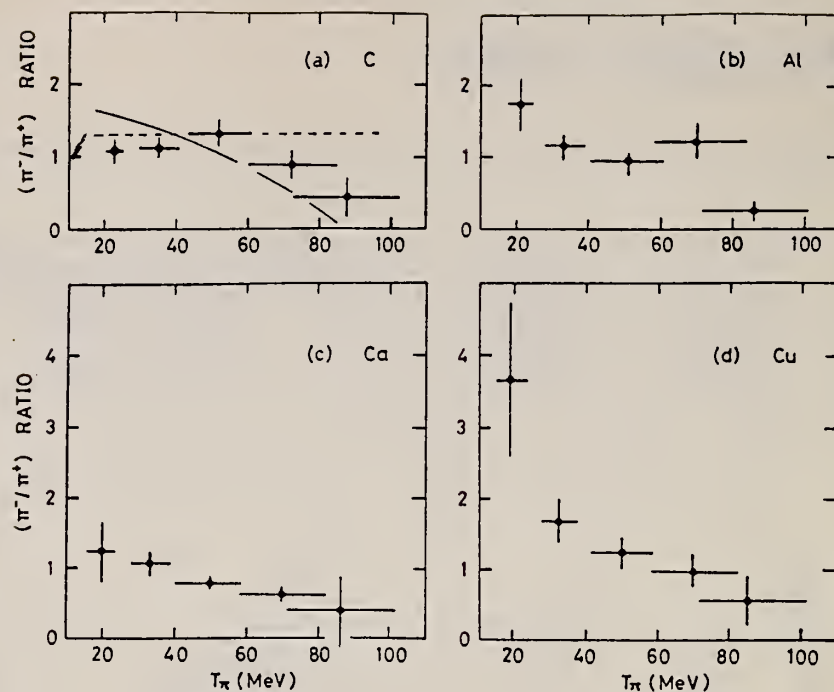


Fig. 3. The π^-/π^+ ratio as a function of the kinetic energy of pions produced from C, Al, Ca, and Cu by 250-MeV bremsstrahlung. The solid curve in (a) is the calculated energy spectrum of π^-/π^+ ratio including the Coulomb potential for C. The dashed curve is the ratio calculated neglecting the Coulomb potential.

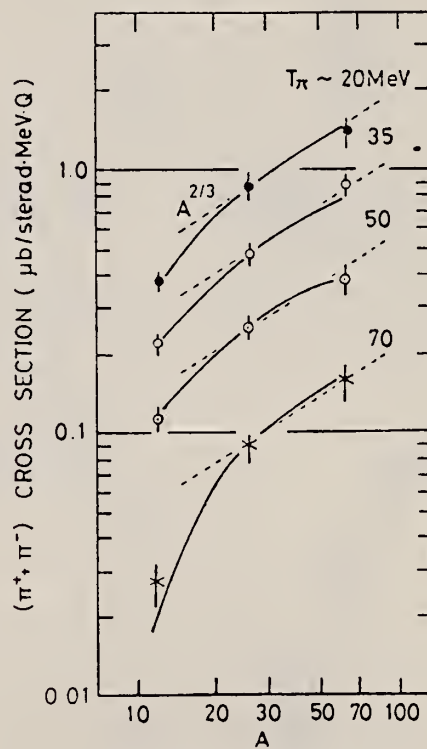


Fig. 4. The A -dependence of the $(\pi^+\pi^-)$ cross sections at the pion kinetic energies of ~ 20 MeV, ~ 35 MeV, ~ 50 MeV and ~ 70 MeV. The solid curves show the relative A -dependence obtained from the theoretical calculation. The dashed lines show $A^{2/3}$ dependence only for guiding eyes.

CA
A=40

CA
A=40

CA
A=40

Method Betatron; photon scattering; NaI spectrometer

Ref. No.

56 Fu 1

EH

Reaction	E or ΔE	E_0	Γ	$\int \sigma dE$	$I \pi$	Notes
Ca (γ, γ)	Bremss. 4-40					Detector at 120° . Cross sections given here are 13% too high due to erroneous $\cos \beta$ factor in denominator of Eq. 5. [See footnote 8 in Phys. Rev. <u>106</u> , 993 (1957)].

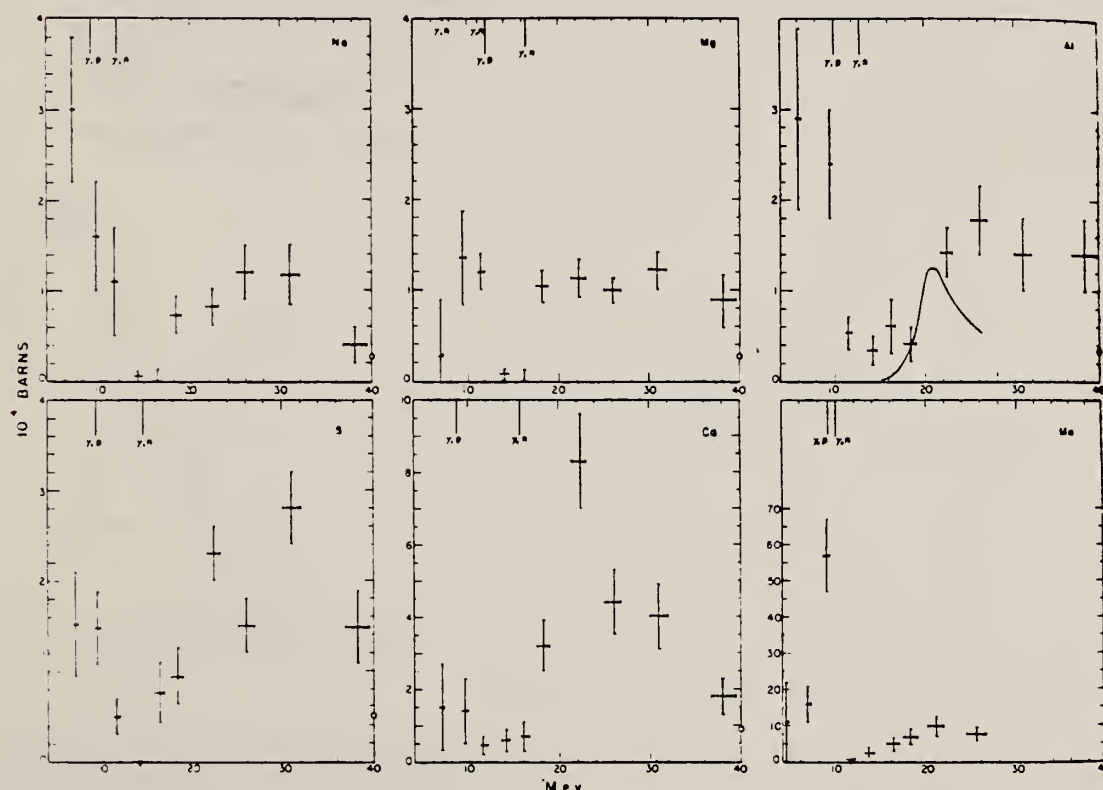


FIG. 4 The elastic scattering cross sections for Na, Mg, Al, S, Ca, and Mn. The indicated spread in energy is the width of the differential discriminator channel, and the standard deviations are based only on the number of counts. The vertical lines at the top represent the particle thresholds for the most important isotopes. The open circles at the extreme right indicate the magnitude of the Thomson cross section for Z free protons scattering coherently. The solid curve superimposed on the Al data is the scattering cross section calculated from the dispersion relation by substituting for $\sigma_e(E)$ in Eq. (6) the sum of the neutron and proton yield¹⁸ cross sections.

REF.

F. D. Schupp, C. B. Colvin and D. S. Martin, Jr.
 Phys. Rev. 107, 1058 (1957)

ELEM. SYM.

A

Z

Ca

40

20

METHOD

REF. NO.

57 Sc 1

JOC

REACTION	RESULT	EXCITATION ENERGY	SOURCE		DETECTOR		ANGLE
			TYPE	RANGE	TYPE	RANGE	
G,3N3P	ABX	35 - 70	C	35 - 70	ACT-I		4PI

70

$$\int_{35}^{70} \sigma dE\gamma = 2.7 \text{ MeV-mb}$$

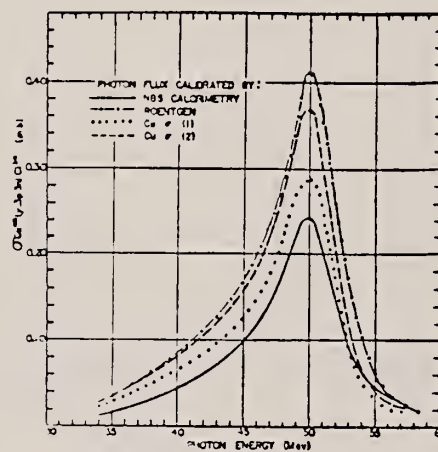


FIG. 3. Cross-section function of $\text{Ca}^{40}(\gamma,3p3n)\text{Cl}^{34}$.

ELEM. SYM.	A	Z
Ca	40	20
REF. NO.		egf
58 Ho 1		

METHOD					
REACTION	RESULT	EXCITATION ENERGY	SOURCE		ANGLE
			TYPE	RANGE	
G, NP	ABX	26- 32	G	26- 32	4PI

(γ ,np) yields include (γ ,d).

Tabelle I

Reaktion	Q-Wert MeV	1 W.O. $\bar{\sigma}$ MeV barn	σ_{\max} mb	E_{\max} MeV	Γ MeV
Ca ⁴⁰ (γ , pn) K ³⁹	-24,3	0,005	2,4	30 \pm 1	2,1
Zn ⁶⁴ (γ , pn) Cu ⁶³	-18,36	0,03			
Zn ⁶⁶ (γ , pn) Cu ⁶⁴	-18,65	0,031	7,2	28 \pm 1	4
Zn ⁶⁸ (γ , p) Cu ⁶⁷	-10,01	0,19	11,4	22,7 \pm 1	6
Sc ⁵⁰ (γ , pn) As ⁴⁸	-20,43	0,02			
Zn ⁶⁴ (γ , 2n) Zn ⁶²	-20,82	0,08			
Mo ⁹² (γ , pn) Nb ⁹⁰	-19,5	0,02			
Sb ¹²³ (γ , pn) Sn ¹²¹	-18,2	0,0006			

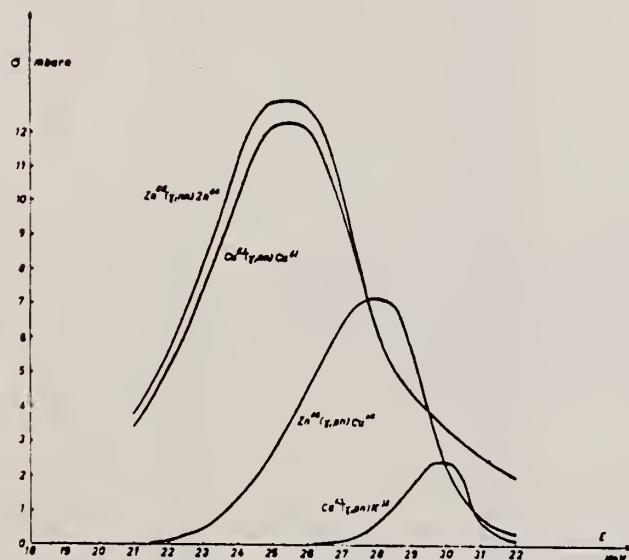


Fig. 1

Gemessene Anregungskurven folgender Reaktionen: Cu⁴⁰(γ , pn) K³⁹, Zn⁶⁴(γ , pn) Cu⁶⁴.
Die Anregungskurve der Zn⁶⁶(γ , nn) Zn⁶⁴-Reaktion wurde mit Hilfe der statistischen Theorie berechnet.
Der Anteil der (γ , d)-Reaktion ist in den entsprechenden (γ , pn)-Anregungskurven enthalten.

Ref. J. Dular, G. Kernel, M. Kregar, M.V. Mihailović, G. Pregl,
M. Rosina, C. Zupančič
Nuclear Phys. 14, 131 (1959)

Elem. Sym.	A	Z
Ca	40	20

Method Compton spectrometer; 30 MeV Betatron

Ref. No.	EH
59 Du 1	

Reaction	E or ΔE	E_0	Γ	$\int \sigma dE$	$J\pi$	Notes
(μ_t)	Bremss. 28.9 30.3					

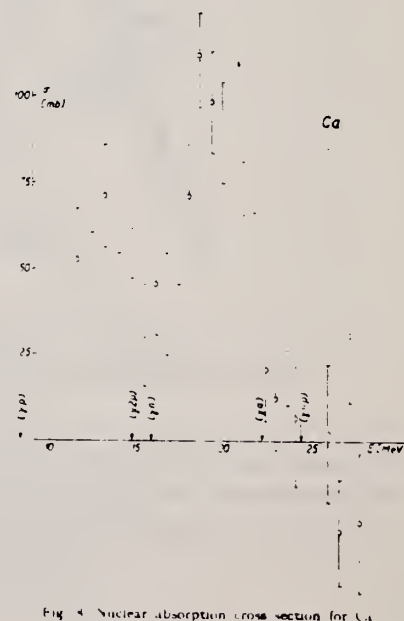


Fig. 4. Nuclear absorption cross section for Ca.

Elem. Sym.	A	Z
Ca	40	20

Method Emulsions; bremsstrahlung

Ref. No.
 59 Em 1
 EH

Reaction	E or ΔE	E_0	Γ	$\int \sigma dE$	$J\pi$	Notes
(γ, xn)	31					<p>Neutron spectrum measured at 90°. 90° neutron yield same for Ca and K for $E_n > 2$ MeV.</p> <p>Calculated spectrum of form $F(E_n) =$ const. $E_n \exp. (-E_n/T)$ with $T = 1.1$ MeV are normalized to data at 2 MeV in 90° spectrum.</p>

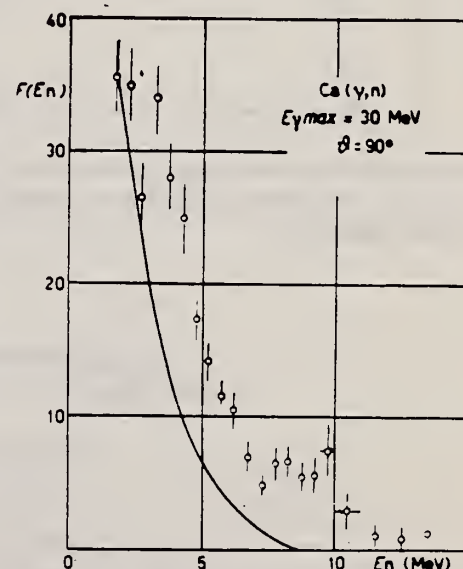


Fig. 3. - Photoneutron spectrum from Ca at $\theta \sim 90^\circ$.
 $F(E_n)$ (arbitrary units) = neutron number ΔE_n .

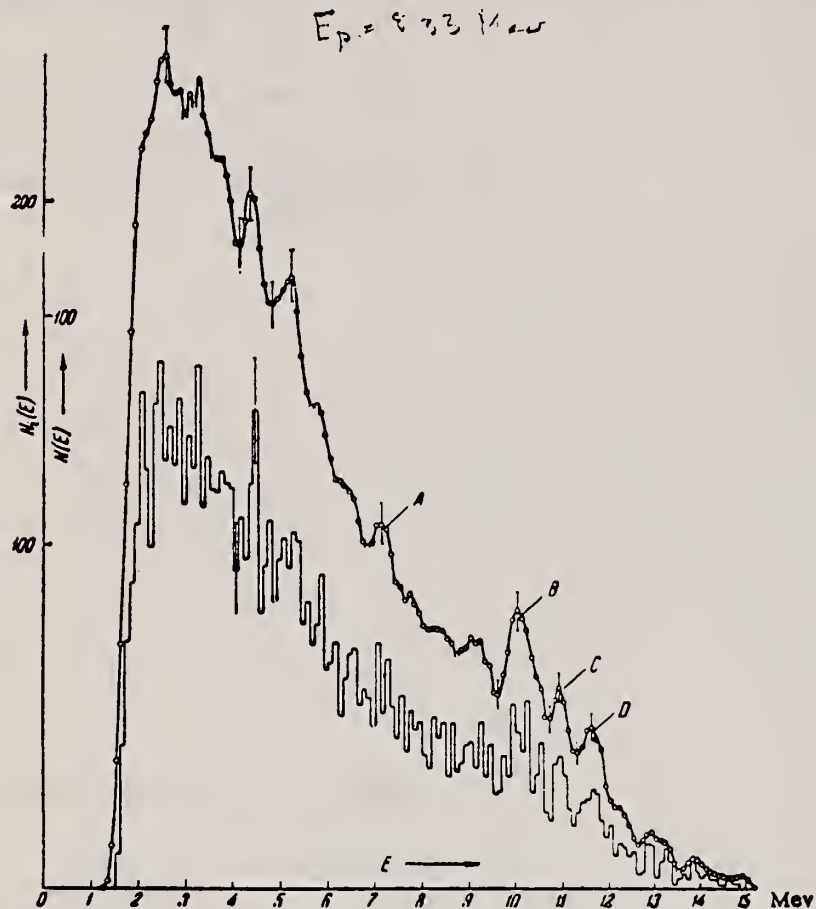
METHOD

REF. NO.

59 Ko 2

EGF

REACTION	RESULT	EXCITATION - - ENERGY - -	SOURCE		DETECTOR		ANGLE
			TYPE	RANGE	TYPE	RANGE	
G,P	SPC	THR - 85	C	85	EMU-D	1-15	DST



$N(E)$ - histogram of the energy distribution of photoprotons from Ca^{40} ; $N_1(E)$ - curve of the same distribution obtained from the histogram according to the Ferreira and Valoshek method [1].

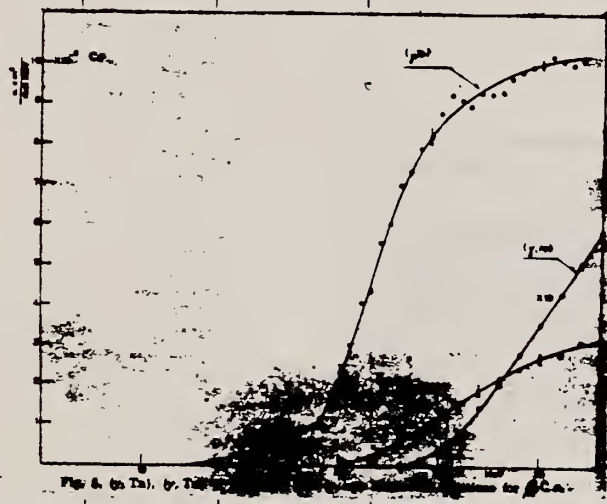
The angular distributions of photoprotons of various energy intervals worked out according to the method of least squares, are described by the following formulas:

from 3.4 to 9.5 Mev	$1 + 0.4 \sin^2 \theta (1 + 0.65 \cos \theta)^2$
from 9.5 to 15 Mev	$1 + 1.2 \sin^2 \theta (1 + 0.5 \cos \theta)^2$
from 6.6 to 7.6 Mev (group A)	$1 + 0.75 \sin^2 \theta (1 + 0.8 \cos \theta)^2$
from 7.5 to 9.5 Mev ("plateau")	$1 + 1.1 \sin^2 \theta (1 + 0.5 \cos \theta)^2$
from 9.7 to 10.8 Mev (group B)	$1 + 1.3 \sin^2 \theta (1 + 0.35 \cos \theta)^2$

Method 31 MeV betatron; activation; NaI; neutron counters

Ref. No.	JHH
60 Fe 1	

Reaction	E or ΔE	E_0	Γ	$\int \sigma dE$	$J\pi$	Notes
(γ, np)	Bremss. 31					Residual nucleus K^{38} ($T_{1/2} = 7.7$ min) decays via $\beta^+ + \gamma$ (2.18 MeV from decay of A^{38}). 2.18 MeV γ , rather than annihilation radiation, gave purest decay curve.
(γ, xn)						Threshold detector using reaction $Si^{28}(n, p)Al^{28}$; $E_n > 5.5$ MeV.
(γ, xn) all energies						1 - meter cube H_2O tank containing Geiger counters surrounded by Rh powder.



Ref. L.A. Kul'chitskii, V. Presperin
Zhur. Eksp. i Teoret. Fiz. 39, 1001 (1960)
Soviet Phys. JETP 12, 696 (1961)

Elem. Sym.	A	Z
Ca	40	20

Method
90 MeV Synchr.; proton recoil counter telescopes

Ref. No.	JH
60 Ku 2	

Reaction	E or ΔE	E ₀	Γ	∫σdE	Jπ	Notes																								
(γ,n)	Bremss.; E _{γmax} =90MeV					Relative yields in table are per nuclear neutron.																								
<table><tr><th>Element</th><th>Relative neutron yield</th><th>Element</th><th>Relative neutron yield</th></tr><tr><td>Li</td><td>1.00±0.05</td><td>Cu</td><td>0.37±0.02</td></tr><tr><td>Be</td><td>1.22±0.09</td><td>Cd</td><td>0.35±0.02</td></tr><tr><td>O</td><td>0.74±0.05</td><td>I</td><td>0.39±0.02</td></tr><tr><td>Al</td><td>0.49±0.03</td><td>Bi</td><td>0.41±0.02</td></tr><tr><td>Ca</td><td>0.33±0.02</td><td></td><td></td></tr></table>							Element	Relative neutron yield	Element	Relative neutron yield	Li	1.00±0.05	Cu	0.37±0.02	Be	1.22±0.09	Cd	0.35±0.02	O	0.74±0.05	I	0.39±0.02	Al	0.49±0.03	Bi	0.41±0.02	Ca	0.33±0.02		
Element	Relative neutron yield	Element	Relative neutron yield																											
Li	1.00±0.05	Cu	0.37±0.02																											
Be	1.22±0.09	Cd	0.35±0.02																											
O	0.74±0.05	I	0.39±0.02																											
Al	0.49±0.03	Bi	0.41±0.02																											
Ca	0.33±0.02																													

METHOD					REF. NO.		NVB
Betatron; neutron cross section; NaI spectrometer; C ¹² (γ,n)C ¹¹					60 Li 2		
monitor							
REACTION	RESULT	EXCITATION ENERGY	SOURCE		DETECTOR		ANGLE
			TYPE	RANGE	TYPE	RANGE	
G, XN	ABI	THR-34	C	34	NAI		

$$\text{Total} \int_0^{33} \sigma(\gamma, n), (\gamma, np), (\gamma, 2n) dE = 116 \pm 17 \text{ MeV-mb}$$

Tabelle. Ergebnisse der Messungen

1 Reaktionen	$(\gamma, n)Ca^{40} + (\gamma, np)K^{39} + \eta(\gamma, 2n)Ca^{40}$	$(\gamma, np)K^{39} + (1-\eta)(\gamma, 2n)Ca^{40}$
2 E_0	34 MeV	29 MeV
3 Gemessene Halbwertszeit	$(0,917 \pm 0,007) \text{ sec}$	$(0,892 \pm 0,010) \text{ sec}$
4 Y/Y(C^{11}) ohne Absorber .	$2,31 \pm 0,05$	$2,5 \pm 0,1$
5 Y/Y(C^{11}) mit Absorber .	$2,38 \pm 0,08$	$0,115 \pm 0,06$
6 D	$0,260 \pm 0,10$	$0,226 \pm 0,16$
7 $\int_0^{33 \text{ MeV}} \sigma dE / \int_0^{33 \text{ MeV}} \sigma(C^{11}) dE$	$2,10 \pm 0,27$	$0,18 \pm 0,04$
8 $\int_0^{33 \text{ MeV}} \sigma dE$	$(107 \pm 16) \text{ MeVmb}$	$(9 \pm 2) \text{ MeVmb}$

Alle angegebenen Fehler sind im wesentlichen die dreifachen statistischen Fehler. Zeile 1: Zusammengefaßt sind einerseits die Reaktionen, die auf Folgeaktivitäten mit Halbwertszeiten von etwa 1 sec führen (kurzlebige Komponente), andererseits diejenigen bei denen K^{39} (Halbwertszeit 7,7 min) entsteht. Siehe hierzu Fig. 1, wo auch die Größe η in der Bildunterschrift erläutert ist. Zeile 2: E_0 bezeichnet die Maximalenergie des Bremsspektrums. Zeile 3: Weitere Erläuterung im Text. Zeile 4 und Zeile 5: Angegeben sind die Ausbeuteverhältnisse relativ zur Reaktion $C^{12}(\gamma, n)$ ohne bzw. mit Zwischenschalten des 20,5 g/cm³ dicken Bleiabsorbers. Zeile 6: Die durch den Bleiabsorber bewirkte Schwächung D der Ausbeute wurde unter Benützung der von SALANDER¹² gemessenen Schwächung für $C^{12}(\gamma, n)$ ($D_C = 0,2569 \pm 0,0015$) aus den Werten von Zeile 4 und 5 berechnet. Zeile 7: Die Verhältnisse der integrierten Wirkungsquerschnitte folgen aus den Zahlen in Zeile 4 und 6 durch Anwendung von Formel (1). Zeile 8: Die integrierten Wirkungsquerschnitte ergeben sich aus den in Zeile 7 angegebenen Verhältnissen, wenn man den Messungen von BARBER, GEORGE und REAGAN⁸ entnimmt, daß der bis 33 MeV integrierte Wirkungsquerschnitt für $C^{12}(\gamma, n)$ $51 \pm 3 \text{ MeVmb}$ beträgt.

¹² SALANDER, C.: Diplomarbeit Heidelberg 1957 (unveröffentlicht).

A. Bussiere de Nercy
J. Phys. Radium 22, 535 (1961) (See 61Bu4)

Ca

40

20

METHOD

Betatron; photon scattering; NaI

REF. NO.

61 Bu 3

NVB

REACTION	RESULT	EXCITATION ENERGY	SOURCE		DETECTOR		ANGLE
			TYPE	RANGE	TYPE	RANGE	
G,G	ABX	15 -32	C	32	NAI-D		DST

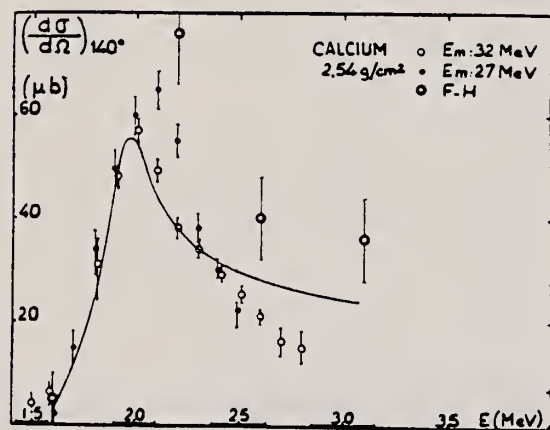


Fig. 4.

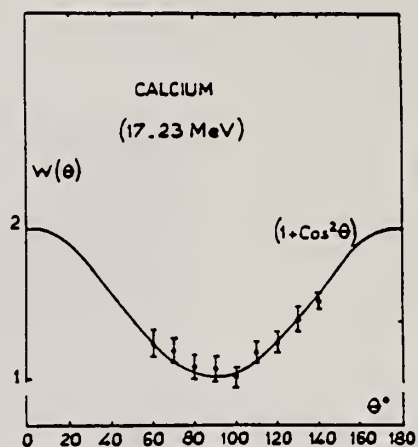


Fig. 6.

METHOD

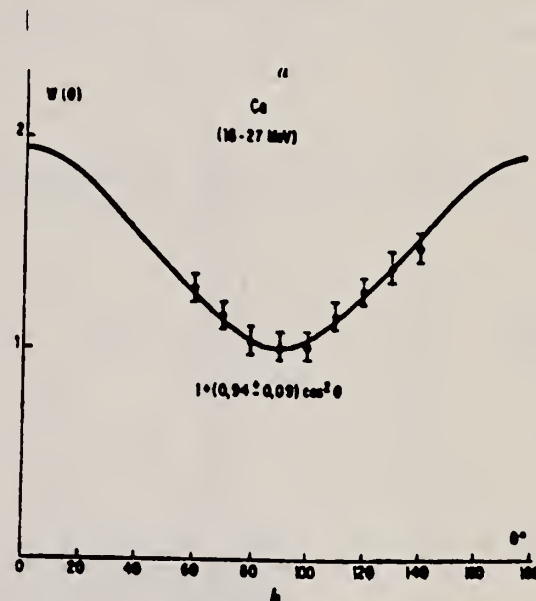
REF. NO.

61 Bu 4

egf

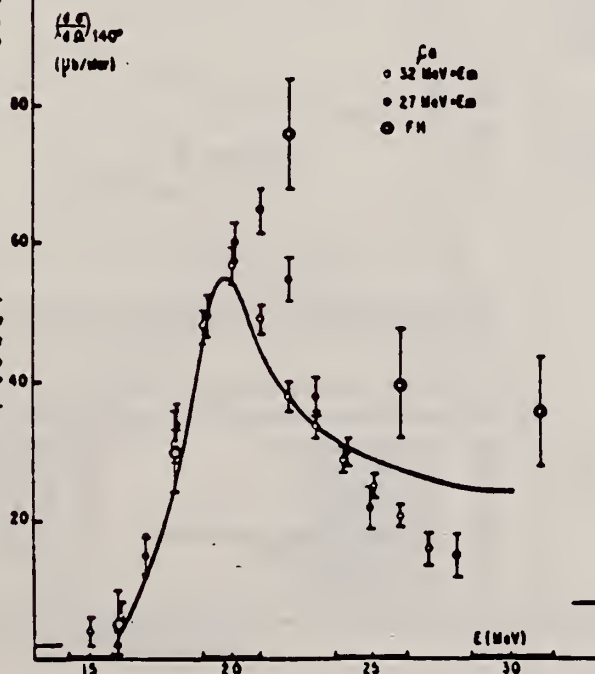
REACTION	RESULT	EXCITATION ENERGY	SOURCE		DETECTOR		ANGLE
			TYPE	RANGE	TYPE	RANGE	
G,G	ABX	15-30	C	27,32	NAI -D		DST

Fig. 24. — Distribution angulaire des photons diffusés par l'aluminium (a) et le calcium (b) (16-27 MeV).



Les courbes en trait plein représentent les sections efficaces prévues par la relation de dispersion.

Fig. 23. — Section efficace différentielle de diffusion γ, γ à 180° pour le calcium.



Elem. Sym.	A	Z
Ca	40	20

Method 3 MeV Van de Graaff; γ 's from $K^{39}(p,\gamma)Ca^{40}$ reaction; NaI.

Ref. No.
61 Ec 1
JHH

Reaction	E or ΔE	E ₀	Γ	∫σdE	Jπ	Notes
(γ,γ)	10.3	10.3	3.6±0.24ev (Γ: γ ₀ ; for other Γ's see Tab.2)		2 +	Data also presented on the K ³⁹ (p,γ)Ca ⁴⁰ reaction: E _p = 2.05MeV. W _{p,γ} (θ _γ)=1-(0.17±0.02)cos ² θ +(0.03±0.03)cos ⁴ θ.

FIG. 10. Nuclear resonant absorption by the 10.3-Mev level of Ca⁴⁰. From top to bottom the curves are for transmission by 11.125, 2.75, and 1.0 in. of calcium metal, respectively, of radiation from the K³⁹(p,γ)Ca⁴⁰ reaction. Note transmission scale breaks between curves.

FIG. 11. Angular distribution of ground state radiation from the 10.3-Mev level of Ca⁴⁰ excited in the K³⁹(p,γ)Ca⁴⁰ reaction.

TABLE II. Parameters of the 10.3-Mev level in Ca⁴⁰.

E ₀	Excitation energy	10.3 ±0.01 Mev
E _p	Proton energy	2.05±0.005 Mev
Γ	Total width	10.3 ±1.7 ev
Γ _p	Proton width	5.8 ±1.8 ev
Γ _γ	Gamma width to ground state	3.6 ±0.24 ev
Γ _γ	Total gamma width	4.5 ±0.55 ev
J ^π	Spin and parity	2 ⁺ (2 ⁻ ,1 [±])

FIG. 12. The energy-level diagram of Ca⁴⁰.

METHOD

Linac; electron scattering; magnetic spectrometer

REF. NO.

61 Pe 1

NVB

REACTION	RESULT	EXCITATION ENERGY	SOURCE		DETECTOR		ANGLE
			TYPE	RANGE	TYPE	RANGE	
$E, E/$	ABX	11-26	D	120-180	MAG-D		DST
		[11-26]					

$E_0 = 15.2 \text{ MeV}$
17 MeV
18 MeV
19.2 MeV
20.5 MeV

97% enriched Ca^{40}

$\int \sigma dE = 0.38 \text{ MeV-b}$ for 120 MeV data
 $= 0.43 \text{ MeV-b}$ for 150 MeV data

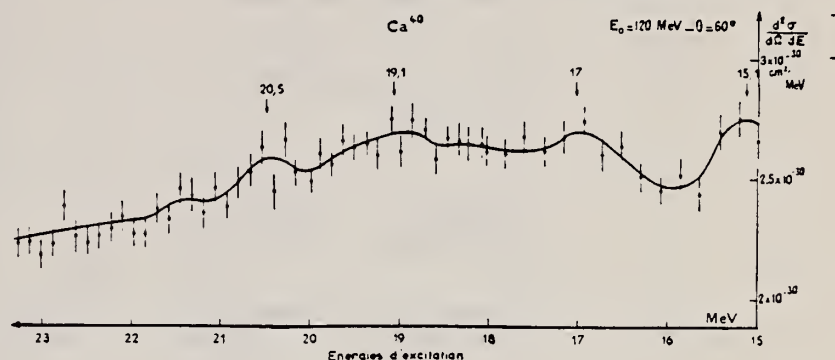


FIG. 2.

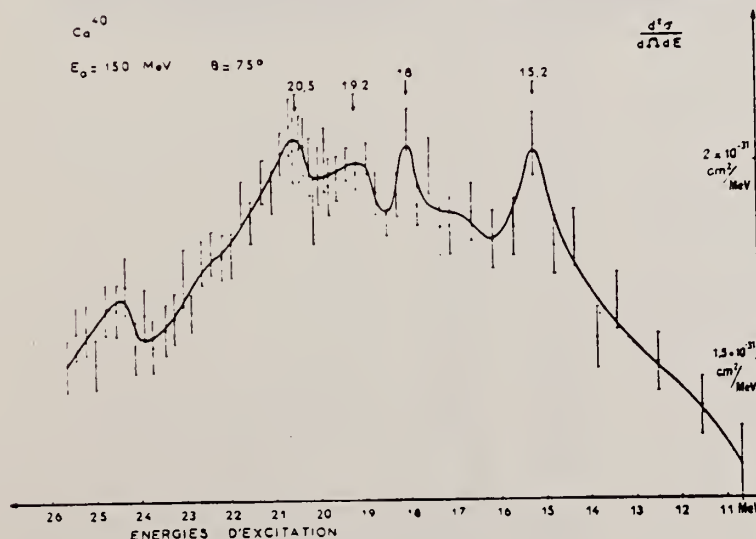


FIG. 3.

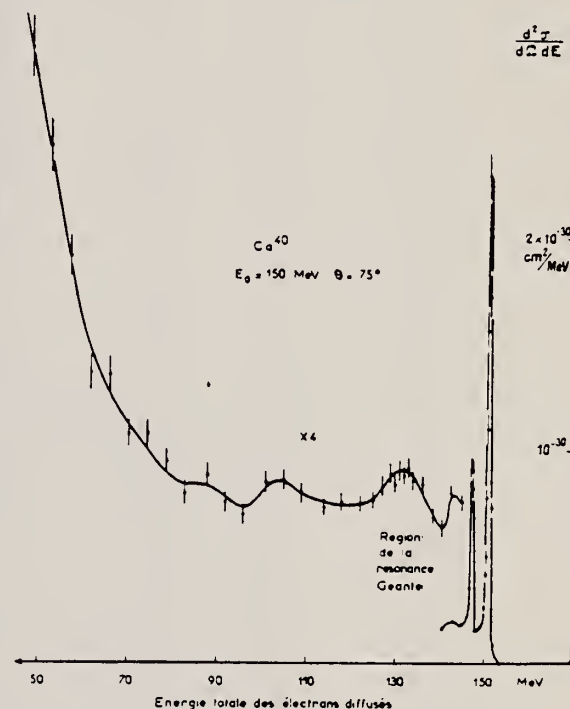


FIG. 1.

On trouve ainsi les lignes à 15,2 MeV, 17 MeV, 18 MeV, 19,2 MeV et 20,5 MeV. La structure de la résonance géante a été prévue théoriquement [14] à l'aide d'un modèle d'interaction particule-trou. Les énergies et intensités des différents dipôles sont données pour deux types d'interaction différents.

Ref. R.A. Pope, D.V. Freck, W.W. Evans
Nuclear Phys. 24, 657 (1961)

Elem. Sym.	A	Z
Ca	40	20

Method Van de Graaff; NaI

Ref. No.	JHH
61 Po 1	

Reaction	E or ΔE	E_0	Γ	$\int \sigma dE$	$J\pi$	Notes
(p, γ)	1.0-2.1	1133.0 ± 1.4 keV	Γ_p : <0.5keV			$E_{\gamma_0} = 9.44$ MeV
		1311.7 ± 1.6 keV	<0.5keV			$E_{\gamma_0} = 9.61$ MeV
		1579.9 ± 1.9 keV	<0.5keV			$E_{\gamma_0} = 9.87$ MeV
		2046.7 ± 2.5 keV	<0.5keV			$E_{\gamma_0} = 10.33$ MeV

ELEM. SYM.	A	Z
Ca	40	20
METHOD		
Tandem		
REF. NO.		
61 Ta 2		JDM

REACTION	RESULT	EXCITATION ENERGY	SOURCE		DETECTOR		ANGLE
			TYPE	RANGE	TYPE	RANGE	
P,G	RLY	18-22	D	9-15	NAI-D	10-25	100

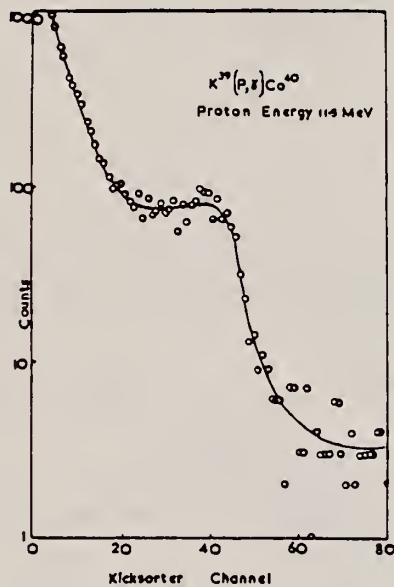


Fig 1.

Figure 1. Spectrum in 6 x 5 in. NaI from proton bombardment of potassium. Proton Energy 11.5 MeV

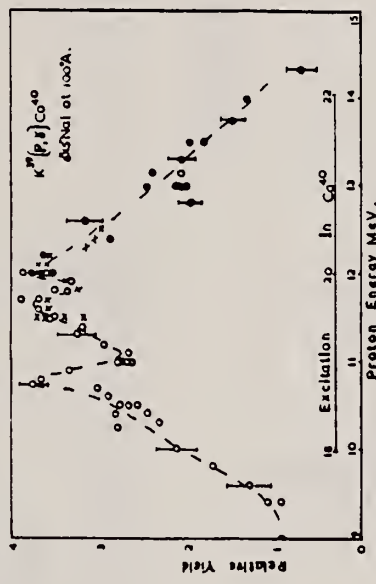


Fig 2.

Figure 2. Excitation function for $K^{39}(p,\gamma)Ca^{40}$

Ref. T. Tohei, M. Sugawara, S. Mori, M. Kimura
J. Phys. Soc. Japan 16, 1657 (1961)

Elem. Sym.	A	Z
Ca	40	20

Method 25 MeV betatron; photon scattering; NaI(Tl) spectrometer;
ion chamber.

Ref. No.	
61 To 1	NVB

Reaction	E or ΔE	E_0	Γ	$\int \sigma dE$	$J\pi$	Notes
----------	-----------------	-------	----------	------------------	--------	-------

Ca(γ, γ)

Bremss.
5-12

8.0

Detector at 120°

Table II from J. Phys. Soc. Japan 18,
17-22 (1963)

References

- 1) E. G. Fuller and E. Hayward: Phys. Rev. **101** (1956) 692.
- 2) see E. Segre: *Experimental Nuclear Physics*, vol. 1, p. 346.
- 3) J. S. Levin and D. J. Hughes: Phys. Rev. **101** (1956) 1328.
- 4) K. Reibel and A. K. Mann: Phys. Rev. **118** (1960) 701.

Table II. The correction of the energy scale.

Energy in Ref. 1 should be read

4.0 Mev	3.3 Mev
6.0	5.5
8.0	7.7
10.0	9.9
12.0	12.1
14.0	14.3

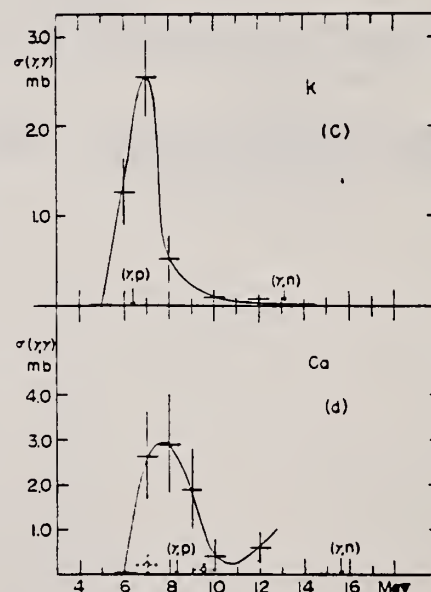


Fig. 6. The elastic scattering cross section of photons. \square : data from the experiment used monochromatic γ rays.
(a): $\sigma(\gamma, \gamma)$ by S. The arrows indicate the positions of the particle threshold energies of S^{36} .
(b): $\sigma(\gamma, \gamma)$ by Al. The arrows indicate the positions of the particle threshold energies of Al^{27} .
(c): $\sigma(\gamma, \gamma)$ by K. The arrows indicate the positions of the particle threshold energies of K^{39} .
(d): $\sigma(\gamma, \gamma)$ by Ca. The arrows indicate the positions of the particle threshold energies of Ca^{40} .

REACTION	RESULT	EXCITATION ENERGY	SOURCE		DETECTOR		ANGLE
			TYPE	RANGE	TYPE	RANGE	
E, E/	FMF	0-9	D	120-220	MAG-D	170-180	DST

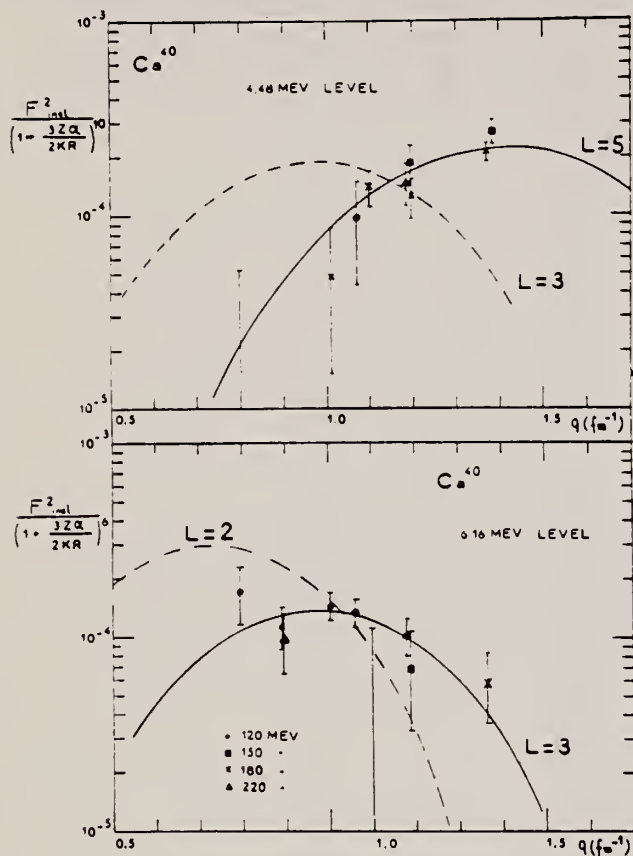


Fig. 2

Table 1

ΔE MeV	$J\pi$	B_{sp}/e^2	$B_{obs} (L \rightarrow 0/e^2)$	G
3.73	3 -	$194f^6$	$1600f^6$	8.25
3.90	2 +	$11.8f^4$	$21.6f^4$	1.83
4.48	5 -	$0.91.10^5 f^{10}$	$2.02.10^5 f^{10}$	2.22
6.16	3 -	$194f^6$	$108f^6$	0.56
6.90	3 -	$194f^6$	$188f^6$	0.97
7.10	2 +	$11.8f^4$	$30.6f^4$	2.60
8.50	(5 -)	$0.91.10^5 f^{10}$	$1.17.10^5 f^{10}$	1.28

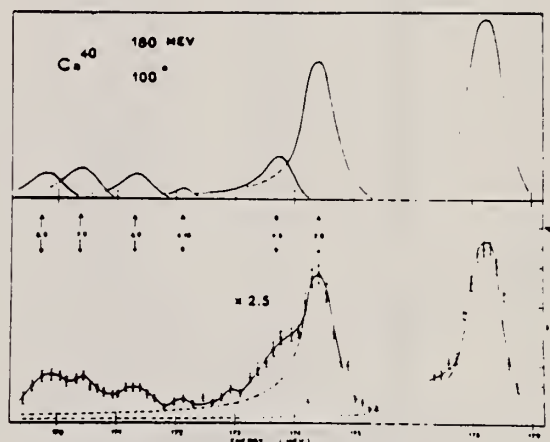


Fig. 1

Table 2

	Experimental Data		Hole Particle Interaction			
			Approximation I		Approximation II	
	E (MeV)	T_R	E (MeV)	T_R	E (MeV)	T_R
E 3	3.73	1	5.55	1	3.84	1
	6.16	0.068	7.26	0.20	7.15	0.062
	6.9	0.118	8.44	0.033	8.34	0.031
			10.7	0.40	10.7	0.090
E 5	4.48	1	5.20	1	4.38	1
	8.5	(0.49)	8.07	0.88	8	0.24

Ref. E.C. Booth, K.A. Wright
Nuclear Phys. 35, 472 (1962)

Elem. Sym.	A	Z
Ca	40	20
Ref. N-		JHH
62 Bo 6-		

Method 4 MeV electron Van de Graaff; brems.; nuclear resonance scattering, ring scatterer; NaI

Reaction	E or ΔE	E_0	Γ	$\int_0^{\infty} dE$	$J\pi$	Notes
$Ca^{40}(\gamma, \gamma)$	Brems. 0 - 4					

Table 8
Mean lifetimes of excited states deduced from the resonance scattering of bremsstrahlung

Nucleus	%	Energy MeV	Spin	J	Γ_0/Γ	ω/Γ	$\tau \times 10^{10} \pm \Delta\tau$ sec.
^{12}C	100	1.46	$1^+ \rightarrow 0^+$	1	0.13	11	0.34g
^{14}N	100	2.06	$1^+ \rightarrow 0^+$	2	0.1	0.76	> 0.06
		3.38	$1^+ \rightarrow 0^+$	2	0.53	11	> 1.6g
		2.64	$1^+ \rightarrow 0^+$	1	0.6	11	> 0.3g
		3.70	$1^+ \rightarrow 0^+$	1	0.11	11	> 0.40g
^{16}O	100	2.96	$1^+ \rightarrow 0^+$	1	0.46	11	0.03g
		1.78	$1^+ \rightarrow 0^+$	1	0.08	0.61	> 0.23
^{18}O	4.71	2.36	$1^+ \rightarrow 0^+$	2	0.216	1	1.5×10^{-4}
		2.43	$1^+ \rightarrow 0^+$	2	11	0.66	1.3
^{20}Ne	100	1.26	$1^+ \rightarrow 0^+$	2	1	0.66	2.3
		2.23	$1^+ \rightarrow 0^+$	2	1	0.79	4.8
		3.13	$1^+ \rightarrow 0^+$	2	11	0.66	0.3
		3.29	$1^+ \rightarrow 0^+$	2	7	0.79	> 1.4(Γ_0/Γ) ²
		3.41	$1^+ \rightarrow 0^+$	2	7	11	> 1.3(Γ_0/Γ) ²
		3.51	$1^+ \rightarrow 0^+$	2	7	0.66	0.66(Γ_0/Γ) ²
^{24}Mg	96	3.76	$0^+ \rightarrow 0^+$	2	1	1	> 0.6(Γ_0/Γ) ²
^{28}Si	4.2	3.127	$0^+ \rightarrow 0^+$	2	1	0.66	> 1.0
^{32}S	78.6	1.33	$1^+ \rightarrow 0^+$	2	1	11	11
		1.76	$1^+ \rightarrow 0^+$	2	11	11	6g
		2.718(66)	$1^+ \rightarrow 0^+$	2	11	11	0.31(Γ_0/Γ) ²
^{36}Ar	78.6	3.01	$1^+ \rightarrow 0^+$	2	7	11	0.37(Γ_0/Γ) ²
		3.1	$1^+ \rightarrow 0^+$	2	7	11	> 0.7(Γ_0/Γ) ²
		3.17	$1^+ \rightarrow 0^+$	2	7	11	> 1.3(Γ_0/Γ) ²
^{40}Ca	94.6	0.620	$1^+ \rightarrow 0^+$	2	1	11	> 1.6g
		1.73	$1^+ \rightarrow 0^+$	2	7	11	> 0.4(Γ_0/Γ) ²
^{48}Ti	86	2.33	$1^+ \rightarrow 0^+$	2	1	11	> 1.6g
		2.63	$1^+ \rightarrow 0^+$	2	1	11	> 1.6g
		3.00	$1^+ \rightarrow 0^+$	2	1	11	0.27g
		3.00	$1^+ \rightarrow 0^+$	2	1	11	> 0.7g
		3.66(7.94)	$1^+ \rightarrow 0^+$	2	7	11	0.14(Γ_0/Γ) ²
^{56}Fe	86	1.96	$0^+ \rightarrow 0^+$	2	1	0.66	> 0.46
^{60}Ni	60	1.33	$1^+ \rightarrow 0^+$	2	11	0.6	> 1.1

The factor ω/Γ is $(M + 1)/2A$ for $1^+ \rightarrow 0^+$ and $(M + 1)/A$ for $2^+ \rightarrow 0^+$.

Ref. V.P. Chizhov, A.P. Komar, L.A. Kulchitsky, A.V. Kulikov,
E.D. Makhnovsky, Yu.M. Volkov
Nuclear Phys. 34, 562 (1962)

Elem. Sym.	A	Z
Ca	40	20

Method 90 MeV Synchrotron; magnetic spectrometer; emulsions;

Ref. No.	JHH
62 Ch 2	

Reaction	E or ΔE	E_0	Γ	$\int \sigma dE$	$J\pi$	Notes
(γ, d)	Bremss.					
	35					
(γ, p)						

Fig. 4 The ratio of the yields of deuterons and protons with energies 15.5 to 30 MeV depending on the mass number of nuclei A for $E_{\max} = 90$ MeV. The solid line stands for the normalized dependence (5).

TABLE I
Experimental data

Elements	E_{\max} (MeV)	Particle energy interval (MeV)	$\frac{Y(\gamma, d)}{Y(\gamma, p)}$	θ	Method
^{40}Ca	30	7.5 to 15	0.003 ± 0.008	90°	[
	43		0.007 ± 0.005		
	90		0.097 ± 0.014		
^{47}Ti	25		0.020 ± 0.030		
	43	7.5 to 15	0.056 ± 0.008	90°	[
	90		0.180 ± 0.054		
^{54}Fe	40	7.5 to 19	0.008 ± 0.002	90°	[
^{62}Ni	35	2.9 to 10	0.009 ± 0.007	$50^\circ - 120^\circ$	[(
^{64}Ni	35	3.7 to 10	0.038 ± 0.017	$50^\circ - 100^\circ$	[(
^{66}Ni	34	4.5 to 15	0.007 ± 0.003	90°	[
^{68}Ni	34	7.5 to 15	0.007 ± 0.003	90°	[
^{70}Ni	70	3 to 10	0.05 ± 0.01	$20^\circ - 50^\circ$	[(
^{70}Zn	70	4 to 10	0.04 ± 0.01	$20^\circ - 50^\circ$	[(
^{90}Zr	90	7 to 19	0.021 ± 0.005	90°	[

[Scintillation telescope method
[(Method of detecting charged particles in magnetic field.

Ref. T.N.Dragnev, B.P.Konstantinov

Zhur.Eksptl. i Teoret.Fiz. 42, 344 (1962);
Soviet PhysJETP 15, 236 (1962)

Elem. Sym.

A

Z

Ca

40

20

Method

synchrotron - nuclear emulsions

Ref. No.

62Dr1

BG

Reaction	E or ΔE	E_0	Γ	$\int \sigma dE$	$J\pi$	Notes
(γ, p)	$E_{\gamma \max} = 22 \text{ MeV}$	$E_p = 4.65$ 10.2				<p>Angular distribution of 4.2-5.4 MeV protons given by</p> $\frac{d\sigma}{d\Omega} = 1 - 0.146 \sin^2\theta (1 - 1.17 \cos\theta)$ <p>essentially isotropic.</p> <p>Angular distribution of 9.5-10.8 MeV protons well represented by</p> $\frac{d\sigma}{d\Omega} = 1 + \sin^2\theta$ <p>Angular distribution of protons with $E > 10.8 \text{ MeV}$ of the form</p> $\frac{d\sigma}{d\Omega} = 1 + 0.48 \sin^2\theta$ <p>Fig.2: below 3 Mev energy distribution cuts off because tracks of less than 10μ length were omitted.</p>

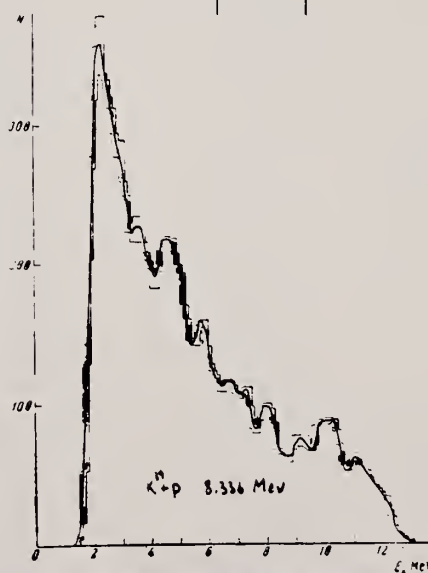


FIG. 2. Energy distribution of the protons.

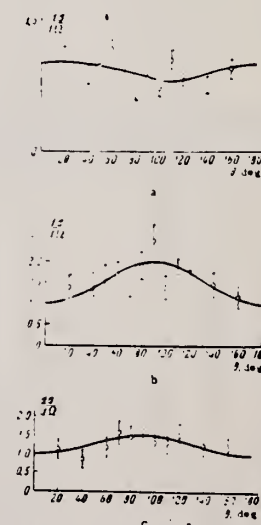


FIG. 3. Angular distributions of protons with the following energies (a) 4.2 - 5.4 MeV, (b) 9.5 - 10.8 MeV, (c) above 10.8 MeV.

Ref. R.D.Edge, G.A.Peterson

Phys.Rev. 128, 2750 (1962)

Elem. Sym.

A

Z

Ca

40

20

Method

Linac - counter telescope

Ref. No.

62Ed1

BG

Reaction	E or ΔE	E_x	Γ	$\int \sigma dE$	$J\pi$	Notes
(e,e')	41.5	no excitations observed below the giant resonance.				Nuclear states excited by 160° electron scattering. M1 transitions assumed.

FORM NBS-418

(8-1-63)

USCOMM-DC 18556-P68

U.S. DEPARTMENT OF COMMERCE
NATIONAL BUREAU OF STANDARDS

REF.

F. W. K. Firk and E. R. Rae
Proc. Padua Conf. 807 (1962)

ELEM. SYM.

A

Z

Ca

40

20

METHOD

Linac

REF. NO.

62 F1 3

JDM

REACTION	RESULT	EXCITATION ENERGY	SOURCE		DETECTOR		ANGLE
			TYPE	RANGE	TYPE	RANGE	
G,N	RLY	16-28	C	32	TOF-D	1-12	

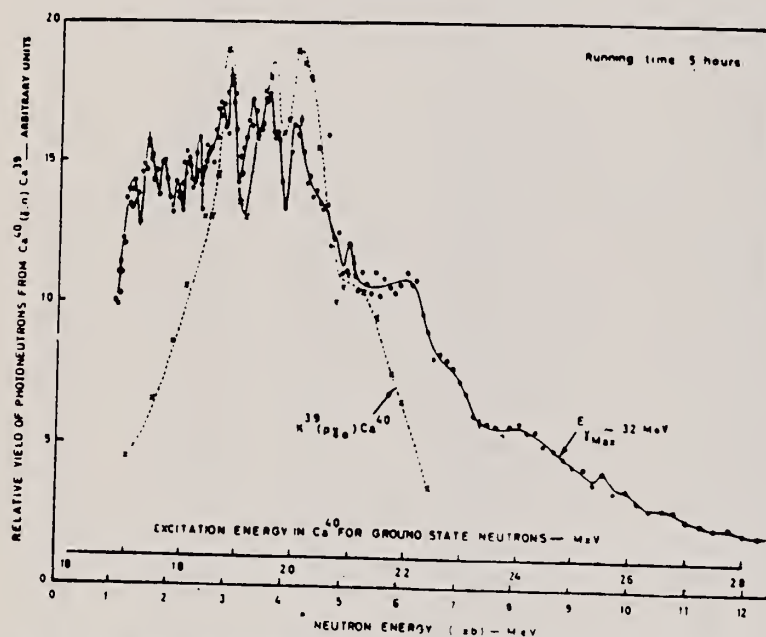


Fig. 1. Energy spectrum of photoneutrons from the reaction $\text{Ca}^{40}(\gamma, n)\text{Ca}^{39}$.

Method 30 - MeV electron synchrotron; emulsions; photon difference method

Ref. No.	JHH
62 Jo 1	

Reaction	E or ΔE	E_0	Γ	$\int \sigma dE$	$J\pi$	Notes
$\text{Ca}^{40}(\gamma, p)$	Bremss. 19.5 20.5					

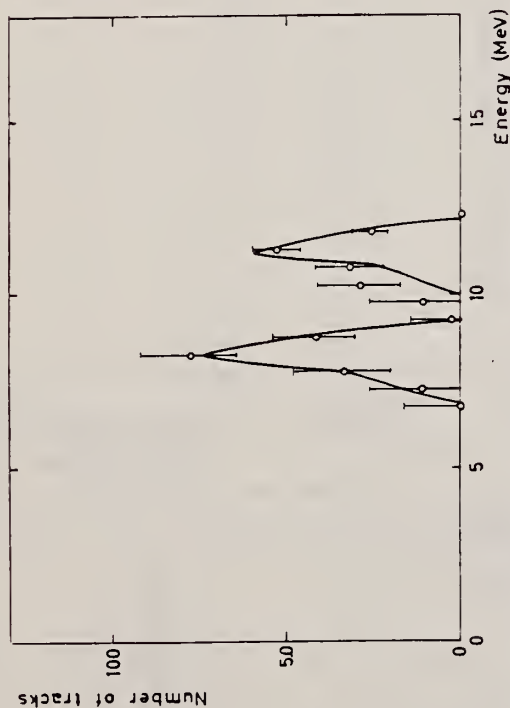


Fig. 3. Difference spectrum between the spectra at 19.5 and 20.5 MeV. This spectrum corresponds to excitation in the range 20 ± 0.5 MeV. The curves show the calculated shape of the peaks.

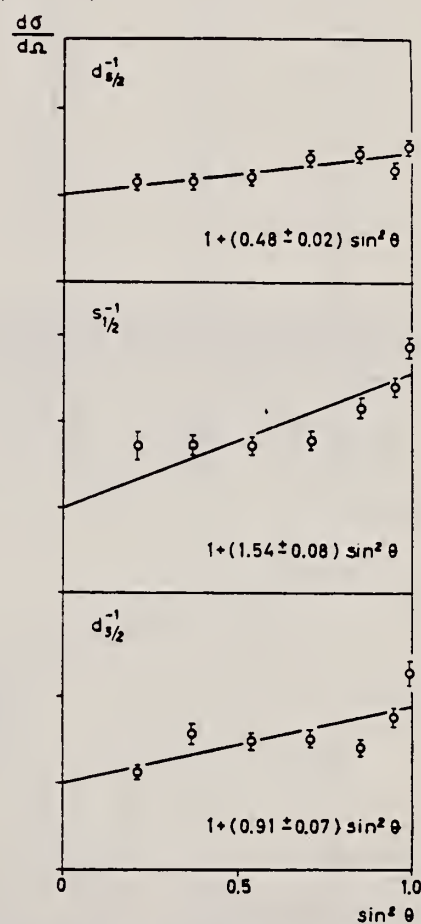


Fig. 4. Angular distribution for the proton groups going to the levels $d_{7/2}^{-1}$, $s_{1/2}^{-1}$ and $d_{3/2}^{-1}$.

Method positron annihilation; neutron yield; 4π neutron; positron current

Ref. No.	
62 Mi 2	JHH

Reaction	E or ΔE	E_0	Γ	$\int \sigma dE$	$J\pi$	Notes
$Ca^{40}(\gamma, n)$	15-25	(19.1) 19.9 (21.4)		$\int_{15}^{23} = 53.5 \text{ MeV-mb}$		

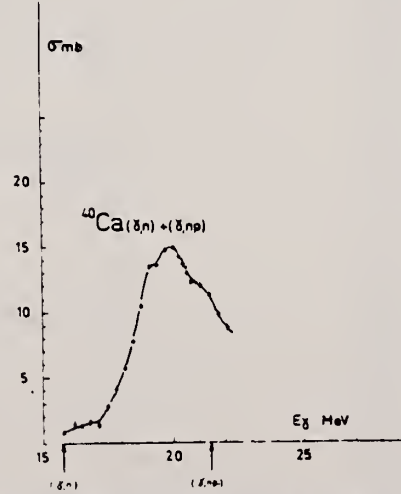


Fig. 3. Section efficace de la réaction (γ, n) sur le calcium.

Tableau 1

Noyau	$\int_{E_{min}}^{E_{max}} (\gamma n + \dots) dE$ (MeV - mb)	Energie des niveaux (MeV)	Largeur des niveaux (MeV)	Sections efficaces intégrées des niveaux discrets (MeV-mb)
C^{12}	24	22.2 23.3		
O^{16}	13	17.5 19.4 21.1 22.2 (23) ≥ 24.2	≈ 1	0.6 1.6 1.4 (4.8) (2.4)
Ca^{40}	53.5	(19.1) 19.9 (21.4)	.	

Elem. Sym.	A	Z
Ca	40	20

Method Van de Graaff; electrostatic proton analyzer; NaI

Ref. No.
62 Ra 1
JHH

Reaction	E or ΔE	E_0	Γ	$\int \sigma dE$	$J\pi$	Notes
(p, γ)	1575.5 ± 0.08 kev	9.87	$\gamma_0 = 1.36 \pm 0.25$ ev		1(+)	73% of γ 's to ground state; $W(\theta) = 1 - (0.08 \pm 0.04)P_2$.
	1580.0 ± 0.08 kev	9.87	0.80 ± 0.26 ev		2+	45% of γ 's to ground state; $W(\theta) = 1 + (0.12 \pm 0.07)P_2 - (0.18 \pm 0.06)P_4$. Widths determined by resonance absorption measurements.

Table III. Partial widths for the 1575.5- and 1580-keV resonance levels in the $K^{(p,\gamma)}Ca^{40}$ and the $K^{(p,\alpha)}Ca^{40}$ reactions. The strengths of the relative transitions to the ground state of Ca^{40} are given in W.u. and the reduced proton widths Γ_p are given in units of $W^{1/2}$. R_{obs} is the observed ratio of the intensities of the transitions to the first excited state and the ground state. R is the ratio of intensities predicted from the single-particle model.

Resonance E (keV)	J π	Γ_0 (eV)	Γ_1 (eV)	Γ_2 (eV)	Γ_p (keV)	Γ_{p1} (eV)	Γ_{p2} (eV)	Type of rad.	$W^{1/2}$	R_{obs}	R
1575.5	1 $^+$	110 ± 30	110 ± 30	13	0.0088	< 0.012	1.46 ± 0.25	1/1	0.087	0.25	0.29
1580.0	2 $^+$	110 ± 30	110 ± 30	15	0.018	< 0.012	1.46 ± 0.25	1/1	0.018	0.25	0.29
1580.0	2 $^+$	1080 ± 300	1080 ± 300	120	0.065	< 0.068	0.40 ± 0.26	2/2	1.27	0.36	0.12

FIG. 2. Proposed decay schemes for the $E_p = 1575.5$ - and 1580 -keV resonances in the $K^{(p,\gamma)}Ca^{40}$ reaction. The prominent cascades are denoted by the heavier lines.

FIG. 3. Angular distributions of ground state γ resonance levels. θ is the angle between the nucleus and the proton beam direction. The solid lines represent fits to the data (obtained by an IBM 650 computer).

Method Betatron; Ca foil target; nuclear emulsion

Ref. No.	
62 Sh 12	NVB

Reaction	E or ΔE	E_0	Γ	$\int \sigma dE$	$J\pi$	Notes
$\text{Ca}^{40}(\gamma, p)$	Bremss. 20.5					

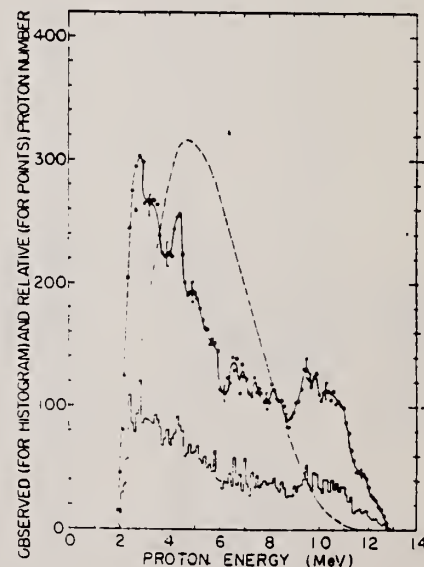


Fig. 2. The energy spectrum of photoprotons from Ca^{40} irradiated by 20.5 Mev bremsstrahlung. The solid line is a smoothed curve. The broken line is a calculated curve using the statistical model with the Weisskopf level density.

Elem. Sym.	A	Z
Ca	40	20
Ref. No.		
63 Ba 1		BG

Method
Linac (Stanford Mark II); counter telescope

Reaction	E or ΔE	E_0	Γ	$\int \sigma dE$	$J\pi$	Notes
$^{40}\text{Ca}(e, e')$	41.5	no resonances				Ground state 0^+ <u>Erratum in Figure 18:</u> 10^{-31} should be 10^{-30}

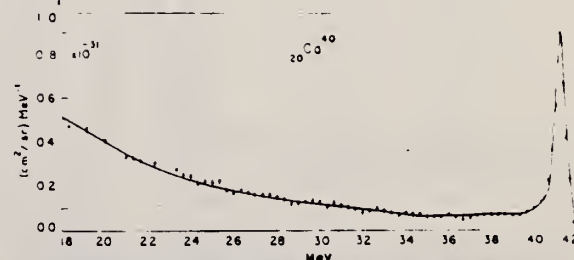


Fig. 18. Spectrum of 41.5 MeV electrons scattered from a calcium target at 180°.

Method
Linac - magnetic spectrum

Ref. No.	63B11	BG
----------	-------	----

Reaction	E or ΔE	E_0	Γ	$\int \sigma dE$	$J\pi$	Notes
(e,e')	120	3.8				Inelastic and elastic form factors determined.
(e,e)	150	4.48				
	180	6.16				
	220	6.9				
		7.9				
		8.5				

Table 1.

Values of B_L , the fitting parameters with the Born approximation inelastic form factors for transition of angular momentum change L . Values of the reduced transition probabilities $B_{exp}(L \rightarrow 0)$ compared with the single particle estimate of Lane (3) $B_{sp}(L \rightarrow 0)$. Their ratio $G = B_{exp}(L \rightarrow 0)/B_{sp}(L \rightarrow 0)$ is also indicated. Values of γ -ray transition rates $\Gamma_{exp}(L \rightarrow 0)$ calculated from the corresponding of $B_{exp}(L \rightarrow 0)$.

E (MeV)	J^π	$B_L \times 10^3$	$B_{exp}(L \rightarrow 0)/e^2$	B_{sp}/e^2	G	$\Gamma_{exp}(L \rightarrow 0)$ (eV)
3.73	3^-	68 ± 7	1425 fm^6	194 fm^6	7.4	5.4×10^{-6}
3.90	2^+	16 ± 6	28.3 fm^4	11.5 fm^4	2.4	21×10^{-3}
4.48	5^-	48 ± 6	$1.87 \times 10^3 \text{ fm}^{10}$	$0.91 \times 10^3 \text{ fm}^{10}$	2.0	0.63×10^{-6}
6.16	3^-	4.8 ± 1.2	104 fm^6	194 fm^6	0.53	13.3×10^{-6}
6.90	3^-	7 ± 2	151 fm^6	194 fm^6	0.79	43×10^{-6}
7.10	2^+	18 ± 2	32.4 fm^4	11.8 fm^4	2.7	0.47
7.90	(6^-)	11 ± 3	$1.06 \times 10^5 \text{ fm}^{10}$	$0.91 \times 10^5 \text{ fm}^{10}$	1.1	400×10^{-13}
8.50	5^-	27 ± 3	$1.06 \times 10^5 \text{ fm}^{10}$	$0.91 \times 10^5 \text{ fm}^{10}$	1.1	400×10^{-13}

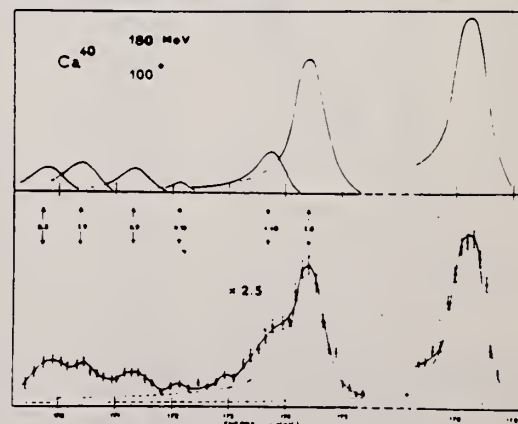


Fig. 1. Scattered electron spectrum from a Ca target at 180 MeV.

Ref.

S. Costa, F. Ferrero, S. Ferromi, B. Minetti, C. Molino
R. Malvano
Phys. Letters 6, 226 (1963)

Elem. Sym.

A

Z

Ca

40

20

Method

100 MeV Synchrotron; 4π neutron detector; calculated integrated
cross sections - fitted with polynomial of degree η

Ref. No.

63 Co 3

BCF

Reaction	E or ΔE	E_0	Γ	$\int \sigma dE$	$J\pi$	Notes
(γ, xn)						$\sigma_b = \int \frac{\sigma(E)}{E} dE$ <p>gets $\langle \vec{v}_p \cdot \vec{v}_n - \vec{v}_n \cdot \vec{v}_{n1} \rangle$</p> $= (k_0^2 - k_p^2 - \frac{3}{\pi^2} \frac{k_F^2}{e^2} \sigma_b \frac{A-1}{A^2}) \times \frac{2}{A-2}$ <p>See "Beren" for plots of this and $\int \sigma dE/60 \text{ ME/A}$.</p>

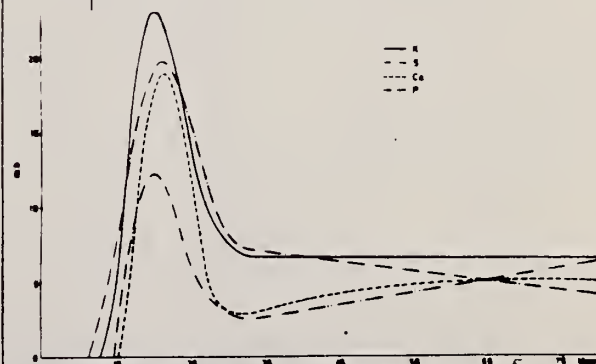


Fig. 1. Photoneutron cross sections for several light elements versus γ -ray energy.

Elem. Sym.	A	Z
Ca	40	20

Method 70 MeV electron synchrotron; BF₃ counters; data unfolded using inverse brems. matrix according to Penfold and Leiss

Ref. No.
63 Mi 2
JHH

Reaction	E or ΔE	E_0	Γ	$\int \sigma dE$	$J\pi$	Notes
(γ, n)	Bremss. 15-30			$\int_{15}^{28} = 76.0 \text{ MeV-mb}$		<u>252</u>

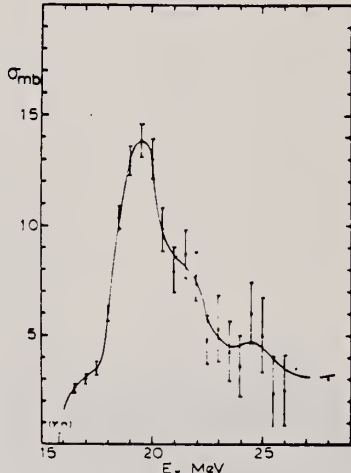


FIG. 1. Photoneutron cross section of calcium unfolded in 1.0-MeV intervals.

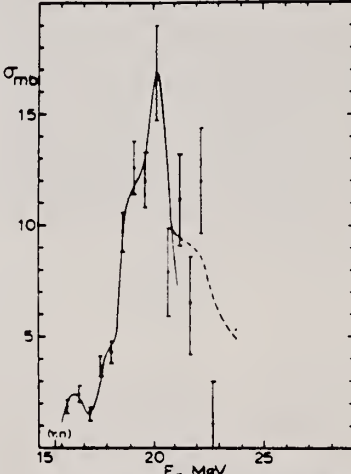


FIG. 2. Photoneutron cross section of calcium unfolded in 0.5-MeV intervals. The solid line represents the superposition of four Gaussian resonance curves listed in Table I.

TABLE I. Parameters of the Gaussian curves which fit the 0.5-MeV interval data. The results are compared with the monochromatic data of Ref. 9.

This experiment					Monochromatic data	
E_0 (MeV)	σ_0 (mb)	Δ (MeV)	Γ (MeV)	$\int \sigma dE$ (MeV-mb)	Energy (MeV)	Photoneutron cross section (mb)
16.6	2.5	0.7	1.1	2.0	16.8	10
18.0	4.0	0.6	1.0	4.1		
19.0	14.4	0.5	0.9	10.6	19	14
20.25	16.8	0.45	1.4	24.5	20	14
21.5	8.1				21.5	11.8
(24.5)	4.5					

Elem. Sym.	A	Z
Ca	40	20
Ref. No.		NVB
63 M1 5		

Method Betatron; proton yield; angular distribution; scintillators;
ion chamber

Reaction	E or ΔE	E_0	Γ	$\int \sigma dE$	$J\pi$	Notes
----------	-----------------	-------	----------	------------------	--------	-------

Ca(γ ,xp)

Bremss.

22

Angular distribution:

$$Y(\theta) = a + b \sin^2 \theta (1 + p \cos \theta)^2$$

where,

$$a = 56 \pm 7$$

$$b = 46 \pm 12$$

$$p = 0.3 \pm 0.2$$

$$b/a = 0.8 \pm 0.2$$

Yield ($E_p > 8$ MeV):

$$(9.5 \pm 1.5) 10^5 \text{ protons/mole-r}$$

Yield ($3.7 < E_p < 14$):

$$(42 \pm 4) 10^5$$

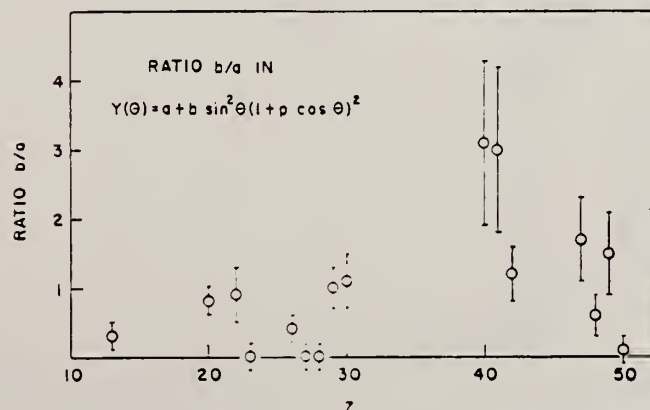
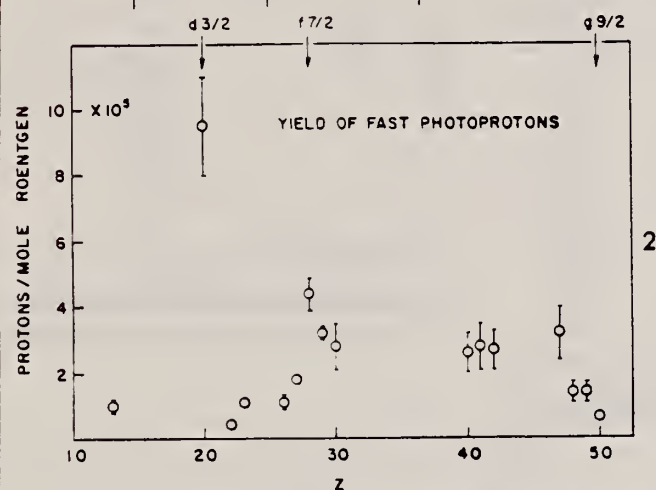


Fig. 2. The yields of fast photoprotons ($E_p > 8$ MeV) obtained from targets of various elements when irradiated with 22-Mev. bremsstrahlung. The target thicknesses range from 21 to 372 mg/cm² (about 8 Mev. for protons). The errors noted are statistical.

Fig. 3. The anisotropy coefficient b/a for fast photoprotons ($E_p > 8$ Mev) from 16 elements. The errors noted are statistical.

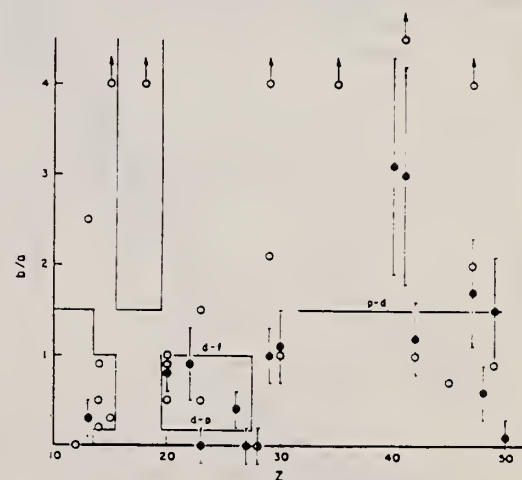


Fig. 4. The values of the fast photoproton anisotropy coefficient b/a found by the present authors. \bullet and other workers (\circ) in the region of the periodic table $10 \leq Z \leq 50$. Arrows indicate off-scale points. The references to the results of other workers are given in Table II. The denunciations are explained in the text.

METHOD

Betatron C^{12} act. and NBS P2 chamber

REF. NO.

64 Ba 1

JOC

REACTION	RESULT	EXCITATION ENERGY	SOURCE		DETECTOR		ANGLE
			TYPE	RANGE	TYPE	RANGE	
G, N	ABX	15-30	C	15-30	ACT-I		4 PI

$$\int_{15.6}^{30} dE_Y \cdot \sigma_{xn} = 81 \pm 4 \text{ MeV-mb}$$

535

TABLE I
 $Ca^{40}(\gamma, n)$ peak energies (MeV)

Brown <i>et al.</i>	Gillet (a)	Gillet (b)	Balashov <i>et al.</i>	Present experiment
16.8	16.0	16.4	16.2	15.9
17.8	17.0*	—	—	17.8
—	—	18.4*	18.4	18.5*
—	—	—	18.7	18.9*
19.2**	—	—	—	19.2*
—	19.5	—	19.6**	19.6**
—	19.9	19.8	—	19.9*
20.6	20.7	—	—	20.8*
—	—	21.7	—	(21.7)
—	22.2*	—	—	22.3
—	—	—	24.4*	24.1
—	—	—	—	(25.4)

Gillet (a): Calculated assuming isotopic spin to be a good quantum number.
(b): Calculated assuming isotopic spin not to be a good quantum number.
Energies of relatively strong transitions are shown with asterisks.

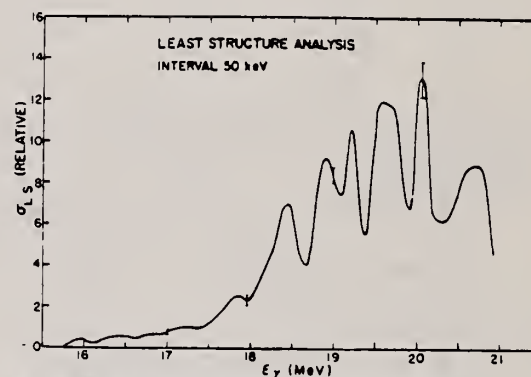


Fig. 8. Photoneutron cross section curve for calcium, as derived by the method of least structure.

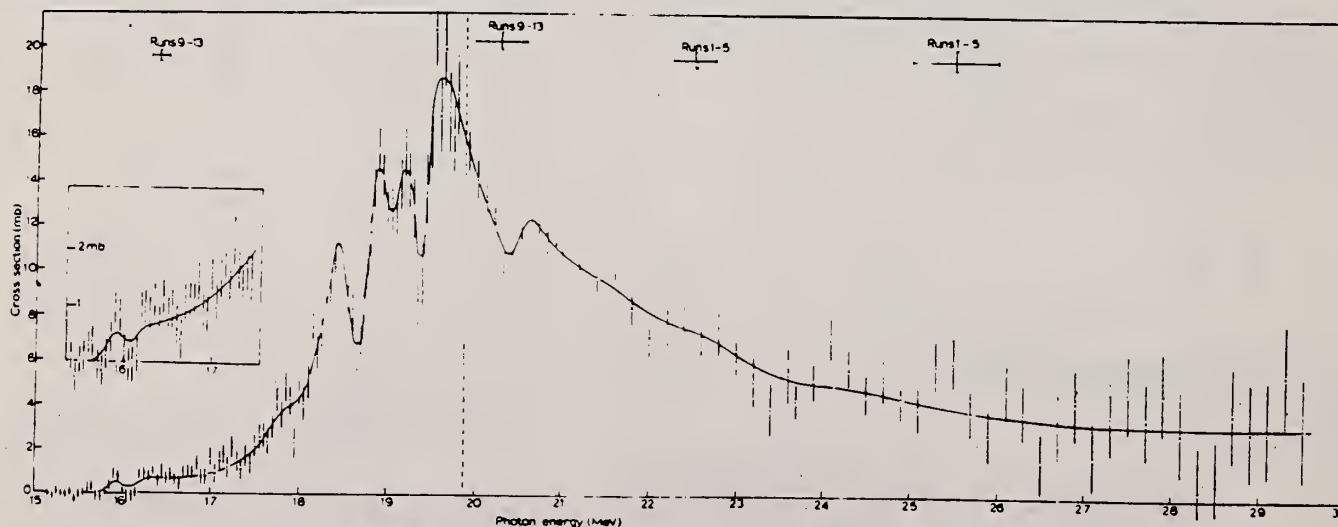


Fig. 7. Photoneutron cross section curve for calcium (Penfold-Leiss analysis).

METHOD			REF. NO.		
Linac /			64 F1 1		JOC
REACTION	RESULT	EXCITATION ENERGY	SOURCE		ANGLE
			TYPE	RANGE	
G, XN	SPC	THR-32	C	25,32	70

TABLE 3
Energy levels in Ca^{40} observed in the reactions $\text{Ca}^{40}(\gamma, n)\text{Ca}^{39}$ and $\text{K}^{39}(p, \gamma_0)\text{Ca}^{40}$

$\text{Ca}^{40}(\gamma, n)\text{Ca}^{39}$ (MeV)	$\text{K}^{39}(p, \gamma_0)\text{Ca}^{40}$ (MeV)
18.15	
18.38	
18.65	
18.78	18.82
19.10 ± 0.05	19.20
19.20	19.30
19.45	19.47
19.70	19.68
19.96	19.95
20.05	20.03
20.02	20.13
20.35	
20.50	20.5
20.75	
21.00	
21.23	21.2
21.5	
22.0	
	21.8

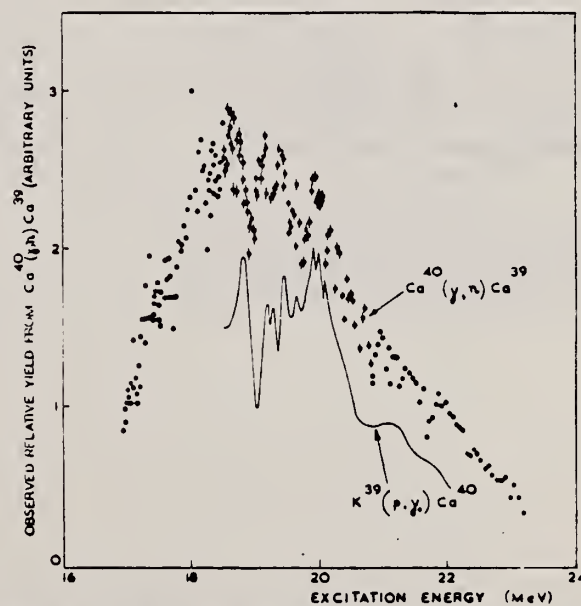


Fig. 4. The observed relative yield of photoneutrons from the reaction $\text{Ca}^{40}(\gamma, n)\text{Ca}^{39}$ for a bremsstrahlung energy of 25 MeV. The $\text{K}^{39}(p, \gamma_0)\text{Ca}^{40}$ data of Feldman ⁴⁰ are included for comparison.

REF.

J. C. Hafele, F. W. Bingham, J. S. Allen
Phys. Rev. 135, B365-70 (1964)

Ca

40

20

METHOD

Cyclotron

REF. NO.

64 Ha 1

NVB

REACTION	RESULT	EXCITATION ENERGY	SOURCE		DETECTOR		ANGLE
			TYPE	RANGE	TYPE	RANGE	
P,G	ABX	14-23	D	6-15	SCI-D		90

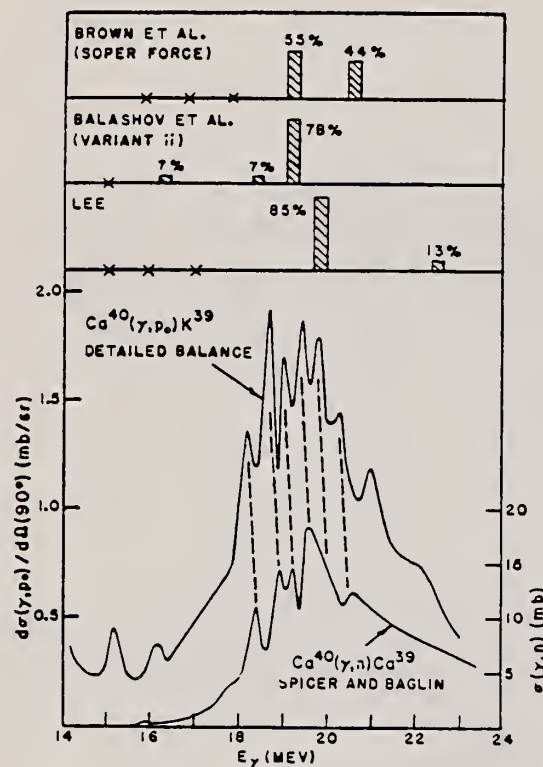
DETAILED BALANCE

FIG. 5. Comparison of the $\text{Ca}^{40}(\gamma, p_0)\text{K}^{39}$ differential cross section at 90° , obtained from the inverse reaction by applying the principle of detailed balance, with the experimental $\text{Ca}^{40}(\gamma, n)\text{Ca}^{39}$ cross section and with theoretical energies and dipole strengths of the dipole states of Ca^{40} . The 'x's indicate energies for dipole states that carry less than 1% of the dipole strength.

REF.

M. Fors, H. Nguyen Ngoc and J. Perez y Jorba
Phys. Letters 2, 40 (1964)

Ca

40

20

METHOD

Linac

[Page 1 of 2]

REF. NO.

64 Ho 1

JOC

REACTION	RESULT	EXCITATION ENERGY	SOURCE		DETECTOR		ANGLE
			TYPE	RANGE	TYPE	RANGE	
E, E/	ABX	10-17	D	80-200	MAG-D		DST

Table 1
Experimental cross sections and their relative errors.

E (MeV)	θ (deg)	σ_{point} (cm ² /sr)	Level at 12.2 MeV		11 MeV		13.9 MeV		14.6 MeV	
			σ_{in} (cm ² /sr)	$\frac{\Delta\sigma_{\text{in}}}{\sigma_{\text{in}}}$	σ_{in} (cm ² /sr)	$\frac{\Delta\sigma_{\text{in}}}{\sigma_{\text{in}}}$	σ_{in} (cm ² /sr)	$\frac{\Delta\sigma_{\text{in}}}{\sigma_{\text{in}}}$	σ_{in} (cm ² /sr)	$\frac{\Delta\sigma_{\text{in}}}{\sigma_{\text{in}}}$
81.74	75	1.75×10^{-27}					3.1×10^{-32}	1	1.0×10^{-31}	0.45
109.8	60	2.47×10^{-27}	3.7×10^{-32}	0.77	1.2×10^{-32}	0.8	1.1×10^{-31}	0.5	2.7×10^{-31}	0.28
120.2	60	2.05×10^{-27}	9.2×10^{-32}	0.46	2.0×10^{-32}	0.8	1.5×10^{-31}	0.5		
140.8	60	1.53×10^{-27}	5.8×10^{-32}	0.31	1.4×10^{-32}	0.8	4.6×10^{-32}	0.45	1.4×10^{-31}	0.28
121.4	75	7.90×10^{-28}							5.2×10^{-32}	0.40
167.8	60	1.055×10^{-27}	6.1×10^{-32}	0.19	1.3×10^{-32}	0.8	7.6×10^{-32}	0.18	1.0×10^{-31}	0.15
106.7	110	1.71×10^{-28}	9.8×10^{-33}	0.19			1.2×10^{-32}	0.5	1.7×10^{-32}	0.40
199.4		7.40×10^{-28}					3.6×10^{-32}		7.2×10^{-32}	
	60		4.8×10^{-32}	0.19	2.2×10^{-32}	0.32		0.28		0.21
201.2		7.32×10^{-28}					2.8×10^{-32}		6.6×10^{-32}	
179.9	75	3.63×10^{-28}	1.9×10^{-32}	0.16			4.0×10^{-33}	1.1	2.4×10^{-32}	0.35
200.7	75	2.91×10^{-28}	1.4×10^{-32}	0.13	7.1×10^{-33}	0.20	2.8×10^{-33}	0.5	2.1×10^{-32}	0.18
179.8	90	1.62×10^{-28}	2.9×10^{-33}	0.77			2.3×10^{-33}	1	7.0×10^{-33}	0.65
189.0	90	1.45×10^{-28}							1.1×10^{-32}	0.23

M. Hors, H. Nguyen Ngoc and J. Perez y Jorba
Phys. Letters 9, 40 (1964)

Ca

40

20

METHOD

Linac

[Page 2 of 2]

REF. NO.

64 Ho 1

JOC

REACTION	RESULT	EXCITATION ENERGY	SOURCE		DETECTOR		ANGLE
			TYPE	RANGE	TYPE	RANGE	

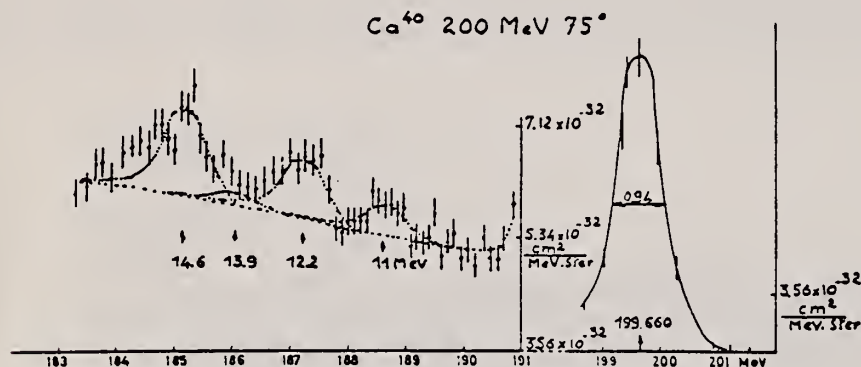


Fig. 1. Spectrum of scattered electrons on Ca^{40} ; 200 MeV 75° .

Table 2

Résumé of different transition hypothesis, reduced transition probabilities $B(f-i)$, radiative transition widths Γ , enhancement factor G in Weisskopf units, and χ^2 analysis under the hypothesis considered.

Excited energy (MeV)	Transition hypo- thesis	$B \times 10^3$	$B(f-i)$	Γ (eV)	G in Weiss- kopf units	χ^2	Corresponding probability
12.20 ± 0.05 $\nu = 8$	E3	2.74 ± 0.20	$42.6 \pm 3.1 \text{ fm}^6$	$(6.43 \pm 0.47) 10^{-4}$	0.44	5.0	0.73
11.0 ± 0.1 $\nu = 5$	E3	1.22 ± 0.20	$19 \pm 3 \text{ fm}^6$	$(1.42 \pm 0.24) 10^{-4}$	0.19	2.77	0.72
	M3	1.32 ± 0.21	$15.4 \pm 2.5 \text{ fm}^6$	$(1.16 \pm 0.19) 10^{-4}$	6.24	1.15	0.94
	E4	2.83 ± 0.47	$515 \pm 85 \text{ fm}^3$	$(1.40 \pm 0.24) 10^{-7}$	0.45	4.08	0.53
	M4	2.61 ± 0.44	$380 \pm 65 \text{ fm}^3$	$(1.03 \pm 0.17) 10^{-7}$		6.0	0.31
	E2	2.28 ± 0.65	to be rejected			28.6	< 0.02
13.9 ± 0.1 $\nu = 9$	E2	1.02 ± 0.13	$1.47 \pm 0.19 \text{ fm}^4$	0.62 ± 0.08	0.18	9.0	0.43
14.6 ± 0.1 $\nu = 9$	E1	0.37 ± 0.03	$0.060 \pm 0.005 \text{ fm}^2$	192 ± 15	0.078	7.42	0.57
	E3	4.14 ± 0.33	$64 \pm 5 \text{ fm}^6$	$(3.37 \pm 0.27) 10^{-3}$	0.66		
	M1	0.37 ± 0.03	$0.03 \pm 0.003 \text{ fm}^2$	96.7 ± 7.7	1.5	8.94	0.43
	E3	4.14 ± 0.33	$64 \pm 5 \text{ fm}^6$	$(3.36 \pm 0.27) 10^{-3}$	0.66		
	M3	3.43 ± 0.28	to be rejected			17.7	0.04
	E1	0.446 ± 0.036					
	E2	1.40 ± 0.11	$2.02 \pm 0.16 \text{ fm}^4$	(1.06 ± 0.08)	0.24	6.08	0.71
	E4	6.35 ± 0.50	$1156 \pm 91 \text{ fm}^8$	$(3.81 \pm 0.30) 10^{-6}$	1.02		
	M2	1.53 ± 0.12	to be rejected			10.3	0.33
	E4	6.38 ± 0.50					
	M4	5.01 ± 0.39	$729 \pm 57 \text{ fm}^3$	$(2.40 \pm 0.19) 10^{-6}$	24	7.11	0.6
	E2	1.50 ± 0.12	$2.17 \pm 0.17 \text{ fm}^4$	1.16 ± 0.09	0.26		

ν is the degree of freedom

Ca	40	20
REF. NO.		NVB
64 Is 2		

METHOD			SOURCE		DETECTOR		ANGLE
Betatron			TYPE	RANGE	TYPE	RANGE	
G, P	ABX	14-32	C	14-32	EMU-D	1-13	DST

Angular distribution isotropic except for 3-5 MeV protons, for which it is $1-0.5 \sin^2\theta$.

SPC

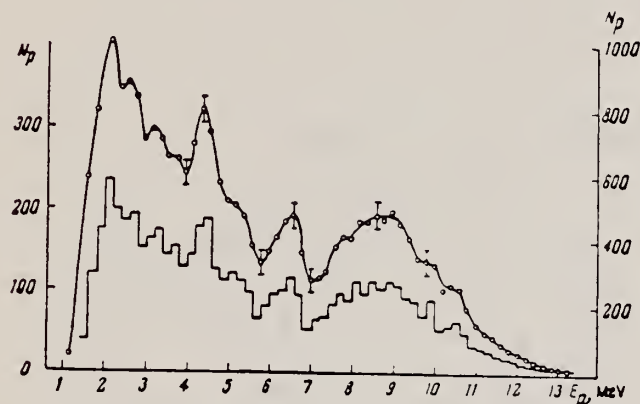


FIG. 1. Energy spectrum of photoprotons from calcium for $E_{\gamma\max} = 22$ MeV. The histogram is plotted to the left ordinate scale, and the curve to the right scale.

Proton energy, MeV	Maximum cross section, mb	Location of peak, MeV	Half-width of peak, MeV	Integrated cross section $\int_{-3\sigma}^{+3\sigma} \sigma dE$ (MeV-mb)
3-5	53 ± 8	20.0 ± 0.5	5.5 ± 0.5	0.42 ± 0.08
5-7	9.0 ± 0.13	21.0 ± 0.5	6.5 ± 0.5	0.07 ± 0.02
≥ 8	19 ± 3	22.0 ± 0.5	6.5 ± 0.5	0.15 ± 0.03
≥ 3	80 ± 12	19.5 ± 0.5	6.5 ± 0.5	0.63 ± 0.12

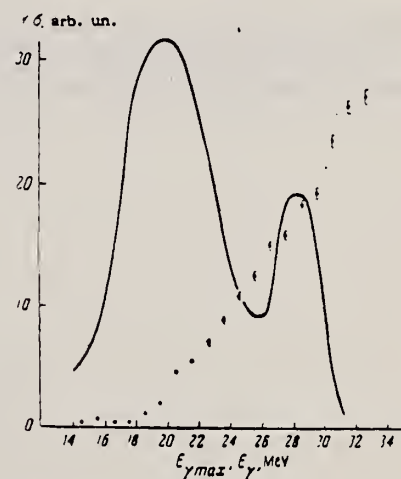


FIG. 2. Variation of the yield of the (γ, p) reaction on calcium with the maximum energy of the bremsstrahlung spectrum (experimental points). The solid curve is the differential cross section for this reaction.

METHOD

REF. NO.

64 Is 3

JDM

REACTION	RESULT	EXCITATION ENERGY	SOURCE		DETECTOR		ANGLE
			TYPE	RANGE	TYPE	RANGE	
G,P	ABX	THR-34	C	18-34	EMU-D	3-15	DST

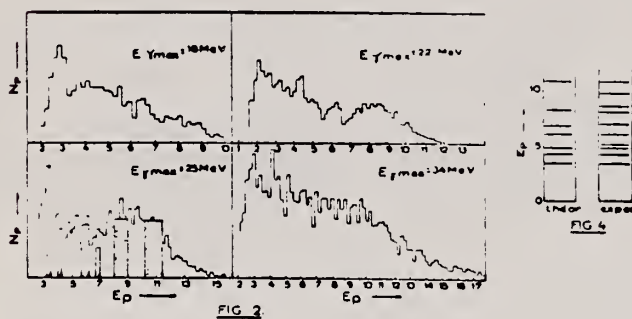
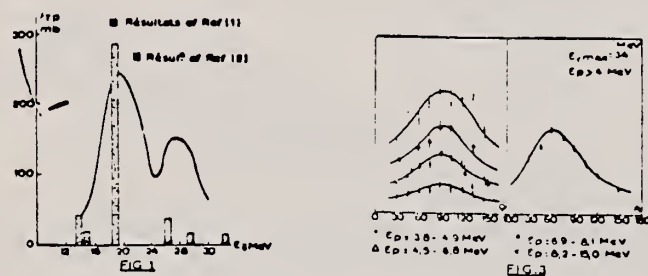


FIG. 1. — Comparison of theoretical and experimental (γ, p) cross-sections for Ca^{40} .
FIG. 2. — Energy distributions of photoprotons.
FIG. 3. — Angular distributions of photoprotons.
FIG. 4. — Comparison of theoretical and experimental spectra for Ca^{40} photoprotons.

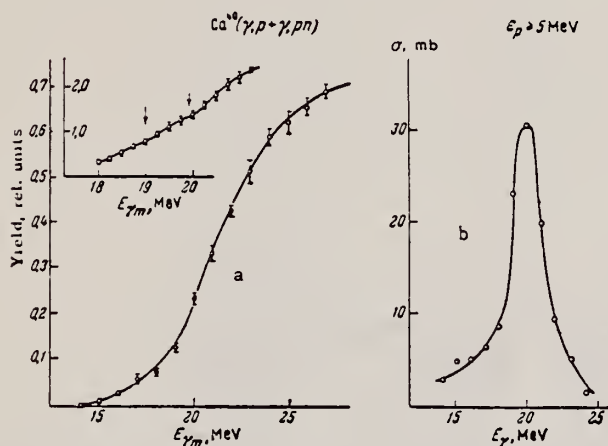
B. S. Ratner
Zhur. Eksp. i Teoret. Fiz. 46, 1480-81 (1964)
Soviet Phys. JETP 19, 1000 (1964)

Ca	40	20
REF. NO. 64 Ra 2		
NVB		

METHOD			SOURCE		DETECTOR		ANGLE
Synchrotron; 10 n chamber monitor			TYPE	RANGE	TYPE	RANGE	
G,P	ABX	14-27	C	30	SCI-I	5-	DST

$$\int_{14}^{27} \sigma dE = (124 \pm 10) \text{ MeV-mb}$$

INCLUDES G,NP
Yield same at 45° , 90° , 135° .



a) Yield of photoprotons of energy $\epsilon_p > 5 \text{ MeV}$ from Ca^{40} as a function of $E_{\gamma m}$. Upper inset: the same quantity, measured every 0.25 MeV for $E_{\gamma m}$ from 18 to 21.5 MeV. The arrows indicate the location of inflection points in the curve. Root-mean-square errors are shown. b) Cross section for emission of photoprotons of energy $\epsilon_p > 5 \text{ MeV}$ from Ca^{40} .

METHOD

K(p, γ)Ca; Van de Graaff

REF. NO.

64 Si 1

NVB

REACTION	RESULT	EXCITATION ENERGY	SOURCE		DETECTOR		ANGLE
			TYPE	RANGE	TYPE	RANGE	
P, γ	NØX	9 - 10	D	1-2	NAI-D		DST

New level at 4.70 MeV.

 J^π of 9.44 MeV level is probably 1^+ or 1^- .

J-PI

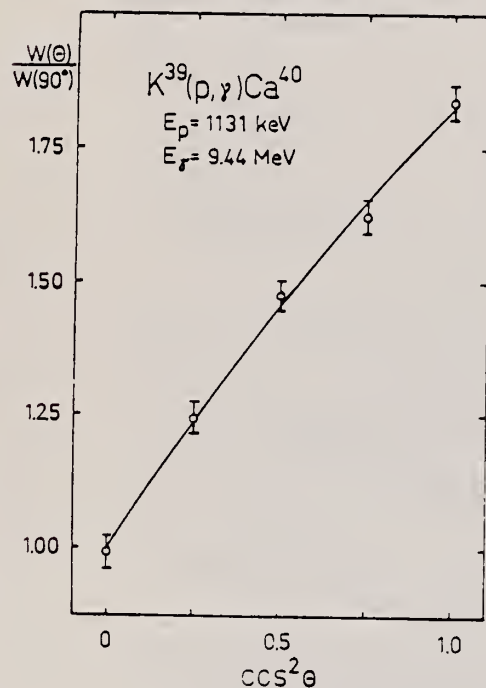
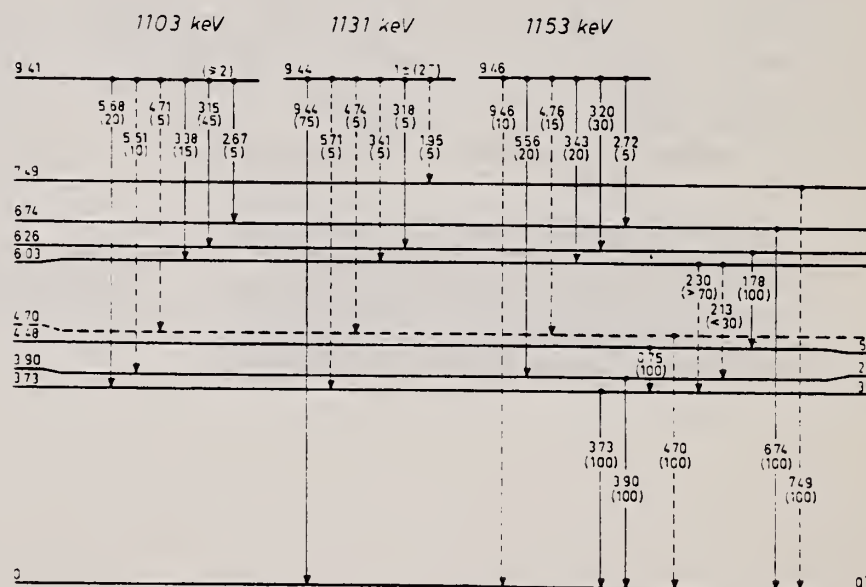


Figure 5. Angular distribution of the 9.44 MeV gamma ray.

Figure 6. Energy levels of Ca^{40} with decay modes found in this work.

METHOD

$K^{39}(p,\gamma)Ca^{40}$ /Tandem

REF. NO.

64 Ta 1

JOC

REACTION	RESULT	EXCITATION ENERGY	SOURCE		DETECTOR		ANGLE
			TYPE	RANGE	TYPE	RANGE	
P,G	RLX		D	9-14	NAI-D		100

Comparison with several other (p, γ) results.

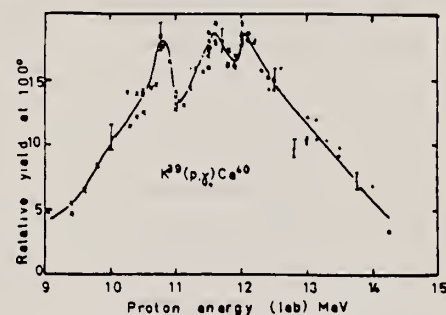


Fig. 6. The excitation function for $K^{39}(p,\gamma)Ca^{40}$ at 100° . The different symbols represent three different runs normalized to each other. The target thickness was about 100 keV.

METHOD			REF. NO.		
Linac; Faraday cup and SEM monitor			65 Cr 1		NVB
REACTION	RESULT	EXCITATION ENERGY	SOURCE		ANGLE
			TYPE	RANGE	
E, E/	ABX	3 - 5	D	250	DST

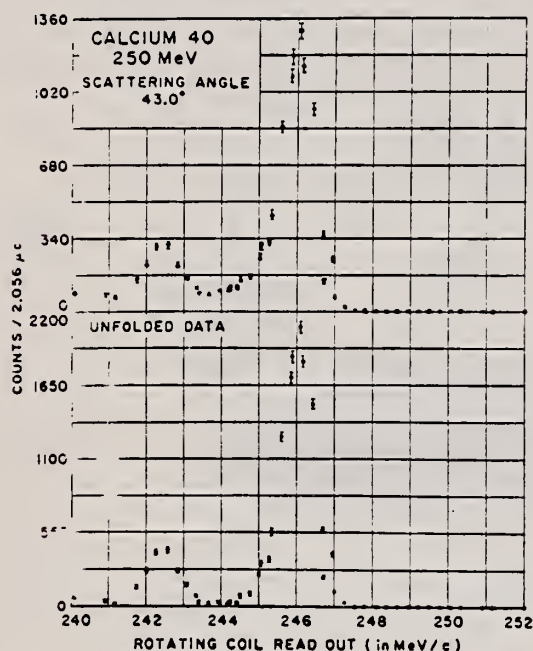


Fig. 1. Elastic and inelastic scattering peaks in Ca^{40} at 250 MeV. The scattering angle is 43° . The data plotted by the computer are shown when the data are not corrected as in (a) above, and when the data are corrected by the computer program of Crannell as in (b) below. The contributions due to the radiative tail associated with the peaks have been subtracted or "unfolded" in Crannell's program.

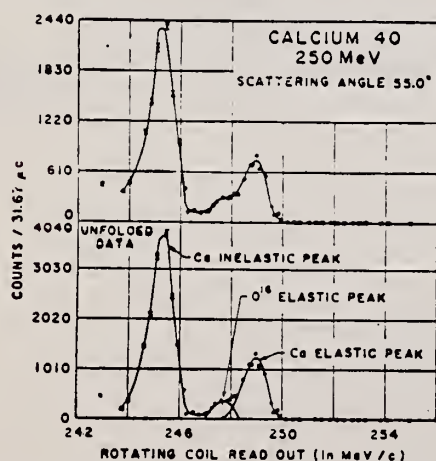


Fig. 2. This figure is similar to Fig. 1 except that the scattering angle is 55° and is near the first diffraction feature of calcium at an energy of 250 MeV. Under these conditions the small impurity of oxygen can be observed. (See text.)

TABLE II. Inelastic electron scattering cross sections in calcium for the combined levels 3.35, 3.73, 3.9, 4.48 MeV. Incident energy = 250 MeV.

θ in degrees	Cross section in cm^2/sr
32	~ 0
35	$17.6 \pm 17.00 \times 10^{-31}$
40	$70.00 \pm 20.00 \times 10^{-31}$
43	$58.66 \pm 8.40 \times 10^{-31}$
45	$52.97 \pm 5.30 \times 10^{-31}$
47	$43.21 \pm 2.70 \times 10^{-31}$
50	$37.00 \pm 1.60 \times 10^{-31}$
53	$21.15 \pm 0.80 \times 10^{-31}$
55	$23.42 \pm 0.80 \times 10^{-31}$
57	$13.16 \pm 0.36 \times 10^{-31}$
60	$10.00 \pm 0.35 \times 10^{-31}$
65	$5.17 \pm 0.36 \times 10^{-31}$
70	$2.92 \pm 0.30 \times 10^{-31}$
75	$1.49 \pm 0.15 \times 10^{-31}$
78	$9.65 \pm 1.00 \times 10^{-32}$
85	$4.02 \pm 0.50 \times 10^{-32}$
90	$2.58 \pm 0.02 \times 10^{-32}$
95	$1.86 \pm 0.40 \times 10^{-32}$
100	$8.80 \pm 4.00 \times 10^{-33}$
105	$5.14 \pm 0.35 \times 10^{-33}$
115	$2.75 \pm 0.27 \times 10^{-33}$
125	$8.94 \pm 2.00 \times 10^{-34}$

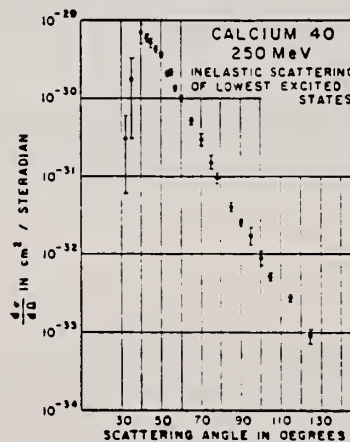


Fig. 4. The inelastic level scattering in calcium at 250 MeV. The figure shows the composite inelastic peak containing the four levels, 3.35, 3.73, 3.9, and 4.48 MeV, of which the middle two are probably the most important.

REF.

B.S. Dolbilkin, V.I. Korin, L.E. Lazareva, and F. A. Nikolaev
Phys. Letters 17, 49 (1965)

ELEM. SYM.

Ca

40

20

METHOD

260 MeV Synchrotron

REF. NO.

65 Do 1

EGF

REACTION	RESULT	EXCITATION ENERGY	SOURCE		DETECTOR		ANGLE
			TYPE	RANGE	TYPE	RANGE	
G, MU-T	ABX	10-28	C	260	MGP	10-28	

$$\int_{11}^{28.5} \sigma dE = 920 \pm 100 \text{ MeV} \cdot \text{mb}$$

$$\int_{19}^{21.1} \sigma dE = 0.6 \text{ of total}$$

Table compares peaks with other data and theory.

$$\sigma_{-1} = 49.6 \pm 4.5 \text{ mb}$$

$$\sigma_{-2} = 2.60 \pm 0.50 \text{ mb/MeV}$$

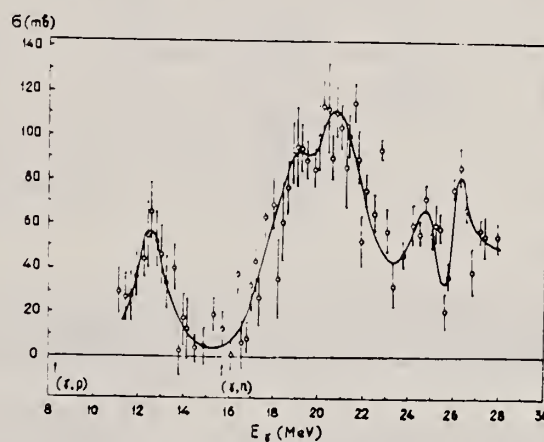


Fig. 1. Nuclear γ absorption cross section of ^{40}Ca as a function of photon energy.

(OVER)

Table 1

Positions of resonance maxima (MeV) from various experiments. The relative values of the integrated cross sections (%) are given in column one.

Calculated energies (MeV) and relative dipole strengths (%) of levels in ^{40}Ca .

From absorption cross section (this experi- ment)	From photoneutron cross section (bremsstrah- lung data) [3]	From photoneutron cross section (monochromatic data) [4]	From photoneutron spectrum (time-of- flight method) [5] ^a	From $\sigma(p, \gamma_0)$, the cross section of the inverse reaction [6]	[11]			
					Ordinary force	Super mixture	[12]	[13]
12.5 (14%) ^c							9.6 (1.5%) 12.3 (1%) 14.3 (11.5%) 15.1 (5%)	
	16.6				13.6 (1%)			
	18.0		19.15 19.38 19.65 18.78		16.6 (1%) 17.6 (9%)	16.8 (1%)		
19.1 (37%) ^{b, c}	19.0	19.1	19.10 19.20 19.45 19.70 19.96 20.02	18.9 19.6	18.5 (80%)	19.2 (55%)	19.1 (79%)	18.4 (90%)
	20.2	19.9	20.05 20.35 20.50 20.75 21.00	20.1				
21.1 (35%)	21.5	21.4	21.23 21.5 22.0		21.5 (9%)	20.6 (44%)	21.4 (2%)	21.7 (10%)
24.7 (8%) 26.1 (6%)	24.5							

- a. The excitation energies were given assuming ground state transitions only, since this is not always the case.
 b. This resonance was observed very distinctly also in the nuclear absorption cross section in ref. 10.
 c. The groups of photoprotons observed in the energy spectra in refs. 7-9 probably correspond to these resonance maxima.

in which two maxima at $E_\gamma=19.1$ and 21.1 MeV are situated, is equal to about 60% of the total integrated cross section. The minus-first moment σ_{-1} and minus-second moment σ_{-2} calculated from the obtained nuclear absorption cross section curve, are 49.6 ± 4.5 mb and 2.60 ± 0.50 mb MeV, respectively.

1. N. A. Burqov, G. V. Danilyan, B. S. Dolbilkin, L. E. Lazareva and F. A. Nikolaev, Zh. Eksp. i Teor. Fiz. 43 (1962) 7; Soviet Phys. JETP 16 (1963) 5.
2. B. S. Dolbilkin, V. A. Zapevalov, V. I. Korin, L. E. Lazareva and F. A. Nikolaev, Nucl. Phys. (in press).
3. K. Min, I. N. Bolen and W. D. Whitehead, Phys. Rev. 132 (1963) 749.
4. J. Miller, C. Schuhl, G. Tamas and C. Tama, Physics Letters 2 (1962) 76.
5. F. W. K. Firk, Nucl. Phys. 52 (1964) 477.
6. N. W. Tanner, G. C. Thomas and E. D. Earle, Nucl. Phys. 52 (1964) 29.
7. T. N. Dragnev and B. P. Konstantinov, Zh. Eksp. i Teor. Fiz. 42 (1962) 344; Soviet Phys. JETP 15 (1962) 236.
8. S. A. E. Johansson and B. Forkman, Nucl. Phys. 36 (1962) 141.
9. K. Shoda, T. Ishizuka, N. Kawamura, K. Abe and M. Kimura, J. Phys. Soc. Japan 17 (1962) 401.
10. J. Dular, G. Kernel, M. Kregar, M. V. Mihanović, G. Pregl, M. Rosina and Č. Zupančič, Nucl. Phys. 14 (1959) 131.
11. G. E. Brown, L. Castillejo and J. A. Evans, Nucl. Phys. 22 (1961) 1.
12. K. V. Shitikova and E. L. Jadrovsky, Izv. Akad. Nauk SSSR (in press).
13. V. Gillet and E. A. Sanderson, Nucl. Phys. 34 (1964) 472.
14. V. V. Balashov, V. G. Shevchenko and N. P. Yudin, Nucl. Phys. 27 (1961) 323.

REF. B. S. Ishkhanov, I. M. Kapitonov, E. N. Kornienko, V. G. Shevchenko,
and B. A. Yur'ev
Izv. Akad. Nauk fiz. 29, 221 (1965)
Bull. Acad. Sci. USSR - Phys. 29, 221 (1965)

ELEM. SYM.	4	2
Ca	40	20
REF. NO.	65 Is 1	EGF

METHOD

[Page 1 of 2]

REACTION	RESULT	EXCITATION ENERGY	SOURCE		DETECTOR		ANGLE
			TYPE	RANGE	TYPE	RANGE	
G,P	SPC	THR-25	C	13-25	EMU-D	2-16	DST

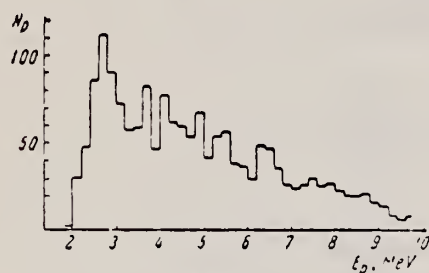


Fig. 1

Fig.1. Photoproton spectrum recorded with E_{γ} max = 18 MeV.

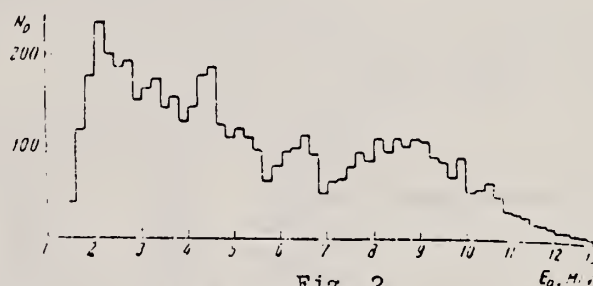


Fig. 2

Fig.2. Photoproton spectrum recorded with E_{γ} max = 22 MeV.

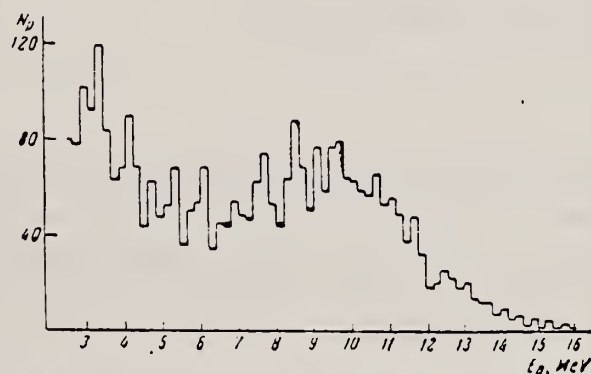


Fig.3. Photoproton spectrum recorded with E_{γ} max = 25 MeV.

REF. B. S. Ishkhanov, I. M. Kapitonov, E. N. Kornienko, V. G. Shevchenko,
and B. A. Yur'ev
Izv. Akad. Nauk fiz. 29, 221 (1965)
Bull. Acad. Sci. USSR - Phys. 29, 221 (1965)

ELEM. SYM.	A	Z
Ca	40	20

METHOD

REF. NO.

65 Is 1

EGF

[Page 2 of 2]

REACTION	RESULT	EXCITATION ENERGY	SOURCE		DETECTOR		ANGLE
			TYPE	RANGE	TYPE	RANGE	

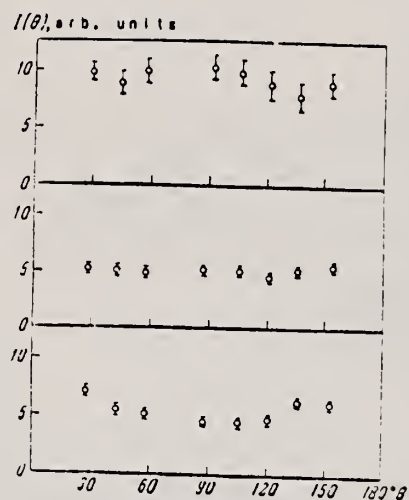


Fig. 4

Fig.4. Angular distributions of different proton groups ($E_{\gamma \text{ max}} = 22 \text{ MeV}$): a - $E_p \geq 7.5 \text{ MeV}$, b - $E_p = 6.0-7.5 \text{ MeV}$, c - $E_p = 3.0-6.0 \text{ MeV}$.

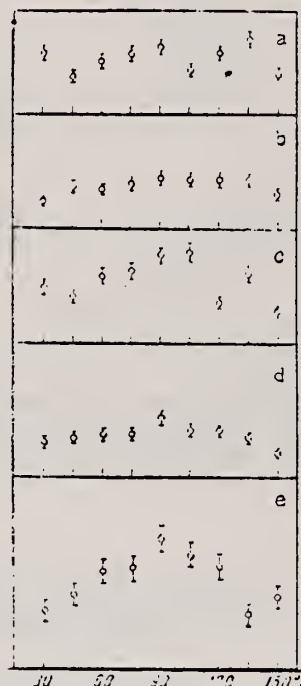


Fig. 5

Fig.5. Angular distributions of different protons groups ($E_{\gamma \text{ max}} = 25 \text{ MeV}$): a - $E_p = 2.7-3.7 \text{ MeV}$, b - $E_p = 3.8-4.9 \text{ MeV}$, c - $E_p = 4.5-6.8 \text{ MeV}$, d - $E_p = 6.9-8.1 \text{ MeV}$, e - $E_p = 8.2-16.0 \text{ MeV}$.

Ca

40

20

METHOD

Betatron; NBS chamber monitor

REF. NO.

65 Va 3

NVB

REACTION	RESULT	EXCITATION ENERGY	SOURCE		DETECTOR		ANGLE
			TYPE	RANGE	TYPE	RANGE	
G, NP	ABI	50 - 300	C	50 - 300	ACT-I		4PI

TABLE 1. Integrated cross sections for the $S^{32}(\gamma, np)P^{30}$,
 $Ca^{40}(\gamma, np)K^{39}$, and $Zn^{66}(\gamma, np)Cu^{64}$ reactions.

E_{max} (MeV)	$\int_0^{E_{max}} \sigma dE$ (MeV mb)		
	$S^{32}(\gamma, np)P^{30}$	$Ca^{40}(\gamma, np)K^{39}$	$Zn^{66}(\gamma, np)Cu^{64}$
50	64 ± 2	31 ± 1	128 ± 3
100	79 ± 5	35 ± 5	160 ± 7
140	81 ± 6	35 ± 7	160 ± 20
200	107 ± 8	43 ± 9	270 ± 30
250	150 ± 10	72 ± 11	370 ± 45
300	190 ± 12	88 ± 14	400 ± 60

METHOD

REF. NO.

Synchrotron; ion chamber monitor

65 Wy 1

NVB

REACTION	RESULT	EXCITATION ENERGY	SOURCE		DETECTOR		ANGLE
			TYPE	RANGE	TYPE	RANGE	
G, MU-T	ABX	10-70	C	90	SCI-D		4PI

55 t

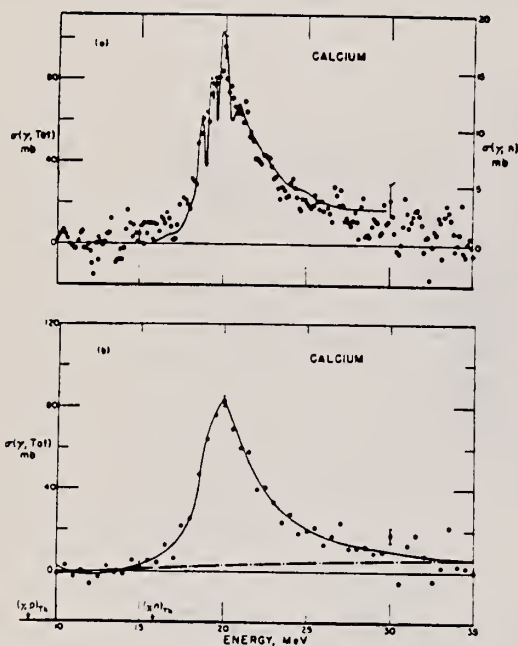


FIG. 21. Calcium total photonuclear cross section. The solid line in (a) represents the $\sigma(\gamma, n)$ data of Baglin and Spicer (Ref. 30) shifted up by 250 keV in energy using the right-hand ordinate scale.

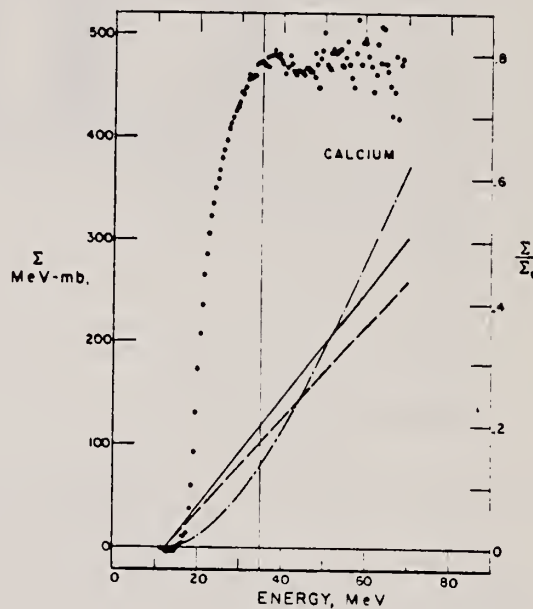


FIG. 22. Calcium total photonuclear cross section integrated over energy.

REF. U. Amaldi Jr., G. Campos Venuti, G. Cortellessa, E. De Sanctis,
S. Frullani, R. Lombard and P. Salvadori
Phys. Letters 22, 593 (1966)

ELEM. SYM.	A	Z
Ca	40	20
REF. NO.	66 Am 1	
	EGF	

REACTION	RESULT	EXCITATION ENERGY	SOURCE		DETECTOR		ANGLE
			TYPE	RANGE	TYPE	RANGE	
E, E/P	SPC	0-120	D	560-760	MAG-D	446-479	51

Proton detector at 62° E_p 113-119 MeV
Electron detector at 51° E 446, 458, 470 or 475 MeV
Incident electron energy varied

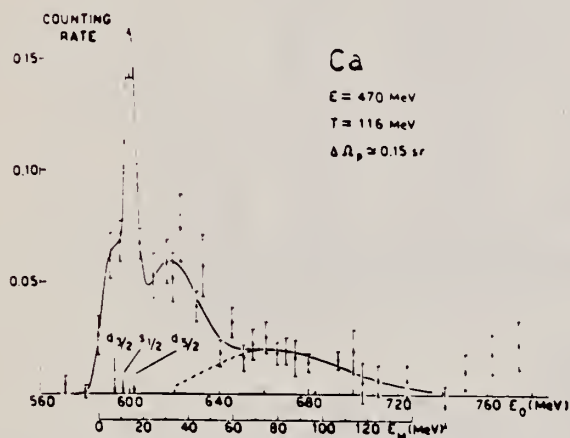


Fig. 1. The electron-proton coincidence rate in calcium as a function of the incoming electron energy E_0 and of the missing energy E_M defined in eq. (1).

Table 1				
	A	B	C	D
E_M	7.7 ± 2.6	14 ± 1	32 ± 4	77 ± 14
σ	13 ± 4	4.8 ± 1.4	23 ± 6	50 ± 31

METHOD

Electron synchrotron; NBS ⁶² Standard Chamber

REF. NO.

66 An 1

JDM

REACTION	RESULT	EXCITATION ENERGY	SOURCE		DETECTOR		ANGLE
			TYPE	RANGE	TYPE	RANGE	
G,XN	RLX	16 - 62	C	16-62	ACT-I		4PI

193

$\int_{\text{Thr}}^{\text{62}} \sigma dE\gamma = 114 \pm 15 \text{ MeV mb}$ and $12 \pm 7 \text{ MeV.mb}$ is due to $(\gamma, 2n)$ processes.

Measured yield of about 1 sec activities

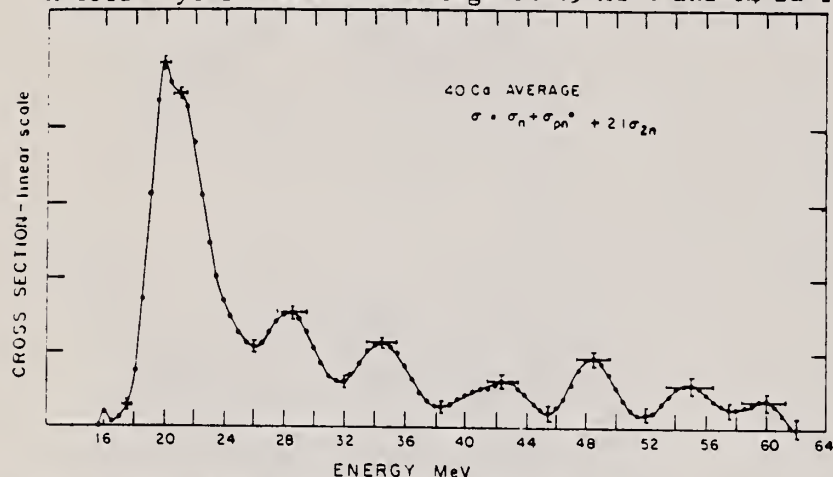
Absolute yield based on average of ⁶³Mi 2 and ⁶⁴Ba 1.*

Fig. 5. The least structure cross section solution for the average of the yield data. Vertical error bars indicate the errors in the cross sections as calculated by the least structure technique. Horizontal error bars indicate the widths the least structure resolution functions at the maxima. Although the figure heading includes only σ_n, σ_{pn} and σ_{2n} the cross sections for other calcium photoreactions leading to positron active products with 1 sec half-life are included in the solution.

TABLE 1

Cross section maxima

A summary of the information for the maxima with energies greater than 26 MeV for calcium.

Energy	$\int(\sigma_p + \sigma_{pn}^* + 1.8\sigma_{2n})dE$	$\int(\sigma_n + \sigma_{pn}^* + 2.4\sigma_{2n})dE$	Experimental resolution (MeV)
28.3 ± 0.3	0.27 ± 0.02	0.27 ± 0.02	2.0
34.7 ± 0.4	0.17 ± 0.02	0.21 ± 0.02	2.0
43.1 ± 0.6	0.14 ± 0.03	0.14 ± 0.03	2.0
48.2 ± 0.3	0.10 ± 0.03	0.18 ± 0.03	2.2
54.6 ± 0.4	0.09 ± 0.02	0.10 ± 0.02	3.0
60.0 ± 0.6	0.07 ± 0.03	0.05 ± 0.03	3.2

The energies of the maxima are given in the first column. The second and third columns show the integrated cross section between successive valley points for each maximum. The integrated cross section values are given as fractions of the integrated cross section to 26 MeV. The second column contains results for the 0.6×2.4 mode of operation. The third column contains results for the 2.4×3.6 mode of operation. The last column gives full-width at half maximum of the least structure resolution function at the energy of each peak.

* K. Min, L. N. Bolen and W. D. Whitehead, Phys. Rev. 132, (1963) 749.

J. E. E. Baglin and B. M. Spicer, Nuclear Physics 54, (1964) 549.

REF. H. Artus, P. Brix, H. G. Clerc, F. Eigenbrod, A. Goldmann,
F. Gudden, E. Spamer, P. Strehl, M. Stroetzel, O. Titze,
and K. J. Wetzel
Proc. Gatlinburg Conference, 314 (1966)

ELEM. SYM.	A	Z
Ca	40	20
REF. NO.		
66 Ar 2		hmg

METHOD

REACTION	RESULT	EXCITATION ENERGY	SOURCE		DETECTOR		ANGLE
			TYPE	RANGE	TYPE	RANGE	
E, E/	LFT	7	D		MAG-D		
		(6.89)					

TABLE I

Summary of Experimental Results^a

Nuclide	E _x (MeV)	Type	Γ _γ (eV)	Γ _γ /Γ _w	R _γ (F)
⁶ Li	2.18	E2	(3.9 ± 0.5) × 10 ⁻⁴	14.4	3.77 ± 0.48
	3.56	M1	8.9 ± 0.4	9.4	2.96 ± 0.11
⁷ Li	11.28 ± 0.05	(M1) or	(1.3 ± 0.4)/g ^b	0.043/g	—
		(M2)	(0.026 ± 0.008)/g	2.6/g	—
⁹ Be	15.97 ± 0.03	M1	(3.7 ± 0.8)/g	0.043/g	—
¹¹ B	4.46	E2 and	0.0173 ± 0.0021	8.2	3.44 ± 0.50
		M1	0.64 ± 0.08	0.34	2.60 ± 0.35
	5.04	M1	1.84 ± 0.14	0.69	2.60 ± 0.11
¹² C	4.43	E2	0.0122 ± 0.0008	5.30	3.14 ± 0.30
¹⁶ O	6.92	E2	0.100 ± 0.015	3.28	3.82 ± 0.46
	11.52	E2	0.52 ± 0.13	1.31	—
²⁴ Mg	9.85 ± 0.04	M1	7.95 ± 1.2	0.38	3.50 ± 0.49
	9.97 ± 0.03				
	10.35 ± 0.03	E2	0.24 ± 0.05	0.58	5.05 ± 0.50
	10.70 ± 0.03	M1	22.2 ± 2.4	0.86	3.60 ± 0.36
	10.93 ± 0.04	E2	0.26 ± 0.11	0.50	—
²⁸ Si	4.97 ± 0.02	C0	(2.0 ± 0.5) × 10 ⁻⁵ ^c	—	6.90 ± 1.20
⁴⁰ Ca	6.89 ± 0.05	E2	0.29 ± 0.04	2.85	4.60 ± 0.50

^a The Born approximation has been used except for ¹⁶O and ⁴⁰Ca.

^b g = (2I_f + 1)/(2I_i + 1).

^c Γ_γ = equivalent to ME = (8.87 ± 1.00) F².

REF.

E. B. Bazhanov, A. P. Komar, A. V. Kulikov and V. I. Ogurtsov
Sov. Phys. Doklady, 11, 332 (1966)

ELEM. SYM.

A

Z

Ca

40

20

METHOD

Synchrotron

REF. NO.

66 Ba 1

JDM

REACTION	RESULT	EXCITATION ENERGY	SOURCE		DETECTOR		ANGLE
			TYPE	RANGE	TYPE	RANGE	
G,XN	ABX	15 - 50	C	15 - 50	BF3-I		4PI

Accuracy of ABX is 10-12%.

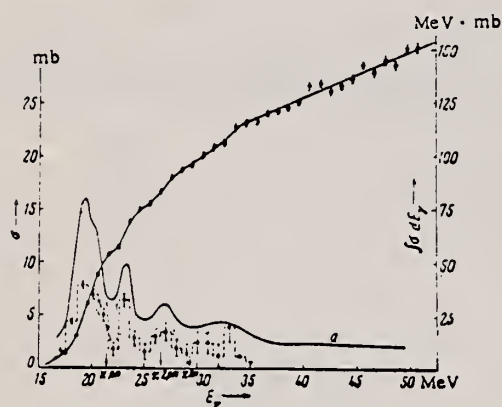


Fig. 1

TABLE 1. Integral Cross Section $\int \sigma dE_\gamma$
MeV · mb

Integration interval $E_1 - E_2$, MeV	Data from the literature	Our data
0-21	43 [5]	48.0 ± 0.8
0-28	75 [5]	91.0 ± 1.2
0-23	60 [6]	62.0 ± 1.0
0-22	53.5 [7]	55.0 ± 0.8
0-29.5	81 ± 4 [3]	95.0 ± 1.2
0-33	115 ± 17 [8]	109 ± 2.0
0-50.5		151 ± 2.2

Note. The errors shown for our data take into account only the statistical accuracy of the experiment.

REF. B. S. Dolbilkin, V. A. Zapevalov, V. I. Korin, L. E. Lazareva
and F. A. Nikolaev
Izv. Akad. Nauk fiz. 30, 349 (1966)
Bull. Acad. Sci. USSR-Phys. 30, 354 (1966)

ELEM. SYM.	A	Z
Ca	40	20
REF. NO.		EGF
66 Do 2		EGF

REACTION	RESULT	EXCITATION ENERGY	SOURCE		DETECTOR		ANGLE
			TYPE	RANGE	TYPE	RANGE	
G-MU-T	ABX	8-30	C	260	MGP-D	6-30	4PI

Resolution 120 keV 10 MeV
220 keV 20 MeV

214

Table 5

Resonances in the calcium cross section

E_{res} , MeV	σ_{max} , mb	Γ , MeV	$\int \sigma dE$, MeV·mb
12,5	60	1,5	130
19,1	80	2,5	310
21,1	100	2,0	320
24,7	50	1,0	60
26,1	70	0,5	60

Sum 930

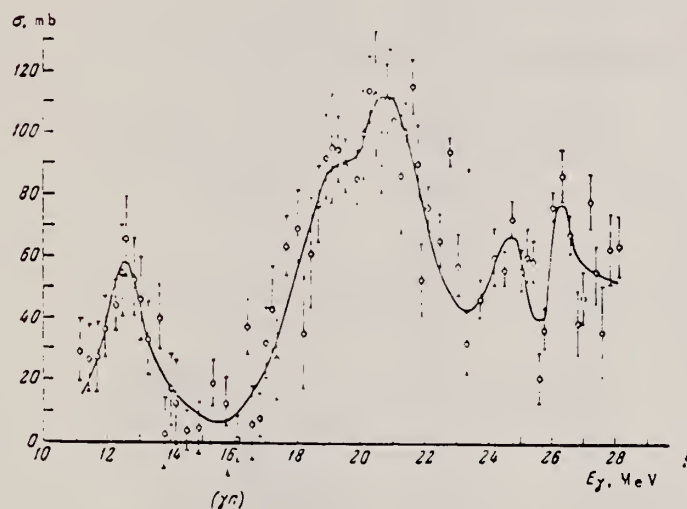


Fig.5. Nuclear absorption cross section of calcium.

ELEM. SYM.	A	Z
Ca	40	20
REF. NO.		
66 Fi 2		hmg

METHOD

/

REACTION	RESULT	EXCITATION ENERGY	SOURCE		DETECTOR		ANGLE
			TYPE	RANGE	TYPE	RANGE	
G,XN	SPC	THR-65	C	65	TOF-D	5-40	90

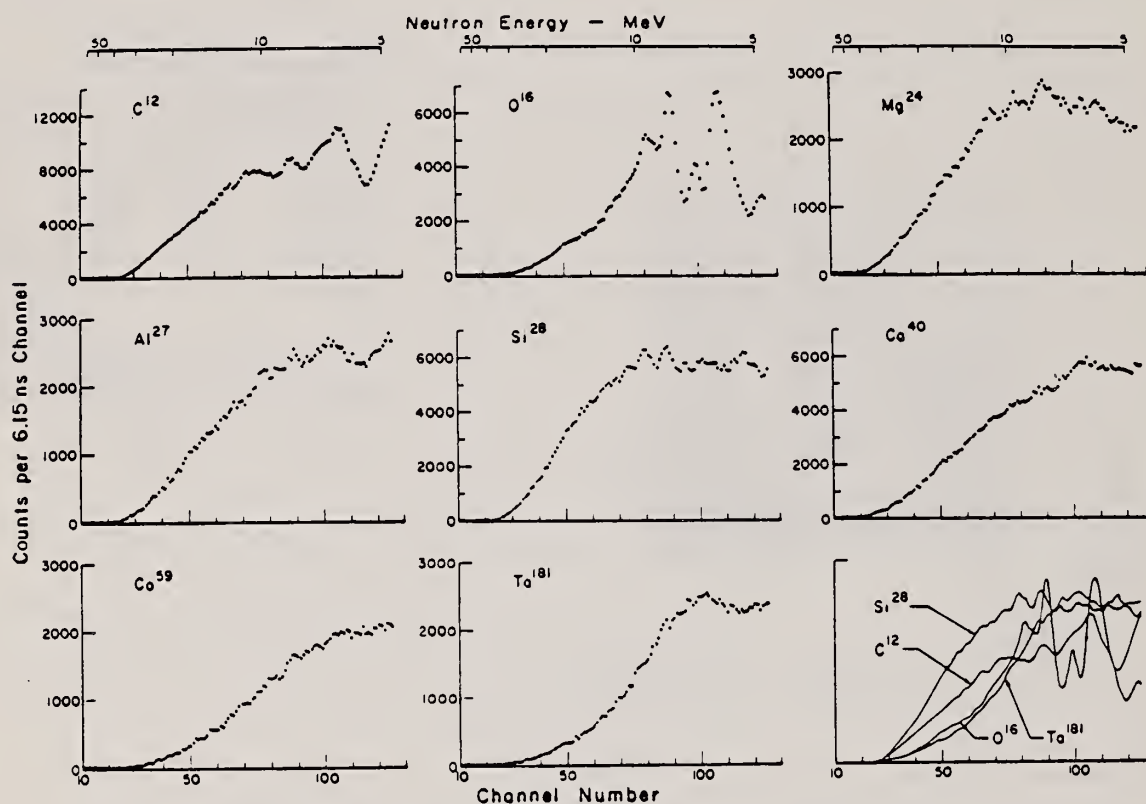


Fig. 1. Observed photoneutron time-of-flight spectra of C, O, Mg, Si, Ca, Co, V, and Ta.

REF.

H.P. Leenhouts and P.M. Endt
Physica 32, 322 (1966)

ELEM. SYM. A Z

Ca

40

20

METHOD

REF. NO.

66 Le 1

JDM

REACTION	RESULT	EXCITATION ENERGY	SOURCE		DETECTOR		ANGLE
			TYPE	RANGE	TYPE	RANGE	
P,G	SPC	9 - 11	D	1 - 3	NAI-D	2 - 12	55

TABLE 1

I, π (keV)	$E_x(^{40}\text{Ca})$ (MeV)	$(2J+1) \Gamma_p \Gamma_n / \Gamma$ (eV)	Ref.	$^{39}\text{K}(p, \gamma)^{40}\text{Ca}$ resonances Decay (in percents)* to lower			
				0	3.35	3.73	3.90
783.2 \pm 1.0	9.100	0.2				70	20
828.1 \pm 1.0	9.143	0.4				70	15
1060.3 \pm 1.0	9.370	0.3	8				
1075.0 \pm 1.0	9.384	0.1				x	x
1085.7 \pm 1.0	9.395	0.2				x	x
1097.6 \pm 1.0	9.407	0.2	8			65	15
1102.5 \pm 1.0	9.411	1.3	8			30	
1116.2 \pm 1.0	9.424	0.8	8			30	
1128.1 \pm 1.0	9.436	0.3				35	
1130.4 \pm 1.0	9.438	3.7	1,8	100			
1153.4 \pm 1.0	9.460	1.5	8			20	
1200.4 \pm 1.0	9.506	0.3				60	
1237.3 \pm 1.0	9.542	1.5				25	15
1237.9 \pm 1.0	9.543			70			30
1305.6 \pm 1.0	9.609	1.7				20	
1307.2 \pm 1.0	9.611	9	1	100			
1337.2 \pm 1.0	9.640	0.3				x	x
1344.4 \pm 1.0	9.646	9	1			40	50
1359.2 \pm 1.0	9.661	0.5		100			
1373.5 \pm 1.0	9.675	5				20	5
1486.6 \pm 1.0	9.786	4.3				20	20
1493.1 \pm 1.0	9.792	1.5		90	10		
1509.1 \pm 1.0	9.807	0.3				70	30
1516.2 \pm 1.0	9.814	0.3		100			
1519.5 \pm 1.0	9.817	0.2				x	
1537.6 \pm 1.0	9.836	0.9				35	45
1543.6 \pm 1.0	9.842	0.6				70	
1563.4 \pm 1.0	9.860	0.7				x	x
1574.6 \pm 1.0	9.872	10	1,7	79	12		5
1578.9 \pm 1.0	9.876	6	1,7	85	10		5
1632.0 \pm 1.0	9.927	0.6				x	
1666.1 \pm 1.0	9.960	5				10	9
1757.1 \pm 1.5	10.049	2.3					30
1766.2 \pm 1.5	10.058	3.4	1			55	20
1854.1 \pm 1.5	10.144	1.0	1			40	20
1930.6 \pm 1.5	10.219	1.1					
1953.8 \pm 1.5	10.241	1.8				100	
1984.6 \pm 1.5	10.273	2.0				15	40
2042.8 \pm 1.5	10.329	26	1	90	7		2
2140.6 \pm 1.5	10.423	7					
2256.9 \pm 2.0	10.538	2.2				90	10
2370.8 \pm 2.0	10.648	10				40	20
2385.4 \pm 2.0	10.661	2.0				25	75
2403.6 \pm 2.0	10.670	14				20	80
2406.0 \pm 2.0	10.672	1.2		100			
2424.9 \pm 2.0	10.700	2.2		x	x		x
2433.1 \pm 2.0	10.708	6				25	60
2473.0 \pm 2.0	10.747	1.9		x		x	
2482.1 \pm 2.0	10.756	10					100
2512 \pm 3	10.785	7		30		15	25
2649 \pm 3	10.919	3.5				x	
2661 \pm 3	10.930	10					x
2817 \pm 3	11.073	9				20	60
all \pm 0.005		all \pm 40%					

a) Crosses indicate the existence of transitions with unknown intensity.

REF.

J. Miller, C. Schuhl, G. Tamas, C. Tzara
J. de Physique 27, 8 (1966)

ELEM. SYM.	A	Z
Ca	40	20
REF. NO.		
66 Mi 2		egf

METHOD

REACTION	RESULT	EXCITATION ENERGY	SOURCE		DETECTOR		ANGLE
			TYPE	RANGE	TYPE	RANGE	
G,N	ABX	15-26	D	15-26	BF3-I		4PI

472

TABLEAU V

 σ_{int} à 26 MeV en MeV.mb

	^{16}O	^{40}Ca	^{12}C	Mg
γ, n	$41,5 \pm 4$	73 ± 7	$29,4 \pm 3$	58 ± 6

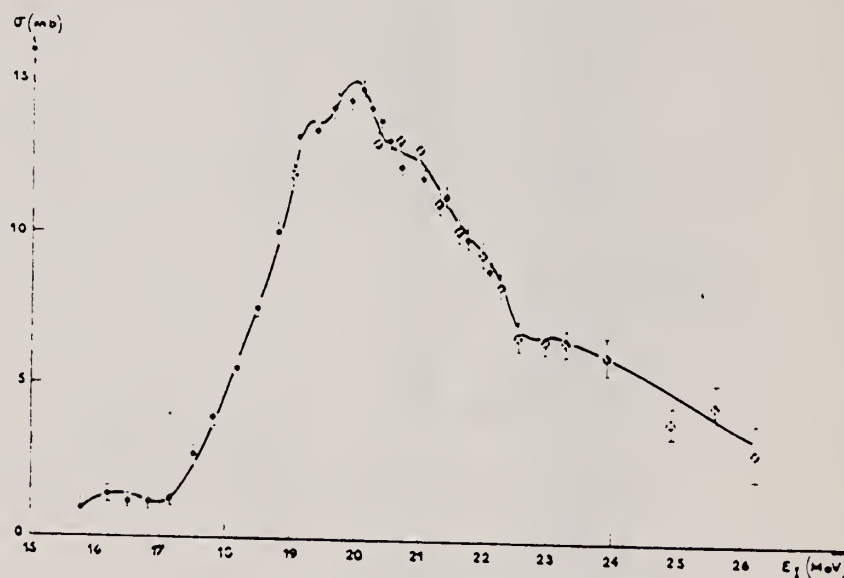


FIG. 2. — $\sigma(\gamma, n)$ dans ^{40}Ca . Points expérimentaux d'avril 1962 (petits cercles noirs) et mai 1963 (grands cercles avec croix blanches). La courbe tient compte de la largeur finie de la raie de photons (400 keV).

METHOD

REF. NO.

67 Dr 2

HMG

REACTION	RESULT	EXCITATION ENERGY	SOURCE		DETECTOR		ANGLE
			TYPE	RANGE	TYPE	RANGE	
G,P	SPC	THR-19	C	16,19	EMU-D		DST

Angular distributions of protons having energies close to the peaks are practically isotropic.

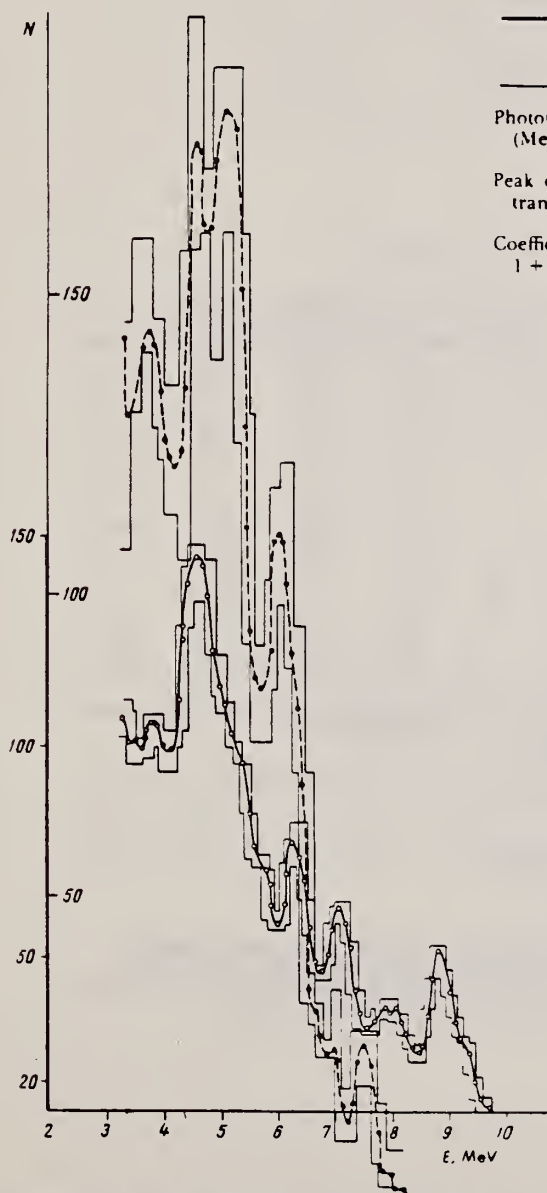


Fig. 1. Proton energy distributions at $E_{\gamma, \max} = 16$ MeV (solid curve) and 19 MeV (dashed curve).

$E_{\gamma, \max}$, MeV	16				19				19-16	
Photoproton peak energy E_p (MeV)-experimental	3.6	4.6	5.1	6.1	4.6	6.2	7.1	8.8	3.7	8.0
Peak energy E_p according to transition scheme (Fig. 3)	3.7	4.7	5.1	6.2	4.7	6.2	7.7	8.7	3.7	7.7
Coefficient α in the formula $1 + \alpha \sin^2 \theta$	0.6	0.3	-0.07	0.2	0.1	3	-0.12	0.3	—	—

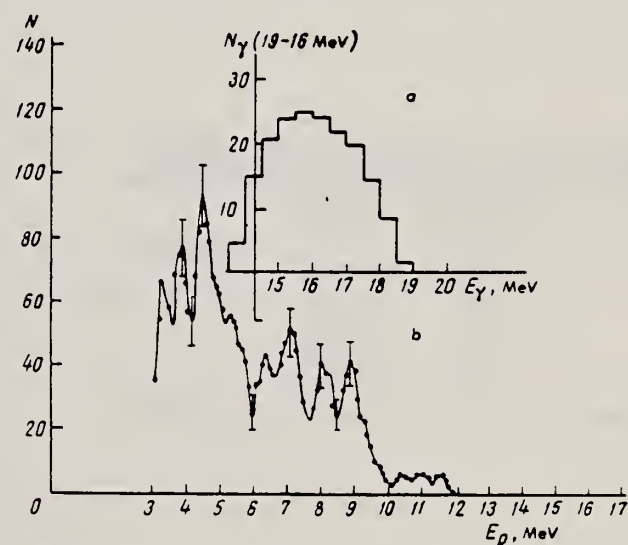


Fig. 2(a). Photon difference spectrum for $\Delta E_{\gamma, \max} = 19-16$ MeV; (b) proton energy distribution for $E_{\gamma, \max} (19-16)$ MeV.

REF.

L. Feldman, B. B. Baliga, and M. Nessim
Phys. Rev. 157, 921 (1967)

ELEM. SYM.	A	Z
Ca	40	20

METHOD

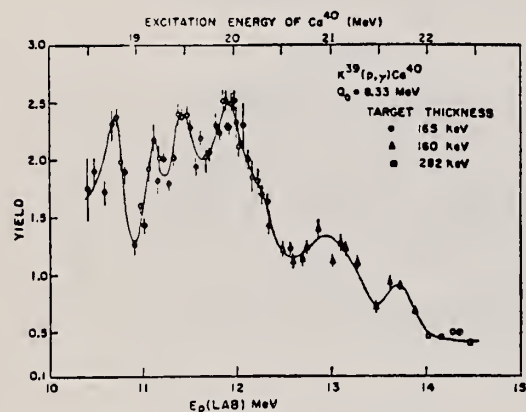
REF. NO.

67 Fe 1

HMG

REACTION	RESULT	EXCITATION ENERGY	SOURCE		DETECTOR		ANGLE
			TYPE	RANGE	TYPE	RANGE	
P,G	ABX	18-23	D	10-15	NAI-D		90

192+

FIG. 13. Yield curve for $K^{39}(p,\gamma)Ca^{40}$.TABLE VI. Absolute cross sections for $K^{39}(p,\gamma)Ca^{40}$, calculated at peaks of yield curve, assuming isotropic angular distributions.

Proton energy (MeV)	Cross sections (μb)
10.75	43.0 ± 9.1
11.18	31.2 ± 7.5
11.45	39.8 ± 9.6
11.94	39.2 ± 8.6
13.04	24.7 ± 7.3
13.75	21.1 ± 5.9

TABLE V. Comparison of Ca^{40} excitation energies (in MeV) at which fine-structure peaks have been observed.

Present experiment	Tanner <i>et al.</i> ^a	Hafele <i>et al.</i> ^b	Firk <i>et al.</i> ^c	Baglin <i>et al.</i> ^d	Mien <i>et al.</i> ^e
(p,γ)	(p,γ)	(p,γ)	(γ,π)	(γ,π)	(γ,π)
...	...	15.2
...	...	16.2	...	15.9	16.6
...	17.3
...	...	18.2	18.1	17.9	18.0
18.8	18.8	18.7	18.7	18.5	...
19.2	...	19.0	19.3	18.9	19.3
19.5	19.6	19.4	...	19.2	...
20.0	20.0	19.8	19.9	19.7	...
...	...	20.3	20.3
21.0	...	21.0	21.0	20.6	21.5
21.7	...	22	22

^a Reference 6.^d Reference 20.^b Reference 18.^e Reference 21.^c Reference 19.^a N. W. Tanner, G. C. Thomas, and E. D. Earle, Nucl. Phys. 52, 29 (1964).^b J. C. Hafele, F. W. Bingham, and J. S. Allen, Phys. Rev. 135, B365 (1964).^c F. W. K. Firk and E. R. Rae (private communication).^d J. E. E. Baglin and B. M. Spicer (private communication).^e K. Mien, L. N. Bolen, and W. D. Whitehead, Bull. Am. Phys. Soc. 8, 358 (1963), and (private communication).

METHOD

[Page 1 of 2]

REACTION	RESULT	EXCITATION ENERGY	SOURCE		DETECTOR		ANGLE
			TYPE	RANGE	TYPE	RANGE	
G,XN	ABY	100-150	C	150	BF3-I		4PI

TABLE 2
Values of the parameters for the best fit to the bremsstrahlung weighted cross sections

$$\int_{E_s}^{E_\gamma} \frac{\sigma(E)}{E} dE = (a_0 + a_1 E_\gamma) E_\gamma$$

	¹² C	¹⁶ O	⁴⁰ Ca
a ₀ (10 ²⁸)	7.03 ± 0.05	7.9 ± 0.5	24.6 ± 0.8
a ₁ (10 ²⁸)	-0.0173 ± 0.0004	-0.0072 ± 0.0036	-0.09 ± 0.006

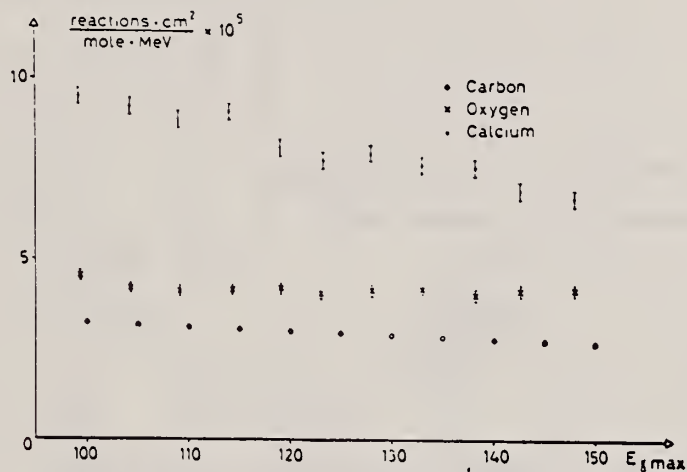


Fig. 3. Yields of the (γ, Tn) reaction for the three nuclei as a function of energy.

REACTION	RESULT	EXCITATION ENERGY	SOURCE		DETECTOR		ANGLE
			TYPE	RANGE	TYPE	RANGE	
G,XN	ABX	100-150	C	150	BF3-I		4PI

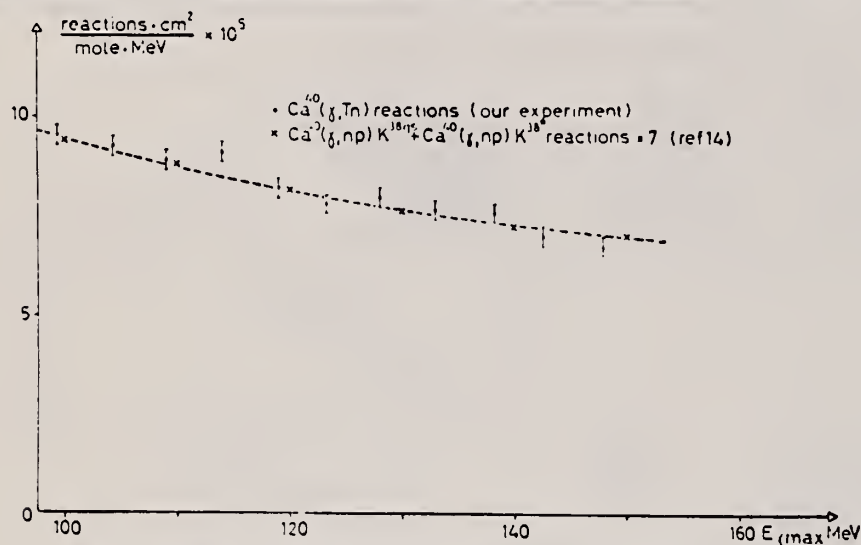


Fig. 5. Comparison between the (γ, Tn) and the (γ, np) yields for calcium (see text).

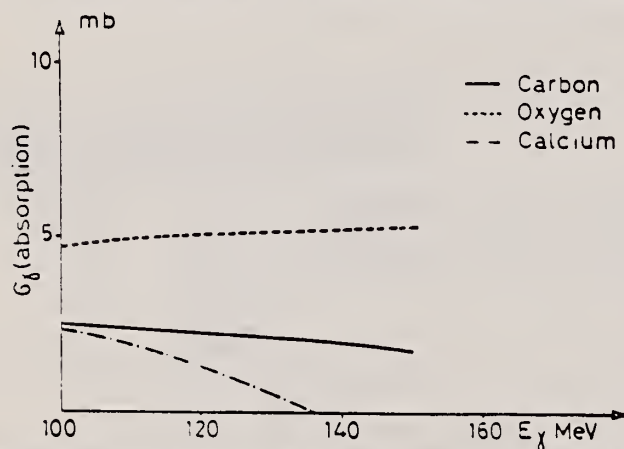


Fig. 6. The absorption cross sections for the three nuclei after all corrections have been applied.

ELEM. SYM.	A	Z
Ca	40	20
REF. NO.		
67 Ge 2		
METHOD		
HMG		

REACTION	RESULT	EXCITATION ENERGY	SOURCE		DETECTOR		ANGLE
			TYPE	RANGE	TYPE	RANGE	
G,XN	ABY	THR-27	C	27	BE ₃ -I		4PI

Table 7. Comparison of neutron yields. Yields are given in units of (neutron cm²/MeV nucleus) × 10⁻²⁸. The estimated uncertainties in Y and Y_c are of the order of 6% and 10%, respectively.

Element	E ₀	Y(E ₀)	UCRL Saclay Va. NBS(Old)				UCRL Saclay Va. NBS(Old)				Ref.
			Y _c				Exp	Exp	Exp	Exp	
							Y _c /Y				
Pb	27	103	86	116			0.83	1.05			26,30
	22	111	92				0.83				
Au	27	89	97	88		115	1.09	0.96		1.25	24,30,38
	22	92	98				1.07				
Ta	27	81	82	77		113	1.01	0.95		1.33	27,30,38
	22	85	79	80			0.93	0.94			
Ho	27	67	75	82		103	1.12	1.19		1.49	27,31,39
	22	69	77				1.12				
Ag	27	36									
	22	34.8									
Cu	27	14.4	13.2	12.4			0.92	0.98			28,30
	22	12.6	11.5				0.91				
Co	27	12.7	12.1		13.5		0.95		1.27		29,34
	22	10.6	9.9				0.94				
Ca	27	1.69		1.13	1.01			0.67	0.60		32,35
P	27	2.35			1.76				0.75		36
Al	27	1.92	1.62		1.38		0.84		0.72		25,37
O ¹⁶	27	0.54	0.42	0.48	0.42		0.78	0.89			16,32,37
C	27	0.50	0.35	0.33	0.46		0.70	0.66			25,32,33

(OVER)

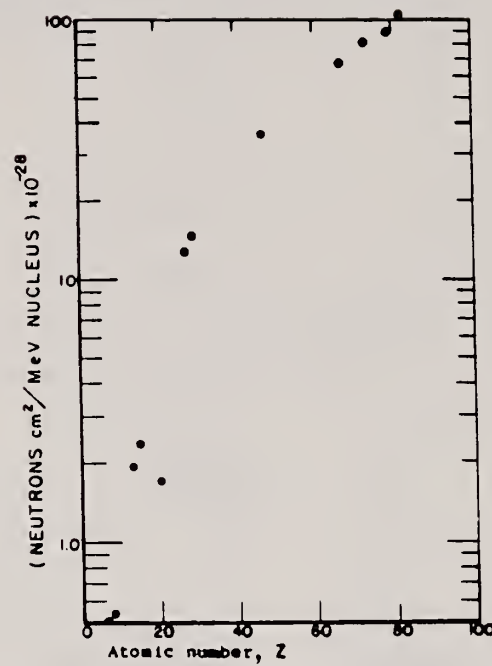


Fig. 31. Absolute neutron yield as a function of atomic number. The neutron yield from calcium ($Z = 20$) is particularly low in comparison with the other elements because its (γ, n) threshold is high compared to the mean energy of the giant resonance.

REF. B. I. Goryachev, B. S. Ishkhanov, B. G. Shevchenko, and B. A. Yur'ev
J. Nucl. Phys. (USSR) 5, 1138 (1967)
Sov. J. Nucl. Phys. 5, 811 (1967)

ELEM. SYM.	A	Z
Ca	40	20
REF. NO.		
67 Go 3		HMG

METHOD

REACTION	RESULT	EXCITATION ENERGY	SOURCE		DETECTOR		ANGLE
			TYPE	RANGE	TYPE	RANGE	
G, XN	ABX	15-30	C	15-30	BF3-I		4PI

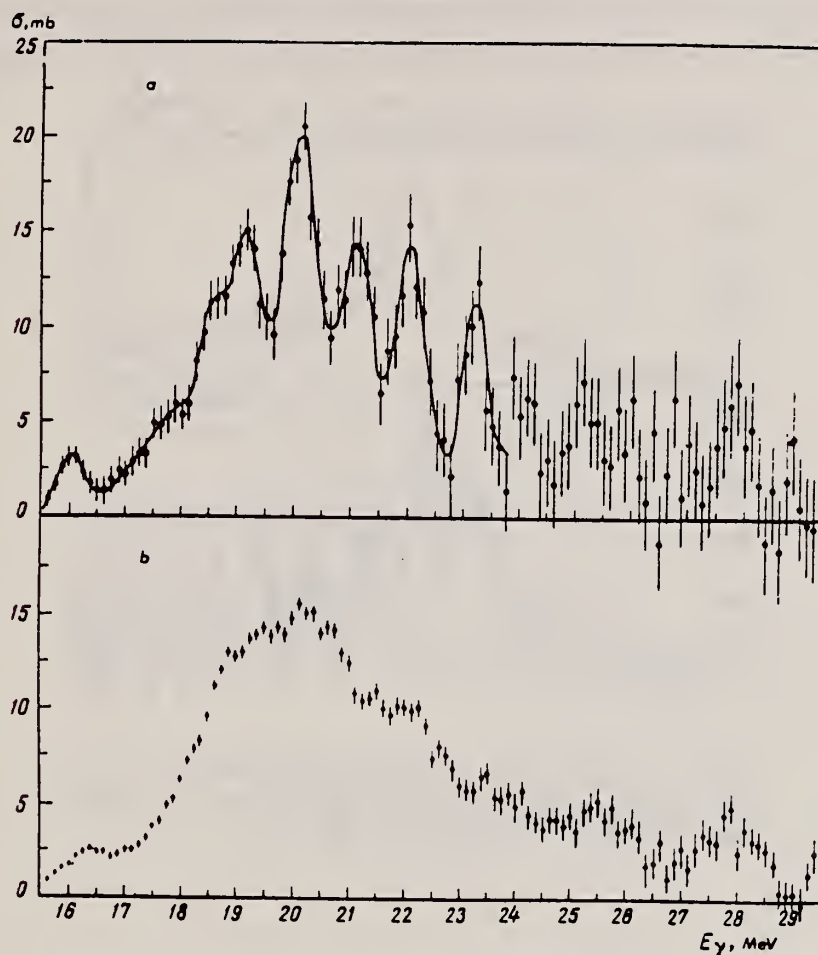


Fig. 1. Cross section of the $\text{Ca}^{40}(\gamma, n)$ reaction. The calculation was made by the Penfold-Leiss method with spacing E of 500 keV (a) and 1 MeV (b).

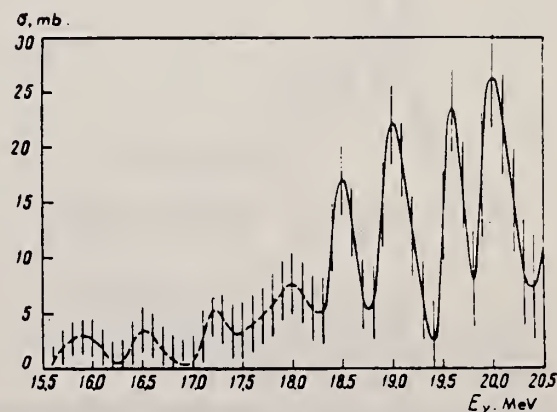


Fig. 2. Calculation of the cross section of the $\text{Ca}^{40}(\gamma, n)$ reaction by the Penfold-Leiss method with spacing $\Delta E = 200$ keV.

REF. B. N. Goryachev, B. S. Ishkhanov, I. M. Kapitonov, I. M. Piskarev, V. G. Shevchenko and O. P. Shevchenko JETP Pis'ma 5, 225 (1967) JETP Letters 5, 180 (1967)			ELEM. SYM.	A	Z
			Ca	40	20
METHOD			REF. NO.		
			67 Go 4		hmg
REACTION	RESULT	EXCITATION ENERGY	SOURCE		ANGLE
			TYPE	RANGE	
G,P	ABX	THR-30	C	12-30	SCD-D
					UNK

$$\sigma_{\text{int}}(30) = 510 \pm 70 \text{ MeV-mb}$$

256

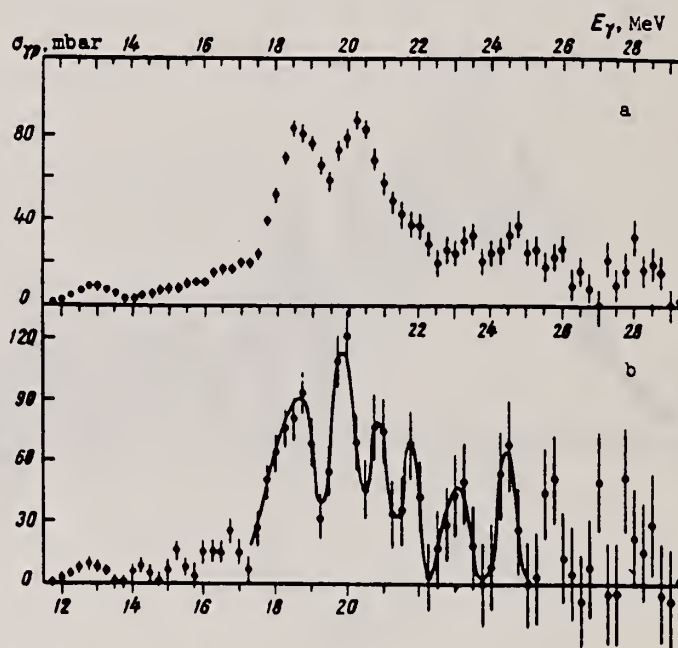


Fig. 1. Cross section of the reaction $\text{Ca}^{40}(\gamma, p)$ ($E_p \geq 2$ MeV) calculated by the Penfold-Leiss method with steps $\Delta E_\gamma = 1.0$ MeV (a) and $\Delta E_\gamma = 0.5$ MeV (b).

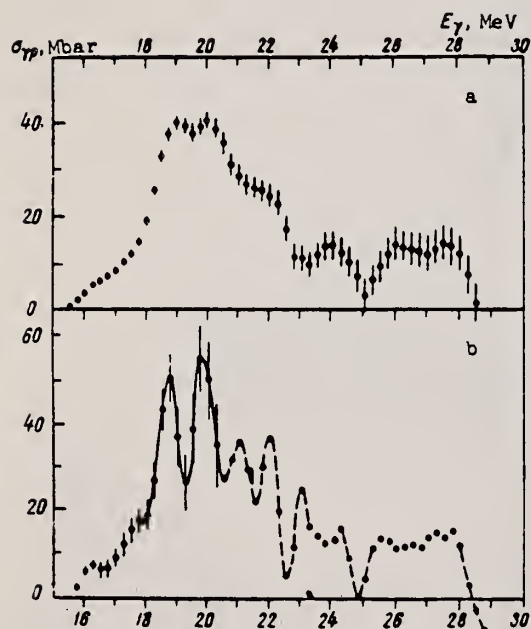


Fig. 2. Cross section of the reaction $\text{Ca}^{40}(\gamma, p)$ ($E_p \geq 7$ MeV) calculated by the Penfold-Leiss method with steps $\Delta E_\gamma = 1.0$ MeV (a) and $\Delta E_\gamma = 0.5$ MeV (b).

REF.

J. M. Loiseaux, J. M. Maison, and M. Langevin
J. de Physique 28, 11 (1967)

ELEM. SYM. A

Z

Ca

40

20

METHOD

REF. NO.

67 Lo 1

JOC

REACTION	RESULT	EXCITATION ENERGY	SOURCE		DETECTOR		ANGLE
			TYPE	RANGE	TYPE	RANGE	
G,G/	ABX	14-30	C	34	NAI-D		DST

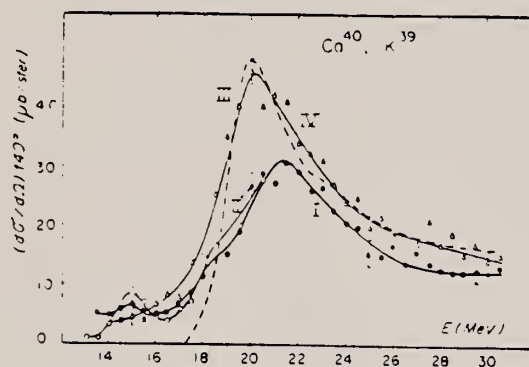


FIG. 9.

Sections efficaces différentielles de diffusion pour ^{40}Ca déterminée à $E_m = 22$ MeV (courbe II), et $E_m = 32$ MeV (courbe I).

Section efficace différentielle de diffusion pour ^{40}Ca déterminée à $E_m = 32$ MeV (courbe III), et prévue par la relation de dispersion (courbe IV).

REF. M. Mishina, E. Tanaka, K. Kageyama, N. Mutsuro, A. Asami,
Y. Kawarasaki and Y. Nakajima
J. Phys. Soc. Japan 23, 919 (1967)

ELEM. SYM.	A	Z
Ca	40	20
REF. NO.		
67 Mi 2		egf

METHOD			SOURCE		DETECTOR		ANGLE
REACTION	RESULT	EXCITATION ENERGY	TYPE	RANGE	TYPE	RANGE	
G, XN	SPC	THR-20	C	23-27	TOF-D	2-12	100

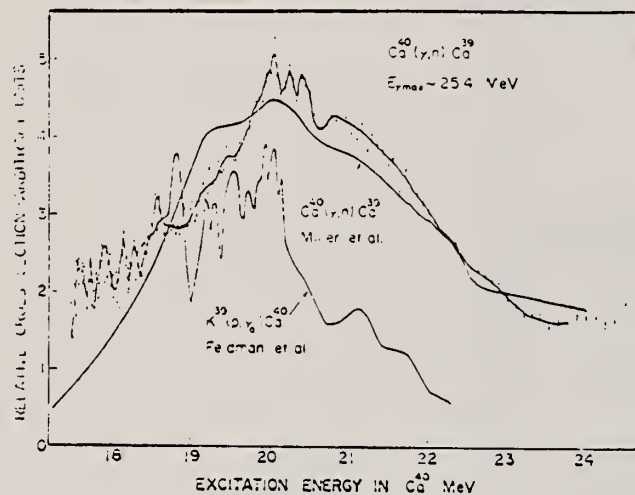


Fig. 9. Relative cross section for $\text{Ca}^{40}(\gamma, n)\text{Ca}^{39}$, deduced from the time spectrum in Fig. 7 assuming the ground state transition only. The results of $\text{Ca}^{40}(\gamma, n)$ cross section by Miller *et al.*³²⁾ and $\text{Ca}^{40}(p, \gamma)$ reaction cross section by Feldman *et al.*³¹⁾ are illustrated simultaneously, in relative units.

REF.

I. L. Smith, J. Garvey, J. G. Rutherglen, and G. R. Brookes
Nucl. Phys. B1, 483 (1967)

ELEM. SYM.

A

Z

Ca

40

20

METHOD

REF. NO.

67 Sm 1

JOC

REACTION	RESULT	EXCITATION ENERGY	SOURCE		DETECTOR		ANGLE
			TYPE	RANGE	TYPE	RANGE	
G, NP	ABX	150-250	C	250	TOF-D		DST

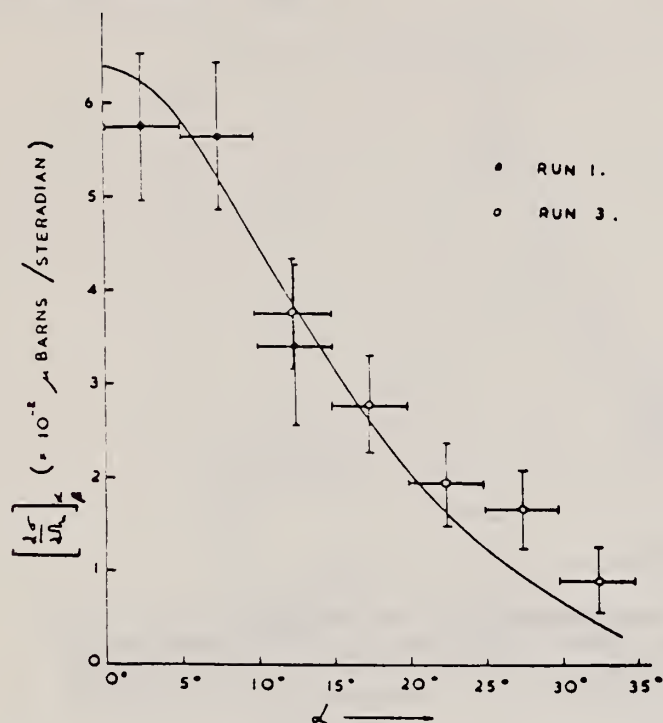


Fig. 6. Vertical angular distribution of coincident protons from calcium (the curve is explained in the text).

ELEM. SYM.	A	Z
Ca	40	20
REF. NO.	68 Ba 1	
	egf	

REACTION	RESULT	EXCITATION ENERGY	SOURCE		DETECTOR		ANGLE
			TYPE	RANGE	TYPE	RANGE	
P,G	RLX	11-14	D	3-6	NAI-D	8-14	0

Table 1

$^{39}\text{K}(p,\gamma)^{40}\text{Ca}$ resonances.

E_p (MeV)	E_x (MeV) ^{a)}	$\frac{(2J+1)}{\Gamma_p \Gamma_{\gamma_0} / \Gamma^b}$ (eV)	Decay modes	Comments
3.863	12.099	5.1	γ_0	
3.875	12.111	3.5	γ_0	
3.970	12.204	2.5	γ_0	
4.104	12.334	3.4	γ_0	
4.195	12.423	2.3	γ_0	
4.380	12.604	5.9	γ_0	
4.425	12.647		γ_1	
4.446	12.658	14.5	γ_0, γ_1	
4.467	12.688	4.4	γ_0	
4.658	12.875	6.1	γ_0, γ_1	
4.766	12.980	4.2	γ_0	
4.783	12.996		γ_1	
4.875	13.086	2.1	γ_0	
4.903	13.113	18.4	γ_0, γ_1	
4.986	13.194	13.9	γ_0, γ_1	$J^\pi = 2^+$
4.995	13.203	6.1	γ_0	
5.083	13.289	8.1	γ_0, γ_1	
5.630	13.822	2.9	γ_0	
5.723	13.913	56.0	γ_0, γ_1	$\Gamma = 20$ keV
5.805	13.993	112.0	γ_0, γ_1	$\Gamma = 20$ keV

196+ 3=2.88; 6=6.03 MEV

all ± 10
keV

all $\pm 30\%$

- a) Calculated using $Q = 8.333$ MeV [17].
b) Calculated taking the strength of the 2.05 MeV resonance to be 26 eV [11].

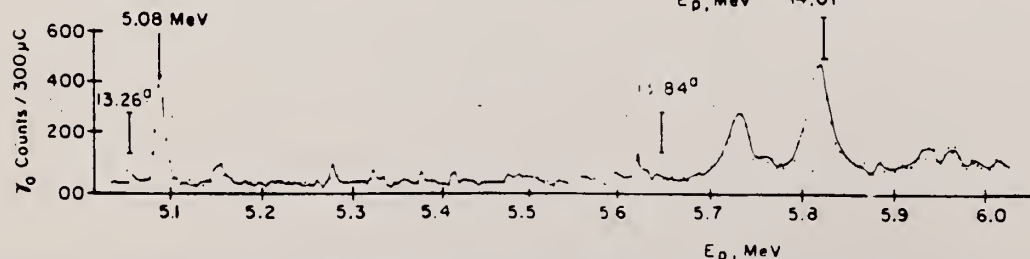
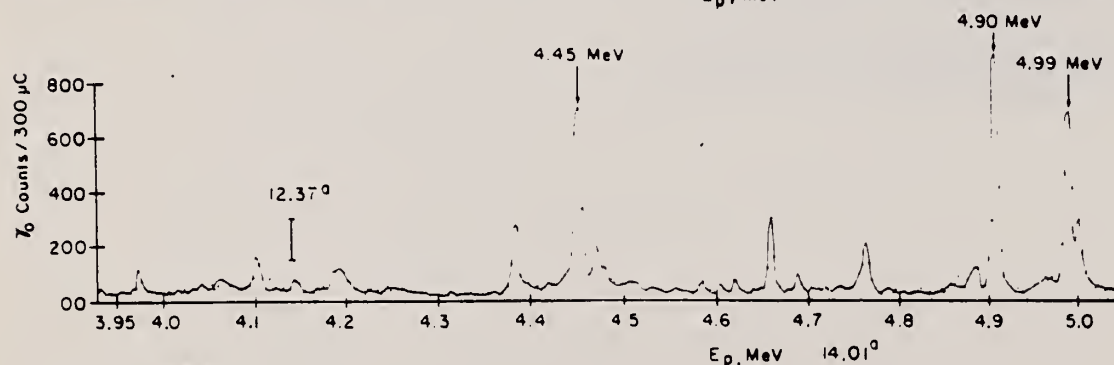
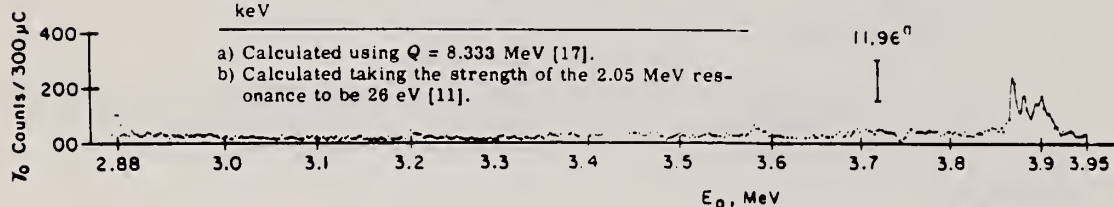


Fig. 1. The excitation function of the ground state gamma ray transition in the $^{39}\text{K}(p,\gamma_0)^{40}\text{Ca}$ reaction from $E_p = 2.88$ to 6.01 MeV. The predicted positions of 1^- states of a recent particle-hole calculation [1] are shown by vertical bars with excitation energies superscripted by an a shown above the bar. The $E_p = 4.99$ MeV resonance was shown to be 2^+

REF. N. Bezic, D. Jamnik, G. Kernel, J. Krajnik and J. Snajder
Nucl. Phys. A117, 124 (1968)

ELEM. SYM.	A	Z
Ca	40	20
REF. NO.		
68 Be 4		egf

METHOD			SOURCE		DETECTOR		ANGLE
REACTION	RESULT	EXCITATION ENERGY	TYPE	RANGE	TYPE	RANGE	
G, MUT	ABX	10-30	C	35	MGC-D	10-30	4PI

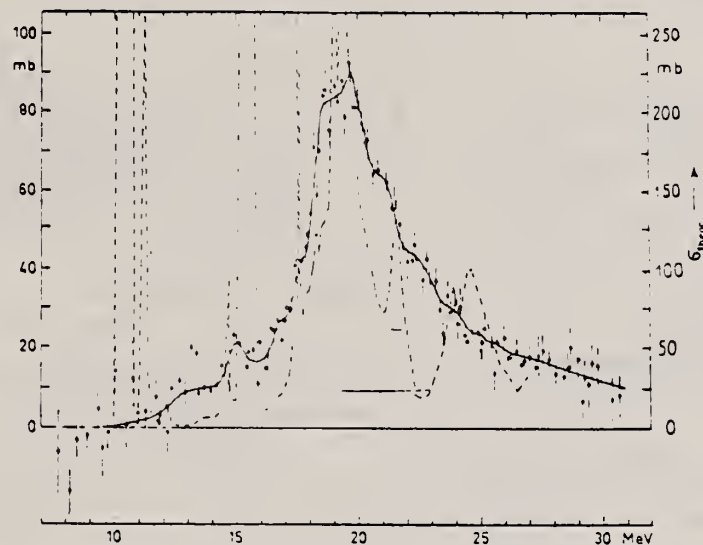


Fig. 3. Nuclear absorption cross section for calcium. The zero line is determined in an absolute way, but a more reasonable zero line may lie 3 mb lower. This value is taken also as an error in the determination of the zero line. For the moments we used the diagram without lowering the zero line. The dashed curve represents a theoretical cross section ¹⁶). Its value is given by the right-hand scale.

¹⁶P. P. Delsanto, H. G. Wahsweiler and W. Greiner,
Phys. Rev. Lett. 19, 700 (1967).

REF. B. I. Goryachev, B. S. Ishkhanov, I. M. Kapitonov, I. M. Piskarev, O. P. Shevchenko, and V. G. Shevchenko Yad. Fiz. 7, 944 (1968) Sov. J. Nucl. Phys. 7, 567 (1968)			ELEM. SYM.	A	Z
			Ca	40	20
METHOD			REF. NO.		
			68 Go 1		hmg
REACTION	RESULT	EXCITATION ENERGY	SOURCE		ANGLE
			TYPE	RANGE	
G, P	ABX	THR-30	C	12-30	10

137

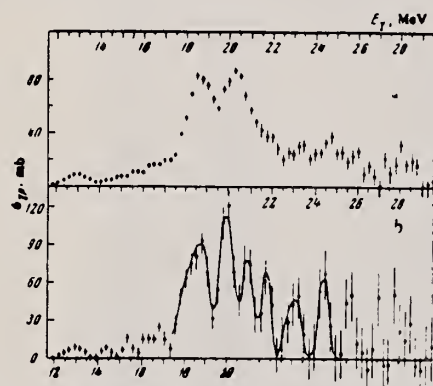


FIG. 1. Cross section for $\text{Ca}^{40}(\gamma, p)$ with $E_p > 2$ MeV photoprotons, calculated from the yield curve by the Penfold-Leiss method, at energy intervals ΔE of (a) 1 MeV and (b) 0.5 MeV.

No smoothing of the yield curve.

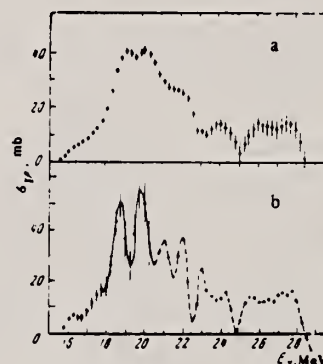


FIG. 2. Cross sections for $\text{Ca}^{40}(\gamma, p)$ for $E_p > 6.5$ MeV protons, calculated from the yield curve by the Penfold-Leiss method, at energy intervals ΔE of (a) 1 MeV and (b) 0.5 MeV.

Yield curve smoothed on the basis of the three closest points.

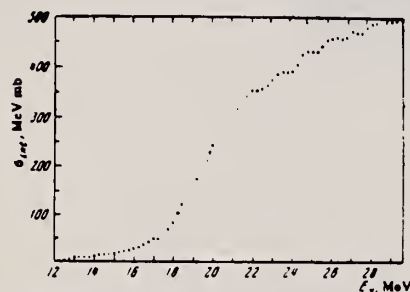


FIG. 3. Energy dependence of the integral cross section for $\text{Ca}^{40}(\gamma, p)$ with $E_p > 2$ MeV photoprotons.

$$\sigma_{\text{int}}(29.5) = 500 \pm 70 \text{ MeV-mb.}$$

Table I. Structural properties of the cross section for $\text{Ca}^{40}(\gamma, p)$ and cross sections for total γ absorption by Ca^{40}

$E_p > 2$ MeV		$E_p > 6.5$ MeV		E^*, MeV	
E^*, MeV	$\sigma_{\text{int}}, \text{MeV-mb}$	E^*, MeV	$\sigma_{\text{int}}, \text{MeV-mb}$	Feldman's Data (private communication)	Data from [10]
12.7 ± 0.2 18.7 ± 0.2	10.7 107	18.7 ± 0.2	58	18.82 19.20, 19.30 19.47, 19.68	18.7
19.9 ± 0.2	104	19.9 ± 0.2	51	19.95, 20.03 20.13	19.5 20.0
20.9 ± 0.2 21.8 ± 0.2 23.2 ± 0.3 24.3 ± 0.2 25.5 ± 0.5 28.0 ± 0.5	51 36 43 41 53 53	(20.9) (21.8) (23.2)	29 24 15	20.5, 21.2, 21.8	21.1
		25-28.5	42		

METHOD					REF. NO.		HMG
					68 Go 6		
REACTION	RESULT	EXCITATION ENERGY	SOURCE		DETECTOR		ANGLE
			TYPE	RANGE	TYPE	RANGE	
G,XN	ABX	15-30	C	15-30	BF3-I		4PI

46.2

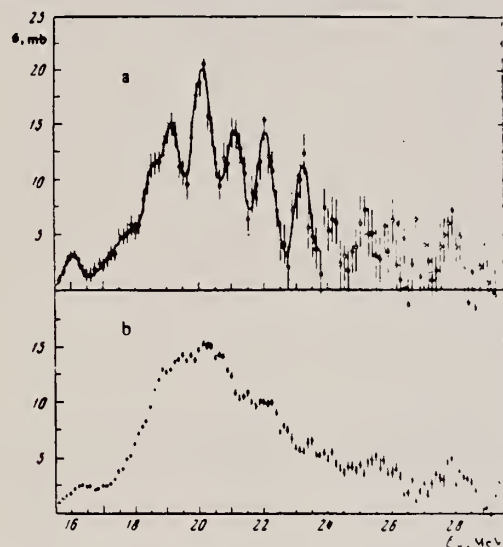


FIG. 4. Cross section for the reaction $\text{Ca}^{40}(\gamma, n)$. The computational step $\Delta E = 0.5$ MeV (a) and 1 MeV (b).

Table III. Parameters of resonances observed in the cross section for $\text{Ca}^{40}(\gamma, n)$

E^*, MeV	$\sigma_{\text{int}}, \text{MeV} \cdot \text{mb}$	E^*, MeV					
Our data		data of [11]	data of [12]	data of [13]	data of [14]	data of [15]	data of [16]
16.1 ± 0.2	1.9			15.9			
17.2 ± 0.1	2.4	16.6	16.8				
17.9 ± 0.1	4.1	18.0		17.8	18.15		
18.5 ± 0.1	5.4			18.5	(18.18; 18.63; 18.78)		
				18.9			
19.1 ± 0.1	7.8	19.0	19.0	19.2	(19.1; 19.2)		19.3
19.6 ± 0.1	6.0			19.6	(19.45; 19.70)		
20.0 ± 0.1	9.7	20.25	20.0	19.9	(19.98; 20.06; 20.02; 20.35)		20-21
21.0 ± 0.1	11			20.8	(20.50; 20.75; 21.00; 21.23; 21.5)		
		(21.5)	(21.5)	(21.7)			
22.0 ± 0.2	10			22.3	22.0		22.5-24.0
23.2 ± 0.2	7						
(24.1)	3.8	24.5		24.1			
25.5 ± 0.3	11.2			(25.4)			
27.9 ± 0.3	7.5						26-28 28.3

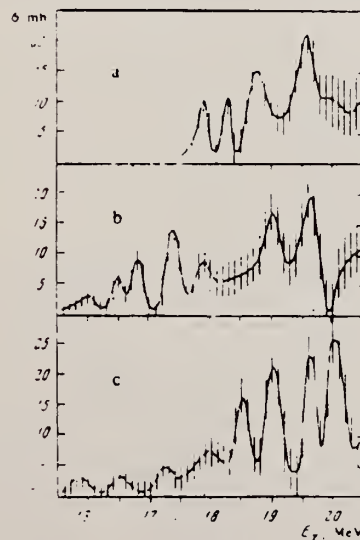


FIG. 5. Cross sections for the reactions: a - $\text{Si}^{28}(\gamma, n)$, b - $\text{S}^{32}(\gamma, n)$, c - $\text{Ca}^{40}(\gamma, n)$. Computational step $\Delta E = 0.2$ MeV

REF. F. R. Metzger
Phys. Rev. 165, 1245 (1968)

ELEM. SYM.	A	Z
Ca	40	20
REF. NO.		
68 Me 2		HMG

METHOD /

REACTION	RESULT	EXCITATION ENERGY	SOURCE		DETECTOR		ANGLE
			TYPE	RANGE	TYPE	RANGE	
G,G	LFT	7.0	D	7.0	SCD-D		DST
		(6.91)					
		(6.95)					

Level	Spin-Parity	To Ground State Trans. Width
6.91 MeV	2+	0.18±0.03 eV
6.95 MeV	1-	0.47±0.06 eV

J-PI

REF. K. Shoda, K. Abe, T. Ishizuka, N. Kawamura, M. Oyamada,
and Baik-Nung Sung
J. Phys. Soc. Japan 25, 664 (1968)

ELEM. SYM.	A	Z
Ca	40	20

METHOD

REF. NO.

68 Sh 3

egf

REACTION	RESULT	EXCITATION ENERGY	SOURCE		DETECTOR		ANGLE
			TYPE	RANGE	TYPE	RANGE	
G ₁ XP	SPC	THR-20	D	20	EMU-D	2-14	DST

Table III. Anisotropic factor B/A of angular distributions estimated for the groups of strong transitions.

	Assumed residual Energy (MeV)	E_{γ} (MeV)	B/A	Used data ^{a)}
²³ Na	1.27	18.8-20.5	0.5 ± 0.4	20.5
	3.3	20.8-22.1	$\infty^{b)}$	<i>D</i>
		22.1-24	$\infty^{b)}$	24.0
	7.0	20.7-22.7	1.5 ± 0.3	<i>D</i>
³¹ P	0	15.7-21	$\infty^{b)}$	24.0, 19.0
	7.0	17.4-20.2	0.5 ± 0.6	<i>D</i>
		20.2-22.7	1.3 ± 1.3	<i>D</i>
³² S	0	14-20	$\infty^{b)}$	(p, γ_0)
		14-14.8	2.4 ± 0.7	17.0
		14.8-16.2	$\infty^{b)}$	17.0
		16.2-17.1	$\infty^{b)}$	17.0
	5.0	19.2-20.1	0.5 ± 0.2	<i>D</i>
		20.1-21.3	0.4 ± 0.2	<i>D</i>
⁴⁰ Ca	0	17.1-20.5	1.5 ± 0.2	20.5
	2.8	17.4-19.9	2.6 ± 0.3	20.5
	6.0	17.2-18.7	0.05 ± 0.09	20.5
		18.7-20.5	0.6 ± 0.1	20.5

- a) The numerical number indicates the maximum energy of the bremsstrahlung irradiated for the data. *D* shows the difference between the two distributions. (p, γ_0) shows the inverse reaction data.
b) The notation ∞ indicates that the distribution is almost $\sin^2 \theta$, i.e., the result has stronger maximum than $1 + 10 \sin^2 \theta$.

Table II. Anisotropic factor B/A of angular distributions determined by least-squares fits with $A + B \sin^2 \theta$.

⁴⁰ Ca	
$(E_{\gamma \text{ max}} = 20.5 \text{ MeV})$	
$E_{\gamma} \text{ (MeV)}$	B/A
2.8-4.2	0.05 ± 0.09
4.2-6.1	0.6 ± 0.1
6.1-8.5	2.6 ± 0.3
8.5- ∞	1.5 ± 0.2
2.8- ∞	0.8 ± 0.1

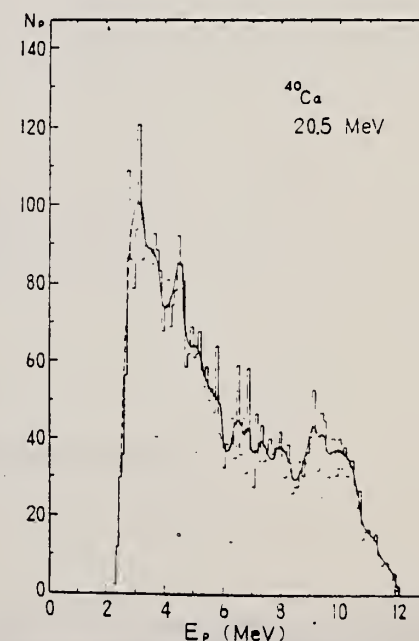


Fig. 4. Energy distributions of photoprotons from ⁴⁰Ca irradiated with 20.5 MeV bremsstrahlung.

REF. P. D. Zimmerman, M. R. Yearian and T. W. Donnelly
Phys. Rev. Letters 21, 1392 (1968)

ELEM. SYM.	A	Z
Ca	40	20
REF. NO.		
68 Zi 2		hmg

METHOD			SOURCE		DETECTOR		ANGLE
REACTION	RESULT	EXCITATION ENERGY	TYPE	RANGE	TYPE	RANGE	
E, E/	ABX	2-25	D	283	MAG-D	257-283	88
				(282.8)			

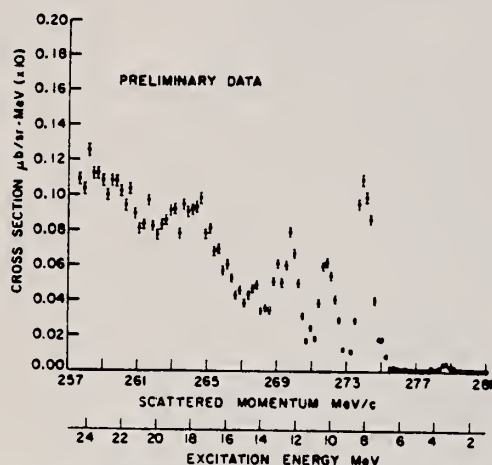


FIG. 1. The spectrum of inelastically scattered electrons from Ca^{40} with an incident energy $E_0 = 282.8$ MeV at an angle $\theta = 88.1^\circ$, after radiative corrections were made.

METHOD

REF. NO.

[Page 1 of 2]

69 Ei 1

hmg

REACTION	RESULT	EXCITATION ENERGY	SOURCE		DETECTOR		ANGLE
			TYPE	RANGE	TYPE	RANGE	
$E, E/$	FMF	3-5	D	42,61	MAG-D	38-57	DST
							(70-150)

B(EL); 3.7-4.5

TABLE V. Experimental form factors for the states of interest in Ca^{40} and Ca^{48} . E_i is the incident electron energy, θ is the scattering angle, q_i is the inelastic momentum transfer, C the ratio of inelastic to elastic peak heights, and $|F_{in}|^2$ the experimental form factor defined by Eq. (10); the sixth column is the percentage error in the experimental form-factor points.

E_i (MeV)	θ (deg)	q_i (F^{-1})	$10^4 C$	$10^2 F_{in}^2$	% error	$10^2 F^{*2}$
Ca^{40}						
3.73 MeV (3-)						
60.36	90.0	0.419	4.62	0.222	6.0	
60.34	110.	0.485	12.91	0.450	2.0	
60.04	130.	0.534	25.30	0.666	2.0	
60.30	150.	0.572	41.90	0.865	6.0	
3.90 MeV (2+)						
60.50	70.0	0.341	2.24	0.145	6.0	
60.36	90.0	0.419	5.73	0.275	4.0	
60.33	110.	0.485	12.83	0.447	4.0	
60.03	130.	0.533	19.75	0.520	4.0	
60.03	150.	0.571	28.50	0.588	6.0	
6.94 MeV (2+, 3-)						
60.51	70.0	0.331	1.90	0.123	4.0	
60.36	90.0	0.407	5.71	0.275	2.0	
60.33	110.	0.471	13.00	0.454	2.0	
60.04	130.	0.519	22.65	0.596	2.0	
60.24	150.	0.555	36.02	0.745	2.0	
Ca^{48}						
3.83 MeV (2+)						
60.21	70.0	0.339	1.87	0.122	5.0	
60.17	90.0	0.418	6.45	0.311	5.0	
60.15	110.	0.484	11.35	0.399	5.0	
60.13	130.	0.535	19.15	0.502	5.0	
60.18	150.	0.570	26.21	0.546	8.0	
41.07	110.	0.325	2.37	0.165	7.0	0.157
41.05	130.	0.359	2.80	0.173	8.0	0.165
41.07	150.	0.383	3.88	0.219	7.0	0.209
4.51 MeV (3-)						
60.21	70.0	0.337	0.35	0.0228	17.0	
60.15	90.0	0.415	1.77	0.0854	8.0	
60.15	110.	0.481	5.51	0.194	8.0	
60.14	130.	0.531	12.11	0.317	4.0	
60.18	150.	0.567	21.94	0.456	8.0	

* F^2 denotes the values of $|F_{in}|^2$ at 41 MeV renormalized to 60.2 MeV.

[over]

TABLE VI. Best-fit values of $B(EL \uparrow)$ and R_w^2 for the states studied in this work. G is the $B(EL \uparrow)$ value expressed in single-particle Weisskopf units. Γ_γ^0 is the partial width for γ decay to the ground state. The column labeled σ_0 is the statistical error in $B(EL \uparrow)$. An additional 12% uncertainty must be included in the final error to account for the dependence of $B(EL \uparrow)$ and R_w^2 on the parameters of the transition charge density. N is the number of degrees of freedom in the fit. The transition charge parameters c_{1r} and l_{1r} are given as ratios to the ground-state parameters, which are different for Ca^{40} and Ca^{48} . See the text.

Nucleus	State energy (MeV)	$B(EL)$ ($e^2 \text{F}^2 L$)	G (spu)	Γ_γ^0 (eV)	σ_0	χ^2/N	Confidence level (σ_0)	c_{1r}/c_0	l_{1r}/l_0	R_w^2 (F^2)
2+ States										
Ca^{40}	3.90	84	2.0	1.23×10^{-4}	2	3.5/3	35	0.880	0.880	19.2
Ca^{40}	6.94	70	1.7	1.94×10^{-4}	2	0.5/3	90	1.0	1.0	24.8
Ca^{48}	3.83	86	1.7	1.14×10^{-4}	2	4.5/6	60	0.984	0.893	20.9
3- States										
Ca^{40}	3.73	21 100	31.7	1.14×10^{-6}	2	0.9/2	65	1.017	1.01	32.3
Ca^{40}	6.94	9 200	13.9	3.83×10^{-6}	3	0.5/3	90	1.00	1.00	31.5
Ca^{48}	4.51	6 500	6.8	1.32×10^{-6}	3	1.5/3	65	0.87	0.99	25.5

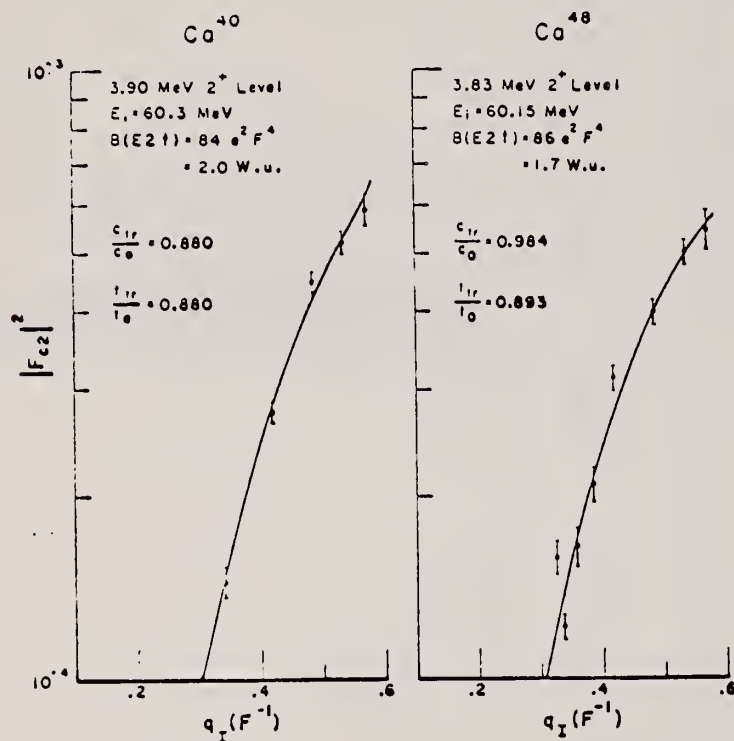


FIG. 8. Experimental form factor points and best theoretical fits to them for the first 2+ states in Ca^{40} and Ca^{48} . The experimental points and their errors are given in Table V.

METHOD

REF. NO.

[Page 2 of 2]

69 Ei 1

hmg

REACTION	RESULT	EXCITATION ENERGY	SOURCE		DETECTOR		ANGLE
			TYPE	RANGE	TYPE	RANGE	

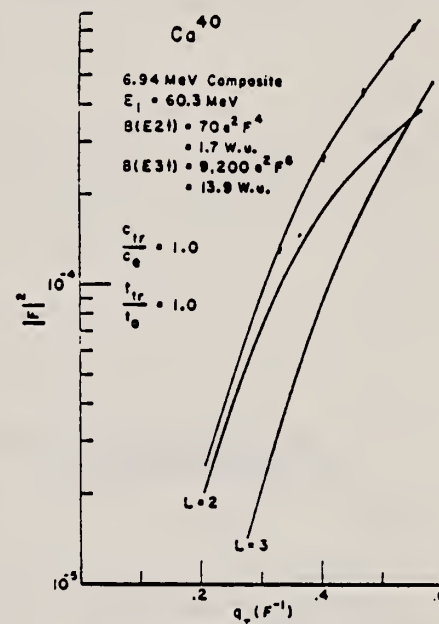


FIG. 10. Experimental points and best theoretical fit to them for the triplet of states near 6.94 MeV. For reasons described in text, only the 2- and 3- states are assumed to contribute to the cross section. These are accounted for by separate form factors generated within the framework of the strict hydrodynamic model. The $B(EL\uparrow)$ values are varied until best fit is obtained. Neither the 2+ nor the 3- form factor alone will fit the data. Both separate and combined form factors are shown in the figure as solid lines.

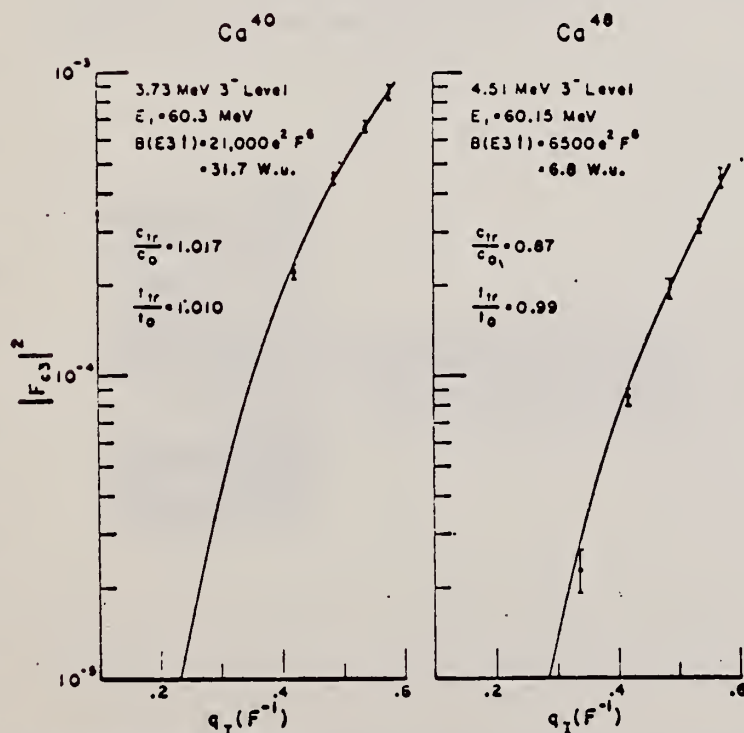


FIG. 9. Experimental form factor points and best theoretical fits to them for the first 3- states in Ca^{40} and Ca^{48} . The experimental values are given in Table V.

METHOD

REF. NO.

69 No 1

egf

REACTION	RESULT	EXCITATION ENERGY	SOURCE		DETECTOR		ANGLE
			TYPE	RANGE	TYPE	RANGE	
G, NA24	ABY	140-999	C	100-999	ACT- I		4PI

999 = 1.2 GEV

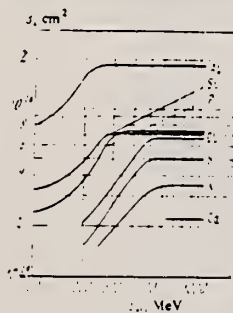


FIG. 2. Cross sections as a function of ray energy.

Table I

Reaction	Nucleons emitted	Threshold*, MeV	Target	Distribution of isotopes, %
Al ²⁷ → Na ²⁴	2p, n	31	Al	100
Si ²⁸ → Na ²⁴	3p, n	43	Si	92.27
P ³¹ → Na ²⁴	4p, 3n	69	P	100
S ³² → Na ²⁴	5p, 3n	74	S	93.02
Cl ³⁵ → Na ²⁴	6p, 5n	104	NH ₄ Cl	75.4
K ³⁹ → Na ²⁴	8p, 7n	140	K ₂ ClO ₃	91.14
Ca ⁴⁰ → Na ²⁴	9p, 7n	148	CaO	96.97

*The threshold was calculated as the binding energy of the emitted nucleons.

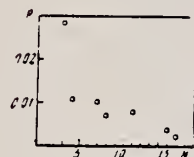


FIG. 3. Dependence of P on number of nucleons which have left the nucleus.

Table II. Cross sections for reactions in the saturation region

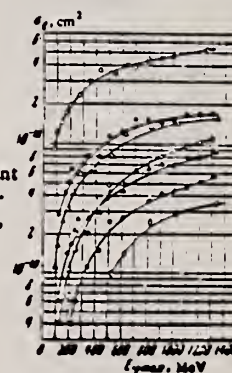
Reaction	σ_{sat} , cm ²	Reaction	σ_{sat} , cm ²
Al ²⁷ → Na ²⁴	185 ± 20	Cl ³⁵ → Na ²⁴	64 ± 7
Si ²⁸ → Na ²⁴	72 ± 4	K ³⁹ → Na ²⁴	45 ± 5
P ³¹ → Na ²⁴	71 ± 8	Ca ⁴⁰ → Na ²⁴	22 ± 5
S ³² → Na ²⁴	52 ± 6		

According to the photomesonic mechanism, the cross section for the reaction can be written in the form

$$\sigma = \sigma_0 A P. \quad (1)$$

Here σ_0 is the total cross section for interaction of the photon with a free nucleon with inclusion of the nucleon motion in the nucleus (σ_0 , as has been shown by Roos and Peterson,⁽⁶⁾ depends only weakly on photon energy for $E_\gamma > 300$ MeV); A is the number of nucleons in the nucleus, and P is the probability that the reaction will proceed by a given channel.

FIG. 1. Cross section σ_Q per equivalent photon as a function of maximum bremsstrahlung energy. Points: O - Al, ● - Si, Δ - P, ▲ - S, □ - Cl, ■ - K, ○ - Ca.



METHOD

REF. NO.

69 U1 1

egf

REACTION	RESULT	EXCITATION ENERGY	SOURCE		DETECTOR		ANGLE
			TYPE	RANGE	TYPE	RANGE	
G, PG	ABY	THR-32	C	32	SCD-D	2-7	120
G, NG	ABY	THR-32	C	32	SCD-D	2-7	120

TABLE 2
Observed yields from the $^{40}\text{Ca}(\gamma, p\gamma')$ and $^{40}\text{Ca}(\gamma, n\gamma')$ reactions

Final state (MeV)	J^π	One-hole configuration	Parent state in ^{40}Ca (MeV)	Yield		Threshold (MeV)
				($10^3/\text{mol} \cdot \text{R}$)	(MeV \cdot mb)	
^{39}Ca : 2.47	$\frac{1}{2}^+$	$(2s_{\frac{1}{2}})^{-1}$	$0^+ 0$	26 ^{a)}	16 ^{a)}	18.2
^{39}K : 2.53				90 ^{a)}	57 ^{a)}	10.8
^{39}Ca : 2.79	$\frac{3}{2}^-$	$(d_{\frac{3}{2}})^{-1}$	$5^- 4.48$	25	15	18.5
^{39}K : 2.82						11.1
^{39}Ca : 3.03	$\frac{1}{2}^-$	$(d_{\frac{1}{2}})^{-1}$	$3^- 3.73$	11	7	18.7
^{39}K : 3.02						11.3
^{39}K : 3.88	$\frac{3}{2}^-$	$(d_{\frac{3}{2}})^{-1}$	$3^- 3.73$	2.4	1.5	14.2
^{39}Ca : 3.88						19.6
^{39}K : 3.94	$\frac{1}{2}, \frac{3}{2}$			3.8	2.5	14.2
^{39}Ca : 3.94						19.6
^{39}K : 4.93				3.2	2.0	13.2
^{39}K : 5.17						13.5
^{39}Ca : 5.13	$(\frac{1}{2}^+), \frac{3}{2}^+$	$(d_{\frac{1}{2}})^{-1}$	$0^+ 0$	4.6 ^{b)}	3.0 ^{b)}	20.8
^{39}K : 5.28				6.0 ^{b)}	3.8 ^{b)}	13.6
^{39}K : 5.62	$(\frac{3}{2}^+), \frac{1}{2}^+$	$(d_{\frac{3}{2}})^{-1}$	$0^- 0$	2.5 ^{b)}	1.6 ^{b)}	13.9
^{39}K : 5.96				1.6 ^{b)}	1.0 ^{b)}	14.3
^{39}Ca : 6.15	$(\frac{1}{2}^+), \frac{3}{2}^+$	$(d_{\frac{1}{2}})^{-1}$	$0^+ 0$	1.4 ^{b)}	0.9 ^{b)}	21.9
^{39}Ca : 6.35				3.2 ^{b)}	2.0 ^{b)}	14.7

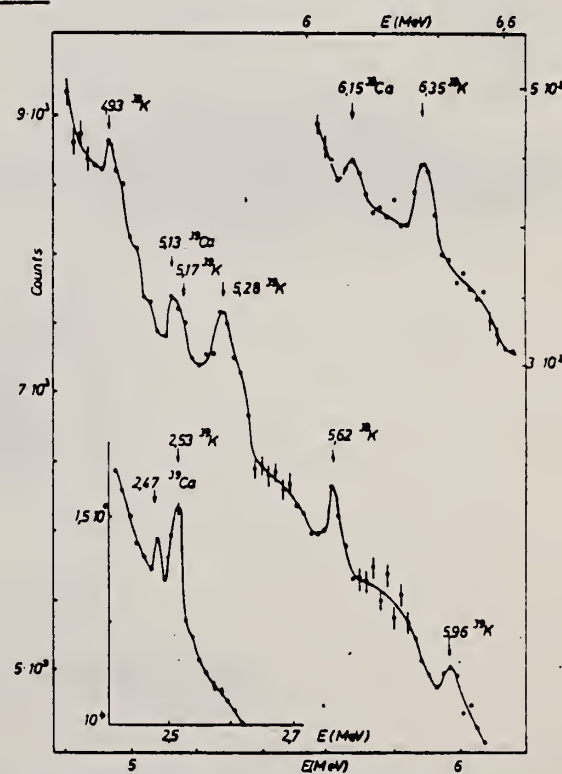
^{a)} Includes possible small contributions from cascade transitions.^{b)} Assuming 100 % ground-state transitions.

Fig. 3. Partial spectra of γ -rays from the calcium target. Level positions of ^{39}K and ^{39}Ca are indicated by arrows. The energy scales correspond to full-energy peaks (lower curve) and double-escape peaks (medium and upper curves), respectively.

METHOD						REF. NO.		EGF
						69 Wu 1		
REACTION	RESULT	EXCITATION ENERGY	SOURCE		DETECTOR		ANGLE	
			TYPE	RANGE	TYPE	RANGE		
G,N 200+	ABX	17-24	D	15-24	TOF-D	2-9	90	
G,P 199+	ABX	17-24	D	15-24	SCD-D	8-15	90	

200+

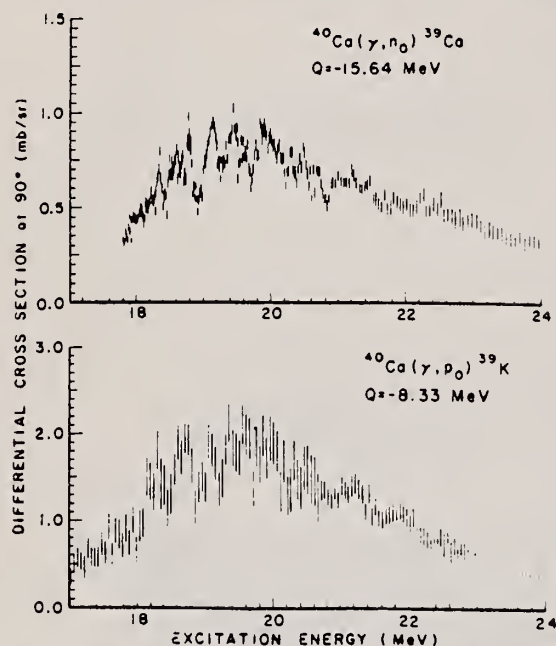


Fig. 1. The observed differential cross sections at 90° for the reactions $^{40}\text{Ca}(\gamma, n_0)^{39}\text{Ca}$ and $^{40}\text{Ca}(\gamma, p_0)^{39}\text{K}$ both measured relative to deuterium cross sections which are known to an accuracy of $\pm 10\%$.

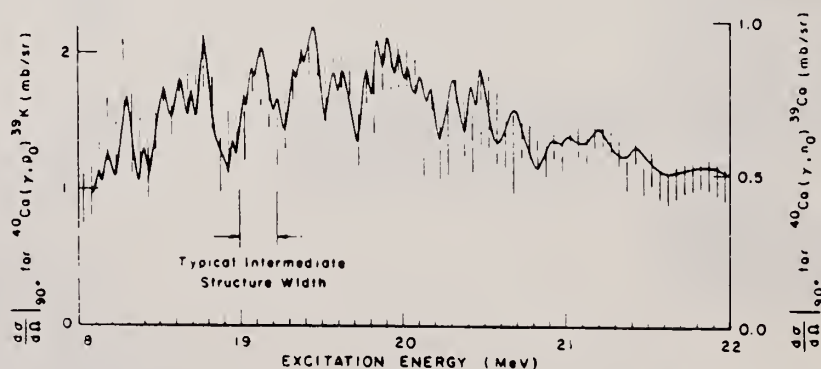


Fig. 2. A comparison between the differential cross sections at 90° for the reactions $^{40}\text{Ca}(\gamma, n_0)^{39}\text{Ca}$ and $^{40}\text{Ca}(\gamma, p_0)^{39}\text{K}$. The data points represent the photoproton results and the solid curve represents the photoneutron results (normalized by a factor of 2.2).

METHOD

REF. NO.

70 Go 3

egf

REACTION	RESULT	EXCITATION ENERGY	SOURCE		DETECTOR		ANGLE
			TYPE	RANGE	TYPE	RANGE	
E, E/	ABX	15-26	D	45-55	MAG-D		DST

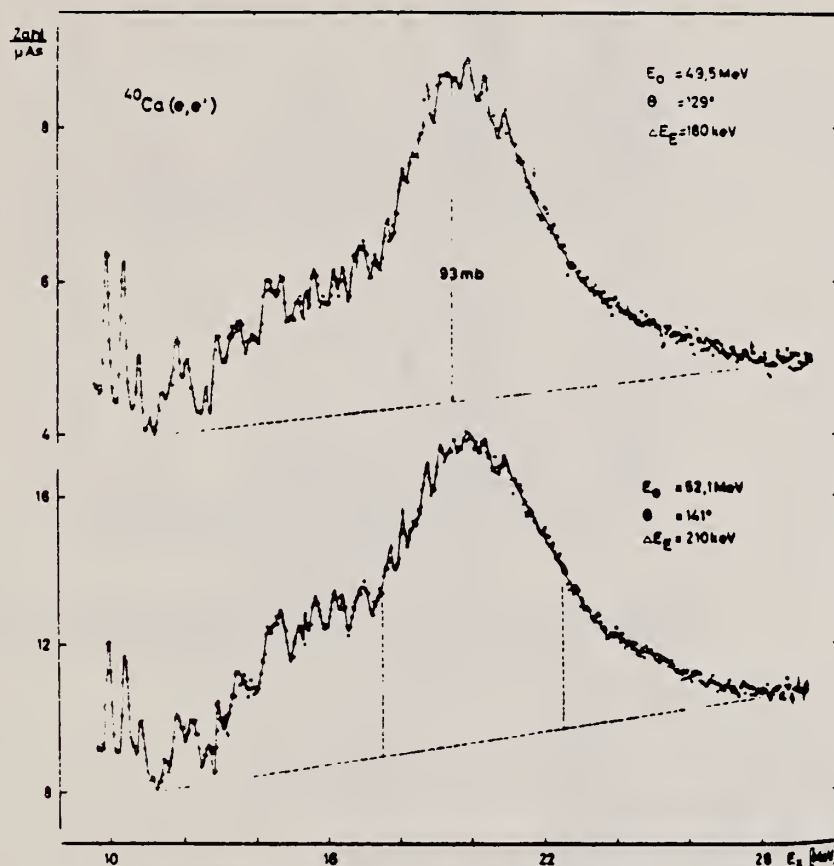


Fig. 5. Riesenresonanz von ^{40}Ca . Beide Spektren sind auf $A_E = 5.0 \cdot 10^3 \text{ MeV}/\mu\text{As}$ normiert. Die gestrichelten Linien geben die im Text erläuterten Integrationsgrenzen und den Untergrund an. Bei $E_x = 19.5 \text{ MeV}$ ergibt die Umrechnung der Zählrate gemäß Gl. (6) und (7) unter Annahme reiner E1-Absorption den Photonenwirkungsquerschnitt $\sigma(\gamma, \text{abs}) \approx 93 \text{ mb}$ ($R_{\text{tr}} = 1.3 R_m$). Die in $^{2-3}$ gemessenen Daten für $\sigma(\gamma, \text{abs})$ haben Maximalwerte bei 19.5 MeV von etwa 85 mb .



METHOD

REF. NO.

70 He 1

egf

REACTION	RESULT	EXCITATION ENERGY	SOURCE		DETECTOR		ANGLE
			TYPE	RANGE	TYPE	RANGE	
P,G	ABX	11-14	D	2-6	NAI-D	6-14	DST

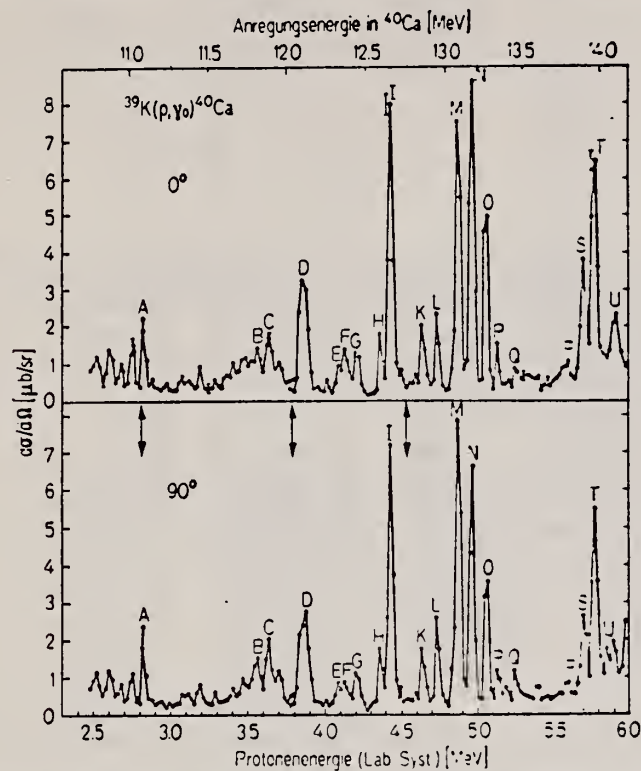


Fig. 3. Anregungsfunktionen der Reaktion $^{39}\text{K}(p, \gamma)^{40}\text{Ca}$ unter 0° und 90° , aufgenommen mit einer Schrittweite von 20 keV. Die Doppelpfeile geben die Energien an bei denen das Target gewechselt wurde

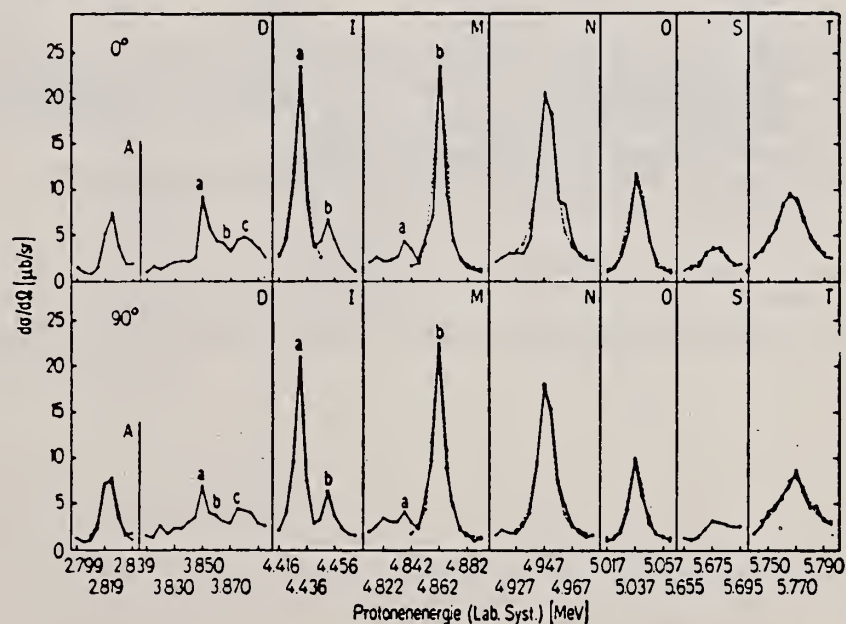


Fig. 4. Teilstücke der Anregungsfunktionen der Reaktion $^{39}\text{K}(p, \gamma)^{40}\text{Ca}$ (Fig. 3), mit 5 keV Auflösung aufgenommen (durchgezogen: Experiment; gestrichelt: angepaßte Form)

Tabelle

1	2	3	4	5	6	7	8
Kennzeichen der Resonanz in Fig. 3 und 4	E_p (Lab. S.) Lage des Maximum aus Messung mit Auflösung von		Γ Totale Breite (aus Messung mit 5 keV Auflösung)	E_x Anregungs- energie in ^{40}Ca ^a	$(2J+1) \Gamma_p \Gamma_{\gamma 0} / \Gamma$ Resonanzstärke aus Messung mit Auf- lösung von		Resonanz- stärke nach Ref. ^{3b}
	20 keV (Fig. 3)	5 keV (Fig. 4)			5 keV	20 keV	
A	2,822 MeV	2,822 MeV	9,6 keV	11,085 MeV	7,2 eV	5,2 eV	
B	3,563			11,807		9,4	
C	3,641			11,883		9,7	
D	3,870	a) 3,850 b) c) 3,880		12,090		19,2	4,7 eV 3,2
E	4,086			12,120			
F	4,124			12,317		8,2	2,6
G	4,201			12,354			
H	4,353			12,429		5,6	1,5
I	4,431	a) 4,431 b) 4,451	7,2	12,578		7,5	7,4
K	4,630			12,654	21,3		13,2
L	4,729			12,674	9,0	31,0	4,0
M	4,866	a) b) 4,862	7,5	12,848		9,0	5,1
N	4,965	4,949	11,7	12,944		11,9	5,2
O	5,050	5,038	12,4 (0°); 9,3 (90°)	13,074	11,9 30,7	40,2	2,2 19,5
P	5,122			13,159	35,2	32,5	10,3
				13,245	15,7	19,3	4,5
				13,327		6,8	5,8

Q	5,240			13,442		6,6	
R	5,590			13,784		6,6	2,2
S	5,693	5,677	23 (0°)	13,868	10,9	20,8	43,0
T	5,772	5,767	24	13,956	25,4	44,6	93,5
U	~ 5,90			~ 14,08		28,4	
Fehler:	relative Lage ± 10 keV, absolute Skala ± 10 keV		$\pm 20\%$	wie Spalten 2 und 3	Relativwerte $\pm 30\%$ absolute Skala $\pm 25\%$		$\pm 30\%$ s. Text

^a Berechnet mit den E_p -Werten aus Spalte 3, wenn verfügbar, sonst aus Spalte 2.

^b Die Werte aus Ref. ³ (Experiment bei 0°) wurden mit dem Verhältnis $d\sigma(90^\circ)/d\sigma(0^\circ)$ multipliziert (s. Text).

Ca

40

20

METHOD

REF. NO.

70 It 2

hmg

[Page 1 of 3]

REACTION	RESULT	EXCITATION ENERGY	SOURCE		DETECTOR		ANGLE
			TYPE	RANGE	TYPE	RANGE	
E, E/	FMF	0-25	D	183, 250	MAG-D		DST

LEVELS: 3-9 MEV

TABLE I. Cross sections for the odd-parity states in ^{40}Ca at the incident energy of 183 MeV. $d\sigma/d\Omega$ are given in units of cm^2/sr with the power of 10 indicated in parenthesis. Errors are expressed as percentage.

E_x θ (deg)	3.74 MeV, 3^- $d\sigma/d\Omega$ error	4.49 MeV, 5^- $d\sigma/d\Omega$ error	5.90 MeV, 1^- $d\sigma/d\Omega$ error	6.29 MeV, 3^- $d\sigma/d\Omega$ error	6.59 MeV, 3^- $d\sigma/d\Omega$ error	6.95 MeV, 1^- $d\sigma/d\Omega$ error
35	4.36(-30) \pm 7.9	1.03(-31) \pm 67.0	5.02(-31) \pm 41.1	9.91(-31) \pm 24.3 8.53(-31) \pm 9.7	6.06(-31) \pm 31.8 4.68(-31) \pm 39.7	4.88(-30) \pm 4.0
45	4.21(-30) \pm 10.5 4.29(-30) \pm 10.3	4.92(-32) \pm 90.0 5.41(-32) \pm 72.0	2.46(-31) \pm 10.0 1.38(-31) \pm 33.3	3.22(-31) \pm 11.5 4.48(-31) \pm 6.6	2.31(-31) \pm 45.7 3.20(-31) \pm 34.6	2.93(-30) \pm 3.5 3.00(-30) \pm 2.5
55	2.97(-30) \pm 10.0 2.59(-30) \pm 10.9	5.99(-32) \pm 25.0 6.63(-32) \pm 12.9	1.06(-31) \pm 8.1 1.30(-31) \pm 10.6	1.65(-31) \pm 9.7 1.90(-31) \pm 5.6	1.44(-31) \pm 10.4 1.13(-31) \pm 9.4	1.44(-30) \pm 3.7 1.38(-30) \pm 3.1
65	1.60(-30) \pm 8.3 1.56(-30) \pm 8.4	5.22(-32) \pm 16.1 5.59(-32) \pm 9.4	4.79(-32) \pm 8.8 4.05(-32) \pm 15.5	6.17(-32) \pm 12.0 5.95(-32) \pm 6.2	4.37(-32) \pm 15.7 4.00(-32) \pm 13.0	5.69(-31) \pm 2.8 5.05(-31) \pm 4.2
75	7.72(-31) \pm 7.3 6.42(-31) \pm 8.8	5.32(-32) \pm 14.3 5.48(-32) \pm 6.7	1.30(-32) \pm 19.6 2.00(-32) \pm 22.5	1.95(-32) \pm 21.7 1.36(-32) \pm 14.6	1.95(-32) \pm 21.7 1.70(-32) \pm 15.0	2.10(-31) \pm 6.6 1.91(-31) \pm 4.5
85	3.23(-31) \pm 8.9	4.58(-32) \pm 13.3	5.30(-33) \pm 48.5	4.50(-33) \pm 50.0	5.95(-33) \pm 40.5	6.80(-32) \pm 9.7
95	1.09(-31) \pm 8.7	3.31(-32) \pm 15.2	1.71(-33) \pm 94.4	<2.85(-33)	1.90(-33) \pm 85.0	1.32(-32) \pm 25.0
105	3.47(-32) \pm 9.9	2.54(-32) \pm 9.9				
115	6.98(-33) \pm 20.1	1.49(-32) \pm 12.9		1.02(-33) \pm 25.0	1.21(-33) \pm 25.0	<7.4 (-34)

TABLE II. Cross sections for the odd-parity states in ^{40}Ca at the incident energy of 250 MeV. $d\sigma/d\Omega$ are given in units of cm^2/sr with the power of 10 indicated in parenthesis. Errors are expressed as percentage.

E_x θ (deg)	3.74 MeV, 3^- $d\sigma/d\Omega$ error	4.49 MeV, 5^- $d\sigma/d\Omega$ error	6.29 MeV, 3^- $d\sigma/d\Omega$ error	6.59 MeV, 3^- $d\sigma/d\Omega$ error	6.95 MeV, 1^- $d\sigma/d\Omega$ error
75	4.96(-32) \pm 24.4	6.08(-32) \pm 13.4	4.08(-33) \pm 22.2	4.84(-33) \pm 31.3	4.94(-33) \pm 23.0
95	3.44(-33) \pm 20.0	3.29(-32) \pm 7.1	3.18(-33) \pm 8.1	3.44(-33) \pm 10.0	3.25(-32) \pm 7.7
95	9.66(-34) \pm 31.6	1.10(-32) \pm 7.8			
105	1.23(-33) \pm 12.5	4.67(-33) \pm 6.6	1.11(-33) \pm 15.0	6.46(-34) \pm 28.6	1.44(-33) \pm 12.9
125	3.16(-34) \pm 32.1	3.50(-34) \pm 22.6	8.37(-35) \pm 64.9	6.11(-35) \pm 72.2	1.59(-34) \pm 50.0
135*	7.47(-35) \pm 22.8	2.41(-33) \pm 17.9			

*Incident energy is 198 MeV.

[over]

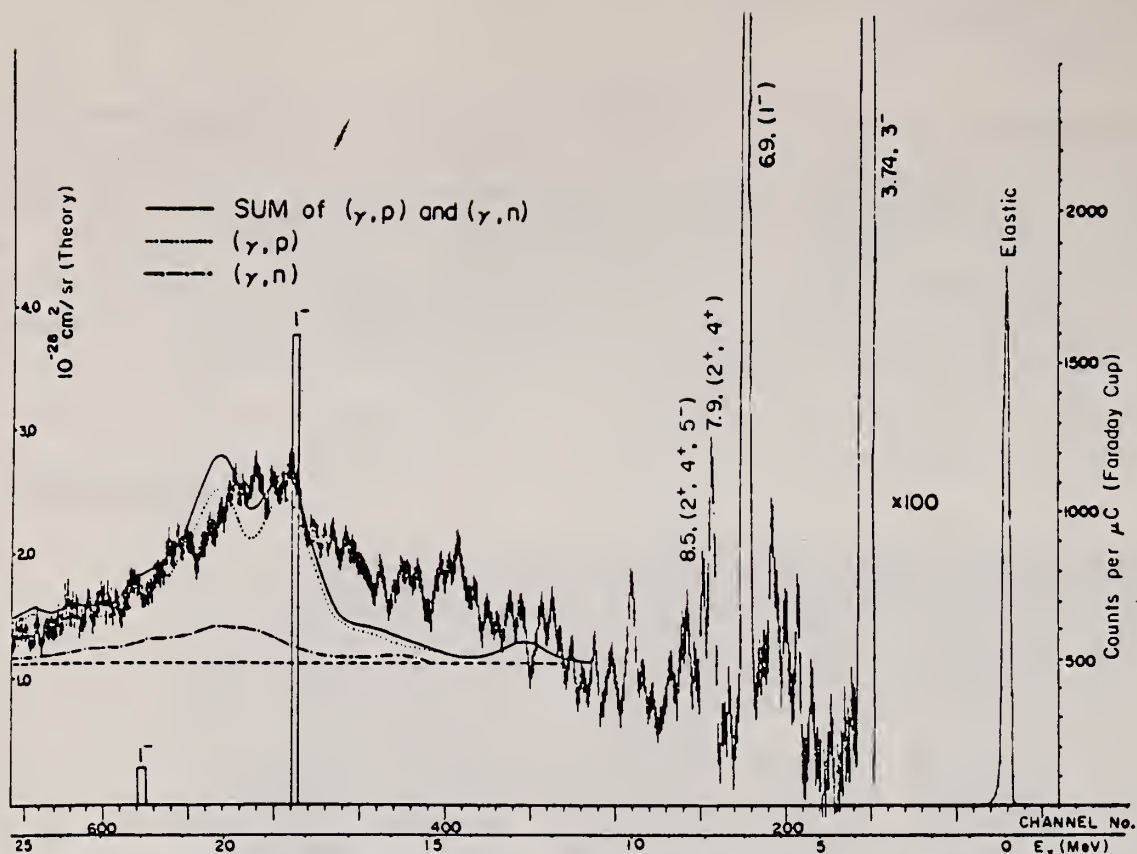


FIG. 3. Spectrum of electrons scattered from ^{40}Ca measured up to the giant-resonance region. The incident energy is 183 MeV and $\theta = 35^\circ$. The radiative corrections have been made. The sum of the cross sections of (γ, p) and (γ, n) reactions are indicated with solid curve on the spectrum.

TABLE VI. Theoretical and experimental reduced transition probabilities for odd-parity states.

E_x (MeV)	J^π	Present	Horie and Yokozawa (Ref. 33)	Gerace and Green (Ref. 34)
3.74	3_1^-	27.3 ± 1.0^a	25.0	$27.2 (23.0)^b$
6.29	3_2^-	4.6 ± 0.4		1.9 (0.5)
6.59	3_3^-	2.5 ± 0.2		2.7 (3.5)
4.49	5^-	17.7 ± 3.8^a	23.4	$20.4 (18.0)$

^aWeighted mean of $B(EL)$ from Tassie-type and shell-model-type transition charge density.

^b $B/B_{w.u.}$ in parentheses were calculated on a different basis of single-particle energy l (see Ref. 34).

³⁴W.J. Gerace and A.M. Green,
Nucl. Phys. A113, 641 (1968).

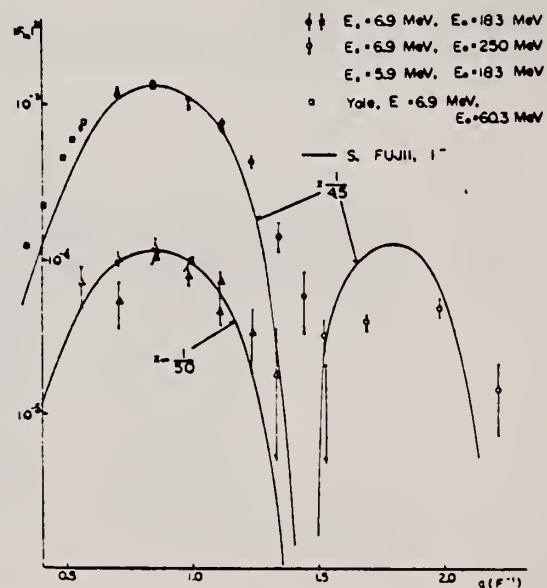


FIG. 7. The experimental $|F_{1n}|^2$ for the 5.9-MeV (1^-) and 6.9-MeV states. The solid curves are calculated by Fujii assuming ρ_{tr} which has the form corresponding to the product of monopole and dipole generators.

REACTION	RESULT	EXCITATION ENERGY	SOURCE		DETECTOR		ANGLE
			TYPE	RANGE	TYPE	RANGE	

$|F_{\theta}|^2$

- Present (e. e')
- Sum of (γ, p) and (γ, n)
- Sum of Longitudinal I² Form Factors

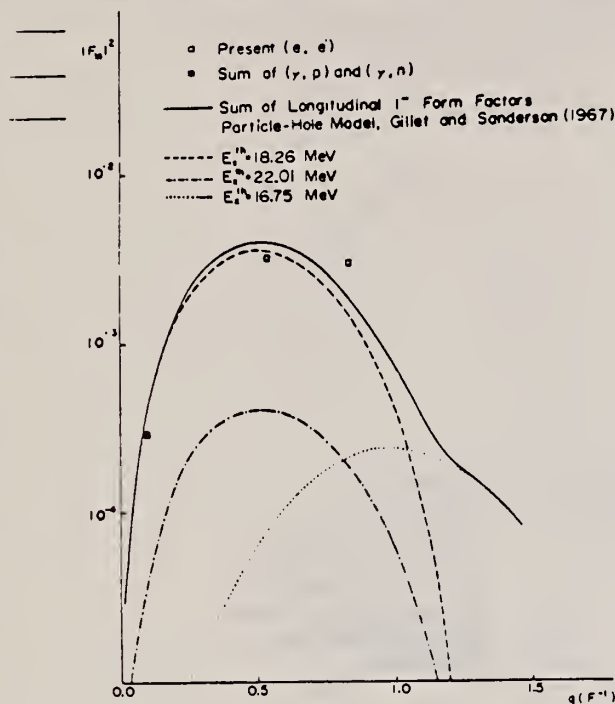


FIG. 8. The experimental form factors of the giant resonance. The data are compared with sum of the theoretical form factors of dipole states calculated with the wave function of Gillet *et al.*

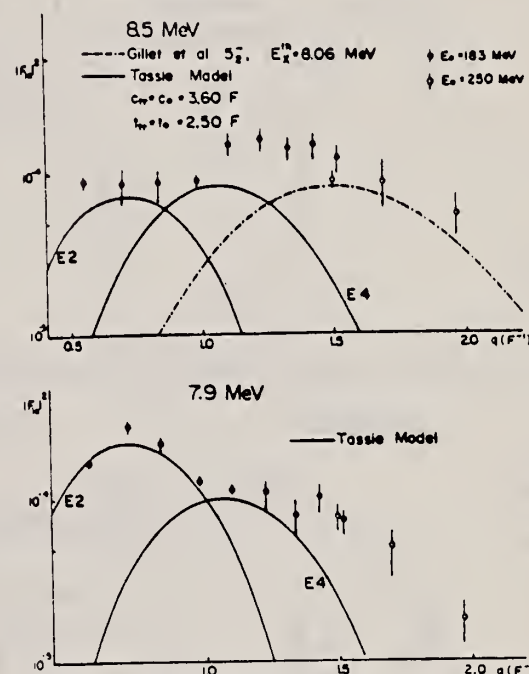


FIG. 16. The experimental $|F_{1n}|^2$ for the 7.9- and 8.5-MeV levels. The curves are calculated by Tassie model, except for $E5$ excitation which is calculated by the wave function of Gillet *et al.*

TABLE V. Reduced transition probabilities for the odd-parity states in ^{40}Ca obtained from the different types of transition charge densities.

E_x (MeV)	J^π	Tassie type		Shell-model type	
		$B(EL)$ ($e^2 F^2 L$)	$B/B_{W.u.}$	$B(EL)$ ($e^2 F^2 L$)	$B/B_{W.u.}$
3.74	3_1^-	18450 ± 670 $c_{tr} = 3.20 F$	27.7 ± 1.0 $t_{tr} = 2.31 F$	18000 ± 670 $\alpha = 1.20, b = 2.07 F$	26.8 ± 1.0
4.49	5^-	$(3.38 \pm_{0.85}^{1.52}) \times 10^6$ $c_{tr} = 2.94 F$	$20.2 \pm_3^9$ $t_{tr} = 1.91 F$	$(2.73 \pm 0.75) \times 10^6$ $\alpha = 0.00, b = 2.05 F$	16.3 ± 4.5
6.29	3_2^-			3040 ± 260 $\alpha = 0.50, b = 2.30 F$	4.6 ± 0.4
6.59	3_3^-			1680 ± 130 $\alpha = 0.45, b = 2.19 F$	2.5 ± 0.2

[over]

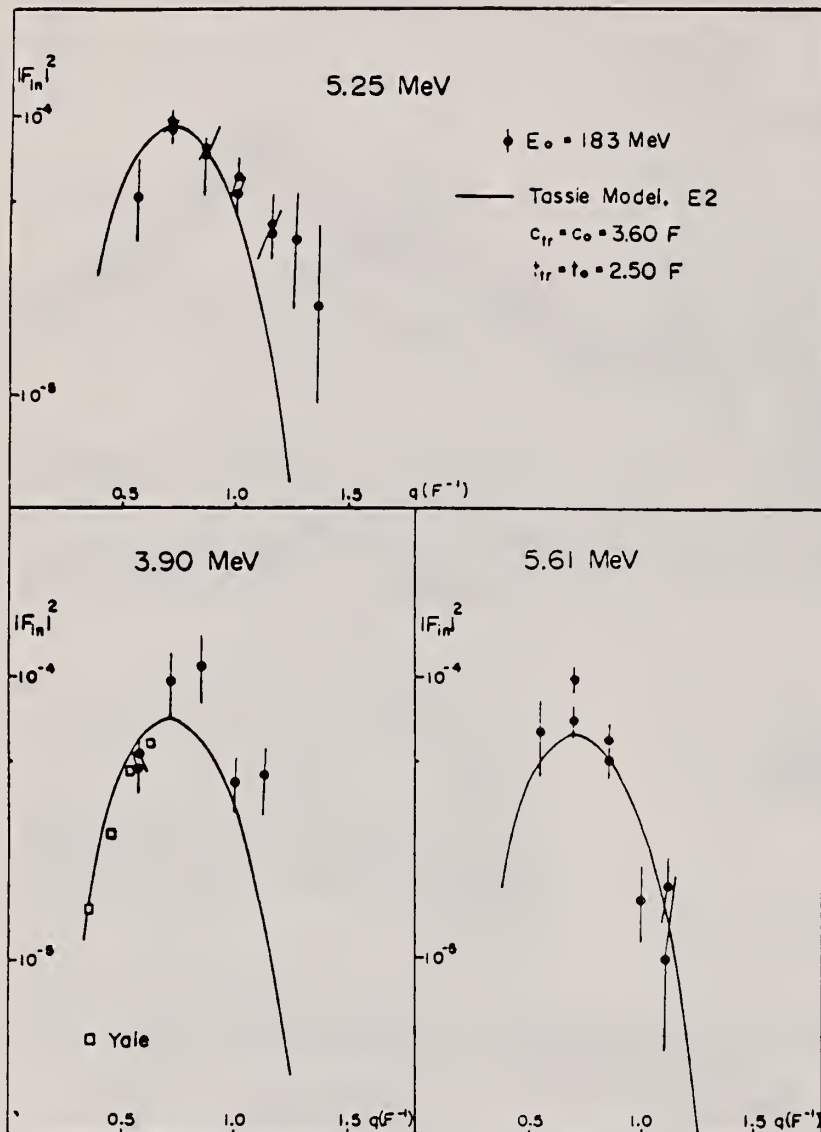


FIG. 15. The experimental $|F_{in}|^2$ for the 3.90-, 5.25-, and 5.61-MeV levels. The curves are calculated by using the strict Tassie model.

REACTION	RESULT	EXCITATION ENERGY	SOURCE		DETECTOR		ANGLE
			TYPE	RANGE	TYPE	RANGE	

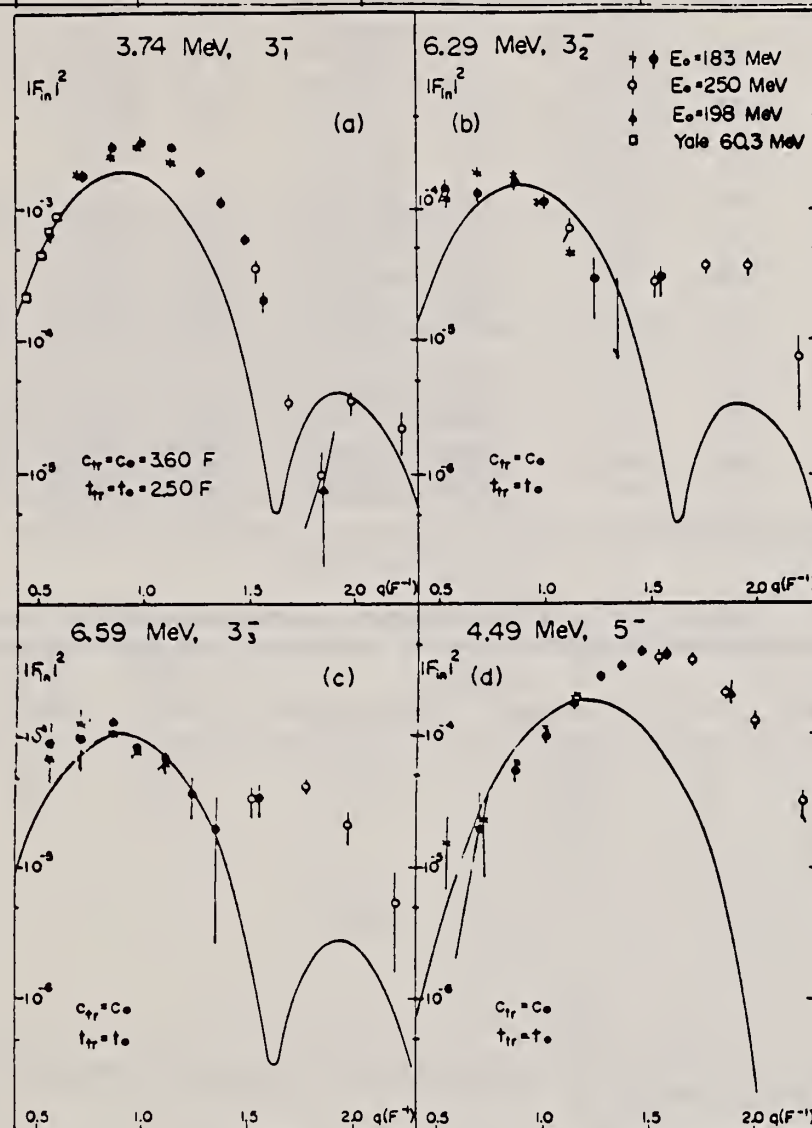


FIG. 5. The experimental F_{1n}^2 for the 3.74- (3_1^-), 6.29- (3_2^-), 6.59- (3_3^-), and 4.49-MeV (5_1^-) states which are defined as $(d\sigma/d\Omega)/\sigma_{\text{Mott}}$ are plotted against momentum transfer q . The curves are theoretical cross sections calculated by DWBA code using the transition charge densities of the strict Tassie model.

[over]

TABLE III. Form factors for the 3^- and 5^- states of ^{40}Ca for the incident energy of 250 MeV. The cross sections at various energies were normalized to those at 250 MeV with the help of the DWBA calculation. Errors are expressed as percentage.

3.74 MeV, 3^-			6.29 MeV, 3^-			6.59 MeV, 3^-			4.49 MeV, 5^-		
θ (deg)	q (F^{-1})	$10^4 \times F_{1n} ^2$	q (F^{-1})	$10^4 \times F_{1n} ^2$	q (F^{-1})	$10^4 \times F_{1n} ^2$	q (F^{-1})	$10^4 \times F_{1n} ^2$	q (F^{-1})	$10^4 \times F_{1n} ^2$	$10^4 \times F_{1n} ^2$
$E_0 = 60.3 \text{ MeV}^a$											
90	0.440	2.22 ± 6.0									
110	0.506	4.50 ± 2.0									
130	0.555	6.66 ± 2.0									
150	0.596	8.65 ± 6.0									
$E_0 = 183 \text{ MeV}$											
35	0.552	6.34 ± 7.9	0.549	1.44 ± 24.3	0.549	0.88 ± 31.8	0.551	0.15 ± 67.0			
				1.24 ± 9.7		0.68 ± 39.7					
45	0.702	17.1 ± 10.5	0.698	1.31 ± 11.5	0.698	0.94 ± 45.7	0.701	0.20 ± 90.0			
		17.4 ± 10.3		1.82 ± 6.6		1.30 ± 34.6		0.22 ± 72.0			
55	0.847	27.8 ± 10.0	0.842	1.55 ± 9.7	0.842	1.35 ± 10.4	0.852	0.56 ± 25.0			
		24.2 ± 10.9		1.78 ± 5.6		1.06 ± 9.4		0.62 ± 12.9			
65	0.985	30.3 ± 8.3	0.987	1.17 ± 12.0	0.979	0.93 ± 15.7	0.993	0.99 ± 16.1			
		29.2 ± 8.4		1.13 ± 6.2		0.76 ± 13.0		1.06 ± 9.4			
75	1.125	26.3 ± 7.3	1.121	0.69 ± 21.7	1.119	0.69 ± 21.7	1.130	1.53 ± 14.3			
		22.7 ± 8.8		0.48 ± 14.6		0.60 ± 15.0		1.94 ± 6.7			
85	1.268	20.1 ± 8.9	1.242	0.28 ± 50.0	1.235	0.37 ± 40.5	1.245	2.85 ± 13.3			
95	1.372	11.5 ± 8.7	1.360	< 0.30	1.350	0.20 ± 85.0	1.353	3.49 ± 15.2			
105	1.480	6.02 ± 9.9					1.455	4.41 ± 9.9			
115	1.570	1.99 ± 20.1	1.570	0.35 ± 25.0	1.560	0.34 ± 25.0	1.568	4.26 ± 12.9			
$E_0 = 250 \text{ MeV}$											
75	1.531	3.28 ± 24.4	1.523	0.27 ± 22.2	1.523	0.32 ± 31.3	1.528	4.02 ± 13.4			
85	1.699	0.40 ± 20.0	1.690	0.37 ± 8.1	1.689	0.40 ± 10.0	1.696	3.82 ± 7.1			
95	1.854	0.19 ± 31.6					1.851	2.17 ± 7.8			
105	1.995	0.40 ± 12.5	1.985	0.36 ± 15.0	1.984	0.21 ± 28.6	1.992	1.52 ± 6.6			
125	2.231	0.22 ± 32.1	2.219	0.074 ± 64.9	2.218	0.054 ± 72.2	2.227	0.31 ± 22.6			
135 ^b	1.845	0.07 ± 22.8					1.841	2.29 ± 17.9			

^aYale data.

^bIncident energy is 198 MeV.

TABLE IV. $B(EL)$ values in Weisskopf units extracted from present (e, e') and other experiments.

E_x (MeV)	J^π	Present		Yale (e, e') (Ref. 5)	Orsay (e, e') (Ref. 4)	MIT (α, α') (Refs. 25, 35)
		Tassie type	Shell-model type			
3.74	3^-	27.7 ± 1.0	26.8 ± 1.0	31.7 ± 4	15.0	23.6 ± 3.5
3.90	2^+	3.0^a		2.0 ± 0.2	3.6	2.9 ± 0.5
4.49	5^-	20.2 ± 3	16.3 ± 4.5		12.3	17.7 ± 2.7
5.25	2^+	0.4^a				
5.61	2^+	0.4^a				
5.90	1^-					0.7 ± 0.2
6.29	3^-		4.6 ± 0.4			6.6 ± 1.0
6.59	3^-		2.5 ± 0.2			3.8 ± 0.6
6.95	1^-					
7.9	2^+	1.3^a				1.8 ± 0.4
7.9	(4^+)	5^a				5.6 ± 0.8
8.5	2^+	0.4^a				0.7
8.5	(5^-)	7.0^a			6.9	$2.1(4^+)$

^aError was not estimated.

REF. K. Kayser, W. Collin, P. Filss, S. Guldbakke, G. Nolte,
H. Reich, J. O. Trier, W. Witschel
Z. Physik 239, 447 (1970)

ELEM. SYM.	A	Z
Ca	40	20
REF. NO.		
70 Ka 2		egf

METHOD					
REACTION	RESULT	EXCITATION ENERGY	SOURCE		ANGLE
			TYPE	RANGE	
G, NP	ABX	20-140	C	20-140	4PI

Investigation of the Photo Nuclear Reactions $^{12}\text{C}(\gamma, n)$, $^{12}\text{C}(\gamma, 2n)$, $^{39}\text{K}(\gamma, n)$ and $^{40}\text{Ca}(\gamma, np)$ up to the Meson Threshold

In order to obtain data on the photon absorption process between the giant resonance and the meson threshold the cross sections of the reactions $^{12}\text{C}(\gamma, n)^{11}\text{C}$, $^{12}\text{C}(\gamma, 2n)^{10}\text{C}$, $^{39}\text{K}(\gamma, n)^{38}\text{K}$, and $^{40}\text{Ca}(\gamma, np)^{38}\text{K}$ have been determined by the analysis of yield curves at the 140 MeV electron synchrotron of the PTB.

Though the (γ, n) cross sections grow small with increasing photon energy they are different from zero up to energies of 60 MeV and above. The cross section of the reaction $^{12}\text{C}(\gamma, 2n)$ is extremely small; its highest value amounts to 0.15% of the highest value of the $^{12}\text{C}(\gamma, n)$ reaction. The measured $^{40}\text{Ca}(\gamma, np)$ cross section is of the order predicted by the naive quasi-deuteron model. The integrated cross sections of the above reactions up to 140 MeV are 85 ± 7 , 0.90 ± 0.10 , 139 ± 16 , and 76 ± 7 MeVmb respectively.

Kernphotoreaktionen an ^{12}C , ^{39}K und ^{40}Ca bis zur Mesonschwelle

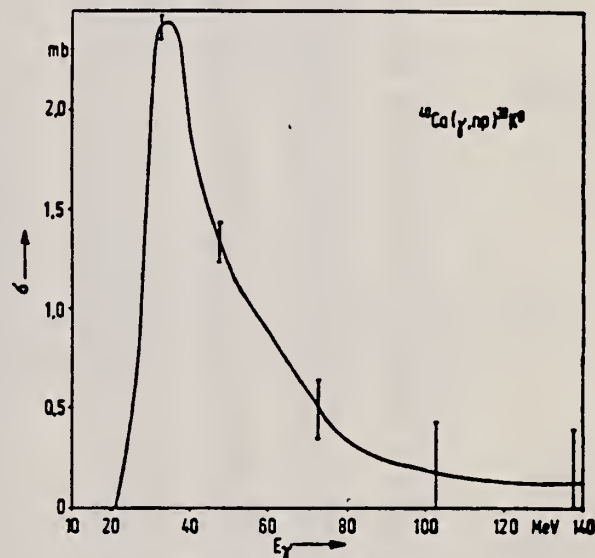


Fig. 6. Wirkungsquerschnitt der Reaktion $^{40}\text{Ca}(\gamma, np)^{38}\text{K}$

ELEM. SYM.	A	Z
Ca	40	20
REF. NO.	70 St 2	
	egf	

REACTION	RESULT	EXCITATION ENERGY	SOURCE		DETECTOR		ANGLE
			TYPE	RANGE	TYPE	RANGE	
E _i E/	ABX	3	D	54	MAG-D		141
		(3.35)		(53.98)			

Tabelle 3. Experimentelle Parameter und Meßwerte. E₀, θ Primärenergie, Streuwinkel im Laborsystem. q unelastischer Impulsübertrag. α/σ_E gemessenes Verhältnis von unelastischem zu elastischem differentiellen Wirkungsquerschnitt; in Klammern ist der statistische Fehler in % angegeben. dσ/dΩ unelastischer differentieller Wirkungsquerschnitt; wegen der Fehlerangaben vgl. Text. Die Meßwerte für Si und S sind als Ergebnisse für ²⁸Si und ³²S aufzufassen (vgl. Text)

3 = 3.35 0+

	E ₀ (MeV)	θ (°)	q ² (fm ⁻²)	α/σ _E (10 ⁻⁴)	dσ/dΩ (10 ⁻³³ cm ² /ster.)
¹² C 7,65 MeV	59,58	117,04	0,231	14,90 (0,6)	24,69 ± 1,60
	56,94	129,02	0,231	13,79 (1,0)	13,68 ± 0,96
	54,12	141,11	0,229	14,98 (0,7)	8,15 ± 0,55
	52,75	153,15	0,231	15,24 (1,0)	6,62 ± 0,47
	51,90	165,05	0,231	15,78 (1,8)	1,16 ± 0,09
	51,18	104,98	0,145	5,80 (0,7)	28,80 ± 1,69
	47,90	117,04	0,145	5,51 (0,7)	17,19 ± 1,01
	45,48	129,02	0,145	5,97 (1,2)	11,14 ± 0,71
	43,57	141,11	0,143	5,95 (1,1)	6,09 ± 0,38
	42,54	153,15	0,145	5,82 (1,4)	2,67 ± 0,18
	37,51	104,98	0,074	1,41 (1,4)	15,38 ± 1,07
	35,08	117,04	0,073	1,33 (1,6)	9,14 ± 0,57
	33,39	129,02	0,073	1,44 (1,7)	5,89 ± 0,37
	32,04	141,11	0,073	1,39 (2,0)	3,11 ± 0,21
	31,36	153,15	0,073	1,39 (3,2)	1,39 ± 0,11
²⁴ Mg 6,44 MeV	59,01	116,94	0,232	5,53 (2,2)	28,28 ± 2,24
	55,81	129,03	0,231	5,41 (1,5)	16,65 ± 1,20
	53,64	140,95	0,231	5,65 (1,6)	9,51 ± 0,70
	52,14	153,00	0,231	5,17 (2,1)	3,95 ± 0,32
	50,98	104,96	0,074	0,59 (2,6)	25,08 ± 1,78
	44,59	116,94	0,074	0,56 (3,2)	15,09 ± 1,16
	42,87	129,03	0,074	0,58 (2,8)	9,37 ± 0,68
	31,72	140,95	0,074	0,58 (3,1)	5,10 ± 0,39
	30,86	153,00	0,074	0,68 (5,5)	2,69 ± 0,27
Si 4,98 MeV	58,38	116,94	0,232	5,61 (1,9)	38,70 ± 2,68
	55,12	129,03	0,231	5,27 (0,9)	21,98 ± 1,34
	52,87	141,11	0,231	5,58 (1,3)	12,72 ± 0,81
	51,28	153,00	0,230	5,69 (1,9)	6,00 ± 0,42
	49,93	104,96	0,145	2,05 (1,6)	49,60 ± 3,13
	49,97	104,96	0,146	2,10 (1,4)	50,68 ± 3,09
	46,77	116,94	0,146	2,23 (2,2)	33,90 ± 2,31
	44,28	129,03	0,146	2,14 (2,0)	19,48 ± 1,29
	42,44	141,11	0,146	2,20 (1,7)	10,98 ± 0,70
	41,23	153,00	0,145	2,45 (2,1)	5,64 ± 0,38
	41,37	153,00	0,146	2,48 (2,5)	5,67 ± 0,40
	36,28	104,96	0,074	0,53 (4,5)	32,51 ± 2,90
	36,26	104,96	0,074	0,56 (4,0)	34,35 ± 2,89
	33,98	116,94	0,074	0,55 (4,3)	21,28 ± 1,83
	32,17	129,03	0,074	0,52 (4,0)	11,98 ± 1,00
Si 6,69 MeV	59,19	104,96	0,210	0,32 (37)	5,17 ± 3,36
	58,80	104,96	0,209	0,27 (45)	4,40 ± 3,30
	53,98	140,95	0,250	0,92 (9)	3,03 ± 1,21

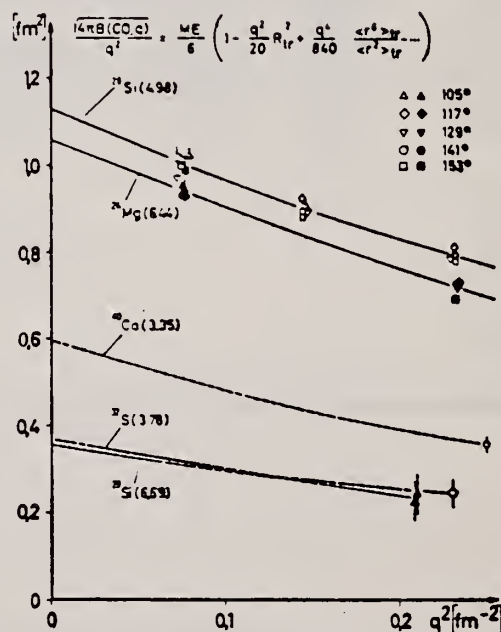


Fig. 3. Meßergebnisse für Monopolübergänge in ²⁴Mg(6,44 MeV), ²⁸Si(4,98 und 6,69 MeV), ³²S(3,78 MeV) und ⁴⁰Ca(3,35 MeV) als Funktion von q². Die eingetragenen Meßpunkte und die zugehörigen Kurven gelten für eine Auswertung mit f_c, x₁ und x₂ nach Modell I. Für ²⁸Si(4,98) sind nur die aus α/σ_E und D^{BA}_{exp} berechneten longitudinalen Anteile aufgetragen (vgl. 5.1), wobei die Meßpunkte bei gleicher Impulsübertragung und gleichem Streuwinkel (vgl. Tabelle 3) zusammengefaßt wurden. Die gestrichelten Kurven zeigen die Extrapolation nach q=0 mit vorgegebenem Übergangsradius

ELEM. SYM.	A	Z
Ca	40	20
REF. NO.		
70 Wu 1		egf

METHOD			SOURCE		DETECTOR		ANGLE
REACTION	RESULT	EXCITATION ENERGY	TYPE	RANGE	TYPE	RANGE	
G ₇ N	ABX	18-20	C	16-22	TOF-D		90

Cross section relative to D(γ ,n)p

GROUND STATE

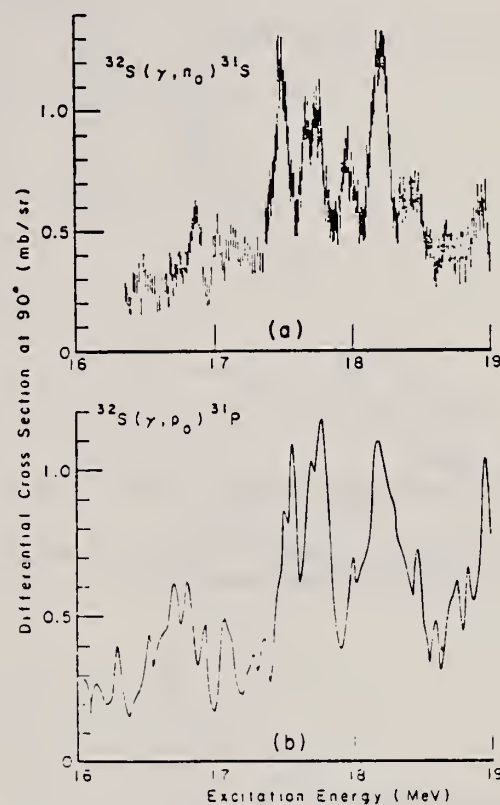


Fig. 5a. The observed $^{32}\text{S}(\gamma, n_0)^{31}\text{S}$ differential cross section at 90° . 5b. The $^{32}\text{S}(\gamma, p_0)^{31}\text{P}$ differential cross section at 90° deduced from the inverse reaction $^{31}\text{P}(p, \gamma)^{32}\text{S}$. The magnitude of the cross section is that of ref. 18), also measured relative to the cross section for the D(γ , n)p reaction.

METHOD

REF. NO.

71 Br 1

egf

REACTION	RESULT	EXCITATION ENERGY	SOURCE		DETECTOR		ANGLE
			TYPE	RANGE	TYPE	RANGE	
G, NP	ABX	19-30	C	19-30	ACT-I		4PI

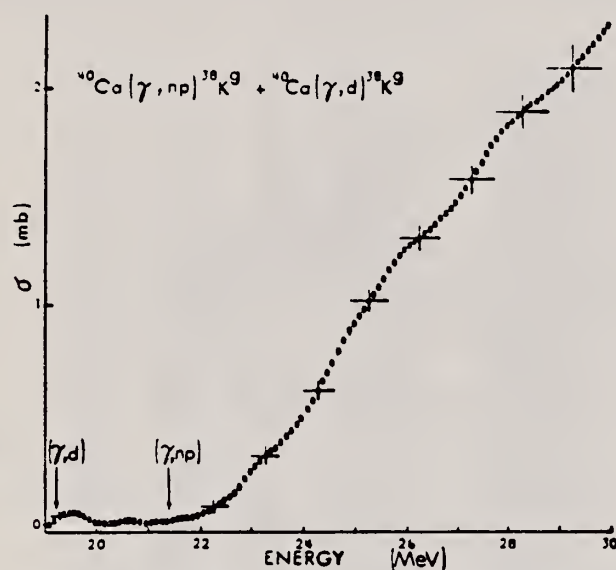


Fig. 3. The experimental $(\gamma, np) + (\gamma, d)$ cross section in ^{40}Ca measured for reactions proceeding through the ^{39}K ground state.

REF.

A. Bussiere, J. Mougey, Phan Xuan Ho, M. Priou, I. Sick
Lettere al Nuovo Cimento 2, 1149 (1971)

ELEM. SYM. A Z

Ca

40

20

METHOD

REF. NO.

71 Bu 2

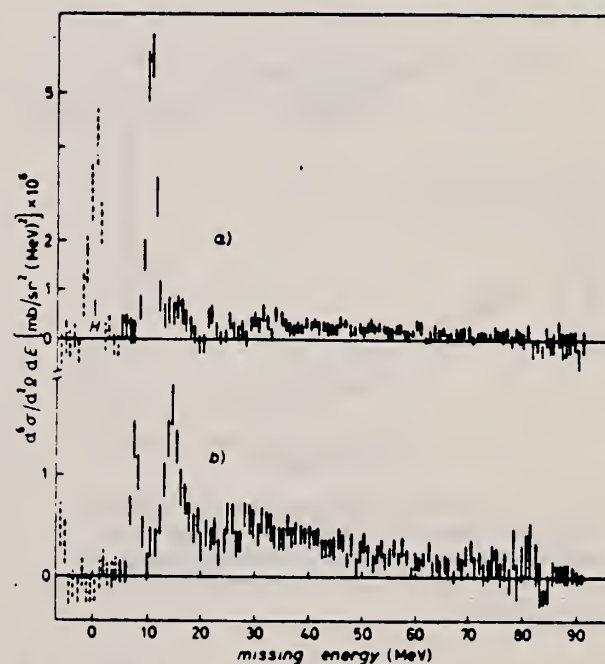
egf

REACTION	RESULT	EXCITATION ENERGY	SOURCE		DETECTOR		ANGLE
			TYPE	RANGE	TYPE	RANGE	
E, E/P	ABX	5-85	D	500	MAG-D		51

PROT P=25,100 MEV/C

TABLE I.

		$p = 25 \text{ MeV/c}$		$p = 100 \text{ MeV/c}$			
		σ_{exp}	σ_{th}	$\sigma_{\text{exp}}/\sigma_{\text{th}}$	σ_{exp}	σ_{th}	$\sigma_{\text{exp}}/\sigma_{\text{th}}$
^{12}C	$1p$	0.25	0.65	0.35	0.83	3.15	0.38
	$1s$	0.38	1.28	0.30	0.31	0.87	0.36
^{40}Ca	$1d_{5/2}$		0.03		0.29	2.62	0.11
	$2s_{1/2}$	1.41	7.24	0.19		0.86	
	$1d_{3/2}$	(0.28)	0.05		0.76	3.94	0.19
	$1p$	(0.65)			(0.93)		
	$1s$	(0.63)			(0.67)		

Cross-sections are given in units $10^{-28} \text{ (cm}^2/\text{MeV/sr)}$.Fig. 2. - $^{40}\text{Ca}(e, e'p)$, $E = 500 \text{ MeV}$, $T' = 86 \text{ MeV}$; a) $p = 25 \text{ MeV/c}$, b) $p = 100 \text{ MeV/c}$.

REACTION	RESULT	EXCITATION ENERGY	SOURCE		DETECTOR		ANGLE
			TYPE	RANGE	TYPE	RANGE	
E, E/	ABX	5-11	D	39, 56	MAG-D		180

4 LEVELS

TABLE I. Differential cross sections, spin and parity, transition radius, and radiation width for energy levels in ^{40}Ca and ^{42}Ca , including DWBA corrections.

Nucleus	Level energy (MeV)	$(d\sigma/d\Omega)_{56}$ (10^{-34} cm ² /sr)	$(d\sigma/d\Omega)_{39}$ (10^{-34} cm ² /sr)	J^π	R (fm)	Γ_0 (eV)
^{40}Ca	5.94 ± 0.07	34 ± 5	23 ± 12	$(1^-, 2^-)$		
	6.94 ± 0.07	38 ± 7	60 ± 19	(1^-)		
	8.43 ± 0.07	102 ± 12	119 ± 21	2^-	4.3 ± 0.5	$2.6^{+1.0}_{-0.9} \times 10^{-2}$
	10.34 ± 0.06	40 ± 13	120 ± 22	(1^+)	$3.5^{+0.4}_{-0.3}$	$7.0^{+1.1}_{-0.9}$
^{42}Ca	8.13 ± 0.07	38 ± 13	104 ± 31	1^+	$3.4^{+0.3}_{-0.2}$	$2.8^{+1.1}_{-0.8}$
	10.82 ± 0.07	48 ± 12	67 ± 37	1^+	$2.0^{+0.2}_{-0.1}$	$2.9^{+1.1}_{-0.8}$
				2^-	$5.0^{+0.2}_{-0.1}$	$7^{+1}_{-1} \times 10^{-2}$
	11.14 ± 0.07	54 ± 12	219 ± 46	1^+	3.9 ± 0.3	$18.9^{+1.1}_{-0.8}$
	11.82 ± 0.07	48 ± 13	123 ± 39	1^+	$3.4^{+0.3}_{-0.2}$	$9.7^{+1.1}_{-0.8}$

^a If the data and equations yield $R^2 < 0$, the lower limit of R is taken to be zero.

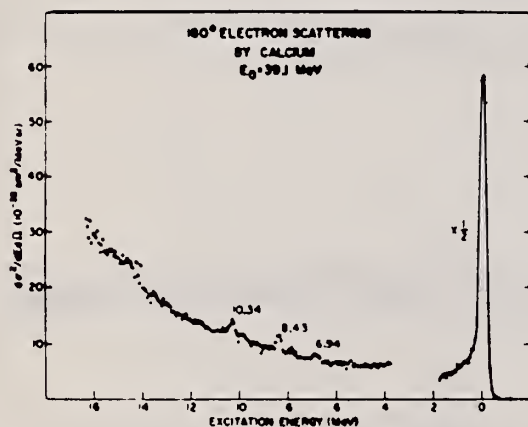


FIG. 1. Differential cross section for 180° scattering of 39.1-MeV electrons from calcium. The gap in the spectrum is present because a preliminary survey, as well as the 56-MeV data, showed no structure of interest in this region.

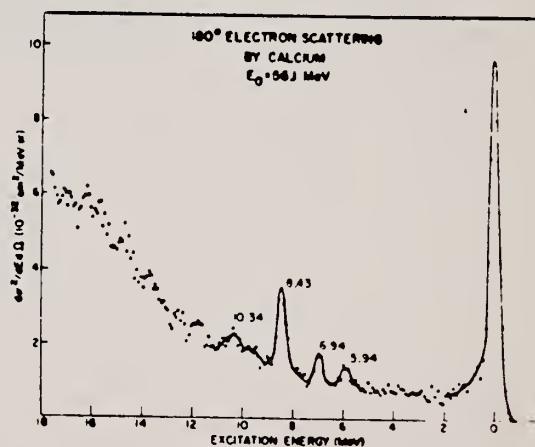


FIG. 2. Differential cross section for 180° scattering of 56.1-MeV electrons from calcium.

REF.

N.V. Goncharov, A.I. Derebchinskii, O.P. Konovalov, S.G. Tonapetyan,
and V.M. Khvorostyan
Yad. Fiz. 14, 31 (1971)
Sov. J. Nucl. Phys. 14, 18 (1972)

ELEM. SYM.

A

Z

Ca

40

20

METHOD

REF. NO.

71 Go 2

hmg

REACTION	RESULT	EXCITATION ENERGY	SOURCE		DETECTOR		ANGLE
			TYPE	RANGE	TYPE	RANGE	
G, PI+	RLY	150-500	C	500	CCH-D		DST

PI-/PI+ YIELD RATIO

Measurements are reported of the relative yield of π^+ mesons and the π^-/π^+ yield ratio for mesons with energy 40 ± 10 MeV emitted in the angular range $\theta_{lab} = 50-160^\circ$ in photon-induced reactions with $E_{max} = 500$ MeV with light and medium nuclei. The charged π -meson detector was a 34-cm Freon bubble chamber with a tube for the beam. The π^-/π^+ yield ratio for He^4 , Li^7 , C^{12} , Si^{28} , S^{32} , Ca^{40} , and Nb^{93} was found to be respectively 0.94 ± 0.14 , 2.15 ± 0.31 , 1.22 ± 0.21 , 1.25 ± 0.15 , 1.0 ± 0.13 , 1.11 ± 0.13 , and 1.53 ± 0.25 . It was established that the π^+ -meson yield follows a $ZA^{-1/3}$ law.

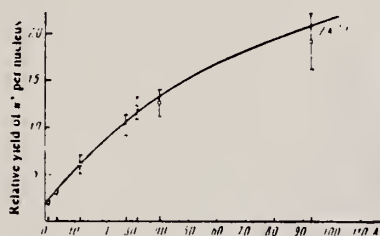


FIG. 2. Relative yield of π^+ mesons per nucleus as a function of mass number A.

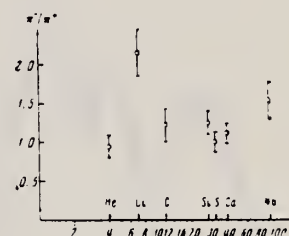


FIG. 3. π^-/π^+ yield ratio as a function of mass number A.



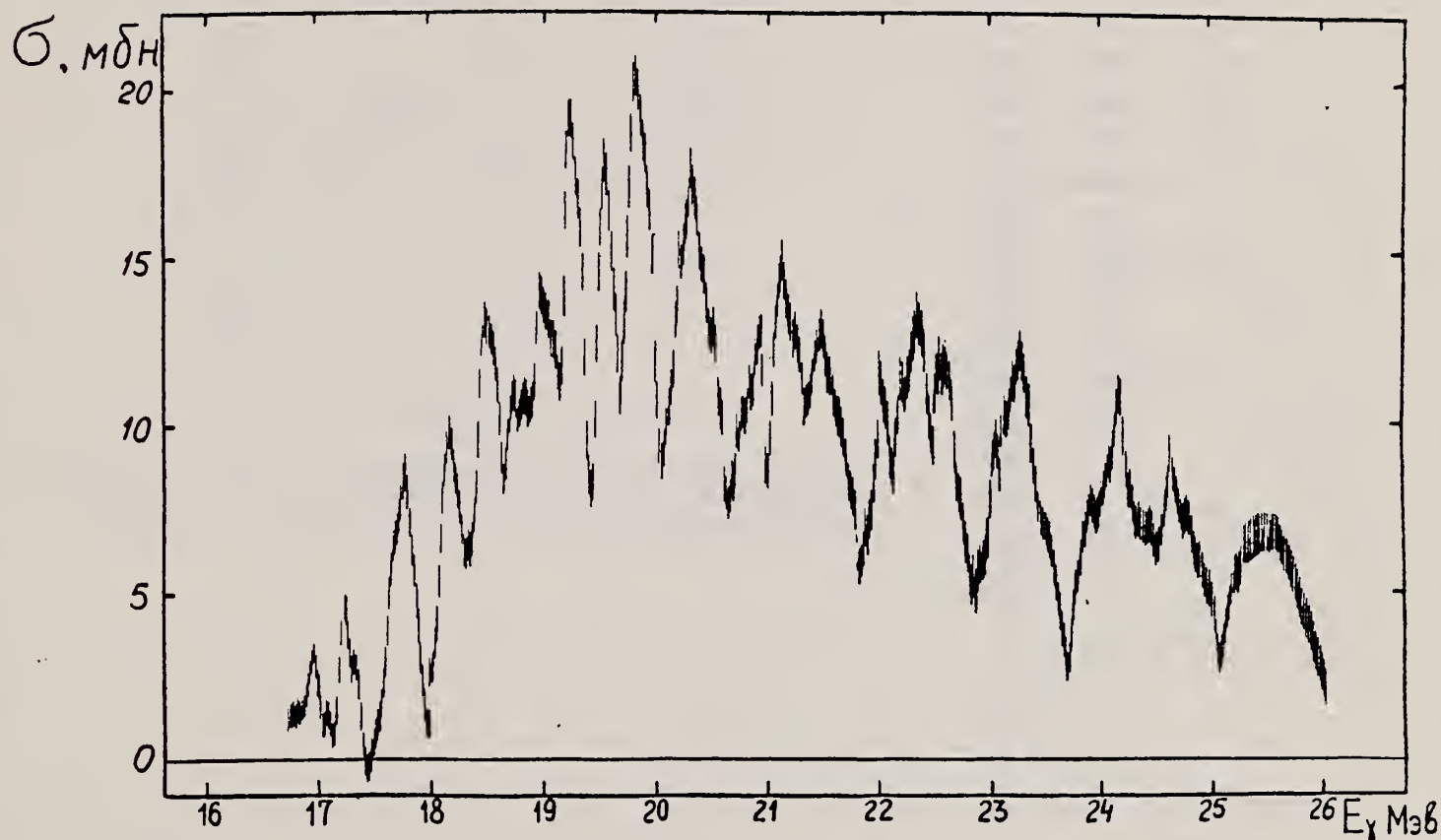
REF.

B.I. Goryachev, B.S. Ishkhanov, and V.G. Shevchenko
 Proceedings of the Second Symposium on the Problems
 of Nuclear Physics, Novosibirsk, USSR, June 1970
 (Kolybasov, V.M., Ed., Izdatel'stvo Nauka, Moscow 1971),
 pp. 362-78,

ELEM. SYM.	A	Z
Ca	40	20

REF. NO.	
71 Go 3	egf

METHOD					
REACTION	RESULT	EXCITATION ENERGY	SOURCE		ANGLE
			TYPE	RANGE	
G, XN	ABX	16- 26	C	16- 26	4PI



Фиг. 3. Сечение реакции $\text{Ca}^{40}(\gamma, n)$.

(over)

Т а б л и ц а 1

Энергии резонансов (Мэв)

C^{12}	O^{16}	Ca^{40}
20,0	16,9	18,9
20,4	17,3	17,2
20,7	17,9	17,8
21,1	18,4	18,2
21,4	18,9	18,5
21,9	19,3	18,8
22,4	19,5	19,0
22,9	20,3	19,3
23,3	20,9	19,8
23,7	21,3	19,9
	21,8	20,4
	22,2	21,0
	22,5	21,2
	22,9	21,5
	23,3	22,0
	23,8	22,4
	24,2	22,8
	24,6	23,3
		24,2
		24,6
		25,5

ELEM. SYM.	A	Z
Ca	40	20
REF. NO.		
71 He 1		egf

REACTION	RESULT	EXCITATION ENERGY	SOURCE		DETECTOR		ANGLE
			TYPE	RANGE	TYPE	RANGE	
E, E/	FMF	3-4	D	198-300	MAG-D		DST

3 LEVELS

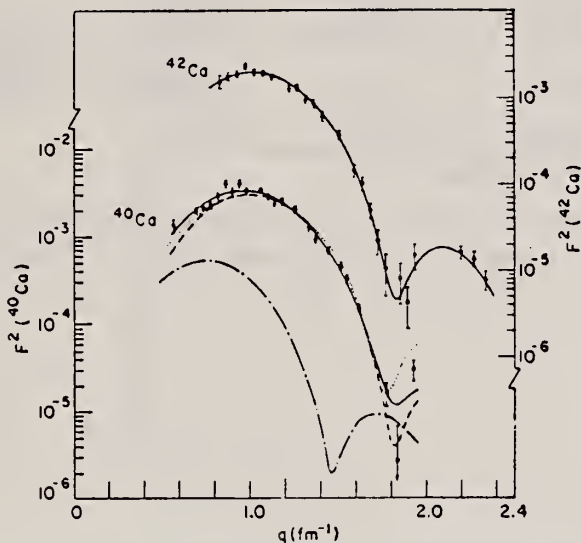


Fig. 3. Fits to ^{42}Ca and ^{40}Ca 3^- levels. Decomposition for ^{40}Ca into contributions of the 3.9 MeV 2^+ level (dash-dot curve) and the 3.75 MeV 3^- level (dashed curve). The solid curve gives the fit to the sum using shape (2), while the dotted curve gives the fit to the sum using shape (3).

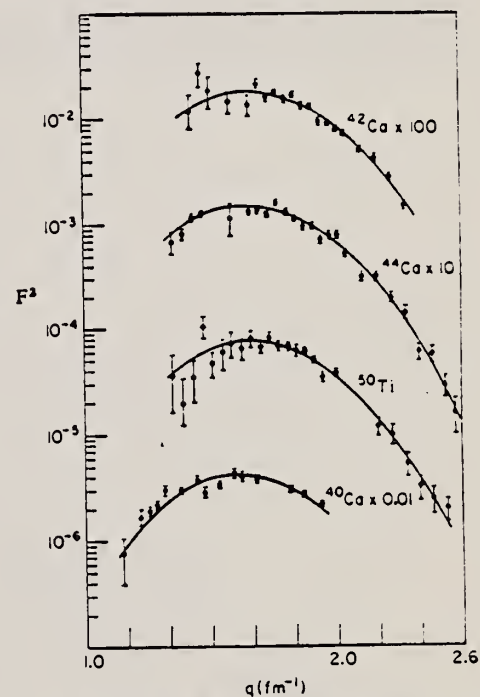


Fig. 7. Fits to ^{42}Ca , ^{40}Ca , ^{44}Ca and ^{50}Ti 5^- levels.

[over]

TABLE 3
Inelastic parameters

Isotope	E^* (MeV)	L	Shape	$c_{ir}^*)$ (fm)	$z_{ir}^*)$ (fm)	$G^*)$ (s.p.u.)	$R_{ir}^*)$ (fm)	$G(\text{s.p.u.})$ heavy-particle scattering ¹⁹⁾
⁴⁰ Ca	3.740	3	2	3.536 ± 0.030	1.483 ± 0.020	24.9 ± 1.0	4.835 ± 0.030	23.6 ± 3.5
	4.480	5	2	3.538 ± 0.050	1.260 ± 0.035	9.7 ± 0.6	4.810	17.7 ± 2.7
			3			17.7 ± 1.5	5.467 ± 0.060	11.3 ± 1.7
⁴² Ca	3.440	3	2	3.565 ± 0.018	1.383 ± 0.014	12.4 ± 0.5	4.719 ± 0.023	12.0 ± 1.8
	4.100	5	2	3.231 ± 0.030	1.404 ± 0.025	3.4 ± 0.3	4.816 ± 0.044	9.0 ± 1.4
⁴⁴ Ca	3.30	3	2	3.555 ± 0.018	1.313 ± 0.013	6.95 ± 0.28	4.618 ± 0.023	8.0 ± 1.2
	2.28	4	2	4.091 ± 0.030	1.268 ± 0.016	2.66 ± 0.15	5.135 ± 0.030	1.3 ± 0.3
	3.91	5	2	3.268 ± 0.030	1.397 ± 0.024	2.30 ± 0.20	4.832 ± 0.045	4.4 ± 0.7
⁴⁶ Ti	2.00	4	2	4.264 ± 0.021	1.229 ± 0.013	7.61 ± 0.30	5.226 ± 0.026	
⁴⁸ Ti	2.286	4	2	4.330 ± 0.021	1.196 ± 0.013	3.37 ± 0.15	5.237 ± 0.026	
⁵⁰ Ti	4.42	3	2	3.645 ± 0.017	1.244 ± 0.012	3.76 ± 0.15	4.600 ± 0.023	5.4 ± 0.8
								$5.9^{20)}$
	2.50	4	2	3.865 ± 0.017	1.347 ± 0.012	4.7 ± 0.15	5.064 ± 0.026	3.3 ± 0.7
	3.20	5	2	3.254 ± 0.032	1.345 ± 0.026	0.83 ± 0.08	4.724 ± 0.045	$2.7^{20)}$
Present experiment								

^{a)} Errors do not reflect any model dependence.

^{b)} Given errors do not include the 6% error of normalization.

¹⁹⁾ A. M. Bernstein, Adv. in Nucl. Phys. **3** (1969) 325.

METHOD

REF. NO.

71 Is 1

hmg

REACTION	RESULT	EXCITATION ENERGY	SOURCE		DETECTOR		ANGLE
			TYPE	RANGE	TYPE	RANGE	
G, XN	ABX	15-26	C	16-26	BF3-I		4PI

414

Data of present work			Data from other articles			
Location of resonances MeV	Integrated cross sections of resonances MeV-mb	Relative contributions to the integrated cross section of the (γ,n) reaction	[1] (γ,n)	[1] (γ,n)	[1] (γ,n)	[1] (γ,n)
16.9	0.71	0.009	15.9	16.1		17.2
17.2	0.72	0.009		17.2		16.2
17.8	2.32	0.029	17.9	17.9		
18.2	3.30	0.028				18.2
18.5	1.46	0.041	18.5	18.5		
18.8	2.79	0.034			18.7	18.7
19.0	1.01	0.037	19.2	19.1		19.0
19.3	4.14	0.051				19.4
19.6	1.79	0.047	19.6	19.6		
19.9	5.79	0.072	19.9	20.0	19.9	19.8
20.4	7.78	0.096				20.1
21.0	1.67	0.045	20.8	21.0	20.9	21.0
21.2	4.22	0.052				
21.5	4.40	0.059	(21.7)			
22.0	2.78	0.074		22.0	21.5	22
22.4	1.65	0.046	22.1			
22.8	1.17	0.040				
23.3	6.46	0.041		23.1	23.2	
24.2	1.40	0.072	24.1	(24.1)	24.4	
24.6	4.12	0.051				
25.5	1.92	0.061	(25.4)	25.5	25.0	
Σ	81		27.0	28.0		

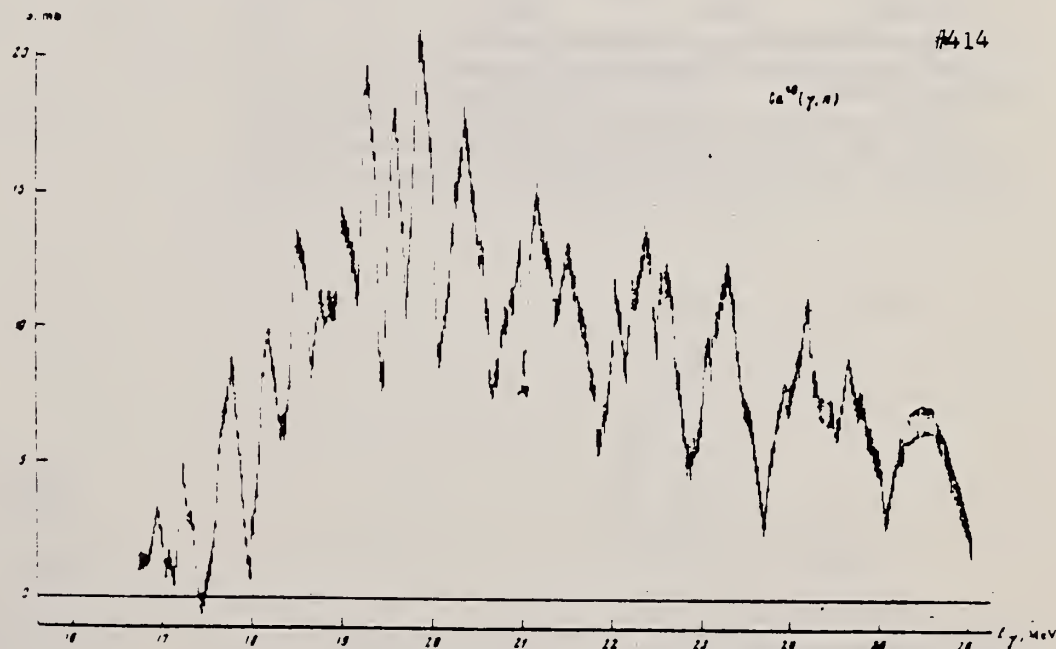


FIG. 1. Structure of the cross section for the reaction $\text{Ca}^{40}(\gamma, n)$.

E. J. Moniz, I. Sick, R. R. Whitney, J. R. Ficenec, R. G. Kephart
and W. P. Trower
Phys. Rev. Letters 26, 445 (1971)

Ca

40

20

REF. NO.

71 Mo 3

hmg

METHOD					
REACTION	RESULT	EXCITATION ENERGY	SOURCE		ANGLE
			TYPE	RANGE	
E, E/	ABX	0-240	D	500	60

Table I. Nuclear Fermi momentum k_F and average nucleon interaction energy $\bar{\epsilon}$ determined by least-squares fit of theory to quasielastic peak.

Nucleus	k_F (MeV/c) ^a	$\bar{\epsilon}$ (MeV) ^b
${}^3\text{Li}^6$	169	17
${}^6\text{C}^{12}$	221	25
${}^{12}\text{Mg}^{24}$	235	32
${}^{20}\text{Ca}^{40}$	251	28
${}^{28}\text{Ni}^{58.7}$	260	36
${}^{39}\text{Y}^{89}$	254	39
${}^{50}\text{Sn}^{118.7}$	260	42
${}^{73}\text{Tl}^{181}$	265	42
${}^{82}\text{Pb}^{208}$	265	44

^aThe fitting uncertainty in these numbers is approximately ± 5 MeV/c.

^bThe fitting uncertainty in these numbers is approximately ± 3 MeV. Simple estimates for $\bar{\epsilon}$ give numbers in reasonable agreement with those in the table.

METHOD

REF. NO.

71 Sh 5

egf

REACTION	RESULT	EXCITATION ENERGY	SOURCE		DETECTOR		ANGLE
			TYPE	RANGE	TYPE	RANGE	
G, P	SPC	12-25	C	18-26	EMU-D		DST

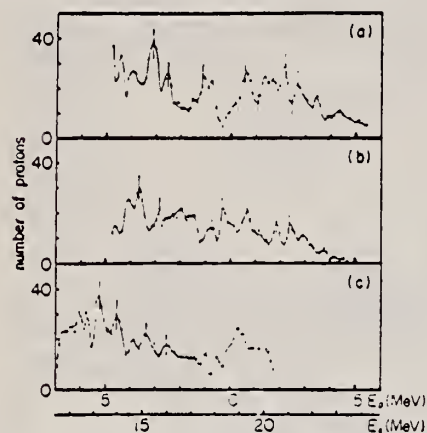


Fig. 5. Difference spectra between two distributions for the different irradiations: (a) 25.5 MeV-(23.0 MeV), (b) 23.0 MeV-(20.5 MeV) and (c) 20.5 MeV-(18.0 MeV).

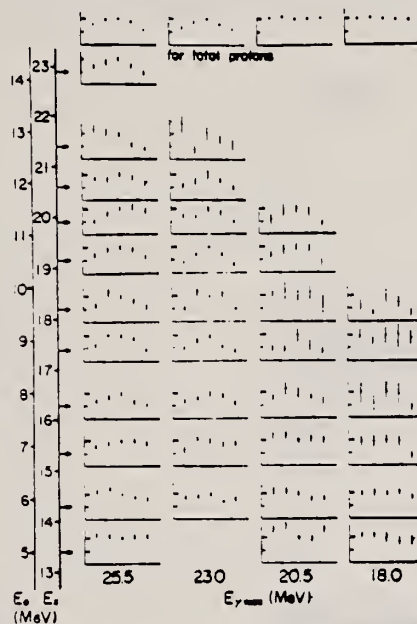


Fig. 3. Experimental angular distributions for each bremsstrahlung maximum energy of 25.5, 23.0, 20.5 and 18.0 MeV. The angular distributions for the total protons are shown at the top. Each distribution is measured at 30°, 60°, 90°, 120° and 150°.

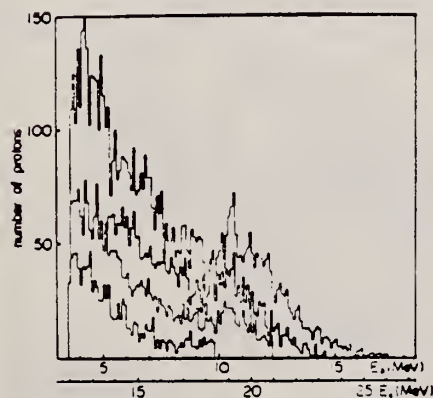


Fig. 1. Histograms of the photoproton energy distributions for the different bremsstrahlung energies of 25.5, 23.0, 20.5 and 18.0 MeV from the top respectively. The abscissa for E_x is excitation energy of ^{40}Ca supposing that all protons decay to the ground state of ^4He . This expression is same in case of Fig. 2, 3, 4 and 5

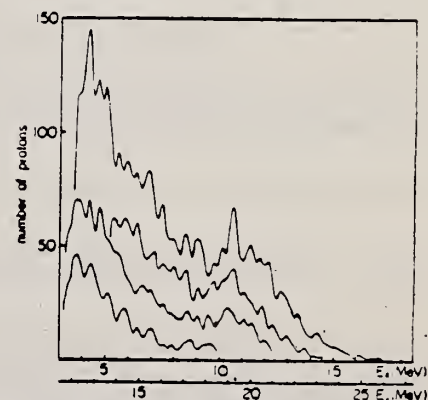


Fig. 2. Smoothed energy spectra of photoprotons from the $^{40}\text{Ca}(\gamma, p)^{39}\text{K}$ reaction with bremsstrahlung maximum energies of 25.5, 23.0, 20.5 and 18.0 MeV.

J. Ahrens, H. Borchert, H. B. Eppler, H. Gimm, H. Gundrum,
 REF. P. Riehn, G. Sita Ram, A. Zieger, M. Kroning, B. Ziegler
 Proc. International Conference on Nuclear Structure Studies
 Using Electron Scattering and Photoreaction, Sendai, Japan
 p. 213 (1972)

ELEM. SYM.	A	Z
Ca	40	20
REF. NO.		
72 Ah 7		egf

REACTION	RESULT	EXCITATION ENERGY	SOURCE		DETECTOR		ANGLE
			TYPE	RANGE	TYPE	RANGE	
G, MUT	ABX	10-140	C	140	MGC-D		4PI

597

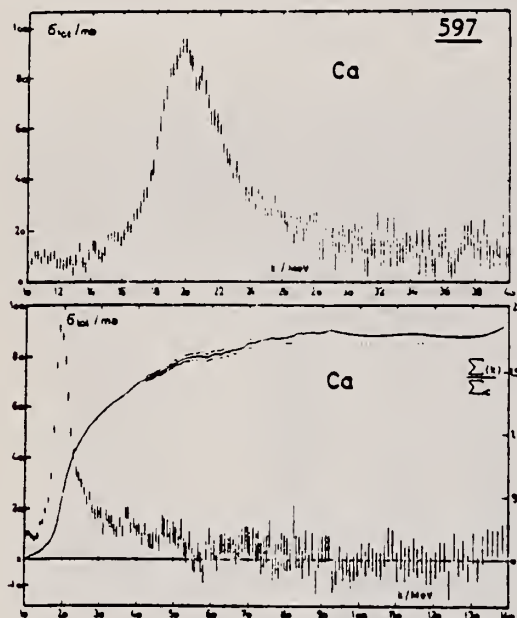
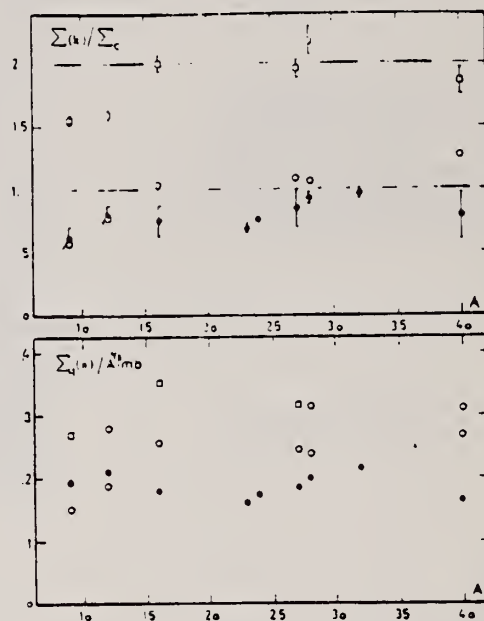


Fig.4-5 Total nuclear cross-sections for Ca



$$\Sigma_c = 60 \frac{\text{mb}}{\text{A}}, \quad \Sigma_1(k) = \int_0^k \delta(k') dk', \quad \Sigma_1(k) = \int_0^k \delta(k') dk'$$

• NBS k: 35 MeV, ○ k: 35 MeV, ○ k: 140 MeV

Fig.11 Integrated cross-sections

METHOD

REF. NO.

72 Br 11

egf

REACTION	RESULT	EXCITATION ENERGY	SOURCE		DETECTOR		ANGLE
			TYPE	RANGE	TYPE	RANGE	
G,P	ABX	12- 26	C	15- 25	SCD-D		90

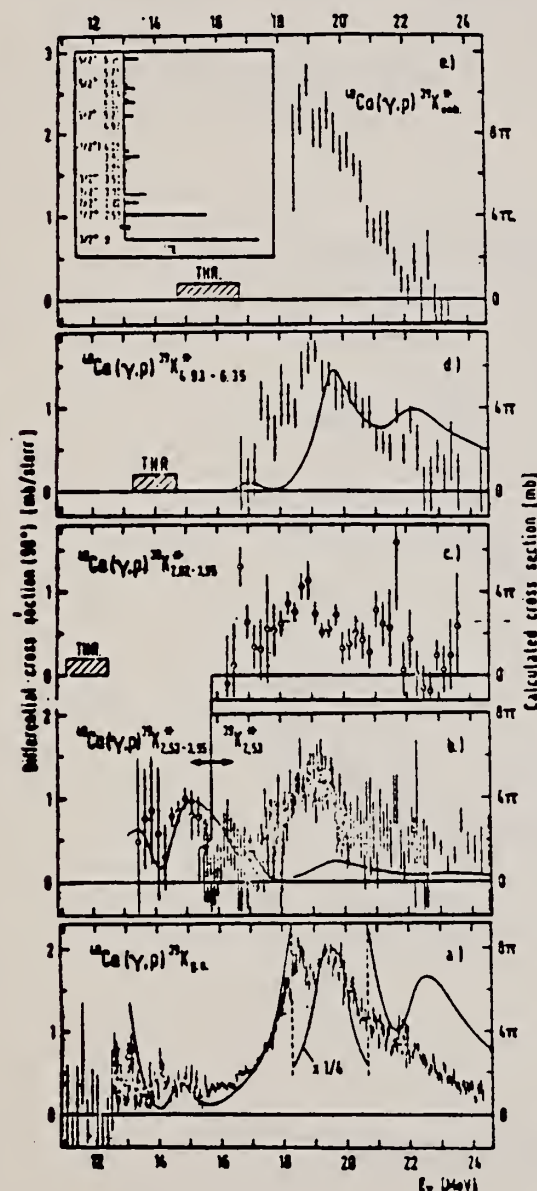


Fig. 1. Experimental points with error bars correspond to the 90° differential cross section of the present experiment, while solid curves show calculated cross sections integrated over angles. The absolute values of the cross sections are given by the scales on the left hand side for the experiment, and on the right hand side for the theory.

- The photoproton cross section (γ, p_0) to the ground state of ^{39}K compared to the calculated cross section for the $1d_{5/2}$ hole proton channel;
- The photoproton cross section to the first excited 2.53 MeV state compared to the calculated value for the $2s_{1/2}$ hole channel. At energies below 15.5 MeV the experimental cross section could not be resolved from the transitions to the states between 2.82 and 3.95 MeV;
- Experimental photoproton cross section to the states of ^{39}K between 2.82 and 3.95 MeV;
- The photoproton cross section to the ^{39}K states in the energy regional between 4.93 and 6.35 MeV compared to the calculated cross-section for the $1d_{5/2}$ proton hole channel;
- The cross section for the (γ, p) reaction, in which the residual nucleus ^{39}K is assumed to be left in the continuum states between 6.4 and 8.5 MeV. The insert shows schematically the population of different excited states of the residual nucleus ^{39}K in the photoproton reaction. It has been obtained independently by measuring the deexcitation gamma-rays resulting from bombardment of a ^{40}Ca target with bremsstrahlung gamma-rays of an end-energy of 30 MeV.



ELEM. SYM.	A	Z
Ca	40	20
REF. NO.		
72 Br 17		egf

REACTION	RESULT	EXCITATION ENERGY	SOURCE		DETECTOR		ANGLE
			TYPE	RANGE	TYPE	RANGE	
G,PG	SPC	11- 24	C	30	SCD-D		90
G,NG	SPC	18- 24	C	30	SCD-D		90
G,P	ABX	11- 24	C	12- 30	SCD-D		DST

Average value $(A_2/A_0) = -0.5$ for transition to
 2.53 MeV $1/2^+$ state in ^{39}K .

* G SPECTRUM

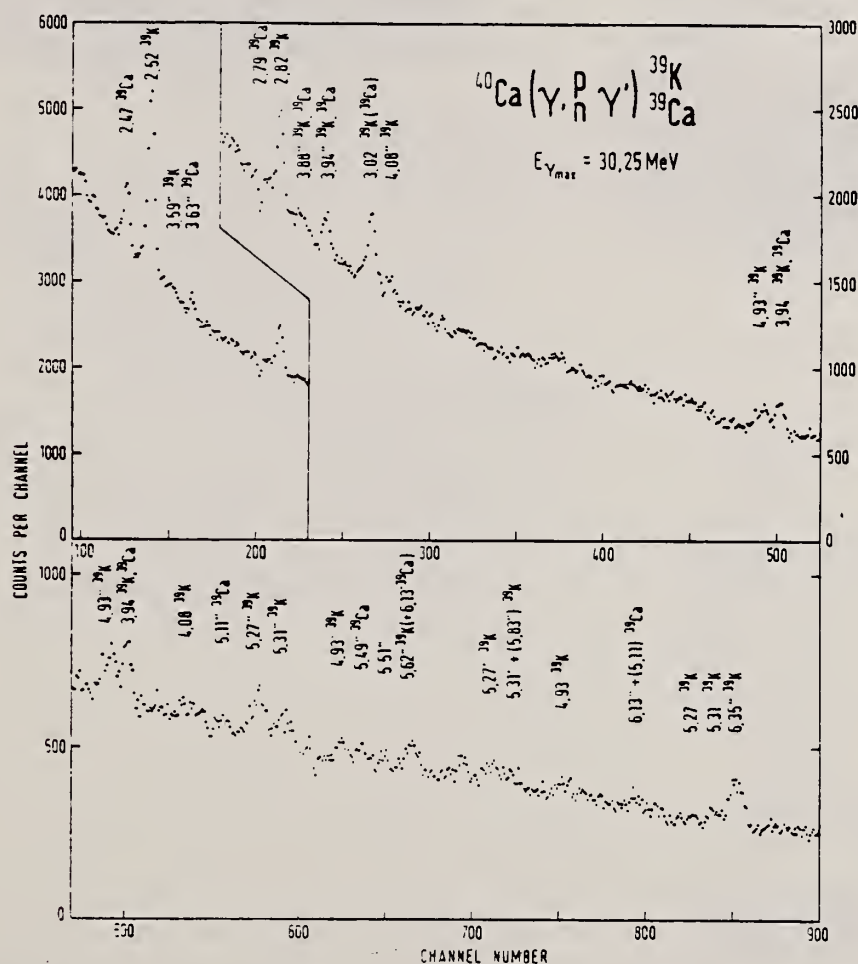


Fig. 4. The deexcitation gamma-ray spectrum obtained with a 570 g natural Ca target at a bremsstrahlung end-point energy 30.25 MeV. The gamma-lines belonging to deexcitations of ^{39}K and ^{39}Ca are indicated in the diagram.

(over)

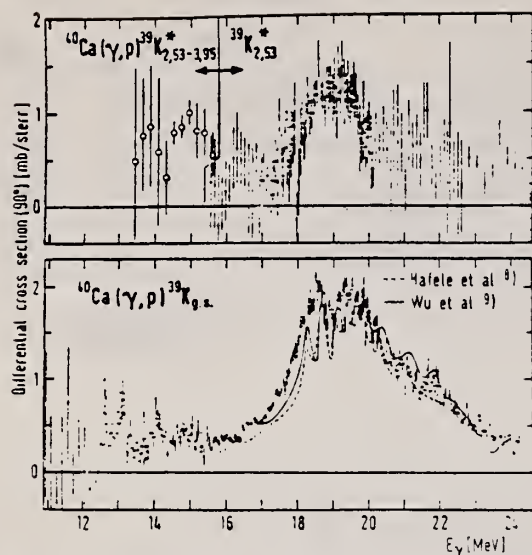


Fig. 5. Two examples of photoproton 90° differential cross sections resulting from the least-squares analysis of the $^{40}\text{Ca}(\gamma, p)^{39}\text{K}$ proton spectra. Present data for the cross section $\sigma(\gamma, p_0)$ to the ground state of ^{39}K (lower diagram) are compared with results from refs. 8 and 9. Below 15.5 MeV the cross section $\sigma(\gamma, p_1)$ to the first excited 2.53 MeV state of ^{39}K (upper diagram) could not be accurately separated from contributions to levels between 2.82 and 3.95 MeV.

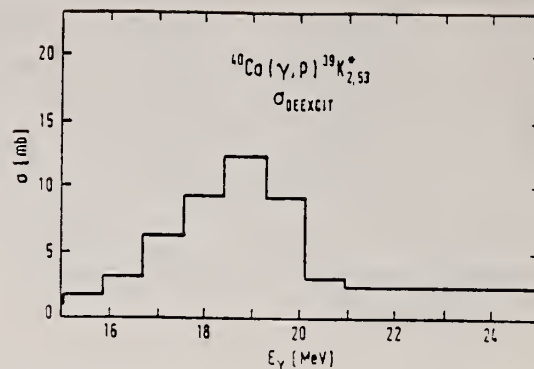


Fig. 6. The cross section integrated over angles for the reaction $^{40}\text{Ca}(\gamma, p_1 \gamma)^{39}\text{K}$. The result was obtained by the matrix inversion method of Penfold and Leiss applied to the yields of the 2.53 MeV deexcitation gamma-line (see fig. 4). Typical errors are ± 2.5 mb.

REF. D. Hiramatsu, T. Kamae, H. Hiramatsu, K. Nakamura, N. Izutsu,
and Y. Watase
PICNS-72, p.429 Sendai (See 73H15)

ELEM. SYM.	A	Z
Ca	40	20

REF. NO.	hvm
72 H1 8	

REACTION	RESULT	EXCITATION ENERGY	SOURCE		DETECTOR		ANGLE
			TYPE	RANGE	TYPE	RANGE	
E,E/P	ABX	0*100	D	700	MAG-D		DST

*SEP ENERGY RANGE

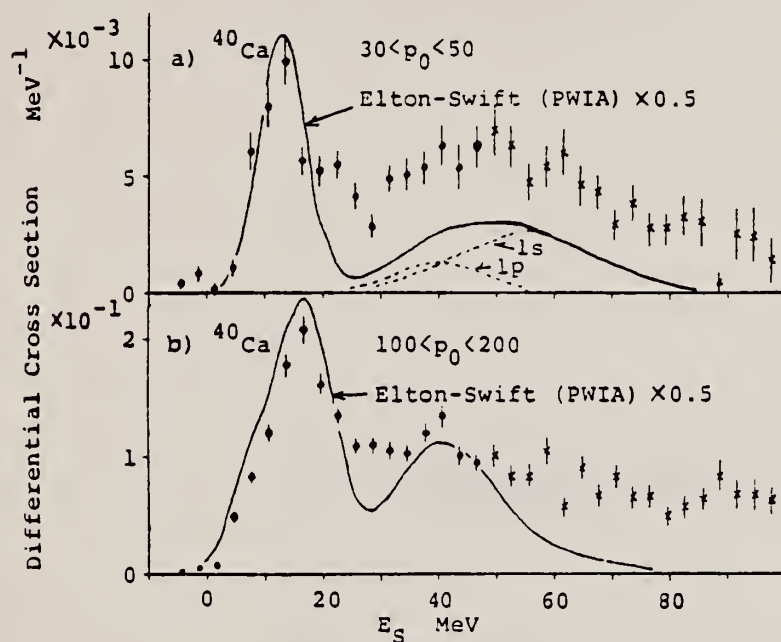


Fig. 5. Separation energy spectra for ^{40}Ca

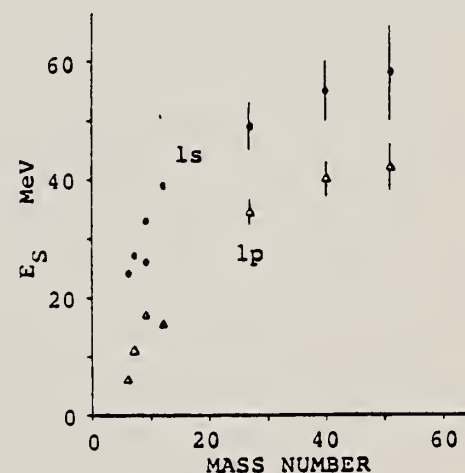


Fig. 6. The separation energy of $1s$ and $1p$ states as a function of the mass number.



REF. J. Ahrens, H.B. Eppler, H. Gimm, H. Gundrum, M. Kroning,
P. Riehn, G. SitaRam, A. Zieger, and B. Ziegler
PICNS-73, Vol.I, p.23 Asilomar

ELEM. SYM.	A	Z
Ca	40	20
REF. NO.		
73 Ah 4		img

METHOD					
REACTION	RESULT	EXCITATION ENERGY	SOURCE		ANGLE
			TYPE	RANGE	
G,MU-T	ABX	10-140	C	140	4PI

Statistics may have been improved over those of 72Ah7.

See figure on other side.

(OVER)

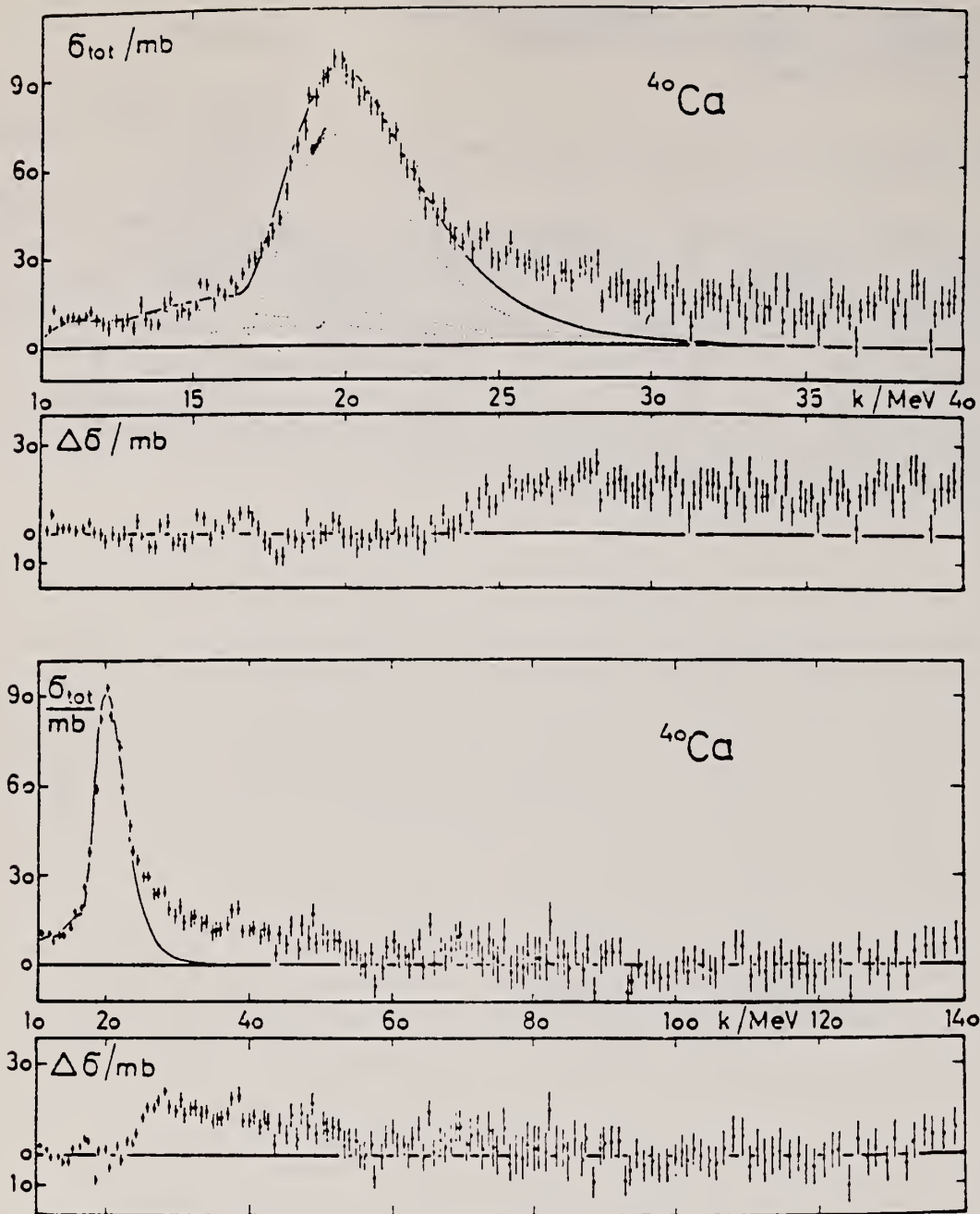


Fig. 3. Same as Fig. 2 for Ca.

REF. R. Bergere, H. Beil, P. Carlos, A. Lepretre, A. Veyssiére
PICNS-73, Vol. I, p. 525 Asilomar

ELEM. SYM.	A	Z
Ca	40	20
REF. NO.		
73 Be 10		hmg

METHOD					
REACTION	RESULT	EXCITATION ENERGY	SOURCE		ANGLE
			TYPE	RANGE	
G,N	ABX	12- 31	D	12- 31	4PI

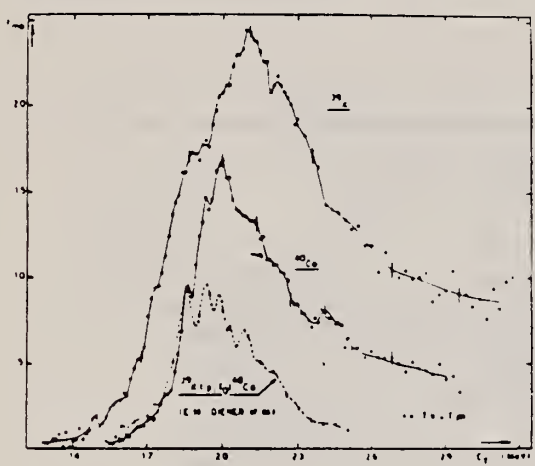


Fig. 8 Comparison of the photoneutron cross-sections of ^{39}K and ^{40}Ca with $^{39}\text{K}(p,\gamma_0)^{40}\text{Ca}$ measured by Diener.¹⁰

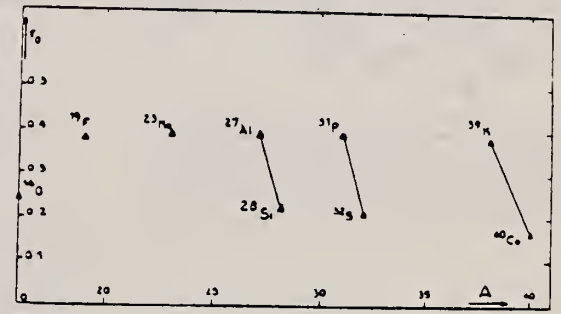


Fig. 13 Integrated photoneutron cross-sections for s-d shell nuclei.

REF. D. Brajnik, D. Jamnik, G. Kernel, U. Miklavzic, and
A. Stanovnik
PICNS-73, Vol. I, p. 537 Asilomar

ELEM. SYM.	A	Z
Ca	40	20
REF. NO.		
73 Br 13		hmg

METHOD						REF. NO.	
						73 Br 13	hmg
REACTION	RESULT	EXCITATION ENERGY	SOURCE		DETECTOR		ANGLE
			TYPE	RANGE	TYPE	RANGE	
G, P	ABX	13- 25	C	15- 25	SCD-D		DST
G, PG*	NOX	16- 31	C	31	SCD-D		DST

DEEXCITATION GAMMAS

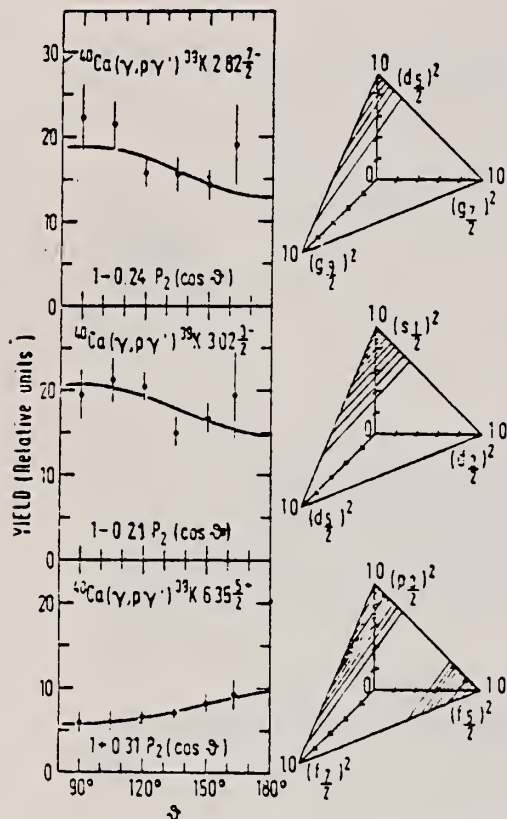


Fig. 2. Examples of angular distributions of deexcitation gamma rays, and corresponding phase space diagrams for possible configurations of reaction channels. The solid lines as the linear phase space diagrams represent extreme expectation values. Experimental errors are denoted by shaded areas. The sum of squared amplitudes is normalized to 1.

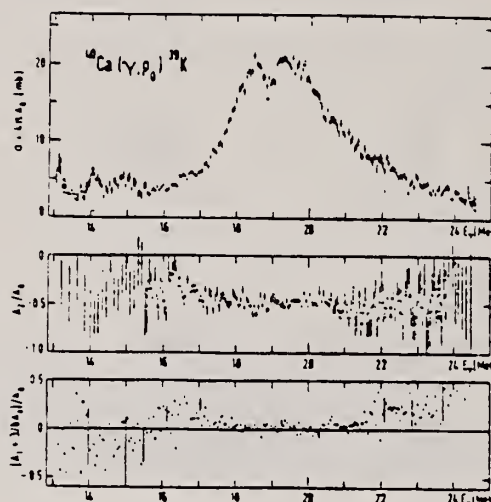


Fig. 1. $^{40}\text{Ca}(\gamma, p_0)^{39}\text{K}$ cross section $\sigma(\gamma, p_0)$, and the angular distribution coefficients from the series $W(\theta) = \sum_{\lambda=0}^{\infty} A_{\lambda} P_{\lambda}(\cos \theta)$.

Table 1

The Legendre polynomial coefficients A_{λ}/A_0 from angular distributions of deexcitation gamma rays

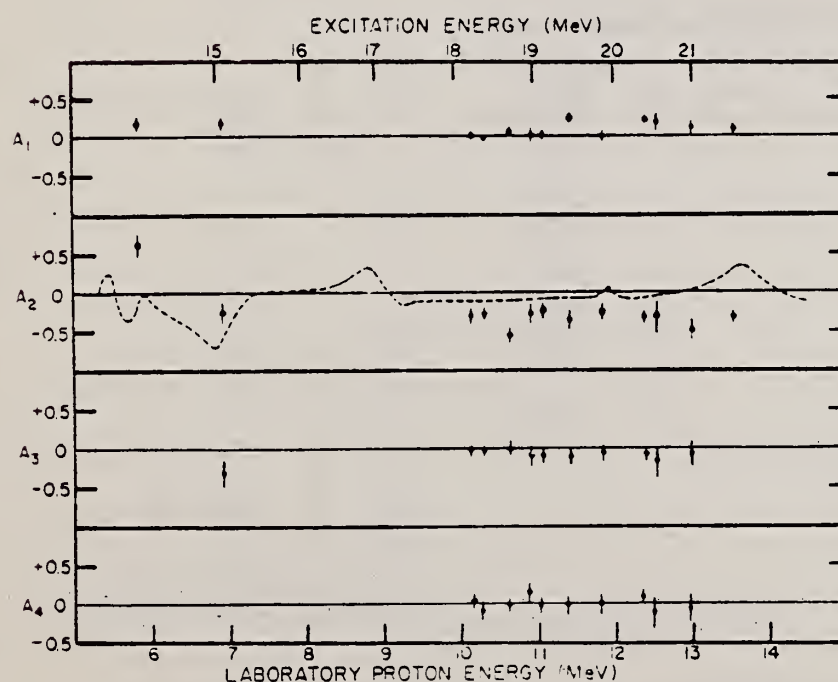
Energy of the intermediate state (MeV)	J^{π}	$\frac{A_2}{A_0}$
2.52	$\frac{1}{2}^{+}$	-0.04 ± 0.07
2.87	$\frac{3}{2}^{+}$	0.04 ± 0.13
2.82	$\frac{3}{2}^{+}$	-0.24 ± 0.14
3.02	$\frac{3}{2}^{+}$	-0.21 ± 0.12
3.94	$\frac{3}{2}^{+}$	-0.21 ± 0.30
4.93	$\frac{7}{2}^{+}$	-0.13 ± 0.15
5.27	$\frac{3}{2}^{+}$	0.23 ± 0.17
5.62	$\frac{3}{2}^{+}$	0.19 ± 0.30
6.35	$\frac{3}{2}^{+}$	0.31 ± 0.15

			Ca	40	20
METHOD			REF. NO.		
			73 D1 1		hmg
REACTION	RESULT	EXCITATION ENERGY	SOURCE		ANGLE
			TYPE	RANGE	
P,G	ABX	14- 26	D	6- 18	NAI-D

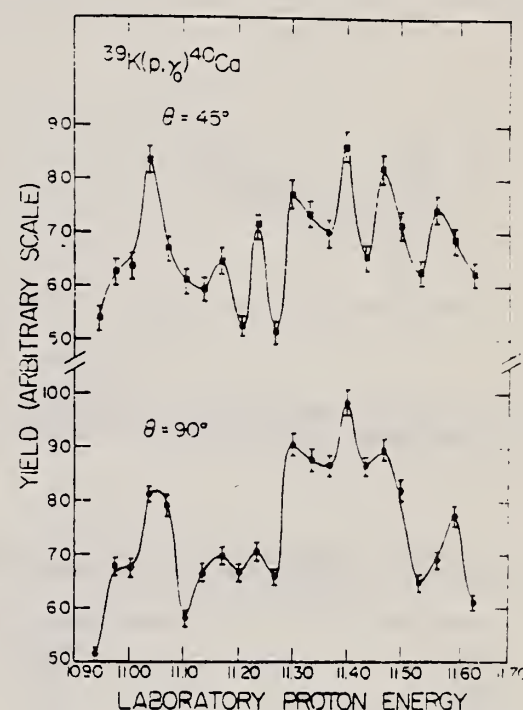
587

TABLE II. Resonance parameters for giant-dipole-resonance peaks in ^{40}Ca .

	Lower peak	Upper peak
$\sigma_0(\gamma, p_\gamma)$ (mb/sr)	1.95 ± 0.1	0.35 ± 0.25
Γ (MeV)	3.1 ± 0.2	3.2 ± 0.5
E_x (MeV)	19.3 ± 0.1	22.0 ± 0.5
% of dipole strength	94 ± 10	15 ± 12

FIG. 4. Plot of Legendre polynomial coefficients A_1 to A_4 determined from $^{39}\text{K}(p, \gamma_0)^{40}\text{Ca}$ angular distribution as a function of bombarding energy. The dashed curve results from the coupled-channel calculation of Ref. 4.

$$W(\theta) = 1 + \sum_{l=1}^4 A_l P_l(\cos\theta)$$

FIG. 3. Comparison of the γ_0 yield function observed at 45° (top) and 90° (bottom) over a segment of the GDR in ^{40}Ca .

(over)

M. Marangoni and A.M. Saruis,
Nucl. Phys. A132, 649 (1969). 431DEPARTMENT OF COMMERCE
NATIONAL BUREAU OF STANDARDS

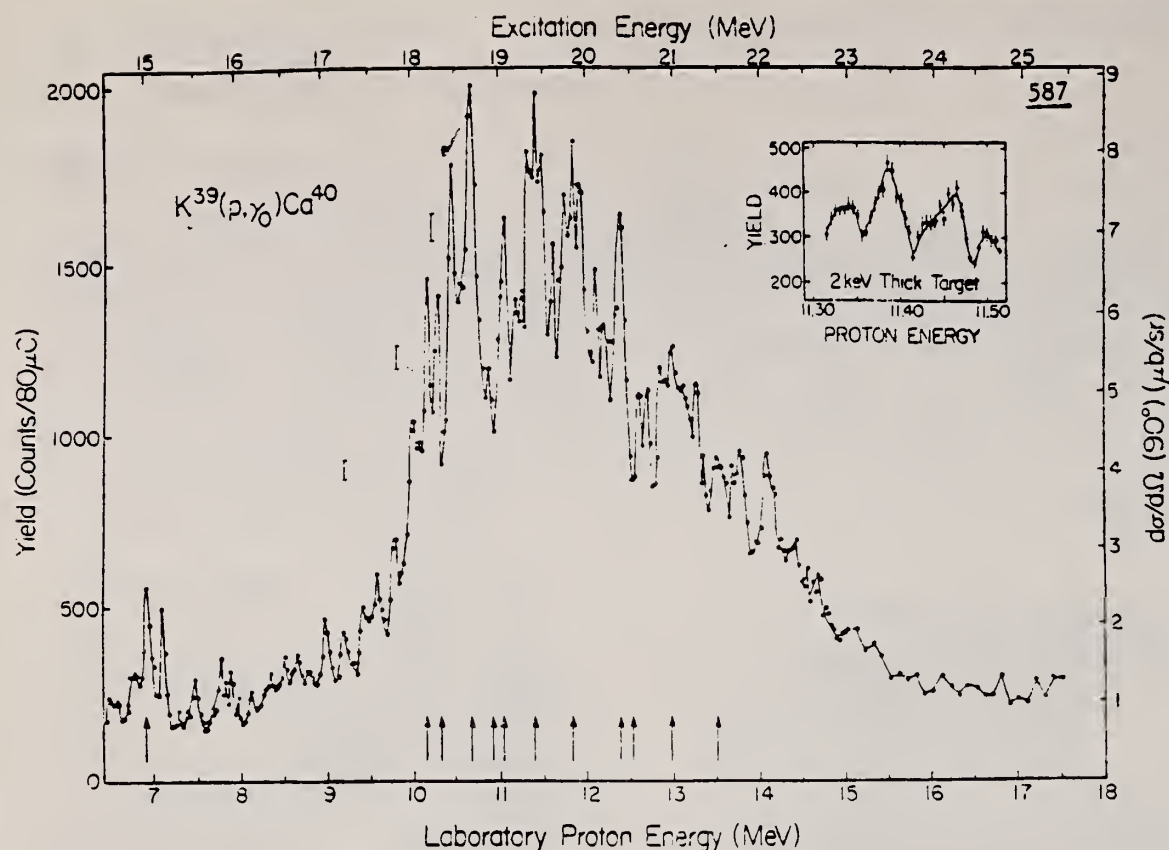


FIG. 2. Excitation function (mostly in 20-keV steps) of the γ , yield at 90° over the GDR regions of ^{40}Ca . Complete angular distributions were taken at energies indicated by arrows. The insert shows the portion from 11.30 to 11.56 MeV taken in 2-keV steps.

TABLE I. Excitation energies (in MeV) of intermediate structure peaks observed in ^{40}Ca .

Present work	$^{39}\text{K}(p, \gamma)^{40}\text{Ca}$ Hafele, Birgham, and Allen (Ref. 5)	$^{40}\text{Ca}(\gamma, p)^{39}\text{K}$ Wu <i>et al.</i> (Ref. 6)
18.25	18.2	18.20
18.68	18.7	18.70
19.07	19.0	19.05
19.45	19.4	19.35
		19.60
19.85	19.8	19.90
20.13 (weak)		
20.43	20.3	20.35
20.65		20.55
20.94 (broad)	21.0	21.20
21.49		
21.69		21.30
22.05	22.0	

ELEM. SYM.	A	Z
Ca	40	20
REF. NO.		
73 Do 9		egf

REACTION	RESULT	EXCITATION ENERGY	SOURCE		DETECTOR		ANGLE
			TYPE	RANGE	TYPE	RANGE	
G,XP	ABY	88-400	C	400	TEL-D		DST

Table 7. Calcium. Bremsstrahlung endpoint energy: 400 MeV. Differential cross-sections in microbarns/sterrad · MeV · eq. quantum. Quoted errors: statistical in percent

Energy	Angle							
	22	30	40	50	60	74	90	110
82.4	10.1 2.5	9.16 2.0	7.98 1.8	6.57 2.0	5.34 2.0	4.30 2.0	3.50 2.0	2.74 2.1
100.3	8.01 3.1	7.08 2.5	5.94 2.3	4.42 2.6	4.05 2.5	3.29 2.5	2.47 2.6	1.76 2.8
104.9	7.08 2.7	6.53 2.1	5.06 3.4	4.11 2.0	3.63 2.4	2.92 2.3	2.12 2.5	1.69 3.1
107.0		5.96 2.5	4.88 2.3					
109.9				4.33 2.2				
117.2	5.11 4.8	4.95 4.2	4.12 4.0	3.37 4.2	2.63 4.3	2.01 4.4	1.65 4.4	1.09 4.6
127.7	5.07 3.4	4.35 2.7	3.43 4.4	2.99 2.0	2.31 3.2	1.78 3.1	1.38 3.2	1.02 4.2
129.5		3.98 3.3	3.28 3.0					
132.0				2.91 2.9				
148.9	3.28 4.3	2.64 3.6	2.38 5.4	2.00 3.1	1.47 4.1	1.16 4.0	0.750 4.4	0.459 6.4
150.7		2.43 4.3	2.17 3.8					
152.9				1.82 3.7				
170.0	2.38 3.8	2.08 2.6	1.71 2.5	1.36 2.8	1.13 2.8	0.791 3.5	0.444 4.6	
187.0	1.37 5.2	1.47 3.2	1.21 3.2	1.05 3.4	0.780 3.6	0.476 4.7	0.253 6.4	
203.8	1.01 6.0	1.06 3.7	0.889 3.7	0.595 4.4	0.467 4.6	0.259 6.3	0.130 8.8	
222.6	0.993 5.7	0.778 4.8	0.638 4.9	0.537 6.1				
238.9	0.600 7.2	0.554 5.9	0.417 6.3	0.360 7.9				
255.3	0.337 9.5	0.369 7.2	0.259 7.9	0.144 12.2				

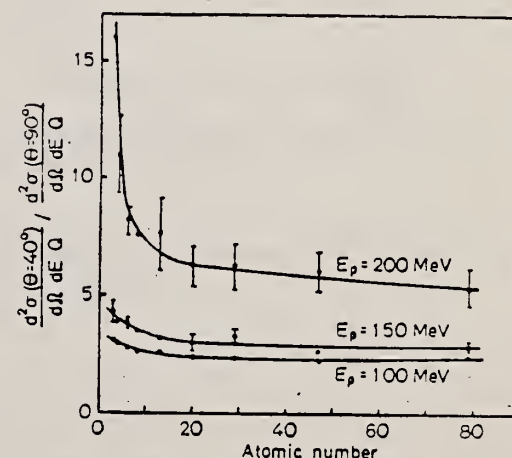


Fig. 6. The ratios of the experimental cross-sections at 40 and 90 degrees for selected proton energies as a function of atomic number

(over)

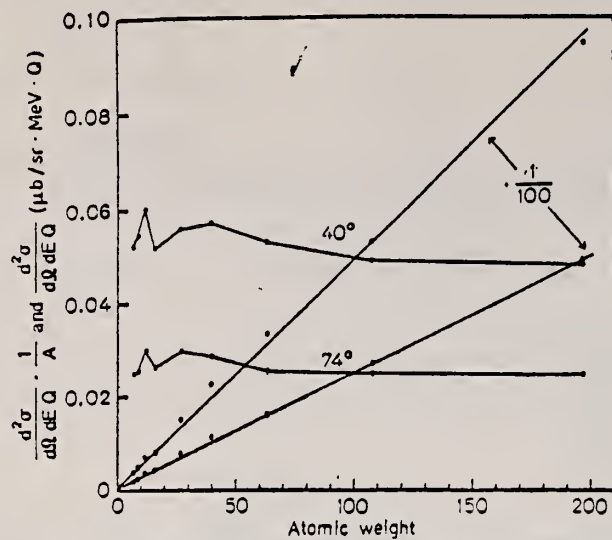


Fig. 9. In this figure, the straight lines show the experimental cross-sections at 40° and 74° for $E_p = 150$ MeV. The other curves are the same cross-sections divided by atomic weight

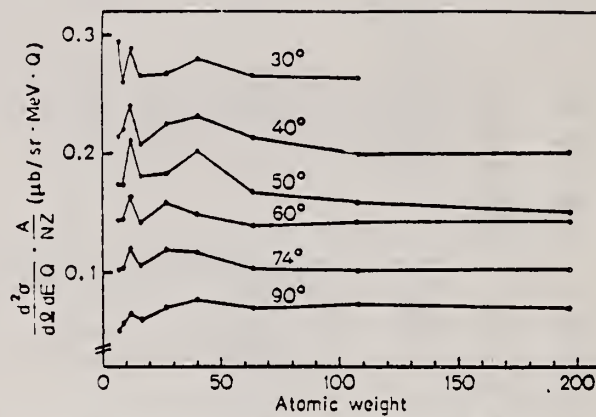


Fig. 8. Experimental cross-sections at various angles for $E_p = 150$ MeV divided by NZ/A plotted as a function of atomic weight

N.V. Goncharov, A.I. Derebchinskii, O.G. Konovalov,
S.G. Tonapetyan, and V.M. Khvorostyan
Yad. Fiz. 17, 242 (1973)
Sov. J. Nucl. Phys. 17, 124 (1973)

ELEM. SYM.	A	Z
Ca	40	20
REF. NO.		
73 Go 5		hmg

REACTION	RESULT	EXCITATION ENERGY	SOURCE		DETECTOR		ANGLE
			TYPE	RANGE	TYPE	RANGE	
G,PI+	ABY	170-400	C	400	BBL-D		90
G,PI-	ABY	170-400	C	400	BBL-D		90
G,P	ABY	80-400	C	400	BBL-D		90

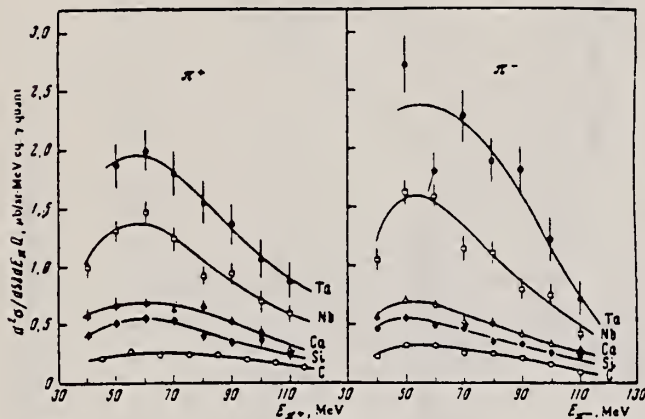


FIG. 2. Energy spectra of π^+ and π^- mesons, $E_{\gamma}^{\max} = 400$ MeV, $\theta_{\text{lab}} = (90 \pm 7)^\circ$.

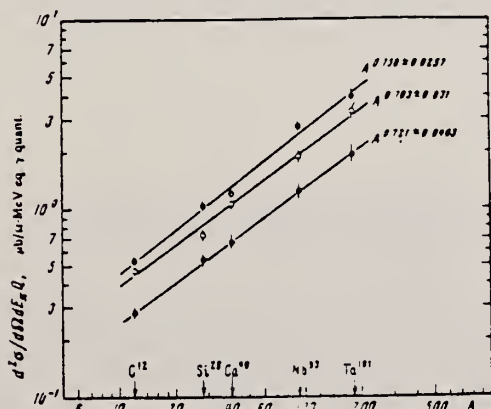


FIG. 4. Charged pion yield vs. the mass number of the nucleus: \bullet — $E_{\pi} = 105 \pm 10$ MeV, \circ — $E_{\pi} = 85 \pm 10$ MeV, \bullet — $E_{\pi} = 65 \pm 10$ MeV.

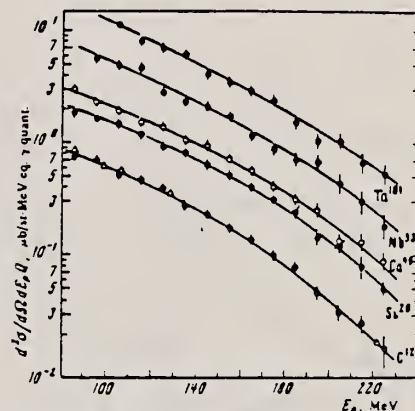


FIG. 3. Energy spectra of protons, $E_{\gamma}^{\max} = 400$ MeV, $\theta_{\text{lab}} = (90 \pm 7)^\circ$. Circles—present data, triangles—from [18].

¹⁸P. Dougan, W. Stiefler, LUSY Preprint, 1001-1003, 1970.

(over)

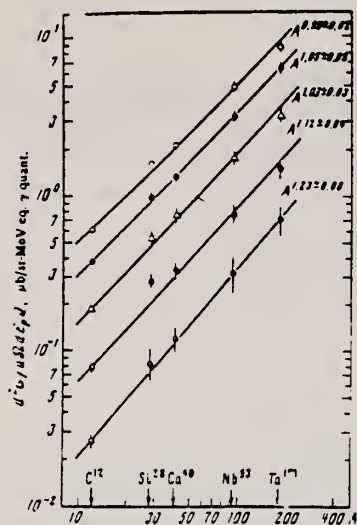


FIG. 5. Proton yields vs. mass number of the nucleus: \circ — $E_p = 100 \pm 10$ MeV, \bullet — $E_p = 125 \pm 15$ MeV, Δ — $E_p = 155 \pm 15$ MeV, \bullet — $E_p = 185 \pm 15$ MeV, \circ — $E_p = 215 \pm 15$ MeV.

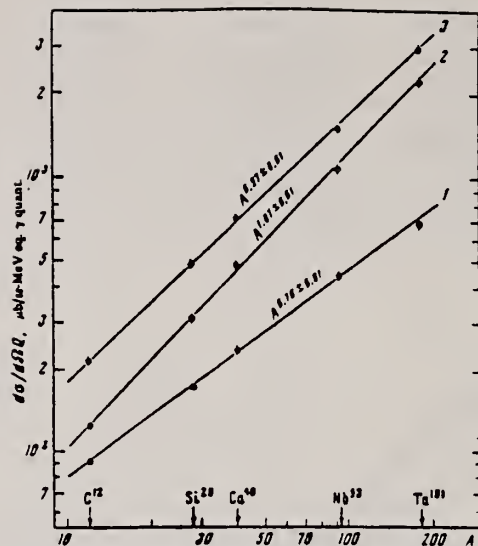


FIG. 6. Pion yield (1), proton yield (2), and summary pion and proton yield (3) vs. the mass number of the nucleus.

METHOD					REF. NO.		egf
					73 Gr 4		
REACTION	RESULT	EXCITATION ENERGY	SOURCE		DETECTOR		ANGLE
			TYPE	RANGE	TYPE	RANGE	
G.PI+	ABX	140-340	C	340	EMU -D		DST
G.PI-	ABX	140-340	C	340	EMU -D		DST

PI+, PI- RATIO

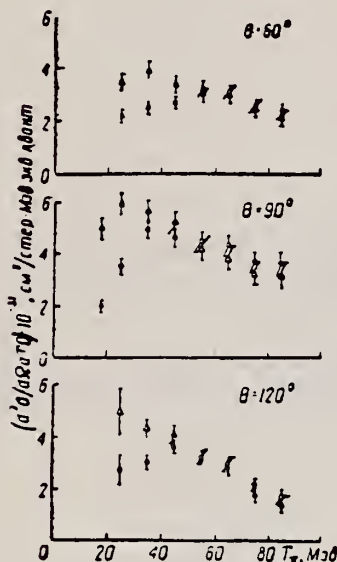
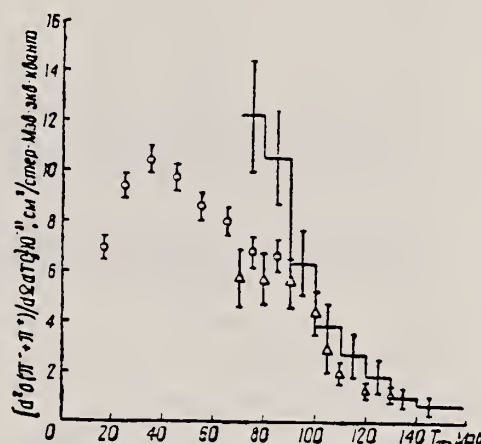


Рис. 1. $E = 340$ Мэв, кружочки — π^+ -мезоны, треугольники — π^- -мезоны.

Рис. 2. $E_0 = 340$ Мэв, $\theta = 90^\circ$, кружочки — данные настоящей работы, треугольники — данные работы [2], ступенчатая линия — расчет работы [6].



4113 CHARGED PION PHOTOPRODUCTION ON ^{40}Ca NUCLEUS AT BREMSSTRAHLUNG MAXIMAL ENERGY 340 MeV. Grishaev, I. A.; Krinitsyn, A. N.; Lapin, N. I.; Nikiforov, V. I.; Pugachev, G. D.; Shramenko, B. I. (Physical-Technical Inst., Kharkov). Ukr. Fiz. Zh. (Russ. Ed.); 18: No. 3, 445-450 (Mar 1973). (In Russian).

Differential cross sections of charged pion photoproduction on ^{40}Ca nucleus are measured at the bremsstrahlung maximal energy $E_0 = 340$ MeV. π^+ - and π^- -mesons with kinetic energies from 20 to 90 MeV were registered using photoemulsions under 60° , 90° , and 120° angles. The π^-/π^+ ratio for kinetic energies from 25 to 85 MeV are found to decrease from 1.53 ± 0.3 to 0.9 ± 0.24 , from 1.69 to 0.88 ± 0.26 from 1.82 ± 0.71 to 0.61 ± 0.3 , for the 60° , 90° and 120° angles respectively. The experimental results are in agreement with volume production of charged mesons on nuclei. The equation for the calculation of the π^-/π^+ ratio is found. (auth)

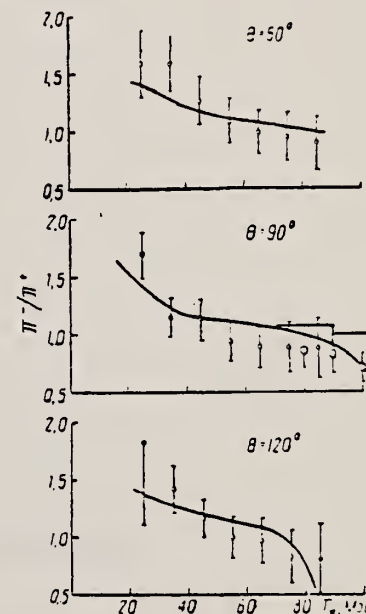
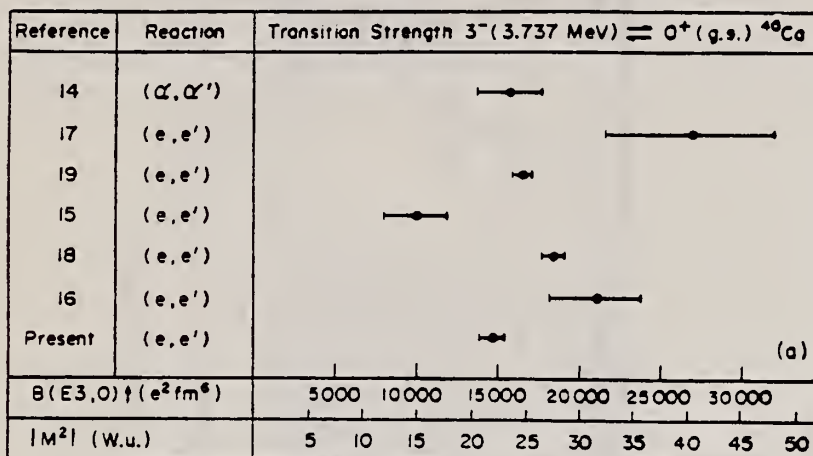


Рис. 3. Сплошная кривая — расчет по формуле (4), ступенчатая — расчет работы [6].



ELEM. SYM.	A	Z
Ca	40	20
REF. NO.		hmg
73 Ha 1		

REACTION	RESULT	EXCITATION ENERGY	SOURCE		DETECTOR		ANGLE
			TYPE	RANGE	TYPE	RANGE	
E, E/	FMF	3- 4	D	61-121	MAG-D		DST



LEVELS 3.74, 3.90 MEV

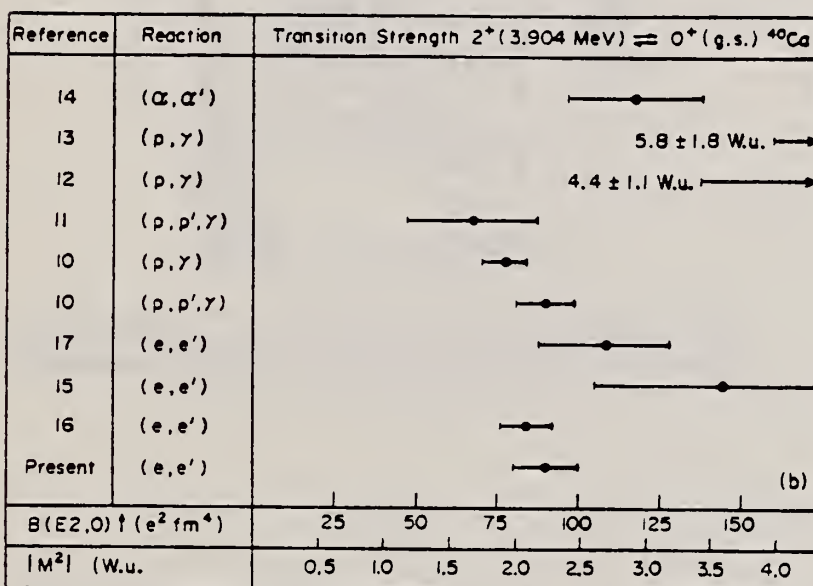


FIG. 6. Comparison of transition strengths for ^{40}Ca levels as derived by various workers. (a) 3^- (3.737-MeV) level.
 (b) 2^+ (3.904-MeV) level.

TABLE V. Transition charge parameters for ^{40}Ca .

Level	$B(EL, 0) \uparrow (e^2 \text{ fm}^{2L})$	$ M^2 \text{ (W.u.)}$	$c_\alpha \text{ (fm)}$	$z_\alpha \text{ (fm)}$	$\langle r^2_\alpha \rangle^{1/2} \text{ (fm)}$	Reference
3^- (3.737)	14870 ± 660	22.4 ± 1.0	3.534	0.430	4.50 ± 0.10	Present work
	21100 ± 2700	31.7 ± 4.0	3.712	0.524	5.68	16
2^+ (3.904)	90.2 ± 10.0	2.22 ± 0.24	3.916	0.417	4.67 ± 0.30	Present work
	84.0 ± 8.4	2.00 ± 0.20	3.212	0.457	4.38	16

(over)

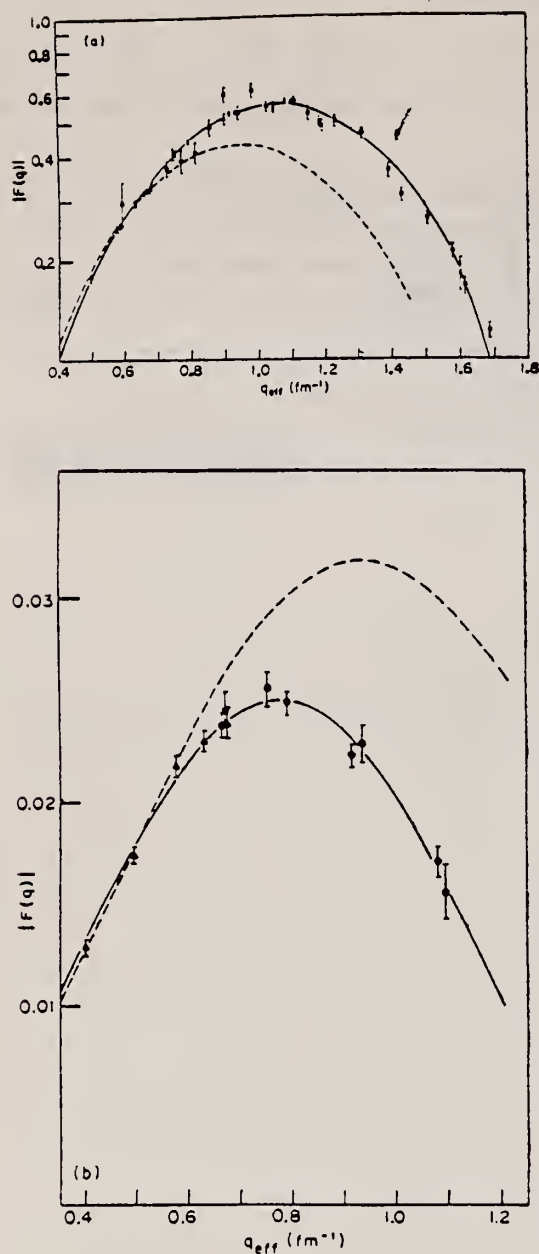


FIG. 5. Phase-shift calculation of the inelastic electron scattering form factors for ^{40}Ca using a Fermi charge distribution (model 3). (a) 3^- (3.737-MeV) level. Solid curve: Best fit form factors based on the present data plus the data of Refs. 16, 18, and 28. Dotted curve: Form factors calculated from the parameters given in Ref. 16. \bullet , present data. ∇ , data of Ref. 16. \times , data of Ref. 18. \blacksquare , data of Ref. 28. (b) 2^+ (3.904-MeV) level. Solid curve: Best fit form factors for the present data plus the data of Ref. 16. Dotted curve: Form factors calculated from the parameters given in Ref. 16. \bullet , present data. \blacktriangle , data of Ref. 16.

TABLE III. Inelastic electron scattering form factors for ^{40}Ca .

Level	θ (deg)	E (MeV)	q (fm^{-1})	$F^2(q)$	
				Value	standard deviation ^c
2^+ (3.904 MeV)	110.75	71.02	0.575	5.43×10^{-4}	0.28×10^{-4}
	110.64	86.05	0.700	5.29×10^{-4}	0.27×10^{-4}
	110.40	101.21	0.825	5.03×10^{-4}	0.22×10^{-4}
	110.64	121.00	0.990	2.96×10^{-4}	0.22×10^{-4}
	145.82	60.88	0.569	5.33×10^{-4}	0.37×10^{-4}
	145.79	68.55	0.643	6.56×10^{-4}	0.39×10^{-4}
3^- (3.737 MeV)	145.40	87.96	0.831	5.42×10^{-4}	0.38×10^{-4}
	145.79	104.59	0.992	2.51×10^{-4}	0.36×10^{-4}
	145.79	104.59	0.992	3.12×10^{-3}	0.09×10^{-3}

^a Laboratory angle.

^b Laboratory kinetic energy.

^c Standard deviation for statistical errors only; estimated $\pm 2\%$ systematic error not included.

¹⁶ R. A. Eisenstein et al., Phys. Rev. **188** 1815 (1969).

¹⁸ K. Itoh et al., Phys. Rev. **G2**, 2181 (1970).

²⁸ J. Heisenberg, private communication.

ELEM. SYM.	A	Z
Ca	40	20
REF. NO.		
73 Ja 3		egf

METHOD					REF. NO.		
					73 Ja 3	egf	
REACTION	RESULT	EXCITATION ENERGY	SOURCE		DETECTOR		ANGLE
			TYPE	RANGE	TYPE	RANGE	
G, NA24	ABY	THR-999	C	100-999	ACT-I		4PI

999=1 GEV

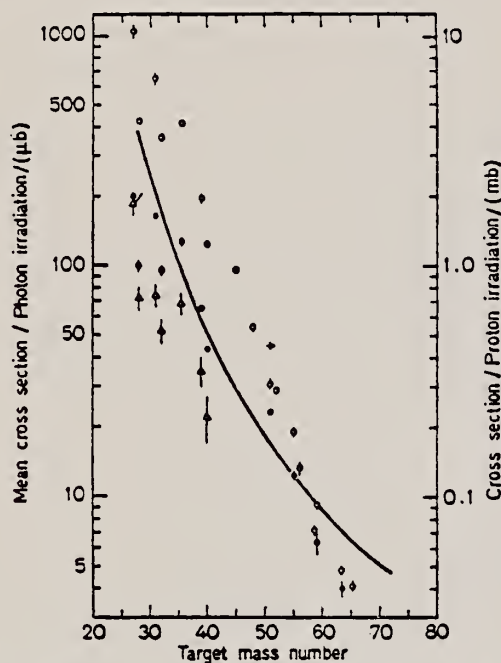


Fig. 7. Mean cross sections for ^{24}Na production as a function of target mass number. Present work filled circles. Noga *et al.* [3] open triangles, Kumbartzi *et al.* [13] cross and Korteling *et al.* [1] 400 MeV protons open circles. The solid line gives the mean cross sections calculated by Jonsson *et al.* [17]

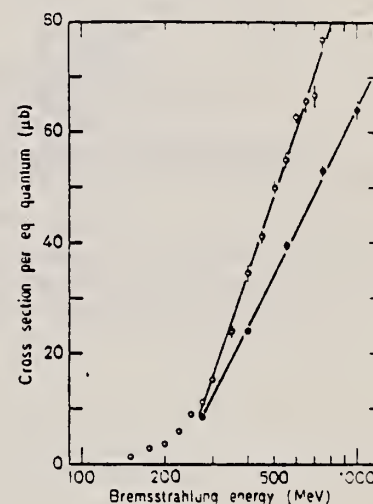


Fig. 4

Fig. 4. The determined yields for the reactions $^{39,40,41}\text{K} \rightarrow ^{24}\text{Na}$ (open circles) and $^{40, \dots}\text{Ca} \rightarrow ^{24}\text{Na}$ (filled circles)

¹Korteling, R.G. *et al.*, J. Inorg. Nucl. Chem. 29, 2863 (1967).

³Noga, V.I. *et al.*, Sov. J. Nucl. Phys. 9, 637 (1969).

¹³Kumbartzi, G. *et al.*, Nucl. Phys. A176, 23 (1971).

¹⁷Jonsson, G.G. *et al.*, LUNP7212, Oct. 1972, to be published in Physica Scripta.

V.G. Vlasenko, N.G. Afanas'ev, V.A. Gol'dshtein, S.V. Dementii,
E.L. Kuplennikov, V.I. Ogurtsov, and V.I. Startsev
Yad. Fiz. 17, 1124 (1973); Sov. J. Nucl. Phys. 17, 585 (1973)

Ca 40 20

METHOD

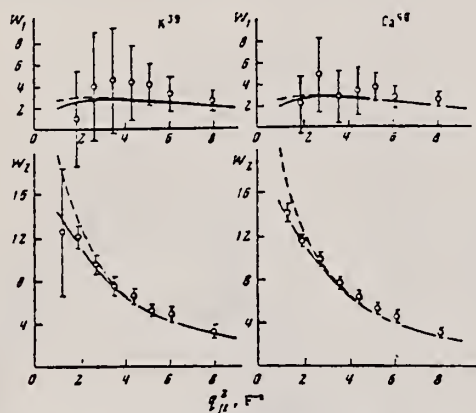
REF. NO.

73 V1 8

hmg

REACTION	RESULT	EXCITATION ENERGY	SOURCE		DETECTOR		ANGLE
			TYPE	RANGE	TYPE	RANGE	
E.E./	FMF	30-180	D	550-999	MAG-D		DST

999=1.15 GEV



Inelastic electromagnetic form factors for K^{39} and Ca^{40} .

ELEM. SYM.	A	Z
Ca	40	20
REF. NO.		
73 Wa 1		egf

METHOD					Page 1 of 3		REF. NO. 73 Wa 1		egf	
REACTION	RESULT	EXCITATION ENERGY	SOURCE		DETECTOR		ANGLE			
			TYPE	RANGE	TYPE	RANGE				
A,G	ABX	12- 22	D	6- 17	NAI-D		DST			

590

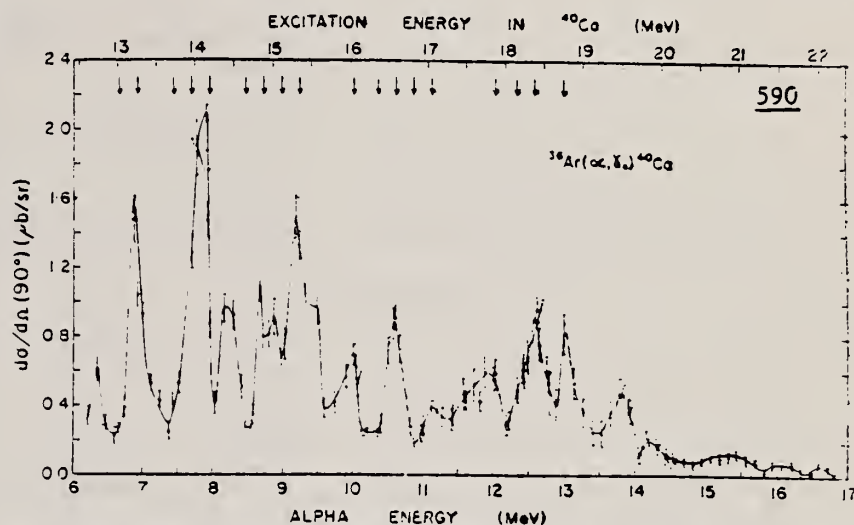


Fig. 2. The absolute differential cross section for the $^{36}\text{Ar}(\alpha, \gamma)^{40}\text{Ca}$ reaction at 90° to the beam direction versus the mean interaction energy in the target gas. The error bars represent statistical errors; the absolute cross sections have an estimated accuracy of $\pm 22\%$.

TABLE I
Properties of resonances in the ^{40}Ca excitation region $E_x = 12.9\text{--}15.0$ MeV

Reso- nance	E_x (MeV)	$E_i(\alpha, \gamma_0)$ (MeV)	$E_i(p, \gamma_0)$ [ref. *)] (MeV)	$E_i(p, \gamma_0)$ [ref. *)] (MeV)	$\Gamma_{c.m.}$ [ref. *)] (keV)	$(2J+1)\Gamma_x\Gamma_{\gamma_0}/\Gamma$ (eV)	$(2J+1)\Gamma_r\Gamma_{\gamma_0}\Gamma$ [ref. *)] (eV)	$\Gamma_x\Gamma_0$
A	6.59	12.97	12.944	12.980		3.4	11.9	0.29
*)			(13.159)	(13.194)	(11.7)		(32.5)	
B	6.90	13.25	13.245	13.289	9.3	9.7	19.3	0.50
C	7.16	13.49	13.442			3.4	6.6	0.52
D	7.42	13.72	13.784	13.822		3.7	6.6	0.56
*)			(13.868)	(13.913)	(23)		(20.8)	
E	7.68	13.95	13.956	13.993	24	14.6	44.6	0.33
F	7.84	14.10	14.080			14.4	28.4	0.51
G	8.20	14.42				4.7		
H	8.30	14.51				4.5		
I	8.70	14.87				6.3		

*) Pair of resonances which are unresolved in the present experiment.

(over)

⁶F. Heimlich and W. Mausberg, Z. Phys. **231** (1970) 397

⁷E. M. Diener, J. F. Amann and P. Paul, Phys. Rev. C, to be published, and private communication

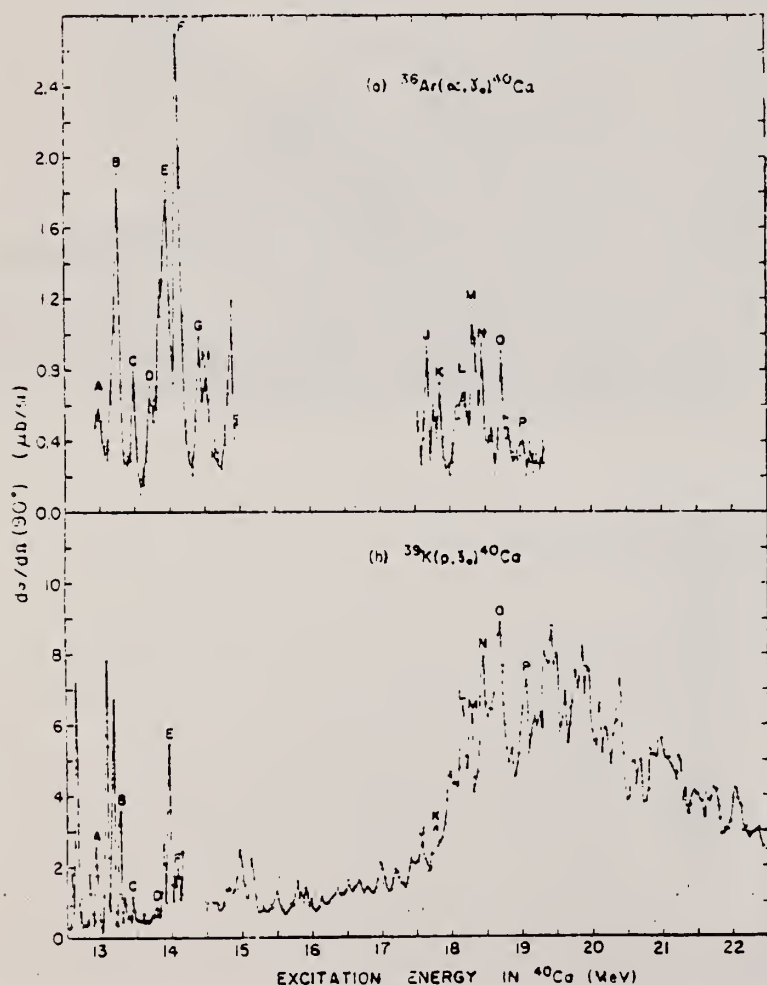


Fig. 3. (a) The absolute differential cross section for the $^{36}\text{Ar}(\alpha, \gamma)^{40}\text{Ca}$ reaction at 90° to the beam direction versus the mean interaction energy in the target gas. The error bars represent statistical errors; the absolute cross sections have an estimated accuracy of $\approx 22\%$. (b) The absolute differential cross section for the $^{39}\text{K}(p, \gamma)^{40}\text{Ca}$ reaction measured at 90° to the beam direction. These data are taken from refs. ^{6,7}.

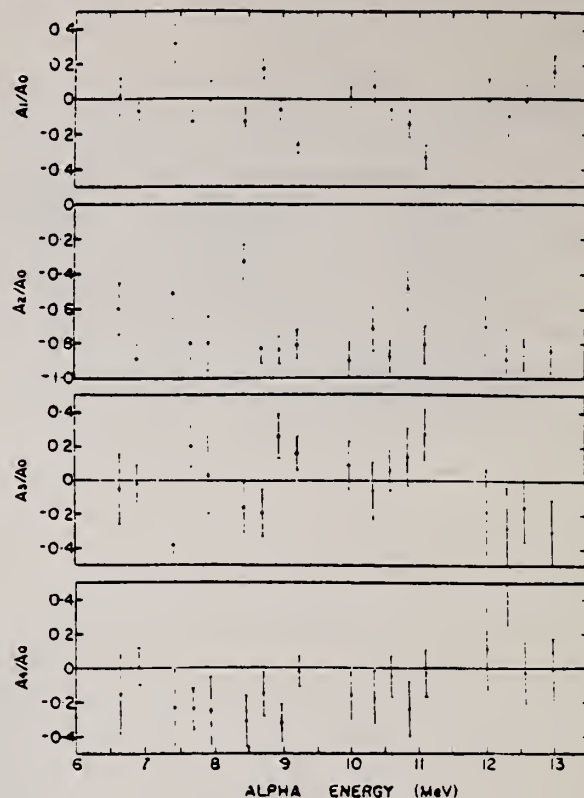


TABLE 2
Properties of resonances in the ^{40}Ca excitation region $E_x = 17.5\text{--}19.3$ MeV

Resonance	E_a (MeV)	$E_x(\alpha, \gamma_0)$ (MeV)	$E_x(p, \gamma_0)$ (ref. 7) (MeV)	$(2J+1) \frac{J^2 J_0^2}{J^2 J_0^2}$ (eV)	ΔE_x (eV)	$\sigma(\gamma, \alpha_0)$ (ref. 7) (mb)	$\sigma(\gamma, p_0)$ (mb)	$\frac{\sigma(\gamma, \alpha_0)}{\sigma(\gamma, p_0)}$
J	11.81	17.67	17.57	5.8	11.6	0.46	6.8	0.068
K	12.02	17.86	17.77	5.4	12.1			
L ^{a)}	12.34	18.15	18.16	11.3	12.1	0.58	12.8	0.045
M	12.54	18.33	18.29	9.4	12.6			
N	12.68	18.45	18.45	6.9	12.6	0.47	17.9	0.026
O ^{b)}	12.99	18.73	18.69	10.3	13.1			
P	13.33	19.04	19.07	4.9	13.1	0.30	16.3	0.018

^{a)} Energy interval used in calculating $\sigma(\gamma, \alpha_0)$ and $\sigma(\gamma, p_0)$.

^{b)} Pair of resonances which are unresolved in the present experiment.

REF.

ELEM. SYM.	A	Z
Ca	40	20
REF. NO.		
73 Wa 1		
egf		

METHOD

Page 3 of 3

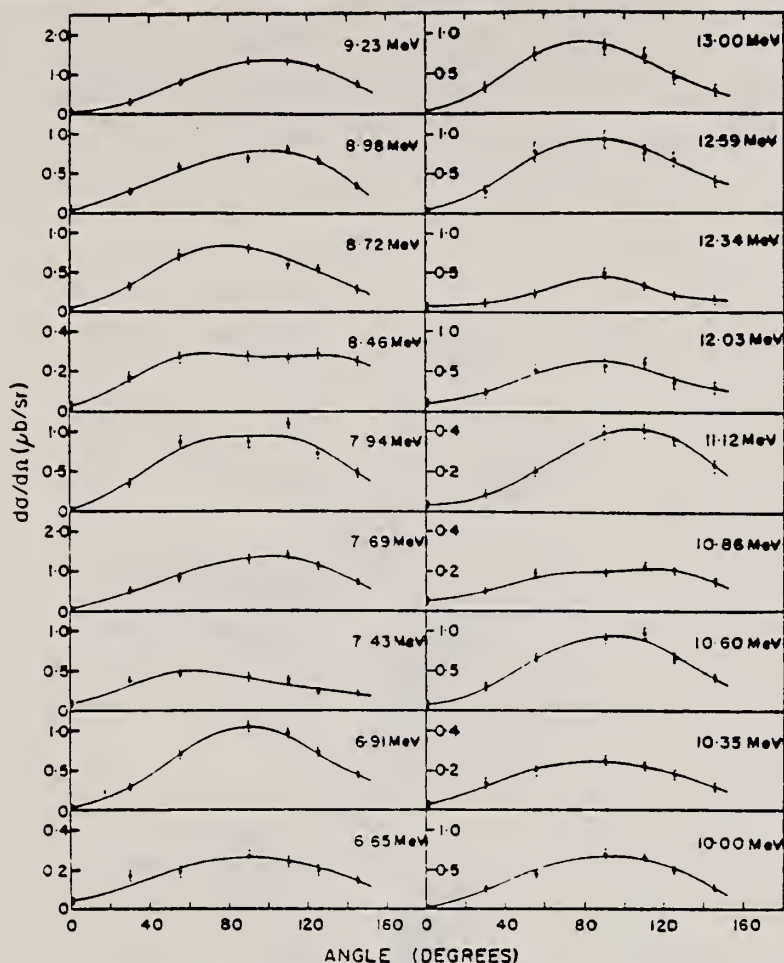


Fig. 4. Gamma-ray angular distributions following the $^{36}\text{Ar}(\alpha, \gamma)^{40}\text{Ca}$ reaction at the bombarding energies indicated.

DETECTOR		ANGLE
TYPE	RANGE	

TABLE 3
The cross sections contributing to the total γ -absorption cross section of ^{40}Ca , averaged over 2 MeV wide energy intervals

E_{γ} (MeV)	$\sigma(\gamma, \alpha_0)^a$ (mb)	$\sigma(\gamma, p_0)^b$ [refs. 6, 7] (mb)	$\sigma(\gamma, p)$ [ref. 9] (mb)	$\sigma(\gamma, n)$ [refs. 10, 11] (mb)	$\sigma(\gamma, \text{total})$ [ref. 12] (mb)	$\sigma(\gamma, \alpha_0)$ $\sigma(\gamma, \text{total})$	$\sigma(\gamma, p_0)$ $\sigma(\gamma, p_0)$
12.5-13.7	0.56	3.8	6	0	9	0.06	0.15
13.7-15.7	0.92	3.3	9	0	15	0.06	0.28
15.7-17.6	0.42	3.9	18	1	24	0.02	0.11
17.6-19.7	0.45	15.2	70	10	70	0.006	0.03
19.7-22.2	0.08	12.9	65	11	65	0.001	0.006

^a) Obtained by detailed balance from the $^{36}\text{Ar}(\alpha, \gamma)^{40}\text{Ca}$ 90° differential cross section shown in fig. 2, assuming an angular distribution of the form $\sin^2\theta$.

^b) Obtained by detailed balance from the $^{39}\text{K}(p, \gamma)^{40}\text{Ca}$ 90° differential cross section shown in fig. 3b, assuming an isotropic angular distribution ⁷).



METHOD

REF. NO.

Page 1 of 4

74 Br 2

hmg

REACTION	RESULT	EXCITATION ENERGY	SOURCE		DETECTOR		ANGLE
			TYPE	RANGE	TYPE	RANGE	
G,P	ABX	8- 31	C	15- 25	SCD-D		DST
G,PG *	ABX	8- 31	C	15- 25	SCD-D		DST
G,NG *	ABX	16- 31	C	15-25	SCD-D		DST

*DEEXCITATION GAMMAS

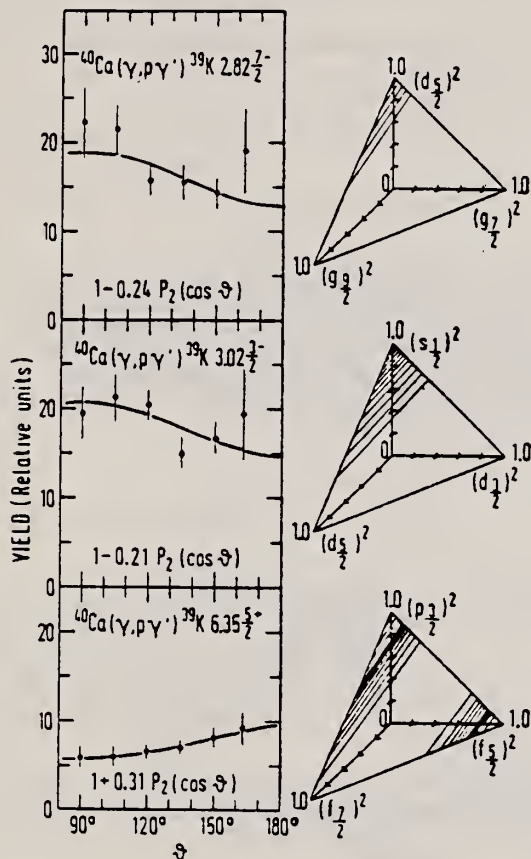


FIG. 12. Angular distributions of deexcitation γ rays from the 2.82-MeV $\frac{1}{2}^-$, 3.02-MeV $\frac{1}{2}^-$, and 6.35-MeV $\frac{3}{2}^-$ levels in ^{39}K measured at 30.25-MeV bremsstrahlung end-point energy. The solid curves are fits to Legendre polynomial expansions $1 + (A_2/A_0) P_2(\cos \theta)$. Configurations of reaction channels are shown on phase-space diagrams (right half of the figure), where the squares of amplitudes are represented as rectangular coordinates of a point on the surface of the plane. The shading density shown represents the precision of the experimentally determined configuration.

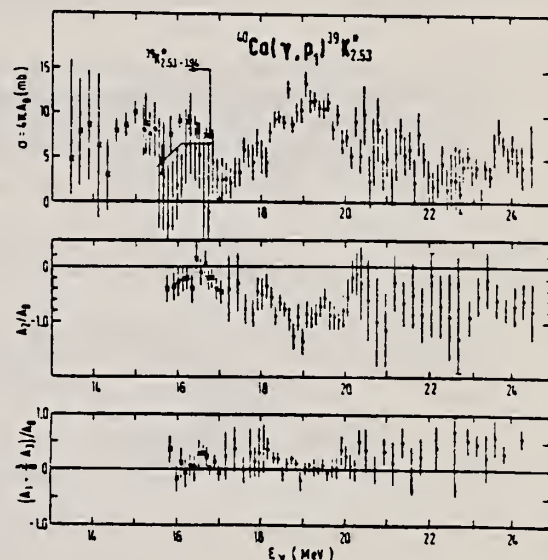


FIG. 5. Energy dependence of the cross section integrated over angles (upper diagram), and the corresponding Legendre polynomial coefficients (lower diagrams) for the $^{40}\text{Ca}(\gamma, p_1)^{39}\text{K}$ reaction in which the residual nucleus is left in the 2.53-MeV $\frac{1}{2}^+$ first excited state. Below $E_\gamma = 17$ MeV separation of this state from higher neighboring states was possible only at 90° ; therefore, at these energies angular distributions (crossed squares in the lower diagrams) were obtained from the sum of cross sections for levels between 2.53-3.94 MeV excitation energy (crossed squares in the upper diagram). Open circles below 17 MeV (upper diagram) represent the (γ, p_1) cross section evaluated from the 90° photo-proton data and angular distributions of the summed cross sections.

(over)

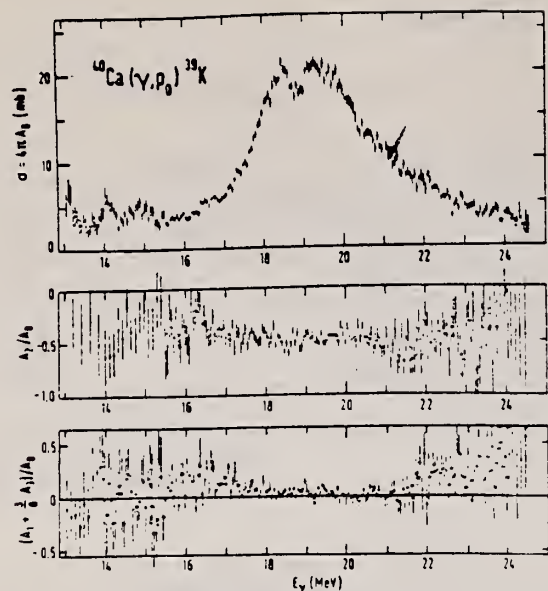


FIG. 4. Energy dependence of the cross section integrated over angles (upper diagram), and the corresponding Legendre polynomial coefficients (lower diagrams) for the $^{40}\text{Ca}(\gamma, p_0)^{39}\text{K}$ reaction in which the residual nucleus is left in the ground state.

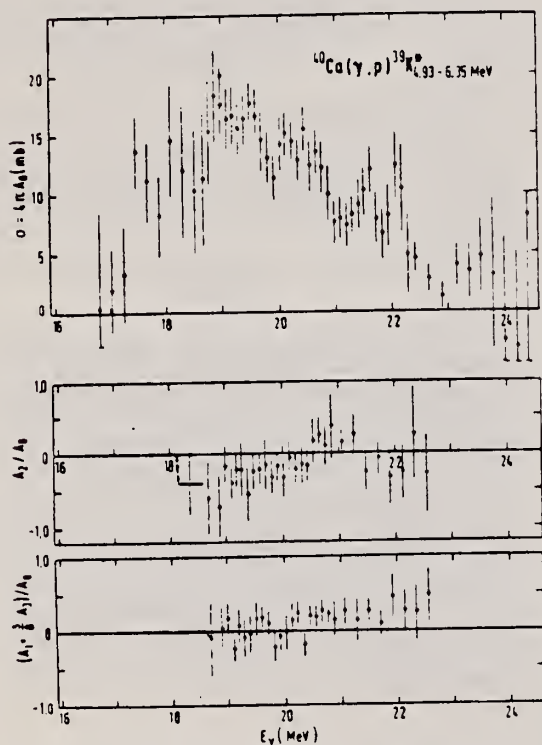


FIG. 7. Energy dependence of the cross section integrated over angles (upper diagram) and the corresponding Legendre polynomial coefficients (lower diagrams) for the $^{40}\text{Ca}(\gamma, p)^{39}\text{K}$ reaction in which states in the residual nucleus between 4.93 and 6.35 MeV excitation energy are populated. Below $E_\gamma = 18$ MeV the cross section was evaluated from the 90° photoproton spectra assuming isotropic angular distribution.

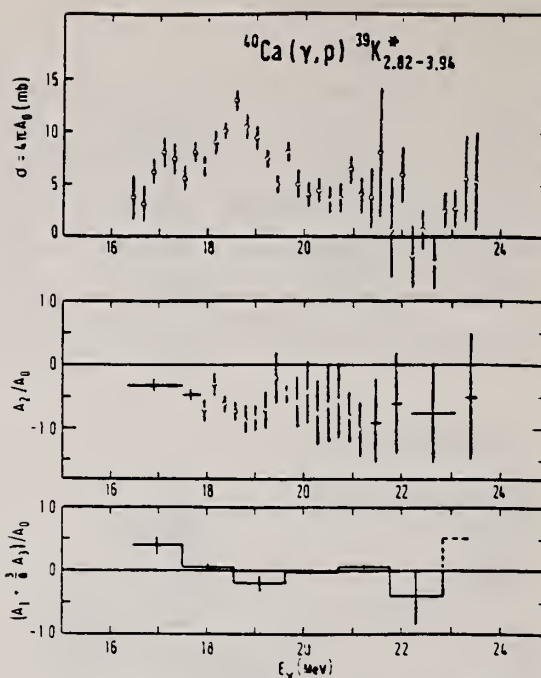


FIG. 6. Energy dependence of the cross section integrated over angles (upper diagram) and the corresponding Legendre polynomial coefficients (lower diagrams) for the $^{40}\text{Ca}(\gamma, p)^{39}\text{K}$ reaction populating states in ^{39}K between 2.82 and 3.94 MeV excitation energy. The main contribution is due to the levels 2.82 MeV $\frac{1}{2}^-$, 3.02 MeV $\frac{1}{2}^-$, and 3.94 MeV (see Fig. 3).

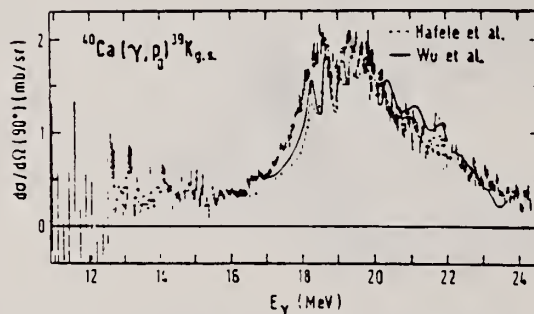


FIG. 15. Comparisons of differential cross sections for the $^{40}\text{Ca}(\gamma, p)^{39}\text{K}_{g.s.}$ reaction at 90° : present work (points with error bars), the data of Wu *et al.* (Ref. 20) (full curve), data from the inverse reaction of Hafele, Bingham, and Allen (Ref. 16) (dashed curve). The solid and dashed curves have been arbitrarily drawn through the experimental points. Errors in the absolute cross-section scale determination are $\pm 6\%$ for the present work, $\pm 10\%$ for Ref. 20, and $\pm 70\%$ for Ref. 16.

REACTION	RESULT	EXCITATION ENERGY	SOURCE		DETECTOR		ANGLE
			TYPE	RANGE	TYPE	RANGE	

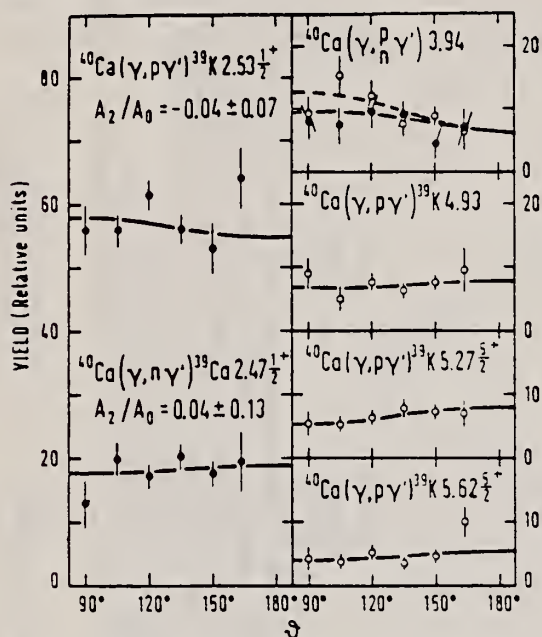


FIG. 13. Angular distributions of deexcitation γ rays from several excited states in ^{39}K and ^{39}Ca listed in Table II. Open and closed circles represent data obtained from full-energy and double escape peaks, respectively. The solid curve is a fit to the Legendre polynomial expansion $1 + (A_2/A_0) P_2(\cos \theta)$.

16

J.C. Hafele, F.W. Bingham, J.S. Allen, Phys. Rev. **135**, B365 (1964).

20

C.P. Wu, J.E.E. Baglin, F.W.K. Firk, and T.W. Phillips, Phys. Lett. **29B**, 359 (1969).

26

N. Bezic, D. Jamnik, G. Kernel, J. Krajnik, and J. Snajder, Nucl. Phys. **A117**, 124 (1968).

27

M. Marangoni, A.M. Saruis, Nucl. Phys. **A132**, 649 (1969); and private communication.

28

R.F. Barrett, L.C. Biedenharn, M. Danos, P.P. Delsanto, W. Greiner, H.G. Wahsweiler, Rev. Mod. Phys. **45**, 44 (1973).

36

V. Gillet and E.A. Sanderson, Nucl. Phys. **A91**, 292 (1967).

42

V. Gillet and E. A. Sanderson, Nucl. Phys. **54**, 472 (1964).

TABLE III. Measured and calculated main decay modes of GDR in ^{40}Ca . Present results are underlined.

Reaction	Residual nucleus		Integrated cross sections relative to the integrated total absorption cross section (%)			
	Energy and spin of the residual state	Dominant shell-model hole config.	Experiment	Coupled-channel calculation ^a	Eigenchannel calculation ^b	Bound state calculation ^c
(γ, p_0)	0 MeV; $\frac{1}{2}^+$, ^{39}K	$(d_{3/2})^{-1}$	<u>21</u>	53	45	24
(γ, n_0)	0 MeV; $\frac{1}{2}^+$, ^{39}Ca		<u>8</u> ^d	20	14	
(γ, p_1)	2.53; $\frac{1}{2}^+$, ^{39}K	$(2s_{1/2})^{-1}$	<u>10.5</u>	9 (2.5%)	25	9
(γ, n_1)	2.47; $\frac{1}{2}^+$, ^{39}Ca		<u>3.5</u>	2	4	
(γ, p)	2.82–4.08, ^{39}K		<u>10.6</u>			
(γ, p)	4.93–8.0, ^{39}K	$(d_{3/2})^{-1}$	<u>34</u> ^f	14	11	67
(γ, n)	5.11–6.13; $\frac{1}{2}^+$, ^{39}Ca		<u>2</u>	2	1	

^a Reference 27. Theoretical integrated total absorption cross section is a sum of the 1p-1h reaction-channel cross sections calculated with absorptive potential.

^b Reference 28.

^c References 36, 42.

^d Reference 20, assuming angular distribution of (γ, p_0) as obtained in the present work.

^e The figure in parentheses represents the part of integrated cross section in the region of the giant resonance.

^f $^{40}\text{Ca}(\gamma, p)^{39}\text{K}_{\gamma, 1, 33}$.

TABLE I. Measured and calculated integrated cross sections for the main residual states. Present data are underlined.

Outgoing particles	Residual nucleus Energy (MeV) and spin	Dominant shell- model hole configuration	Integrated cross sections up to E_γ (MeV mb)			Comparison of bremsstrahlung yields ^a at an end-point energy $E_{\gamma \max}$ (MeV mb) Present meas. Ullrich and Krauth (Ref. 55) Integrated over angles $\theta = 120^\circ$ ($E_{\gamma \max} = 30.25$ MeV) ($E_{\gamma \max} = 32$ MeV)
			Experiment ($E_\gamma = 24.6$ MeV) Deceleration γ rays	Coupled-channel calculation with absorptive potential	Elgenchannel calculation without absorptive potential	
p_0	0 : $\frac{3}{2}^+$	$(d_{3/2})^{-1}$		255	350	
n_0	0 : $\frac{3}{2}^+$			90	110	
p_1	2.53; $\frac{1}{2}^+$	$(2s_{1/2})^{-1}$	48 ± 6	44 (12) ^d	190	59 ± 4
n_1	2.47; $\frac{1}{2}^+$		16 ± 3	11	30	18 ± 2
p	2.82; $\frac{1}{2}^-$		11 ± 3			17 ± 2
n	2.79; $\frac{1}{2}^-$		2 ± 2^e			3 ± 2
$p + (n)^f$	3.02; $\frac{3}{2}^-$		14 ± 3			15
p	3.59; $\frac{3}{2}^-$		2 ± 1^e			15 ± 2
n	3.63; $\frac{3}{2}^-$					2.3 ± 1.0
$p + n$	3.88		2.8 ± 0.8^e			2.9 ± 0.7
$p + (n)^f$	3.94		11 ± 4			10.2 ± 1.5
p	4.08		3.6 ± 1.0^e			3.5 ± 0.7
p	4.93		5 ± 1^e			5.4 ± 0.8
n	5.13; $\frac{3}{2}^+$	$(d_{3/2})^{-1}$	1 ± 1^e			2.0 ± 0.7
p	5.27; $\frac{3}{2}^+$		8 ± 1^e			6.5 ± 1
p	5.31		3.5 ± 1.5^e			3.8 ± 0.6
n	5.48; $\frac{3}{2}^+$		2 ± 1^e			2.2 ± 0.6
p	5.62; $\frac{3}{2}^+$		9 ± 3^e			6 ± 1
p	5.83		$< 1^e$			2 ± 1
p	5.96		$< 1^e$			1 ± 1
n	6.15; $\frac{3}{2}^+$	$(d_{3/2})^{-1}$	2 ± 1^e			1.5 ± 0.8
p	6.35; $\frac{3}{2}^+$		6 ± 1^e			7 ± 1
p_{unb}	6.5-8.0	$(d_{3/2})^{-1}$				2.0
Total absorption			480 $\pm 40^h$			
Total p			363 ± 25			
Total n			67 $\pm 4^i$			
			74 $\pm 7^j$			

^a Listed yields are equal to the energy-integrated cross sections, assuming that they have shapes identical to the absorption cross section.

^b Estimated from Ref. 20 assuming for the (γ, n_0) reaction the same angular distribution as for the (γ, p_0) .

^c In the region below $E_\gamma = 16$ MeV where (γ, p_1) could not be resolved, the integrated cross section for residual states between 2.53 and 4 MeV (amounting to 14 MeV mb) was assumed to be shared between (γ, p_1) and higher states in the same proportion as corresponding deexcitation γ -ray yields.

^d The figure inside the brackets represents the part of integrated cross section in the region of the giant resonance.

^e Because of low intensity, integrated cross sections are obtained by the method of Ref. (4).

^f The contribution of neutron channel is negligible due to the high reaction threshold (see Fig. 11).

^g The cross section for (γ, p_{unb}) has been extrapolated below $E_\gamma = 18.5$ MeV according to the shape of the transmission coefficients (extrapolated value of the cross section amounts to 23 ± 8 MeV mb).

^h From Ref. 26.

ⁱ J. E. E. Baglin and B. M. Spicer, Nucl. Phys. 54, 549 (1964).

^j B. S. Ishanov, I. M. Piskarev, I. M. Kapitonov, V. S. Sopov, and V. G. Shevchenko, Yad. Fiz. 13, 1141 (1971) [transl.: Sov. J. Nucl. Phys. 13, 655 (1971)].

METHOD						REF. NO.	
						74 Da 2	egf
REACTION	RESULT	EXCITATION ENERGY	SOURCE		DETECTOR		ANGLE
			TYPE	RANGE	TYPE	RANGE	
G,P	ABY	13-450	C	450	TEL-D		90
G,T	ABY	30-450	C	450	TEL-D		90
G,HE *	ABY	29-450	C	450	TEL-D		DST
G,A	ABY	17-450	C	450	TEL-D		DST

* HE=HE3

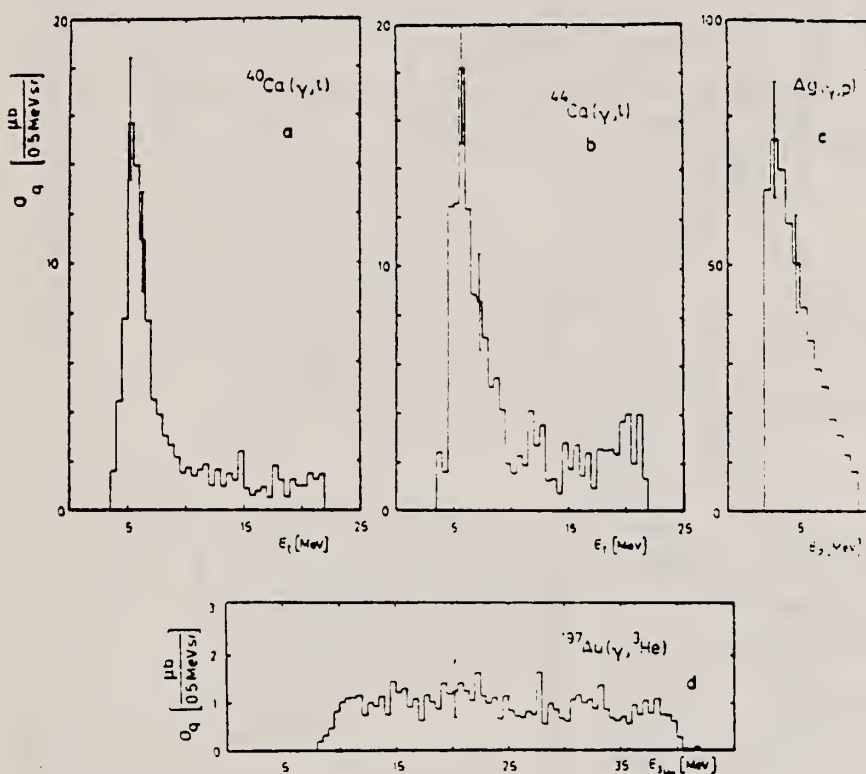


Fig. 3. Characteristic measured spectra of p, t, ^3He and ^4He from the target nuclei ^{27}Al , $^{40,44}\text{Ca}$, ^{197}Ag , ^{197}Au .

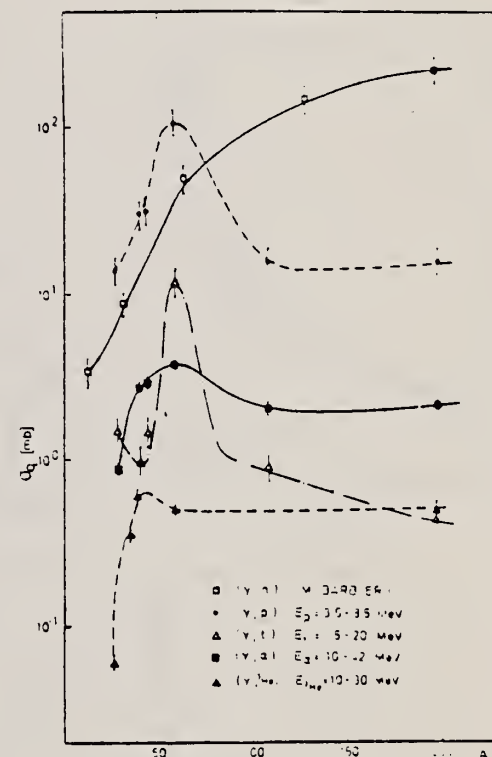


Fig. 5. Yield of protons, tritons, ^3He and ^4He depending on mass number A [ref. 23]. The lines through the points are to guide the eye.

23) M. Barbier, Induced radioactivity
(North-Holland, Amsterdam, 1969)

(over)

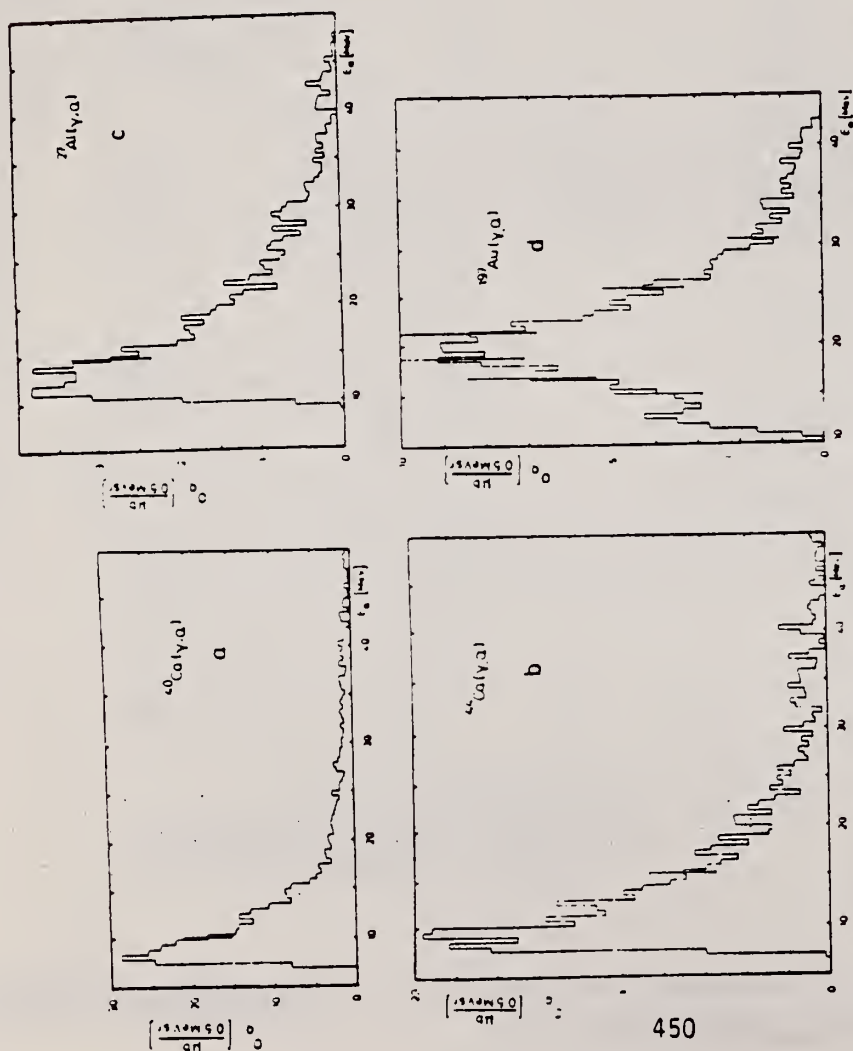


Fig. 4. Characteristic measured spectra of p, t, ^3He and ^4He from the target nuclei ^{27}Al , $^{40,44}\text{Ca}$, ^{89}Ag , ^{197}Au .

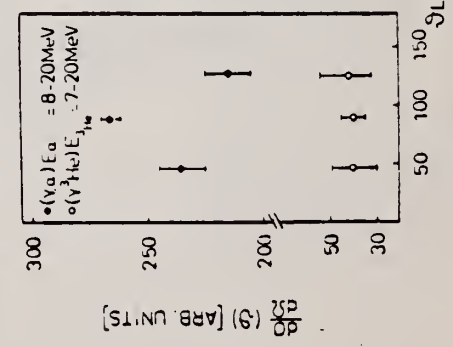


Fig. 9. Angular distributions of $^{40}\text{Ca}(\gamma, \alpha)$ and $^{40}\text{Ca}(\gamma, ^3\text{He})$ reactions at $E_{\gamma}^{\text{max}} = 450 \text{ MeV}$.

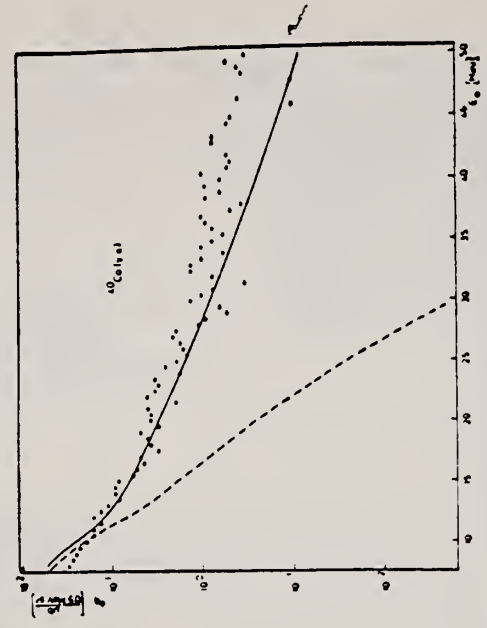


Fig. 7. Same as fig. 6 but for $^{40}\text{Ca}(\gamma, \alpha)$, $^{92}\text{Nb}(\gamma, \alpha)$ and $^{197}\text{Au}(\gamma, \alpha)$.

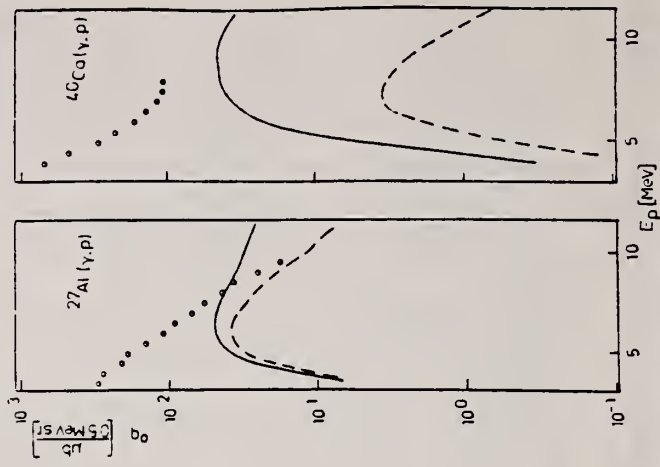


Fig. 6. Experimental data with statistical model calculations for the reactions $^{27}\text{Al}(\gamma, p)$ and $^{40}\text{Ca}(\gamma, p)$ for $E_{\gamma}^{\text{max}} = 50 \text{ MeV}$ (calculation). Full line for $^{27}\text{Al}(\gamma, p)$ and dashed line for $^{40}\text{Ca}(\gamma, p)$.

ELEM. SYM.	A	Z
Ca	40	20
REF. NO.		
74 Fo 4		egf

METHOD					REF. NO.		
					74 Fo 4	egf	
REACTION	RESULT	EXCITATION ENERGY	SOURCE		DETECTOR		ANGLE
			TYPE	RANGE	TYPE	RANGE	
G.A	ABX	13- 20	D	6- 14	NAI-D		90

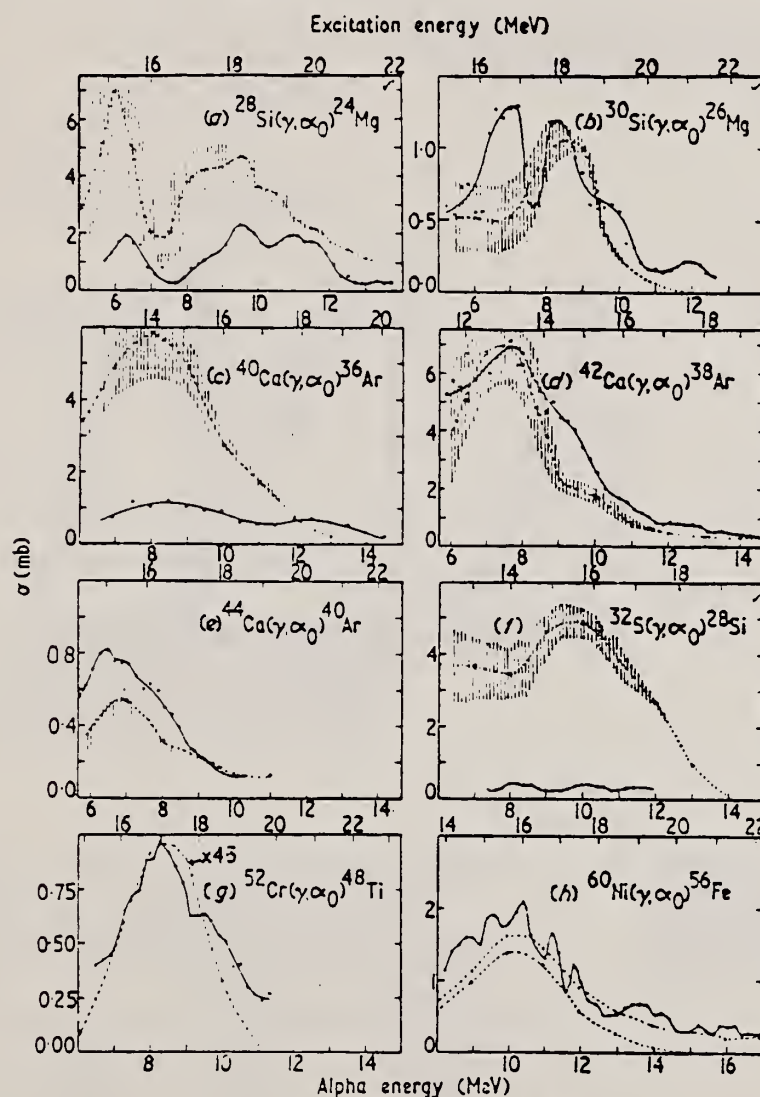
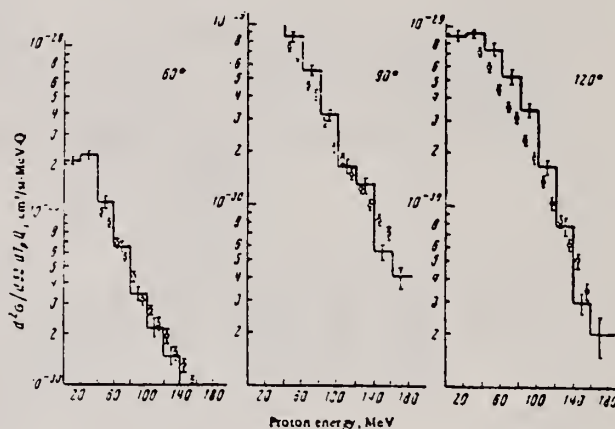


Figure 1. Excitation functions for the (γ, α) reaction obtained from α capture data using the principle of detailed balance. The data shown in (a) and (f) are from Meyer-Shutzmeister *et al* (1963). Those in (b) are from Watson *et al* (1973). The relative experimental errors are approximately $\pm 10\%$. The absolute errors are $\pm 25\%$. The broken curves are the results of calculations (see text). The vertical lines indicate the relative errors due to uncertainties in the total photonuclear cross sections where they are greater than $\pm 10\%$. The crosses indicate the energies at which transmission coefficients were calculated.

METHOD						REF. NO.		
						74 Gr 6		hmg
REACTION	RESULT	EXCITATION ENERGY	SOURCE		DETECTOR		ANGLE	
			TYPE	RANGE	TYPE	RANGE		
G,P	ABY	38-168	C	340	EMU-D		DST	

The emulsion method has been used to measure the cross sections for photoproduction of protons with kinetic energies from 30 to 160 MeV at angles of 60, 90, and 120° in the laboratory system from the nucleus ⁴⁰Ca with 340-MeV bremsstrahlung. The proton energy spectra are in good agreement with calculations based on the cascade model.



ELEM. SYM.	A	Z
Ca	40	20

METHOD	REF. NO.	
	74 Na 1	hmg

REACTION	RESULT	EXCITATION ENERGY	SOURCE		DETECTOR		ANGLE
			TYPE	RANGE	TYPE	RANGE	
E, E/P	SPC	0* 80	D	700-750	SPK-D		UKN

*SEPARATION ENERGY

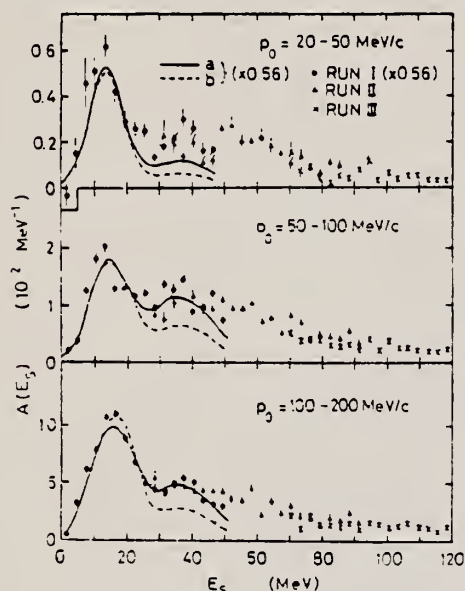


FIG. 1. Distorted spectral function integrated over p_0 . Superimposed curves are DWIA calculation for $2s$, $1d$, and $1p$ using Elton-Swift wave functions with parameters given in Table I (solid curves a) and with shell-model occupation numbers (dashed curves b).

TABLE I. Parameters for the solid curves a in Fig. 1 ($1d_{3/2}$, $2s_{1/2}$, $1d_{5/2}$, and $1p$ states) and for the dot-dashed curves in Fig. 2 ($1s$ state).

State	C_{n1j}	Peak energy (MeV)	Width (FWHM) (MeV)
$1d_{3/2}$	1.04 ± 0.40	10.4 ± 1.4	9.2 ± 1.3
$2s_{1/2}$	1.02 ± 0.06	13.6 ± 0.4	12.0 ± 0.9
$1d_{5/2}$	0.78 ± 0.26	18.4 ± 1.6	9.9 ± 1.4
$1p$	1.70 ± 0.15	35.3 ± 0.5	23.5 ± 2.3
$1s$	1.87 ± 0.09	58.4 ± 1.1	31.9 ± 1.1

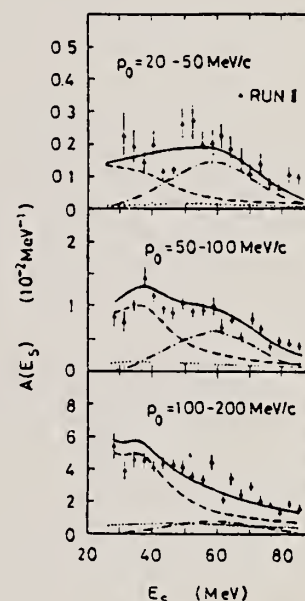


FIG. 2. Data obtained in run II. Superimposed curves are radiative ($e, e'p$) cross section (dashed curves) and multiple collision background (dotted curves); $1s$ contribution (dot-dashed curves); sum of all the contributions (solid curves).



REF

A. Veyssiere, H. Beil, R. Bergere, P. Carlos, A. Lepretre, and
A. De Miniac
Nucl. Phys. A227, 513 (1974)

REF. NO.

74 Ve 1

egf

REACTION	RESULT	EXCITATION ENERGY	SOURCE		DETECTOR		ANGLE
			TYPE	RANGE	TYPE	RANGE	
G,N *	ABX	15- 30	D	15- 30	BF3-I		4PI

* 905

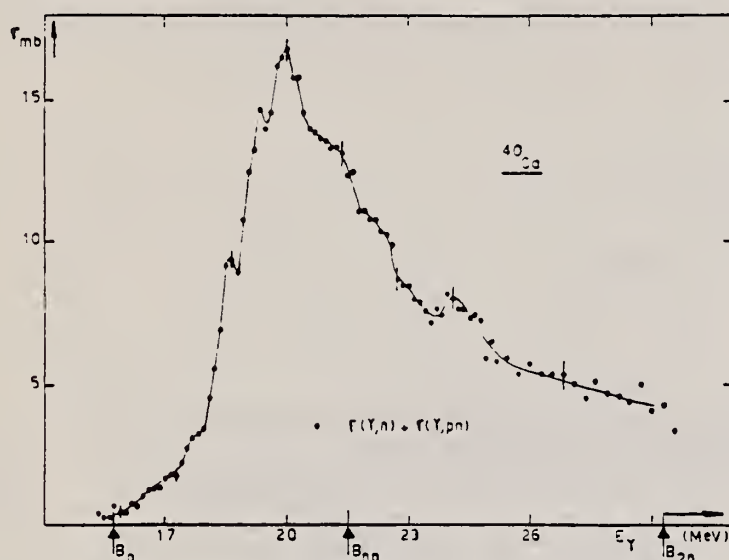


Fig. 11. The $[\sigma(\gamma, n) + \sigma(\gamma, pn)]$ photoneutron cross section of ^{40}Ca .

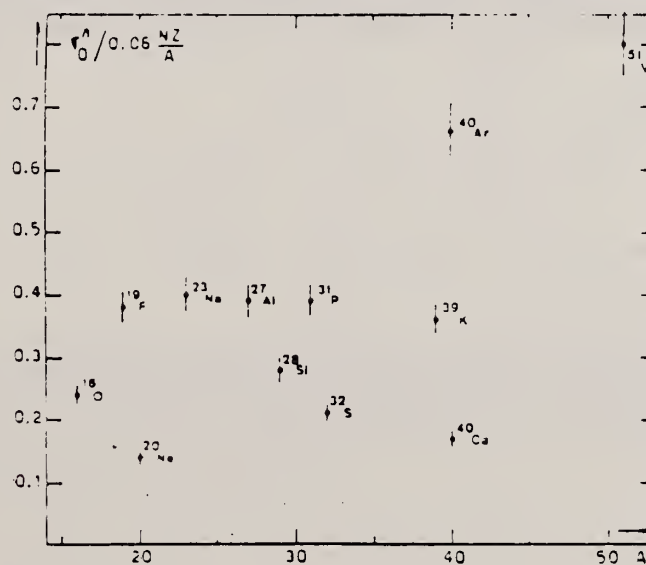


Fig. 22. Ratio of experimental integrated photoneutron cross section σ_0^{exp} over the Thomas, Reiche and Kuhn sum rule $[0.06 NZ^2/A]$. Numerical values and upper integration limits E_{γ} are taken from table 3. Also $\Delta\sigma_0^{\text{exp}} = \pm 7\%$ for all nuclei.

(over)

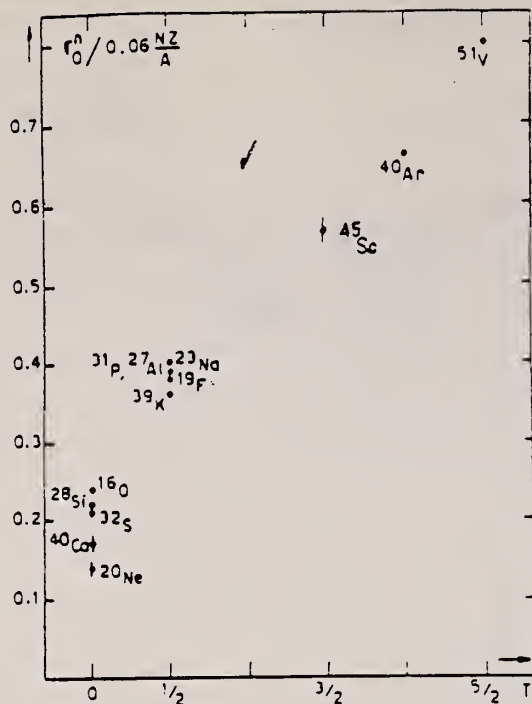


Fig. 24. The $[\sigma_0^n/(0.06 NZ/A)]$ ratio as a function of isospin T . Possible overall errors of $\pm 7\%$ at $T=0$ to be applied to all nuclei shown.

TABLE 3
Experimental integrated photoneutron cross sections $\sigma_0^n = \int_0^{E_{\gamma}} \sigma_{Tn}(E) dE$ compared with the classical sum rule $[0.06 NZ/A]$ of Thomas, Reich and Kuhn

	$T=0$					$T=\frac{1}{2}$					$T=\frac{3}{2}$	$T=2$	$T=\frac{5}{2}$
Nucleus	^{16}O	^{20}Ne	^{28}Si	^{32}S	^{40}Ca	^{19}F	^{23}Na	^{27}Al	^{31}P	^{39}K	^{43}Sc	^{40}Ar	^{51}V
σ_0^n (MeV · mb)	58 ± 4	42 ± 3	94 ± 7	98 ± 7	100 ± 7	108 ± 7	137 ± 9	158 ± 10	182 ± 12	210 ± 14	383 ± 25	393 ± 28	602 ± 42
$\sigma_0^n/(0.06 NZ/A)$	0.24	0.14	0.22	0.21	0.17	0.38	0.40	0.39	0.39	0.36	0.57	0.66	0.8
E_{γ} (MeV)	30	26.7	30	30	29.5	29	30	30	29	30	28.1	26.7	28

METHOD		ELEM. SYM.		A	Z
		Ca		40	20
		REF. NO.			
		74 Wh 3		hmg	
REACTION	RESULT	EXCITATION ENERGY	SOURCE		ANGLE
			TYPE	RANGE	
E, E/	ABX	0-300	D	500	60

See further analysis of this data in reference 79Zi1

QUASIELASTIC SCAT

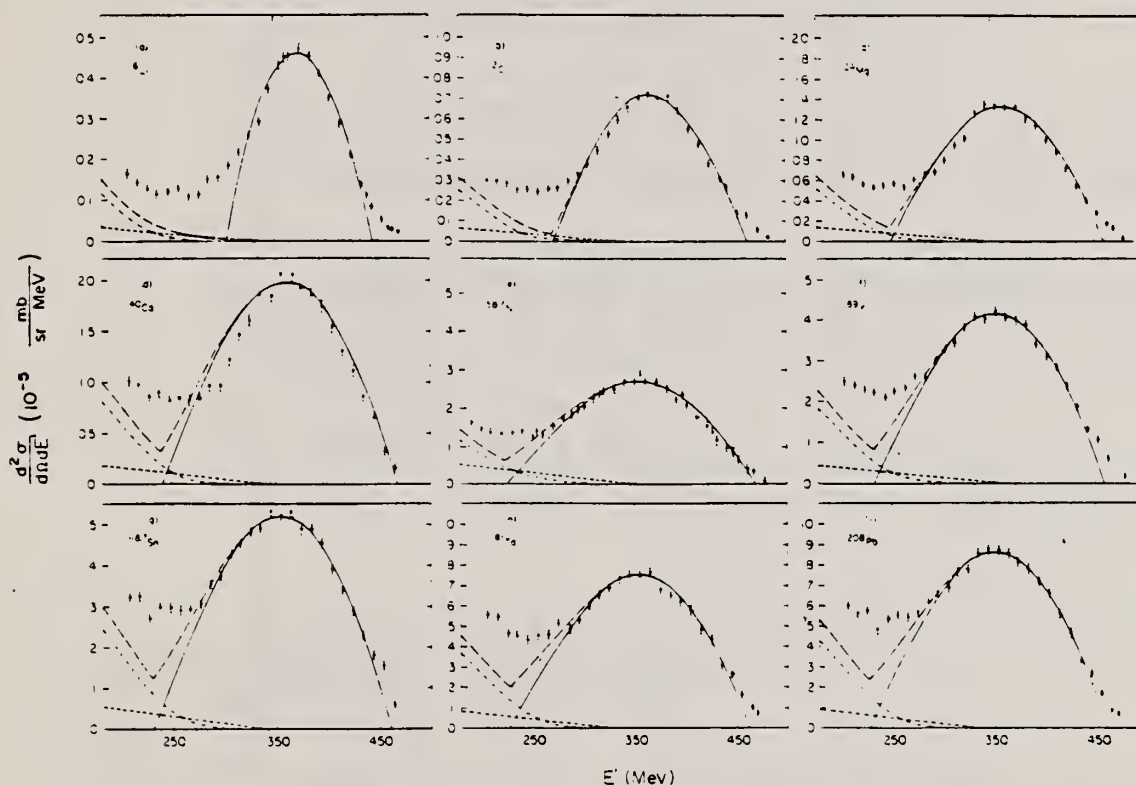


FIG. 1. The measured quasielastic peaks; the errors on the data points do not include an over-all 3% normalization uncertainty. The solid curve is a fit by the Fermi-gas model which yielded k_F (in MeV/c) and $\bar{\epsilon}$ (in MeV) as follows: (a) ^6Li (169, 17); (b) ^{12}C (221, 25); (c) ^{24}Mg (235, 32); (d) ^{40}Ca (249, 33); (e) ^{58}Ni (260, 36); (f) ^{89}Y (254, 39); (g) ^{118}Sm (260, 42); (h) ^{181}Ta (265, 42); (i) ^{208}Pb (265, 44). The fitting uncertainty in k_F is ± 5 MeV/c and in $\bar{\epsilon}$ it is ± 3 MeV. The small-amplitude dashed curve is the s-wave π -production contribution, the dot-dashed curve is the isobar excitation, and the large-amplitude dashed curve is the total result.

(over)

REF.

J. Ahrens, H. Borchert, K.H. Czock, H.B. Eppler, H. Gimm,
H. Gundrum, M. Kroning, P. Riehn, G. Sita Ram, A. Ziegler,
and B. Ziegler
Nucl. Phys. A251, 479 (1975)

ELEM. SYM.

A

Z

Ca

40

20

METHOD

REF. NO.

75 Ah 3

egf

REACTION	RESULT	EXCITATION ENERGY	SOURCE		DETECTOR		ANGLE
			TYPE	RANGE	TYPE	RANGE	
G, MU-T	ABX	10-160	C	140-275	MGC-D		4PI

TABLE 2

934+

The moments of the experimental nuclear cross section distributions integrated from 10 MeV to the energy E , and their statistical errors

	E (MeV)	Σ_{-2} (mb·MeV) \pm (%)	Σ_{-1} (mb) \pm (%)	Σ_0 (mb·MeV) \pm (%)	Σ_{+1} (b·MeV ²) \pm (%)	Σ_{+2} (b·MeV ³) \pm (%)
Li	100	0.196	1.1	4.64	1.0	143
	140	0.197	1.1	4.79	1.0	161
	210	0.198	1.1	5.03	1.0	206
Be	100	0.192	2.5	5.19	1.5	173
	140	0.194	2.5	5.33	1.5	189
	210	0.195	2.5	5.58	1.5	236
C	100	0.313	1.7	8.81	1.1	291
	140	0.316	1.7	9.18	1.2	334
O	100	0.580	1.6	14.50	1.3	432
	140	0.585	1.6	15.10	1.3	508
Al	100	1.10	1.8	25.70	1.5	739
	140	1.11	1.8	26.3	1.7	807
Ca	100	2.22	1.2	45.5	1.5	1120
	140	2.23	1.2	46.8	1.7	1290

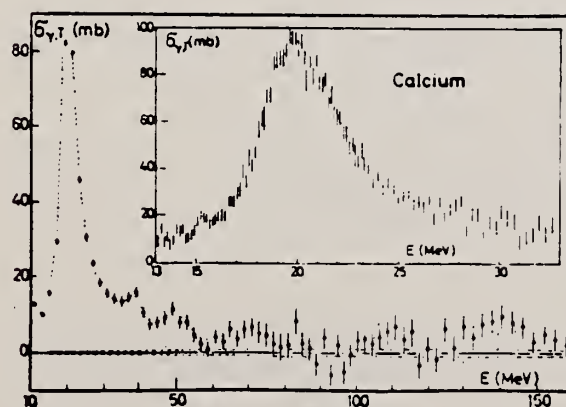


Fig. 8. The same as fig. 2 for Ca.

Fig. 2. Total photonuclear cross section for natural Li. The error bars indicate one standard deviation of counting statistics from the main spectrometer. The dashed lines along the abscissa indicate the uncertainty due to counting statistics in the normalizing spectrometer. Oscillations of the base line within this area are possible, the period of these oscillations, however, must not be smaller than 10% in photon energy. The dashed and dotted lines through the cross section values have been drawn to guide the eye.

REF.

V. di Napoli, G. Rosa, F. Salvetti, M. L. Terranova,
H. G. de Carvalho, J. B. Martins, O. A. P. Tavares
J. Inorg. Nucl. Chem. **37**, 1101 (1975)

ELEM. SYM.

A

Z

Ca

40

20

METHOD

REF. NO.

75 Di 4

egf

REACTION	RESULT	EXCITATION ENERGY	SOURCE		DETECTOR		ANGLE
			TYPE	RANGE	TYPE	RANGE	
G,F18	ABY	THR-999	C	300-999	ACT-I		4PI
G,NA22	ABY	THR-999	C	300-999	ACT-I		4PI
G,NA24	ABY	THR-999	C	300-999	ACT-I		4PI

999 = 1 GEV

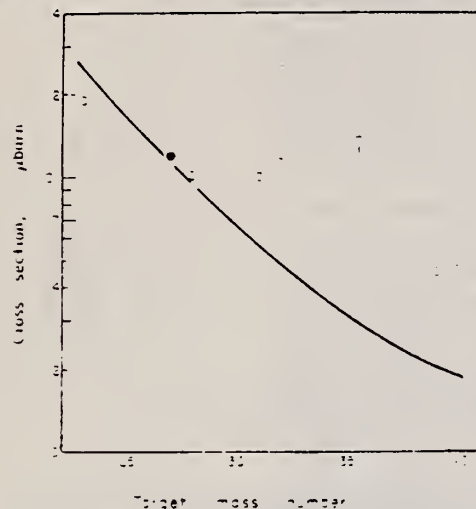


Fig. 2. Mean absolute cross section of ^{18}F photoproduction vs the target mass number. Open triangle: energy range 0.15-0.72 GeV, Ref. [18]. Filled circle, energy range 0.3-1 GeV, Ref. [3]. Open circles: present work. The curve has been calculated by means of Eqn (1).

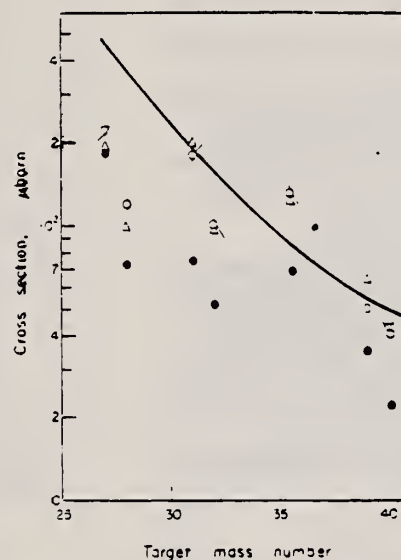


Fig. 4. Mean absolute cross section of ^{24}Na photoproduction vs the target mass number. Filled circles: energy range 0.1-1 GeV, Ref. [20]. Reversed open triangle: energy range 0.3-1 GeV, Ref. [8]. Open triangles, energy range 0.25-1 GeV, Ref. [19]. Open circles: present work. The curve has been calculated by means of Eqn (1).

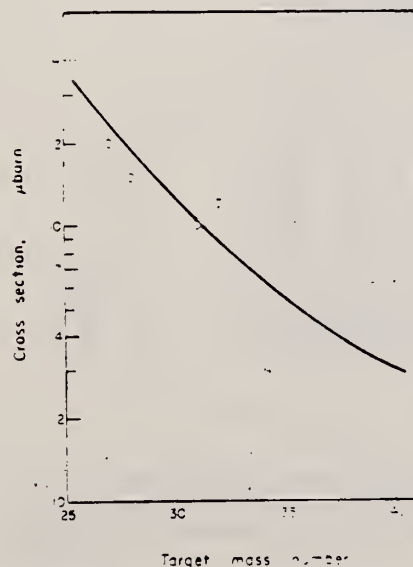


Fig. 3. Mean absolute cross section of ^{22}Na photoproduction vs the target mass number. The curve has been calculated by means of Eqn (1).

Table 2. Cross-section per equivalent quantum $\sigma_0(\mu\text{b})$ of photoproduction of ^{18}F

Target nucleus	Bremsstrahlung maximum energy $E_0(\text{GeV})$				
	0.30	0.40	0.55	0.75	1.00
^{22}Na	590 \pm 30	640 \pm 30	720 \pm 30	780 \pm 30	830 \pm 30
$^{27}\text{Al}^a$	116 \pm 7	172 \pm 6	202 \pm 6	245 \pm 5	270 \pm 5
^{28}Si	80 \pm 10	110 \pm 10	145 \pm 10	170 \pm 10	200 \pm 10
^{31}P	60 \pm 10	90 \pm 10	130 \pm 10	150 \pm 10	180 \pm 10
^{32}S	55 \pm 10	90 \pm 10	125 \pm 10	160 \pm 10	190 \pm 10
$^{35,37}\text{Cl}$	185 \pm 20	230 \pm 20	270 \pm 20	310 \pm 20	350 \pm 20
^{39}K	35 \pm 5	50 \pm 5	65 \pm 5	75 \pm 5	90 \pm 5
^{40}Ca	5 \pm 2	20 \pm 3	35 \pm 5	45 \pm 5	60 \pm 5

^aThe results for ^{27}Al have already been published (see [3]) and are reported for comparison.

(over)

2. V. di Napoli and M. L. Terranova, *J. inorg. nucl. Chem.* **36**, 3633 (1974).
3. V. di Napoli, A. M. Lacerenza, F. Salvetti, S. M. Terenzi, H. G. de Carvalho and J. B. Martins, *J. inorg. nucl. Chem.* **35**, 1419 (1973).
4. C. M. Lederer, J. M. Hollander and I. Perlman, *Table of Isotopes*, 6th Edn Wiley, New York (1967).
5. R. G. Korteling and A. A. Caretto, Jr., *J. inorg. nucl. Chem.* **29**, 2863 (1967).
6. R. G. Korteling and A. A. Caretto, Jr., *Phys. Rev. C1*, 193 (1970).
7. R. G. Korteling and A. A. Caretto, Jr., *Phys. Rev. C1*, 1960 (1970).
8. V. di Napoli, A. M. Lacerenza, F. Salvetti, H. G. de Carvalho and J. B. Martins, *Lett. Nuovo Cimento* **1**, 835 (1971).
9. I. Halpern, R. J. Debs, J. T. Eisinger, A. W. Fairhall and H. G. Richter, *Phys. Rev.* **97**, 1327 (1955).
10. C. B. Fulmer, K. S. Toth, I. R. Williams, T. H. Handley, C. F. Dell, E. L. Callis, T. M. Jenkins and J. M. Wyckoff, *Phys. Rev. C2*, 1371 (1970).
11. G. J. Kumbartzki, U. Kim and C. K. Kwan, *Nucl. Phys.* **A160**, 237 (1970).
12. G. J. Kumbartzki and U. Kim, *Nucl. Phys.* **A176**, 23 (1971).
13. K. Lindgren and G. G. Jonsson, *Nucl. Phys.* **A197**, 71 (1972).
14. C. E. Roos and V. Z. Peterson, *Phys. Rev.* **124**, 1610 (1961).
15. T. A. Gabriel and R. G. Alsmiller, Jr., *Phys. Rev.* **182**, 1035 (1969).
16. G. G. Jonsson and K. Lindgren, *Phys. Scr.* **7**, 49 (1973).
17. G. Rudstam, *Z. Naturf.* **21a**, 1027 (1966).
18. A. Masaike, *J. phys. Soc. Japan* **19**, 427 (1964).
19. A. Järund, B. Friberg and B. Forkman, Private communication to G. G. Jonsson and K. Lindgren, quoted in Ref. [16]; see also A. Järund, B. Friberg and B. Forkman, University of Lund Report No. LLNP-7303, 1973 (unpublished).
20. V. I. Noga, Yu. N. Ranyuk and P. V. Sorokin, *Yad. Fiz.* **9**, 1152 (1969) (transl.: *Sov. J. Nucl. Phys.* **9**, 673 (1969)).
21. T. Methasiri and S. A. E. Johansson, *Nucl. Phys.* **A167**, 97 (1971).
22. J. R. Nix and E. Sassi, *Nucl. Phys.* **81**, 61 (1966).
23. W. D. Myers and W. J. Swiatecki, *Nucl. Phys.* **81**, 1 (1966).

Table 3. Cross-section per equivalent quantum $\sigma_0(\mu\text{b})$ of photoproduction of ^{24}Na

Target nucleus	Bremsstrahlung maximum energy E_0 (GeV)				
	0.30	0.40	0.55	0.75	1.00
^{27}Al	490 \pm 20	560 \pm 20	667 \pm 20	690 \pm 20	745 \pm 20
^{28}Si	290 \pm 20	330 \pm 20	380 \pm 20	430 \pm 20	470 \pm 20
^{31}P	230 \pm 20	250 \pm 20	290 \pm 20	330 \pm 20	350 \pm 20
^{32}S	206 \pm 10	240 \pm 10	280 \pm 10	320 \pm 10	350 \pm 10
^{35}Cl	230 \pm 10	260 \pm 10	290 \pm 10	320 \pm 10	350 \pm 10
^{39}K	30 \pm 3	50 \pm 5	65 \pm 5	80 \pm 5	100 \pm 5
^{40}Ca	5 \pm 2	20 \pm 3	45 \pm 5	60 \pm 5	60 \pm 5

Table 4. Cross-section per equivalent quantum $\sigma_0(\mu\text{b})$ of photoproduction of ^{24}Na

Target nucleus	Bremsstrahlung maximum energy E_0 (GeV)				
	0.30	0.40	0.55	0.75	1.00
$^{27}\text{Al}^*$	370 \pm 10	440 \pm 10	500 \pm 20	550 \pm 20	660 \pm 20
^{28}Si	100 \pm 10	140 \pm 10	160 \pm 10	210 \pm 10	240 \pm 10
^{31}P	100 \pm 20	160 \pm 20	200 \pm 20	270 \pm 20	310 \pm 20
^{32}S	120 \pm 10	160 \pm 10	180 \pm 10	210 \pm 10	240 \pm 10
^{35}Cl	65 \pm 10	100 \pm 10	140 \pm 10	190 \pm 10	220 \pm 10
^{39}K	20 \pm 5	35 \pm 5	55 \pm 5	65 \pm 5	80 \pm 5
^{40}Ca	12 \pm 3	25 \pm 5	35 \pm 5	50 \pm 5	60 \pm 5

*The results for ^{27}Al have already been published (see [8]) and are reported for comparison.

Table 5. Mean absolute cross-section $\bar{\sigma}_0(\mu\text{b})$ in the energy range 0.3–1 GeV

Target nucleus	Produced radionuclide		
	^{18}F	^{24}Na	^{26}Na
^{23}Na	190 \pm 30		
$^{27}\text{Al}^*$	120 \pm 10	200 \pm 20	220 \pm 20
^{28}Si	100 \pm 10	150 \pm 20	120 \pm 10
^{31}P	100 \pm 10	100 \pm 20	180 \pm 20
^{32}S	110 \pm 10	120 \pm 10	100 \pm 10
^{35}Cl	135 \pm 20	100 \pm 10	130 \pm 10
^{39}K	45 \pm 5	60 \pm 5	50 \pm 5
^{40}Ca	46 \pm 5	60 \pm 5	40 \pm 5

*The results for the photoproduction of ^{18}F and ^{24}Na from ^{27}Al have already been published (Ref. [3] and [8], respectively).

REF.	Y. Torizuka, K. Itoh, Y. M. Shin, Y. Kawazoe, H. Matsuzaki, G. Takeda Phys. Rev. C11, 1174 (1975)			ELEM. SYM.	A	Z	
				Ca	40	20	
METHOD				REF. NO.			
				75 To 2		hmg	
REACTION	RESULT	EXCITATION ENERGY	SOURCE		DETECTOR		ANGLE
			TYPE	RANGE	TYPE	RANGE	
E,E/	FMF	10- 35	D	150-250	MAG-D		DST

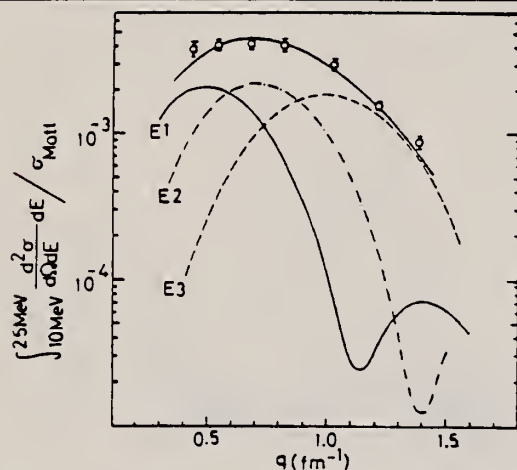


FIG. 2. The experimental form factor over the range 10-25 MeV. The solid, dash-dotted, dashed, and thick solid lines are the E1, E2, and E3 components and their sum, respectively.

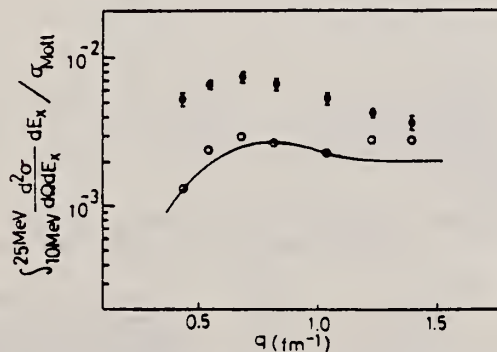


FIG. 5. The integrated values over 10-25 MeV for the cross section (closed circles), theoretical background (full line), and phenomenological background (open circles).

B(EL), GDR REGION

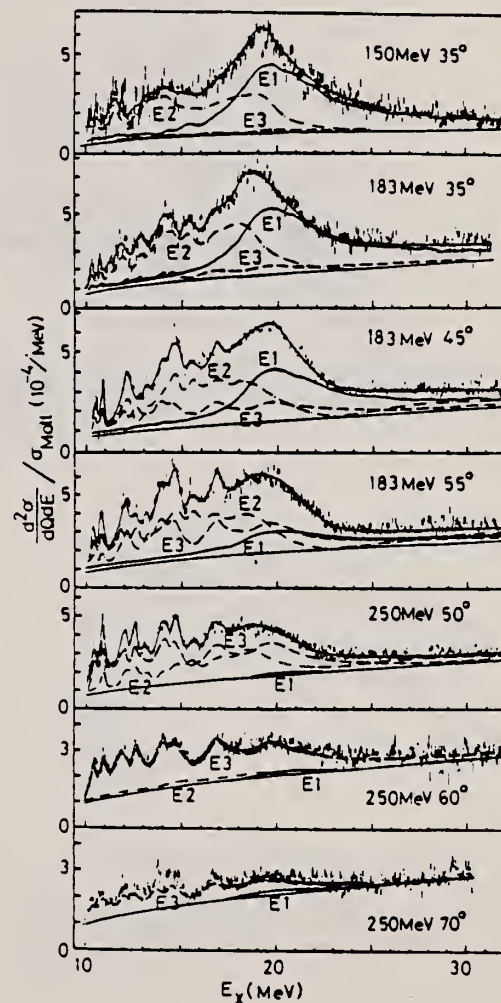


FIG. 1. The spectra of ^{40}Ca at various momentum transfers. The E1 (thick solid), E2 (dash-dotted), E3 (dashed), and the sum (thin solid) as well as the underlying background (smooth line) are shown.

(over)

TABLE II. Values of $B(EL)$ and $|M(0)|^2$ and the percentage of the isoscalar energy-weighted sum rule (EWSR). The errors are +15% and -30%.

E_x (MeV)	L	$B(EL)$ ($e^2 \text{fm}^{2L}$)	Percentage of EWSR ($T=0$)
10-13	2	72	8.2
	0	117	12.6
	3	2.97×10^3	6.3
13-16	2	144	20.6
	0	235	31.7
	3	2.93×10^3	7.9
16-19	2	148	25.6
	0	241	39.4
	3	2.71×10^3	8.8
19-22	2	57	11.6
	0	93	17.8
	3	2.43×10^3	9.2
22-25	2	0	0
	3	1.03×10^3	4.4
10-25	2	421	66
	0	688 ^a	102
	3	1.21×10^4	36.6

^a $|M(0)|^2 = |\langle \sum_i \frac{1}{2} r_i^2 \rangle|^2$ in fm^4

REF. S. G. Tonapetyan, N. V. Goncharov, and V. M. Khvorostyan
Yad. Fiz. 22, 440 (1975)
Sov. J. Nucl. Phys. 22, 226 (1976)

ELEM. SYM.	A	Z
Ca	40	20

REF. NO.	hmg
75 To 4	

REACTION	RESULT	EXCITATION ENERGY	SOURCE		DETECTOR		ANGLE
			TYPE	RANGE	TYPE	RANGE	
G,PI+	ABY	150-400	C	300,400	BBL-D		90
G,PI-	ABY	150-400	C	300,400	BBL-D		90
G,P	ABY	88-400	C	300,400	BBL-D		90

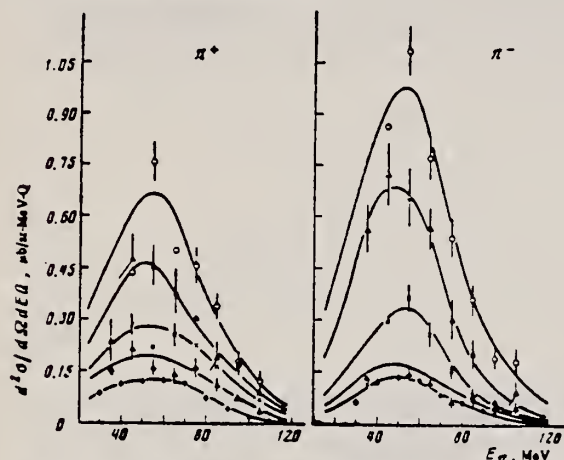


FIG. 1. Energy spectra of π^+ and π^- mesons. $E_{\pi}^{\text{max}} = 300$ MeV, $\theta_{\text{lab}} = 90 \pm 7^\circ$. Points: \circ — ^{12}C , \triangle — ^{28}Si , \times — ^{40}Ca , \diamond — ^{93}Nb , \square — ^{181}Ta .

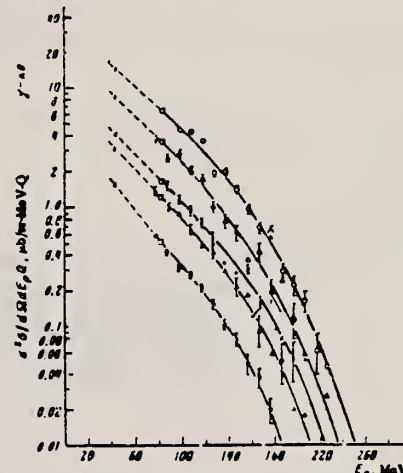


FIG. 3. Energy spectra of protons, $E_p^{\text{max}} = 300$ MeV, $\theta_{\text{lab}} = 90 \pm 7^\circ$. Points: \circ — ^{12}C , \triangle — ^{28}Si , \times — ^{40}Ca , \diamond — ^{93}Nb , \square — ^{181}Ta , \square —data from ref. 5, \diamond —data from ref. 6.

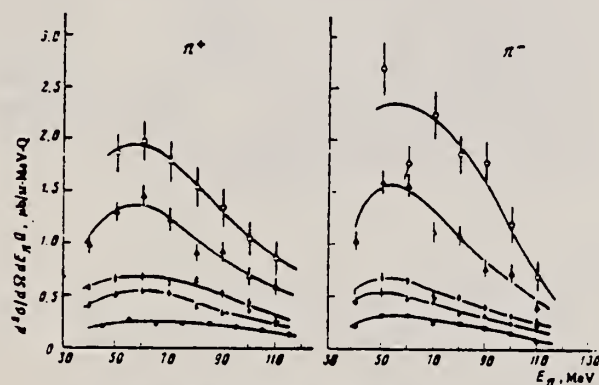


FIG. 2. Energy spectra of π^+ and π^- mesons. $E_{\pi}^{\text{max}} = 400$ MeV, $\theta_{\text{lab}} = 50 \pm 7^\circ$. The points are the same as in Fig. 1.

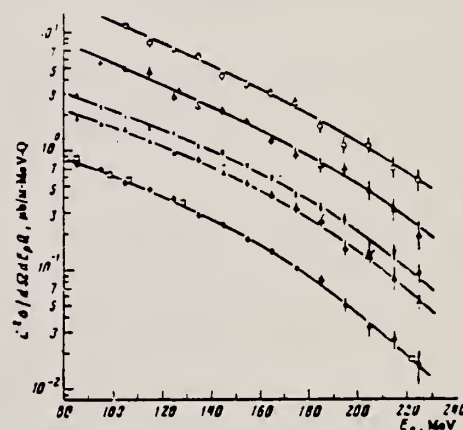
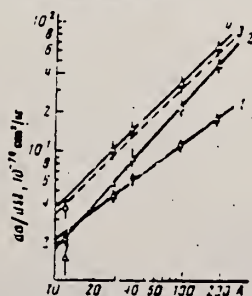


FIG. 4. Energy spectra of protons, $E_p^{\text{max}} = 400$ MeV, $\theta_{\text{lab}} = 90 \pm 7^\circ$. The points are the same as in Fig. 1; \square —data from ref. 7.

FIG. 5. Dependence of yields of π mesons 1, protons 2, and the sum of π -meson and proton yields 4 as a function of mass number of the nucleus. The dashed line 3 is the theory. Points: \square —experimental differential cross sections for pions of all signs, \triangle —differential cross sections for protons emitted at the same angle $\theta_{\text{lab}} = 90^\circ$, \circ —combined values of these differential cross sections. The statistical errors are shown.



⁵P.C. Murray et al., Phys. Rev. 94, 764 (54).

⁶C. Levinthal et al., Phys. Rev. 82, 822 (51).

⁷P. Dougan et al., LUSY Prep. 1002 (1970).

REF. A. S. Danagulyan, N. A. Demekhina
Yad. Fiz. 24, 681 (1976)
Sov. J. Nucl. Phys. 24, 355 (1976)

ELEM. SYM.	A	Z
Ca	40	20

METHOD	REF. NO.	
	76 Da 4	hmg

REACTION	RESULT	EXCITATION ENERGY	SOURCE		DETECTOR		ANGLE
			TYPE	RANGE	TYPE	RANGE	
G, NA24	ABX	THR* 5	C	2* 5	ACT-I		4PI

*ENERGY, GEV

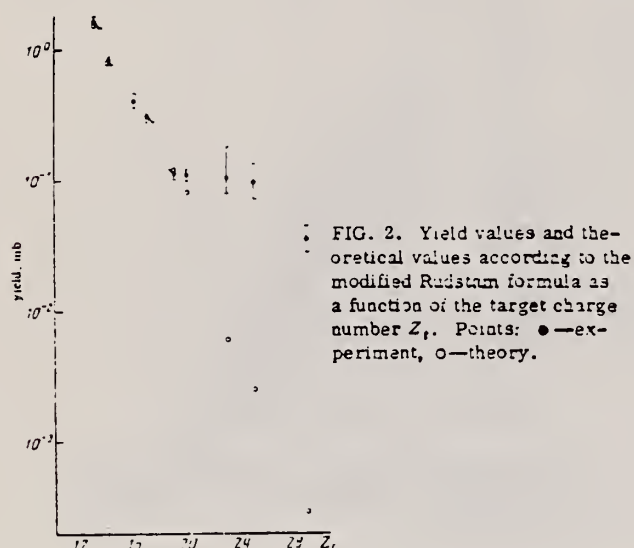


TABLE I. Experimental yields and reaction cross sections obtained in the measurements at the Erevan electron accelerator.

Target nucleus	Reaction yield, mb					Reaction cross section, mb
	$E_{\gamma \text{ max}}$, GeV					
	2	3	4	4.5	5	
²⁷ Al	0.81±0.08	0.87		0.87		0.07213±0.0348
²⁸ Si	0.27±0.02	0.28		0.29		0.0287±0.013
³² S	0.24±0.02	0.22		0.27		0.0323±0.0155
Cl	0.28±0.11	0.30		0.23		—
³⁹ K	0.1±0.01	0.125		0.13		0.06±0.0238
⁴⁰ Ca	0.086±0.01	0.09		0.115		0.035±0.0168
⁴⁴ V	0.083±0.02	0.094±0.02	0.009±0.02		0.062±0.025	0.019
⁵⁵ Mn	0.073±0.02	0.073±0.01	0.067±0.017		0.088±0.015	0.04078±0.0058
Cu	0.029±0.008	0.037±0.007	0.046±0.007		0.034±0.007	0.00347±0.0025

Note. The reaction cross sections have been calculated in the $1/E$ approximation of the bremsstrahlung spectrum.

ELEM. SYM.	A	Z
Ca	40	20
REF. NO.		
76 Li 7	egf	

REACTION	RESULT	EXCITATION ENERGY	SOURCE		DETECTOR		ANGLE
			TYPE	RANGE	TYPE	RANGE	
G,PN	ABX	150 - 800	C	80-800	ACT-I		4PI
G,3P3N	ABX	50 - 800	C	80-800	ACT-I		4PI

The yields of the reactions $^{40}\text{Ca}(\gamma, pn)^{38}\text{K}$ and $^{40}\text{Ca}(\gamma, 3p3n)^{34}\text{mCl}$ have been measured by the activation method in the energy range 80-800 MeV. From the measured yields the cross sections are deduced. The experimental cross sections are compared to calculations with a cascade-evaporation model for photo-induced reactions.

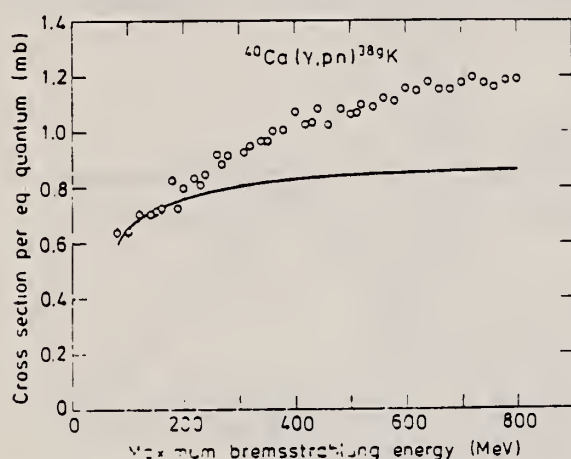


Fig. 1. The maximum yield of ^{38}K as a function of the maximum bremsstrahlung energy. The solid curve is calculated from low energy cross section data as described in the text.

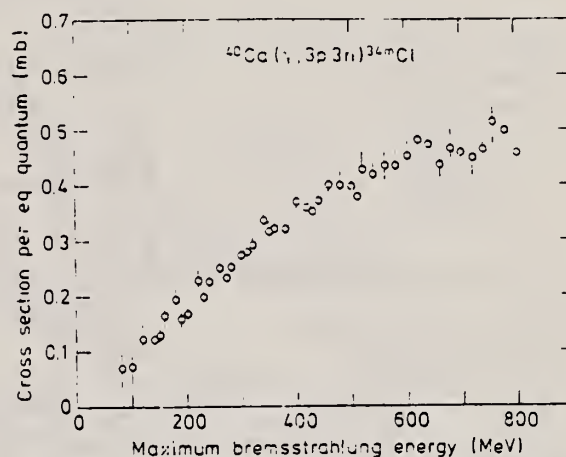


Fig. 2. The measured yield of ^{34}mCl as a function of the maximum bremsstrahlung energy.

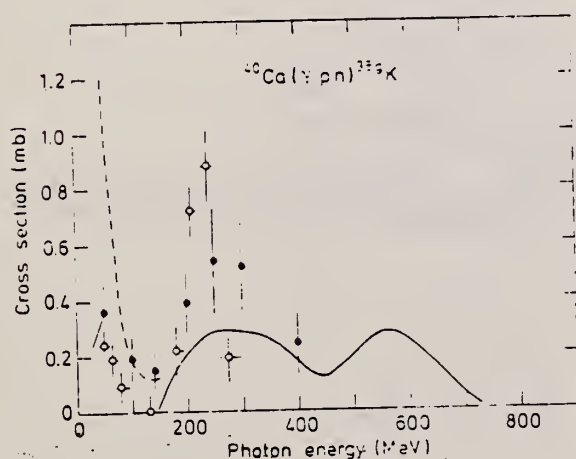


Fig. 3. The cross section for ^{38}K as a function of photon energy. The present result is given by the solid curve. The results in Refs. 3 and 5 are given by the dashed curve and open circles respectively. Filled circles are calculated values.

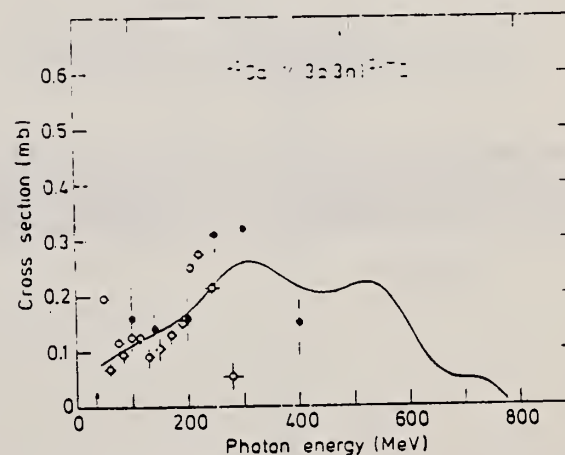


Fig. 4. The same as Fig. 3, but for ^{34}mCl .

- ³ Kayser, K., Collin, W., Filss, P., Guldbakke, S., Nolte, G., Reich, H., Trier, J.O., Witschel, W.: Z. Physik 239, 447 (1970)
⁵ Meyer, R.A.: Thesis, Univ. of Illinois, 1963, unpublished

REF.

J. Mougey, M. Bernheim, A. Bussiere, A. Gillebert, Phan
Xuan Ho, M. Priou, D. Royer, I. Sick, G. J. Wagner
Nucl. Phys. A262, 461 (1976)

ELEM. SYM.

A

Z

Ca

40

20

METHOD

REF. NO.

76 Mo 5

egf

REACTION	RESULT	EXCITATION ENERGY	SOURCE		DETECTOR		ANGLE
			TYPE	RANGE	TYPE	RANGE	
E, E/P	ABX	8* 80	D	497	MAG-D		53

*MISSING ENERGY

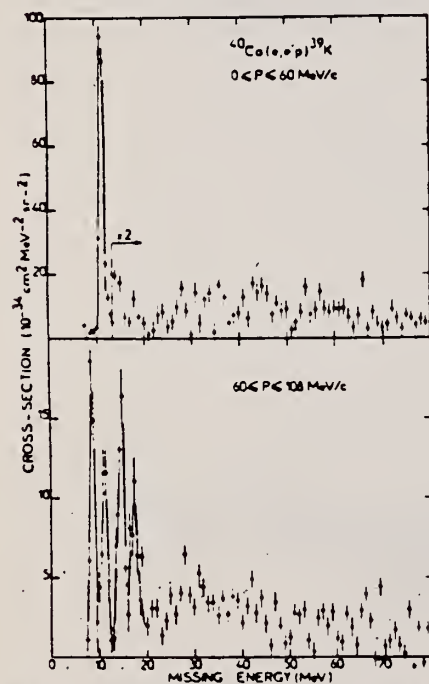
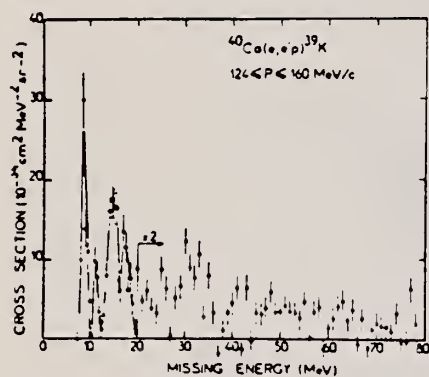


Fig. 13. Missing energy spectra from $^{40}\text{Ca}(e, p)$: (a) $0 \leq P \leq 60$ MeV/c, (b) $60 \leq P \leq 108$ MeV/c and (c) $124 \leq P \leq 160$ MeV/c.

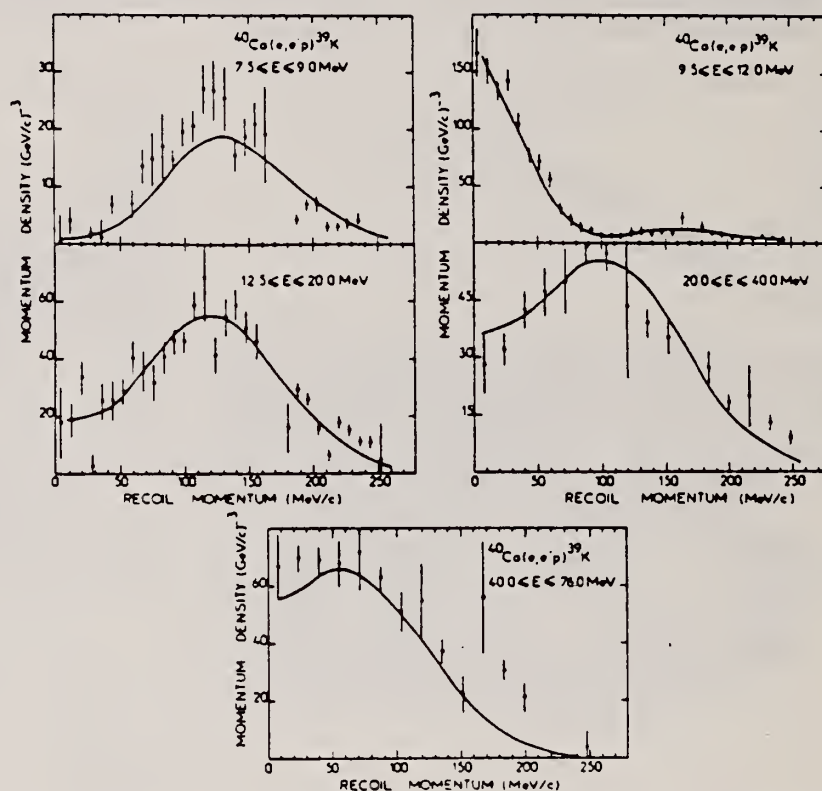


Fig. 14. Momentum distribution from $^{40}\text{Ca}(e, p)$: (a) $7.5 \leq E \leq 9$ MeV, (b) $9.5 \leq E \leq 12$ MeV, (c) $12.5 \leq E \leq 20$ MeV, (d) $20 \leq E \leq 40$ MeV and (e) $40 \leq E \leq 70$ MeV. The solid line represents the DWIA calculation.

REF.

K. Nakamura, S. Hiramatsu, T. Kamae, H. Muramatsu,
N. Izutsu, Y. Watase
Nucl. Phys. A271, 221 (1976)

ELEM. SYM.	A	Z
Ca	40	20

REF. NO.	
76 Na 3	egf

METHOD

REACTION	RESULT	EXCITATION ENERGY	SOURCE		DETECTOR		ANGLE
			TYPE	RANGE	TYPE	RANGE	
E, E/P	SPC	0*130	D	700-750	MAG-D		DST

Abstract: Information on proton hole states has been obtained for ^{27}Al , ^{40}Ca and ^{51}V through the (e, e'p) reaction. Lower-lying hole states have been identified. For ^{40}Ca an extensive analysis has been performed to study the structure of the 1s hole state. For ^{27}Al and ^{51}V , the properties of the 1s hole states have also been determined. The separation energies of the 1p and 1s states seem to be constant (40 and 60 MeV, respectively) for $A > 30$.

*SEPARATION ENERGY

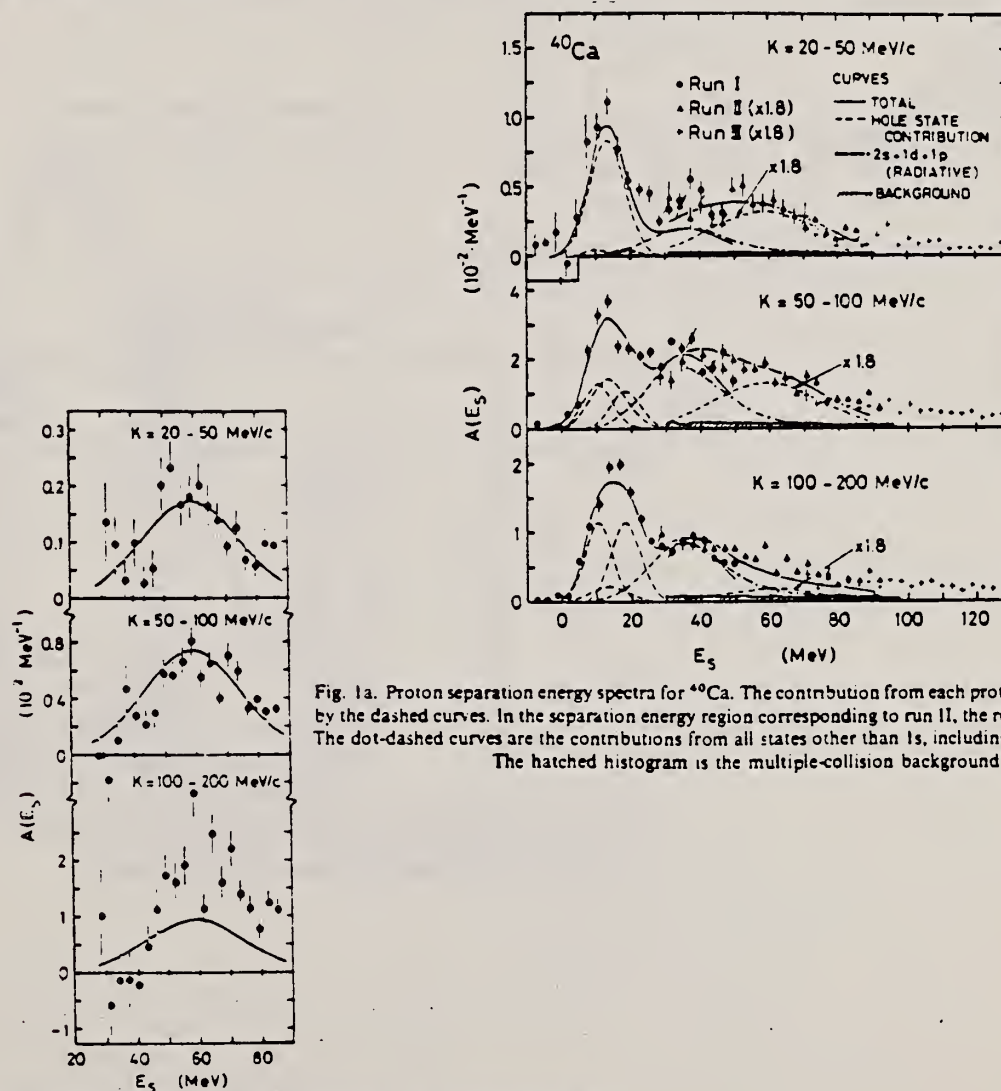


Fig. 1a. Proton separation energy spectra for ^{40}Ca . The contribution from each proton hole state is shown by the dashed curves. In the separation energy region corresponding to run II, the result of fit A is shown. The dot-dashed curves are the contributions from all states other than 1s, including the radiative effects. The hatched histogram is the multiple-collision background.

Fig. 3. The proton separation energy spectra in the 1s region after subtraction of the contributions from the 2s, 1d and 1p states. The 1s contribution is clearly evident. The solid curves show the result of fit A (see text).

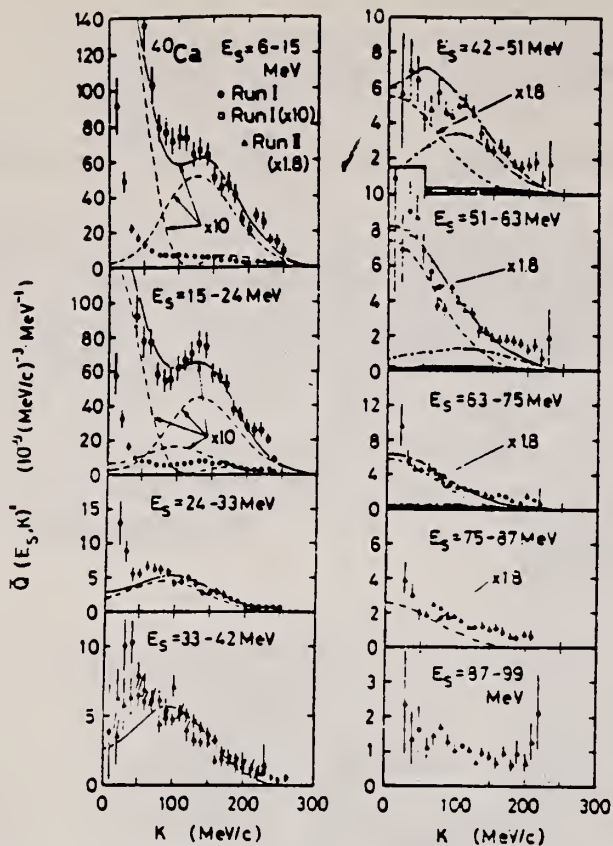


Fig. 1b. Recoil momentum distributions for ^{40}Ca . The curves are as in fig. 1a.

TABLE 6
Results of the PWIA analysis

Nucleus	α	Z'_α	Peak energy (MeV)	Width (FWHM) ^{a)} (MeV)	Oscillator const (MeV c)
^{27}Al	2s	0.12 ± 0.01	14.3 ± 0.2	4 ± 3	82 ± 4
	1d	1.6 ± 0.1	14.0 ± 0.6	12 ± 2	91 ± 1
	1p	2.4 ± 0.2	34 ± 1	31 ± 3	100 ± 1
	1s ^{b)}		57 ± 3	31 ± 9	148 ± 4
^{40}Ca	1d _{3/2}	1.1 ± 0.3	10.9 ± 0.7	9 ± 1	76 ± 4
	2s	0.9 ± 0.1	14.4 ± 0.3	13 ± 1	83 ± 5
	1d _{5/2}	1.5 ± 0.3	19.0 ± 1.1	10 ± 1	93 ± 4
	1p	1.8 ± 0.4	35 ± 1	21 ± 3	85 ± 3
	1s ^{b)}		59 ± 3	34 ± 10	144 ± 6
^{51}V	1f	0.4 ± 0.1	10.3 ± 1.1	5 ± 3	115 ± 8
	2s	0.3 ± 0.1	15.1 ± 0.2	5 ± 2	99 ± 5
	1d	1.7 ± 0.3	19.5 ± 0.5	19 ± 2	94 ± 6
	1p	1.1 ± 0.1	40 ± 1	25 ± 4	91 ± 4
	1s ^{b)}		60 ± 3	36 ± 11	143 ± 4

The errors are statistical only except for those assigned to the peak energies and widths for the 1s states.

^{a)} The experimental energy resolution (≈ 7 MeV) is not unfolded.

^{b)} Parameters were determined from the fit to the data of run II.

ELEM. SYM.	A	Z
Ca	40	20
REF. NO.		
76 Zi 1		egf

Comment: Mean Separation energy 33 ± 3 MeV

REACTION	RESULT	EXCITATION ENERGY	SOURCE		DETECTOR		ANGLE
			TYPE	RANGE	TYPE	RANGE	
E,E/	ABX	40-280	D	*	MAG-D		120

See further analysis of this data in reference 79Zi1

TRANS 3-Q CONST

Measurements of average separation energies and of Fermi momenta for ^{40}Ca and ^{48}Ca are reported. Evidence for the possible existence of "bump" structure in the quasi-elastic scattering of electrons from ^{48}Ca is also presented.

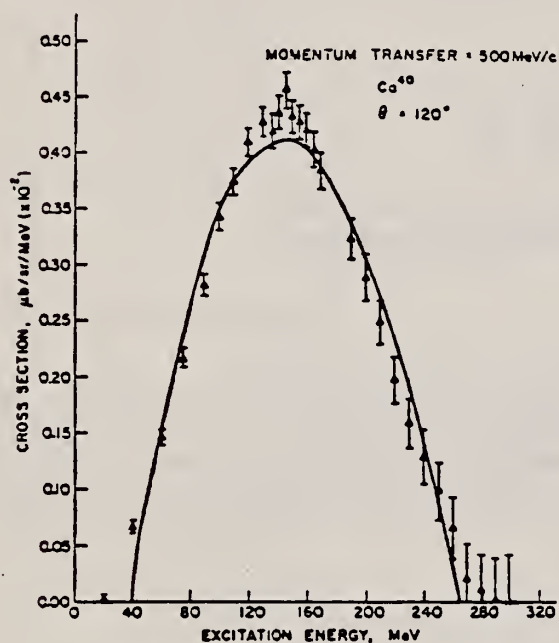


Fig. 1. Quasi-elastic spectrum obtained from ^{40}Ca at $|q| = 500$ MeV/c and a scattering angle of 120° . The smooth curve is the theoretical spectrum of the Moniz Fermi-gas model. The errors indicated at large energy loss are primarily due to the radiative corrections

REF. J.-O. Adler, B. Bulow, G.G Jonsson and K. Lindgren
Nuc1. Phys. A280, 325 (1977)

ELEM. SYM.	A	Z
Ca	40	20
REF. NO.		
77 Ad 3		egf

METHOD						
REACTION	RESULT	EXCITATION ENERGY	SOURCE		DETECTOR	
			TYPE	RANGE	TYPE	ANGLE
G,NG	ABY	18-750	C	100-750	SCD-D	135
G,PG	ABY	11-750	C	100-750	SCD-D	135

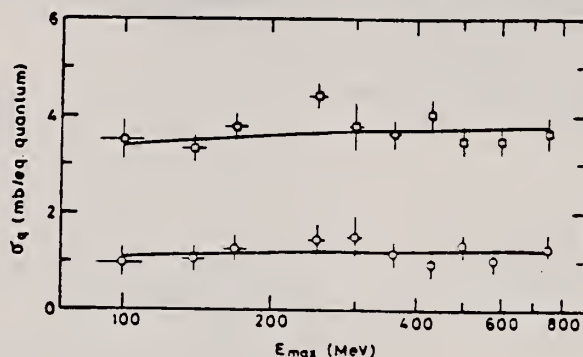


Fig. 2. Measured yields σ_q for reactions leading to the 2.47 MeV state in ^{39}Ca (circles) and the 2.52 MeV state in ^{39}K (squares). The solid curves show low energy and pion contributions fitted to the experimental points as described in text.

TABLE I

Experimentally determined mean yields in the energy range 100-750 MeV and thresholds for different one-nucleon removal channels

Final state		Emitted particle	$\bar{\sigma}_q$ (mb eq q.)	Threshold (MeV)
E^* (MeV)	J^π			
2.47	$\frac{1}{2}^+$	n_1	1.2 ± 0.2	18.2
2.52	$\frac{1}{2}^+$	p_1	3.7 ± 0.4	10.8
2.79	$\frac{1}{2}^-$	n_2	0.2 ± 0.1	18.5
2.81	$\frac{1}{2}^-$	p_2	1.2 ± 0.3	11.1
3.02	$\frac{1}{2}^-$	n_3	1.1 ± 0.4	18.7
3.01	$\frac{1}{2}^-$	p_3		11.3

TABLE 2

Comparison between the present one-nucleon yields and results from experiments at lower bremsstrahlung end-point energies

Experiment	E_{max} (MeV)	Relative yields				
		n_1	p_1	n_2	p_2	$(n_3 + p_3)$
present work	100-750	0.32 ± 0.06	1	0.05 ± 0.03	0.32 ± 0.09	0.30 ± 0.11
ref. ¹⁾	30-25	0.31 ± 0.04	1	0.05 ± 0.04	0.29 ± 0.04	0.25 ± 0.04
ref. ²⁾	32	0.28 ± 0.14	1	0.26 ± 0.13		0.12 ± 0.06

ELEM. SYM.	A	Z
40	Ca	20
REF. NO.		
77 As 10		hmg

REACTION	RESULT	EXCITATION ENERGY	SOURCE		DETECTOR		ANGLE
			TYPE	RANGE	TYPE	RANGE	
G, BE7 G, Na22	ABY	THR*5	C	2*5	SCD-D		UKN
G, Na24				(4.5)			

Photonuclear reactions in the targets ^{27}Al , ^{28}Si , ^{31}P , ^{32}S , and ^{40}Ca have been studied for maximum bremsstrahlung energies of 2, 2.4, 3, and 4.5 GeV. The yields of the residual nuclei ^7Be , ^{11}C , ^{12}N , ^{18}F , ^{22}Na , and ^{24}Na were measured by means of a germanium-lithium semiconductor detector with a sensitive volume of 30 cm³. In discussion of the results we took into account the contribution of the low energy part of the bremsstrahlung spectrum. Comparison of the measured yields with estimates calculated by Rudstam's formula permitted us to conclude that there is a difference in the mechanism of formation of the light fragments ^7Be , ^{11}C , and ^{12}N from that of the other residual nuclei ^{18}F , ^{22}Na , and ^{24}Na .

*GEV 5=4.5 GEV

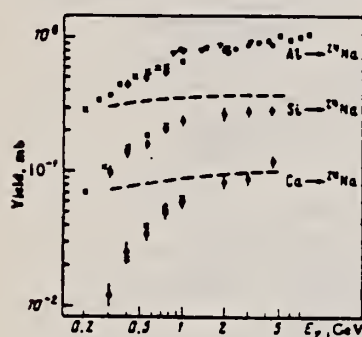


FIG. 1. Yields of the isotope ^{24}Na from targets of Al, Si, and Ca. x—Data of Ref. 4, o—data of Ref. 2, v—data of Ref. 6, o—data of Ref. 10, ●—data of the present work. The dashed lines show the contributions of the low energy part of the bremsstrahlung spectrum to the yields of the reactions $\text{Al}-^{24}\text{Na}$, $\text{Si}-^{24}\text{Na}$ according to the data of Ref. 4 and the results of the calculations of the present work.

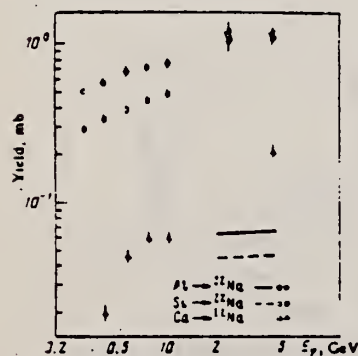


FIG. 2. Yields of ^{22}Na from targets of Al, Si, and Ca. The hollow symbols show the data of Ref. 2, and the solid symbols the data of the present work. The lines indicate the results of the calculations of the present work, which determine the contribution of the low-energy part of the bremsstrahlung spectrum to the yields of the reactions $\text{Al}-^{22}\text{Na}$ and $\text{Si}-^{22}\text{Na}$ for $2 \text{ GeV} \leq E_{\gamma} \leq 4.5 \text{ GeV}$.

TABLE II.

Residual nucleus	Reaction yield, mb/O					Normalized yield	σ_{theo} mb/g
	$\lambda_{\gamma} \text{ max} = 1 \text{ GeV}$	2 GeV	3 GeV	4 GeV	4.5 GeV		
Al target							
^{24}Na	0.06 ± 0.02	0.81	0.81	0.87	0.87	0.98	0.33
^{22}Na	0.74 ± 0.02		1.02 ± 0.13		1.07 ± 0.1	0.666	0.86
^{18}F	0.27 ± 0.003	0.38 ± 0.02		0.4 ± 0.02	0.39 ± 0.01	0.296	1.6
^{12}N		0.021 ± 0.004		0.025 ± 0.003	0.022 ± 0.004	0.0127	2.54
^{11}C	0.117 ± 0.013	0.104 ± 0.011		0.12 ± 0.02	0.107 ± 0.015	0.191	$3.3 \cdot 10^4$
^7Be	0.29 ± 0.03		0.37 ± 0.06		0.3 ± 0.05	0.216	$1.2 \cdot 10^4$
Si target							
^{24}Na	0.24 ± 0.01	0.274 ± 0.024	0.27 ± 0.02	0.29 ± 0.02	0.29 ± 0.02	0.14	0.43
^{22}Na	0.17 ± 0.02		1.22 ± 0.2		1.22 ± 0.1	1.17	2.39
^{18}F	0.2 ± 0.01	0.38 ± 0.03		0.39 ± 0.02	0.39 ± 0.02	0.39	2.89
^{12}N		0.033 ± 0.01		0.037 ± 0.01	0.039 ± 0.01	0.0217	7.26
^{11}C		0.108 ± 0.02		0.115 ± 0.025	0.121 ± 0.027	0.107	$1.2 \cdot 10^4$
^7Be			0.368 ± 0.05		0.32 ± 0.04	0.291	$8.2 \cdot 10^4$
P target							
^{24}Na	0.31 ± 0.02				0.35 ± 0.02	0.428	0.72
^{22}Na	0.35 ± 0.02				0.35 ± 0.02	0.421	2.03
^7Be					0.35 ± 0.02	0.208	$8.81 \cdot 10^4$
S target							
^{24}Na	0.24 ± 0.01	0.23 ± 0.02	0.25 ± 0.02	0.24 ± 0.02	0.27 ± 0.02	0.117	1.1
^{22}Na	0.35 ± 0.01			0.34 ± 0.02	0.34 ± 0.02	0.398	3.88
^{18}F	0.19 ± 0.01	0.26 ± 0.01		0.22 ± 0.01	0.27 ± 0.01	0.284	4.73
^{12}N		0.047 ± 0.02		0.053 ± 0.02	0.056 ± 0.025	0.054	$2.66 \cdot 10^4$
^{11}C	0.122 ± 0.013	0.163 ± 0.028		0.112 ± 0.028	0.13 ± 0.02	0.136	$1.23 \cdot 10^4$
^7Be	0.25 ± 0.02		0.36 ± 0.02		0.34 ± 0.04	0.314	$1 \cdot 10^4$
Cl target							
^{24}Na	0.22 ± 0.01	0.28 ± 0.03		0.3 ± 0.03	0.29 ± 0.03	0.297	1.8
^{22}Na	0.35 ± 0.02	0.21 ± 0.01				0.18	7.52
K target							
^{24}Na	0.08 ± 0.005	0.1 ± 0.01		0.125 ± 0.012	0.15 ± 0.013	0.16	2
^{22}Na	0.09 ± 0.003	0.11 ± 0.02				0.1	7.58
Ca target							
^{24}Na	0.16 ± 0.003	0.088 ± 0.01		0.09 ± 0.01	0.12 ± 0.012	0.147	2.2
^{22}Na	0.08 ± 0.003				0.21 ± 0.02	0.21	6.37
^7Be					0.245 ± 0.023	0.23	$1.2 \cdot 10^4$

Data for Cl and K targets previously published in Reference 11.

¹¹G. A. Vartapetyan *et al.*, Yad. Fiz. 17, 685 (1973) [Sov. J. Nucl. Phys. 17, 350 (1973)].

REF.

H.D. Graf, V. Heil, A. Richter, E. Spamer, W. Stock and
O. Titze
Phys. Lett. **72B**, 179 (1977)

ELEM. SYM.	A	Z
Ca	40	20
REF. NO.	77 Gr 2	
	egf	

METHOD

REACTION	RESULT	EXCITATION ENERGY	SOURCE		DETECTOR		ANGLE
			TYPE	RANGE	TYPE	RANGE	
E, E/	ABX	7	D	31- 67	MAG-D		DST

7=6.95

The isospin forbidden electroexcitation of the $1^-, T=0$ state at 6.95 MeV in ^{40}Ca has been investigated for momentum transfers $q = (0.18-0.51) \text{ fm}^{-1}$. The longitudinal form factor exhibits a minimum at $q = 0.19 \text{ fm}^{-1}$ indicating a destructive interference of the isoscalar and isovector parts. This behaviour is reproduced by a continuum shell-model calculation. A description of the transverse form factor leads to an effective proton charge of 0.5 for the $\Delta T = 0$ convection current.

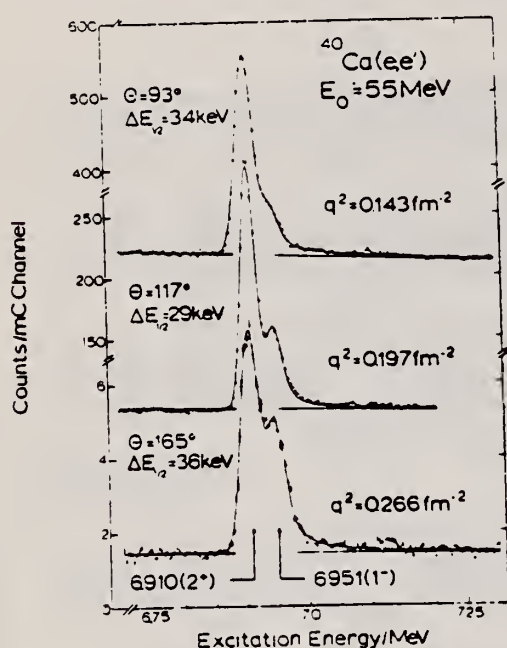


Fig. 1. Spectra of inelastically scattered electrons from an enriched (99.97%) ^{40}Ca target at three different momentum transfers. The counting rate, normalized to one detection channel and 1 mC of collected beam charge, is plotted as a function of excitation energy.

⁹F.R. Metzger, Phys. Rev. **165**, 1245 (1968)

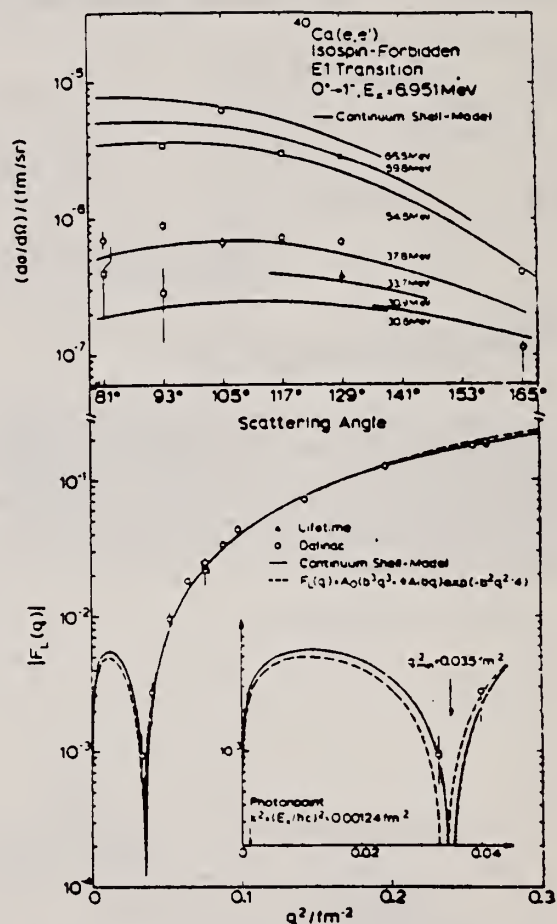


Fig. 2. Differential cross sections for the excitation of the $1^-, T=0$ state at 6.95 MeV in ^{40}Ca as a function of scattering angle at different energies (upper part). The lower part shows the absolute value of the longitudinal form factor $F_L(q)$ as a function of q^2 . The theoretical ratios of longitudinal to transverse cross sections were used to eliminate the transverse contributions. Besides the present measurements at the DALINAC the value calculated from the lifetime [9] is indicated. The full lines represent the results of the continuum shell-model calculation. Here, $d\sigma/d\Omega$ and $|F_L|^2$ were scaled by a factor of 0.81. The dashed line was obtained by a least-squares fit of eq. (2) to the experimental data.

ELEM. SYM.	A	Z
Ca	40	20
REF. NO.		
77 La 3		egf

METHOD					
REACTION	RESULT	EXCITATION ENERGY	SOURCE		ANGLE
			TYPE	RANGE	
G,G	G.G	7	D	7	DST

Abstract: The strengths of the isospin forbidden E1 ground-state transitions from the 1^- , 6.95 MeV state of ^{40}Ca and the 1^- , 7.12 MeV state of ^{16}O were determined in a γ -ray resonance scattering experiment; the partial widths are $\Gamma_0 = 0.41 \pm 0.03$ eV and 0.06 ± 0.01 eV, respectively. The results are in good agreement with previous determinations, confirming the unusually large strengths of these E1 transitions. In addition, the widths of the 2^+ , 6.91 MeV state of ^{40}Ca and the 2^+ , 6.92 MeV state of ^{16}O were measured as $\Gamma_0 = 0.13 \pm 0.05$ eV and 0.094 ± 0.010 eV, respectively.

6.95, 6.91 MeV

TABLE I
Widths of ^{40}Ca states

E_x (keV)		J^π	Γ_0 (eV)			Γ_0/Γ	
this work	ref. ^{a)}		this work	ref. ^{a)} ^{c)}	theory	this work	ref. ^{a)}
6914 \pm 2	6911 \pm 2	2^+	0.13 \pm 0.06	0.18 \pm 0.03	0.08 ^{a)}	> 0.7	> 0.65
6954 \pm 2	6954 \pm 3	1^-	0.41 \pm 0.08	0.47 \pm 0.06	0.36 ^{b)}	> 0.8	> 0.75

^{a)} Ref. ⁷⁾. ^{b)} Ref. ⁴⁾. ^{c)} In calculating Γ_0 it was assumed that $\Gamma_0/\Gamma = 1$.

- ⁴ D.H. Glockner and R.D. Lawson, Phys. Lett. 56B, 301 (1975)
⁷ W.J. Gerace and A.M. Green, Nuc1. Phys. A123, 241 (1969)

ELEM. SYM.	A	Z
Ca	40	20
REF. NO.		
78 Fi 7		

METHOD					
REACTION	RESULT	EXCITATION ENERGY	SOURCE		ANGLE
			TYPE	RANGE	
G,P	SPC	45-85	C	60-100	DST

Experimental data on the (γ, p) reaction at $E_\gamma = 60-100$ MeV for targets in the range $A = 7-93$ are compared with predictions based on a single-particle knock-out mechanism using shell model wavefunctions. The results show that this mechanism is more important than has generally been believed

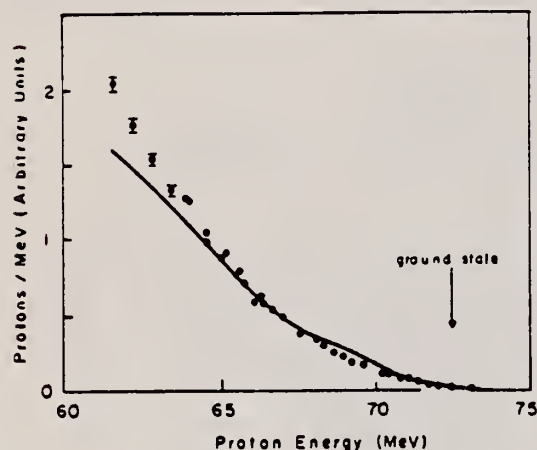


Fig. 1. The experimental proton spectrum at 45° from ^{40}Ca produced by 80 MeV bremsstrahlung is shown as circles. The ratio of the calculated and experimental spectra was obtained by a least-squares fitting procedure. The calculated proton spectrum, normalised by this ratio, is shown as a line.

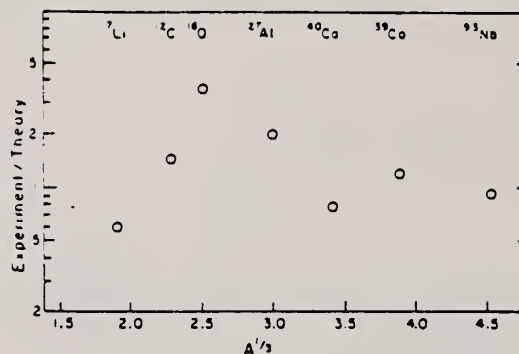


Fig. 2. The ratio of the measured photoproton emission populating low-lying states to the single-particle direct knock-out predictions is shown as a function of nuclear mass A for 80 MeV bremsstrahlung. Errors in the ratio, due to uncertainties in our calculations, are estimated to be a factor of ≈ 1.5 . Errors in the experimental data are negligible.

REF. H.D. Gräf, H. Feldmeier, P. Manakos, A. Richter, E. Spamer and
D. Strottman
Nucl. Phys. A295, 319 (1978)

ELEM. SYM.	A	Z
Ca	40	20
REF. NO.		
78 Gr 1		rs

REACTION	RESULT	EXCITATION ENERGY	SOURCE		DETECTOR		ANGLE
			TYPE	RANGE	TYPE	RANGE	
E, E/	ABX	3	D	34- 60	MAG-D		DST

3=3.353

Abstract: Monopole transitions from the 0_1^+ ground states to 0_2^+ excited states at 3.353 MeV (^{40}Ca), 1.837 MeV (^{42}Ca), 1.884 MeV (^{44}Ca) and 4.272 MeV (^{48}Ca) have been investigated with high resolution inelastic electron scattering (FWHM ≈ 30 keV) at low momentum transfer ($0.29 \leq q \leq 0.53 \text{ fm}^{-1}$). The respective monopole matrix elements are $2.53 \pm 0.41 \text{ fm}^2$, $5.24 \pm 0.39 \text{ fm}^2$, $5.45 \pm 0.41 \text{ fm}^2$ and $2.28 \pm 0.49 \text{ fm}^2$. These results are used together with known ground state charge radii and the average number of holes in the sd shell in the ground state to estimate the number of particle-hole excitations in the wave functions of the excited 0_2^+ states.

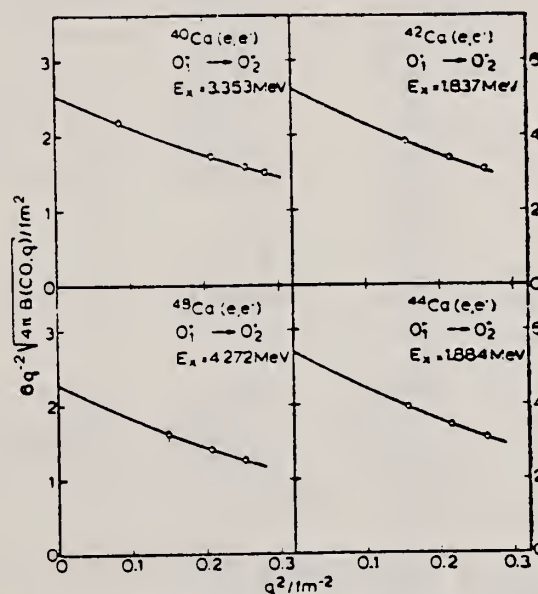


Fig. 3. Extrapolation of the measured $B(C0, q)$ values (dots) to $q = 0$ with the two parameter expression of eq. (1).

(OVER)

TABLE 2
Elastic and inelastic cross sections $(d\sigma/d\Omega)_{el}$ (10^{-3} fm² sr) and $(d\sigma/d\Omega)_{inel}$ (10^{-3} fm² sr), respectively, and DWBA correction factors f_c for the monopole transitions studied

Nucleus E_i (MeV)	E_0 (MeV)	θ (deg)	q^2 (fm ⁻²)	$(d\sigma/d\Omega)_{el}$	$(d\sigma/d\Omega)_{inel}$	f_c
⁴⁰ Ca 3.353	59.76	128.9	0.282	4.52	2.91 (6.5)	1.46
	54.73	140.9	0.256	3.11	1.95 (11.7)	1.53
	54.70	116.9	0.210	14.65	4.84 (8.9)	1.55
	33.67	128.9	0.086	40.70	2.47 (34.7)	1.91
⁴² Ca 1.837	54.73	140.9	0.263	3.05	6.53 (5.8)	1.48
	54.70	116.9	0.215	14.21	20.51 (4.3)	1.51
	54.70	92.9	0.156	64.99	45.23 (3.9)	1.54
⁴⁴ Ca 1.834	54.73	140.9	0.263	3.15	6.44 (7.3)	1.47
	54.72	116.9	0.215	14.83	20.91 (4.0)	1.50
	54.72	92.9	0.156	66.24	45.39 (3.5)	1.53
⁴⁸ Ca 4.272	54.73	140.9	0.252	2.99	1.11 (30.8)	1.46
	54.73	116.9	0.206	14.20	3.09 (5.6)	1.49
	54.73	92.9	0.149	64.09	7.38 (13.4)	1.53

The values in parentheses denote the statistical error of the cross sections in percent.

TABLE 3
Results of the present (e, e') experiment for monopole matrix elements, transition radii and pair decay widths together with results from other experiments and theoretical predictions

Nucleus	ME (fm ²)	R_{tr} (fm)	Γ_{π} (μ eV)	Exp.	Theory
⁴⁰ Ca	3.6 \pm 1.1	6.3	0.37 \pm 0.23	(e, e') ^{a)}	
			0.21 \pm 0.01	b)	
	2.6 \pm 0.1			(p, p') ^{c)}	d)
	2.44				e)
	5.53				f)
⁴² Ca	2.53 \pm 0.41	6.1 \pm 0.9	0.18 \pm 0.06	this work	
	5.93 \pm 0.52			(p, p') ^{g)}	
	5.58				d)
	4.19				f)
	5.24 \pm 0.39	6.3 \pm 0.4	0.016 \pm 0.002	this work	
⁴⁴ Ca	5.39 \pm 1.79			(p, p') ^{h)}	
	5.56			(x, p') ⁱ⁾	
	5.45 \pm 0.41	6.5 \pm 0.4	0.021 \pm 0.003	this work	
⁴⁸ Ca	1.52 \pm 0.07			(p, p') ^{j)}	
	2.28 \pm 0.49	6.8 \pm 1.4	0.63 \pm 0.27	this work	

a) Ref. ¹¹⁾; b) Ref. ¹²⁾; c) Ref. ⁹⁾; d) Ref. ¹⁾; e) Ref. ⁴⁾; f) Ref. ²²⁾; g) Ref. ²³⁾.

³W.J. Gerace and A.M. Green, Nucl. Phys. A93, 110 (1967);
A123, 241 (1969)

⁴P. Federman and S. Pittel, Phys. Rev. 186, 1106 (1969);
Nucl. Phys. A139, 108 (1969)

⁹M. Ulrickson, N. Benczer-Koller, J.R. MacDonald and
J.W. Tape, Phys. Rev. C15 186 (1977)

¹¹P. Strehl, Z. Phys. 234, 416 (1970)

¹²P.M. Endt and C. van der Leun, Nucl. Phys. A235, 27 (1974)

²²L.D. Skouras, Nucl. Phys. A220, 604 (1974)

²³J.D. McCullen and D.J. Donahue, Phys. Rev. C8, 1406 (1973)

METHOD					REF. NO.	
					78 Gr 5	hmg
REACTION	RESULT	EXCITATION ENERGY	SOURCE		DETECTOR	
			TYPE	RANGE	TYPE	RANGE
E, E/	ABX	3	D	31-67	MAG-D	
		(3.353)				

Abstract: Monopole transitions from the 0_1^+ ground states to 0_2^+ excited states at 3.353 MeV (^{40}Ca), 1.837 MeV (^{42}Ca), 1.884 MeV (^{44}Ca) and 4.272 MeV (^{48}Ca) have been investigated with high resolution inelastic electron scattering (FWHM ≈ 30 keV) at low momentum transfer ($0.29 \leq q \leq 0.53 \text{ fm}^{-1}$). The respective monopole matrix elements are $2.53 \pm 0.41 \text{ fm}^2$, $5.24 \pm 0.39 \text{ fm}^2$, $5.45 \pm 0.41 \text{ fm}^2$ and $2.28 \pm 0.49 \text{ fm}^2$. These results are used together with known ground state charge radii and the average number of holes in the sd shell in the ground state to estimate the number of particle-hole excitations in the wave functions of the excited 0^+ states.

NUCLEAR REACTIONS $^{40,42,44,48}\text{Ca}(e, e')$, $E = 31-67$ MeV; measured $\sigma(E; E_0; \theta)$.
 $^{40,42,44,48}\text{Ca}$ 0^+ level deduced E0 matrix elements. Shell model calculation.

TABLE 2
Elastic and inelastic cross sections ($d\sigma/d\Omega$), ($10^{-1} \text{ fm}^2/\text{sr}$) and ($d\sigma/d\Omega$) ($10^{-1} \text{ fm}^2/\text{sr}$), respectively, and DWBA correction factors f_c for the monopole transitions studied

Nucleus E_0 (MeV)	E_0 (MeV)	θ (deg)	q^2 (fm^{-2})	$(d\sigma/d\Omega)_0$	$(d\sigma/d\Omega)_{\text{DWBA}}$	f_c
^{40}Ca 3.353	59.76	128.9	0.282	4.52	2.91 (6.5)	1.46
	54.73	140.9	0.256	3.11	1.95 (11.7)	1.53
	54.70	116.9	0.210	14.65	4.84 (8.9)	1.55
	33.67	128.9	0.086	40.70	2.47 (34.7)	1.91
^{42}Ca 1.837	54.73	140.9	0.263	3.05	6.53 (5.8)	1.48
	54.70	116.9	0.215	14.21	20.51 (4.3)	1.51
	54.70	92.9	0.156	64.99	45.23 (3.9)	1.54
^{44}Ca 1.884	54.73	140.9	0.263	3.15	6.44 (7.3)	1.47
	54.72	116.9	0.215	14.83	20.91 (4.0)	1.50
	54.72	92.9	0.156	66.24	45.39 (3.5)	1.53
^{48}Ca 4.272	54.73	140.9	0.252	2.99	1.11 (30.8)	1.46
	54.73	116.9	0.206	14.20	3.09 (5.6)	1.49
	54.73	92.9	0.149	64.09	7.38 (13.4)	1.53

The values in parentheses denote the statistical error of the cross sections in percent.

TABLE 3
Results of the present (e, e') experiment for monopole matrix elements, transition radii and pair decay widths together with results from other experiments and theoretical predictions

Nucleus	ME (fm^2)	R_{00} (fm)	Γ_0 (μeV)	Exp.	Theory
^{40}Ca	3.6 ± 1.1	6.3	0.37 ± 0.23	(e, e') ^{a)}	
	2.6 ± 0.1		0.21 ± 0.01	^{b)}	
	2.44			(p, p') ^{c)}	^{d)}
	5.53			this work	^{e)}
^{42}Ca	2.53 ± 0.41	6.1 ± 0.9	0.18 ± 0.06	this work	
	5.93 ± 0.52			(p, p') ^{c)}	^{d)}
	5.58			this work	^{e)}
^{44}Ca	4.19	6.3 ± 0.4	0.016 ± 0.002	this work	
	5.39 ± 1.79			(p, p') ^{c)}	^{d)}
	5.56			(a, p') ^{c)}	^{e)}
^{48}Ca	5.45 ± 0.41	6.5 ± 0.4	0.021 ± 0.003	this work	
	1.52 ± 0.07			(p, p') ^{c)}	^{d)}
	2.28 ± 0.49	6.8 ± 1.4	0.63 ± 0.27	this work	^{e)}

^{a)} Ref. ¹¹⁾, ^{b)} Ref. ¹²⁾, ^{c)} Ref. ⁹⁾, ^{d)} Ref. ⁶⁾, ^{e)} Ref. ²¹⁾.

(OVER)

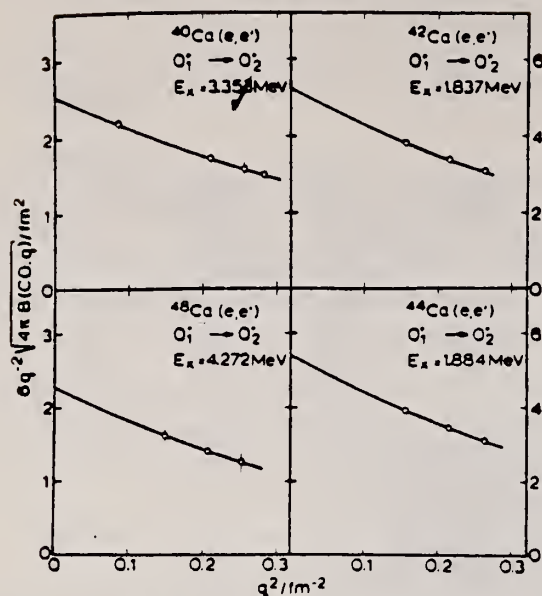


Fig. 3. Extrapolation of the measured $B(C0, q)$ values (dots) to $q = 0$ with the two parameter expression of eq. (1).

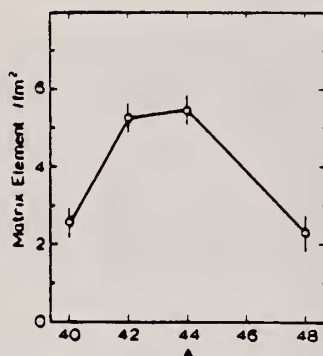


Fig. 4. The determined monopole matrix elements as a function of mass number for the four Ca isotopes. The line which connects the experimental points has no theoretical significance.

- 3) W. J. Gerace and A. M. Green, Nucl. Phys. A93 (1967) 110, A123 (1969) 241
- 4) P. Federman and S. Pittel, Phys. Rev. 186 (1969) 1106; Nucl. Phys. A139 (1969) 108
- 5) M. Sakakura, A. Arima and T. Sebe, Phys. Lett. 61B (1976) 335
- 6) N. Benczer-Koller, G. G. Seaman, M. C. Bertin, J. W. Tape and J. R. MacDonald, Phys. Rev. C2 (1970) 1037
- 7) J. C. Adloff, K. H. Souw, D. Disdier, F. Scheibling, P. Chevallier and Y. Wolfson, Phys. Rev. C10 (1974) 1819
- 8) M. Ulrickson, W. Hartwig, N. Benczer-Koller, J. R. MacDonald and J. W. Tape, Phys. Rev. C13 (1976) 536
- 9) M. Ulrickson, N. Benczer-Koller, J. R. MacDonald and J. W. Tape, Phys. Rev. C15 (1977) 186
- 10) P. Strehl and Th. H. Schucan, Phys. Lett. 27B (1968) 641
- 11) P. Strehl, Z. Phys. 234 (1970) 416
- 12) P. M. Endt and C. van der Leun, Nucl. Phys. A235 (1974) 27
- 13) R. F. Frosch, R. Hofstadter, J. S. McCarthy, G. K. Nöldeke, K. J. van Oostrum, M. R. Yearian, B. C. Clark, R. Herman and D. G. Ravenhall, Phys. Rev. 174 (1968) 1380
- 14) P. Doll, G. J. Wagner, K. T. Knöpfle and G. Maurle, Nucl. Phys. A263 (1976) 210
- 15) J. A. Nolen, Jr. and R. J. Gleitsmann, Phys. Rev. C11 (1975) 1159
- 16) K. K. Seth, A. Saha, W. Benenson, W. A. Lanford, H. Nann and B. H. Wildenthal, Phys. Rev. Lett. 33 (1974) 233
- 17) C. R. Fischer and G. H. Rawitscher, Phys. Rev. 135 (1964) B377
- 18) C. W. de Jager, H. de Vries and C. de Vries, Atomic Data and Nucl. Data Tables 14 (1974) 479
- 19) H. Theissen, Springer Tracts in Modern Phys. 65 (1972) 1
- 20) S. Krewald, R. Rosenfelder, J. E. Galonska and A. Faessler, Nucl. Phys. A269 (1976) 112
- 21) Th. H. Schucan, Nucl. Phys. 61 (1965) 417
- 22) L. D. Skouras, Nucl. Phys. A220 (1974) 604
- 23) J. D. McCullen and D. J. Donahue, Phys. Rev. C8 (1973) 1406

REF. P.D. Zimmerman, J.M. Finn, C.F. Williamson, T. de Forest Jr.,
and W.C. Hermans
phys. Lett. 80B, 45 (1978)

ELEM. SYM.	A	Z
Ca	40	20
REF. NO.		rs
78 Zi 3		

METHOD			SOURCE		DETECTOR		ANGLE
REACTION	RESULT	EXCITATION ENERGY	TYPE	RANGE	TYPE	RANGE	
E, E/	RLX	0-250	D	150-250	MAG-D		160

Deep-inelastic electron scattering data from ^{40}Ca were obtained at several bombarding energies and a 160° scattering angle at the Bates Linear Accelerator. The data, and calculations illustrate two processes which may contribute, are presented.

QUASI-ELASTIC

See further analysis of this data in reference 79Zi1

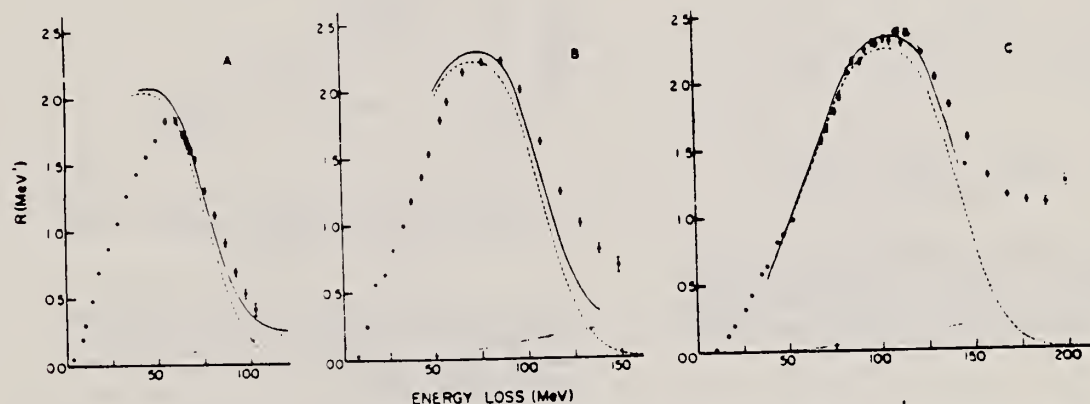


Fig. 1. Response function for ^{40}Ca at 160° scattering angle versus energy lost by the electron. Figures a, b, c show data taken at bombarding energies of 150, 200, and 250 MeV, respectively. The dashed lines represent the quasi-elastic contribution calculated using the H.O. shell model; the dotted lines represent the MEC contribution; the solid lines are the sum of these two terms. The sum and MEC calculations have not been continued beyond pion threshold; the one-body calculation has been continued to the ends of the plots.

$$\sigma_M R(q, \omega) = \frac{d^2\sigma}{d\Omega dE_f}$$

ELEM. SYM.	A	Z
Ca	40	20
REF. NO.		
79Gr2		hg

METHOD					REF. NO.	
					79Gr2	hg
REACTION	RESULT	EXCITATION ENERGY	SOURCE		DETECTOR	
			TYPE	RANGE	TYPE	RANGE
E, E/	ABX	10	D	36-58	MAG-D	
		(10.319)				

LEVEL 10.319, J-PI, B(ML)

An unusually strong magnetic dipole transition from the ground state to a state at $E_x = 10.319$ MeV in ^{40}Ca has been observed in high-resolution inelastic electron scattering, contrary to expectations from the pure independent particle shell model. The transition strength, however, can be accounted for by coherent spin-flip transitions due to strong ground-state correlations.

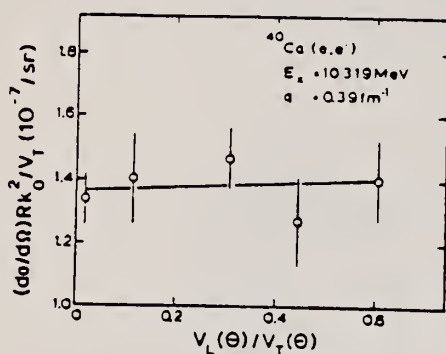


Fig. 2. Angular dependence of the cross section at constant momentum transfer $q = 0.39 \text{ fm}^{-1}$. The quantities on the axes are defined in the main text. The slope of the angular distribution is compatible with zero, i.e. with a pure transverse transition.

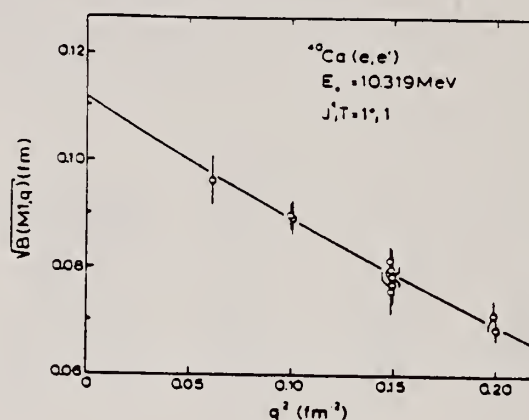


Fig. 3. Square root of the reduced transition probability as a function of q^2 . The extrapolation of the fitted curve through the data points to the photon point $q = k = E_x/\hbar c$ yields the $B(M1)$ transition strength.

REF. W. Steffen, H.-D. Gräf, W. Gross, D. Meuer, A. Richter, E. Spamer;
O. Titze, W. Knüpfer
Phys. Lett. 95B, 23 (1980)

EL. SYD.	A	Z
Ca	40	20
REP. NO.		
80 St 7		hy

METHOD

REACTION	RESULT	EXCITATION ENERGY	SOURCE		DETECTOR		ANGLE
			TYPE	RANGE	TYPE	RANGE	
E, E/	SPC	8-12	D	30-50	MAG-D		151

LEV 8.43, 9.87, 10.32

The search for magnetic dipole transitions from the ground state of the even-even Ca isotopes to high lying $J^\pi = 1^+$ states by means of low momentum transfer but high resolution inelastic electron scattering is described. The previously detected strongly excited $J^\pi = 1^+$ state at $E_x = 10.319$ MeV [$B(M1) \uparrow = 1.12 \pm 0.27 \mu_N^2$] in ^{40}Ca has been confirmed, but – contrary to the expectations of the independent particle shell model – only a fairly weak M1 transition is observed in ^{42}Ca [$E_x = 11.235$ MeV, $B(M1) \uparrow = 0.59 \pm 0.05 \mu_N^2$] and none in ^{44}Ca between $E_x = 8.2$ –12.2 MeV. In ^{48}Ca , however, a very strong M1 transition [$B(M1) \uparrow = 4.0 \pm 0.3 \mu_N^2$] to a single state at $E_x = 10.227$ MeV has been discovered.

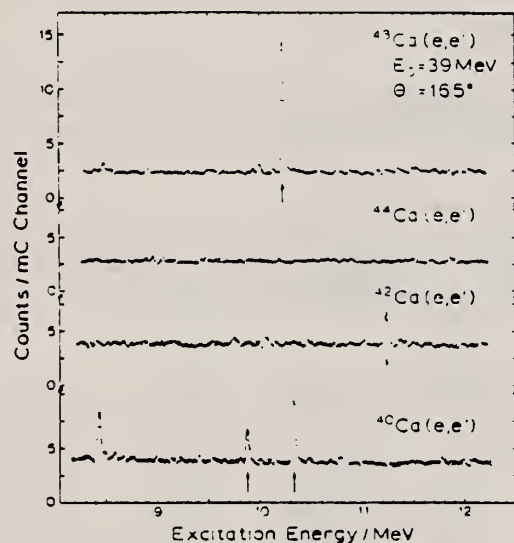


Fig. 1. High-resolution inelastic electron scattering spectra of $^{40,42,44,48}\text{Ca}$ all measured at $\theta = 165^\circ$ and $E_0 = 39$ MeV. Magnetic dipole transitions are denoted by an arrow.

Ca	40	20
REF. NO.		
81 Ch 1		hg

METHOD			SOURCE		DETECTOR		ANGLE
REACTION	RESULT	EXCITATION ENERGY	TYPE	RANGE	TYPE	RANGE	
P,G	LFT	9, 11	D	1 - 2	SCD-D		DST
				(1.130-2.043)			

The absolute strengths of the $^{39}\text{K}(p,\gamma)^{40}\text{Ca}$ resonances at $E_p = 1130, 1344$, and 2043 keV have been determined to be $S_{1m} = 1.6 \pm 0.2, 4.1 \pm 0.5$, and 14.3 ± 1.3 eV, respectively. Relative strengths were measured for resonances in the range $0.7 < E_p < 2.9$ MeV. The astrophysical reaction rates of hydrogen burning of ^{39}K in explosive oxygen burning in the stellar temperature region of $T = (1.0-7.0) \times 10^8$ K are compared with Hauser-Feshbach calculations. The effect of the revised reaction rates on the ^{39}K abundance is discussed.

9.43, 10.32 MeV

On a déterminé que les forces absolues des resonances $^{39}\text{K}(p,\gamma)^{40}\text{Ca}$ pour $E_p = 1130, 1344$ et 2043 keV avaient respectivement les valeurs $S_{1m} = 1.6 \pm 0.2, 4.1 \pm 0.5$ et 14.3 ± 1.3 eV. Les forces relatives étaient mesurées pour les resonances dans l'intervalle $0.7 < E_p < 2.9$ MeV. Les vitesses des reactions astrophysiques de fusion ^{39}K -hydrogene au cours de la combustion explosive de l'oxygene, dans la region de temperatures stellaires $T = (1.0-7.0) \times 10^8$ K sont comparées avec les calculs Hauser-Feshbach. On discute l'effet des valeurs revisees des vitesses de reaction sur l'abondance de ^{39}K .

[Traduit par le journal]

Can. J. Phys. 59, 238 (1981)

TABLE 2. Summary of the angular distribution results and comparison with previous values

E_p (keV)	Transition (MeV)	a_2		a_4	
		Present ^a	Ref. 2	Present ^a	Ref. 2
1130	$r \rightarrow 0$	0.35 ± 0.03		0.00 ± 0.04	
1344	$r \rightarrow 3.74$	0.09 ± 0.03	0.06 ± 0.05	-0.15 ± 0.03	-0.08 ± 0.05
	$r \rightarrow 3.31$	-0.25 ± 0.03	-0.12 ± 0.04	0.02 ± 0.04	0.04 ± 0.05
2043	$r \rightarrow 0$	-0.065 ± 0.012	0.036 ± 0.010	-0.003 ± 0.014	0.001 ± 0.010

^aThe coefficients are corrected for the solid angle of the detector

TABLE 3. Summary of the present absolute strength measurements

E_p (keV)	Target	Transition (MeV)	Branching (%)	$\mu_{r10}(55)^\dagger$	$\epsilon(E_p)^\ddagger$ (eV $(10^{13} \text{ mol cm}^{-3})$)	S_{1m} (eV)
1130	KCl	$r \rightarrow 0$	91 ± 3	1.000 ± 0.014	18.3	1.6 ± 0.2
1344	KCl	$r \rightarrow 3.74$	41 ± 3	1.049 ± 0.014	17.1	4.1 ± 0.7
		$r \rightarrow 3.90$	46 ± 3	0.993 ± 0.014		4.0 ± 0.8
2043	KCl	$r \rightarrow 0$	53 ± 3	1.000 ± 0.006	12.9	14.5 ± 1.5
	K ₂ SO ₄				20.6	14.1 ± 2.1
						14.3 ± 1.3

^aAs deduced from the angular distribution data obtained in the present experimental geometry. Thus the solid angle attenuation is taken into account experimentally.

[†]Deduced from the data given in ref. 10. Error limits estimated to be $\pm 5\%$.

REF. P.E. Burt, L.W. Fagg, H. Crannell, D.I. Sober, W. Stapor,
J.T. O'Brien, X.K. Maruyama, J.W. Lightbody, R.A. Lindgren
Physical Review C25, 2805 (1982)

EL. SYM.	A	Z
Ca	40	20
REF. NO.		egf
82 Br 10		

METHOD

REACTION	RESULT	EXCITATION ENERGY	SOURCE		DETECTOR		ANGLE
			TYPE	RANGE	TYPE	RANGE	
E, E/	FMF	10	D	31-65	MAG-D		DST

Values of the form factor for the 10.32 MeV transition in ^{40}Ca have been measured at six different low momentum transfers corresponding to incident electron energies between 31 and 65 MeV and scattering angles of 127.8° and 162.4°. Analysis of the data shows that the transition is transverse and M1. Our data in conjunction with that of earlier workers yield a value of $\Gamma_0(M1) = 4.82 \pm 0.26$ eV for the ground state transition width. It is shown that in the low momentum transfer range covered in this work, $q < 0.55 \text{ fm}^{-1}$, this result is essentially model independent. Results for the transition at 9.86 MeV state are also discussed.

9.86 AND 10.32 MEV LVS

[NUCLEAR REACTIONS $^{40}\text{Ca}(e, e')$, $E_0 = 31-65$ MeV; measured $d\sigma/d\Omega$ at $\theta = 127.8^\circ, 162.4^\circ$; deduced multipolarity and transition width, Γ_0 .]

TABLE I. Values of cross section and form factors squared for the 9.86 and 10.32 MeV transition. The % errors apply to both the cross section and the form factor squared.

Level (MeV)	q (fm^{-1})	E_0 (MeV)	θ (deg)	$\frac{d\sigma}{d\Omega}$ ($\text{fm}^2/\text{sr} \times 10^{-6}$)	F^2 ($\times 10^{-6}$)	Error %
9.86	0.260	30.93	162.4	0.613	2.74	10.6
9.86	0.336	41.78	127.8	1.40	8.50	11.7
9.86	0.342	39.12	162.4	0.647	4.62	17.1
9.86	0.442	49.15	162.4	0.447	5.04	9.9
9.86	0.547	59.59	162.4	0.307	5.09	13.6
9.86	0.546	64.97	127.8	1.13	16.6	5.3
10.32	0.258	30.92	162.4	1.34	3.84	6.6
10.32	0.334	41.80	127.8	1.21	5.31	11.6
10.32	0.340	39.12	162.4	1.03	5.46	13.3
10.32	0.440	49.15	162.4	0.560	5.23	8.8
10.32	0.544	59.60	162.4	0.290	5.00	14.5
10.32	0.544	64.97	127.8	0.334	4.73	12.9

The form factors squared for the 9.86 MeV transition are given in terms of F^2/T_0 ; while those for the 10.32 MeV transition are in terms of F_T^2 .

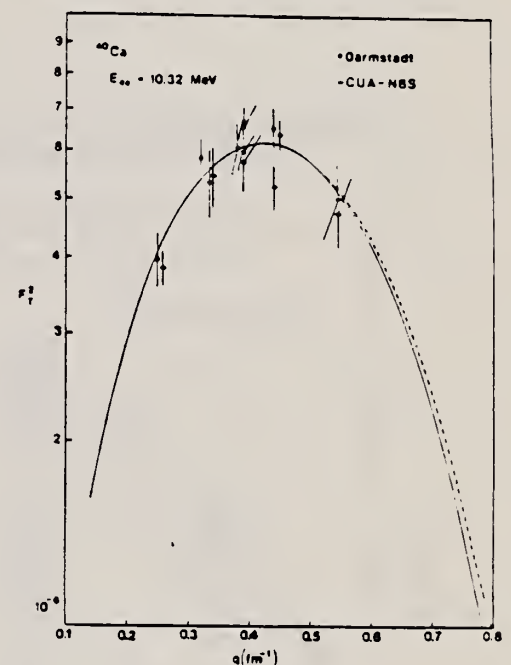


FIG. 3. Transverse form factors squared as a function of the momentum transfer q . Experimental points from this work as well as those of Ref. 4 are plotted. The solid and dashed curves fitted to the data points correspond to oscillator shell model form factor calculations assuming $f_{1/2} \rightarrow f_{1/2}$ and $d_{3/2} \rightarrow d_{3/2}$ transition configurations and oscillator parameters $b = 1.84$ and 2.11 fm, respectively.

REF. G.W. Dodson, E.C. Booth, F.L. Milder, B.E. Parad, B.L. Roberts,
D.R. Tieger, J. Comuzzi
Phys. Rev. C26, 2548 (1982)

ELEM. SYM.	A	Z
Ca	40	20
REF. NO.		
82 Do 3		egf

METHOD

REACTION	RESULT	EXCITATION ENERGY	SOURCE		DETECTOR		ANGLE
			TYPE	RANGE	TYPE	RANGE	
G,PI0	ABY	THR*20	C	140-155	CKV-I		1PI

Photoproduction of π^0 mesons off targets of ${}^6\text{Li}$, ${}^{12}\text{C}$, ${}^{28}\text{Si}$, ${}^{40}\text{Ca}$, natural Cd, and natural Pb was studied using a bremsstrahlung beam with endpoint energies of 140, 145, 150, and 155 MeV. Photoproduction from a liquid hydrogen target was employed as a normalization. The measured yields were found to be in disagreement with published theoretical cross sections for ${}^6\text{Li}(\gamma, \pi^0){}^6\text{Li}$ and also in disagreement with a simple schematic model which assumed only coherent contributions from the M_{1+} multipole. The schematic model, however, did approximately predict the relative magnitudes of the yield curves for the energy range 14–20 MeV over threshold.

*MEV ABOVE THR

NUCLEAR REACTIONS ${}^6\text{Li}$, ${}^{12}\text{C}$, ${}^{28}\text{Si}$, ${}^{40}\text{Ca}$, Cd, Pb, (γ, π^0) ;
 $E_\gamma = 140-155$ MeV; measured σ ; test of reaction model.

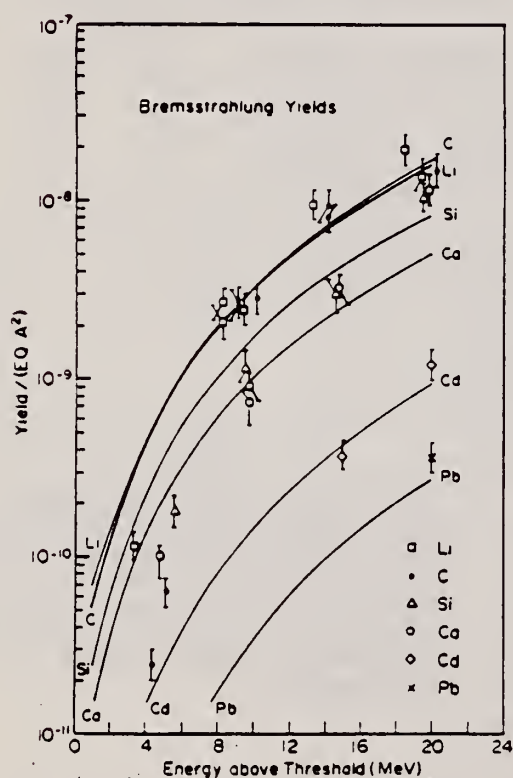


FIG. 6. The experimental and calculated yields for (γ, π^0) off a range of complex nuclei. The data were scaled so that the ${}^{12}\text{C}(\gamma, \pi^0){}^{12}\text{C}$ experimental yield fit the calculated yield at 9.7 MeV over threshold (see text).

REF. R. Moreh, W.M. Sandefur, W.C. Sellyey, D.C. Sutton, R. Vodhanel
Phys. Rev. C25, 1824 (1982)

ELEM. SYM.	A	Z
Ca	40	20
REF. NO.		egf
82 Mo 10		

METHOD					REF. NO.	
					82 Mo 10	egf
REACTION	RESULT	EXCITATION ENERGY	SOURCE		DETECTOR	
			TYPE	RANGE	TYPE	RANGE
G,G	LFT	4-10	C	9-12	SCD-D	127

Resonance fluorescence is used for measuring the widths of 13 levels in ^{40}Ca below 10.4 MeV among which nine $E2$ transitions were identified. The total $E2$ strength of those nine levels together with some other known 2^+ levels below 10 MeV exhausts $\sim 22\%$ of the energy weighted sum rule. The partial and total widths of the strong $M1$ state at 10.32 MeV are compared with theory.

13 LEVELS 3.9-10.3 MEV

[NUCLEAR REACTIONS $^{40}\text{Ca}(\gamma, \gamma')$, $E = 8.5, 11.3, 11.7$ MeV bremsstrahlung. Deduced Γ_0 , $\Gamma(E2)$, $\Gamma(M1)$. Natural target.]

TABLE I. Excitation energies, spins, and measured widths of levels in ^{40}Ca photoexcited in the present work. Asterisks indicate calibration energies taken from Ref. 9.

E_x (keV)	Present			Others	
	J^π	Γ_0 (meV)	Γ_0/Γ_i	Γ_0^* (meV)	J^π
3904.4 \pm 0.2*	2 ⁺		1.00	13.4 \pm 0.8	2 ⁺
5628.0 \pm 1.0	2 ⁺	7 \pm 3	0.9 \pm 0.05 ^c	8.7 \pm 2.4	2 ⁺
5902.0 \pm 1.0	1	25 \pm 5	1.00	11 \pm 4	1 ⁻
6422.4 \pm 1.0 ^b	2 ⁺	50 \pm 6	1.00 ^b		
6909.1 \pm 0.3*	2 ⁺	190 \pm 20	1.00	160 \pm 35	2 ⁺
6950.9 \pm 0.3*	1	450 \pm 20	1.00	506 \pm 39	1 ⁻
7872.9 \pm 0.8	2 ⁺	190 \pm 17	0.84 \pm 0.06	>30	2 ⁺
8091.4 \pm 0.8	2 ⁺	150 \pm 10	1.00	>15	2 ⁺
8113.4 \pm 1.3	1	12 \pm 5	1.00	>30	
8578.9 \pm 0.8	2 ⁺	94 \pm 12	1.00	>20	2 ⁺
8747.6 \pm 1.2	2 ⁺	65 \pm 12	1.00		(1,2) ⁺
8980.6 \pm 1.2 ^d	2 ⁺	54 \pm 10	1.00 ^d		
9866.0 \pm 2.0		3600 \pm 1450 ^e	0.0122 ^e	1360 \pm 250	1
10318.0 \pm 2.0	1	5500 \pm 800	0.21 \pm 0.02 ^f	4740 \pm 300 ^g	1 ⁺ ^g

*Reference 9.

^bThis is a new level whose Γ_0/Γ_i was taken to be 1.00.

^cThis value of Γ_0/Γ_i was taken from Ref. 9.

^dThis is a new level. Another level at 8980 \pm 5 keV, listed in Ref. 9 and reported to have $J^\pi = (5-7)^+$, is obviously not identifiable with this level.

^eThis Γ_0 was obtained using $\Gamma_0/\Gamma_i = 0.0122$ taken from Ref. 9. Our measurement yielded a value of Γ_0^2/Γ_i of 44 \pm 18 meV to be compared with a value of 16.6 \pm 5.0 meV deduced from Ref. 9.

^fThis is our measured value and is reported for the first time.

^gReference 5.

TABLE III. $B(E2)$ values and the percentage of transition strength in units of the EWSR in ^{40}Ca as measured in the present work. Asterisks indicate data taken from Ref. 9.

E_x (MeV)	J^π	$B(E2)$ ($e^2\text{fm}^4$)	(EWSR) (%)
3.904	2^+	18.40 ± 1.10	3.59 ± 0.21
5.249	2^+	1.28 ± 0.33	0.34 ± 0.09
5.630	2^+	1.53 ± 0.65	0.43 ± 0.12
6.422	2^+	5.68 ± 0.68	1.82 ± 0.22
6.909	2^+	15.00 ± 1.50	5.17 ± 0.52
7.467	2^+	3.52 ± 2.10	1.32 ± 0.80
7.873	2^+	7.79 ± 0.70	3.07 ± 0.27
8.091	2^+	5.36 ± 0.37	2.17 ± 0.15
8.579	2^+	2.51 ± 0.33	1.08 ± 0.14
8.748	2^+	1.57 ± 0.29	0.69 ± 0.14
8.981	2^+	1.15 ± 0.29	0.52 ± 0.12
9.388*	2^+		
9.564*	2^+		
9.808*	$(1,2^+)$		
9.869*	$(1,2^+)$	$(10.60 \pm 3.45)^a$	$(5.23 \pm 1.70)^a$
$\Sigma 0-10$			$\geq 22 \pm 2^b$

*This level was reported (Ref. 9) to have $\Gamma_0 = 0.80 \pm 0.27$ eV. Because of the uncertainty due to its large strength, it was not included in calculating the total EWSR below 10 MeV.

^bIn calculating this total strength, the $B(E2)$ value for each of the levels at 9.388, 9.564, and 9.808 MeV was assumed to be $0.7 e^2\text{fm}^4$. With such a transition strength, those levels could have been easily missed in the present measurement especially because the levels are unbound and the value of Γ_0/Γ_1 could very likely be < 1 .

CA
A=41

CA
A=41

CA
A=41

REF.

I. Bergqvist, D. Drake, and D. K. McDaniels
PICNS-73, II, p. 945 (1973) Asilomar

ELEM. SYM.

A

Z

Ca

41

20

METHOD

REF. NO.

73 Be 6

egf

REACTION	RESULT	EXCITATION ENERGY	SOURCE		DETECTOR		ANGLE
			TYPE	RANGE	TYPE	RANGE	
N,G	RLY	18- 24	D	10- 15	NAI-D		UKN

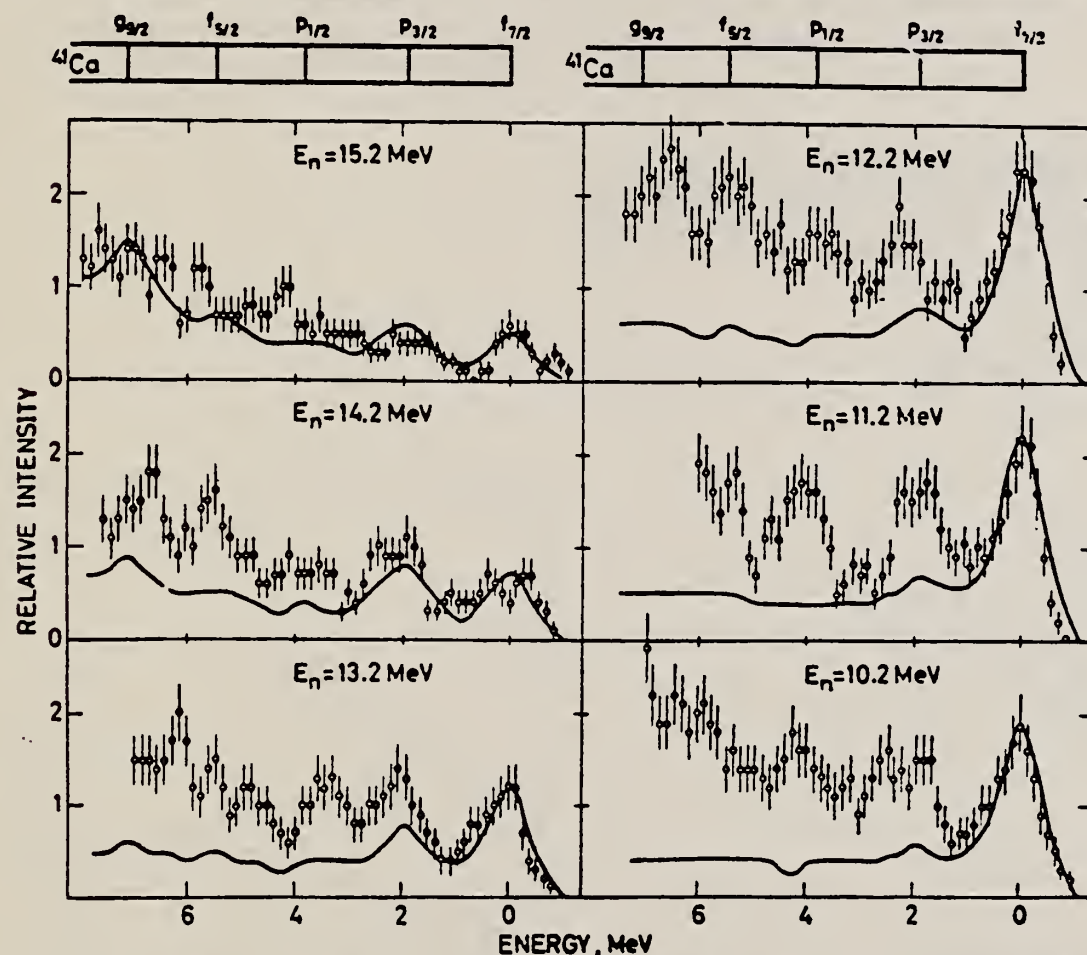


FIG. 1. Experimental γ -ray spectra from the $^{40}\text{Ca}(n,\gamma)^{41}\text{Ca}$ reaction at neutron energies from 10.2 to 15.2 MeV. The relative γ -ray intensity is plotted as a function of the excitation energy of the approximate location of the single-particle levels in ^{41}Ca . The solid lines represent spectra calculated from the semi-direct capture theory of Clement, Lane, and Rook.⁴ The peaks corresponding to the $f_{7/2}$ ground state transitions have been used to normalize the theoretical spectra to the experimental ones.

⁴C.F. Clement, A.M. Lane, and J.R. Rook, Nucl. Phys. **66**, 273, 293 (1965);

L. Rosen, J.G. Beery, A.S. Goldhaber, and E.M. Auerbach, Ann. Phys. **34**, 96 (1965).



ELEM. SYM.	A	Z
Ca	41	20

REF. NO.	
74 Be 7	egf

REACTION	RESULT	EXCITATION ENERGY	SOURCE		DETECTOR		ANGLE
			TYPE	RANGE	TYPE	RANGE	
N,G	ARX	15- 27	D	6- 18	NAI-D		90

Cross section value assumes isotopes angular distribution (see 72Be7, I. Bergqvist, D.M. Drake, D.K. McDaniels, Nucl. Phys. A191, 641 (1972)).

Fig. 3. Experimental (n, γ) cross section for γ -ray transitions to excited levels between 1.9 and 2.7 MeV. The differential cross section at 90° was multiplied by 4π and obtained from eq. (2) of the text. The theoretical cross sections (see caption to fig. 2) were calculated for an assumed $p_{3/2}$ neutron state located at the centroid energy $E_x = 2.07$ MeV, of the observed $p_{3/2}$ levels and with the spectroscopic factor $S = 1.0$ and (lower curves) for a $d_{3/2}$ neutron state at $E_x = 2.02$ MeV with $S = 0.2$.

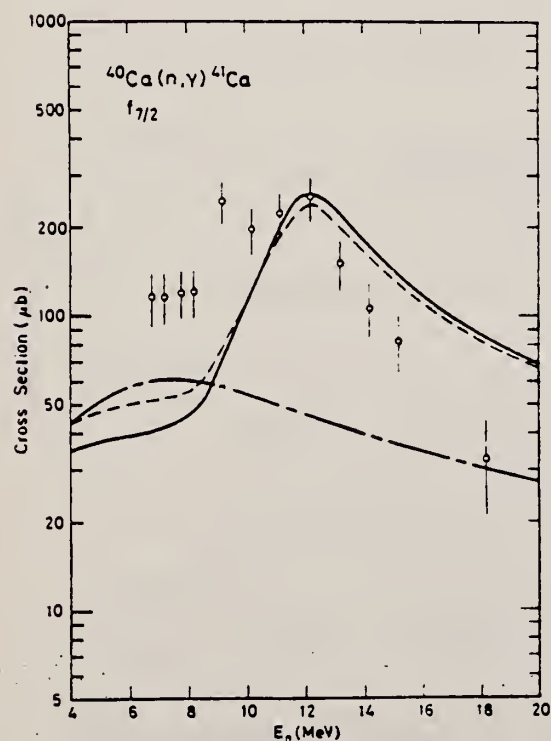
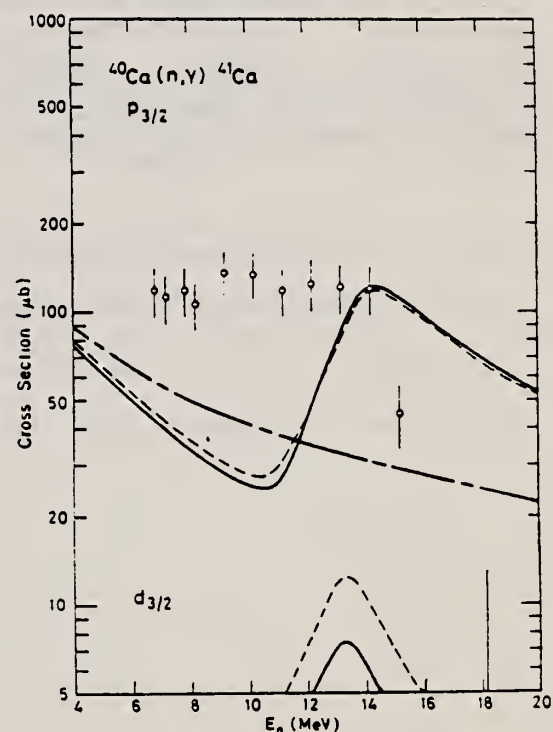


Fig. 2. Total (n, γ) cross section for the γ -ray transition to the $f_{7/2}$ ground state of ^{41}Ca . The differential cross section at 90° was multiplied by 4π and obtained from eq. (2) of the text. The direct cross section (dash-dot line) was calculated from the theory of Lane⁴⁾ and the semidirect cross sections from Clement *et al.*¹⁰⁾ using two different form factors for the particle-vibration coupling: a surface peaked form factor originally used⁹⁾ (solid line) and a volume form described by Longo and Saporetti²⁸⁾ (dashed line). Interference between direct and semidirect capture is taken into account.



(over)

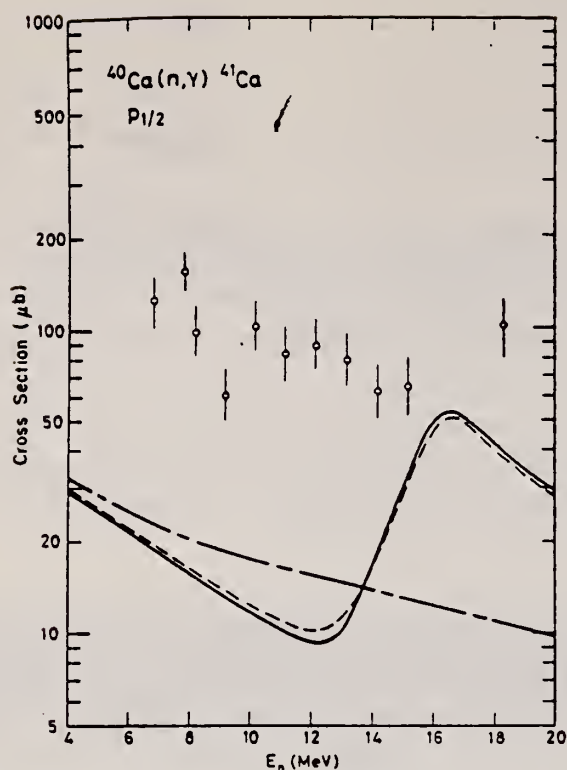


Fig. 4. Experimental (n, γ) cross section for γ -ray transitions to excited levels between 3.5 and 4.8 MeV. The differential cross section at 90° was multiplied by 4π and obtained from eq. (2) of the text. The theoretical cross sections (see caption to fig. 2) were calculated for an assumed $p_{1/2}$ neutron state located at the centroid energy $E_c = 4.13$ MeV, of the observed $p_{1/2}$ levels and with the spectroscopic factor $S = 1.0$.

4

A.M. Lane, Nucl. Phys. 11 (1959) 625

9

G.E. Brown, Nucl. Phys. 57 (1964) 339

10

C.F. Clement, A.M. Lane, and J.R. Rook, Nucl. Phys. 66 (1965) 273,293

28

G. Longo and F. Saporetti, Nucl. Phys. 199 (1973) 530

REF. E. D. Arthur, D. M. Drake, I. Halpern
Phys. Rev. Lett. 35, 914 (1975).

ELEM. SYM.	A	Z
Ca	41	20
REF. NO.		
75 Ar 5		
hmg		

REACTION	RESULT	EXCITATION ENERGY	SOURCE		DETECTOR		ANGLE
			TYPE	RANGE	TYPE	RANGE	
N,G	NOX	22	D	14	NAI-D		DST
		(22.4)					

Relative yields of capture photons have been observed for four nuclei at angles of 55°, 90°, and 125° in bombardments with 14-MeV neutrons. The yields from ^{10}B , ^{29}Si , and ^{40}Ca show smaller fore-aft anisotropies than those observed in corresponding proton captures. This suggests that the forward peaking in (p, γ) reactions is due mainly to direct rather than collective capture amplitudes. Photons from $^{12}\text{C}(n, \gamma)^{13}\text{C}$ peak backward, but this peaking cannot be straightforwardly accounted for in terms of the interference between the collective excitations dominant in this energy region.

TABLE I. Angular distribution coefficients.

Reaction	E^0 (MeV)	a_2	$R_n = 0.57a_1 - 0.39a_2$	R_p
$^{10}\text{B}(n, \gamma)^{11}\text{B}$	25	-0.44 ± 0.28	0.05 ± 0.08	$^{10}\text{B}(p, \gamma)^{11}\text{C} \sim 0.3^a$
$^{12}\text{C}(n, \gamma)^{13}\text{C}$	18	-0.08 ± 0.18	-0.15 ± 0.06	$^{12}\text{C}(p, \gamma)^{13}\text{N} \sim 0.3^b$
$^{29}\text{Si}(n, \gamma)^{30}\text{Si}$	24	0.2 ± 0.24	0.02 ± 0.1	
$^{40}\text{Ca}(n, \gamma)^{41}\text{Ca}$	22	0.03 ± 0.20	-0.06 ± 0.08	$^{39}\text{K}(p, \gamma)^{40}\text{Ca} \sim 0.2^c$

^aRef. 13.

^bRef. 14.

^cRef. 15.

¹³H.M. Kuan, Nucl. Phys. A151, 129 (1970).

¹⁴M. Hasinoff, private communication.

¹⁵E.M. Diener et al., Phys. Rev. C7, 695 (1973); E.M. Diener et al., Phys. Rev. C7, 705 (1973).

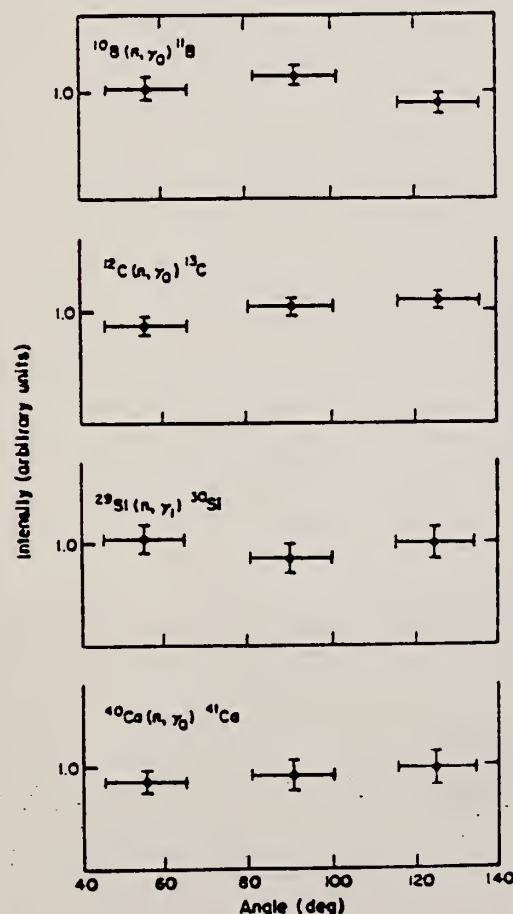


FIG. 3. Angular distributions obtained for 14-MeV neutron capture leading to the designated final states. The horizontal bars show the angular widths subtended by the capture targets.

$$W(\theta_{n\gamma}) \sim 1 + \sum_{n=1} a_n P_n$$



REF. S.A. Wender, N.R. Roberson, M. Potokar, H.R. Weller and
D.R. Tilley
Phys. Rev. Lett. 41, 1217 (1978)

ELEM. SYM.	A	Z
Ca	41	20
REF. NO.		
78 We 1		rs

METHOD						REF. NO.	
						78 We 1	rs
REACTION	RESULT	EXCITATION ENERGY	SOURCE		DETECTOR		ANGLE
			TYPE	RANGE	TYPE	RANGE	
N,G	ABX	15- 21	D	6- 13	NAI-D		DST

Differential cross sections have been measured for the reaction $^{40}\text{Ca}(n,\gamma)^{41}\text{Ca}$ at seven angles in 1-MeV steps and at $\theta_{\text{lab}} = 90^\circ$ in 200-keV steps for incident neutron energies of 6-13 MeV. The extracted a_2 coefficients and the fore-aft asymmetry are in good agreement with a direct-semidirect model calculation if the isoscalar giant quadrupole resonance is included.

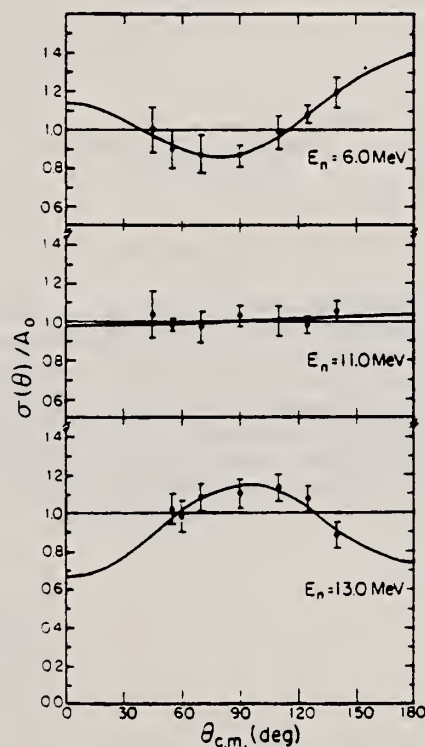


FIG. 2. Typical data at three energies for the quantity $\sigma(\theta)/A_0$. The solid curves are the results of fitting the data by Legendre polynomials to second order.

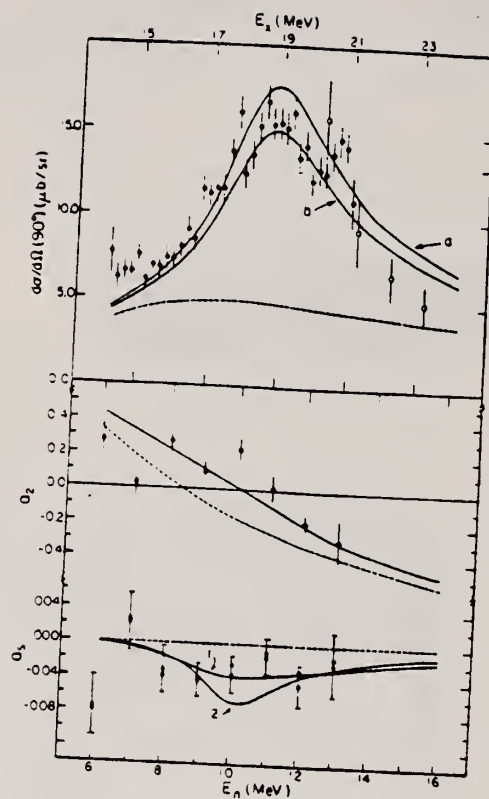


FIG. 3. Comparison of the a_2 coefficients, a_3 coefficients, and 90° yield curve with a DSD reaction model calculation as described in the text. For a_2 , the solid circles are from second-order fits while the open circles are from third-order fits. The dashed curves for the yield curve and a_2 coefficients are from a pure direct dipole calculation, while the dashed curve for the a_3 coefficients is from a calculation that assumes DSD dipole terms but only a direct quadrupole term.

REF. H.R. Weller, R.A. Blue, P.L. Von Behren, N.R. Roberson, C.R. Gould
D.R. Tilley and S.A. Wender
Phys. Rev. C 17, 1260 (1978)

ELEM. SYM.	A	Z
Ca	41	20
REF. NO.		hg
78 We 3		

REACTION	RESULT	EXCITATION ENERGY	SOURCE		DETECTOR		ANGLE
			TYPE	RANGE	TYPE	RANGE	
N,GO	NOX	16, 20	D	8, 12	TOF-D		DST

Angular distributions have been measured for neutron energies of 8 and 12 MeV for the $^{40}\text{Ca}(\pi, \gamma_0)^{41}\text{Ca}$ reaction. The extracted a_2 coefficients are in good agreement with recent direct-semidirect calculations. The behavior of a_2 is examined in light of recent results from polarized proton capture measurements on $^{54,56,58}\text{Fe}$.

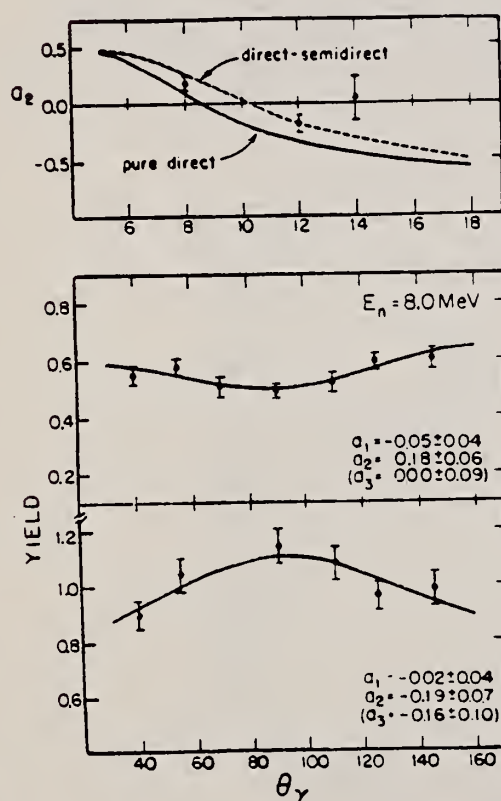


FIG. 1. Angular distributions obtained for 8 and 12 MeV neutrons. The solid lines were obtained from a least squares fit in terms of Legendre polynomials through $P_2(\cos\theta)$. Above is a plot of the calculated values of a_2 from Ref. 2 for the pure direct model (solid line) and direct-semidirect model with a complex form factor. In addition to the a_2 points obtained in the present work, the value from Ref. 4 at $E_n = 14$ MeV is shown.

2 A. Likar, M. Potokar, and F. Cvelbar, Nucl. Phys. A280, 49 (1977)

4 E.D. Arthur, D.M. Drake, and I. Halpern, Phys. Rev. Lett. 35, 914 (1975)

REF. M. Jensen, D.R. Tilley, H.R. Weller, N.R. Roberson, S.A. Wender,
T.B. Clegg
Phys. Rev. Lett. 43, 609 (1979)

ELEM. SYM.	A	Z
Ca	41	20
REF. NO.		hg
79 Je 1		

METHOD						REF. NO.	
						79 Je 1	hg
REACTION	RESULT	EXCITATION ENERGY	SOURCE		DETECTOR		ANGLE
			TYPE	RANGE	TYPE	RANGE	
\$ N,G	ABX	18	D	10	NAI-D		DST

Preliminary data at $E_n=8,9,11$ MeV give similar results to the 10 MeV measurements but no reliable E2 cross sections have yet been extracted.

$\$$ POL NEUTRONS

The capture of fast polarized neutrons incident on ^{40}Ca has been measured at an incident neutron energy of 10.0 MeV. The results indicate a significant non-E1 contribution in the giant-dipole-energy region of ^{40}Ca . When the data at $E_n=10$ MeV are analyzed with the use of a model, they are found to be consistent with an E2 strength which is $(3.2 \pm 2.7)\%$ of the total capture cross section. Some of the implications of this result are discussed.

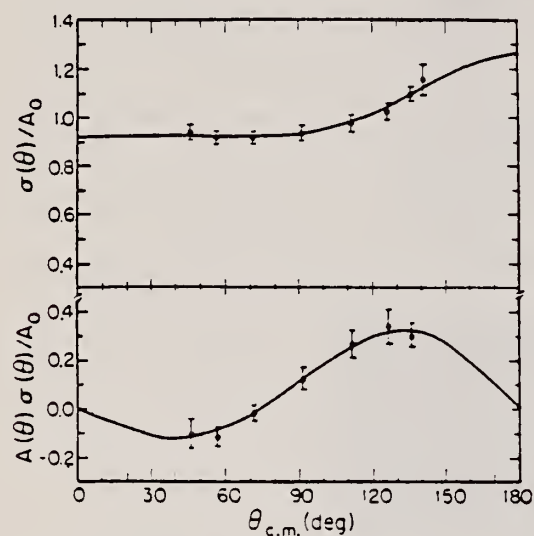


FIG. 1. The cross section and analyzing powers obtained for the reaction $^{40}\text{Ca}(n_{001}, \gamma)^{41}\text{Ca}$ at $E_n = 10.0$ MeV. The solid lines are the curves generated by fitting the data with the T -matrix amplitudes and phases described in the text.

The cross-section data shown here are a composite of the present results along with the previous 10 MeV data from Ref. 8.

S. A. Wender, N. R. Roberson, M. Potokar, H. R. Weller, and D. R. Tilley, Phys. Rev. Lett. 41, 1217 (1978).

ELEM. SYM.	A	Z
Ca	41	20
REF. NO.		
80 Li 4		hg

METHOD			SOURCE		DETECTOR		ANGLE
			TYPE	RANGE	TYPE	RANGE	
N, G	ABX	11-17	D	3-9	NAI-D		90

Abstract: Gamma-ray spectra from radiative capture of neutrons in calcium, nickel, yttrium and radiogenic lead have been recorded at neutron energies between 0.5 and 11 MeV. The γ -radiation was detected by a large NaI(Tl) scintillation detector using time-of-flight techniques to suppress background radiation. Cross sections for capture to bound final states, mainly ground states, were determined.

Measured cross sections and data from previous experiments are compared with predictions of the direct-semidirect and compound-nucleus models. For neutron energies below 4 MeV the compound-nucleus model accounts reasonably well for the observed cross sections. Above 7 MeV the direct-semidirect model gives a good description of the experimental data. In the energy region from 4 to 7 MeV the contributions from the two models are of the same order of magnitude and interference between the two capture processes might be important.

E NUCLEAR REACTIONS ^{40}Ca , ^{58}Ni , ^{84}Y , $^{208}\text{Pb}(n, \gamma)$; $E = 0.5\text{--}11$ MeV; measured $\sigma(E)$; compound nucleus, direct-semidirect model analyses.

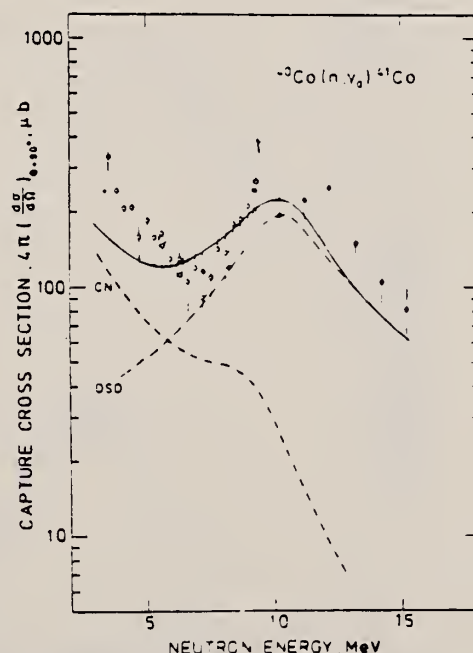


Fig. 1. Cross sections for the $^{40}\text{Ca}(n, \gamma)^{41}\text{Ca}$ reaction. The experimental data are from ref. 5) (solid circles) and from the present experiment (open circles). The error bars include the uncertainty in the absolute scale. The extensive data set of ref. 22) in agreement with the present data is not included. The compound-nucleus (CN) and direct-semidirect (DSD) curves are obtained from calculations described in the text. The full curve is the sum of the two others.

ELEM. SYM.	A	Z
Ca	41	20
REF. NO.		
80 Ni 3		hg

METHOD					
REACTION	RESULT	EXCITATION ENERGY	SOURCE		ANGLE
			TYPE	RANGE	
P,G	ABX	17-26	D	8-17	90

Assumes $=10.786 \frac{d\sigma}{d\Omega} (90)$ i.e. constant $a_2 = -0.33$, $a_4=0$

Differential 90° cross sections for $^{40}\text{K}(p,\gamma)^{41}\text{Ca}$ were measured over the entire giant dipole resonance region. The data are compared with similar results for the $^{40}\text{Ca}(n,\gamma)^{41}\text{Ca}$ reaction and with calculations based on the direct-semidirect capture model. An observed energy difference of about 1.5 MeV between the centroids of the (p,γ) and (n,γ) cross-section curves is interpreted as the result of isospin selection rules.

[NUCLEAR REACTIONS $^{40}\text{K}(p,\gamma)^{41}\text{Ca}$ in the giant dipole energy region. Shows evidence for a shift of GDR due to isospin splitting.]

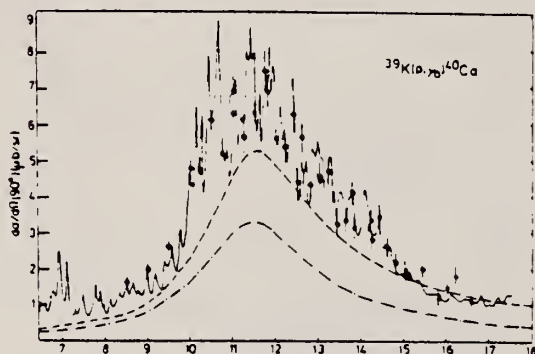


FIG. 1. The $^{39}\text{K}(p,\gamma)^{40}\text{Ca}$ cross section from Ref. 5 (full curve) and from the present work (closed circles). The smooth curves represent calculations based on the DSD capture model using optical potential parameters of Ref. 15 (dashed curve) and Ref. 14 (dot-dashed curve).

The uncertainties in the absolute scale are about 20-25% in the three experiments, implying that the data are in agreement within errors. To

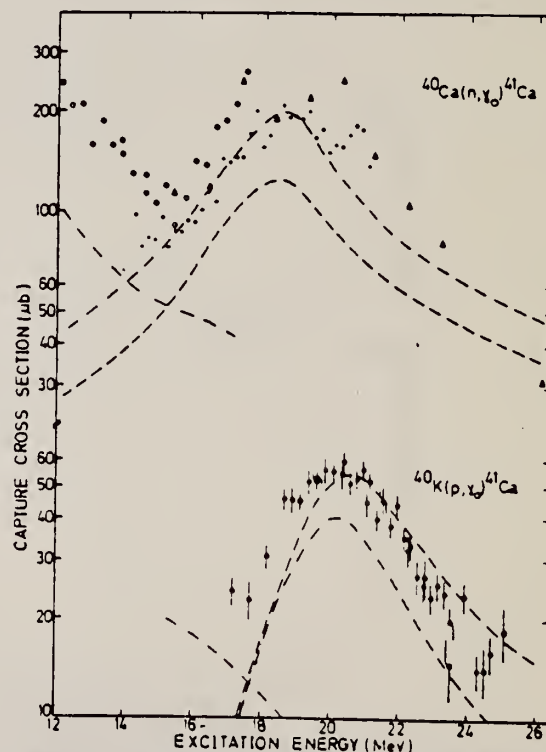


FIG. 2. Cross sections for the $^{40}\text{Ca}(n,\gamma)^{41}\text{Ca}$ reaction from Ref. 7 (open triangles), Ref. 8 (open circles), and Ref. 9 (crosses), and for the $^{40}\text{K}(p,\gamma)^{41}\text{Ca}$ reaction from the present work (closed circles) plotted against the excitation energy of the capturing state in ^{41}Ca . The dashed and dot-dashed curves represent DSD calculations (as in Fig. 1); the double dot-dashed curves are obtained from CN capture calculations.

CA
A=42

CA
A=42

CA
A=42

Ref. L. Simons, K-E. Nystén, E. Spring, L. Kåld, H. Junger,
P. Holmberg, I. Forsblom
Phys. Letters 7, 344 (1963)

Elem. Sym.	A	Z
Ca	42	20

Method
Van de Graaff; NaI

Ref. No.	JHH
63 Si 2	

Reaction	E or ΔE	E_0	Γ	$\int \sigma dE$	$J\pi$	Notes
$K^{41}(p, \gamma)$	1.050- 1.200					
	$E_{p0} =$ 1.111	$E_{\gamma 0} =$ 11.4				For this resonance, $(2J_r + 1)$ $(\Gamma_p \Gamma_\gamma / \Gamma) = 8.5 (\pm 50\%)$

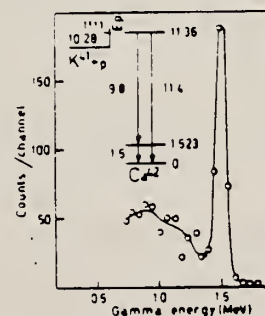


Fig. 3. Spectrum in coincidence with gamma rays of energy 8.5 - 10.5 MeV at the 1111 keV resonance.

REF.

F.R. Metzger and G.K. Tandon
Phys. Rev. 148, B1133 (1966)

ELEM. SYM.	A	Z
Ca	42	20

METHOD

Nuclear Resonance Fluorescence

REF. NO.

66 Me 3

JDM

REACTION	RESULT	EXCITATION ENERGY	SOURCE		DETECTOR		ANGLE
			TYPE	RANGE	TYPE	RANGE	
G,G	LFT	1.52	D	1.52	NAI		

$$\tau = 1.4 \times 10^{-12} \text{ secs.}$$

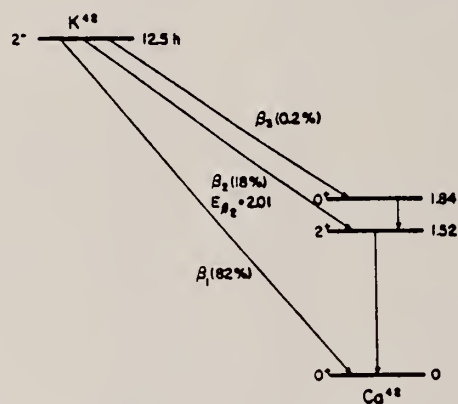


FIG. 1. Portion of the decay scheme of K^{48} relevant to this study.
Energies are given in MeV.

METHOD

REF. NO.

71 He 1

egf

REACTION	RESULT	EXCITATION ENERGY	SOURCE		DETECTOR		ANGLE
			TYPE	RANGE	TYPE	RANGE	
E, E/	FMF	1-4	D	198-300	MAG-D		DST

3 LEVELS

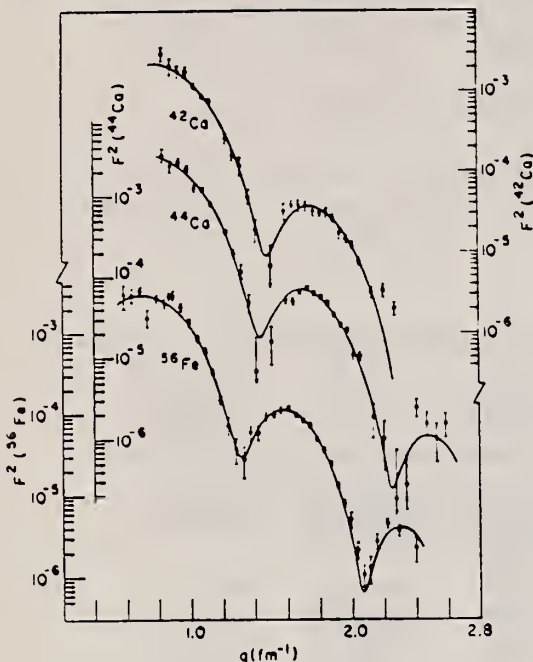


Fig. 1. Fits to the ^{42}Ca , ^{44}Ca and ^{56}Fe 2^+ levels.

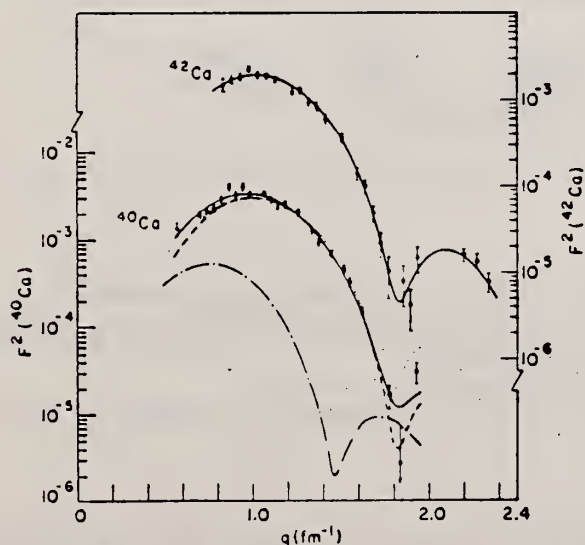


Fig. 3. Fits to ^{42}Ca and ^{40}Ca 3^- levels. Decomposition for ^{40}Ca into contributions of the 3.9 MeV 2^+ level (dash-dot curve) and the 3.75 MeV 3^- level (dashed curve). The solid curve gives the fit to the sum using shape (2), while the dotted curve gives the fit to the sum using shape (3).

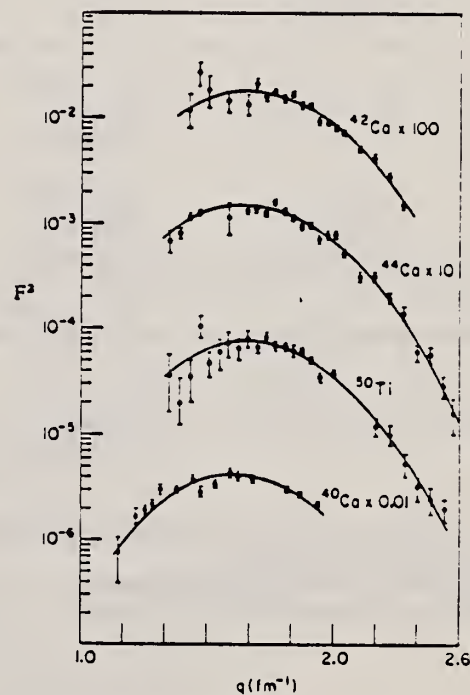


Fig. 7. Fits to ^{42}Ca , ^{40}Ca , ^{44}Ca and ^{50}Ti 5^- levels.

TABLE 3
Inelastic parameters

Isotope	E^* (MeV)	L	Shape ✓	c_{ir}^* (fm)	z_{ir}^* (fm)	G^* (s.p.u.)	R_{ir}^* (fm)	G (s.p.u.) heavy-particle scattering ¹⁹⁾
⁴⁰ Ca	3.740	3	2	3.536 ± 0.030	1.483 ± 0.020	24.9 ± 1.0	4.835 ± 0.030	23.6 ± 3.5
	4.480	5	2	3.538 ± 0.050	1.260 ± 0.035	9.7 ± 0.6	4.810	17.7 ± 2.7
			3			17.7 ± 1.5	5.467 ± 0.060	11.3 ± 1.7
⁴² Ca	3.440	3	2	3.565 ± 0.018	1.383 ± 0.014	12.4 ± 0.5	4.719 ± 0.023	12.0 ± 1.8
	4.100	5	2	3.231 ± 0.030	1.404 ± 0.025	3.4 ± 0.3	4.816 ± 0.044	9.0 ± 1.4
⁴⁴ Ca	3.30	3	2	3.555 ± 0.018	1.313 ± 0.013	6.95 ± 0.28	4.618 ± 0.023	8.0 ± 1.2
	2.28	4	2	4.091 ± 0.030	1.268 ± 0.016	2.66 ± 0.15	5.135 ± 0.030	1.3 ± 0.3
	3.91	5	2	3.268 ± 0.030	1.397 ± 0.024	2.30 ± 0.20	4.832 ± 0.045	4.4 ± 0.7
	2.00	4	2	4.264 ± 0.021	1.229 ± 0.013	7.61 ± 0.30	5.226 ± 0.026	
⁴⁶ Ti	2.286	4	2	4.330 ± 0.021	1.196 ± 0.013	3.37 ± 0.15	5.237 ± 0.026	
⁵⁰ Ti	4.42	3	2	3.645 ± 0.017	1.244 ± 0.012	3.76 ± 0.15	4.600 ± 0.023	5.4 ± 0.8
								$5.9^{20)}$
	2.50	4	2	3.865 ± 0.017	1.347 ± 0.012	4.7 ± 0.15	5.064 ± 0.026	3.3 ± 0.7
	3.20	5	2	3.254 ± 0.032	1.345 ± 0.026	0.83 ± 0.08	4.724 ± 0.045	$2.7^{20)}$
Present experiment								

^{a)} Errors do not reflect any model dependence.

^{b)} Given errors do not include the 6% error of normalization.

¹⁹⁾ A. M. Bernstein, Adv. in Nucl. Phys. 2 (1969) 325.

TABLE 2
Inelastic parameters for 2⁺ levels

Isotope	E^* (MeV)	$B(E2)$ Coulomb Excit. ($e^2 \cdot \text{fm}^4$)	Shape	c_{ir}^* (fm)	z_{ir}^* (fm)	Fitted $B(E2)$ ($e^2 \cdot \text{fm}^4$) ^{b)}	R_{ir}^* (fm)	$B(E2)$ ($e^2 \cdot \text{fm}^4$) heavy-particle scattering
⁴² Ca	1.520	$364 \pm 82^*)$	2	3.541 ± 0.025	1.459 ± 0.020	320 ± 20	4.619 ± 0.030	$476 \pm 74^{19)}$
⁴⁴ Ca	1.160	$350 \pm 70^{10)}$	2	3.691 ± 0.027	1.428 ± 0.020	480 ± 30	4.704 ± 0.030	$507 \pm 100^{19)}$
			1	3.454 ± 0.025	0.690 ± 0.010	1270 ± 85	5.553 ± 0.030	
⁴⁶ Ti	3.259		2			54 ± 10		
	0.885	$830 \pm 170^{14)}$	2	3.807 ± 0.014	1.397 ± 0.010	740 ± 20	4.763 ± 0.017	$867^{20)}$
⁴⁸ Ti		$560 \pm 100^{12)}$	1	3.562 ± 0.014	0.669 ± 0.005	1680 ± 50	5.510 ± 0.020	$738^{11)}$
	0.984	$700 \pm 140^{14)}$	2	3.777 ± 0.014	1.340 ± 0.010	537 ± 15	4.671 ± 0.017	$788 \pm 120^{19)}$
		$310 \pm 70^{12)}$	1	3.539 ± 0.014	0.633 ± 0.005	1110 ± 30	5.321 ± 0.020	$673^{11)}$
⁵⁰ Ti								$659^{20)}$
	2.420		2			49 ± 8		$57 \pm 10^{19)}$
	1.530	$240 \pm 20^{12)}$	2	3.768 ± 0.014	1.255 ± 0.010	307 ± 10	4.567 ± 0.017	$349^{20)}$
⁵⁶ Fe			1	3.535 ± 0.014	0.576 ± 0.005	515 ± 17	5.047 ± 0.020	$260^{21)}$
	4.320		2			51 ± 8		$431^{24)}$
	0.850	$877 \pm 70^*)$	2	4.048 ± 0.024	1.357 ± 0.014	945 ± 45	4.919 ± 0.025	$72^{24)}$
			1	3.878 ± 0.024	0.651 ± 0.006	1570 ± 70	5.454 ± 0.030	
Present experiment								

^{a)} Errors do not reflect any model dependence.

^{b)} Given errors do not include the 6% error of normalization.

^{c)} Average for $B(E2)$ formed from values of refs. ¹²⁻¹⁸⁾.

¹²⁾ J. Simpson, J. Cookson, D. Eccleshall and M. Yates, Nucl. Phys. 62 (1965) 385

¹³⁾ G. M. Temmer and N. P. Heydenburg, Phys. Rev. 104 (1956) 967

¹⁴⁾ D. S. Andreyev, A. P. Grinberg, K. I. Erokhina and I. Kh. Lemberg, Nucl. Phys. 19 (1960) 400

¹⁵⁾ E. R. Metzger, Nucl. Phys. 27 (1961) 612

¹⁶⁾ W. H. Kelly and G. B. Beard, Nucl. Phys. 27 (1961) 138

¹⁷⁾ R. B. Buzhanov, A. A. Islamov, D. K. Knipov and Yu. K. Shubnyi, JETP (Sov. Phys.) 17 (1963) 94

Ca	42	20
REF. NO.		hmg
73 D1 2		

METHOD			SOURCE		DETECTOR		ANGLE
REACTION	RESULT	EXCITATION ENERGY	TYPE	RANGE	TYPE	RANGE	
P,G	ABX	14- 23	D	4- 13	NAI-D		DST

585

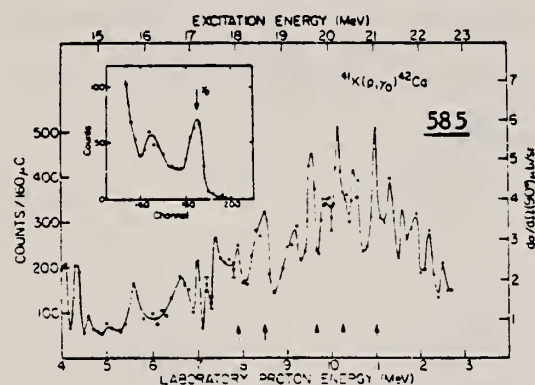


FIG. 1. Excitation function of the $^{41}\text{K}(p, \gamma_0)^{42}\text{Ca}$ reaction taken over the giant dipole region of ^{42}Ca , at $\theta = 90^\circ$. Complete angular distributions were taken at the indicated bombarding energies. The insert shows the high-energy portion of the γ spectrum obtained at $E_p = 10.5$ MeV. The arrow labels the γ_0 transition.

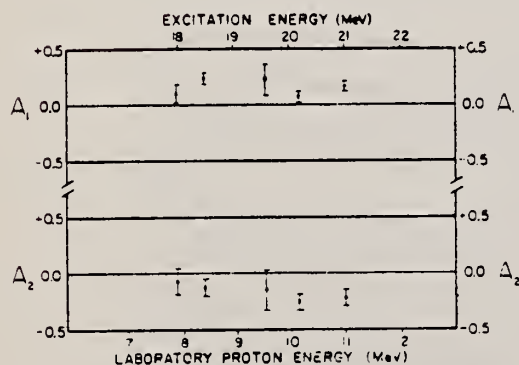


FIG. 2. Plot of Legendre polynomials coefficients A_1 and A_2 obtained from angular distributions at various energies in the GDR of ^{42}Ca .

$$W(\theta) = 1 + A_1 P_1(\cos\theta) + A_2 P_2(\cos\theta)$$

TABLE I. Comparison of the GDR gross structure observed in ^{40}Ca (Ref. 4) and ^{42}Ca in radiative proton capture.

E_x (MeV)	$\sigma_0(\gamma, p_1)$ (mb/sr)	% of (γ, p_0) strength	Γ (MeV)	
17.4 ± 0.1	0.13 ± 0.1	13 ± 2	3.3 ± 0.5	^{42}Ca
20.4 ± 0.1	0.64 ± 0.1	97 ± 4	4.4 ± 0.1	
19.3 ± 0.1	1.95 ± 0.1	84 ± 13	3.1 ± 0.2	^{40}Ca
22.0 ± 0.5	0.35 ± 0.25	16 ± 12	3.2 ± 0.5	

⁴E.M. Diener, et al., Phys. Rev. C7, 695 (1973).

ELEM. SYM.	A	Z
Ca	42	20
REF. NO.		
74 Fo 4		egf

METHOD					REF. NO.		
					74 Fo 4		egf
REACTION	RESULT	EXCITATION ENERGY	SOURCE		DETECTOR		ANGLE
			TYPE	RANGE	TYPE	RANGE	
G.A	ABX	11- 19	D	6- 14	NAI-D		90

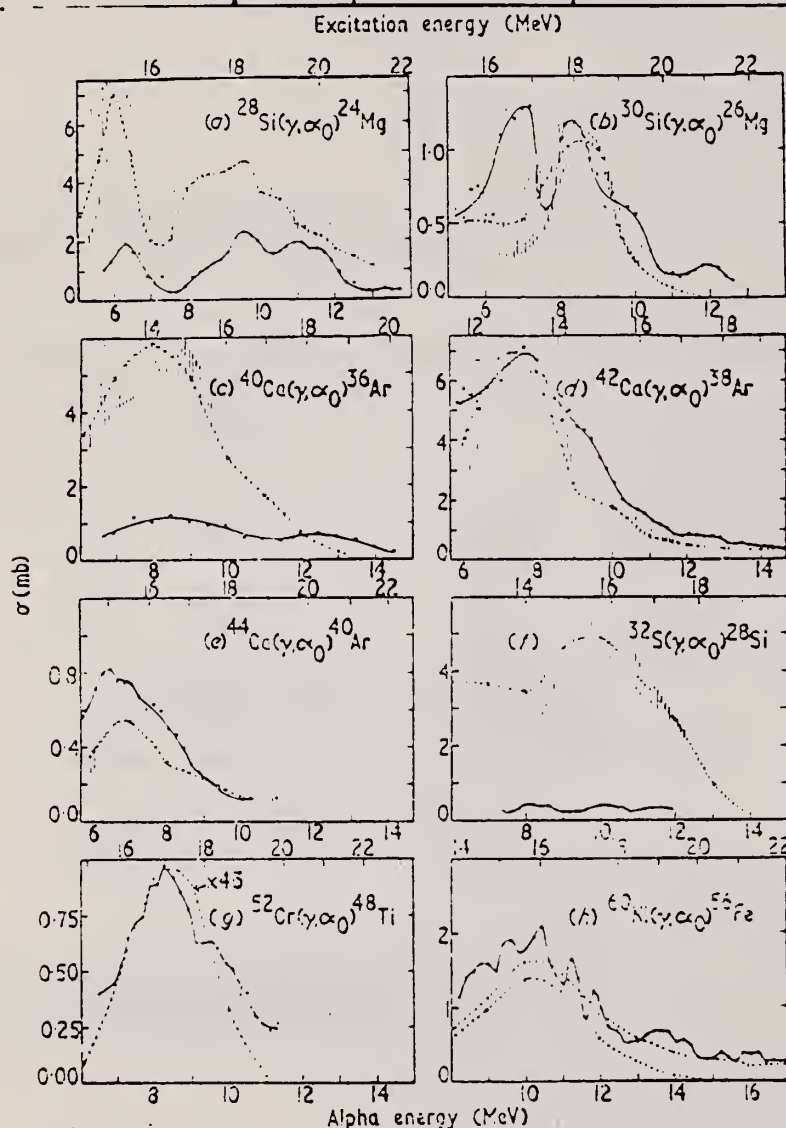


Figure 1. Excitation functions for the (γ, α) reaction obtained from α capture data using the principle of detailed balance. The data shown in (a) and (f) are from Meyer-Shutzmeister *et al* (1963). Those in (b) are from Watson *et al* (1973). The relative experimental errors are approximately $\pm 10\%$. The absolute errors are $\pm 25\%$. The broken curves are the results of calculations (see text). The vertical lines indicate the relative errors due to uncertainties in the total photonuclear cross sections where they are greater than $\pm 10\%$. The crosses indicate the energies at which transmission coefficients were calculated.

REF.

G. S. Foote, D. Branford, D. C. Weisser, N. Shikazono,
R.A.I. Bell, F.C.P. Huang
Nucl. Phys. **A263**, 349 (1976)

ELEM. SYM.	A	Z
Ca	42	20

METHOD

REF. NO.

76 Fo 2

egf

REACTION	RESULT	EXCITATION ENERGY	SOURCE		DETECTOR		ANGLE
			TYPE	RANGE	TYPE	RANGE	
A,G	ABX	11- 21	D	5- 16	NAI-D		DST

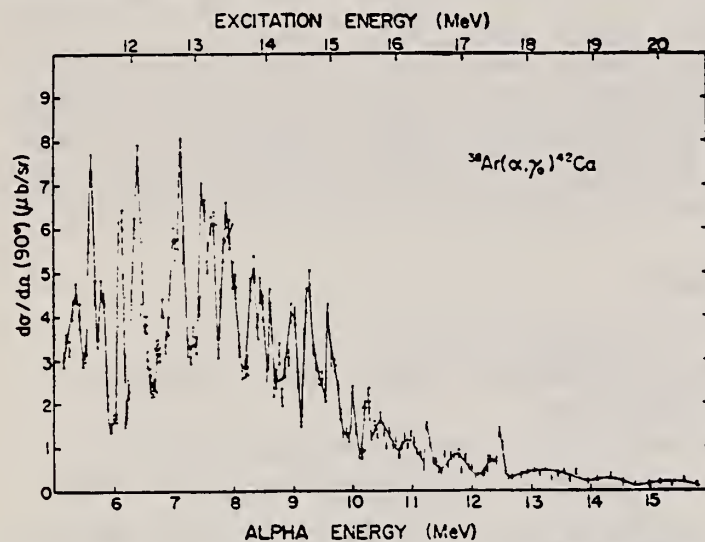


Fig. 2. Absolute differential cross sections for the $^{38}\text{Ar}(\alpha, \gamma)^{42}\text{Ca}$ reaction measured at 90° to the beam direction versus bombarding energy. The error bars represent relative statistical errors. The absolute error is $\pm 30\%$. The continuous line is a guide to the eye.

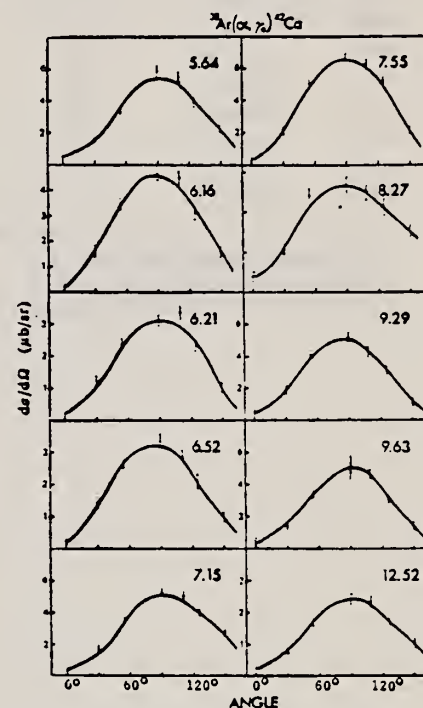


Fig. 5. Angular distribution measurements for the $^{38}\text{Ar}(\alpha, \gamma)^{42}\text{Ca}$ reaction at the bombarding energies (MeV) indicated. Only relative statistical errors are shown. The continuous lines represent Legendre polynomial fits to the data.

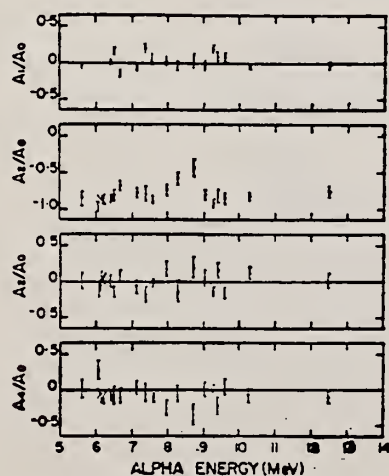


Fig. 8. Normalised Legendre polynomial coefficients determined by linear least squares fitting of the γ -ray angular distributions measured for the $^{38}\text{Ar}(\alpha, \gamma)^{42}\text{Ca}$ reaction.

(over)

TABLE 3

Comparisons of energy integrated (γ, α) cross sections, peak energies of the broad structures in the (γ, α) excitation functions and the particle threshold energies

Final ^{a)} nucleus	Range of integration (MeV)	$\int \sigma(\gamma, \alpha) dE^b$ (mb · MeV)	$\int \sigma(\gamma, \alpha) dE^b$ cds (%)	Particle threshold energies			E^c (MeV)	Exp. peak energy (MeV)	GDR energy (MeV)	Refs.
				α (MeV)	n (MeV)	p (MeV)				
²⁸ Si	14.5–22.5	9.6	2.3	9.99	17.18	11.59	15.2	18.0	20	¹⁾
³⁰ Si	14.0–22.0	5.3	1.2	10.65	10.62	13.51	15.7	16.5	18	¹⁾
³² Si	13.1–22.7	2.7	0.57	6.95	15.09	8.87	13.0	16	20	¹⁾
⁴⁰ Ca	12.5–22.2	4.8	0.8	7.04	15.62	8.33	14.2	14.0	20	⁶⁾
⁴² Ca	11.0–20.5	30.2	4.8	6.25	11.49	10.28	13.3	13.0	17.4	this work
⁴⁴ Ca	13.5–18.8	2.6	3.09	8.84	11.13	12.16	15.9	15.3	17	this work
⁴⁴ Ca*	13.5–18.8	0.76	0.12				15.9		18.5	this work
⁴⁴ Ti	10.5–20.6	6.1	0.9	5.18	5.18	8.66	13.9	14.0		¹⁵⁾
⁵² Ti	12.7–20.4	≈ 0.3	≈ 0.04	7.67	7.80	13.53	16.1			¹⁵⁾
⁵² Cr	15.0–20.5	2.9	0.38	9.35	12.05	10.52	17.6	17.0	18	this work
⁵² Cr*	15.0–20.5	0.51	0.07				17.6			this work
⁶⁰ Ni	13.9–22.8	9.6	1.07	6.29	11.39	9.53	15.7	15.8	16.6	³⁾
⁶⁰ Ni*	13.9–22.8	1.7	0.18	4.96			15.7		17.9	³⁾

^{a)} The asterisk denotes first excited state.

^{b)} The errors are approximately $\pm 30\%$.

^{c)} E is the α -particle threshold energy plus Coulomb barrier height (see text).

- ¹ L. Meyer-Schutzmeister et al., Nucl. Phys. A108, 180 (1968).
- ³ G. S. Foote et al., Nucl. Phys. A220, 505 (1974).
- ⁶ R. B. Watson et al., Nucl. Phys. A203, 209 (1973).
- ¹⁵ R. E. Peshel et al., Nucl. Phys. A232, 269 (1974).

REF. H.D. Gräf, H. Feldmeier, P. Manakos, A. Richter, E. Spamer and
D. Strottman
Nucl. Phys. A295, 319 (1978)

ELEM. SYM.	A	Z
Ca	42	20
REF. NO.		
78 Gr 1		rs

METHOD					
REACTION	RESULT	EXCITATION ENERGY	SOURCE		ANGLE
			TYPE	RANGE	
E, E/	ABX	2	D	34- 60	DST

2=1.837

Abstract: Monopole transitions from the 0_1^+ ground states to 0_2^+ excited states at 3.353 MeV (^{40}Ca), 1.837 MeV (^{42}Ca), 1.884 MeV (^{44}Ca) and 4.272 MeV (^{48}Ca) have been investigated with high resolution inelastic electron scattering (FWHM ≈ 30 keV) at low momentum transfer ($0.29 \leq q \leq 0.53 \text{ fm}^{-1}$). The respective monopole matrix elements are $2.53 \pm 0.41 \text{ fm}^2$, $5.24 \pm 0.39 \text{ fm}^2$, $5.45 \pm 0.41 \text{ fm}^2$ and $2.28 \pm 0.49 \text{ fm}^2$. These results are used together with known ground state charge radii and the average number of holes in the sd shell in the ground state to estimate the number of particle-hole excitations in the wave functions of the excited 0_2^+ states.

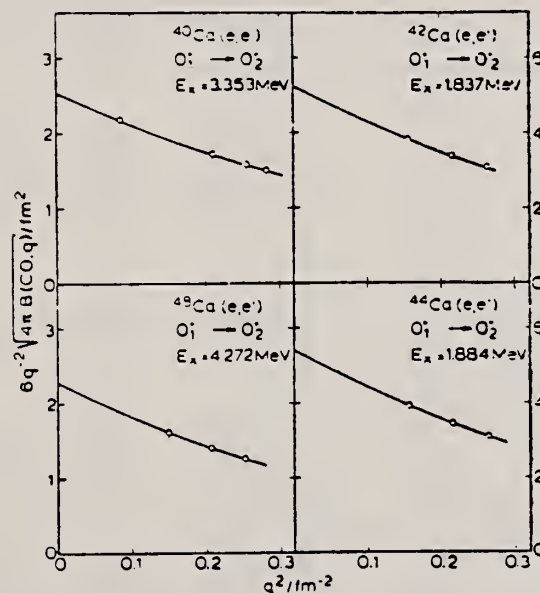


Fig. 3. Extrapolation of the measured $B(C0, q)$ values (dots) to $q = 0$ with the two parameter expression of cq (1).

(OVER)

TABLE 2
Elastic and inelastic cross sections ($d\sigma/d\Omega$)_{el} (10^{-3} fm² sr) and ($d\sigma/d\Omega$)_{inel} (10^{-3} fm² sr), respectively, and DWBA correction factors f_c for the monopole transitions studied

Nucleus E_i (MeV)	E_0 (MeV)	θ (deg)	q^2 (fm ⁻²)	($d\sigma/d\Omega$) _{el}	($d\sigma/d\Omega$) _{inel}	f_c
⁴⁰ Ca 3.353	59.76	128.9	0.282	4.52	2.91 (6.5)	1.46
	54.73	140.9	0.256	3.11	1.95 (11.7)	1.53
	54.70	116.9	0.210	14.65	4.84 (8.9)	1.55
	33.67	128.9	0.086	40.70	2.47 (34.7)	1.91
⁴² Ca 1.837	54.73	140.9	0.263	3.05	6.53 (5.8)	1.48
	54.70	116.9	0.215	14.21	20.51 (4.3)	1.51
	54.70	92.9	0.156	64.99	45.23 (3.9)	1.54
⁴⁴ Ca 1.884	54.73	140.9	0.263	3.15	6.44 (7.3)	1.47
	54.72	116.9	0.215	14.83	20.91 (4.0)	1.50
	54.72	92.9	0.156	66.24	45.39 (3.5)	1.53
⁴⁸ Ca 4.272	54.73	140.9	0.252	2.99	1.11 (30.8)	1.46
	54.73	116.9	0.206	14.20	3.09 (5.6)	1.49
	54.73	92.9	0.149	64.09	7.38 (13.4)	1.53

The values in parentheses denote the statistical error of the cross sections in percent.

TABLE 3
Results of the present (e, e') experiment for monopole matrix elements, transition radii and pair decay widths together with results from other experiments and theoretical predictions

Nucleus	ME (fm ²)	R_{tr} (fm)	Γ_e (eV)	Exp	Theory
⁴⁰ Ca	3.6 ± 1.1	6.3	0.37 ± 0.23	(e, e') ^{a)}	
			0.21 ± 0.01	" ^{b)}	
	2.6 ± 0.1			(p, p') ^{c)}	" ^{d)}
	2.44				" ^{e)}
	5.53				
⁴² Ca	2.53 ± 0.41	6.1 ± 0.9	0.18 ± 0.06	this work	
	5.93 ± 0.52			(p, p') ^{c)}	" ^{d)}
	5.58				" ^{e)}
⁴⁴ Ca	4.19				
	5.24 ± 0.39	6.3 ± 0.4	0.016 ± 0.002	this work	
	5.39 ± 1.79			(p, p') ^{c)}	
⁴⁸ Ca	5.56			(x, p') ^{c)}	
	5.45 ± 0.41	6.5 ± 0.4	0.021 ± 0.003	this work	
⁴⁸ Ca	1.52 ± 0.07			(p, p') ^{c)}	
	2.28 ± 0.49	6.8 ± 1.4	0.63 ± 0.27	this work	

^{a)} Ref. ¹¹⁾; ^{b)} Ref. ¹²⁾; ^{c)} Ref. ³⁾; ^{d)} Ref. ³⁾; ^{e)} Ref. ⁴⁾; ^{f)} Ref. ²²⁾; ^{g)} Ref. ²³⁾.

³⁾ W.J. Gerace and A.M. Green, Nucl. Phys. **A93**, 110 (1967);
A123, 241 (1969)

⁴⁾ P. Federman and S. Pittel, Phys. Rev. **186**, 1106 (1969);
Nucl. Phys. **A139**, 108 (1969)

⁹⁾ M. Ulrickson, N. Benczer-Koller, J.R. MacDonald and
J.W. Tape, Phys. Rev. **C15** 186 (1977)

¹¹⁾ P. Strehl, Z. Phys. **234**, 416 (1970)

¹²⁾ P.M. Endt and C. van der Leun, Nucl. Phys. **A235**, 27 (1974)

²²⁾ L.D. Skouras, Nucl. Phys. **A220**, 604 (1974)

²³⁾ J.D. McCullen and D.J. Donahue, Phys. Rev. **C8**, 1406 (1973)

METHOD

REF. NO.

78 Gr 5

hmg

REACTION	RESULT	EXCITATION ENERGY	SOURCE		DETECTOR		ANGLE
			TYPE	RANGE	TYPE	RANGE	
E, E/	ABX	1	D	31-67	MAG-D		DST
		(1.837)					

Abstract: Monopole transitions from the 0_1^+ ground states to 0_2^+ excited states at 3.353 MeV (^{40}Ca), 1.837 MeV (^{42}Ca), 1.884 MeV (^{44}Ca) and 4.272 MeV (^{48}Ca) have been investigated with high resolution inelastic electron scattering (FWHM ≈ 30 keV) at low momentum transfer ($0.29 \leq q \leq 0.53 \text{ fm}^{-1}$). The respective monopole matrix elements are $2.53 \pm 0.41 \text{ fm}^2$, $5.24 \pm 0.39 \text{ fm}^2$, $5.45 \pm 0.41 \text{ fm}^2$ and $2.28 \pm 0.49 \text{ fm}^2$. These results are used together with known ground state charge radii and the average number of holes in the sd shell in the ground state to estimate the number of particle-hole excitations in the wave functions of the excited 0_2^+ states.

E

NUCLEAR REACTIONS $^{40, 42, 44, 48}\text{Ca}(e, e^-)$, $E = 31-67 \text{ MeV}$; measured $\sigma(E; E_e; \theta)$.
 $^{40, 42, 44, 48}\text{Ca}$ 0_2^+ level deduced E0 matrix elements. Shell model calculation.

TABLE 2

Elastic and inelastic cross sections ($d\sigma/d\Omega$), ($10^{-1} \text{ fm}^2 \text{ sr}$) and ($d\sigma/d\Omega$) ($10^{-1} \text{ fm}^2 \text{ sr}$), respectively, and DWBA correction factors f_c for the monopole transitions studied

Nucleus E_i (MeV)	E_0 (MeV)	θ (deg)	q^2 (fm^{-2})	$(d\sigma/d\Omega)_i$	$(d\sigma/d\Omega)_{\text{DWBA}}$	f_c
^{40}Ca 3.353	59.76	128.9	0.282	4.52	2.91 (6.5)	1.46
	54.73	140.9	0.256	3.11	1.95 (11.7)	1.53
	54.70	116.9	0.210	14.65	4.84 (8.9)	1.55
	33.67	128.9	0.086	40.70	2.47 (34.7)	1.91
^{42}Ca 1.837	54.73	140.9	0.263	3.05	6.53 (5.8)	1.48
	54.70	116.9	0.215	14.21	20.51 (4.3)	1.51
	54.70	92.9	0.156	64.99	45.23 (3.9)	1.54
^{44}Ca 1.884	54.73	140.9	0.263	3.15	6.44 (7.3)	1.47
	54.72	116.9	0.215	14.83	20.91 (4.0)	1.50
	54.72	92.9	0.156	66.24	45.39 (3.5)	1.53
^{48}Ca 4.272	54.73	140.9	0.252	2.99	1.11 (30.8)	1.46
	54.73	116.9	0.206	14.20	3.09 (5.6)	1.49
	54.73	92.9	0.149	64.09	7.38 (13.4)	1.53

The values in parentheses denote the statistical error of the cross sections in percent.

TABLE 3

Results of the present (e, e^-) experiment for monopole matrix elements, transition radii and pair decay widths together with results from other experiments and theoretical predictions

Nucleus	ME (fm^2)	R_{tr} (fm)	f_c (μeV)	Exp.	Theory
^{40}Ca	3.6 ± 1.1	6.3	0.37 ± 0.23 0.21 ± 0.01	(e, e^-) ^{a)} ^{b)}	^{a)} ^{c)}
	2.6 ± 0.1			(p, p') ^{a)}	^{a)}
	2.44				^{a)}
	5.53			this work	
	2.53 ± 0.41	6.1 ± 0.9	0.18 ± 0.06		
^{42}Ca	5.93 ± 0.52			(p, p') ^{a)}	^{a)}
	5.58				^{a)}
	4.19			this work	
^{44}Ca	5.24 ± 0.39	6.3 ± 0.4	0.016 ± 0.002		
	5.39 ± 1.79			(p, p') ^{a)}	
	5.56			(α, α') ^{a)}	
^{48}Ca	5.45 ± 0.41	6.5 ± 0.4	0.021 ± 0.003	this work	
	1.52 ± 0.07			(p, p') ^{a)}	
	2.28 ± 0.49	6.8 ± 1.4	0.63 ± 0.27	this work	

^{a)} Ref ¹¹⁾, ^{b)} Ref ¹²⁾, ^{c)} Ref ⁹⁾, ^{d)} Ref ¹⁾, ^{e)} Ref ²⁾, ^{f)} Ref ¹³⁾

(OVER)

ELECTRIC MONOPOLE TRANSITIONS

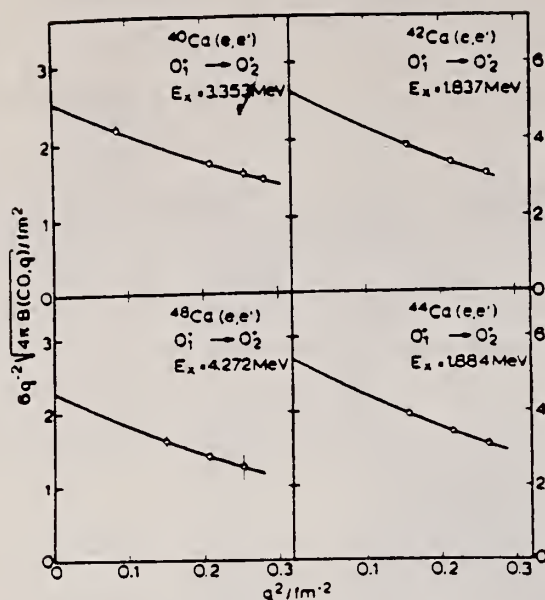


Fig. 3. Extrapolation of the measured $B(C0, q)$ values (dots) to $q = 0$ with the two parameter expression of eq. (1).

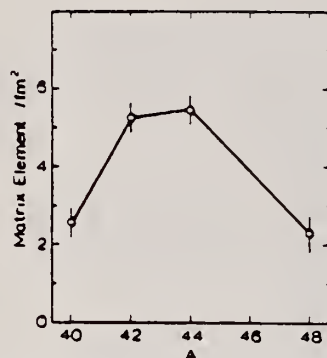


Fig. 4. The determined monopole matrix elements as a function of mass number for the four Ca isotopes. The line which connects the experimental points has no theoretical significance.

- 3) W. J. Gerace and A. M. Green, Nucl. Phys. A93 (1967) 110, A123 (1969) 241
- 4) P. Federman and S. Pittel, Phys. Rev. 186 (1969) 1106, Nucl. Phys. A139 (1969) 108
- 5) M. Sakakura, A. Arima and T. Sebe, Phys. Lett. 61B (1976) 335
- 6) N. Benczer-Koller, G. G. Seaman, M. C. Bertin, J. W. Tape and J. R. MacDonald, Phys. Rev. C2 (1970) 1037
- 7) J. C. Adloff, K. H. Souw, D. Disdier, F. Scheibling, P. Chevallier and Y. Wolfson, Phys. Rev. C10 (1974) 1819
- 8) M. Ulrickson, W. Hartwig, N. Benczer-Koller, J. R. MacDonald and J. W. Tape, Phys. Rev. C13 (1976) 536
- 9) M. Ulrickson, N. Benczer-Koller, J. R. MacDonald and J. W. Tape, Phys. Rev. C15 (1977) 186
- 10) P. Strehl and Th. H. Schucan, Phys. Lett. 27B (1968) 641
- 11) P. Strehl, Z. Phys. 234 (1970) 416
- 12) P. M. Endt and C. van der Leun, Nucl. Phys. A235 (1974) 27
- 13) R. F. Frosch, R. Hofstadter, J. S. McCarthy, G. K. Nöldeke, K. J. van Oostrum, M. R. Yearian, B. C. Clark, R. Herman and D. G. Ravenhall, Phys. Rev. 174 (1968) 1380
- 14) P. Doll, G. J. Wagner, K. T. Knöpfle and G. Mairle, Nucl. Phys. A263 (1976) 210
- 15) J. A. Nolen, Jr. and R. J. Gleitsmann, Phys. Rev. C11 (1975) 1159
- 16) K. K. Seth, A. Saha, W. Benenson, W. A. Lanford, H. Nann and B. H. Wildenthal, Phys. Rev. Lett. 33 (1974) 233
- 17) C. R. Fischer and G. H. Rawitscher, Phys. Rev. 135 (1964) B377
- 18) C. W. de Jager, H. de Vries and C. de Vries, Atomic Data and Nucl. Data Tables 14 (1974) 479
- 19) H. Theissen, Springer Tracts in Modern Phys. 65 (1972) 1
- 20) S. Krewald, R. Rosenfelder, J. E. Galonska and A. Faessler, Nucl. Phys. A269 (1976) 112
- 21) Th. H. Schucan, Nucl. Phys. 61 (1965) 417
- 22) L. D. Skouras, Nucl. Phys. A220 (1974) 604
- 23) J. D. McCullen and D. J. Donahue, Phys. Rev. C8 (1973) 1406

METHOD					REF. NO.	
/					80 Py 6	hg
REACTION	RESULT	EXCITATION ENERGY	SOURCE		DETECTOR	
			TYPE	RANGE	TYPE	RANGE
E, P	ABX	10-29	D	15-29	MAG-D	90
E, P \emptyset	ABX	10-29	D	15-29	MAG-D	90
E, A \emptyset	ABX	6-29	D	15-29	MAG-D	90

Abstract

Experimental results are presented for the cross sections measured at 90° of the reactions $^{42}\text{Ca}(\gamma, p)$, $^{42}\text{Ca}(\gamma, p_0)$ and $^{42}\text{Ca}(\gamma, x_0)$ between excitation energies 16 and 28 MeV.

VIRT. PHOTON ANALYSIS

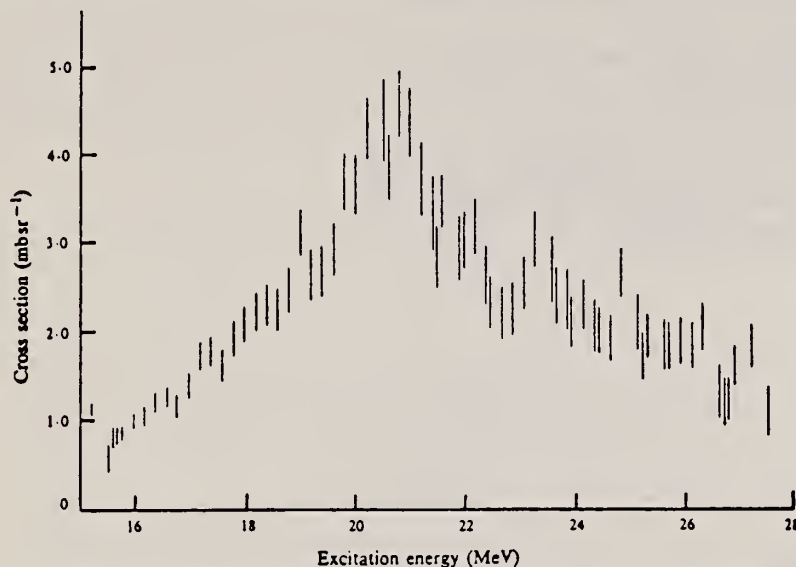


Fig. 1. Differential photoproton cross section of $^{42}\text{Ca}(\gamma, p)$ for $E_p > 3.7$ MeV at a detection angle of 90° to the beam direction. Error bars are statistical only; there is a 15% uncertainty in the absolute cross section scale.

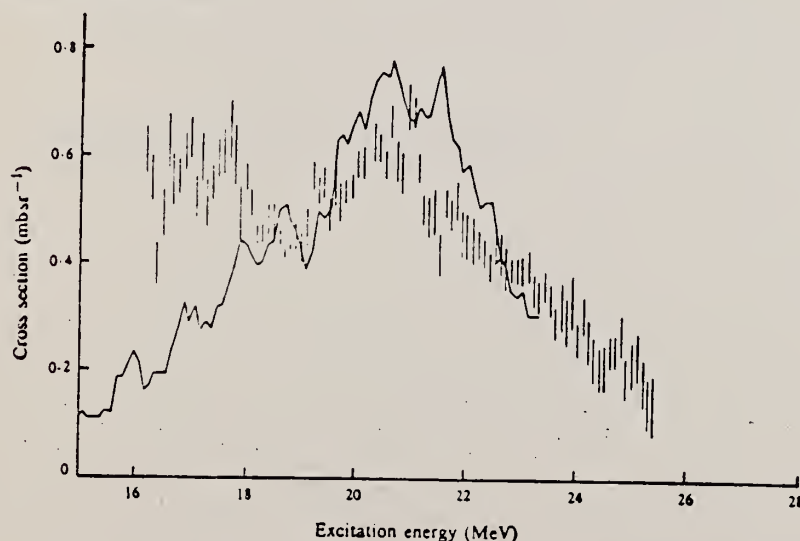


Fig. 2. Differential cross section of $^{42}\text{Ca}(\gamma, p_0)$ at $\theta = 90^\circ$. Error bars are statistical only; there is a 15% uncertainty in the absolute cross section scale. The solid curve is the $^{42}\text{Ca}(\gamma, p_0)$ cross section derived by detailed balance from the $^{41}\text{K}(p, \gamma)$ data of Diener *et al.* (1973) and smoothed with a 0.5 MeV sliding interval.

Diener, E. M., Amann, J. F., Paul, P., and Vergados, J. D. (1973). *Phys. Rev. C* **7**, 705. 73 D, 2

(OVER)

U.S. DEPARTMENT OF COMMERCE
NATIONAL BUREAU OF STANDARDS

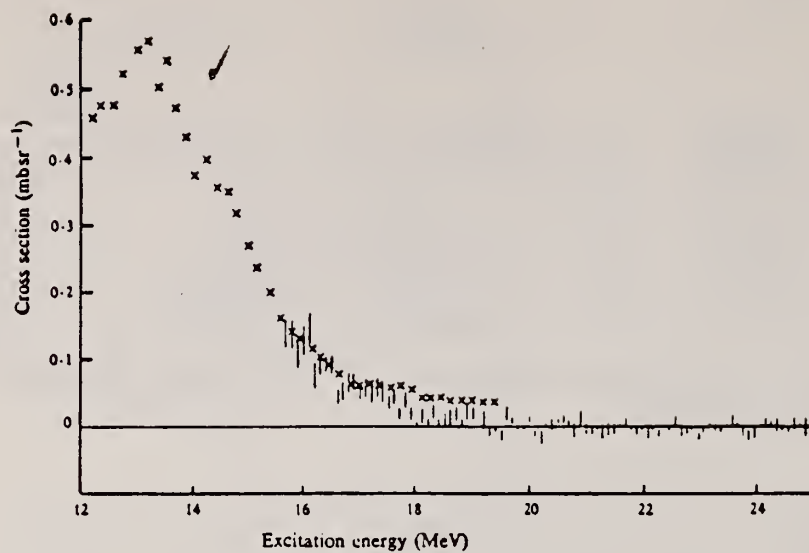


Fig. 3. Differential cross section of $^{41}\text{Ca}(\gamma, \gamma_0)$ at $\theta = 90^\circ$. Error bars are statistical only; there is a 15% uncertainty in the absolute cross section scale. Crosses indicate the differential cross section for $^{41}\text{Ca}(\gamma, \gamma_0)$ derived from the cross section measured by Foote *et al.* (1976). The scale in this case is assigned on the assumption of an isotropic angular distribution.

REF. W. Steffen, H.-D. Gräf, W. Gross, D. Meuer, A. Richter, E. Spamer,
O. Titze, W. Knüpfer
Phys. Lett. 95B, 23 (1980)

ELEM. SYM.	A	Z
Ca	42	20
REF. NO.		
80 St 7		hg

METHOD					
REACTION	RESULT	EXCITATION ENERGY	SOURCE		ANGLE
			TYPE	RANGE	
E, E/	SPC	8-12	D	30-50	DST

The search for magnetic dipole transitions from the ground state of the even-even Ca isotopes to high lying $J^\pi = 1^+$ states by means of low momentum transfer but high resolution inelastic electron scattering is described. The previously detected strongly excited $J^\pi = 1^+$ state at $E_x = 10.319$ MeV [$B(M1) \uparrow = 1.12 \pm 0.27 \mu_N^2$] in ^{40}Ca has been confirmed, but – contrary to the expectations of the independent particle shell model – only a fairly weak M1 transition is observed in ^{42}Ca [$E_x = 11.235$ MeV, $B(M1) \uparrow = 0.59 \pm 0.05 \mu_N^2$] and none in ^{44}Ca between $E_x = 8.2$ –12.2 MeV. In ^{48}Ca , however, a very strong M1 transition [$B(M1) \uparrow = 4.0 \pm 0.3 \mu_N^2$] to a single state at $E_x = 10.227$ MeV has been discovered.

Level 11.235, BEL

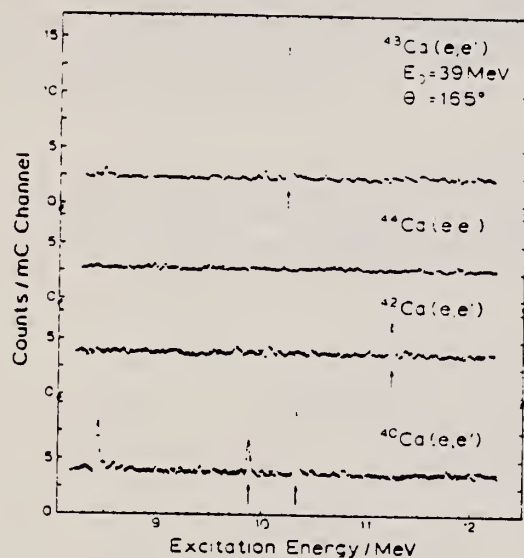


Fig. 1. High-resolution inelastic electron scattering spectra of $^{40,42,44,48}\text{Ca}$ all measured at $\theta = 165^\circ$ and $E_0 = 39$ MeV. Magnetic dipole transitions are denoted by an arrow.

REF. Y.I. Assafiri, M.N. Thompson
Nuc1. Phys. A357, 429 (1981)

ELEM. SYM.	A	Z
Ca	42	20
REF. NO.		hg
81 As 12		

METHOD

REACTION	RESULT	EXCITATION ENERGY	SOURCE		DETECTOR		ANGLE
			TYPE	RANGE	TYPE	RANGE	
G,SN	ABX	11 - 28	C	10 - 28	BF3-I		4PI
		(11.5 - 28)					

(γ ,sn) cross section obtained from the $\sigma(\gamma,xn)$ by using the statistical model for the neutron multiplicity correction

STATISTICS XN TO SN

Abstract: The reaction $^{42}\text{Ca}(\gamma, n)^{41}\text{Ca}$ has been measured from 10.5 MeV to 28 MeV using an enriched metal target and the yield curve technique. The resultant cross section shows gross structure which is shown to be consistent with predictions of isospin splitting of the giant dipole resonance.

E

NUCLEAR REACTIONS $^{42}\text{Ca}(\gamma, n)$, $E = 10.5 - 28$ MeV, bremsstrahlung, measured $\sigma(E)$. ^{42}Ca deduced evidence for isospin splitting. Enriched target.

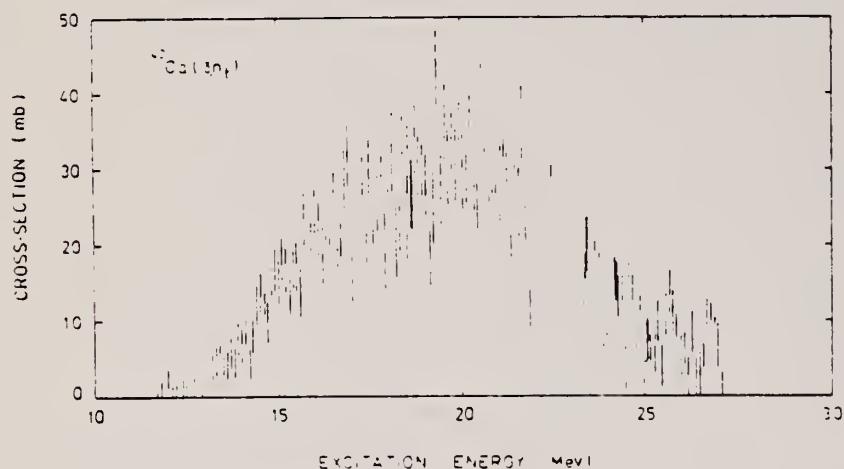


Fig. 4 The $^{42}\text{Ca}(\gamma, n)$ cross section

ELEM. SYM.	A	Z
Ca	42	20
REF. NO.	hg	
81 It 2		

REACTION	RESULT	EXCITATION ENERGY	SOURCE		DETECTOR		ANGLE
			TYPE	RANGE	TYPE	RANGE	
E, E/	FMF	9 - 35	D	150 - 250	MAG-D		DST

We present the giant electric-dipole and electric-quadrupole cross sections of ^{42}Ca and ^{44}Ca measured by inelastic electron scattering with incident energies between 124 and 250 MeV. Spectra were decomposed into dipole, quadrupole, and other higher multipole components. The giant dipole resonances in both nuclei have a large width of approximately 12 MeV, with at least two gross resonance structures. The quadrupole resonances are distributed in several clusters between 10 and 22 MeV, depleting $(61 \pm 9)\%$ in ^{42}Ca and $(46 \pm 7)\%$ in ^{44}Ca of the isoscalar energy-weighted sum rule, respectively. Higher multipole resonances were also found in the same excitation energy region. The observed structure in the dipole and quadrupole resonances are examined in terms of the collective model, and it is suggested that the splitting of the dipole resonance revealed in ^{44}Ca may reflect the effect of nuclear deformation.

B(CL)

NUCLEAR REACTIONS $^{42}\text{Ca}(e,e')$ and $^{44}\text{Ca}(e,e')$, $E=124-250$ MeV, $q=0.4-1.2 \text{ fm}^{-1}$, enriched target, measured $\sigma(E, \theta)$ up to 35 MeV in excitation energy; deduced electric-dipole, electric-quadrupole, and higher multipole strength in the giant resonance region.

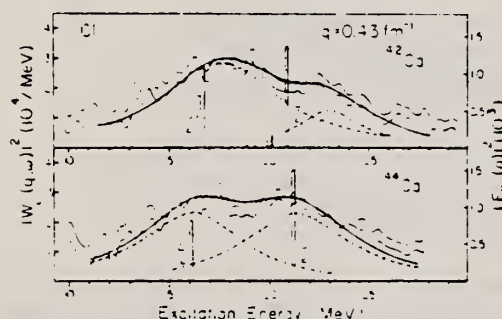


FIG. 5. The longitudinal dipole differential form factors of ^{42}Ca and ^{44}Ca at $q=0.43 \text{ fm}^{-1}$. The shaded area shows the errors arising from the least square method. The two gross resonances in both isotopes are fitted by two Breit-Wigner shape cross sections. The K splitting of the Suzuki-Rowe model (Refs. 40 and 42) is compared with the spectra. Shell model calculation (Ref. 9) is also shown by solid lines for the $T_{<}$ state and dashed lines for the $T_{>}$ state. Both $T_{<}$ and $T_{>}$ strengths are multiplied by a factor of 2.

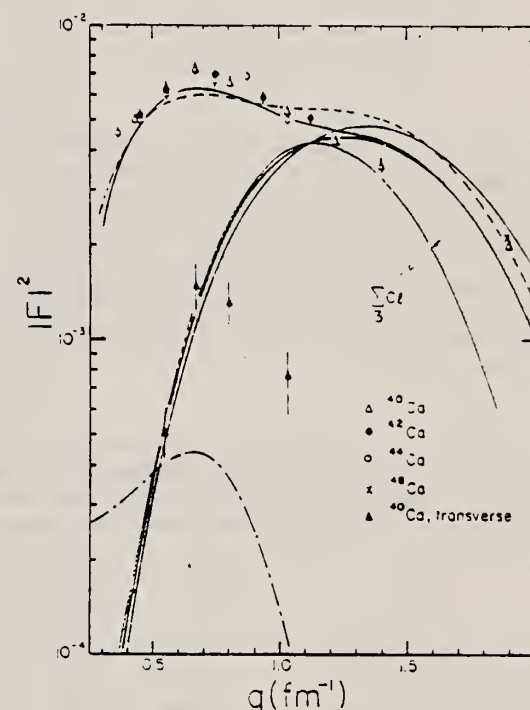


FIG. 1. The total form factor integrated from 10 to 25 MeV for ^{42}Ca and ^{44}Ca , together with the experimental results of ^{40}Ca (Ref. 3). The measured form factors at $q=1.9 \text{ fm}^{-1}$ are taken from Ref. 27. The shaded area labeled $\Sigma Cl (l \geq 3)$ is the investigated range of the contributions of the higher multipole excitation for ^{42}Ca . The solid and dashed curves are the sum of the all multipole excitations in ^{42}Ca and ^{44}Ca , respectively. Also the measured transverse form factor of ^{40}Ca integrated in the same energy range is shown. The electric-dipole transverse form factor calculated using the particle-hole wave functions (Ref. 32) is shown by the dot-dashed curve.

OVER

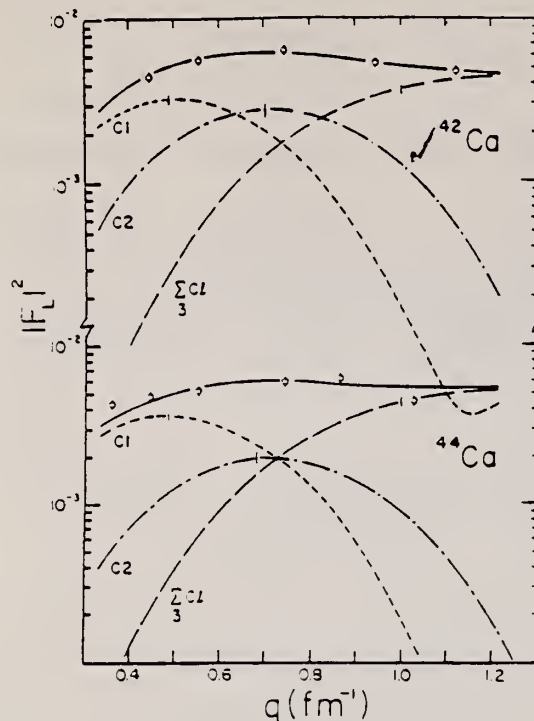


FIG. 4. The longitudinal form factors integrated from 10 to 25 MeV for ^{42}Ca and ^{44}Ca , together with the result of the multipole expansion. The dashed, dash-dotted, and long dashed curves are the $C1$, $C2$, and $\Sigma C1$ ($l \geq 3$) components, respectively. The solid curve is the sum of the all multipole excitation. The occasional error bars on the $C1$, $C2$, and $\Sigma C1$ ($l \geq 3$) curves include statistical error and model dependence of the higher multipole excitations.

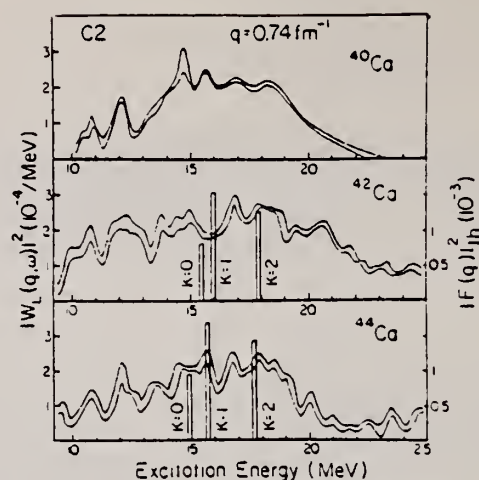


FIG. 7. The longitudinal quadrupole differential form factors of ^{42}Ca and ^{44}Ca at $q = 0.74 \text{ fm}^{-1}$ are compared with the result of ^{40}Ca (Ref. 3). The shaded area for ^{40}Ca was obtained by combining the result of ^{40}Ca at $q = 0.67 \text{ fm}^{-1}$ and $q = 0.81 \text{ fm}^{-1}$, while those of ^{42}Ca and ^{44}Ca show the errors arising from the least square method. The K splitting of the Suzuki-Rowe model is also shown.

TABLE II. Reduced transition probabilities $B(C1, 1)$ obtained by the multipole expansion and the depletion of the isovector electric dipole EWSR (S_1). The positions of dipole peaks are indicated in square brackets. Errors in $B(C1)$ and S_1 are $\pm 10\%$, which include errors arising from the model dependence on the higher multipole transitions.

^{42}Ca			^{44}Ca		
ω (MeV)	$B(C1)$ ($e^2 \text{ fm}^2$)	S_1 (%)	ω (MeV)	$B(C1)$ ($e^2 \text{ fm}^2$)	S_1 (%)
9.0 ~ 12.5 [9.4, 11.2]	1.49	10.2	9.0 ~ 12.1 [10.0, 11.7]	1.46	9.4
12.5 ~ 14.5 [13.3, 13.9]	1.34	11.5	12.1 ~ 14.5 [13.0, 14.1]	1.60	13.3
14.5 ~ 18.0 [16.2, 17.5]	3.06	31.9	14.5 ~ 18.5 [15.3, 16.2, 17.3]	3.78	38.4
18.0 ~ 21.0 [18.3, 19.2]	2.81	35.1	18.5 ~ 23.0 [19.6, 20.3, 21.4, 22.0]	4.33	55.3
21.0 ~ 26.0 [22.5]	3.19	48.1	23.0 ~ 25.0 [22.9]	1.52	22.4
26.0 ~ 30.0 [26.7]	1.39	25.0	25.0 ~ 27.0	0.96	15.3
30.0 ~ 35.0	0.64	13.3			
10.0 ~ 25.0	11.0	129	10.0 ~ 25.0	12.2	138
9.0 ~ 35.0	13.9	173			

ELEM. SYM.	A	Z
Ca	42	20
REF. NO.		
81 It 2		hg

REACTION	RESULT	EXCITATION ENERGY	SOURCE		DETECTOR		ANGLE
			TYPE	RANGE	TYPE	RANGE	
E, E/	FMF	9 - 35	D	150-250	MAG-D		DST

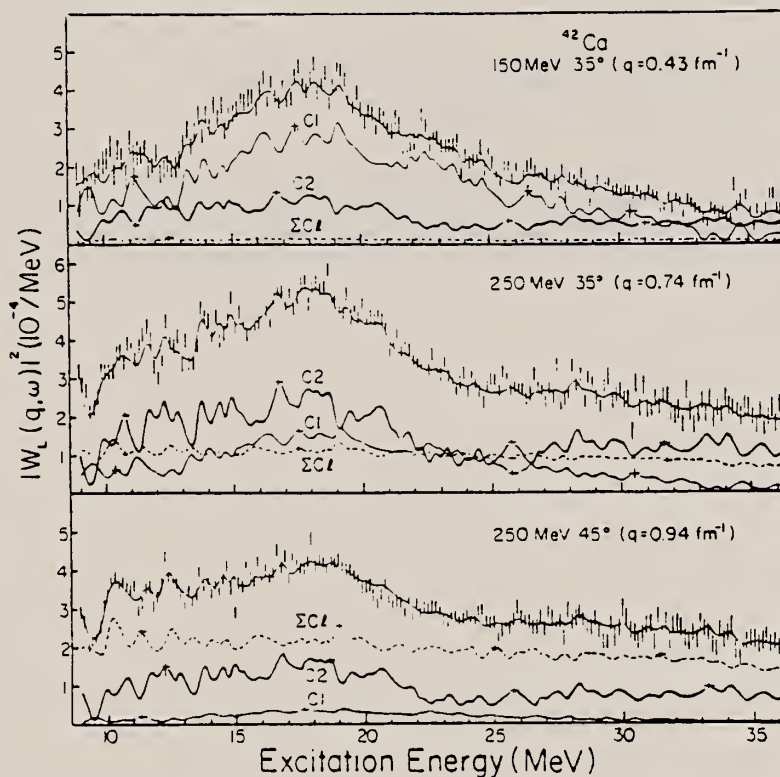


FIG. 2. The longitudinal differential form factor of ^{42}Ca at various momentum transfers. The error bars show the experimental results sorted by 150 keV. The thin curve, thick curve, and dashed curve show the dipole, quadrupole, and higher multipole ($3 \leq Cl \leq 6$) excitations, respectively. Also shown is the sum of the all multipole excitations by thin curve. The occasional error bars on the curves indicate errors associated with the least square method.

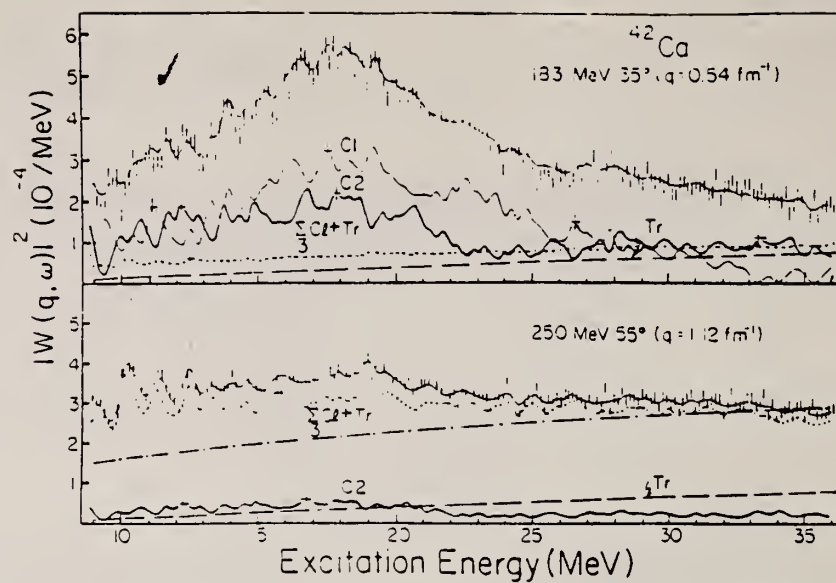


FIG. 8. The total differential form factor of ^{42}Ca at 183 MeV 35° and 250 MeV 55° . The short-dashed curve is the sum of the transverse excitations (labeled T_r) and the higher multipole ($l \geq 3$) excitations. The dot-dashed curve in the lower figure indicates the phenomenological shape for the continuum, which was used to deduce the resonant part of the octupole strength. The contribution of the dipole strength to the spectra at 250 MeV 55° is negligibly small.

CA
A=44

CA
A=44

CA
A=44

Ref. P. Brix, U. Hegel, K.H. Lindenberger, D. Quitmann
Z. Physik 150, 461 (1958)

Elem. Sym.	A	Z
Ca	44	20

Method 35 MeV betatron; radioactivity; absorption measurement; ionization chamber

Ref. No.	EH
58 Br 1	

Reaction	E or ΔE	E_0	Γ	$\int \sigma dE^-$	$I\pi$	Notes
$Ca^{44}(\gamma, p)$	Bremss. 31			$\int^{31} = 0.12 \pm 0.02$ MeV- ab b		Experiment done with and without filter 18mm of Pb & difference taken to get integrated σ ; $Cl^{35}(\gamma, n)$ σ is standard [Barber <u>et al</u> , Phys. Rev. <u>98</u> , 73 (1955)].

REF.

Y. Oka, T. Kato, K. Nomura, T. Saito, Hui-Tuh Tsai
Bull. Chem. Soc. Japan 41, 380 (1968)

ELEM. SYM.

A

Z

Ca

44

20

METHOD

REF. NO.

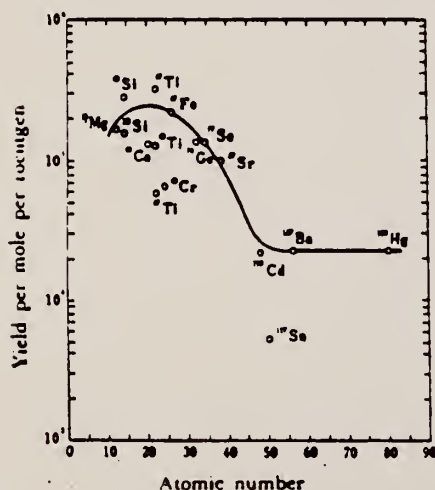
68 Ok 3

egf

REACTION	RESULT	EXCITATION ENERGY	SOURCE		DETECTOR		ANGLE
			TYPE	RANGE	TYPE	RANGE	
G _p	ABY	THR-20	C	20	ACT-I		4PI

TABLE 1. SUMMARY OF DATA ON (γ, p) REACTIONS WITH 20 MeV BREMSSTRAHLUNG

Nuclide		S_p (MeV)	Observed γ -ray			Yield determined	
Parent (Natural abundance, %)	Residual (Half-life)		Energy (MeV)	Branching ratio (%)	Type of multipole transition	$\mu\text{Ci/mg}^a$	Yield/mol·R
²³ Mg (10.11)	²⁴ Na (15 hr)	12.06	1.37	100	E2	1.48×10^{-1}	1.7×10^3
²⁸ Si (4.71)	²⁹ Al (2.27 min)	12.33	1.78	100	E2	1.91	2.8×10^3
³⁰ Si (3.12)	³⁰ Al (6.56 min)	13.59	1.28	93.8	E2 + M1	6.51×10^{-1}	1.5×10^3
⁴⁰ Ca (2.06)	⁴¹ K (22.4 hr)	12.17	0.374	85	E2 + M1	7.86×10^{-2}	1.3×10^3
⁴⁷ Ti (7.32)	⁴⁸ Sc (84.1 d)	10.47	0.887	100	E2	7.11×10^{-2}	3.1×10^3
⁴⁸ Ti (73.99)	⁴⁷ Sc (3.4 d)	11.44	0.160	100	E2 + M1	6.83×10^{-2}	1.2×10^3
⁴⁸ Ti (5.46)	⁴⁸ Sc (1.8 d)	11.35	1.31	100	E2	4.40×10^{-2}	5.8×10^3
⁵² Cr (9.55)	⁵² V (3.8 min)	11.15	1.43	100	E2	5.01×10^{-1}	6.6×10^3
⁵⁴ Fe (2.17)	⁵⁴ Mn (2.58 hr)	10.57	1.81	23.5	E2 + M1	8.10×10^{-2}	2.1×10^3
⁷⁶ Ge (36.74)	⁷⁵ Ga (4.8 hr)	10.92	0.295	97	(E2)	3.70×10^{-1}	1.3×10^3
⁷⁸ Se (7.58)	⁷⁶ As (26.5 hr)	9.61	0.559	41	E2	1.48×10^{-2}	1.3×10^3
⁸⁷ Sr (7.02)	⁸⁶ Rb (19 d)	9.41	1.08	9	E2	5.15×10^{-4}	9.9×10^3
¹¹³ Cd (12.26)	¹¹² Ag (3.2 hr)	9.74	1.39	35	E2	1.91×10^{-2}	2.1×10^3
¹¹⁷ Sn (7.57)	¹¹⁶ In (34 min)	9.58	1.27	84	E2	9.80×10^{-2}	6.9×10^3
¹³⁷ Ba (11.32)	¹³⁶ Cs (13 d)	8.67	0.830	100	E2	1.68×10^{-2}	2.2×10^3
¹⁹⁸ Hg (16.84)	¹⁹⁷ Au (2.7 d)	7.27	0.412	100	E2	8.43×10^{-4}	2.2×10^3

a) The value corrected at the end of 1 hr irradiation (9.4×10^6 R/min).Fig. 2. The yield curve for the (γ, p) reaction with 20 MeV bremsstrahlung.

METHOD

REF. NO.

71 He 1

egf

REACTION	RESULT	EXCITATION ENERGY	SOURCE		DETECTOR		ANGLE
			TYPE	RANGE	TYPE	RANGE	
E, E/	FMF	1-4	D	198-300	MAG-D		DST

5 LEVELS

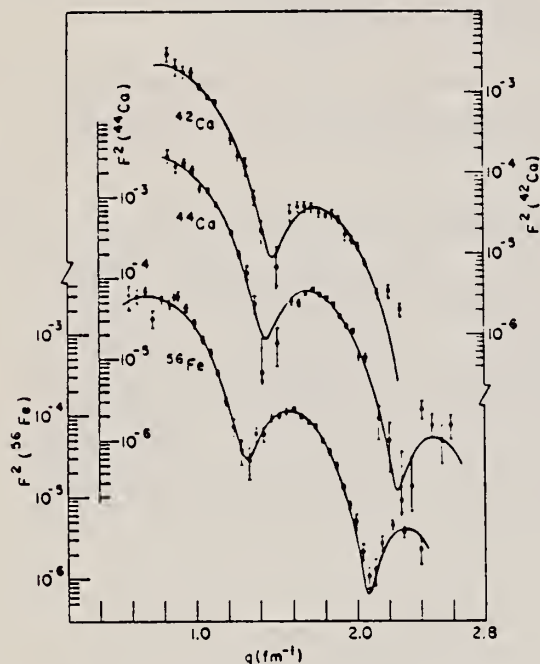


Fig. 1. Fits to the ^{42}Ca , ^{44}Ca and ^{56}Fe 2^+ levels.

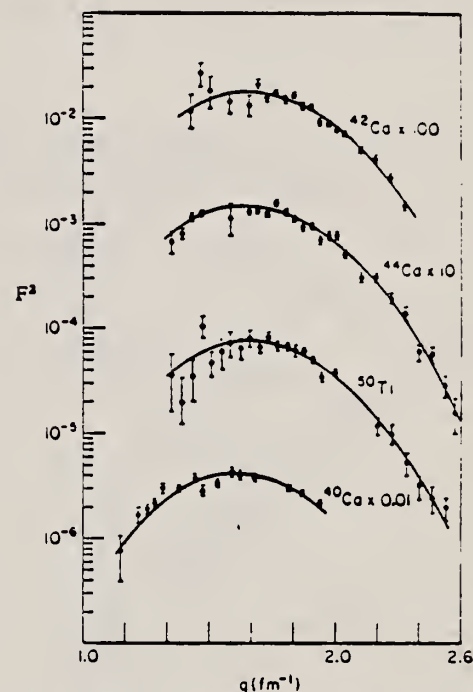


Fig. 7. Fits to ^{42}Ca , ^{40}Ca , ^{44}Ca and ^{30}Ti 5^- levels.

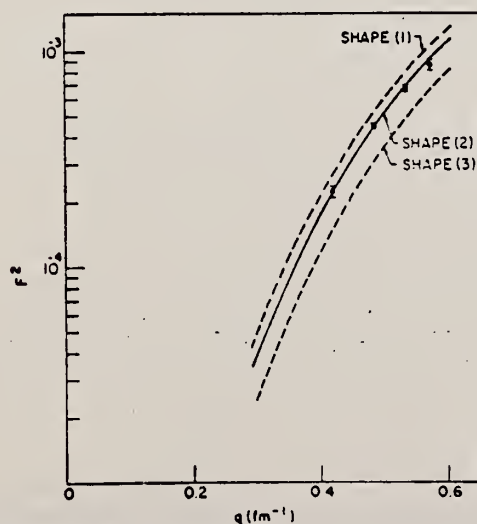


Fig. 5. Low-energy data for ^{40}Ca 3^- level from ref. ⁸). The curves represent the best fits to our high-energy data using shapes (1), (2) and (3) as explained in the text.

[over]

TABLE 3
Inelastic parameters

Isotope	E^* (MeV)	L	Shape	c_{10}^* (fm)	z_{10}^* (fm)	G^* (s.p.u.)	R_{10}^* (fm)	$G(\text{s.p.u.})$ heavy-particle scattering ¹⁹⁾
⁴⁰ Ca	3.740	3	2	3.536 ± 0.030	1.483 ± 0.020	24.9 ± 1.0	4.835 ± 0.030	23.6 ± 3.5
	4.480	5	2	3.538 ± 0.050	1.260 ± 0.035	9.7 ± 0.6	4.810	17.7 ± 2.7
			3			17.7 ± 1.5	5.467 ± 0.060	11.3 ± 1.7
⁴² Ca	3.440	3	2	3.565 ± 0.018	1.383 ± 0.014	12.4 ± 0.5	4.719 ± 0.023	12.0 ± 1.8
	4.100	5	2	3.231 ± 0.030	1.404 ± 0.025	3.4 ± 0.3	4.816 ± 0.044	9.0 ± 1.4
⁴⁴ Ca	3.30	3	2	3.555 ± 0.018	1.313 ± 0.013	6.95 ± 0.28	4.618 ± 0.023	8.0 ± 1.2
	2.28	4	2	4.091 ± 0.030	1.268 ± 0.016	2.66 ± 0.15	5.135 ± 0.030	1.3 ± 0.3
	3.91	5	2	3.268 ± 0.030	1.397 ± 0.024	2.30 ± 0.20	4.832 ± 0.045	4.4 ± 0.7
	2.00	4	2	4.264 ± 0.021	1.229 ± 0.013	7.61 ± 0.30	5.226 ± 0.026	
⁴⁶ Ti	2.286	4	2	4.330 ± 0.021	1.196 ± 0.013	3.37 ± 0.15	5.237 ± 0.026	
⁵⁰ Ti	4.42	3	2	3.645 ± 0.017	1.244 ± 0.012	3.76 ± 0.15	4.600 ± 0.023	5.4 ± 0.8 $5.9^{20)}$
	2.50	4	2	3.865 ± 0.017	1.347 ± 0.012	4.7 ± 0.15	5.064 ± 0.026	3.3 ± 0.7 $2.7^{20)}$
	3.20	5	2	3.254 ± 0.032	1.345 ± 0.026	0.83 ± 0.08	4.724 ± 0.045	

Present experiment

^{a)} Errors do not reflect any model dependence.

^{b)} Given errors do not include the 6% error of normalization.

¹⁹⁾ A. M. Bernstein, Adv. in Nucl. Phys. 3 (1969) 325.

For data on 2^+ levels, see Table 2 on ⁴²Ca (for ⁴⁴Ca).

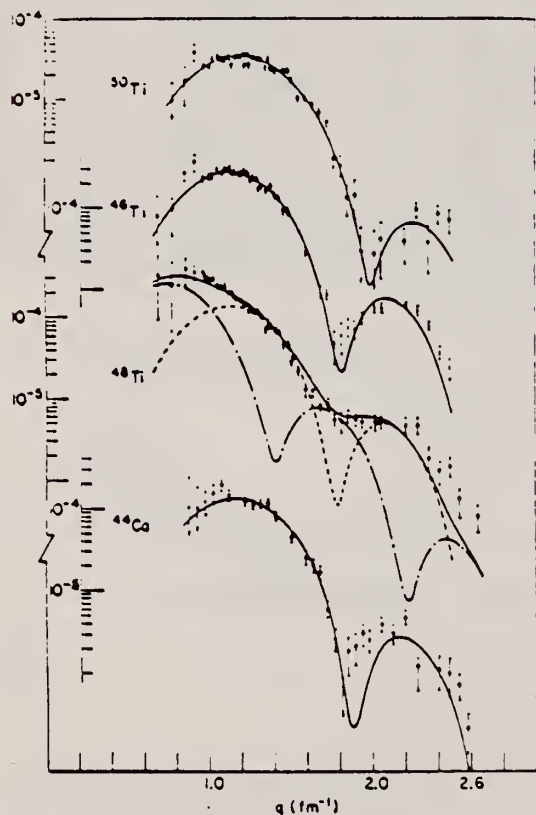


Fig. 6. Fits to ⁵⁰Ti, ⁴⁶Ti, ⁴⁸Ti and ⁴⁴Ca 4^+ levels. For ⁴⁶Ti we show the decomposition into contributions of the 2.42 MeV 2^+ level (dash-dot curve) and the 2.286 MeV 4^+ level (dashed curve).

REF. D. Branford, G.S. Foote, R.A.I. Bell, D.C. Weissner,
F.C.P. Huang and R.B. Watson
PICNS-73, Vol.II, p.943 (1973) Asilomar

ELEM. SYM.	A	Z
Ca	44	20

METHOD

REF. NO.	
73 Br 7	egf

REACTION	RESULT	EXCITATION ENERGY	SOURCE		DETECTOR		ANGLE
			TYPE	RANGE	TYPE	RANGE	
G,A	ABX	- 25	D	16	NAI-D		DST

NO ANG DST DATA

Table 1. Preliminary Results with Relative Errors; Absolute Errors \approx 30%

Reaction	$\int \sigma(\gamma_0, \alpha_0) dE$ mb. MeV	$\int \sigma(\gamma_1, \alpha_0) dE$ mb. MeV	Excitation Energy (MeV)
$^{40}\text{Ar}(\alpha, \gamma)^{44}\text{Ca}$	1.4 ± 0.3	0.42 ± 0.08	15.5
$^{48}\text{Ti}(\alpha, \gamma)^{52}\text{Cr}$	3.0 ± 0.6	0.48 ± 0.10	17.0
$^{56}\text{Fe}(\alpha, \gamma)^{60}\text{Ni}$	7.8 ± 1.5	1.52 ± 0.30	16.0

ELEM. SYM.	A	Z
Ca	44	20
REF. NO.		hmg
73 To 1		

REACTION	RESULT	EXCITATION ENERGY	SOURCE		DETECTOR		ANGLE
			TYPE	RANGE	TYPE	RANGE	
E, E/	FMF	7- 35	D	124-250	MAG-D		DST

Table I. The $B(EL)$ and $|M_{if}|^2$ values and fractions of the energy weighted sum rule (EWSR) for the giant resonances in ^{44}Ca .

	E_x (MeV)	$B(EL)$ or $ M_{if} ^2$	fraction of T=0 EWSR(%)	fraction of T=1 EWSR(%)
E2	17*	$884 e^2\text{fm}^4$	148	123
E0	17*	1550 fm^4	240	
E1	17*	$8.9 e^2\text{fm}^2$		92

* Center of energy from 10 to 28 MeV

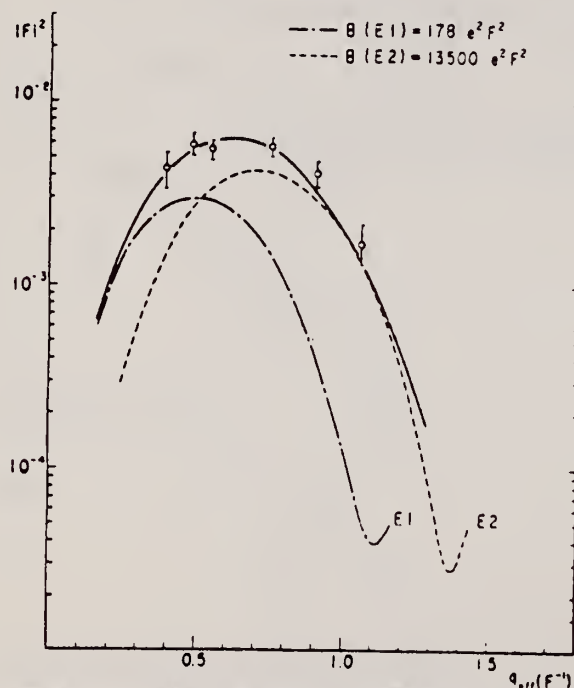


Fig. 2. The form factor integrated over the range from 10 to 28 MeV in ^{44}Ca . The form factor was decomposed to E1 and E2 components.

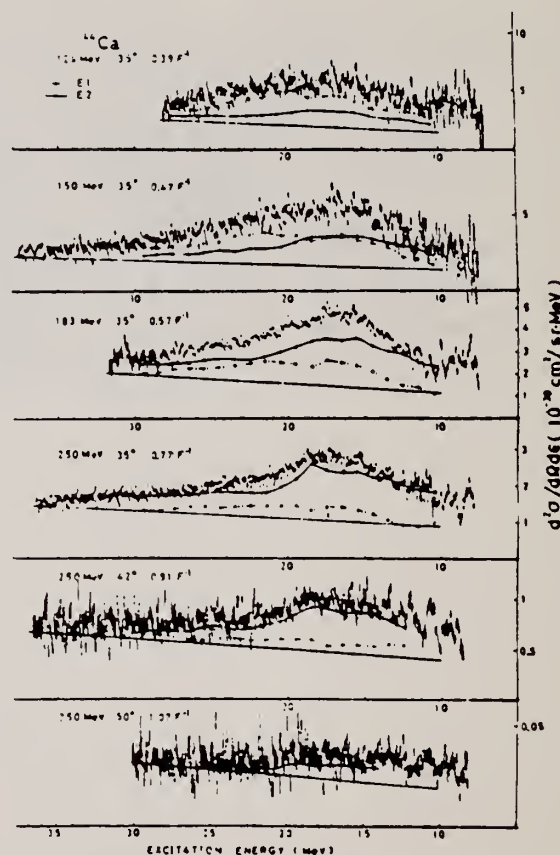


Fig. 1. Inelastic electron scattering spectra of the giant resonance region in ^{44}Ca . The spectra were decomposed to E1(dotted line) and E2(solid line) components.

P. David, J. Debrus, F. Lubke, H. Mommsen, R. Schoenmackers,
and G. Stein
Nucl. Phys. A221, 145 (1974)

Ca

44

20

METHOD

REF. NO.

74 Da 2

egf

REACTION	RESULT	EXCITATION ENERGY	SOURCE		DETECTOR		ANGLE
			TYPE	RANGE	TYPE	RANGE	
G,P	ABY	THR-400	C	450	TEL-D		90
G,T	ABY	THR-400	C	450	TEL-D		90
G,HE	ABY	THR-400	C	450	TEL-D		90
G,A	ABY	THR-400	C	450	TEL-D		90

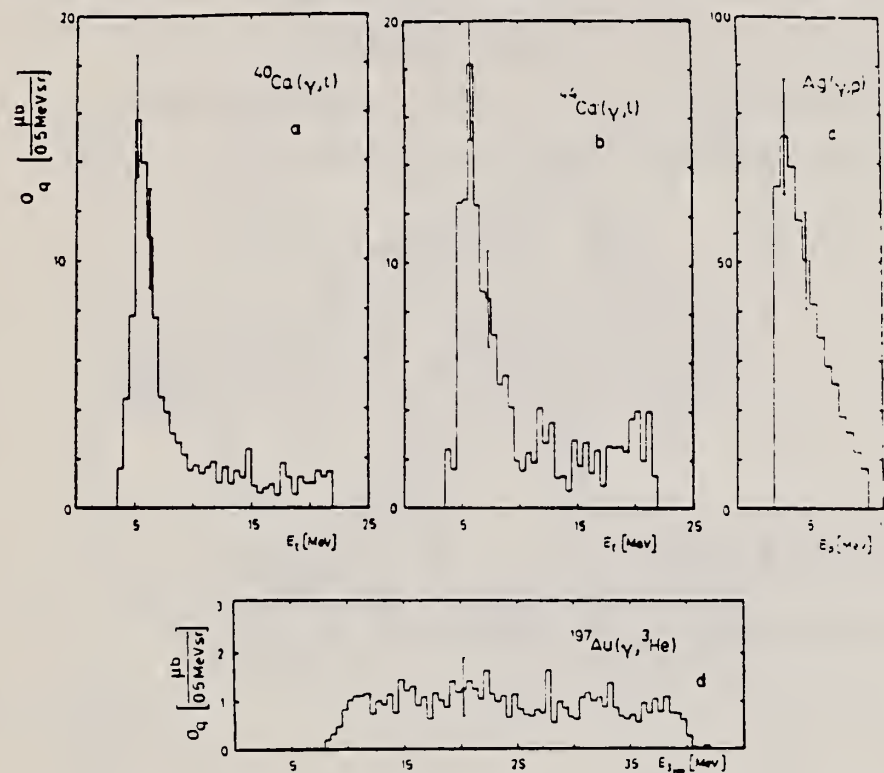


Fig. 3. Characteristic measured spectra of p, t, ^3He and ^4He from the target nuclei ^{27}Al , $^{40,44}\text{Ca}$, ^{107}Ag , ^{197}Au .

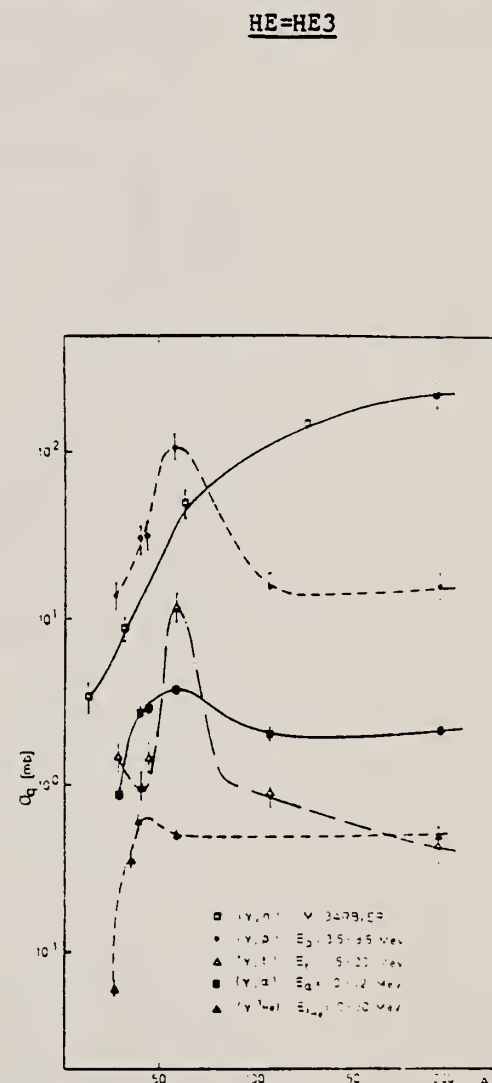


Fig. 5. Yield of protons, tritons, ^3He and ^4He depending on mass number A [ref. 23]. The lines through the points are to guide the eye.

23) M. Barbier, Induced Radioactivity
(North-Holland, Amsterdam, 1969)

(over)

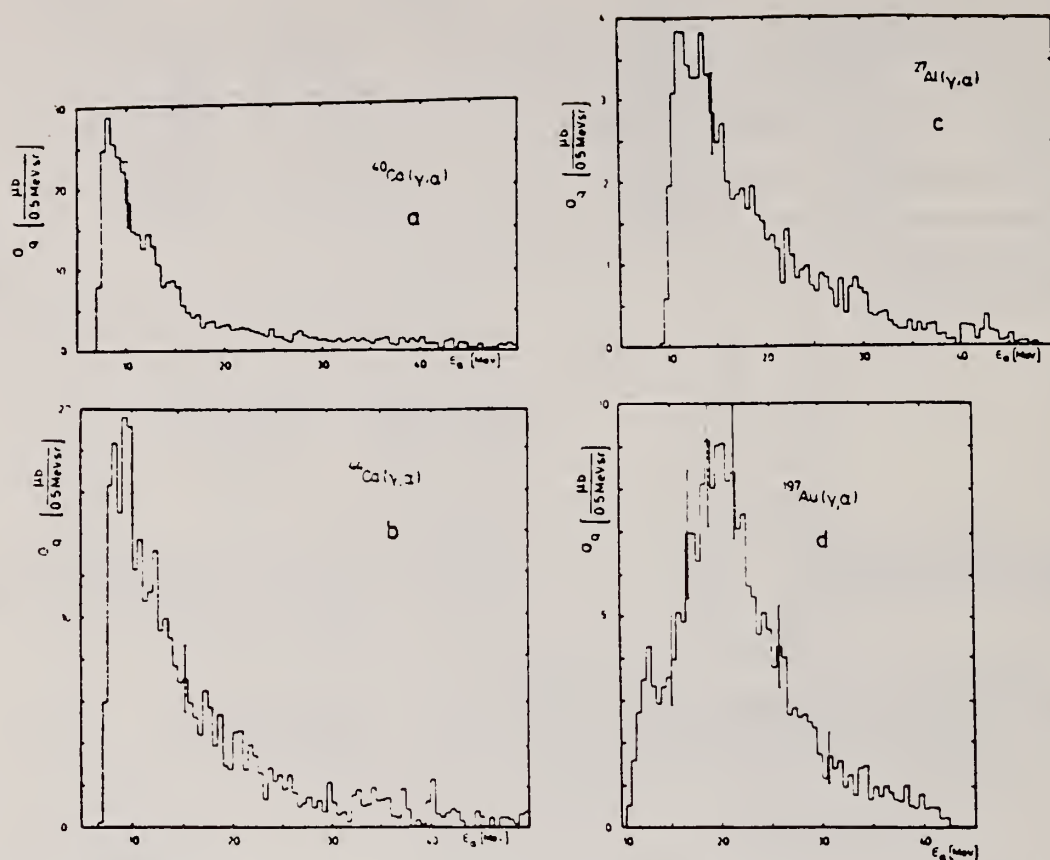


Fig. 4. Characteristic measured spectra of p, t, ^3He and ^4He from the target nuclei ^{27}Al , $^{40,44}\text{Ca}$, ^{181}Ag , ^{197}Au .

REF. G.S. Foote, D. Branford, D.C. Weissner, N. Shikazono, and
F.C.P. Huang
J. Phys. A: Math., Nucl. Gen., 7, L4 (1974)

ELEM. SYM.	A	Z
Ca	44	20
REF. NO.		
74 Fo 4		egf

METHOD			SOURCE		DETECTOR		ANGLE
REACTION	RESULT	EXCITATION ENERGY	TYPE	RANGE	TYPE	RANGE	
G.A	ABX	14- 19	D	6- 10	NAI-D		90

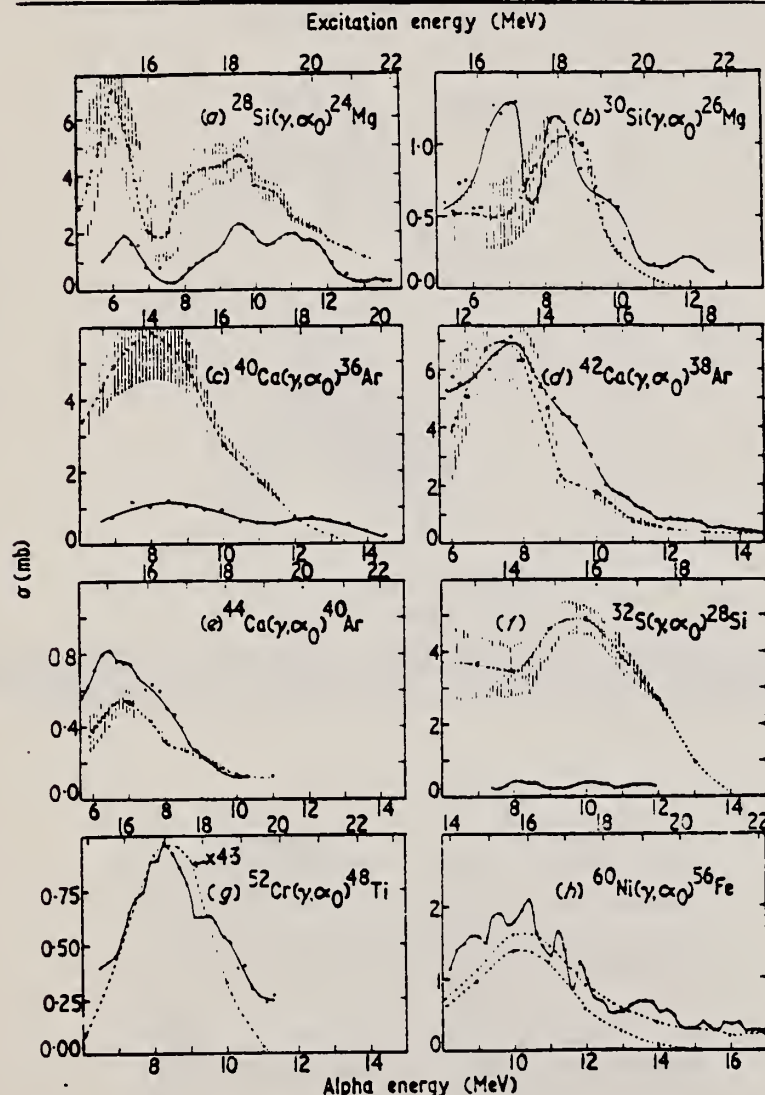


Figure 1. Excitation functions for the (γ, α) reaction obtained from a capture data using the principle of detailed balance. The data shown in (a) and (f) are from Meyer-Shutzmeister *et al* (1968). Those in (b) are from Watson *et al* (1973). The relative experimental errors are approximately $\pm 10\%$. The absolute errors are $\pm 25\%$. The broken curves are the results of calculations (see text). The vertical lines indicate the relative errors due to uncertainties in the total photonuclear cross sections where they are greater than $\pm 10\%$. The crosses indicate the energies at which transmission coefficients were calculated.

REF.

G. S. Foote, D. Branford, D. C. Weissner, N. Shikazono,
R.A.I. Bell, F.C.P. Huang
Nucl. Phys. **A263**, 349 (1976)

ELEM. SYM.

A

Z

Ca

44

20

METHOD

REF. NO.

76 Fo 2

egf

REACTION	RESULT	EXCITATION ENERGY	SOURCE		DETECTOR		ANGLE
			TYPE	RANGE	TYPE	RANGE	
A,G	ABX	13- 19	D	5- 11	NAI-D		DST

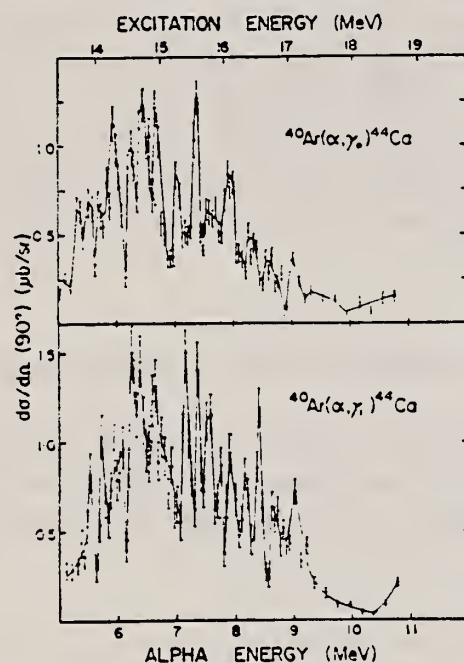


Fig. 3. Absolute differential cross sections for the $^{40}\text{Ar}(\alpha, \gamma_0)^{44}\text{Ca}$ and $^{44}\text{Ar}(\alpha, \gamma_1)^{44}\text{Ca}$ reactions measured at 90° to the beam direction versus bombarding energy. The error bars represent relative statistical errors. The absolute error is $\pm 30\%$. The continuous line is a guide to the eye.

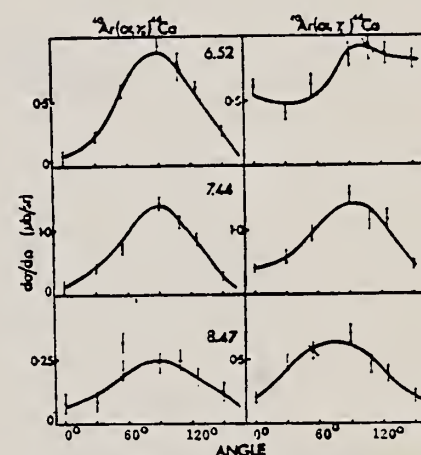


Fig. 6. Angular distribution measurements for the $^{40}\text{Ar}(\alpha, \gamma_0)^{44}\text{Ca}$ reaction and the $^{44}\text{Ar}(\alpha, \gamma_1)^{44}\text{Ca}$ reaction at the bombarding energies (MeV) indicated. Only relative statistical errors are shown. The continuous lines represent Legendre polynomial fits to the data.

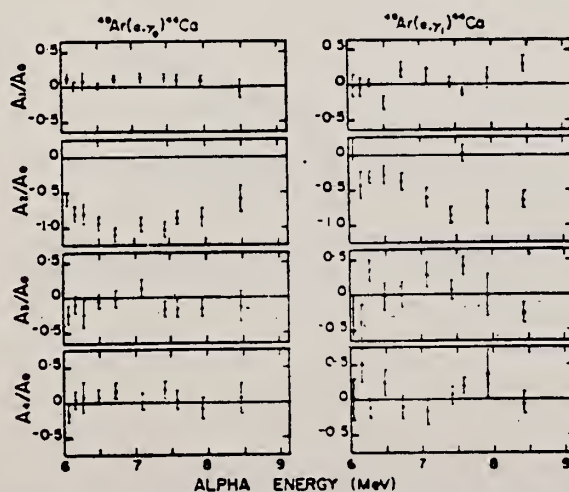


Fig. 9. Normalised Legendre polynomial coefficients determined by linear least squares fitting of the γ -ray angular distributions measured for the $^{40}\text{Ar}(\alpha, \gamma_0)^{44}\text{Ca}$ and $^{44}\text{Ar}(\alpha, \gamma_1)^{44}\text{Ca}$ reaction.

(over)

U.S. DEPARTMENT OF COMMERCE
NATIONAL BUREAU OF STANDARDS

TABLE 3
Comparisons of energy integrated (γ, α) cross sections, peak energies of the broad structures in the (γ, α) excitation functions and the particle threshold energies

Final ^{a)} nucleus	Range of integration (MeV)	$\int \sigma(\gamma, \alpha) dE^b)$ (mb · MeV)	$\int \frac{\sigma(\gamma, \alpha) dE^b)}{cds}$ (%)	Particle threshold energies			$E^c)$ (MeV)	Exp. peak energy (MeV)	GDR energy (MeV)	Refs.
				α (MeV)	n (MeV)	p (MeV)				
²⁸ Si	14.5-22.5	9.6	2.3	9.99	17.18	11.59	15.2	18.0	20	¹⁾
³⁰ Si	14.0-22.0	5.3	1.2	10.65	10.62	13.51	15.7	16.5	18	¹⁾
³² Si	13.1-22.7	2.7	0.57	6.95	15.09	8.87	13.0	16	20	¹⁾
⁴⁰ Ca	12.5-22.2	4.8	0.8	7.04	15.62	8.33	14.2	14.0	20	⁶⁾
⁴² Ca	11.0-20.5	30.2	4.8	6.25	11.49	10.28	13.3	13.0	17.4	this work
⁴⁴ Ca	13.5-18.8	2.6	3.09	8.84	11.13	12.16	15.9	15.3	17	this work
⁴⁴ Ca*	13.5-18.8	0.76	0.12				15.9		18.5	this work
⁴⁴ Ti	10.5-20.6	6.1	0.9	5.18	5.18	8.66	13.9	14.0		¹⁵⁾
⁵² Ti	12.7-20.4	≈ 0.3	≈ 0.04	7.67	7.80	13.53	16.1			¹⁵⁾
⁵² Cr	15.0-20.5	2.9	0.38	9.35	12.05	10.52	17.6	17.0	18	this work
⁵² Cr*	15.0-20.5	0.51	0.07				17.6			this work
⁶⁰ Ni	13.9-22.8	9.6	1.07	6.29	11.39	9.53	15.7	15.8	16.6	³⁾
⁶⁰ Ni*	13.9-22.8	1.7	0.18	4.96			15.7		17.9	³⁾

^{a)} The asterisk denotes first excited state.

^{b)} The errors are approximately $\pm 30\%$.

^{c)} E is the α -particle threshold energy plus Coulomb barrier height (see text).

- ¹ L. Meyer-Schutzmeister et al., Nucl. Phys. A108, 180 (1968).
- ³ G. S. Foote et al., Nucl. Phys. A220, 505 (1974).
- ⁶ R. B. Watson et al., Nucl. Phys. A203, 209 (1973).
- ¹⁵ R. E. Peshel et al., Nucl. Phys. A232, 269 (1974).

ELEM. SYM.	A	Z
Ca	44	20
REF. NO.		
77 01 1		egf

METHOD							
REACTION	RESULT	EXCITATION ENERGY	SOURCE		DETECTOR		ANGLE
			TYPE	RANGE	TYPE	RANGE	
E,P	ABX	15-25	D	15-25	MAG-D		90
E,A	ABX	14-17	D	14-17	MAG-D		90

Abstract: The cross sections of the (e, e'p) reaction on ^{44}Ca , ^{45}Sc and ^{46}Ti have been measured and used to deduce (p, p) cross sections. Together with (p, n) cross sections from others, these data allow an estimate of the T_1 and T_2 GDR cross sections. The experimental results seem to be consistent with the theory on the isospin splitting. The (p, p₀) or (p, p₀ + p₁) and (p, x₀) cross sections have also been measured. The ratio of (p, p₀) to (p, p) indicates a contribution of a statistical nature in the T_1 GDR region and some additional direct modes in the T_2 GDR region. The contribution of one (^{45}Sc) or two (^{46}Ti) extra protons is discussed and it is found that the valence nucleons contribute to GDR in an independent way.

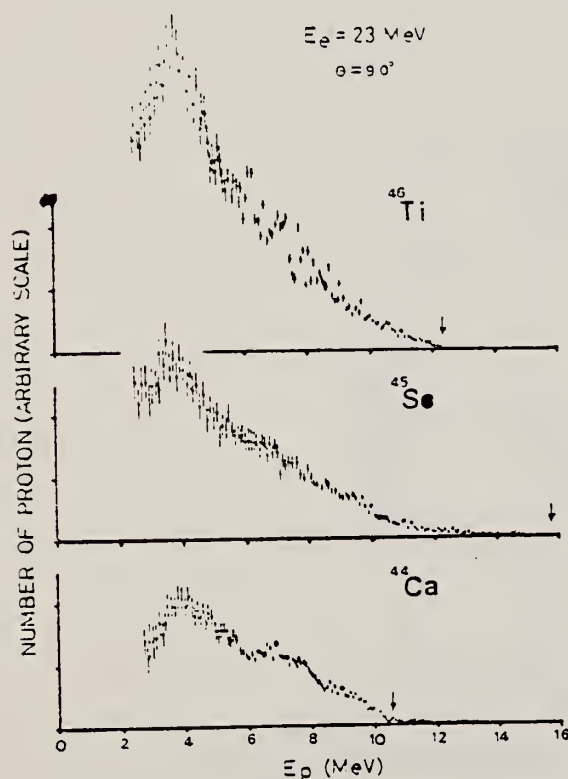


Fig. 4. Example of proton energy distribution obtained with 23 MeV electron beam. Arrows show the proton end point energy

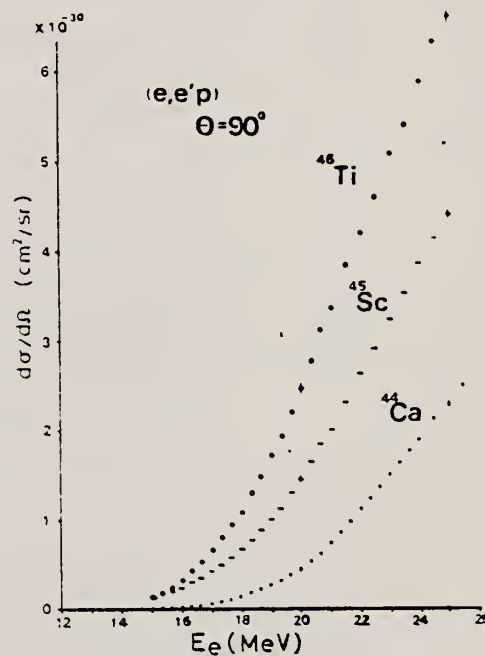


Fig. 5. The differential cross sections at $\theta = 90^\circ$ of the (e, e'p) reaction

(over)

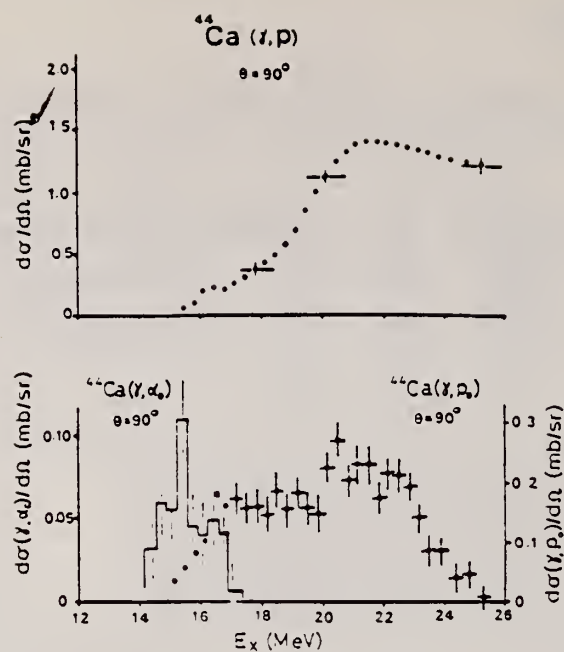


Fig. 6. The differential cross sections at $\theta = 90^\circ$ of the (γ, p) , (γ, p_0) and (γ, α) reactions of ^{44}Ca .

REF. H.D. Gräf, H. Feldmeier, P. Manakos, A. Richter, E. Spamer and
D. Strottman
Nucl. Phys. A295, 319 (1978)

ELEM. SYM.	A	Z
Ca	44	20
REF. NO.		
78 Gr 1		rs

METHOD					
REACTION	RESULT	EXCITATION ENERGY	SOURCE		ANGLE
			TYPE	RANGE	
E, E/	ABX	2	D	34- 60	DST

2=1.884

Abstract: Monopole transitions from the 0_1^+ ground states to 0_2^+ excited states at 3.353 MeV (^{40}Ca), 1.837 MeV (^{42}Ca), 1.884 MeV (^{44}Ca) and 4.272 MeV (^{46}Ca) have been investigated with high resolution inelastic electron scattering (FWHM ≈ 30 keV) at low momentum transfer ($0.29 \leq q \leq 0.53 \text{ fm}^{-1}$). The respective monopole matrix elements are $2.53 \pm 0.41 \text{ fm}^2$, $5.24 \pm 0.39 \text{ fm}^2$, $5.45 \pm 0.41 \text{ fm}^2$ and $2.28 \pm 0.49 \text{ fm}^2$. These results are used together with known ground state charge radii and the average number of holes in the sd shell in the ground state to estimate the number of particle-hole excitations in the wave functions of the excited 0^+ states.

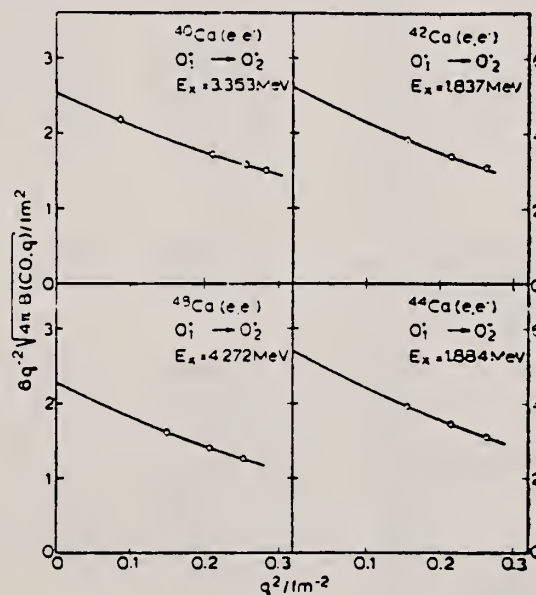


Fig. 3. Extrapolation of the measured $B(C0, q)$ values (dots) to $q = 0$ with the two parameter expression of eq. (1).

TABLE 2
Elastic and inelastic cross sections ($d\sigma/d\Omega$)_{el} (10^{-1} fm² sr) and ($d\sigma/d\Omega$)_{inel} (10^{-1} fm² sr), respectively, and DWBA correction factors f_c for the monopole transitions studied

Nucleus E_i (MeV)	E_0 (MeV)	θ (deg)	q^2 (fm ⁻²)	($d\sigma/d\Omega$) _{el}	($d\sigma/d\Omega$) _{inel}	f_c
⁴⁰ Ca 3.353	59.76	128.9	0.282	4.52	2.91 (6.5)	1.46
	54.73	140.9	0.256	3.11	1.95 (11.7)	1.53
	54.70	116.9	0.210	14.65	4.84 (8.9)	1.55
	33.67	128.9	0.026	40.70	2.47 (34.7)	1.91
⁴² Ca 1.837	54.73	140.9	0.263	3.05	6.53 (5.8)	1.48
	54.70	116.9	0.215	14.21	20.51 (4.3)	1.51
	54.70	92.9	0.156	64.99	45.23 (3.9)	1.54
⁴⁴ Ca 1.884	54.73	140.9	0.263	3.15	6.44 (7.3)	1.47
	54.72	116.9	0.215	14.83	20.91 (4.0)	1.50
	54.72	92.9	0.156	66.24	45.39 (3.5)	1.53
⁴⁸ Ca 4.272	54.73	140.9	0.252	2.99	1.11 (30.8)	1.46
	54.73	116.9	0.206	14.20	3.09 (5.6)	1.49
	54.73	92.9	0.149	64.09	7.38 (13.4)	1.53

The values in parentheses denote the statistical error of the cross sections in percent.

TABLE 3
Results of the present (e, e') experiment for monopole matrix elements, transition radii and pair decay widths together with results from other experiments and theoretical predictions

Nucleus	ME (fm ²)	R_{tr} (fm)	Γ_e (μ eV)	Exp	Theory
⁴⁰ Ca	3.6 \pm 1.1	6.3	0.37 \pm 0.23	(e, e') ^{a)}	
	2.6 \pm 0.1		0.21 \pm 0.01	^{b)}	
	2.44			(p, p') ^{c)}	^{d)}
	5.53				^{e)}
	2.53 \pm 0.41	6.1 \pm 0.9	0.18 \pm 0.06	this work	
⁴² Ca	5.93 \pm 0.52			(p, p') ^{c)}	
	5.58				^{d)}
	4.19				^{e)}
	5.24 \pm 0.39	6.3 \pm 0.4	0.016 \pm 0.002	this work	
⁴⁴ Ca	5.39 \pm 1.79			(p, p') ^{c)}	
	5.56			(x, p') ^{c)}	
	5.45 \pm 0.41	6.5 \pm 0.4	0.021 \pm 0.003	this work	
⁴⁸ Ca	1.52 \pm 0.07			(p, p') ^{c)}	
	2.28 \pm 0.49	6.8 \pm 1.4	0.63 \pm 0.2 ^{e)}	this work	

^{a)} Ref. ¹¹⁾ ^{b)} Ref. ¹²⁾ ^{c)} Ref. ⁹⁾ ^{d)} Ref. ³⁾ ^{e)} Ref. ⁴⁾ ^{f)} Ref. ²²⁾ ^{g)} Ref. ²³⁾

³⁾ W.J. Gerace and A.M. Green, Nucl. Phys. A93, 110 (1967);
A123, 241 (1969)

⁴⁾ P. Federman and S. Pittel, Phys. Rev. 186, 1106 (1969);
Nucl. Phys. A139, 108 (1969)

⁹⁾ M. Ulrickson, N. Benczer-Koller, J.R. MacDonald and
J.W. Tape, Phys. Rev. C15 186 (1977)

¹¹⁾ P. Strehl, Z. Phys. 234, 416 (1970)

¹²⁾ P.M. Endt and C. van der Leun, Nucl. Phys. A235, 27 (1974)

²²⁾ L.D. Skouras, Nucl. Phys. A220, 604 (1974)

²³⁾ J.D. McCullen and D.J. Donahue, Phys. Rev. C8, 1406 (1973)

ELEM. SYM.	A	Z
Ca	44	20
REF. NO.		hmg
78 Gr 5		

REACTION	RESULT	EXCITATION ENERGY	SOURCE		DETECTOR		ANGLE
			TYPE	RANGE	TYPE	RANGE	
E, E/	ABX	1	D	31-67	MAG-D		DST
		(1.884)					

Abstract: Monopole transitions from the 0_1^+ ground states to 0_2^+ excited states at 3.353 MeV (^{40}Ca), 1.837 MeV (^{42}Ca), 1.884 MeV (^{44}Ca) and 4.272 MeV (^{48}Ca) have been investigated with high resolution inelastic electron scattering (FWHM ≈ 30 keV) at low momentum transfer ($0.29 \leq q \leq 0.53 \text{ fm}^{-1}$). The respective monopole matrix elements are $2.53 \pm 0.41 \text{ fm}^2$, $5.24 \pm 0.39 \text{ fm}^2$, $5.45 \pm 0.41 \text{ fm}^2$ and $2.28 \pm 0.49 \text{ fm}^2$. These results are used together with known ground state charge radii and the average number of holes in the sd shell in the ground state to estimate the number of particle-hole excitations in the wave functions of the excited 0_2^+ states.

E NUCLEAR REACTIONS $^{40,42,44,48}\text{Ca}(e, e^-)$, $E = 31-67$ MeV; measured $\sigma(E; E_e; 0)$.
 $^{40,42,44,48}\text{Ca}$ 0_2^+ level deduced E0 matrix elements. Shell model calculation.

TABLE 2

Elastic and inelastic cross sections ($d\sigma/d\Omega_{el}$ ($10^{-1} \text{ fm}^2 \text{ sr}$) and ($d\sigma/d\Omega$) ($10^{-1} \text{ fm}^2 \text{ sr}$), respectively, and DWBA correction factors f_c for the monopole transitions studied

Nucleus E_i (MeV)	E_0 (MeV)	θ (deg)	q^2 (fm^{-2})	$(d\sigma/d\Omega)_{el}$	$(d\sigma/d\Omega)_{in}$	f_c
^{40}Ca 3.353	59.76	128.9	0.282	4.52	2.91 (6.5)	1.46
	54.73	140.9	0.256	3.11	1.95 (11.7)	1.53
	54.70	116.9	0.210	14.65	4.84 (8.9)	1.55
	33.67	128.9	0.086	40.70	2.47 (34.7)	1.91
^{42}Ca 1.837	54.73	140.9	0.263	3.05	6.53 (5.8)	1.48
	54.70	116.9	0.215	14.21	20.51 (4.3)	1.51
	54.70	92.9	0.156	64.99	45.23 (3.9)	1.54
^{44}Ca 1.884	54.73	140.9	0.263	3.15	6.44 (7.3)	1.47
	54.72	116.9	0.215	14.83	20.91 (4.0)	1.50
	54.72	92.9	0.156	66.24	45.39 (3.5)	1.53
^{48}Ca 4.272	54.73	140.9	0.252	2.99	1.11 (30.8)	1.46
	54.73	116.9	0.206	14.20	3.09 (5.6)	1.49
	54.73	92.9	0.149	64.09	7.38 (13.4)	1.53

The values in parentheses denote the statistical error of the cross sections in percent.

TABLE 3

Results of the present (e, e⁻) experiment for monopole matrix elements, transition radii and pair decay widths together with results from other experiments and theoretical predictions

Nucleus	ME (fm^2)	R_e (fm)	Γ_e (μeV)	Exp.	Theory
^{40}Ca	3.6 ± 1.1	6.3	0.37 ± 0.23	(e, e ⁻) ^{a)}) ^{a)}) ^{b)}
	2.6 ± 0.1		0.21 ± 0.01	(p, p ⁺) ^{c)}	
	2.44			this work	
	2.53 ± 0.41	6.1 ± 0.9	0.18 ± 0.06	this work	
^{42}Ca	5.93 ± 0.52			(p, p ⁺) ^{c)}) ^{a)}) ^{b)}
	5.58			this work	
	4.19			this work	
^{44}Ca	5.24 ± 0.39	6.3 ± 0.4	0.016 ± 0.002	(p, p ⁺) ^{c)}) ^{a)}) ^{b)}
	5.39 ± 1.79			(p, p ⁺) ^{c)}	
	5.56			(p, p ⁺) ^{c)}	
^{48}Ca	5.45 ± 0.41	6.5 ± 0.4	0.021 ± 0.003	this work) ^{a)}) ^{b)}
	1.52 ± 0.07			(p, p ⁺) ^{c)}	
	2.28 ± 0.49	6.8 ± 1.4	0.63 ± 0.27	this work	

^{a)} Ref. ¹¹⁾, ^{b)} Ref. ¹²⁾, ^{c)} Ref. ¹³⁾, ^{d)} Ref. ¹⁴⁾, ^{e)} Ref. ¹⁵⁾, ^{f)} Ref. ¹⁶⁾

ELECTRIC MONOPOLE TRANSITIONS

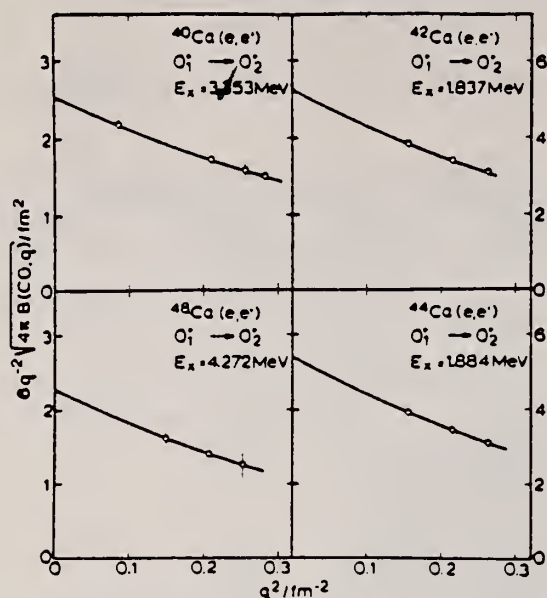


Fig. 3. Extrapolation of the measured $B(C0, q)$ values (dots) to $q = 0$ with the two parameter expression of eq. (1).

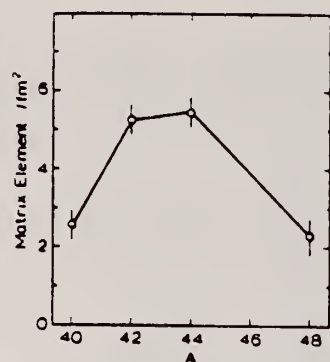


Fig. 4. The determined monopole matrix elements as a function of mass number for the four Ca isotopes. The line which connects the experimental points has no theoretical significance.

- 3) W. J. Gerace and A. M. Green, Nucl. Phys. A93 (1967) 110, A123 (1969) 241
- 4) P. Federman and S. Pittel, Phys. Rev. 186 (1969) 1106; Nucl. Phys. A139 (1969) 108
- 5) M. Sakakura, A. Arima and T. Sebe, Phys. Lett. 61B (1976) 335
- 6) N. Benczer-Koller, G. G. Seaman, M. C. Bertin, J. W. Tape and J. R. MacDonald, Phys. Rev. C2 (1970) 1037
- 7) J. C. Adloff, K. H. Souw, D. Disdier, F. Scheibling, P. Chevallier and Y. Wolfson, Phys. Rev. C10 (1974) 1819
- 8) M. Ulrickson, W. Hartwig, N. Benczer-Koller, J. R. MacDonald and J. W. Tape, Phys. Rev. C13 (1976) 536
- 9) M. Ulrickson, N. Benczer-Koller, J. R. MacDonald and J. W. Tape, Phys. Rev. C15 (1977) 186
- 10) P. Strehl and Th. H. Schucan, Phys. Lett. 27B (1968) 641
- 11) P. Strehl, Z. Phys. 234 (1970) 416
- 12) P. M. Endt and C. van der Leun, Nucl. Phys. A235 (1974) 27
- 13) R. F. Frosch, R. Hofstadter, J. S. McCarthy, G. K. Nöldeke, K. J. van Oostrum, M. R. Yearian, B. C. Clark, R. Herman and D. G. Ravenhall, Phys. Rev. 174 (1968) 1380
- 14) P. Doll, G. J. Wagner, K. T. Knöpfle and G. Mairle, Nucl. Phys. A263 (1976) 210
- 15) J. A. Nolen, Jr. and R. J. Giletsmann, Phys. Rev. C11 (1975) 1159
- 16) K. K. Seth, A. Saha, W. Benenson, W. A. Lanford, H. Nann and B. H. Wildenthal, Phys. Rev. Lett. 33 (1974) 233
- 17) C. R. Fischer and G. H. Rawitscher, Phys. Rev. 135 (1964) B377
- 18) C. W. de Jager, H. de Vries and C. de Vries, Atomic Data and Nucl. Data Tables 14 (1974) 479
- 19) H. Theissen, Springer Tracts in Modern Phys. 65 (1972) 1
- 20) S. Krewald, R. Rosenfelder, J. E. Galonska and A. Faessler, Nucl. Phys. A269 (1976) 112
- 21) Th. H. Schucan, Nucl. Phys. 61 (1965) 417
- 22) L. D. Skouras, Nucl. Phys. A220 (1974) 604
- 23) J. D. McCullen and D. J. Donahue, Phys. Rev. C8 (1973) 1406

ELEM. SYM.	A	Z
Ca	44	20

METHOD				REF. NO.	
				78 Ma 10	hg
REACTION	RESULT	EXCITATION ENERGY	SOURCE		ANGLE
			TYPE	RANGE	
G,P	ABY	12-68	C	30-68	4PI

Analysis is made of reactions interfering with photon activation analysis procedures.

The activation yield curves have been presented for a number of photonuclear reactions in the energy range from 30 to 68 MeV, in order to evaluate quantitatively the interferences due to competing reactions in multielement photon activation analysis. The general features of the yields as functions of both target mass number and excitation energy were elucidated from the data obtained, discussion being given on the results in terms of the reaction mechanism.

Simultaneous neutron activation due to appreciable neutron production from the converter and surrounding materials has also been studied, and, finally, the magnitudes of interferences in real multielement analysis were given in the form of their energy dependences.

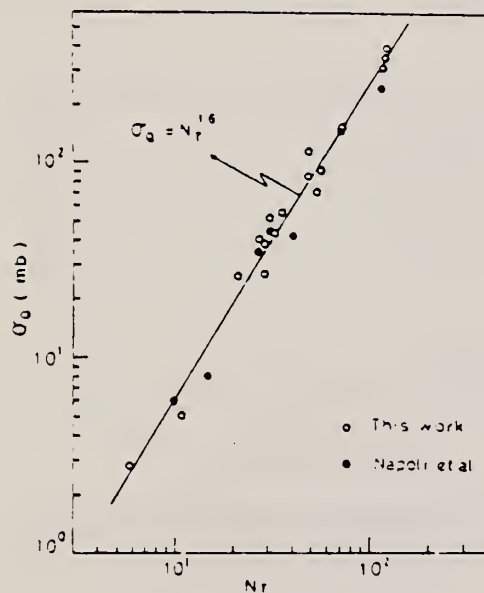


Fig. 2. Yield per equivalent quanta versus target neutron number.

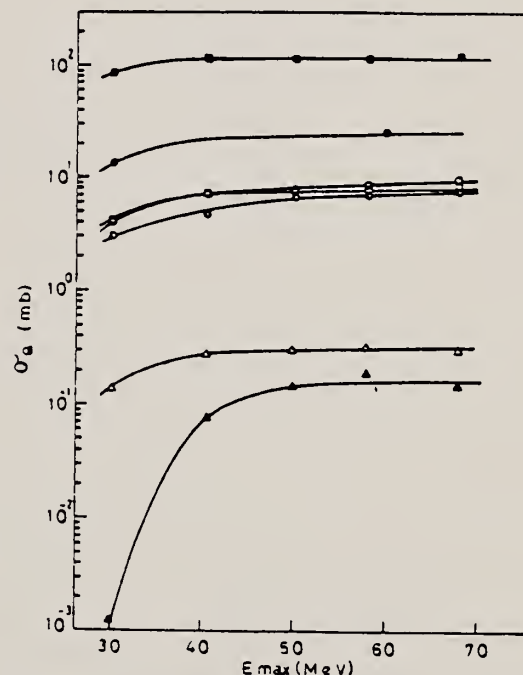


Fig. 4. Activation yield curves for the reactions on Ca, Ti and V
 ■ $^{48}\text{Ca}(\gamma, n)^{47}\text{Ca}$, □ $^{44}\text{Ca}(\gamma, p)^{43}\text{K}$, ● $^{46}\text{Ti}(\gamma, n)^{45}\text{Ti}$,
 ○ $^{48}\text{Ti}(\gamma, p)^{47}\text{Sc}$, ○ $^{49}\text{Ti}(\gamma, p)^{48}\text{Sc}$, △ $^{51}\text{V}(\gamma, \alpha)^{47}\text{Sc}$,
 ▲ $^{51}\text{V}(\gamma, zn)^{49}\text{Sc}$.

(over)

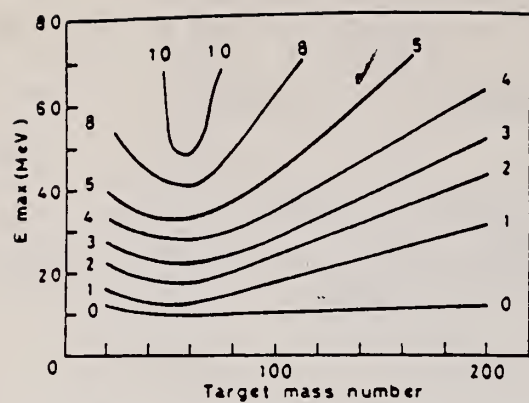


Fig. 10. Yields of the (γ, p) reactions as a function of bremsstrahlung maximum energy and target mass number. The numerical values in the figure are yields per equivalent quanta in mb.

REF. W. Steffen, H.-D. Gräf, W. Gross, D. Meuer, A. Richter, E. Spamer,
O. Titze, W. Knüpfner
Phys. Lett. 95B, 23 (1980)

ELEM. SYM.	A	Z
Ca	44	20
REF. NO.		hg
80 St 7		

METHOD					
REACTION	RESULT	EXCITATION ENERGY	SOURCE		ANGLE
			TYPE	RANGE	
E, E/	SPC	8-12	D	30-50	DST

The search for magnetic dipole transitions from the ground state of the even-even Ca isotopes to high lying $J^\pi = 1^+$ states by means of low momentum transfer but high resolution inelastic electron scattering is described. The previously detected strongly excited $J^\pi = 1^+$ state at $E_x = 10.319$ MeV [$B(M1) \uparrow = 1.12 \pm 0.27 \mu_N^2$] in ^{40}Ca has been confirmed, but – contrary to the expectations of the independent particle shell model – only a fairly weak M1 transition – observed in ^{42}Ca [$E_x = 11.235$ MeV, $B(M1) \uparrow = 0.59 \pm 0.05 \mu_N^2$] and none in ^{44}Ca between $E_x = 8.2-12.2$ MeV. In ^{43}Ca , however, a very strong M1 transition [$B(M1) \uparrow = 4.0 \pm 0.3 \mu_N^2$] to a single state at $E_x = 10.227$ MeV has been discovered.

NO TRANS 8.2-12.2 MEV

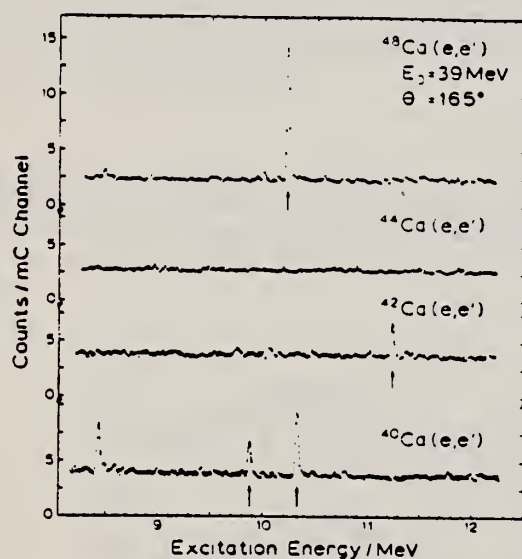


Fig. 1. High-resolution inelastic electron scattering spectra of $^{40,42,44,48}\text{Ca}$ all measured at $\theta = 165^\circ$ and $E_0 = 39$ MeV. Magnetic dipole transitions are denoted by an arrow.

METHOD					REF. NO.		
					81 It 2	hg	
REACTION	RESULT	EXCITATION ENERGY	SOURCE		DETECTOR		ANGLE
			TYPE	RANGE	TYPE	RANGE	
E, E/	FMF	9 - 35	D	124 - 250	MAG-D		DST

We present the giant electric-dipole and electric-quadrupole cross sections of ^{42}Ca and ^{44}Ca measured by inelastic electron scattering with incident energies between 124 and 250 MeV. Spectra were decomposed into dipole, quadrupole, and other higher multipole components. The giant dipole resonances in both nuclei have a large width of approximately 12 MeV, with at least two gross resonance structures. The quadrupole resonances are distributed in several clusters between 10 and 22 MeV, depleting $(61 \pm 9)\%$ in ^{42}Ca and $(46 \pm 7)\%$ in ^{44}Ca of the isoscalar energy-weighted sum rule, respectively. Higher multipole resonances were also found in the same excitation energy region. The observed structure in the dipole and quadrupole resonances are examined in terms of the collective model, and it is suggested that the splitting of the dipole resonance revealed in ^{44}Ca may reflect the effect of nuclear deformation.

NUCLEAR REACTIONS $^{42}\text{Ca} (e, e')$ and $^{44}\text{Ca} (e, e')$, $E = 124 \sim 250$ MeV, $q = 0.4 \sim 1.2 \text{ fm}^{-1}$, enriched target, measured $\sigma(E, \theta)$ up to 35 MeV in excitation energy; deduced electric-dipole, electric-quadrupole, and higher multipole strength in the giant resonance region.

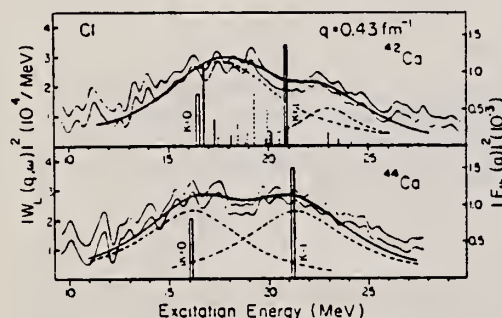


FIG. 5. The longitudinal dipole differential form factors of ^{42}Ca and ^{44}Ca at $q = 0.43 \text{ fm}^{-1}$. The shaded area shows the errors arising from the least square method. The two gross resonances in both isotopes are fitted by two Breit-Wigner shape cross sections. The K splitting of the Suzuki-Rowe model (Refs. 40 and 42) is compared with the spectra. Shell model calculation (Ref. 9) is also shown by solid lines for the T_{-} state and dashed lines for the T_{+} state. Both T_{-} and T_{+} strengths are multiplied by a factor of 2.

B(CL)

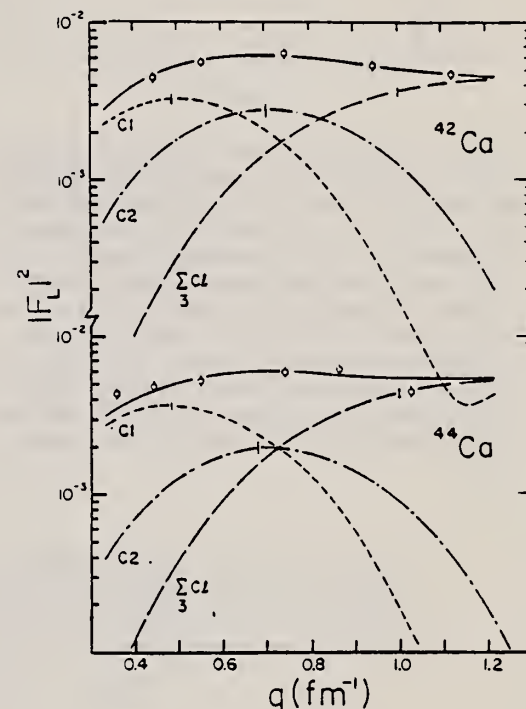


FIG. 4. The longitudinal form factors integrated from 10 to 25 MeV for ^{42}Ca and ^{44}Ca , together with the result of the multipole expansion. The dashed, dash-dotted, and long dashed curves are the C_1 , C_2 , and ΣC_L ($L \geq 3$) components, respectively. The solid curve is the sum of the all multipole excitation. The occasional error bars on the C_1 , C_2 , and ΣC_L ($L \geq 3$) curves include statistical error and model dependence of the higher multipole excitations.

OVER

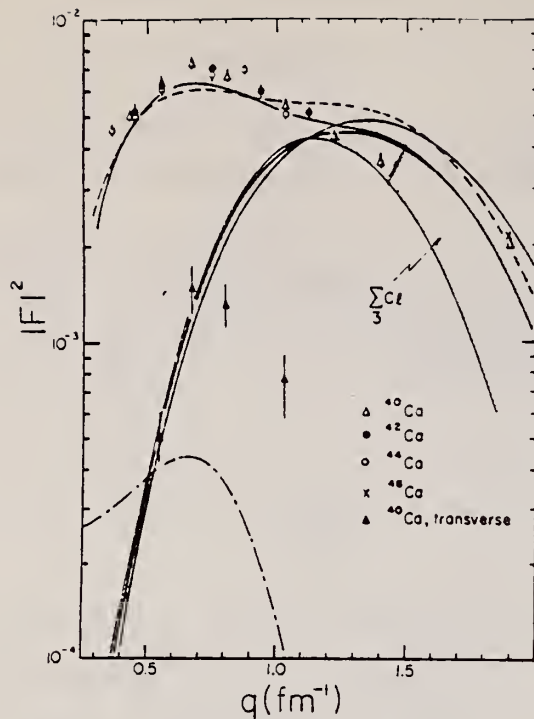


FIG. 1. The total form factor integrated from 10 to 25 MeV for ^{42}Ca and ^{44}Ca , together with the experimental results of ^{40}Ca (Ref. 3). The measured form factors at $q = 1.9 \text{ fm}^{-1}$ are taken from Ref. 27. The shaded area labeled ΣCl ($l \geq 3$) is the investigated range of the contributions of the higher multipole excitation for ^{42}Ca . The solid and dashed curves are the sum of the all multipole excitations in ^{42}Ca and ^{44}Ca , respectively. Also the measured transverse form factor of ^{40}Ca integrated in the same energy range is shown. The electric-dipole transverse form factor calculated using the particle-hole wave functions (Ref. 32) is shown by the dot-dashed curve.

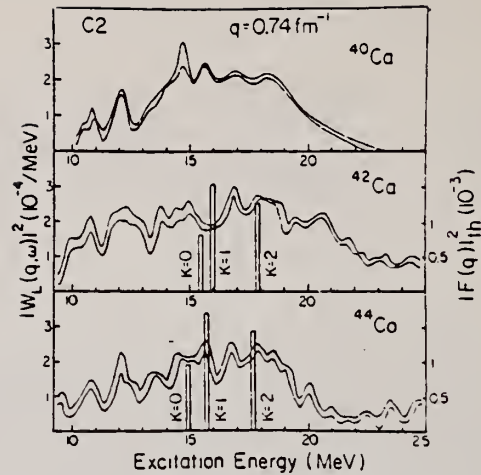


FIG. 7. The longitudinal quadrupole differential form factors of ^{42}Ca and ^{44}Ca at $q = 0.74 \text{ fm}^{-1}$ are compared with the result of ^{40}Ca (Ref. 3). The shaded area for ^{40}Ca was obtained by combining the result of ^{40}Ca at $q = 0.67 \text{ fm}^{-1}$ and $q = 0.81 \text{ fm}^{-1}$, while those of ^{42}Ca and ^{44}Ca show the errors arising from the least square method. The K splitting of the Suzuki-Rowe model is also shown.

TABLE II. Reduced transition probabilities $B(C1, 1)$ obtained by the multipole expansion and the depletion of the isovector electric dipole EWSR (S_1). The positions of dipole peaks are indicated in square brackets. Errors in $B(C1)$ and S_1 are $\pm 10\%$, which include errors arising from the model dependence on the higher multipole transitions.

^{42}Ca			^{44}Ca		
ω (MeV)	$B(C1)$ ($e^2 \text{fm}^2$)	S_1 (%)	ω (MeV)	$B(C1)$ ($e^2 \text{fm}^2$)	S_1 (%)
9.0 ~ 12.5 [9.4, 11.2]	1.49	10.2	9.0 ~ 12.1 [10.0, 11.7]	1.46	9.4
12.5 ~ 14.5 [13.3, 13.9]	1.34	11.5	12.1 ~ 14.5 [13.0, 14.1]	1.60	13.3
14.5 ~ 18.0 [16.2, 17.5]	3.06	31.9	14.5 ~ 18.5 [15.3, 16.2, 17.3]	3.78	38.4
18.0 ~ 21.0 [18.3, 19.2]	2.81	35.1	18.5 ~ 23.0 [19.6, 20.3, 21.4, 22.0]	4.33	55.3
21.0 ~ 26.0 [22.5]	3.19	48.1	23.0 ~ 25.0 [22.9]	1.52	22.4
26.0 ~ 30.0 [26.7]	1.39	25.0	25.0 ~ 27.0	0.96	15.3
30.0 ~ 35.0	0.64	13.3			
10.0 ~ 25.0	11.0	129	10.0 ~ 25.0	12.2	138
9.0 ~ 35.0	13.9	173			

Continuation		
ELEM. SYM.	A	Z
Ca	44	20
REF. NO.		
81 It 2		hg

METHOD					
REACTION	RESULT	EXCITATION ENERGY	SOURCE		ANGLE
			TYPE	RANGE	
E, E/	FMF	9 - 35	D	124-250	DST

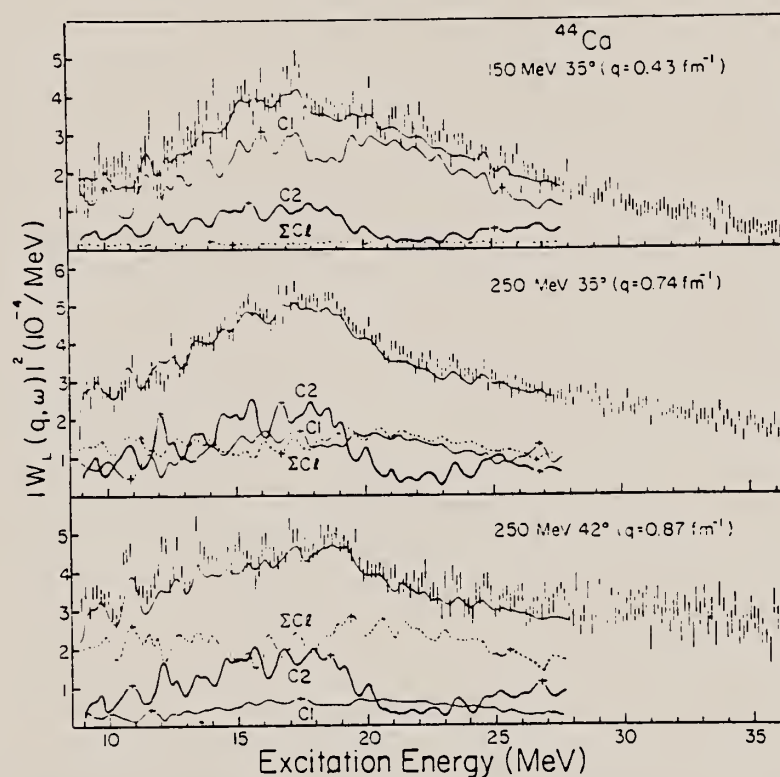


FIG. 3. The longitudinal differential form factor of ^{44}Ca at various momentum transfers. See caption of Fig. 2.

CA
A=48

CA
A=48

CA
A=48

REF.

P. D. Zimmerman, M. R. Yearian and T. W. Donnelly
 Phys. Rev. Letters 21, 1392 (1968)

ELEM. SYM.

A

Z

Ca

48

20

METHOD

REF. NO.

68 Zi 2

hmg

REACTION	RESULT	EXCITATION ENERGY	SOURCE		DETECTOR		ANGLE
			TYPE	RANGE	TYPE	RANGE	
$E_e E_i$	ABX	2-25	D	283	MAG-D	257-283	88
				(282.8)			

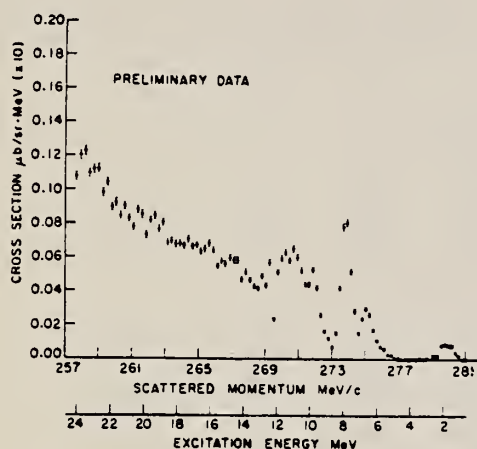


FIG. 2. The spectrum of inelastically scattered electrons from Ca^{48} with an incident energy $E_0 = 282.8$ MeV at an angle $\theta = 88.1^\circ$, after radiative corrections were made.

METHOD					REF. NO.	
					69 E1 1	hmg
REACTION	RESULT	EXCITATION ENERGY	SOURCE		DETECTOR	
			TYPE	RANGE	TYPE	RANGE
E, E/	FMF	3-5	D	42, 61	MAG-D	38-57
						(70-150)

B(EL); 3.7-4.5

TABLE V. Experimental form factors for the states of interest in Ca^{40} and Ca^{48} . E_i is the incident electron energy, θ is the scattering angle, q_i is the inelastic momentum transfer, C the ratio of inelastic to elastic peak heights, and $|F_{in}|^2$ the experimental form factor defined by Eq. (10); the sixth column is the percentage error in the experimental form-factor points.

E_i (MeV)	θ (deg)	q_i (F^{-1})	$10^4 C$	$10^2 F_{in}^2$	$\% \text{ error}$	$10^2 F^* \cdot$
Ca^{40}						
3.73 MeV (3-)						
60.36	90.0	0.419	4.62	0.222	6.0	
60.34	110.	0.485	12.91	0.450	2.0	
60.04	130.	0.534	25.30	0.666	2.0	
60.30	150.	0.572	41.90	0.865	6.0	
3.90 MeV (2+)						
60.50	70.0	0.341	2.24	0.145	6.0	
60.36	90.0	0.419	5.73	0.275	4.0	
60.33	110.	0.485	12.83	0.447	4.0	
60.03	130.	0.533	19.75	0.520	4.0	
60.03	150.	0.571	28.50	0.588	6.0	
6.94 MeV (2+, 3-)						
60.51	70.0	0.331	1.90	0.123	4.0	
60.36	90.0	0.407	5.71	0.275	2.0	
60.33	110.	0.471	13.00	0.454	2.0	
60.04	130.	0.519	22.65	0.596	2.0	
60.24	150.	0.555	36.02	0.745	2.0	
Ca^{48}						
3.83 MeV (2+)						
60.21	70.0	0.339	1.87	0.122	5.0	
60.17	90.0	0.418	6.45	0.311	5.0	
60.15	110.	0.484	11.35	0.399	5.0	
60.13	130.	0.535	19.15	0.502	5.0	
60.18	150.	0.570	26.21	0.546	8.0	
41.07	110.	0.325	2.37	0.165	7.0	0.157
41.05	130.	0.359	2.80	0.173	8.0	0.165
41.07	150.	0.383	3.88	0.219	7.0	0.209
4.51 MeV (3-)						
60.21	70.0	0.337	0.35	0.0228	17.0	
60.15	90.0	0.415	1.77	0.0854	8.0	
60.15	110.	0.481	5.51	0.194	8.0	
60.14	130.	0.531	12.11	0.317	4.0	
60.18	150.	0.567	21.94	0.456	8.0	

* F^* denotes the values of $|F_{in}|^2$ at 41 MeV renormalized to 60.2 MeV.

TABLE VI. Best-fit values of $B(EL \uparrow)$ and R_{tr}^2 for the states studied in this work. G is the $B(EL \uparrow)$ value expressed in single-particle Weisskopf units. Γ_γ^0 is the partial width for γ decay to the ground state. The column labeled σ_c is the statistical error in $B(EL \uparrow)$. An additional 12% uncertainty must be included in the final error to account for the dependence of $B(EL \uparrow)$ and R_{tr}^2 on the parameters of the transition charge density. N is the number of degrees of freedom in the fit. The transition charge parameters c_{tr} and l_{tr} are given as ratios to the ground-state parameters, which are different for Ca^{40} and Ca^{48} . See the text.

Nucleus	State energy (MeV)	$B(EL)$ ($e^2 F^2 L$)	G (spu)	Γ_γ^0 (eV)	σ_c	χ^2/N	Confidence level (σ_c)	c_{tr}/c_0	l_{tr}/l_0	R_{tr}^2 (F^2)
2+ States										
Ca^{40}	3.90	84	2.0	1.23×10^{-3}	2	3.5/3	35	0.880	0.880	19.2
Ca^{40}	6.94	70	1.7	1.94×10^{-1}	2	0.5/3	90	1.0	1.0	24.8
Ca^{48}	3.83	86	1.7	1.14×10^{-3}	2	4.5/6	60	0.984	0.893	20.9
3- States										
Ca^{40}	3.73	21 100	31.7	1.14×10^{-3}	2	0.9/2	65	1.017	1.01	32.3
Ca^{40}	6.94	9 200	13.9	3.83×10^{-3}	3	0.5/3	90	1.00	1.00	31.5
Ca^{48}	4.51	6 500	6.8	1.32×10^{-3}	3	1.5/3	65	0.87	0.99	25.5

ELEM. SYM.	A	Z
Ca	48	20
REF. NO.		egf
69 La 3		

METHOD			SOURCE		DETECTOR		ANGLE
REACTION	RESULT	EXCITATION ENERGY	TYPE	RANGE	TYPE	RANGE	
G,A	ABY	23-55	C	39-55	ACT-I		4PI
G,AN	ABY	33-55	C	39-55	ACT-I		4PI
G,N	ABY	10-55	C	39-55	ACT-I		4PI

ABY UPPER LIMIT

TABLE 1. Relative Photonuclear Yield from Bremsstrahlung Irradiation

Bremsstrahlung End Point, Mev	Ar ⁴⁰ (γ, α)	Ar ⁴² ($\gamma, \alpha n$)	Ca ⁴⁷ (γ, n)
39	3.0		9.2×10^3
48	20	0.91	27×10^3
55	27	1.8	51×10^3

The relative yields of Ar⁴⁰, the 6-minute activity attributed to Ar⁴², and Ca⁴⁷ are shown in Table 1. Using cross-section measurements [Fultz et al., 1966] and yield curves measured in our irradiation geometry (P. E. Wilkness, Chemical Oceanography Branch, USNRL, private communication, 1969) for the Ca⁴⁷(γ, n)C⁴⁶ reaction, a maximum of approximately 0.02 mb (with coarse resolution) was calculated for the Ca⁴⁷ (γ, α) Ar⁴⁰ cross section up to 55 Mev, assuming a slow variation in cross section from 30 to 55 Mev. Since Ca⁴⁷ has more neutrons than Ca⁴⁰, one might expect competing reactions such as (γ, n) and ($\gamma, 2n$) to be more probable relative to (γ, α) in this isotope than in Ca⁴⁰. Thus 0.1 mb is considered the upper limit for the Ca⁴⁷ (γ, α) Ar⁴⁰ effective cross section over a smooth distribution of γ -ray energies up to 55 Mev.

ELEM. SYM.	A	Z
Ca	48	20
REF. NO.		
76 Zi 1		
egf		

Comment: Mean separation energy 34 ± 3 MeV

REACTION	RESULT	EXCITATION ENERGY	SOURCE		DETECTOR		ANGLE
			TYPE	RANGE	TYPE	RANGE	
E, E/	ABX	20-280	D	*	MAG-D		DST

See further analysis of this data in reference 79Zi1

TRANS 3-Q CONST

Measurements of average separation energies and of Fermi momenta for ^{40}Ca and ^{48}Ca are reported. Evidence for the possible existence of "bump" structure in the quasi-elastic scattering of electrons from ^{48}Ca is also presented.

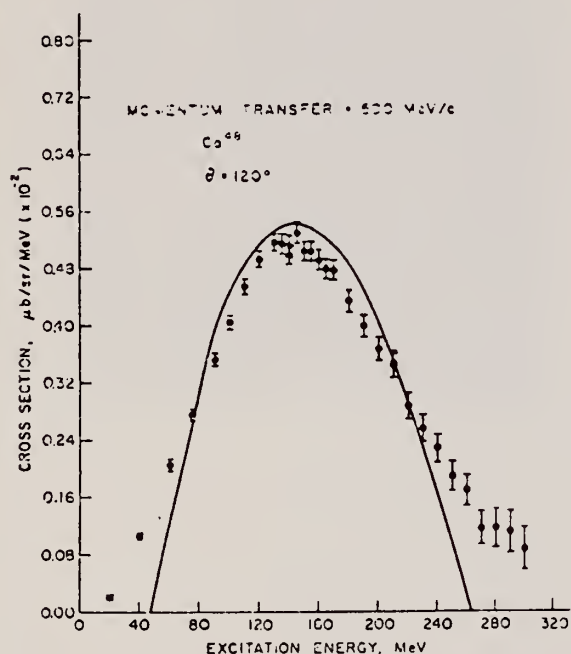


Fig. 2. Quasi-elastic spectrum from ^{48}Ca at the same kinematics as in Figure 1. The curve is once again the Moniz model. A systematic under-estimation by the Fermi gas model of the cross section at large energy losses is apparent.

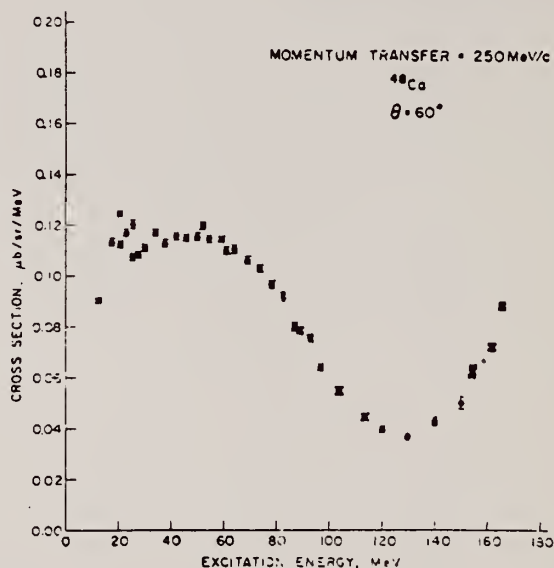


Fig. 3. Quasi-elastic cross-section obtained from ^{48}Ca at a fixed three-momentum transfer of 250 MeV/c at a scattering angle of $(\theta)^2$.

ELEM. SYM.	A	Z
Ca	48	20
REF. NO.		
78 Gr 1		rs

REACTION	RESULT	EXCITATION ENERGY	SOURCE		DETECTOR		ANGLE
			TYPE	RANGE	TYPE	RANGE	
E,e/	ABX	4	D	34- 60	MAG-D		DST

4=4.272

Abstract: Monopole transitions from the 0_1^+ ground states to 0_2^+ excited states at 3.353 MeV (^{40}Ca), 1.837 MeV (^{42}Ca), 1.884 MeV (^{44}Ca) and 4.272 MeV (^{48}Ca) have been investigated with high resolution inelastic electron scattering (FWHM ≈ 30 keV) at low momentum transfer ($0.29 \leq q \leq 0.53 \text{ fm}^{-1}$). The respective monopole matrix elements are $2.53 \pm 0.41 \text{ fm}^2$, $5.24 \pm 0.39 \text{ fm}^2$, $5.45 \pm 0.41 \text{ fm}^2$ and $2.28 \pm 0.49 \text{ fm}^2$. These results are used together with known ground state charge radii and the average number of holes in the sd shell in the ground state to estimate the number of particle-hole excitations in the wave functions of the excited 0_2^+ states.

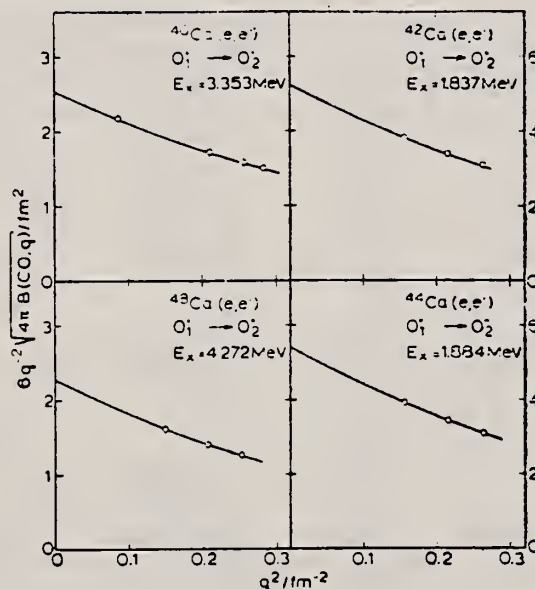


Fig. 3. Extrapolation of the measured $B(C0, q)$ values (dots) to $q = 0$ with the two parameter expression of eq. (1)

over

TABLE 2
Elastic and inelastic cross sections ($d\sigma/d\Omega$)_{el} (10^{-3} fm² sr) and ($d\sigma/d\Omega$) (10^{-3} fm² sr), respectively, and DWBA correction factors f_c for the monopole transitions studied

Nucleus E_i (MeV)	E_0 (MeV)	θ (deg)	q^2 (fm $^{-2}$)	$(d\sigma, d\Omega)_{el}$	$(d\sigma, d\Omega)_{inel}$	f_c
^{40}Ca 3.353	59.76	128.9	0.282	4.52	2.91 (6.5)	1.46
	54.73	140.9	0.256	3.11	1.95 (11.7)	1.53
	54.70	116.9	0.210	14.65	4.84 (8.9)	1.55
	33.67	128.9	0.086	40.70	2.47 (34.7)	1.91
^{42}Ca 1.837	54.73	140.9	0.263	3.05	6.53 (5.8)	1.48
	54.70	116.9	0.215	14.21	20.51 (4.3)	1.51
	54.70	92.9	0.156	64.99	45.23 (3.9)	1.54
^{44}Ca 1.884	54.73	140.9	0.263	3.15	6.44 (7.3)	1.47
	54.72	116.9	0.215	14.83	20.91 (4.0)	1.50
	54.72	92.9	0.156	66.24	45.39 (3.5)	1.53
^{48}Ca 4.272	54.73	140.9	0.252	2.99	1.11 (30.8)	1.46
	54.73	116.9	0.206	14.20	3.09 (5.6)	1.49
	54.73	92.9	0.149	64.09	7.38 (13.4)	1.53

The values in parentheses denote the statistical error of the cross sections in percent.

TABLE 3
Results of the present (e, e') experiment for monopole matrix elements, transition radii and pair decay widths together with results from other experiments and theoretical predictions

Nucleus	ME (fm ²)	R_{tr} (fm)	Γ_e (μ eV)	Exp	Theory
⁴⁰ Ca	3.6 \pm 1.1	6.3	0.37 \pm 0.23	(e, e') ^{a)}	
			0.21 \pm 0.01	^{b)}	
	2.6 \pm 0.1			(p, p') ^{c)}	^{d)}
	2.44				^{e)}
	5.53				
⁴² Ca	2.53 \pm 0.41	6.1 \pm 0.9	0.18 \pm 0.06	this work	
	5.93 \pm 0.52			(p, p') ^{c)}	^{d)}
	5.58				^{e)}
	4.19				
⁴⁴ Ca	5.24 \pm 0.39	6.3 \pm 0.4	0.016 \pm 0.002	this work	
	5.39 \pm 1.79			(p, p') ^{c)}	
	5.56			(x, p') ^{f)}	
	5.45 \pm 0.41	6.5 \pm 0.4	0.021 \pm 0.003	this work	
⁴⁸ Ca	1.52 \pm 0.07			(p, p') ^{c)}	
	2.28 \pm 0.49	6.8 \pm 1.4	0.63 \pm 0.27	this work	

^{a)} Ref. ¹¹⁾, ^{b)} Ref. ¹²⁾, ^{c)} Ref. ⁹⁾, ^{d)} Ref. ³⁾, ^{e)} Ref. ⁴⁾, ^{f)} Ref. ²²⁾, ^{g)} Ref. ²³⁾.

³⁾ W.J. Gerace and A.M. Green, Nucl. Phys. A93, 110 (1967);
A123, 241 (1969)

⁴⁾ P. Federman and S. Pittel, Phys. Rev. 186, 1106 (1969);
Nucl. Phys. A139, 108 (1969)

⁹⁾ M. Ulrickson, N. Benczer-Koller, J.R. MacDonald and
J.W. Tape, Phys. Rev. C15 186 (1977)

¹¹⁾ P. Strehl, Z. Phys. 234, 416 (1970)

¹²⁾ P.M. Endt and C. van der Leun, Nucl. Phys. A235, 27 (1974)

²²⁾ L.D. Skouras, Nucl. Phys. A220, 604 (1974)

²³⁾ J.D. McCullen and D.J. Donahue, Phys. Rev. C8, 1406 (1973)

ELEM. SYM.	A	Z
Ca	48	20

METHOD	REF. NO.
	78 Gr 5

ANGLE
hmg

REACTION	RESULT	EXCITATION ENERGY	SOURCE		DETECTOR		ANGLE
			TYPE	RANGE	TYPE	RANGE	
E, E/	ABX	4	D	31-67	MAG-D		DST
		(4.272)					

Abstract: Monopole transitions from the 0_1^+ ground states to 0_2^+ excited states at 3.353 MeV (^{40}Ca), 1.837 MeV (^{42}Ca), 1.884 MeV (^{44}Ca) and 4.272 MeV (^{48}Ca) have been investigated with high resolution inelastic electron scattering (FWHM ≈ 30 keV) at low momentum transfer ($0.29 \leq q \leq 0.53 \text{ fm}^{-1}$). The respective monopole matrix elements are $2.53 \pm 0.41 \text{ fm}^2$, $5.24 \pm 0.39 \text{ fm}^2$, $5.45 \pm 0.41 \text{ fm}^2$ and $2.28 \pm 0.49 \text{ fm}^2$. These results are used together with known ground state charge radii and the average number of holes in the sd shell in the ground state to estimate the number of particle-hole excitations in the wave functions of the excited 0_2^+ states.

E NUCLEAR REACTIONS $^{40,42,44,48}\text{Ca}(e, e')$, $E = 31-67 \text{ MeV}$; measured $\sigma(E; E_e; \theta)$.
 $^{40,42,44,48}\text{Ca}$ 0_1^+ level deduced E0 matrix elements. Shell model calculation.

TABLE 2
Elastic and inelastic cross sections ($d\sigma/d\Omega$) ($10^{-3} \text{ fm}^2/\text{sr}$) and ($d\sigma/d\Omega$) ($10^{-7} \text{ fm}^2/\text{sr}$), respectively, and DWBA correction factors f_c for the monopole transitions studied

Nucleus E_i (MeV)	E_0 (MeV)	θ (deg)	q^2 (fm^{-2})	$(d\sigma/d\Omega)_i$	$(d\sigma/d\Omega)_{\text{DWBA}}$	f_c
^{40}Ca 3.353	59.76	128.9	0.282	4.52	2.91 (6.5)	1.46
	54.73	140.9	0.256	3.11	1.95 (11.7)	1.53
	54.70	116.9	0.210	14.65	4.84 (8.9)	1.55
	33.67	128.9	0.086	40.70	2.47 (34.7)	1.91
^{42}Ca 1.837	54.73	140.9	0.263	3.05	6.53 (5.8)	1.48
	54.70	116.9	0.215	14.21	20.51 (4.3)	1.51
	54.70	92.9	0.156	64.99	45.23 (3.9)	1.54
^{44}Ca 1.884	54.73	140.9	0.263	3.15	6.44 (7.3)	1.47
	54.72	116.9	0.215	14.83	20.91 (4.0)	1.50
	54.72	92.9	0.156	66.24	45.39 (3.5)	1.53
^{48}Ca 4.272	54.73	140.9	0.252	2.99	1.11 (30.8)	1.46
	54.73	116.9	0.206	14.20	3.09 (5.6)	1.49
	54.73	92.9	0.149	64.09	7.38 (13.4)	1.53

The values in parentheses denote the statistical error of the cross sections in percent.

TABLE 3
Results of the present (e, e') experiment for monopole matrix elements, transition radii and pair decay widths together with results from other experiments and theoretical predictions

Nucleus	ME (fm^2)	R_{tr} (fm)	f_c (μeV)	Exp.	Theory
^{40}Ca	3.6 ± 1.1	6.3	0.37 ± 0.23	(e, e') ^{a)}	
	2.6 ± 0.1		0.21 ± 0.01	(p, p') ^{b)}	
	2.44				
	5.53				
^{42}Ca	2.53 ± 0.41	6.1 ± 0.9	0.18 ± 0.06	this work	
	5.93 ± 0.52			(p, p') ^{c)}	
	5.58				
	4.19				
^{44}Ca	5.24 ± 0.39	6.3 ± 0.4	0.016 ± 0.002	this work	
	5.39 ± 1.79			(p, p') ^{d)}	
	5.56			(α, α') ^{e)}	
	5.45 ± 0.41	6.5 ± 0.4	0.021 ± 0.003	this work	
^{48}Ca	1.52 ± 0.07			(p, p') ^{f)}	
	2.28 ± 0.49	6.8 ± 1.4	0.63 ± 0.27	this work	

^{a)} Ref. ¹¹⁾, ^{b)} Ref. ¹²⁾, ^{c)} Ref. ⁹⁾, ^{d)} Ref. ¹⁾, ^{e)} Ref. ²¹⁾, ^{f)} Ref. ²¹⁾.

ELECTRIC MONOPOLE TRANSITIONS

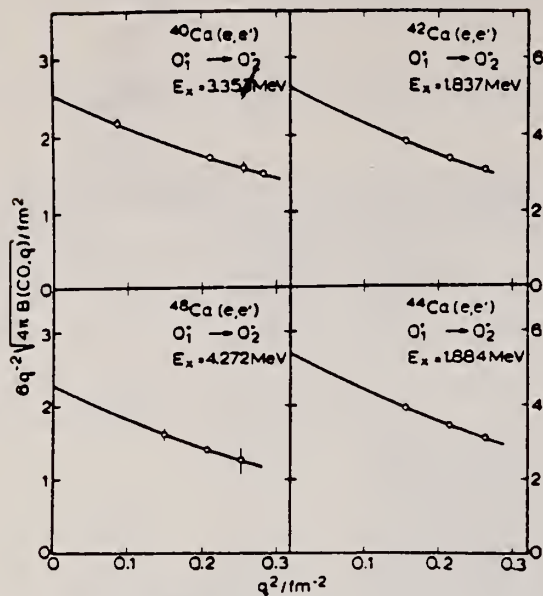


Fig. 3. Extrapolation of the measured $B(C0, q)$ values (dots) to $q = 0$ with the two parameter expression of eq. (1).

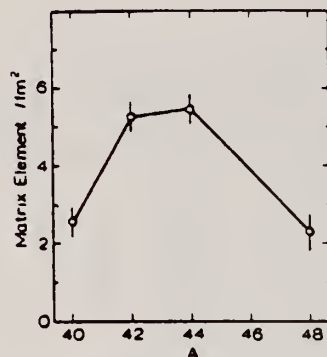


Fig. 4. The determined monopole matrix elements as a function of mass number for the four Ca isotopes. The line which connects the experimental points has no theoretical significance.

- 3) W. J. Gerace and A. M. Green, Nucl. Phys. A93 (1967) 110, A123 (1969) 241
- 4) P. Federman and S. Pittel, Phys. Rev. 186 (1969) 1106; Nucl. Phys. A139 (1969) 108
- 5) M. Sakakura, A. Arima and T. Sebe, Phys. Lett. 61B (1976) 335
- 6) N. Benczer-Koller, G. G. Seaman, M. C. Bertin, J. W. Tape and J. R. MacDonald, Phys. Rev. C2 (1970) 1037
- 7) J. C. Adloff, K. H. Souw, D. Disdier, F. Scheibling, P. Chevallier and Y. Wolfson, Phys. Rev. C10 (1974) 1819
- 8) M. Ulrickson, W. Hartwig, N. Benczer-Koller, J. R. MacDonald and J. W. Tape, Phys. Rev. C13 (1976) 536
- 9) M. Ulrickson, N. Benczer-Koller, J. R. MacDonald and J. W. Tape, Phys. Rev. C15 (1977) 186
- 10) P. Strehl and Th. H. Schucan, Phys. Lett. 27B (1968) 641
- 11) P. Strehl, Z. Phys. 234 (1970) 416
- 12) P. M. Endt and C. van der Leun, Nucl. Phys. A235 (1974) 27
- 13) R. F. Frosch, R. Hofstadter, J. S. McCarthy, G. K. Nöldeke, K. J. van Oostrum, M. R. Yearian, B. C. Clark, R. Herman and D. G. Ravenhall, Phys. Rev. 174 (1968) 1380
- 14) P. Doll, G. J. Wagner, K. T. Knöpfle and G. Mairle, Nucl. Phys. A263 (1976) 210
- 15) J. A. Nolen, Jr. and R. J. Gleitsmann, Phys. Rev. C11 (1975) 1159
- 16) K. K. Seth, A. Saha, W. Benenson, W. A. Lanford, H. Nann and B. H. Wildenthal, Phys. Rev. Lett. 33 (1974) 233
- 17) C. R. Fischer and G. H. Rawitscher, Phys. Rev. 135 (1964) B377
- 18) C. W. de Jager, H. de Vries and C. de Vries, Atomic Data and Nucl. Data Tables 14 (1974) 479
- 19) H. Theissen, Springer Tracts in Modern Phys. 65 (1972) 1
- 20) S. Krewald, R. Rosenfelder, J. E. Galonska and A. Faessler, Nucl. Phys. A269 (1976) 112
- 21) Th. H. Schucan, Nucl. Phys. 61 (1965) 417
- 22) L. D. Skouras, Nucl. Phys. A220 (1974) 604
- 23) J. D. McCullen and D. J. Donahue, Phys. Rev. C8 (1973) 1406

METHOD

REF. NO.

78 Ma 10

hg

REACTION	RESULT	EXCITATION ENERGY	SOURCE		DETECTOR		ANGLE
			TYPE	RANGE	TYPE	RANGE	
G,N	ABY	10-68	C	30-68	ACT - \bar{L}		4PI

Analysis is made of reactions interfering with photon activation analysis procedures.

The activation yield curves have been presented for a number of photonuclear reactions in the energy range from 30 to 68 MeV, in order to evaluate quantitatively the interferences due to competing reactions in multi-element photon activation analysis. The general features of the yields as functions of both target mass number and excitation energy were elucidated from the data obtained, discussion being given on the results in terms of the reaction mechanism.

Simultaneous neutron activation due to appreciable neutron production from the converter and surrounding materials has also been studied, and, finally, the magnitudes of interferences in real multi-element analysis were given in the form of their energy dependences.

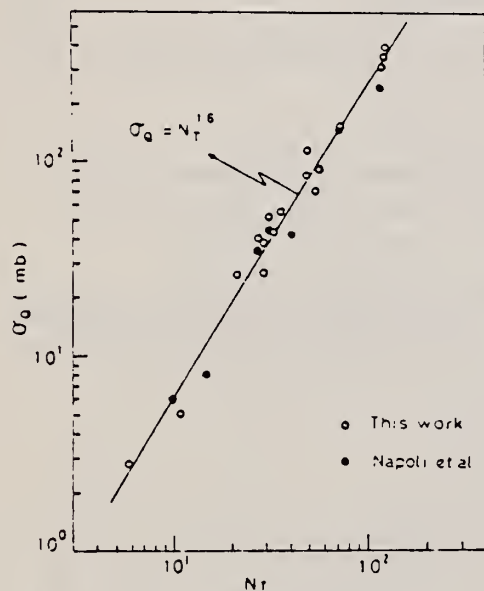


Fig. 2. Yield per equivalent quanta versus target neutron number.

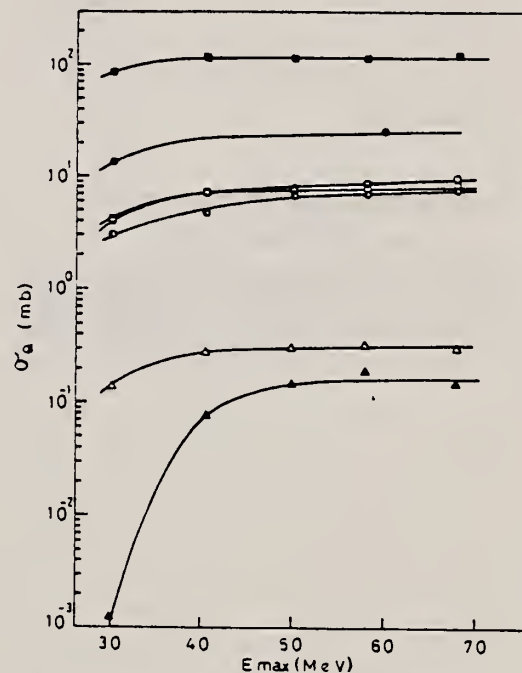


Fig. 4. Activation yield curves for the reactions on Ca, Ti and V.

■ $^{48}\text{Ca}(\gamma, n)^{47}\text{Ca}$, □ $^{44}\text{Ca}(\gamma, p)^{43}\text{K}$, ● $^{46}\text{Ti}(\gamma, n)^{45}\text{Ti}$,
 ○ $^{48}\text{Ti}(\gamma, p)^{47}\text{Sc}$, ● $^{49}\text{Ti}(\gamma, p)^{48}\text{Sc}$, Δ $^{51}\text{V}(\gamma, \alpha)^{47}\text{Sc}$,
 ▲ $^{51}\text{V}(\gamma, xn)^{48}\text{Sc}$.

(over)

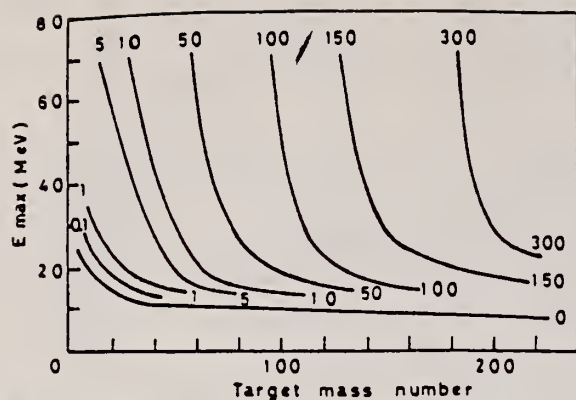


Fig. 9. Yields of the (γ, n) reactions as a function of bremsstrahlung maximum energy and target mass number. The numerical values in the figure are yields per equivalent quanta in mb.

REF. W. Steffen, H.-D. Gräf, W. Gross, D. Meuer, A. Richter, E. Spamer,
O. Titze, W. Knüpfner
Phys. Lett. **95B**, 23 (1980)

ELEM. SYM.	A	Z
Ca	48	20
REF. NO.	80 St 7	
	hg	

METHOD					REF. NO. 80 St 7		hg
REACTION	RESULT	EXCITATION ENERGY	SOURCE		DETECTOR		ANGLE
			TYPE	RANGE	TYPE	RANGE	
E,E/	SPC	8-12	D	30-50	MAG-D		DST

The search for magnetic dipole transitions from the ground state of the even-even Ca isotopes to high lying $J^\pi = 1^+$ states by means of low momentum transfer but high resolution inelastic electron scattering is described. The previously detected strongly excited $J^\pi = 1^+$ state at $E_x = 10.319$ MeV [$B(M1) \uparrow = 1.12 \pm 0.27 \mu_N^2$] in ^{40}Ca has been confirmed, but – contrary to the expectations of the independent particle shell model – only a fairly weak M1 transition is observed in ^{42}Ca [$E_x = 11.235$ MeV, $B(M1) \uparrow = 0.59 \pm 0.05 \mu_N^2$] and none in ^{44}Ca between $E_x = 8.2$ –12.2 MeV. In ^{48}Ca , however, a very strong M1 transition [$B(M1) \uparrow = 4.0 \pm 0.3 \mu_N^2$] to a single state at $E_x = 10.227$ MeV has been discovered.

LEVEL 10.23, BEL

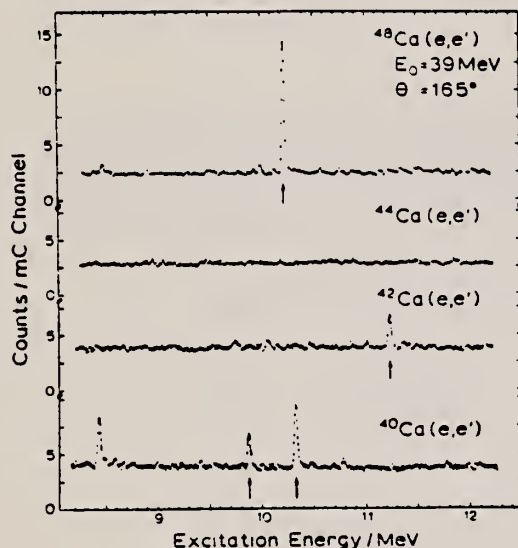


Fig. 1. High-resolution inelastic electron scattering spectra of $^{40,42,44,48}\text{Ca}$ all measured at $\theta = 165^\circ$ and $E_0 = 39$ MeV. Magnetic dipole transitions are denoted by an arrow.

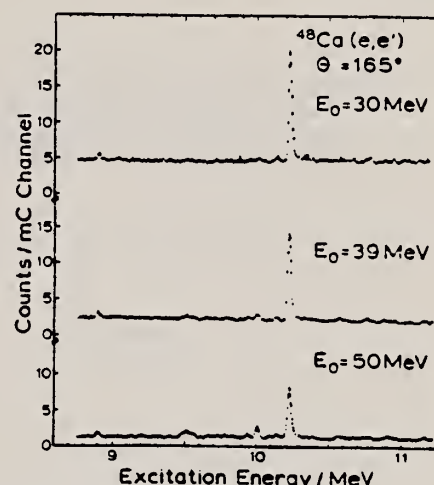


Fig. 2. Three $^{48}\text{Ca}(e, e')$ spectra all taken at $\theta = 165^\circ$ but at different bombarding energies $E_0 = 30, 39$ and 50 MeV displaying the behaviour of the isolated and strongly excited $J^\pi = 1^+$ state at $E = 10.23$ MeV.

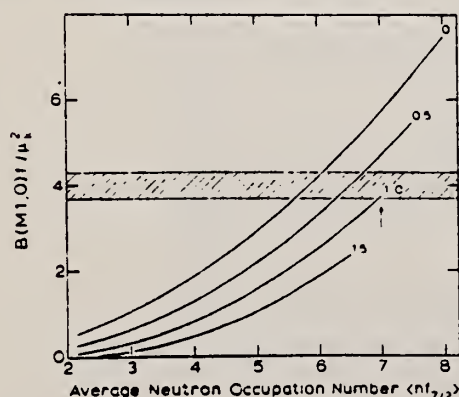


Fig. 3. Dependence of the M1 strength in ^{48}Ca on the average occupation number $(n f_{7/2})$. The numbers written on the right side of the solid lines denote the average occupation number $(n f_{7/2})$. The experimentally determined transition strength and its uncertainty is plotted in the form of a band. If there is one neutron missing in the closed $f_{7/2}$ shell (indicated by the arrow) the experiment tells that between 1 and 0.75 neutrons might be in the $f_{5/2}$ shell.



REF. G. Eulenberg, D.I. Sober, W. Steffen, H.-D. Gräf, G. Küchler,
A. Richter, E. Spamer, B.E. Metsch, W. Knüpfer
Phys. Lett. 116B, 113 (1982)

ELEM. SYM.	A	Z
Ca	48	20
REF. NO.		
82 Eu 1		egf

METHOD		REF. NO.			
		82 Eu 1		egf	
REACTION	RESULT	EXCITATION ENERGY	SOURCE		ANGLE
			TYPE	RANGE	
E, E/	ABX	8-12	D	30-58	DST

$$\Sigma B(M1) \uparrow = 4.6 \pm 0.5 \mu_N^2$$

M1 STRENGTH

Following the recent discovery of a very strong magnetic dipole transition in ^{48}Ca to a state at 10.23 MeV in high-resolution inelastic electron scattering, results of a detailed search for M1 strength in the other $N = 28$ isotones ^{50}Ti , ^{52}Cr and ^{54}Fe are described. The M1 strength found in the investigated region of excitation energy $E_x \approx 7-12$ MeV is very fragmented and considerably quenched in comparison to predictions of shell model calculations in a model space that includes up to $2p-2h$ excitations.

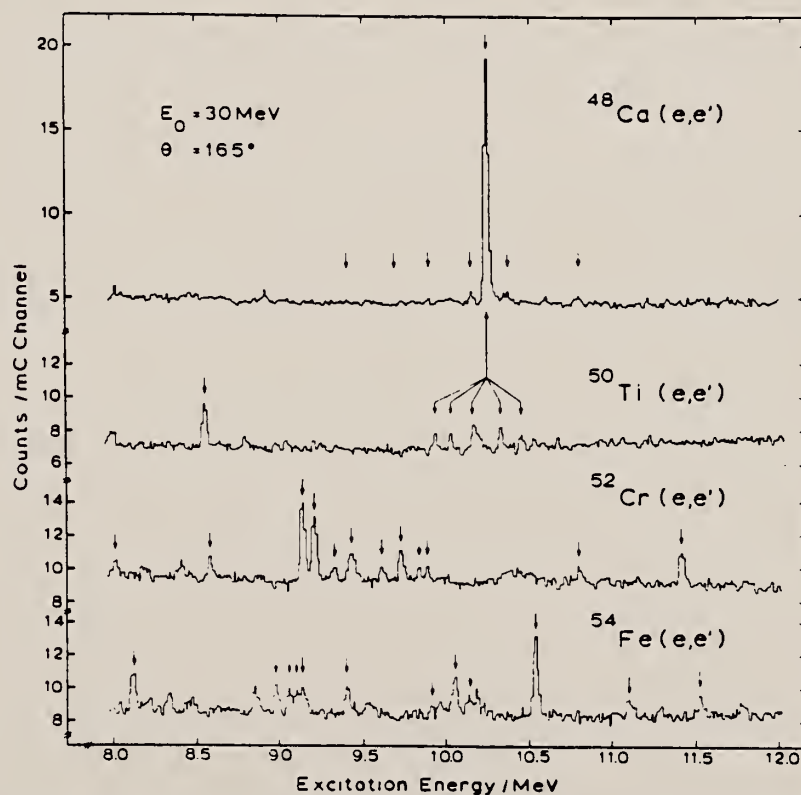


Fig. 1. High-resolution inelastic electron scattering spectra of the $N = 28$ isotones all measured at $E_0 = 30$ MeV and at $\theta = 165^\circ$. The strongest magnetic dipole transitions are indicated by arrows.

DEFINITIONS OF ABBREVIATIONS AND SYMBOLS

Note: In this list definitions are given for various photoneutron reactions in which the following symbols are used: N, NL, nN, SN and XN. Corresponding definitions apply for reactions involving other nuclear particles where the symbols N (neutron) is replaced by, e.g. P, D, T, HE, A etc. Where unknown reactions result in the production of a specific radionuclide, the chemical symbol and mass number is listed as the reaction product, e.g. a G,NA22 reaction in ⁵⁹Co.

A	alpha particle		response function. Contrast with D = discrete.
ANAL	analysis		
ABI	absolute integrated cross-section data	CCH	cloud chamber
		CF	compared with
ABX	absolute cross-section data	CHRGD	charged
ABY	absolute yield data. Often means cross-section per equivalent quantum is listed.	CMPT	Compton
		COIN COINC	coincidence, coincide
ACT	measurement of induced radio-activity of the target	COH	coherent
ASM	asymmetric, asymmetry	CK	Cerenkov
AVG	average	D	deuteron or discrete. When discrete, it is used to describe a photon source or a detector response function. Contrast with C = continuous.
BBL	bubble chamber		
BEL B(EL)	reduced electric radiative transition probability	DLTE	energy loss
BF3	BF ₃ neutron counter with moderator e.g., Halpern detector, long counter	DLTQ	momentum transfer
		DST	distribution
BML	reduced magnetic radiative transition probability, B(ML)	DT BAL	detailed balance
BREAKS	levels located by "breaks" in the yield curve	E	electron
		E/	inelastically scattered electron
BRKUP	breakup	E+	positron
BRMS	bremsstrahlung		
BTW	between	EDST	energy distribution or spectrum
C	continuous. Used to describe a photon source or a detector	E/N	used only to indicate a coincidence experiment as in (E,E/N).

	N stands for any outgoing particle measured in coincidence with an inelastically scattered electron. Distinguish from eg., (E,N) which is used to represent an electron induced reaction when only the outgoing particle N is detected.	KE	kinetic energy
EMU	emulsions (photographic plates)	L	may be an integer or zero that always follows a reaction product symbol. This is used to indicate transitions to specific states in the residual nuclide. When the letter is used as in (G,NL) the cross section given is that for the sum of transitions to two or more specific final states.
EXCIT	excited	LFT	excited state lifetime
F	fission	LIM	limit
FMF	form factor	LV,LVS	level, levels
FM-1	inverse femtometers	LQD	liquid
FRAG	fragment	MAG	magnetic spectrometer
G	photon	MEAS	measurement(s)
G/	inelastically scattered photon	MGC	magnetic Compton spectrometer
G-WIDTH	gamma-ray transition width	MGP	magnetic pair spectrometer
HAD	hadrons, hadron production	MOD	moderated neutron detector <u>not</u> employing a BF ₃ counter, e.g. rhodium foil, Szilard-Chalmers reaction, ³ He, ⁶ Li reactions, GD loaded liquid scintillator, etc.
HE He3	³ He particle	MSP	mass spectrometer
INT	interaction, integral, intensity	MULT	multiple, multipole, multiplicity
INC	includes	MU-T	used only in combination with G to indicate a total photon absorption cross section measurement, i.e. (G,MU-T)
ION	ionization chamber	N	neutron (see also XN and SN). The notation (G,N) is used to indicate a reaction in which only a single neutron is emitted, i.e. the reaction that can, in many cases, be measured by observing the radioactive decay of the residual nuclide.
ISOB	isobaric		
ISM	isomer		
J	multiplicity of particle defined by following symbol e.g. (G,PJN) with remark J = 2,3,5,7		
JPI J-PI	spin and parity of a nuclear state		
K	second multiplicity index, e.g. (G,JPKN) with both J & K positive integers greater than 1		

nN	where n is any integer. (G,nN) indicates the sum over all reaction cross sections in which n neutrons are emitted.	SN	sum of neutron producing reactions, $\sigma(\gamma,SN)=\sigma(\gamma,N) + \sigma(\gamma,NP) + \sigma(\gamma,2N) + \sigma(\gamma,3N) + \text{etc.}$
NAI	NaI(Tl) spectrometer	SPC	photon or particle energy spectrum
NEUT	neutron(s)	SPK	spark chamber
NOX	no cross-section data	SPL	spallation
P	proton (see also XP)	STAT	statistical
PART	particle(s)	SYM	symetric, symmetry
PHOT	photon(s)	T	triton
PI	pion, usually written as PI+, PI-, PIO to indicate charge	TEL	counter telescope
POL	polarized or polarization	THR	threshold for reaction or threshold detector, e.g., $^{29}\text{Si}(n,p)^{29}\text{Al}$.
Q-SQUAR	momentum transfer squared (q^2)	TOF	time-of-flight detector
RCL	recoil	TRK	tracks of particles or fragments observed in solid materials (glass, mylar, etc.)
REL	relative	TRNS	transition
RLI	relative integrated cross-section data	UKN	unknown
RLX	relative cross-section data	UNK	
RSP	reaction spectrometer	VIB	vibrational
RLY	relative yield data	VIR PHOT	virtual photon(s)
SCTD	scattered	XN	all neutrons, total neutron yield, $\sigma(\gamma,XN) = \sigma(\gamma,N) + 2\sigma(\gamma,2N) + 3\sigma(\gamma,3N) + \sigma(\gamma,NP) + \text{etc.}$
SCD	semiconductor (solid state) detector	XP	all protons, total proton yield $\sigma(\gamma,XP) = \sigma(\gamma,P) + \sigma(\gamma,NP) + 2\sigma(\gamma,2P) + \text{etc.}$
SCI	scintillator detector other than NaI, e.g., CsI, KI, organic (liquid or solid), stilbene, He	XX	reaction products defined in REMARKS
SEP	separation	XXX	
SEP ISOTP	separated isotope used	YLD	yield
SIG	SIGMA (cross section)		

4PI a 4π geometry was used or a method like radioactivity or a total absorption measurement

999 energy defined in REMARKS

\$ indicates the measurement involved beams or targets that were either polarized or aligned, or that the polarization of the reaction

products was determined. The polarized particle is indicated in REMARKS.

* or @

symbols used to indicate that the units associated with the numerals on one or both sides of the symbol in a specific column are not MeV. The units are defined in REMARKS.

U.S. DEPT. OF COMM. BIBLIOGRAPHIC DATA SHEET (See instructions)		1. PUBLICATION OR REPORT NO.	2. Performing Organ. Report No.	3. Publication Date
4. TITLE AND SUBTITLE Photonuclear Data-Abstract Sheets 1955-1982				
5. AUTHOR(S) E.G. Fuller and Henry Gerstenberg				
6. PERFORMING ORGANIZATION (If joint or other than NBS, see instructions) NATIONAL BUREAU OF STANDARDS DEPARTMENT OF COMMERCE WASHINGTON, D.C. 20234			7. Contract/Grant No.	8. Type of Report & Period Covered
9. SPONSORING ORGANIZATION NAME AND COMPLETE ADDRESS (Street, City, State, ZIP)				
10. SUPPLEMENTARY NOTES				
<input type="checkbox"/> Document describes a computer program; SF-185, FIPS Software Summary, is attached.				
11. ABSTRACT (A 200-word or less factual summary of most significant information. If document includes a significant bibliography or literature survey, mention it here) These abstract sheets cover most classes of experimental photonuclear data leading to information of the electromagnetic matrix element between the ground and excited states of a given nucleus. This fifteen volume work contains nearly 7200 abstract sheets and covers 89 chemical elements from hydrogen through americium. It represents a twenty-seven year history of the study of electromagnetic interactions. The sheets are ordered by target element, target isotope, and by an assigned bibliographic reference code. Information is given on the type of measurement, excitation energies studied, source type and energies, detector type, and angular ranges covered in the measurement. For a given reference, the relevant figures and tables are mounted on a separate sheet for each nuclide studied.				
12. KEY WORDS (Six to twelve entries; alphabetical order; capitalize only proper names; and separate key words by semicolons) data-abstract sheets, elements, experimental, isotopes, nuclear physics, photonuclear reactions				
13. AVAILABILITY <input type="checkbox"/> Unlimited <input checked="" type="checkbox"/> For Official Distribution. Do Not Release to NTIS <input type="checkbox"/> Order From Superintendent of Documents, U.S. Government Printing Office, Washington, D.C. 20402. <input type="checkbox"/> Order From National Technical Information Service (NTIS), Springfield, VA. 22161			14. NO. OF PRINTED PAGES 15. Price	

